INFLUENCE OF ACTIVE SITE LIGANDS AND NANOPARTICLE SURFACES ON HUMAN CARBONIC ANHYDRASE ISOZYMES

A Dissertation
Submitted to the Graduate Faculty
of the
North Dakota State University
of Agriculture and Applied Science

By

Sumathra Manokaran

In Partial Fulfillment of the Requirements
for the Degree of
DOCTOR OF PHILOSOPHY

Major Department:
Chemistry and Biochemistry

August 2010

Fargo, North Dakota

North Dakota State University
Graduate School

Title

Influence of Active site Ligands and Nanoparticle Surfaces on Human Carbonic Anhydrase Isozymes

By

Sumathra Manokaran

The Supervisory Committee certifies that this ***disquisition*** complies with North Dakota State University's regulations and meets the accepted standards for the degree of

DOCTOR OF PHILOSOPHY

ABSTRACT

Manokaran, Sumathra, Ph.D., Department of Chemistry and Biochemistry, College of Science and Mathematics, North Dakota State University, August 2010. Influence of Active Site Ligands and Nanoparticle Surfaces on Human Carbonic Anhydrase Isozymes. Major Professor: Dr. D. K. Srivastava.

Carbonic anhydrase (CA) is an ubiquitously distributed zinc containing metallo enzyme that catalyzes the reversible hydration of carbon dioxide to form bicarbonate and a proton. Existence of 16 isoenzymes of CA in the animal kingdom has been known so far with varying subcellular and tissue distributions. Due to their involvement in many physiological and pathological processes, these isozymes have been the target for drug designing for the past 6 decades. The present study was designed with the aim of understanding the effect of active site ligands and nanoparticle surfaces on human carbonic anhydrase isozymes.

In an effort to identify a fluorescent probe for carbonic anhydrases, the quantum yields and binding affinities of a variety of naphthalenesulfonamide derivatives with human carbonic anhydrase isozymes (hCAs) were determined. In this pursuit, a highly sensitive fluorescent probe, JB2-48 was identified. Experiments involving the above flurophore with hCA I unraveled the contributions of the sulfonamide moiety and the hydrophobic regions of the ligand structure on the spectral, kinetic, and thermodynamic properties of the enzyme-ligand complex. The fluorescence data revealed that the deprotonation of the sulfonamide moiety of the enzyme-bound ligand increases the fluorescence emission intensity as well as the lifetime of the ligand. This is manifested via the electrostatic interaction between the active site resident Zn^{2+} cofactor and the negatively charged sulfonamide group of the ligand. Evidence was provided that the

anionic and neutral forms of JB2-48 are stabilized by the complementary microscopic/conformational states of the enzyme.

Investigations on the binding of the sulfonamide inhibitor, benzene sulfonamide (BS), with hCA isozymes II and VII, revealed that the binding is stabilized by polar interactions in the former case and hydrophobic interactions in the latter case. In addition, it was found that the binding of BS with hCA II is enthalpically driven at low temperatures, whereas it is entropically driven for its binding with hCA VII.

Due to the prevalence of bipolar distribution of charges on hCA XII, the effects of the interaction of differently charged quantum dots, liposomes and polylysine on hCA XII were investigated. These charged particles were found to differently modulate the active site of the enzyme. The data revealed that whereas polylysine and liposomes exhibited no influence on the binding and catalytic features of the enzyme, quantum dots had significant influence on the above features. Arguments were presented that the above differential feature exhibited by quantum dots, liposomes and polylysine is encoded in the rigidity versus flexibility of the charged molecules.

Studies on the denaturation of hCA isozymes II and XII unraveled their unfolding mechanism. It was found that the unfolding of hCA XII followed a simple two state model from native to unfolded state; however hCA II unfolded with the formation of a stable intermediate.

ACKNOWLEDGEMENTS

Working towards a Ph.D. degree, in my opinion, is truly a roller-coaster ride. Through this journey, I have had the opportunity of interacting and working with several people who were directly or indirectly involved in making this thesis possible. Though it is impossible to express all my thanks to them in this available limited space, I will still try.

First and foremost, I would like to thank my advisor, Dr. D.K. Srivastava for his great guidance and support. His immense knowledge and enthusiasm towards research motivated not only me but the whole group to do good science. I appreciate his valuable time and ideas that helped in conducting this research.

I would also like to thank my committee members, Dr. Sparks, Dr. Sun and Dr. Mallik for their encouragement, valuble comments and questions.

The past and the present members of Dr. D.K. Srivastava's group have contributed immensely towards my personal and professional time. I would like to thank Shakila, my first buddy in the group, for her constant professional and moral support. I would like to express my thanks and gratitude to Al Berg for his help with the experimental design and data analysis even after he moved out from the lab. I am very thankful to Raushan for always having helped me out in experiments and for sharing his knowledge in molecular biology. I have been extremely fortunate to have known Nitesh and his wife Preeti who have been extremely supportive both in professional and personal fronts. They have been a part of our family ever since we became friends. They helped me stay sane through difficult times. Special thanks to Nitesh for proof reading every single line of my thesis. I

would also like to extend my thanks Abir, Kunley, and Bratati for being excellent colleagues.

I would like to thank all the members of the department who in one way or the other helped me in carrying out my research all these years. I am thankful to the financial support by NSF-EPSCoR.

None of this would have been possible without the love and support of my family. I would like to thank my parents and parent's in-laws for their ever lasting love, encouragement and support. I would like to thank my husband Rajesh without whom I would not even have considered pursuing a Ph.D degree. His constant love, support, encouragement, and confidence in me helped me move forward. Lastly, but most importantly I would like to thank my son Srijeev. He has been an excellent child from day one and is a source of my energy and inspiration. To him, I present this thesis.

TABLE OF CONTENTS

LIST OF TABLES

LIST OF FIGURES

Figure Page

LIST OF ABBREVIATIONS

AZM ..... Acetazolamide

AL ..... Anionic liposome

BS ..... Benzene sulfonamide

BSA ..... Bovine serum albumin

CA ..... Carbonic anhydrase

CD ..... Circular dichroism

CL ..... Cationic liposome

CNS ..... Central nervous system

DMSO ..... Dimethylsulfoxide

DNSA ..... Dimethyl naphthalene sulfonic acid

DSC ..... Differential scanning calorimetry

FPLC ..... Fast protein liquid chromatography

GdmCl ..... Guanidinium chloride

HEPES ..... 4-(2-Hydroxyethyl)piperazine-1-ethanesulfonic acid

hCA ..... Human carbonic anhydrase

hCAs ..... Human carbonic anhydrase isozymes

IDA ..... Iminodiacetic acid

IPTG ..... Isopropyl thio-β-galactopyranoside

kDa ..... Kilo Dalton

MES ..... 2-Morpholinoethanesulfonic acid

min ..... Minute

NCBI ..... National center for biotechnology information

NMR..... Nuclear magnetic resonance

NL ..... Neutral liposome

PAGE ..... Polyacrylamide gel electrophoresis

Pfu ..... Polymerase chain reaction

PMSF..... Phenylmethylsulfonyl fluoride

Qds ..... Quantum dots

Qds^{+}..... Cationic quantum dots

Qds^{-} ..... Anionic quantum dots

s ..... Second

SDS ..... Sodium dodecyl sulfate

Xho..... *Xanthomonas holcicola*

CHAPTER 1. INTRODUCTION

1.1. A literature review detailing the carbonic anhydrase family

1.1.1. Discovery of carbonic anhydrase

Carbon dioxide (CO_2), the major end product of aerobic metabolism is released into the blood and is transported to lungs for exhalation. Untill the early 1900s, scientists did not have a clue as to the mode of CO_2 transport in blood and its release in lung capillaries. Two major theories, namely the "direct combination theory" and the "bicarbonate theory" were proposed to explain the above process. According to the "direct combination theory", direct reversible combination of bicarbonate (HCO_3^-) to blood proteins, especially Hb, leads to its transport (*1-5*). According to the "bicarbonate theory", bicarbonate (HCO_3^-) is the main carrier of CO_2 in the blood and when the blood reaches the lungs, the blood proteins that act as weak acids convert the bicarbonate into carbonic acid (H_2CO_3), which is then dehydrated to water (H_2O) and CO_2 (*6-9*). The latter is then released through lungs by exhalation. Studies conducted from 1917-1925 revealed that under physiological conditions, majority of CO_2 in blood exists in the form of free CO_2, HCO_3^-, and H_2CO_3 and the amount of its existence in any other form is negligible. The reaction according to the bicarbonate theory proceeds in two steps.

$$HP\ (\text{Protein acid}) + NaHCO_3 \longrightarrow NaP\ (\text{Protein salt}) + H_2CO_3 \qquad (1.1)$$

$$H_2CO_3 \longrightarrow CO_2 + H_2O \qquad (1.2)$$

Of the two steps involved in bicarbonate theory, (1.1) is very rapid as it is ionic. Therefore, the second step was considered as a rate limiting step and it was of interest to determine the rate of that step.

In 1913, Theil found that when OH^- was added to a CO_2 solution containing a pH indicator, the color of the solution changed slowly, indicating a drop in pH (*10*). In 1924, Faurholt measured the kinetics of the carbon dioxide hydration by mixing CO_2 and H_2O and rapidly adding $BaCl_2$ and an amine to the above mixture, which resulted in the formation of $Ba(HCO_3^-)_2$ and carbamine. Both the products being soluble permitted their analysis in solution on a slower time scale (*11*). According to these experiments, the rate of CO_2 dissociation from bicarbonate was slow. All these experimental outcomes were not in favor of the bicarbonate theory, since by then it was known that the amount of time the blood spends in active circulation in capillaries was only 1 s. The importance of studying the kinetics of the above reaction in blood was then pointed out by Hartridge and Roughton after their measurements of the rate of assosiation and dissociation of oxygen with Hb (*10*) Using the rate constants obtained by Theil and Farrholt, other scientists including Henriques calculated that in the second step, the rate of CO_2 formation under physiological conditions would be much lower than actually observed in the exhaled air. Henriques then came up with the startling conclusion that either one or both of the following conditions must be met: (a) there must be a catalyst in the blood for the second step; (b) CO_2 must be transported by some other means besides bicarbonate in the blood. In 1928, Henriques compared the rate of CO_2 formation from blood and serum samples by shaking them vigorously in vacuo. He found that whereas CO_2 evolved from the blood samples at the very early stages of shaking, the rate of its escape from serum was similar to the ones calculated by Faurholt. Based on this result, he concluded that a very rapid reversible reaction between CO_2 and Hemoglobin (Hb) takes place (similar to the reaction between Hb and O_2) the catalytic mechanism of which could not be explained. He gave the name

carbHb to the hypothetical complex between Hb and CO_2 (*10*). Hawkins and van Slyke (1930) and Brinkman and Margaria (1931) showed that, addition of very dilute blood or Hb to buffers of physiological pH resulted in the rapid evolution of CO_2 (*12*)

Eventually in 1932, Meldrum and Roughton isolated a white substance from ox blood which accelerated the reaction even when it was diluted to 1 part in 10,000,000. This substance free from Hb and other heme compounds had properties of an enzyme distinct from other known enzymes of blood and was given the name "Carbonic anhydrase (CA)" (*11*). Soon after its discovery, Meldrum and Roughton purified the enzyme from red blood corpuscles and studied its properties. They found the enzyme to be stable between the pH range of 3.0 and 12.0 and inactivated when heated for 30 minutes at 65°C. Various compounds including CO, cyanides, sulphides, azides, Cu, Ag, Au, Zn(II), Hg, phenyl urethane were also found to inhibit the enzyme activity (*11*).

1.1.2. CA families

It is speculated that Carbonic anhydrases (CAs) are the first enzymes to have appeared as they catalyze a very basic chemical reaction, the reversible hydration of CO_2 to form HCO_3^- and H^+ ions. Homologous forms of CA genes are found in certain algae and bacteria, which could possibly be the first gene that arose before the evolution of prokaryotes and eukaryotes almost half a billion years ago. During the course of evolution, these genes underwent significant duplications, resulting in new genes (*13*).

CAs are encoded by five, evolutionarily unrelated gene families, namely alpha (α), beta (β), gamma (γ), delta (δ) and epsilon (ε). The five classes of CA families have no sequence identities, which is indicative of their independent evolutionary origin (*14-19*) .

1.1.2.1. The alpha (α) CAs

The CAs that belong to mammals are all classified as α CAs which are the best characterized family. In vertebrates, at least 16 different CAs (CA I-CA XV) are identified to date. They possess zinc as the active site metal (*20-22*). Their sub cellular locations and kinetic parameters for CO_2 hydration reaction are listed in Table 1.1. The catalytic mechanism and structural features of the enzymes of this class are detailed in the next section (section 1.1.7 and 1.1.10).

1.1.2.1.1. Mammalian CAs (isozymes of the alpha class of the family)

1.1.2.1.1.1. Background of discovery

Until thirty years after the discovery of CAI from bovine erythrocytes, scientists were unaware of the existence two distinct forms of this enzyme in the erythrocytes. These two forms of the enzymes had very different rates of activity. The isozyme that is present at high concentrations had a low catalytic activity, and the one present at low concentrations had a higher catalytic activity (at least 5 to 6 fold higher than the other form) and were named as CA I and CA II (*23*, *24*) respectively. To be specific, CA II, the most efficient enzyme catalyst of this family known till date, has a turnover number of 10^6 s^{-1} for CO_2 hydration at pH 9, 25°C (*24*), whereas CA I is less efficient with a turnover number for CO_2 hydration equal to 2×10^5 s^{-1} (*25*).

Until 1976, only two isoforms of CAs were known to exist. In 1976, high concentrations of another enzyme in human muscle cells were identified with CA activity (*26*). The activity of this enzyme was far lower than the other CA isozymes (only 5 % as compared to that of CA I) due to the absence of the proton shuttle residue, His64. Interestingly, this particular isoform of the enzyme was found to be insensitive to

acetazolamide, a potent inhibitor of CAs (*27*). The sequence of this form closely resembled that of CA I and CA II (*28*) indicating common evolutionary ancestory. The muscle enzyme was later named CA III.

After the discovery of CA III, many isoforms of this class have been identified to date. CA IV was the first membrane bound enzyme identified within the CA family. This enzyme is anchored to the membrane surface by a glycosylphosphatidylinositol (GPI) tail (*29-31*). CA IV is known to be a highly active enzyme with a pH-independent k_{cat} value of $1.1 \times 10^6\ s^{-1}$ (*32*).

CA V was the next class of the enzyme identified in the mitochondria of guinea pig liver (*33*, *34*). The cDNA for human mitochondrial CA V was recently cloned from a human liver cDNA library (*35*, *36*) and was also found to be highly expressed in rat and mouse islet cells (*37*). Two forms of CA V are known to exist, CA VA and CA VB. Whereas CA VA is expressed abundantly in liver, CA VB is expressed in a normal human heart and skeletal muscle (*34*, *35*). The highly conserved amino acid residue His64 in murine CA V is replaced by a tyrosine (*38*). Although tyrosine is considered as a poor proton shuttle residue, it still achieves a maximal turnover in CO_2 hydration of $3 \times 10^5\ s^{-1}$ at pH > 9 (*39*).

Ferney et al. discovered CA VI in sheep saliva (*14*) which was later purified from human saliva (*40*). Up to 10-14 mg of CA VI is expressed per day in saliva. This enzyme exhibits only 2% of the catalytic activity exhibited by CA II (*40*, *41*). Although this enzyme is normally secreted, it is also found to be expressed intracellularly in response to stress. Both these forms of the enzyme are regarded to be the products of the same gene but under the control of different promoters (*42*).

CA VII, although expressed in low amounts, is widely distributed. The gene for this enzyme was isolated from the human genomic library by Montgomery et al in 1991 (*43*). The catalytic activity of the enzyme was found to be very high with a k_{cat} value of 9.4 x 10^5. However, the tissue expression of this enzyme is not yet known (*44*).

CA IX was first discovered in HeLa cells, which were obtained from a human cervical carcinoma line (ref). It is not found in normal cervical cells (*45*). CA IX is a membrane associated glycoprotein with an extracellular facing catalytic domain and a transmembrane anchor followed by a short C-terminal cytoplasmic tail. The N-terminal side of CA IX is extended with a proteoglycan -like region which is unique to this isoform (*45*, *46*).

CA XII is another membrane bound protein, belonging to this class of the enzyme. Although CA XII mRNA was found to be expressed in non malignant tissues, it was originally identified as a tumor associated gene expressed in renal and lung cancer cells (*47*, *48*). CA XII is a dimeric, bitopic membrane protein with a N-terminal extracellular catalytic domain, a membrane-spanning α-helix, and a small intracellular C-terminal domain (*49*).

Analysis of the human and mouse genomic data identified another new isozyme of this class viz., CA XIII. The catalytic activity of this isozyme is similar to that of cytosolic CA I and mitochondrial CA V (*50*). Similar to CA II, CA XIII is widely distributed in several organs including the thymus, small intestine and colon (*50*).

CA XIV is a transmembrane protein comprised of an extracellular catalytic domain, a single transmembrane helix, and a short intracellular polypeptide segment. It is found in kidney, liver, brain, skeletal muscle, heart, and lung (*51-53*).

The latest member of this class was first identified and isolated from mouse kidney in 2005. Like CA IV (*31*), CA XV is also a GPI anchored enzyme (*54*). It is expressed in several species in vertebrates; however, in humans and chimpanzees, the gene has become non functional (*54*).

Apart from the above mentioned catalytically active CAs, some non catalytic CAs also form a part of this class. These are termed as CA – related proteins (CA-RP). The roles of CA-RP VIII, X and XI are not clear at this point. The amino acid sequences of CA-RPs are strictly conserved, suggesting that they may have important functions associated with binding to molecules in the cytosol or cellular structures (*55*).

1.1.2.2. The beta (β) CAs

Initially, this class of CA was thought to be present only in plants, but later found to be widely distributed in algae, bacteria and archaea (*17*, *56-63*). The first crystal structure of this class, from the red alga *Porphyridium purpureum*, revealed a novel catalytic site for CO_2 hydration (*17*). The enzymes of this class are different from that of α and γ CAs in that these enzymes are often dimers, tetramers, hexamers and octamers whereas the α CAs has either monomeric or dimeric enzymes and γ CAs are trimeric enzymes. Crystal structures of four β CAs are available to date (*17*, *57*, *59*, *60*, *62*). The zinc ion present in the catalytic site is ligated by two conserved cysteine residues and one conserved histidine residue. For some members belonging to this class, it was found that the water molecule that is usually bound to the catalytic zinc was absent. Thus it has been suggested that the active site of CAs belonging to this group is blocked at pH 7.5 or lower, and was reasoned

Table 1.1. Subcellular localizations and kinetic parameters for CO_2 hydration reaction by CAs.
The kinetic parameters were obtained for human CA (hCA) and murine CA (mCA) isozymes at 20°C and pH 7.5. The Table is adapted and modified from reference (*20*)

Isozyme	K_{cat} (s^{-1})	K_m (mM)	K_{cat}/K_m ($M^{-1}s^{-1}$)	Subcellular localization	Refs
hCA I	2.0×10^5	4.0	5.0×10^7	Cytosol	(*20*, *64*, *65*)
hCA II	1.4×10^6	9.3	1.5×10^8	Cytosol	(*20*, *64*, *65*)
hCA III	1.0×10^4	33.3	3.0×10^5	Cytosol	(*20*, *64*, *65*)
hCA IV	1.1×10^6	21.5	5.1×10^7	Membrane-bound	(*64*, *65*)
hCAVA	2.9×10^5	10.0	2.9×10^7	Mitochondria	(*66*)
hCAVB	9.5×10^5	9.7	9.8×10^7	Mitochondria	(*66*)
hCAVI	3.4×10^5	6.9	4.9×10^7	Secreted (saliva, milk)	(*67*)
hCAVII	9.5×10^5	11.4	8.3×10^7	Cytosol	(*68*)
hCAVIII	ND	ND	ND	Cytosol	(*20*, *64*, *65*)
hCA IX	3.8×10^5	6.9	5.5×10^7	Transmembrane	(*56*, *20*, *64*, *65*, *69*)
hCAX	ND	ND	ND	Cytosol	(*20*, *64*, *65*)
hCAXI	ND	ND	ND	Cytosol	(*20*, *64*, *65*)
hCAXII	3.8×10^5	12.0	3.5×10^7	Transmembrane	(*49*)
hCAXIII	1.5×10^5	13.8	1.1×10^7	Cytosol	(*50*)
hCAXIV	3.1×10^5	7.9	3.9×10^7	Transmembrane	(*70*)
mCAXV	4.7×10^5	14.2	3.3×10^7	Membrane-bound	(*54*)

that at pH below 7.5, the carboxylate of an aspartic acid coordinates to the Zn(II) ion as the fourth ligand. However, at pH values above 8.3, aspartate forms a salt bridge with arginine thereby leading to opening of the active site and making way for a water molecule to bind the zinc ion. It has been proposed that, once the water molecule binds to the active site, it would have a mechanism similar to that of α CAs for catalyzing the CO_2 hydration and dehydration. According to phylogenitic analysis, this class is more diverse than others. Sequence alignment of the available enzymes of this class indicated that only 5 residues, two cysteines and one histidine (that chelate the zinc ion) plus an aspartate and arginine are conserved (*17, 59-62*).

1.1.2.3. The gamma (γ) CAs

The γ CAs are found in methane-producing bacteria and archea. The enzymes of this class are thought to have evolved between 3.0 and 4.5 billion years ago (*18*). The enzyme "Cam" from the archaeon *Methanosarcina thermophila* is a homo trimer with a left handed parallel beta helical fold. As this enzyme is active when zinc is substituted with cobalt and iron, it is possible that it has a different catalytic metal other than zinc in *Methanosarcina thermophila*. The crystal structure of Cam showed several differences between this class and other classes of CAs. The zinc ion in the active site of Cam is coordinated by three histidine residues and 2 water molecules forming trigonal bipyramidal coordination geometry. When zinc is substituted with cobalt, the coordination becomes octahedral. Surprisingly, it was found that of the three histidine residues coordinating the catalytic metal ion, two comes from one monomer and the third is from the other monomer. Thus, the active sites are located at the interface between pairs of monomers. It has also been suggested that this class of CA would probably follow the same catalytic mechanism

as that of α CAs and that the zinc ion probably transitions between the tetrahedral and trigonal bipyramidal geometry (*71-73*).

1.1.2.4. The delta (δ) CAs

The δ class of CAs is found in diatoms. X-ray structures of a 27-kDa monomeric CA from the marine diatom *Thalassiosira weissflogii* showed that the catalytic zinc atom is coordinated by three histidine residues and a water molecule similar to that of the enzymes from the α CAs. This suggested that the catalytic mechanism of this class would also be similar to those of the α CAs (*61*).

1.1.2.5. The epsilon (ε) CAs

This class of CAs is found in bacteria, chemolithotrophs and marine cyanobacterias. It was found in chemolithoautotroph *H. neapolitanus*. The enzymes of this class are a catalytically functional component of the shell of cso-carboxysomes. This class has some structural resemblance to the β CAs near the catalytic metal ion site although significant sequence similarity between these classes was not observed (*74*)

1.1.3. Distribution of α CAs

The α CAs are widely distributed in many cells and tissues of the body and is summarized in Table 1.2.

1.1.4. Physiological reaction catalyzed by CAs

The interconversion between carbon dioxide and bicarbonate (Eqn 1. 3), a very simple physiological reaction, is catalyzed by CAs (*65*, *75*)

$$CO_2 + H_2O \rightleftharpoons HCO_3^- + H^+ \qquad (1.3)$$

The above reaction takes place even in the absence of CAs. However, their first order rate constants for the hydration and dehydration of the above reaction are 3.5×10^2 and 20 sec^{-1}

Table 1.2. Distribution of CAs.

α CAs	Distribution	References
CAI	Red blood cells, vascular endothelium and gastrointestinal epithelia, tissues such as corneal endothelium, lens and ciliary body epithelium of the eye, sweat glands, salivary glands, adipose cells and myoepithelial cells.	(*20*, *64*, *65*, *21*, *76*)
CAII	Widely distributed in cells of almost all the tissues such as osteoclasts of bone, oligodendrocytes of brain, ciliary body, lens and retina of the eye, perivenous cells of liver, kidney tubules, acinar cells of salivary glands, ductal cells of pancreas, parietal cells of stomach, uterus etc.	(*20*, *64*, *65*, *21*, *76*)
CAIII	Skeletal muscle, salivary glands, smooth muscle, red cells, prostate gland, lung, kidney, brain colon, mammary gland, and testis.	(*20*, *65*, *21*, *76*, *77*)
CAIV	Capillary endothelium of lungs, brush borders of the tubular cells of kidney, muscle, liver and gastrointestinal mucosal cells.	(*65*, *21*, *76*, *77*)
CAV	CA VA –liver ; CA VB- heart and skeletal muscle pancreas, kidney, spinal cord, GI tract.	(*35*, *36*, *65*)
CAVI	Salivary glands and mammary glands.	(*78-81*)
CAVII	Central nervous system (CNS).	(*82*, *83*)

Table 1.2. continued

CA VIII	Central nervous system (CNS).	(*84*, *85*)
CA IX	Tumors and gastrointestinal mucosa.	(*86-94*)
CA X	Central nervous system (CNS).	(*20*, *77*, *85*)
CA XI	Central nervous system (CNS).	(*20*, *77*, *85*)
CA XII	Renal, intestinal, reproductive epithelia, eye, tumors.	(*49*, *20*, *86*, *87*, *94-97*)
CA XIII	Kidney, brain, lung, gut, reproductive tract.	(*50*, *21*, *98*, *99*)
CA XIV	Kidney, brain, liver	(*70*)
CA XV	Kidney	(*54*, *21*)

respectively. These rates are not fast enough to accomplish the dehydration and excretion of CO_2 through lungs and hydration of respiratory CO_2 in blood in the physiological system (*100*, *101*) and this discrepancy between the rates led to the discovery of the CAs (*11*, *102*).The above reaction catalyzed by CAs is involved in a variety of physiological and biochemical processes due to which its physiological significance is vast as detailed below.

Although, CAs catalyze a variety of other reactions (Figure 1.1), in addition to the reversible hydration of CO_2 to bicarbonate (Eqn 3), it is unclear at this moment whether these reactions have any physiological significance (*65*, *21*, *77*).

1.1.5. Physiological roles of CA isozymes

The major role of CA is the transport and excretion of CO_2. CO_2 produced by the citric acid cycle diffuses from the tissues into the blood stream. CA present in the blood

favors the forward reaction of Eqn 1.3. Whereas the H^+ formed are buffered by the Hemoglobin (Hb) present in the blood, the HCO_3^- ions diffuse in to the plasma in exchange

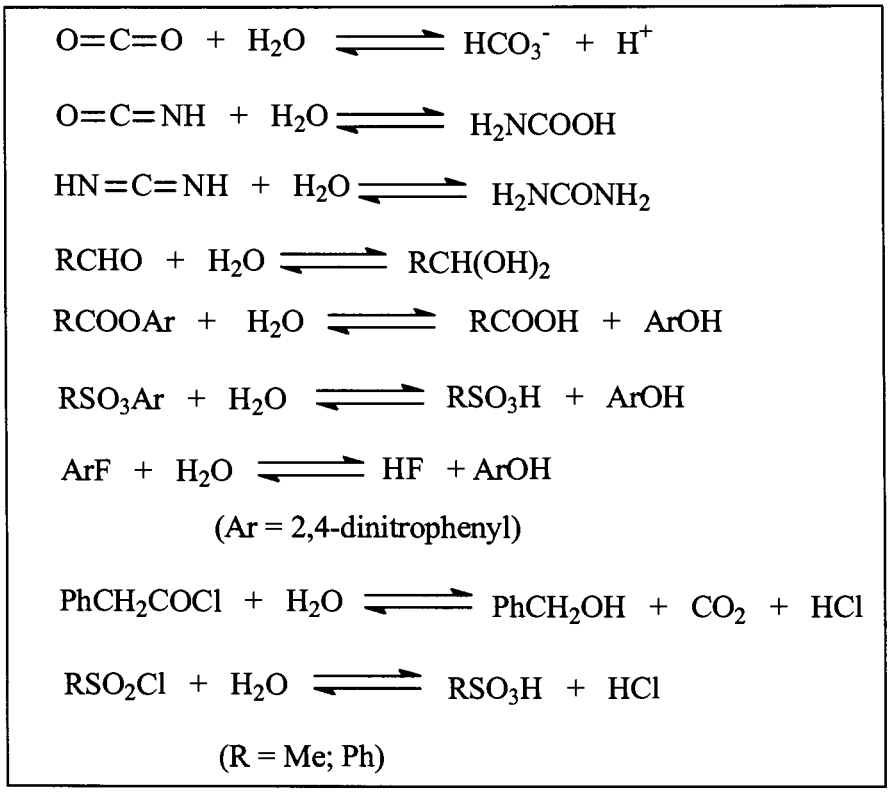

Figure 1.1. Reactions catalyzed by α- Carbonic anhydrases.
The Figure is adapted from reference (*21*).

for Cl^- ions. This process removes the end products of CO_2 hydration, ie, H^+ and HCO_3^- ions from tissues. At the respiratory surface, the reverse reaction of Eqn. 3 takes place and the carbon dioxide that is formed is excreted from the body (*100*, *103*, *104*). Another role of CA is its ability to aid O_2 and CO_2 transport with in the RBC. As Hb present in the blood buffers the H^+ ions formed from the hydration reaction, its affinity for oxygen decreases and oxygen is released from the RBCs. Conversely, the large amount of oxygen at the respiratory surface reduces Hb's affinity to bind protons. This is referred to as the Haldane

effect, where the deoxygenated blood carries more CO_2 than oxygenated blood (*105*, *106*). The release of free protons from Hb (due to excess oxygen) and release of CO_2 across the respiratory surface causes CAs to catalyze the dehydration reaction which inturn produces more CO_2 which is then released from the body.

In muscle, CA IV located on the capillary walls helps in the transport of CO_2 into the capillaries by facilitating the hydration of CO_2, and thus maintains the concentration gradient of CO_2 between muscle and blood. In mammals, this is important during physical activity when CO_2 concentration in the muscle increases (*106*). Because of the fast production of H^+ in RBC (due to presence of CA) and the slow production of H^+ in plasma (due to absence of CA), pH disequilibrium between RBC and plasma takes place. CA IV, bound to the capillary surface produces H^+ in plasma and maintains the pH between RBCs and plasma (*106*).

The CA IV in muscle fibers (*107*) and cardiac muscle present on the surface of sarcolemma and sarcoplasmic reticulum (*108*) provides HCO_3^- to the interstitial space. HCO_3^- ions act as a buffer and are very important for maintaining the lactate efflux. The protons that diffuse out of the cell along with lactate through the H^+- lactate co-transporter are buffered by the HCO_3^- present in the interstitial space (*106*).

Evidence suggests that CA plays a major role in calcification in both vertebrates and invertebrates (*109-112*). In 1997, Lucas and Knapp demonstrated the importance of CA in calcification of leptogorgia virgulata (*113*). Regulation of calcium transport and its accumulation is very important in living organisms especially in calcification. Calcified hard tissues provide structural support and integrity to the body. This calcium is usually precipitated in the form of calcium carbonate and calcium phosphate. In mammals, CA has

been suggested to have a role in cartilage calcification, but no clear evidence for this suggestion is available till date. Studies suggest that, just before the calcification process takes place in the cartilage matrix, CA is secreted from hypertrophic chondrocytes into the extra cellular matrix (*80, 114-116*). It is suggested that the high pH of the cartilage extra cellular fluid that helps in calcium phosphate precipitation is due to the presence of CA in the growth plate cartilage which facilitates CO_2 transport (*117*).

CA plays an important role in the ciliary body of the eye by maintaining the mechanism of sodium transport into the eye (*118*). The influx of sodium ions into the eye is accompanied by the transport of water; both processes are important in maintaining the aqueous humor secretion (*119, 120*).

CAs present in the nervous system also facilitates many functions. CA is the primary contributor of cerebrospinal fluid in the choroid plexus (*121*). CAs are also found in oligodendrocytes and glial cells and sensory neurons of the brain and plays a significant role in signal processing, long-term synaptic transformation, and attentional gating of memory storage (*120, 122, 123*).

CA II present in the salivary glands and gastric surface epithelial cells catalyzes the production of bicarbonate into the saliva and gastric juice (*124*). CA VI is also expressed in the serous acinar and demilune cells of the sub mandibular and parotid glands (*79, 80*). Studies suggest that CA II and CA VI may have an important role in the regulation of the acid- base balance in the upper alimentary canal and at the appearance of acid peptic disease is linked to decreased secretion of CA VI and bicarbonate. Presence of CA II in the salivary glands and esophageal and gastric mucosal epithelium might be involved in enhancing the buffer capacity of the saliva and gastric secretions by supplying these fluids

with bicarbonate, thus creating a bicarbonate barrier on the mucosal surface (*79*, *80*). Salivary CA VI might, in turn, be responsible for accelerating the removal of excessive acid in the form of carbon dioxide by catalyzing the reversible reaction of carbon dioxide hydration. This suggests that low secretion of CA VI may retard the neutralizing effect of saliva and bicarbonate ions, and thus contribute to other factors responsible for the appearance of acid peptic diseases (*125*).

Apart from these functions, CAs also provide bicarbonate for a variety of enzyme-catalyzed carboxylation reactions. Gluconeogenesis requires mitochondrial CA V to provide bicarbonate for pyruvate carboxylase, a key enzyme that replenishes intermediates in the synthesis of fatty acids, amino acids, neurotransmitters, and porphyrins (*33*, *126-128*).

1.1.6. Pathological roles of CA isozymes

1.1.6.1. Diuretics

The CAs present in the kidney play an important role in maintaining the acid-base balance by the secretion and excretion of protons aided by the CO_2 hydration reaction catalyzed by them. They are also involved in the reabsorption of bicarbonate and excretion of ammonium ions (*129*, *130*). CA inhibitors (acetazolamide and many other sulfonamide inhibitors) have been widely used as diuretic agents as their administration leads to an increase in the volume of urine which leads to increased bicarbonate, Na^+ and K^+ elimination as well as decreased chloride elimination. This occurs due to the inhibition of CA in the proximal tubule which in turn leads to inhibition of H^+ secretion by nephrons. The net effect of these processes is the transport of sodium bicarbonate from the tubular lumen to the interstitial space, followed by movement of the isotonically obligated water,

and augmented diuresis. CA inhibitors are also used to treat hypertension and congestive heart failure (*20*, *77*, *129*, *130*).

1.1.6.2. Glaucoma

Glaucoma is a chronic eye disease, caused by high intraocular pressure (IOP). The high IOP in turn leads to irreversible damage to the optic nerve head, resulting in the progressive loss of visual function and eventually blindness (*131-133*). As CAs plays an important role in secreting the aqueous humor of the eye, its inhibition decreases the production of bicarbonate, which subsequently lowers the intraocular pressure. This makes CA inhibitors effective therapeutics in the treatment of glaucoma (*77*, *131-138*). Presently, acetazolamide, brinzolamide, dorzolamide and methazolamide are the sulfonamide inhibitors that have been approved by FDA for the treatment of glaucoma. The CA inhibitors are also used in the treatment of macular degeneration and macular edema, the disorders that affect the central retina (*119*, *132*, *139*, *140*).

1.1.6.3. Obesity

CAV (A and B) present in mitochondria is involved in several biosynthetic processes, such as ureagenesis, gluconeogenesis and lipogenesis. These two isozymes along with cytosolic CA II are involved in the supply of bicarbonate, the substrate involved in several biosynthetic processes (*33*, *34*, *141*). Studies suggest that CA inhibitors could potentially be used as anti-obesity drugs. For example, topiramate was found to decrease energy and fat gain in zucker rats.. It also serves as an effective inhibitor of CAV. In addition, when this drug was administered to patients to treat epilepsy, it also resulted in the loss of body weight. Administration of zonisamide, an aliphatic CA inhibitor, to obese female patients who are on low caloric diet, resulted in a 11 pound weight loss as compared

to the obese female patients, who are on low calorie diet alone. Thus, it has been proposed that inhibition of CA V and CA II might represent targets for novel anti-obesity drugs by reducing lipogenesis (*20*, *141-143*).

1.1.6.4. Osteoporosis

CA II present in the bone is responsible for the supply of protons, formed from the hydration of CO_2, to an ATP-dependent proton pump which uses them in the mobilization of calcium from the bone. This is required for the dissolution of the inorganic matrix that precedes the enzymatic removal of organic bone matrix. Exposure of low concentrations of inhibitor in rat osteoclast cultures lead to increased osteoclast number and bone resorption activity, whereas higher concentrations affected cell survival. It also causes intracellular acidification in osteoclasts. The inhibiton experiments conducted in vivo and in vitro provide evidence that transport metabolons are involved in the regulation of intracellular pH and CA inhibitors could be used in the design of novel anti-osteoporosis therapies(*20*, *144*). Inhibition of CA also leads to reduced bone loss in postmenopausal osteoporosis, a disease in which bones become extremely porous, are subject to fracture, and heal slowly (*145*).

1.1.6.5. Cancer

Two membrane CA isozymes, CA IX and CA XII have been known to be associated with tumors (*86*, *87*, *89-91*, *93-95*, *146-149*). CA IX shows a high ectopic expression in a variety of hypoxic human tumors and is an endogenous marker of cellular hypoxia (*64*, *89*, *96*, *150-156*). CA IX expression was found to be upregulated in carcinoma cells derived from various organs including oesophagus, lung, kidney, colon and rectum, breast, cervix, and bladder (*64*, *89*, *96*, *150-156*). The expression of CA IX is dramatically

up regulated under hypoxic conditions by direct transcriptional activation of the CA IX gene by the hypoxia inducible factor (HIF) transcription factor , and is down regulated by the wild-type von Hippel- Lindau tumor suppressor protein (pVHL) (*69*, *154*, *157-163*). CA IX participates in the regulation of extracellular pH contributing to acidification of tumor microenvironment thereby increasing the invasive behavior of cancer cells, distant metastasis and resistance to radio/chemotherapy (*164*). Svastova et al. showed that control of acidification of the tumoral extracellular pH is achieved by CA IX only under hypoxic conditions, and this process can be perturbed by inhibiting CA IX with selective sulfonamide inhibitors. CA IX also influences other processes in the cell microenvironment that promotes cell proliferation, invasion, and metastasis. Since CAIX is highly expressed in many hypoxic tumors and plays a role in tumor acidification, it is considered as an important target for anticancer therapy (*69*, *163-166*).

1.1.6.6. CA IX mediated pH regulation in hypoxia

Insufficient supply of oxygen in tumors leads to hypoxia. Hypoxic tumor cells undergo metabolic alterations and thus they are prone to mutations, which then lead to increased resistance to anti-cancer treatment. Since CA IX is not expressed in normal cells, but is expressed in tumor cells, it is considered as an important target for cancer therapy (*92*, *167*). Expression of CA IX is regulated at the level of transcriptional activation. In contrast to other CA isozymes, the catalytic activity of CA IX is insensitive to high lactate concentrations (*167-169*). This helps them to work efficiently in the hypoxic tumor microenvironment rich in lactate, produced by anaerobic glycolysis (*167-169*). However, bicarbonate ions inhibit the activity of CA IX indicating that CA IX may preferentially catalyze the hydration reaction of CO_2 producing bicarbonate which are then transported to

the interior of the cell with the help of bicarbonate transporters. The transport of bicarbonate ions from one side of the plasma membrane to the other is required for the regulation of intra cellular pH (*168-170*). Two possibilities have been proposed in favor of the role of CA IX in pH regulation in hypoxic cells: It contributes to the extracellular microenvironment acidification in hypoxic tumor cells (*92*, *164*, *166-168*), and minimizes the intracellular pH gradient thereby helps in neutralizing the pH of hypoxic tumor cells (*152*, *168*). It is known that the bicarbonate ions produced by CA IX are imported to cytoplasm where it combines with intracellular protons by entering in to a dehydration reaction (catalyzed by cytosolic CAII) thereby maintaining neutral intracellular pH. On the otherhand, it acidifies the extracellular environment as the protons produced by hydration of CO_2 remains outside the cells and contribute to acidosis (Figure 1.2). As the cell proliferation and its survival require maintenance of neutral intracellular pH, it is hypothesized that the pH regulation by CA IX would promote growth of the tumor (*168*, *171*).

CA inhibitors are also involved in treating ulcers as they can suppress the secretion of gastric acid (*119*, *172*).

The structures of CA isozymes have been determined by both X-ray crystallography and NMR spectroscopy. Whereas X-ray crystallography has provided useful structural data about wild type and mutant CAs with and without ligands, NMR has provided information about the structural dynamics of the enzyme along with its bound ligands in the solution phase. The structural features of human CA II (hCA II), the most thoroughly studied isozyme will be discused in detail in the next section along with the structures of other isozymes.

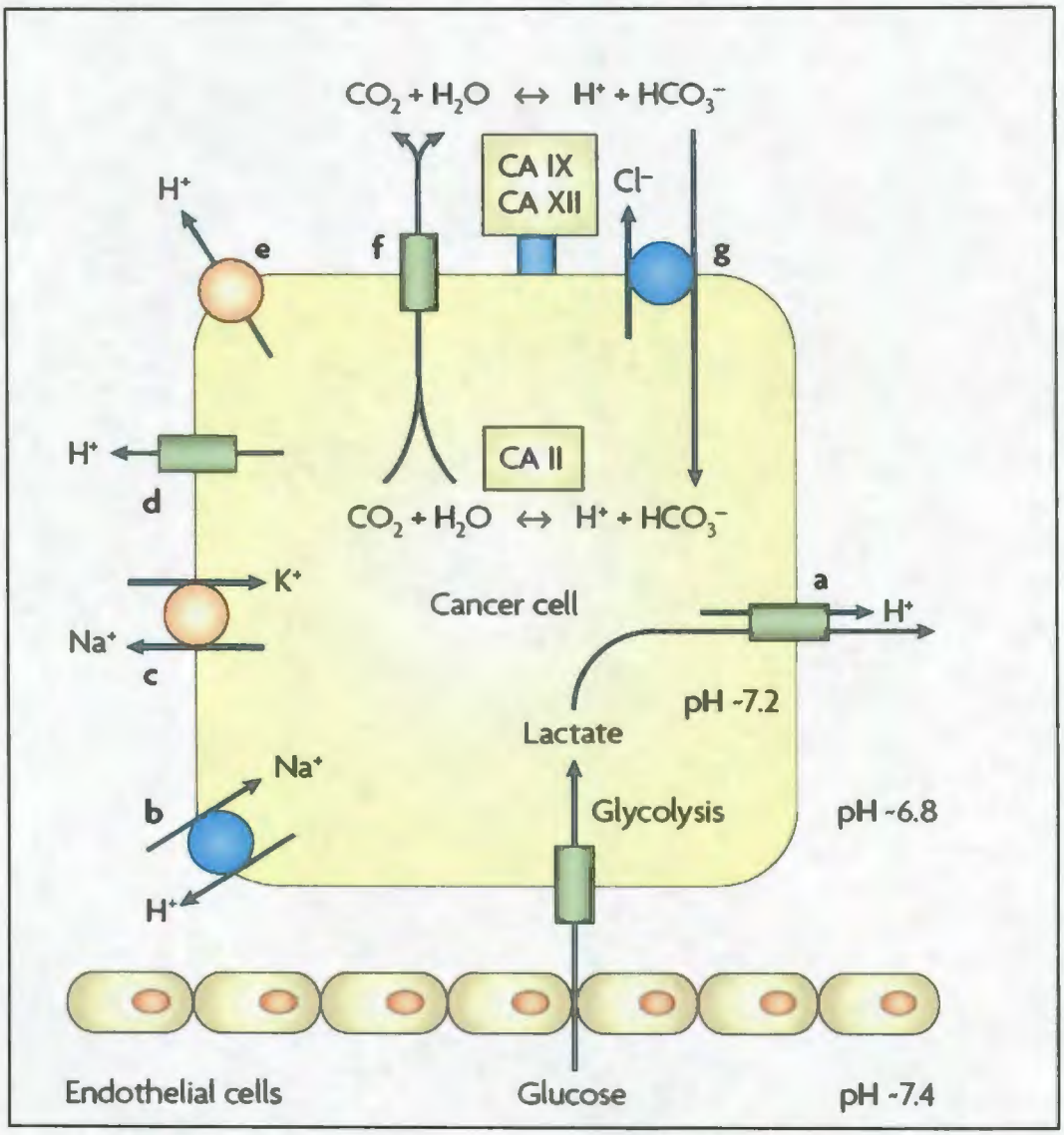

Figure 1.2. pH regulation in tumor cells.
CAIX and/or hCA XII present on the membranes catalyze the hydration reaction of CO_2 producing bicarbonate which is then transported to the cell interior by the bicarbonate transporters. The cytosolic CAII catalyzes the dehydration reaction producing CO_2 and H_2O. The H^+ ions produced in the extra cellular fluid contributes to its acidity. The Figure is adapted from reference (*20*).

1.1.7. Structural features of CA isozymes

1.1.7.1. Structure of hCA II

The X-ray crystallographic studies revealed that the structure of hCA II is an ellipsoid and is divided into two halves by a 10 stranded twisted beta sheet structure and contains α-helices surrounding the β sheets (*173*). The enzyme is characterized by the presence of a C-terminal knot. Two β strands crossover each other such that the knot would still remain in the protein even if the polypeptide chains were pulled from both ends. It also contains an extensive hydrophobic core between the beta sheet and the secondary structural elements on the surface (Figure 1.3).

The hydrophobic core consists of 34 residues of which 10 are aromatic. Of these aromatic residues, 8 are conserved in hCA I and hCA II. To a lesser extent, the aliphatic residues present in this region are also conserved between the two isozymes. A comparatively smaller core of hydrophobic residues present in the upper half is conserved in most CAs. The upper half contains the active site region and the N-terminal residues. A basic patch is seen on the front side of the enzyme. Polar residues are present on the surface of the enzyme opposite to that containing the active site. The substrate binds in the hydrophobic pocket and the large polar patches are proposed to facilitate entry and exit of bicarbonate to and from the active site (*173*).

The active site of hCA II is conical in shape (Figure 1.4) and is about 15 Å deep. The zinc ion present at the bottom of the active site is tetrahedrally ligated by three histidine residues (His94, His96 and His119) and a water molecule (Figure 1.4) (*173*). The pK_a of the zinc bound water is 6.8 for hCA II (*176*). The hydrogen bond between Glu106

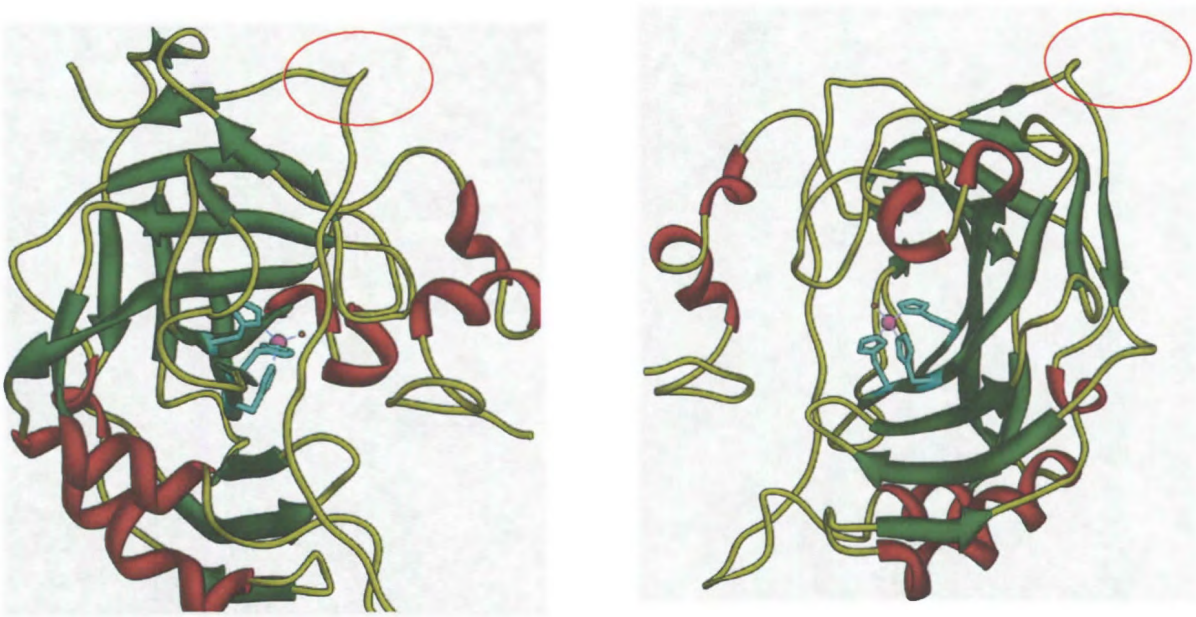

Figure 1.3. Ribbon structure of hCA II.
Ribbon structure of hCA II (PDB ID: 2CBA) (*174*) from two perspectives modeled by UCSF Chimera® software (*175*). α - helices are depicted in red, β – sheets are in green and the random coil turns in yellow. The residues coordinating zinc, His94, His96 and His119 are shown in cyan and zinc is shown in red. The red oval in both the cases represents the C-terminal knot.

and Thr199 helps in aligning the Oγ1 atom on Thr199 in order to accept a hydrogen bond from the Zn(II)-bound hydroxide ion and to orient the lone pair of the hydroxide ion for nucleophilic attack on CO_2 (*173*, *177*, *178*). The hydrogen bonded network in the zinc binding site of hCA II is depicted in Figure 1.5. The hydrogen bond network between Thr199, and Glu106 and 6 water molecules present in the active site interacting tightly with zinc bound water, is responsible for proton transfer into the bulk solution via His64 (*174*, *179-181*). This network along with Thr200, His64, Tyr7, Asn62, Asn67, Gln32 and Glu106 forms the hydrophilic side of the cavity (*182*). Hydrophobic core of the cavity is created by

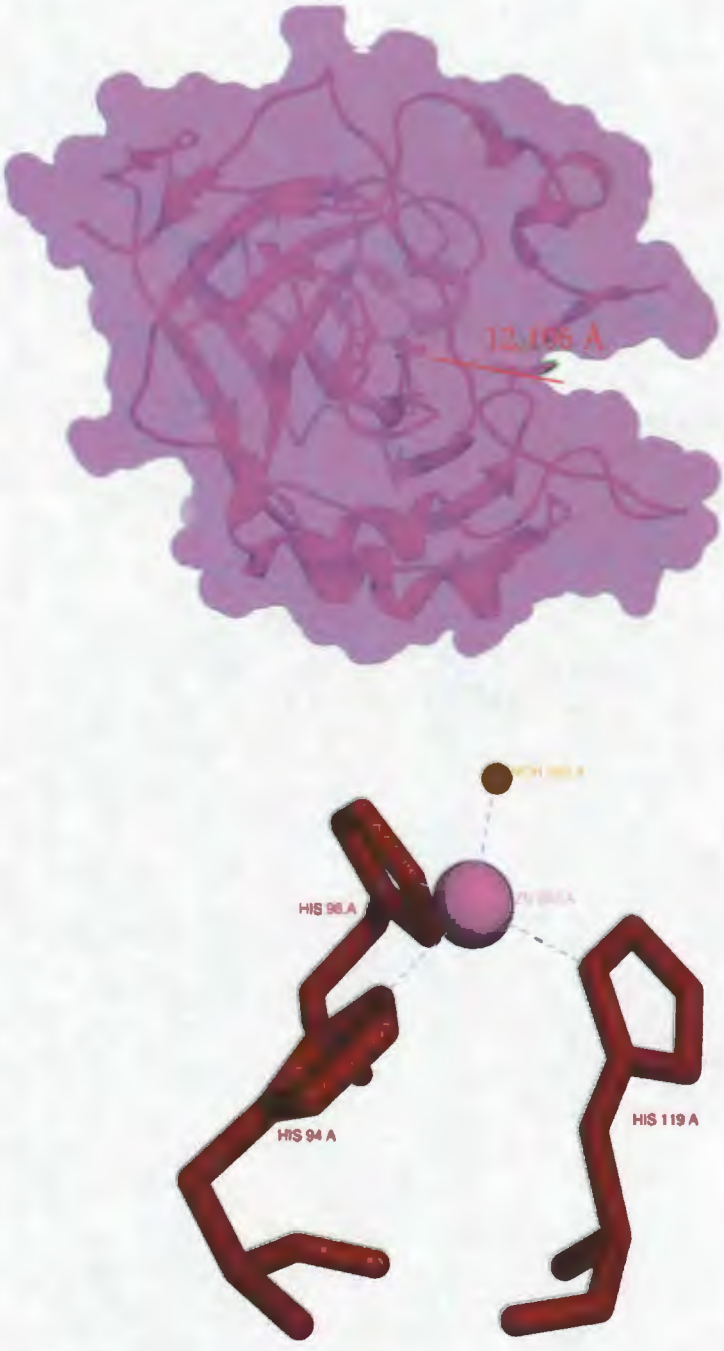

Figure 1.4. Surface diagram and active site of hCA II.
Upper panel shows the surface diagram of hCA II (PDB ID: 2CBA) (*174*). The distance between catalytic zinc and His64 present at the active site entrance is shown. The bottom panel is the close up view of the active site of hCA II. The catalytic zinc ligated to three histidines and a water molecule is shown. The Figure is modeled by UCSF Chimera® software (*175*).

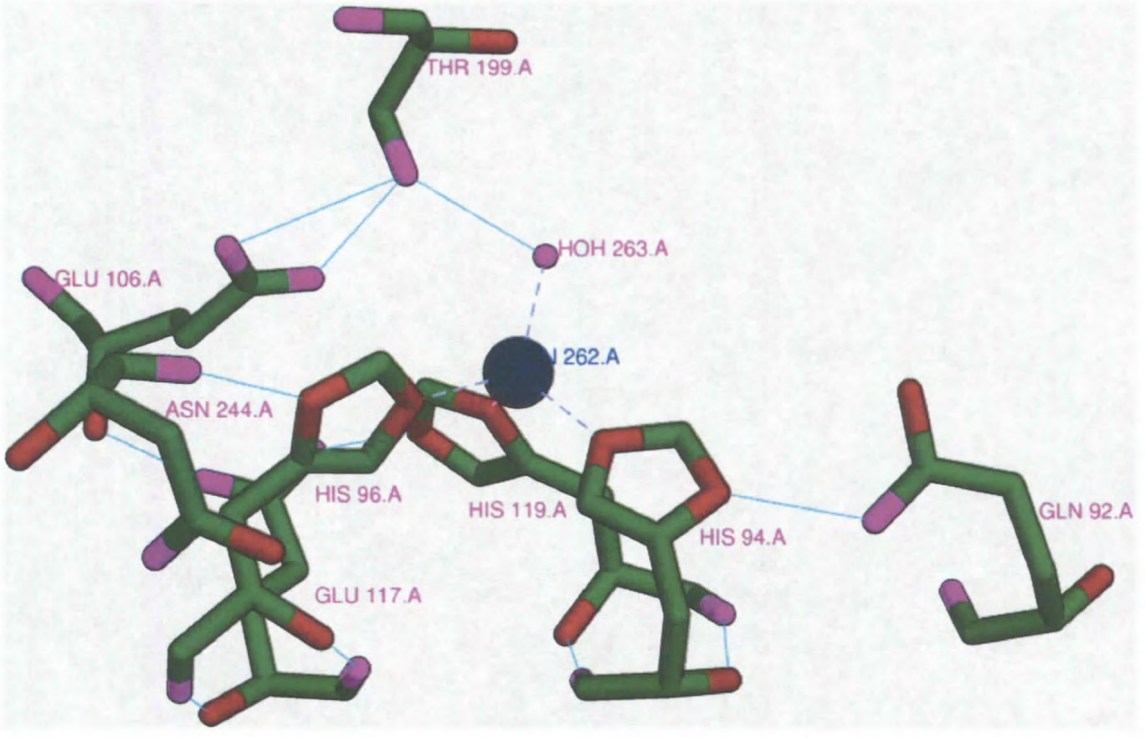

Figure 1.5. Hydrogen bond network in the active site of hCA II.
Hydrogen bond network in the active site of hCA II (PDB ID: 2CBA) (*174*) is shown. Hydrogen bonds are shown as blue lines. The Figure is modeled by UCSF Chimera® software (*175*).

residues Val121, Phe131, Val135, Val143, Leu198, Val207 and Trp209 (*75*, *119*, *183-185*). Computational, NMR and X-ray studies suggest that the binding of CO_2 in the hydrophobic pocket displaces water338 that forms a hydrogen bond with the amide back bone of Thr199 (*183*, *186-190*). X-ray structures showed that cyanate (NCO^-), which is structurally and electronically similar to CO_2, is able to accept a hydrogen bond from Thr199, although, it could not displace the zinc bound water (*190*).

The X-ray crystallographic studies indicated very minimal changes in the global structure of hCA II in the pH range between 5.7 and 8.4. suggesting that the changes in the ligand binding properties at different pH values are due to chemical effects in the active site, such as protonation of the enzyme or ligand rather than global structural effects. Binding of ligands and removal of active site zinc also produced minimal changes in the global structure of the enzyme (*173*, *174*, *182*, *191*, *192*). The structural integrity of the tetrahedral coordination of Zn(II) ion was also unchanged over a broad pH range (pH 5-10). The only difference between hCA II structures over a pH range of 5.1-10 is the positional occupancy of the His64 side chain (Figure 1.6). When the position of the side chain of His64 occupies a conformation oriented away from the zinc ion, it is termed as the "out" conformation and when it occupies a conformation oriented towards zinc ion, it is termed as the "in" conformation. It was found that the occupancy of the "in" conformation increased from 60 – 80 % over the pH range of pH 6.1 and 7.0. However, at pH 5.1, the His64 chain is 90% in the "in" conformation and is suggested to be due to the electrostatic attraction between the imidazolium side chain of His64 and the Zn(II) bound SO_4^{2-}. At physiological pH, the "in" and "out" conformations are at near–equivalent occupancies. It was suggested that in the hydration direction the "in" conformation of His64 may accept a proton from the zinc bound water and becomes the "out" conformation to deliver the proton to solution (*193*). It is argued that as the majority of α CA isozymes are structurally similar, the findings for hCA II is likely to be relevant for other isozymes (*173*, *174*, *182*, *191*, *192*).

1.1.7.1.1. pK_a of the zinc bound water

The changes in the esterase and hydratase activities of hCA II as a function of pH

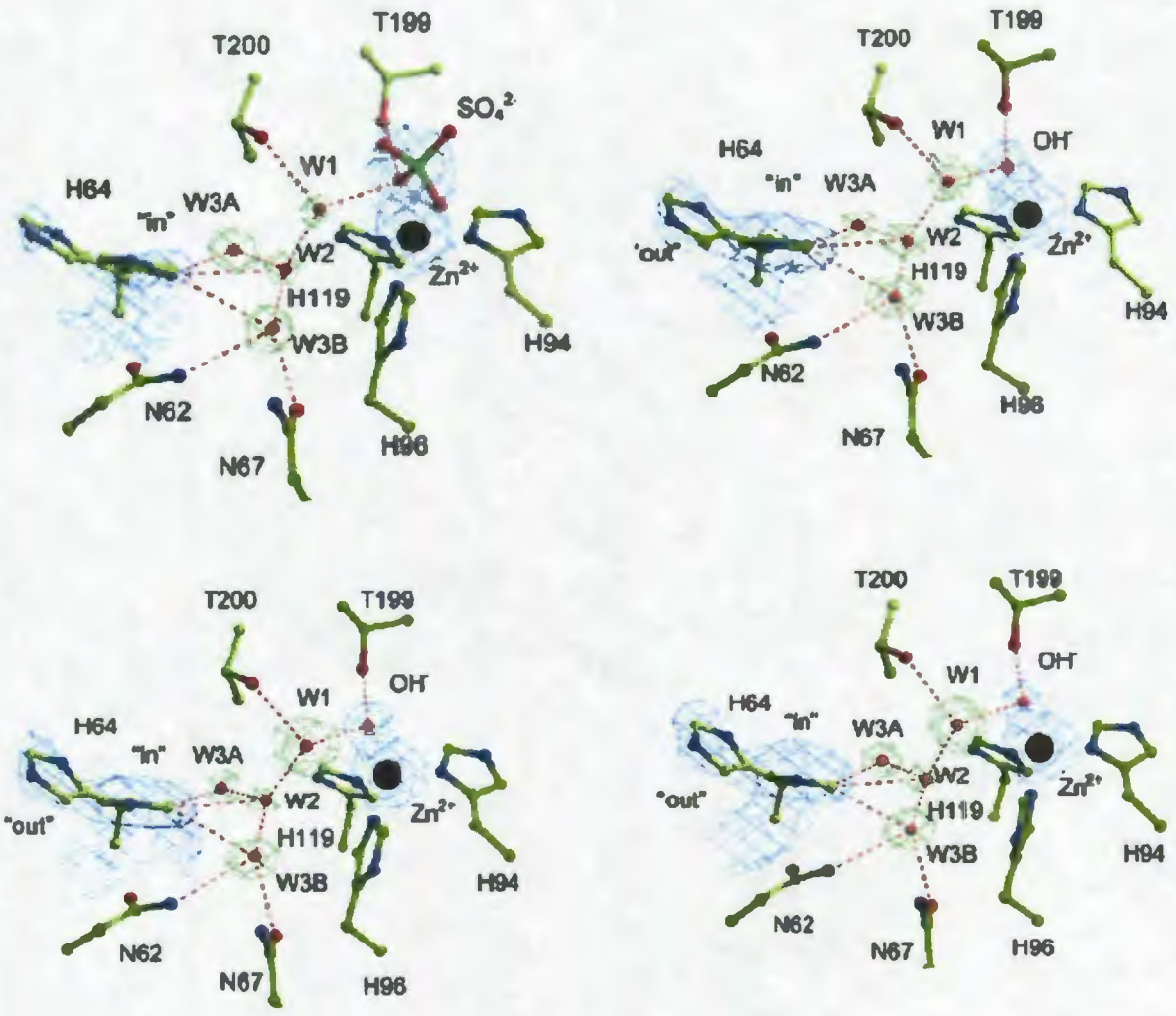

Figure 1.6. Crystal structures of hCA II showing the different positions of His64 at different pH.
All the panels depict the active site in the same orientation. The top left and the right panels show the conformation of active site residues at pH 5.1 and 6.1. The bottom left and right panels show the conformation of active site residues at pH 7.0 and 10.0. The Figure was adapted from reference (*193*).

suggest the presence of a single ionizable group with pK_a of 6.8 which has been widely accepted to be the zinc bound water 263 (*75*, *176*, *194-196*). This pK_a is influenced by the environment of the active site metal. For example, mutation of threonine and the residues that are directly or indirectly coordinated to zinc, alter the pK_a values significantly (*176*,

197, 198). Several groups attempted to determine the influence of pK_a on ligand binding using enzyme activity. However, the protonation of Zn-OH at lower pH led to the reduced activity preventing such determination (*196, 199, 200*). The binding of several aryl sulfonamides to Co(II)-bCA II was monitored by Lindskog using the stopped-flow method. They concluded that, two ionizable groups are involved in ligand binding, one on the inhibitor and one each on the protein. The pK_a value on the protein was found to be 6.6 using a series of inhibitors and this was assigned to the Zn(II)-OH group (*201*). Based on this and other studies (*201, 202*), it was concluded that the same ionizable group of hCA, which is presumably the Zn(II)-bound water263, is involved in ligand binding and catalysis.

1.1.7.2. Structure of hCA I

Human CA I is approximately ellipsoidal, with the active site situated in a dead end cavity similar to that of hCA II, leading to the center of the molecule where the zinc ion is located. On either side of a large beta-structure formed by 10 polypeptide segments, six right-handed helices are present. In addition, a number of smaller beta sheets and three distinct clusters consisting of aromatic residues located at similar distances from the zinc ion are present. Twisted β-pleated sheets are the predominant structural feature observed in hCA I, comprising about 40% of all the residues (Figure 1.7). The active site of hCA I is divided into hydrophilic and hydrophobic cones. Where as the hydrophobic part of the cavity consists of Ser206, Ala121 and 135, Val207, Phe91, Leu131, 138, 146, and 109, and Pro201 and 202, the hydrophilic part of the cavity is comprsed of His64, 67, and 200, Asn69, and Gln92, Thr199, Tyr7, and Val62. Comparison of the structure of hCA I and

Figure1.7. Ribbon structure of hCAI.
The structure of hCA I (PDB ID: 2CAB) (*203*) is modeled by UCSF Chimera® software (*175*). The helices and the beta sheets are represented in red and green color. The catalytic zinc is shown as a round ball in majenta and the ligands (His94, His96 and His119) coordinating the catalytic zinc is shown in cyan.

hCA II reveals very similar shape and tertiary structural features (Figure 1.8) of these enzymes.Despite the fact that the sequences of hCA I and hCA II are not very similar, all the helices, β-sheets and reverse bends are located homologously in the tertiary structures. The location of the active site and the hydrogen bonded network involving His94, His96,

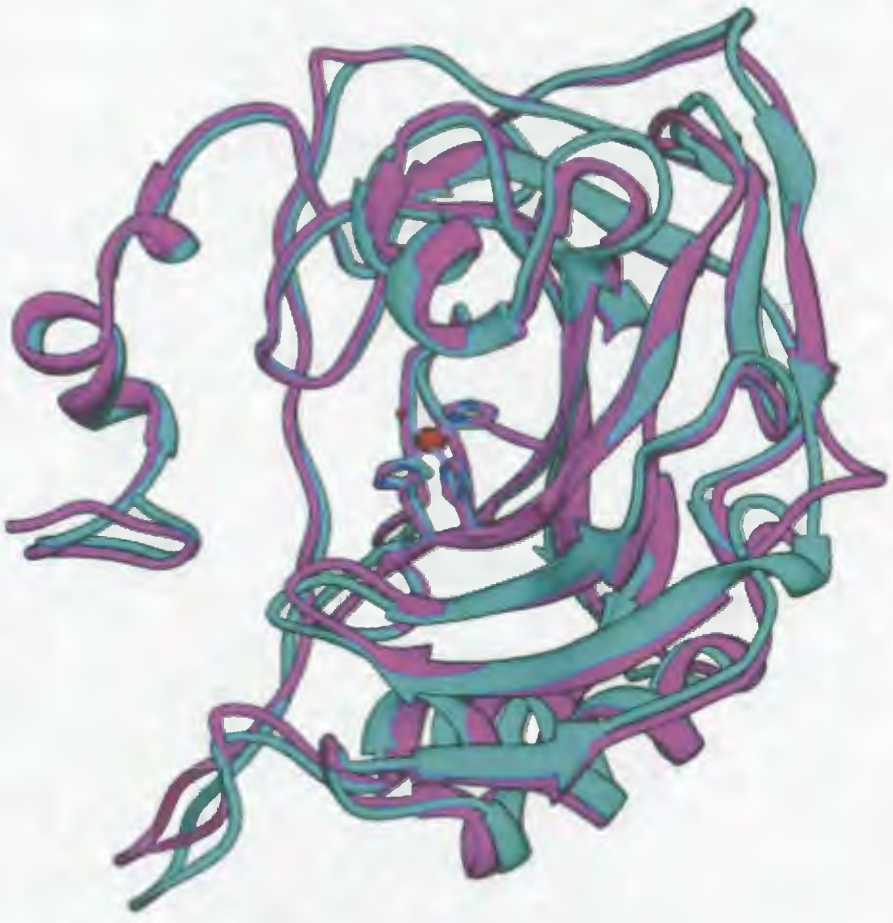

Figure 1.8. Tertiary structure of hCA I and hCA II.
Overlay of hCA I (majenta) and hCA II (cyan) tertiary structure (PDB ID: hCA I-2CAB; hCA II-2 CBA) (*174*, *203*) modeled by Chimera® software (*175*).

and His119, Glu117, His107, Tyr194, Ser29, and Trp209 are also similar in the two isozymes. In addition, the hydrophobic and hydrophilic halves are also similarly situated in these two isozymes. However, the active site cavity shows some important differences in the immediate vicinity of zinc. These differences arise from the replacement of Thr200 and Asn67 in hCA II by histidines in hCA I, Ile91 and Phe131 in hCA II by Phe and Leu in

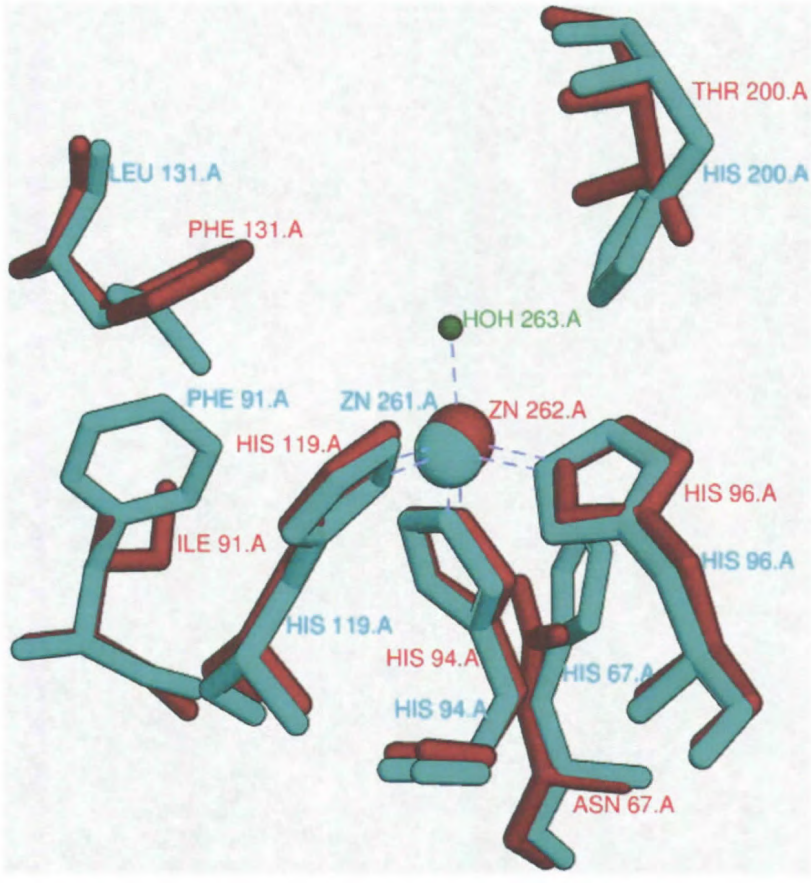

Figure 1.9. Overlay of the active site residues of hCA I and hCA II.
Overlay of the active site residues of hCA I (2CAB) (cyan) (*203*) and hCA II 2CBA (red) (*174*). The structures were modeled by the UCSF Chimera® software (*175*).

hCA I (Figure 1.9). Moreover, the hydrophobic cavity in hCA II is more hydrophobic than that of hCA I (*203-205*).

1.1.7.3. Structure of hCA I Michigan I

Human CA I Michigan I, a variant of hCA I was discovered in three generations of a European Caucasian family residing in Michigan (*206*). This genetic variant is a result of a single point mutation (CAT to CGT) that changes His67 to Arg in a critical region of the

active site (*207*). The enzyme variant shows that a single amino acid substitution within the active site of hCA I affects both its catalytic and inhibition properties even though the mutated residue is not directly involved in the coordination of the catalytic metal ion and the overall global structure (Figure 1.10) of the mutant enzyme is similar to the native enzyme (*208*).

A comparison of the relative positions of some of the active site residues of native and mutant enzymes showed no significant changes in the distances and the angles of the Zn(II) coordination polyhedron (Figure 1.11) The hydrogen bonding between Thr199-Glu106 that is involved in stabilizing and orientating the catalytic zinc bound hydroxide for catalysis is also unaltered in the variant. Comparison of the hCA I Michigan I with and without added zinc ion showed that in the absence of added zinc, Arg67 in the variant adopts a conformation pointing out of the active site in contrast to its histidine counterpart in the native hCA I which adopts an "in" conformation. However, this situation is reversed in the presence of added zinc ions where the arginine turns into the active site to coordinate with a second Zn(II) ion bound in the active site. The binding of the second zinc ion also causes additional minor conformational changes to several other active site residues, including His64 and His200. These active site modifications resulted in an enhancement of the variant's esterase activity toward α and β-naphthyl acetates (*208*).

1.1.7.4. Structure of hCA III

The overall tertiary structure of hCA II (*173*) and hCA III (*209*) are similar with some important differences in the active site that are responsible for the drastic difference in the catalytic activity between the two isozymes. The main difference is at position 64.

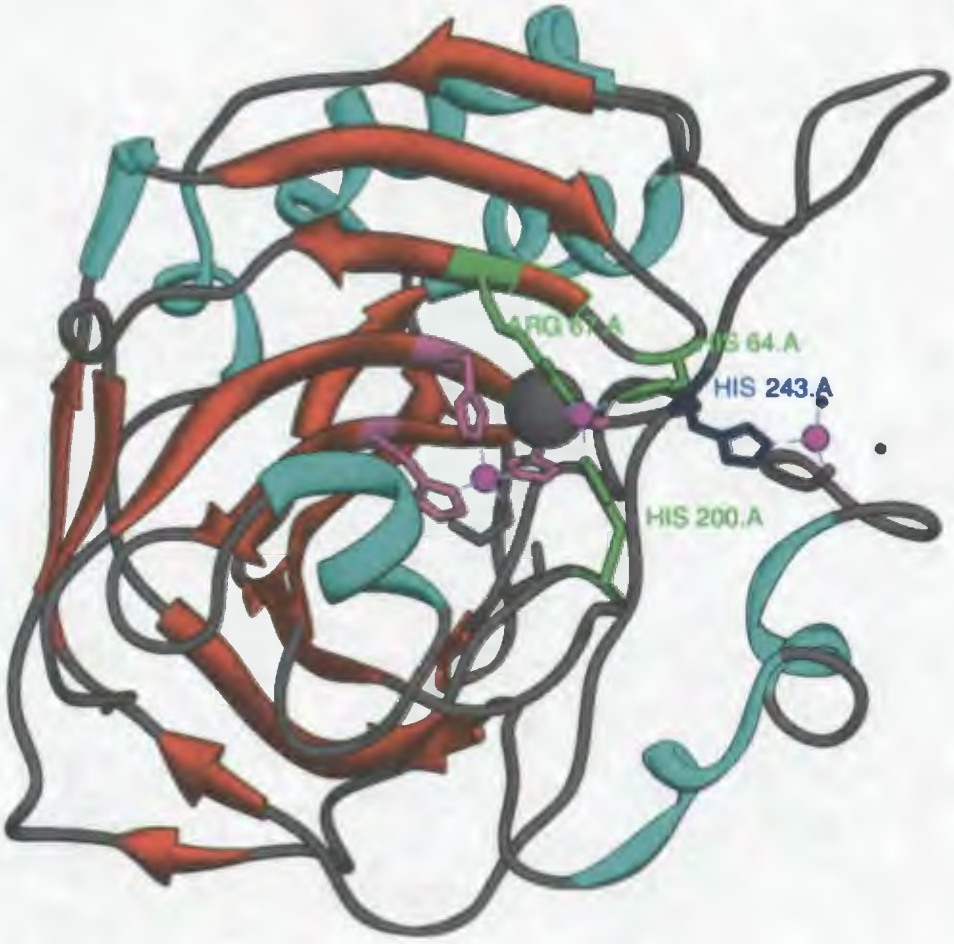

Figure 1.10. Ribbon diagram of CAI Michigan I.
The ribbon diagram of CAI Michigan I (PDB ID: 1JV0) (*208*) is modeled by UCSF Chimera® software (*175*). The α - helices, β - sheets and coils are represented in cyan, orange red and grey colors respectively. The zinc atoms and the three His residues (His94, 96 and 119) are are in majenta. The other active site residues Arg67, His200 and His64 are in green and His243 occupying an out conformation is shown in blue.

Where as His is present at position 64 in hCA II and serves as an efficient proton shuttle, in hCAIII it is replaced by a Lys residue which is hydrogen bonded to Trp5 and points away from the active site. Another difference exists at position 198 which is Phe in hCA III and Leu in hCA II. Comparison of the crystal structures of hCA III and Phe198Leu hCA III

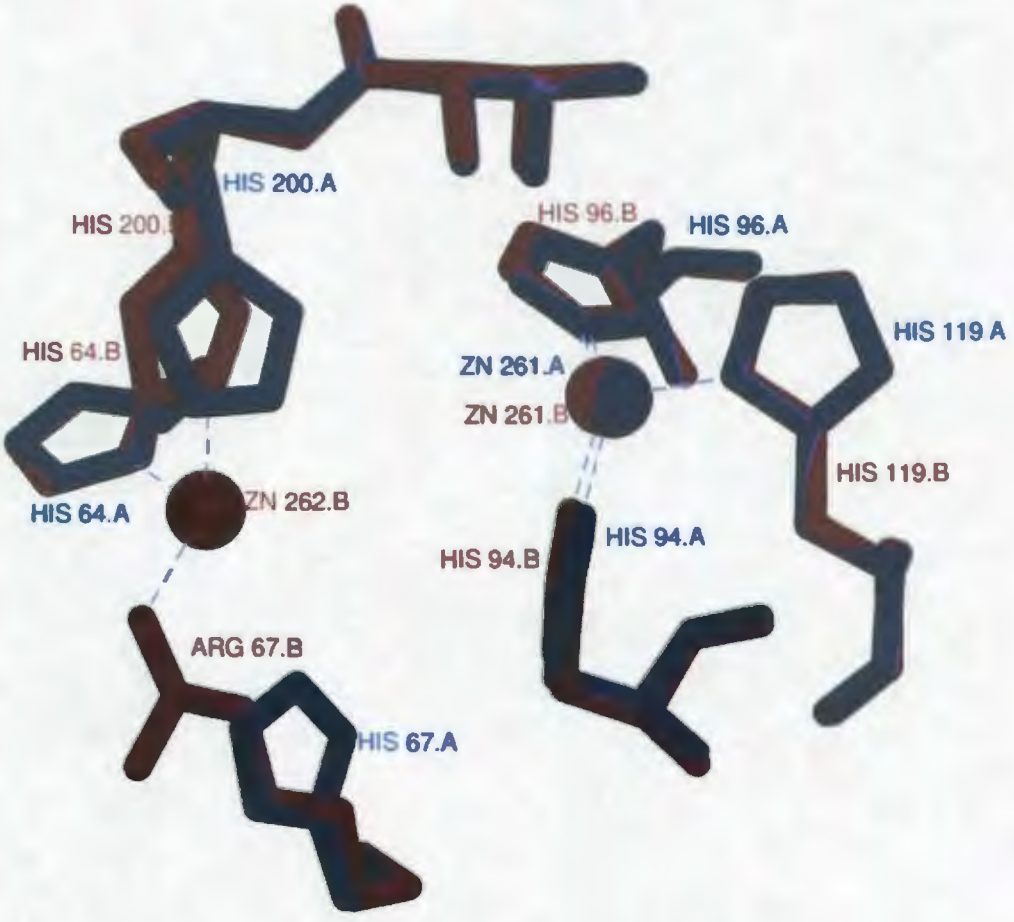

Figure 1.11. Overlay of the active site structure of hCA I and hCA I Michigan I.
The active site structures of hCA I (PDB ID: 2CAB) (*203*) and hCA I Michigan I (PDB ID: 1JV0) (*208*) are shown. The former and the later enzymes are represented in blue and brown colors respectively. The structures were modeled using the by UCSF Chimera® software (*175*).

muatants revealed that the Cγ of Phe198 is almost 0.5-0.7 Å closer to zinc compared to that of Phe198Leu mutant. Duda et al. (*210*) suggested that the presence of the bulkier Phe198 in hCA III brings its side chain closer to the zinc in addition to the constraints in the active site. This extra constraint was suggested to be one of the contributors for the decrease in

the catalytic activity of hCA III. Comparison of the active site structures of hCA II, hCA III and Phe198Leu hCA III is shown in Figure 1.12.

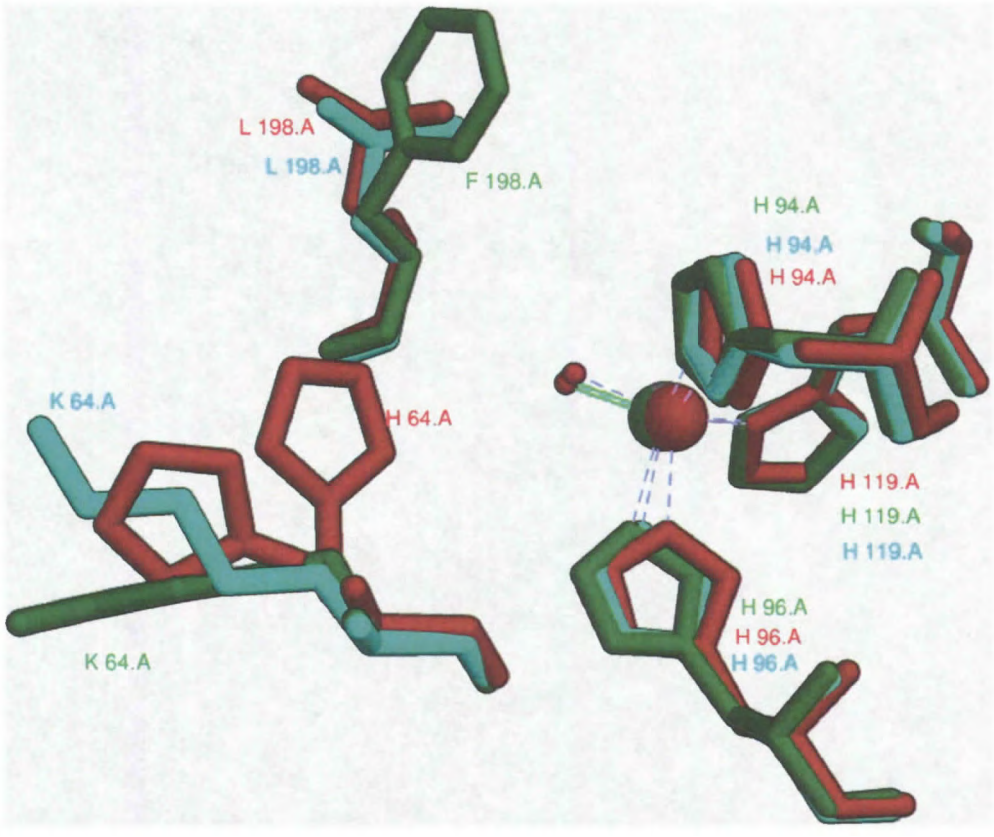

Figure 1.12. Overlay of the active site structure of hCA II, hCA III and Phe198Leu hCA III.
Overlay of the active site structure of hCA II (red) (PDB ID: 2CBA) (*174*), hCA III (PDB ID: 1Z93) (cyan) (*210*) and Phe198Leu hCA III (green) (PDB ID: 1Z97) (*210*) are shown in green, red and cyan respectively. The structures were modeled using the by UCSF Chimera® software (*175*).

1.1.7.5. Structure of hCA IV

The X-ray crystallographic data of the structure of the secretory form of hCA IV was reported by Stams et al. in 1996. According to the structure determination, the overall fold of hCA IV is similar to that of hCA II and is dominated by a central, eight-stranded β-

sheet superstructure (Figure 1.13). The active site structure of hCA IV is also similar to hCA II. The active site metal ligands, His94, 96 and 119, the substrate binding pocket, the

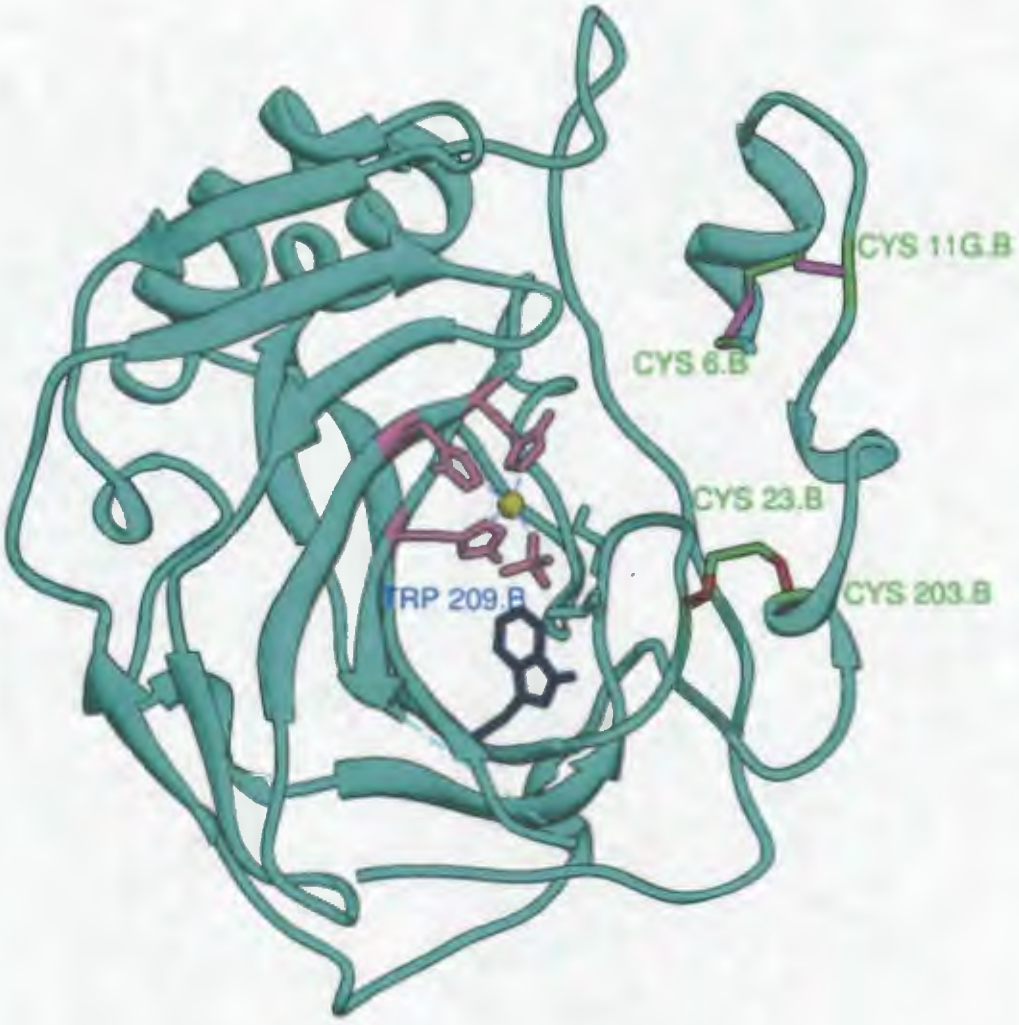

Figure 1.13. Ribbon diagram of hCA IV.
Ribbon diagram of hCA IV (PDB ID: 1ZNC) (*212*) modeled by the UCSF Chimera® software (*175*). The zinc ion in the center is shown in yellow and the three ligands, His94, His96, His99 are represented in majenta. The disulfide bonds beween the cysteine residues are shown in green.

catalytic proton shuttle residue, His64 are also conserved between the two isozymes. At pH 5.1, the side chain of His64 occupies the "out" conformation, similar to hCA II. Although

the immediate vicinity of the active site of hCA IV is similar to that of hCA II, some significant structural differences are observed in the greater active site clefts of hCA IV and hCA II. The significant difference is the presence of two disulfide linkages in hCA IV between Cys 6 -11, and Cys 23-203 which contribute to its exceptional stability to solubilization in 5% SDS (*29, 211, 212*). The disulfide bond between Cys23 and Cys203 plays an important role in stabilizing the polypeptide loop containing the catalytically important residue, Thr199, which helps in proper orientation of the zinc-bound hydroxide for catalysis. Whereas Val131 present in hCA IV is found within an extended loop, Phe131 of hCA II is found within a short alpha helix. The positively charged side chains of Lys37, 39, 42, 43, 187, 188, 258, Arg46, 189A, 213 and His190 present in hCA IV create a significant electropositive surface potential around the C- terminus of hCA IV. Of the above mentioned amino acids, only Lys39 and Arg213 are conserved in other hCA isozymes. These residues were proposed to facilitate the interaction of hCA IV with the negatively charged phosphate groups of the phospholipid membrane (*173, 212*). 1.1.7.6. Structure of CA V

The three-dimensional structure of murine (m) mitochondrial CA V was determined and refined by Boriack-sjodin et.al in 1995 (*38*). The first 21 amino acid residues of CA V, which in hCA II forms a small, partly α-helical segment on the surface of the enzyme adjacent to the active site, is deleted. But this deletion neither affects the activity nor the structure of mCA V(*38, 39*). Although the structure of mCA V superimposes well with hCA II (Figure 1.14) and the three His residues and their hydrogen bonding interactions within the active site residues are conserved between the two isozymes, some differences

are also observed. Insertion of Ser125 in the mCA V sequence extends a loop connecting strand βE to helix αD. This in turn shifts helix αD 2Å towards the zinc. The hydrophobic region and the substrate association pocket are conserved with the exception of one key

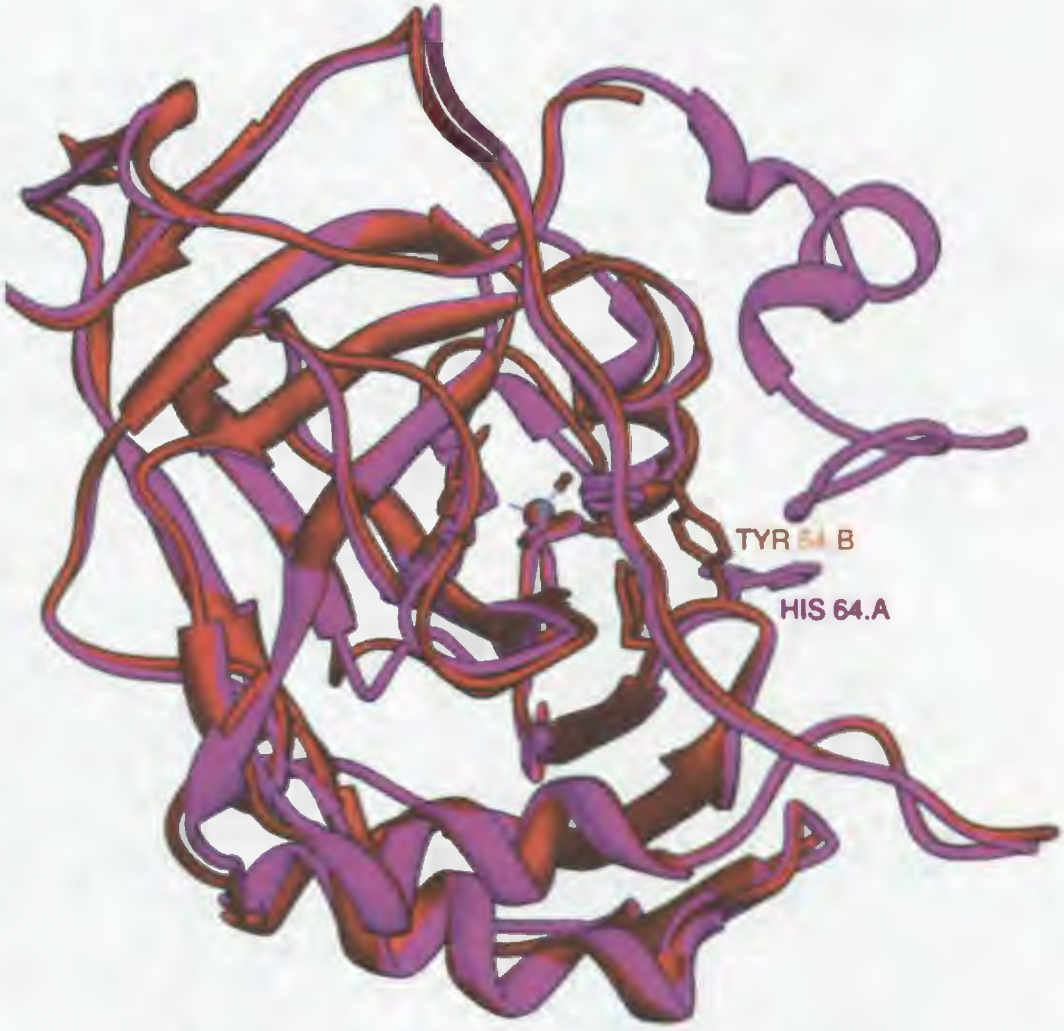

Figure 1.14. Overlay of the tertiary structure of hCA II and mCA V.
Overlay of the tertiary structure of hCA II (PDB ID: 2CBA) (*174*) and mCA V (PDB ID: 1DMX) (*38*). hCA II and mCA V are shown in majenta and orange red. The residue His64 in hCA II is replaced by Tyr in m CAV. The Figure is modeled by the UCSF Chimera® software (*175*).

amino acid substitution at position 131 (*38*, *173*, *213*, *214*). Phe31 of hCA II is substituted by Tyr in mCA V. Tyr131 is located on helix αD and is directed towards the active site.

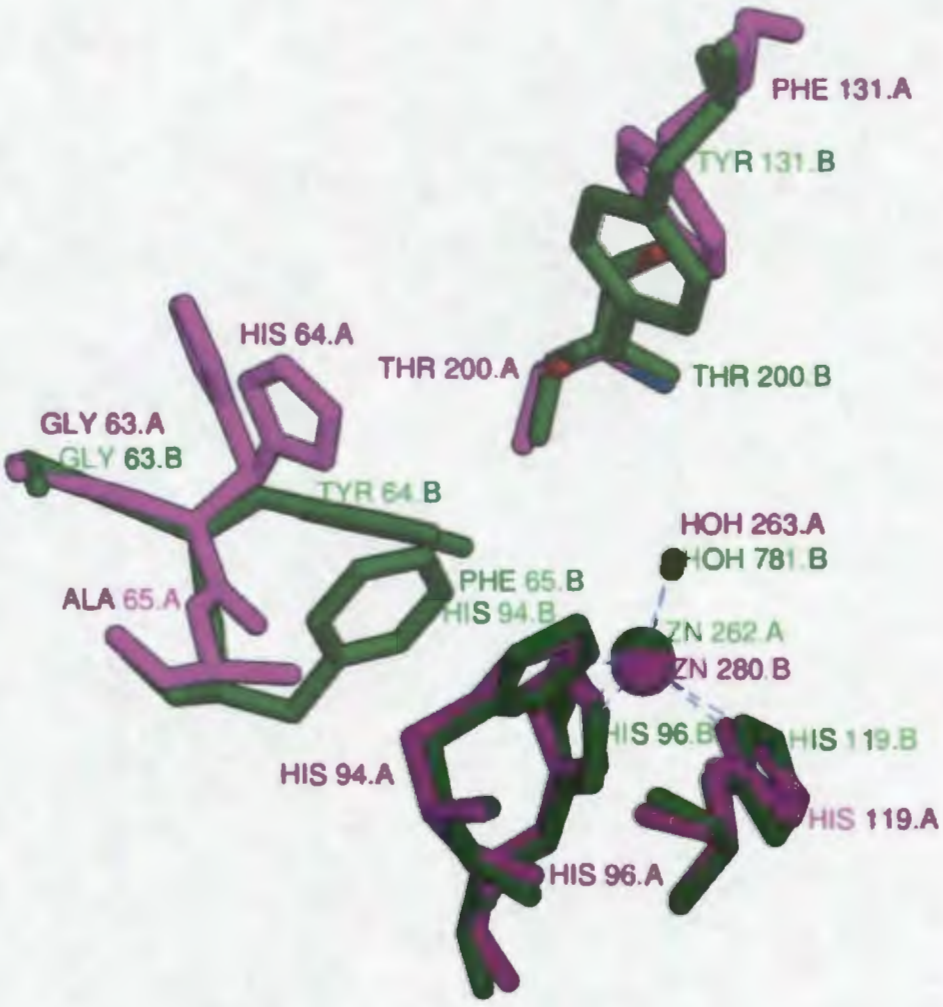

Figure 1.15. Overlay of the active site structure of hCA II and mCA V.
Overlay of the active site structure of hCA II (PDB ID: 2CBA) (*174*) and mCA V (PDB ID: 1DMX) (*38*). mCA V and hCA II are represented in green and majenta colors respectively. The structures were modeled using the by UCSF Chimera® software (*175*).

The amino acid substitution and the shift of helix αD, has strong implications on the catalytic proton transfer. In addition, the catalytic proton shuttle of hCA II, His64, is

replaced by Tyr in mCA V (Figure 1.15). This reside is flanked by Gly63 and Ala65 in hCA II whereas in mCAV, it is flanked by Gly63 and Phe65. The conformation of Tyr64 in mCA V is also different from that of His64 in hCA II and could be due to the steric hindrance created by the bulky side chain of Phe65. Comparison of the crystal structures of hCA II and mCA V complexed with acetazolamide revealed a similar mode of binding in both the isozymes except for a small difference at position 131. The hydrogen bonding between the inhibitor and the hydroxyl group of Tyr131 observed in mCA V is not possible with Phe131 of hCA II (*38*, *173*).

1.1.7.7. Structure of hCA IX

The cDNA coding human hCA IX was first cloned and investigated by Pastorek et al in 1994 (*45*). Human CA IX is a multi domain protein consisting of an N-terminal proteoglycan like domain, a catalytic domain, a transmembrane domain and an intracytoplasmic tail (*46*, *215*). The proteoglycan domain is absent in other CAs and resembles the keratan sulfate attachment domain of a large aggregating proteoglycan such as aggrecan. However, the catalytic domain shows 30 – 40 % sequence homology with other CA isozymes (*215*). Like hCA XII (*49*), hCA IX is also a dimeric protein (*216*) and the dimerization is mediated by an intermolecular disulfide bond between Cys41 of the two monomers. Apart from the intermolecular disulfide bond, hCA IX possess an intramolecular disulfide bond between cys23 and cys203 similar to that found in hCA IV (*212*) and hCA XII (*49*). The formation of hCA IX dimer involves a contact area comprising the region Ala39 to Ala43. This region contains Cys41 that is involved in intermolecular disulfide bonding. The C_α - C_α distance between these two residues was found to be around 5.3 Å. The structure based sequence alignment revealed the presence of

Asp residue at this position in other CAs and was suggested to be the reason for the absence of oligomerization inspite of the high sequence homology observed between hCA IX and other CAs. It has been suggested that the bulky side chain of Asp could be responsible for destabilizing the interactions at the CA dimer interface making it incompatible for oligomerization. Crystal structures of the mutant hCA IX (Cys41 to Ser) showed that the two serine residues did not interact with each other and pointed towards opposite directions (Figure 1.16). Inspite of the above mutation, the hCA IX crystalized as a dimer which is stabilized by numerous van der Waals interactions and two hydrogen bonds involving Arg137 side chain and the carbonyl oxygen of Ala127. However, it is not known whether this form is a dimer in solution.

Comparison of the catalytic domain of hCA IX (*216*) with other membrane associated hCAs (*49*, *70*, *212*) exhibited substantial three dimensional similarity (Figure 1.17).The N-terminal regions and the portions involving residues 232-238 of hCA isozymes showed main differences where a large sequence deletion is present in hCA IX. As these regions are present far away from the active site, it has been proposed that this would not affect the binding and catalytic function of hCA IX. Superimposition of the active site region of hCA IX with hCA IV, hCA XII and mCA XIV showed only minor differences in the 125-137 region. This has been atrributed to the sequence deletion of a few amino acids in this region. Only eight amino acids (*66*, *68*, *127*, *128*, *131*, *132*, *199*, *217*) in the active site region are different among the above four isozymes and could be potentially used in the design of selective hCA IX inhibitors (*216*).

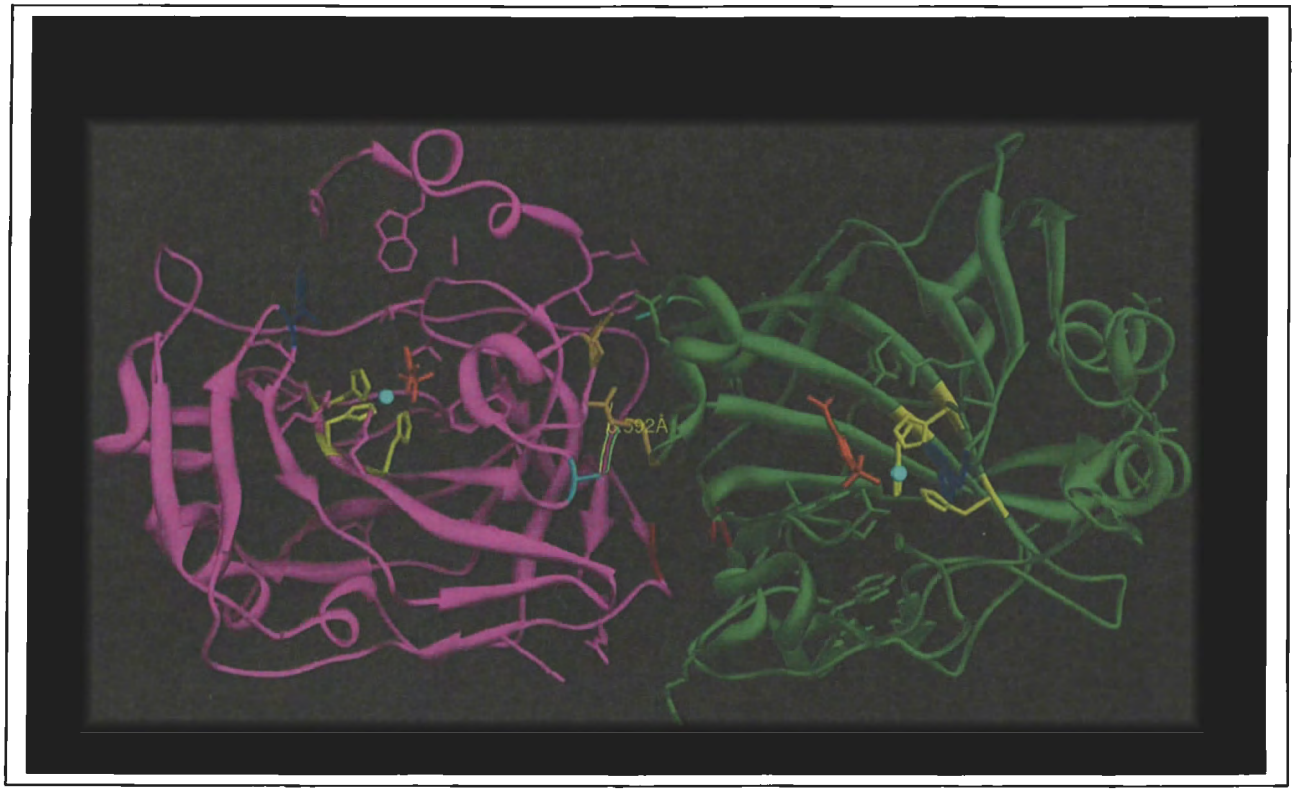

Figure 1.16. Tertairy structure of hCA IX.
Tertairy structure of hCA IX (PDB ID: 3IAI) dimer (*216*). The 3 His residues coordinating the catalytic zinc (cyan) are depicted in yellow. His64 in both the chains were colored blue. Cys 41 in native protein is replaced by serine (red) in this mutant. The Figure is modeled by the UCSF Chimera® software (*175*).

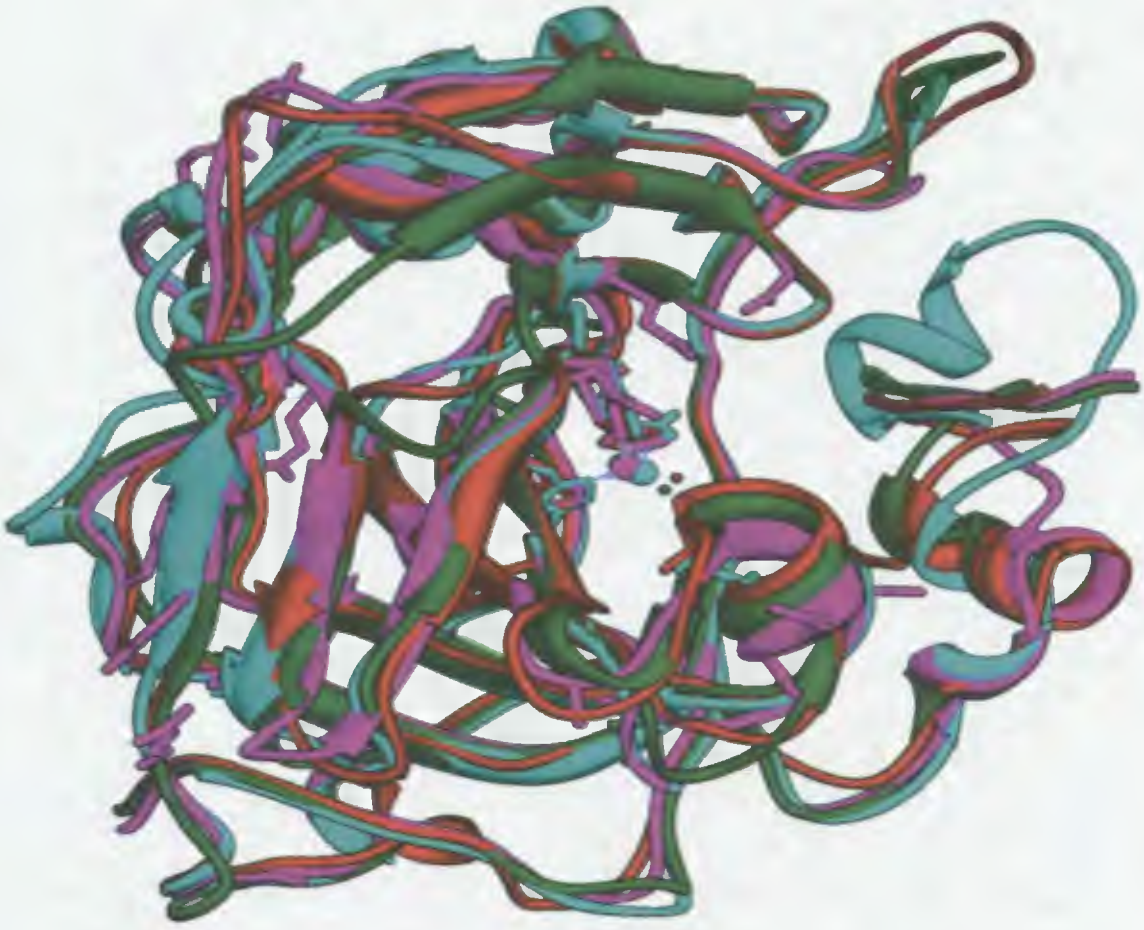

Figure 1.17. Overlay of tertiary structure of hCA IX, hCA XII, hCA IV and hCA II. Overlay of tertiary structure of hCA IX (majenta) with hCA XII (orange red), hCA IV (cyan), hCA II (green). The structures were modeled using UCSF Chimera® software (*175*). The PDB IDs are 3IAI (*216*), 1JCZ (*71*) , 1ZNC (*215*) , 2CBA (*174*) for hCA IX, hCA XII, hCA IV and hCA II respectively.

1.1.7.8. Structure of hCA XII

Human CA XII, like hCA IX is a bitopic (single-pass) transmembrane protein. It contains an N-terminal extracellular CA domain, a transmembrane α-helix, and an intracellular C-terminal domain consisting of 30-residues which possesses potential

phosphorylation sites. Whittington et al solved the x-ray crystal structure of the extracellular catalytic domain of hCA XII at 1.55-Å resolution, and in the presence of acetazolamide at 1.50-Å resolution (*49*). Human hCA XII was found to be a dimer in both crystal structures and in solution (as indicated by its elution profile on Sephacryl S-300 column with a molecular mass of 60 kDa) (*49*).

The two domains of hCA XII interact to bury 2,200 $Å^2$ of total surface area. Both conserved residues and residues unique to hCA XII are present at the dimer interface. The dimer interface is stabilized by 19 hydrogen bond interactions and Gln249, a highly conserved residue involved in two of the hydrogen bond interactions. The dimer is assembled such that the active site clefts are oriented towards the extracellular mileu and the C- terminus is anchored to the cell membrane (Figure 1.18).

The two glycosylation sites, Asn52 and Asn136, are also exposed on the surface. Two signature motifs, GXXXG and GXXXS, present in the transmembrane segment of hCA XII serve as the framework for the dimerization of transmembrane α-helices (*49*, *218*, *219*).

The overall fold of hCA XII is similar to that observed for other isozymes of this class. However, larger loops are seen in hCA XII in the regions of Ala54A–Asn54B, Pro102A, and Arg240A–Glu240B in comparison with hCA II (*49*, *173*) (Figure 1.19). The enzyme also has a single disulfide linkage between Cys23 and Cys203 similar to that observed in hCA IV and hCA IX (*49*, *212*, *216*). The active site of hCAXII is identical to that of the cytosolic hCA II (Figure 1.20). The zinc ion present at the bottom of the deep active site cleft is ligated by His94, His96, His119, a water molecule, and an acetate anion. The zinc-bound water ionizes to yield zinc-bound hydroxide ion at high pH conditions.

The catalytic metal ion is also coordinated to one of the oxygen atoms of the acetate anion present in the crystallization buffer and the carbonyl oxygen atom of the acetate accepts hydrogen bonds from the zinc-bound water molecule and the backbone NH of Thr199. Acetate, like bicarbonate, protrudes into the hydrophobic substrate binding pocket, lined by residues Val121, 143, 207, Leu141, 198 and Trp209 (*49*, *220*, *221*). His64, the catalytic proton shuttle residue, is conserved in hCA XII and occupies the ''out'' conformation at low pH. The active site of hCA XII varies from that of other CAs, in the vicinity of Thr91, Gln92, and the ''130's segment'' (Ala131–Ala134). Presence of Ala 131 (which is Phe in hCA II) in hCA XII, results in a comparatively wider canyon in the active site cleft of hCA XII than hCA II. As a consequence, the side chain of Ser135 is exposed. These features in the active site of hCA XII is not observed in any other isozyme and could possibly be utilized in the design of hCA XII-specific inhibitors (*49*, *222-225*).

The crystal structure of hCA XII complexed with acetazolamide showed similar interactions with the active site residues as that of the hCA II-acetazolamide complex except for the presence of two additional hydrogen bonds between the hydroxyl group of Thr200 and the two nitrogen atoms of the 1,3,4-thiadiazole ring. It was suggested that an inhibitor molecule larger than acetazolamide has the potential to interact within the wider canyon adjacent to the 130's segment, thereby providing hCA XII-specific binding (*49*, *226*).

1.1.8. General features of the active site cavity of catalytically active α - CAs

The active site cavity of all CAs is conical in shape and includes three functional regions. (1) The primary coordination sphere around zinc: This region consists of three histidine residues and a water molecule. These histidine residues are direct zinc ligands

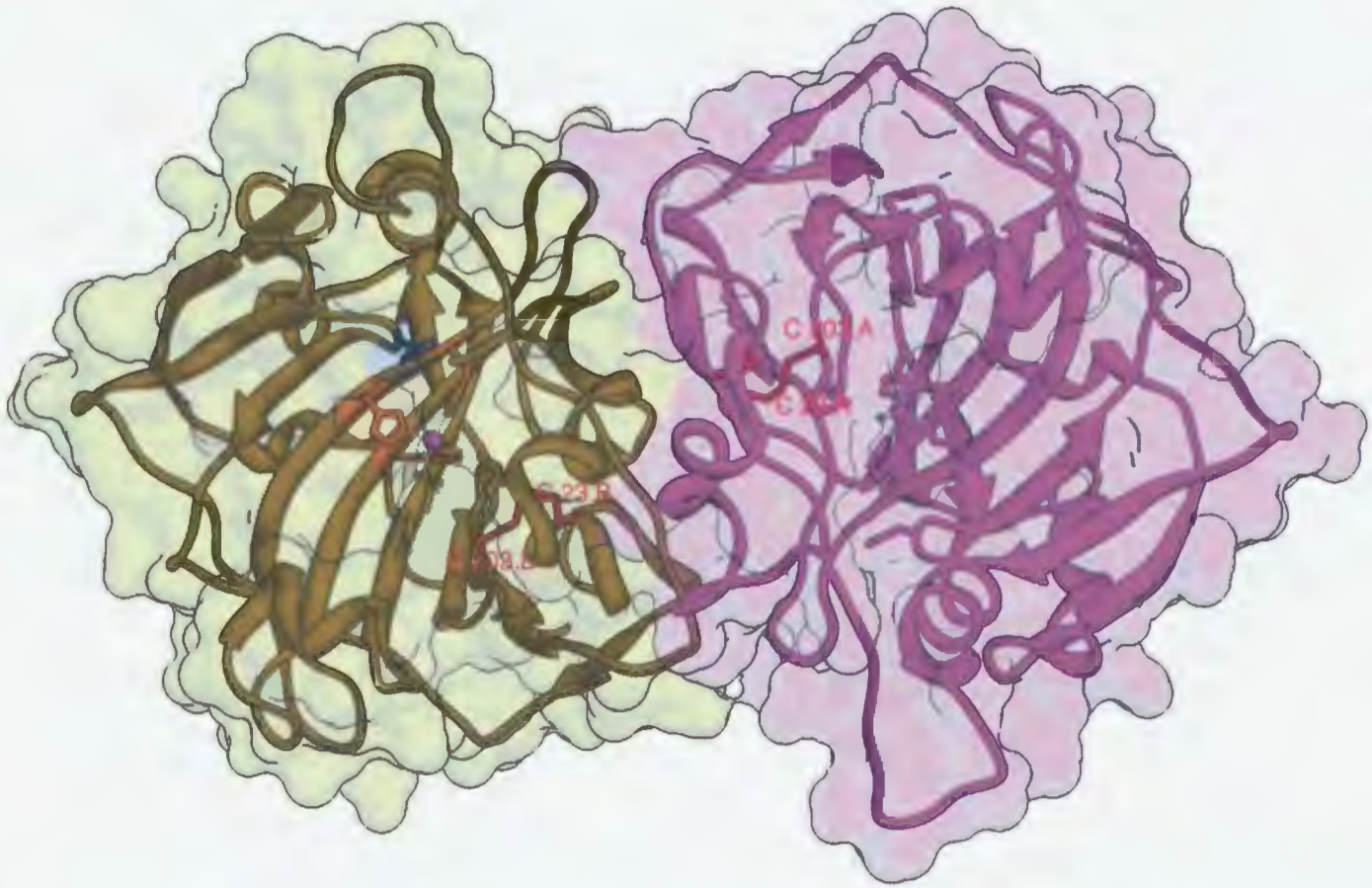

Figure 1.18. Tertiary structure of dimeric hCA XII.
Tertiary structure of dimeric hCA XII (PDB ID: 1JCZ) (*49*) was modeled using UCSF Chimera ® software (*175*). The cysteine residues Cys 23 and Cys 203 and the disulfide bond between these residues in the two monomers are shown in red.

Figure 1.19. Overlay of the tertiary structure of hCA XII and hCA II.
The structures were modeled using UCSF Chimera® software (*175*). The catalytic zinc is shown as a ball in the center. The PDB IDs are 1JCZ (*49*), 2CBA (*174*) for hCA XII and hCA II respectively. The larger loops of hCA XII are shown in red ovals.

(*119*). Apart from direct ligands, CAs also possesses indirect ligands. For example, the indirect ligands in hCA II are Gln92, Glu117 and the backbone carbonyl of Asn244 (Figure 1.21). The hydrogen bonding interactions between these residues and the three histidine residues that are ligated to zinc, and Thr199 enhance the basicity of direct histidine ligands and positions them for optimal metal coordination (*176*, *178*, *227-229*).

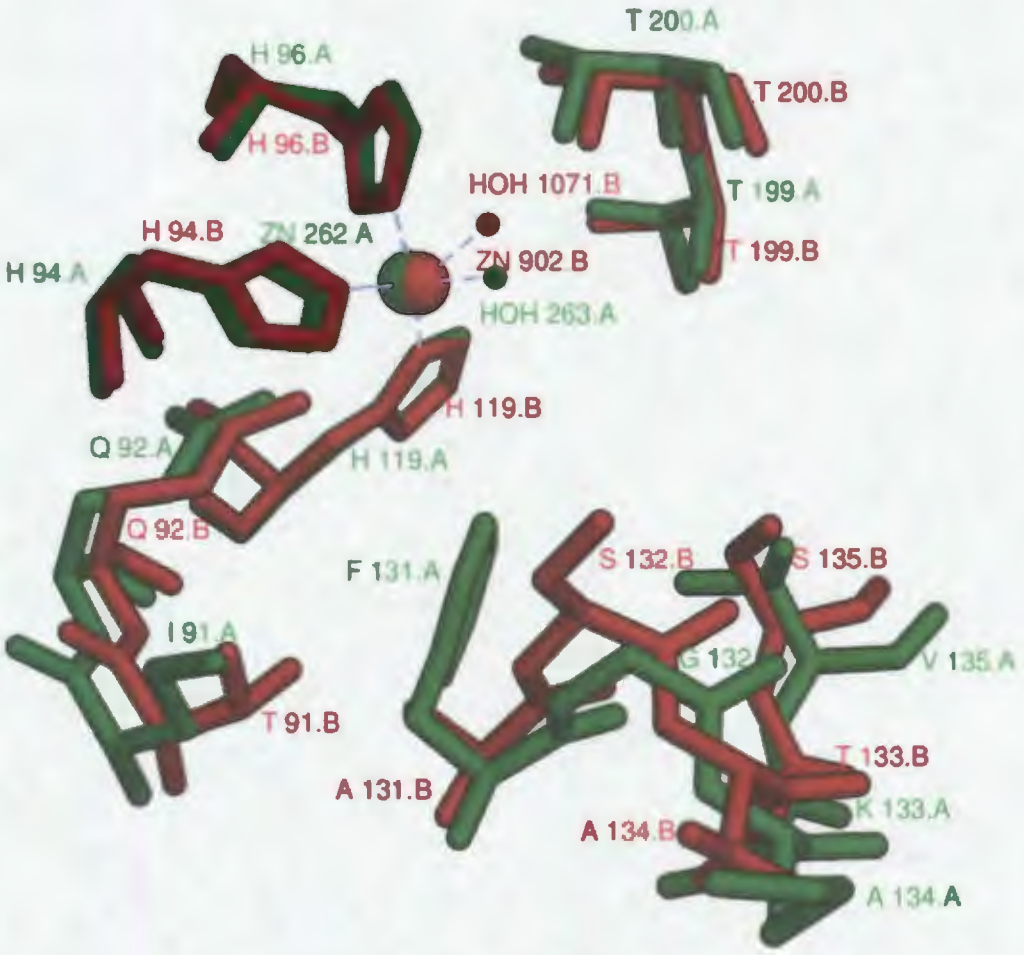

Figure 1.20. Overlay of the active site structure of hCA XII and hCA II.
The active site structure of hCA XII (red), and hCA II (green)tructures were modeled using UCSF Chimera® software (*175*). The catalytic zinc is shown as a ball in the center. The PDB IDs are 1JCZ (*49*), 2CBA (*174*) for hCA XII and hCA II respectively.

(2) The primary and secondary hydrophobic faces: This is the region where the substrate and inhibitors bind (Figure 1.22). The primary hydrophobic site of CAs is composed of Val121, Val143, Leu198, and Trp209. The secondary hydrophobic site is located far away from the active site in comparison to the primary site. Inhibitors having long chain linkers

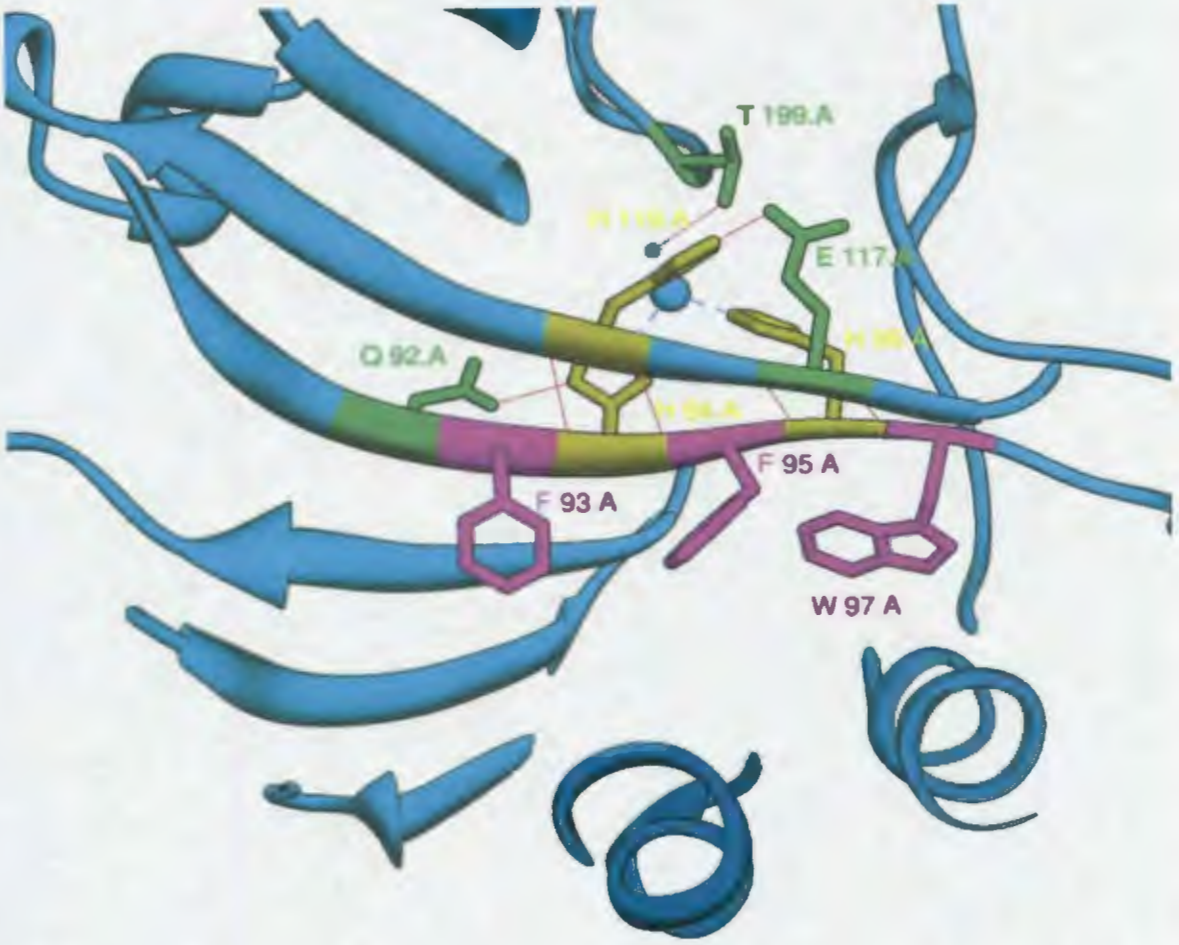

Figure 1.21. Close view of the active site of hCA II.
Close view of the active site of hCA II (PDB ID:2CBA) (*174*). The direct ligands of the catalytic zinc (blue ball) are shown in yellow. The hydrogen bonds are depicted as red lines. Indirect zinc ligands are colored green. The hydrophobic residues located opposite to His94, 96 and Lys 92 are shown in magenta. The structure is modeled using UCSF Chimera® software (*175*).

between a hydrophobic tail and the zinc binding head group were found to interact with the secondary hydrophobic face (*184*, *185*).

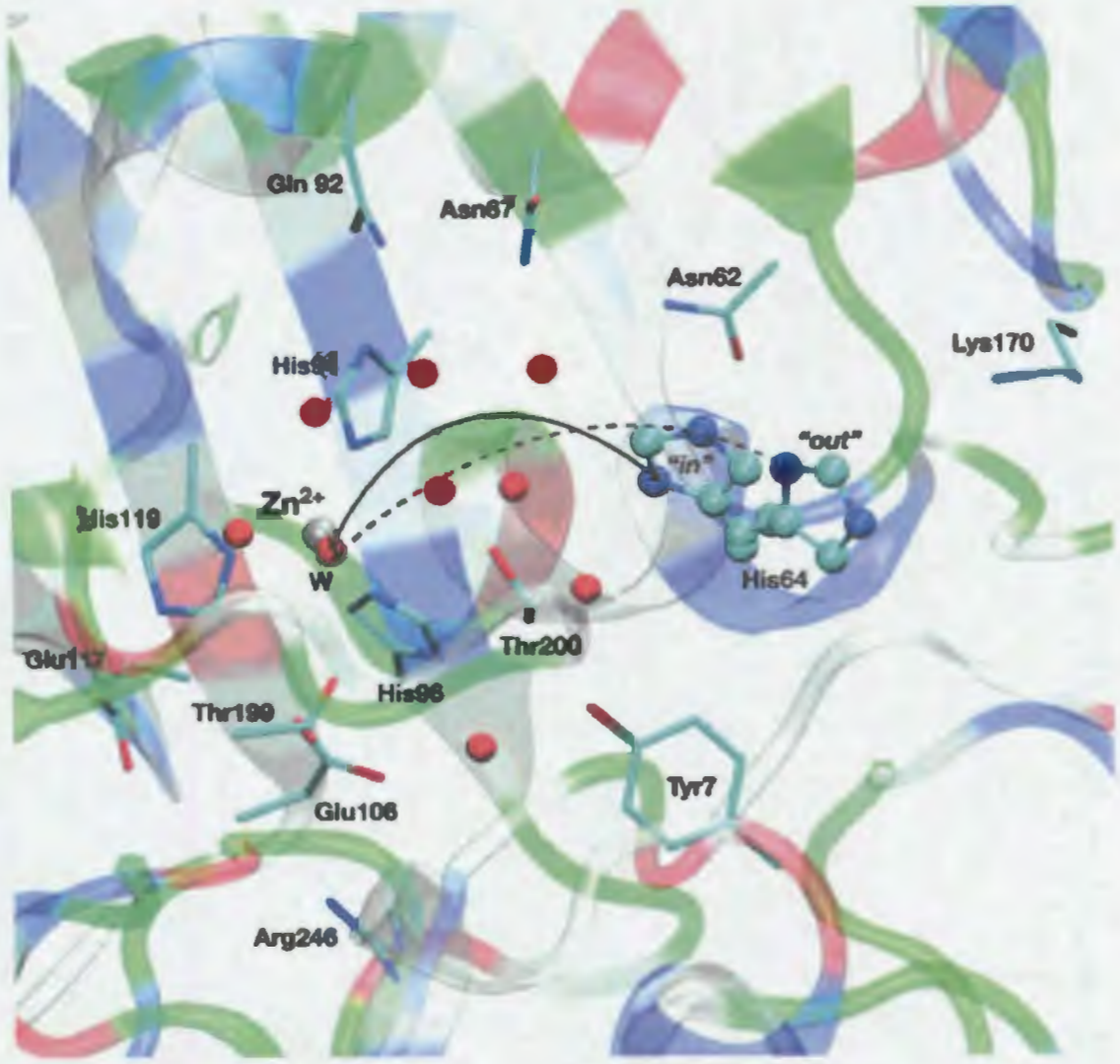

Figure 1.22. Active site of hCA II showing the primary and secondary hydrophobic residues along with the hydrophilic site.
Water molecules involved in proton transfer are shown in red and the proton shuttle residue, His64 is shown as ball and stick conformer. Figure is adapted from reference (*230*).

(3) A hydrophilic face: This region facilitates proton shuttle and thereby regenerates the catalytic activity of the protein (Figure 1.22) (*119*). The hydrophilic face consists of 8 residues of which Thr199 and Thr200 are located near the active site cavity. Tyr7, Asn62, Asn67, Gln92, and Glu106, are involved in the hydrogen bond network with nine ordered water molecules in the active site. Glu117, His107, Asn244, and Arg246 help in the orientation of sidechains that line the active site cavity and thereby are indirectly involved in the hydrogen bonding network of water molecules. Thus, whereas the hydrophilic face of the active site is essential for catalysis, the hydrophobic face is important for inhibitor binding (*173*, *231-233*). Although the global structure of CAs remains unchanged with changes in pH, some significant changes occur in the active site. Changes in the location of various water molecules in and around the active site are noticed as the pH increases from 6.0 to 7.8 (*174*, *234*). However, the metal coordination geometry remains unaffected (*174*).

1.1.9. Metallo enzyme variants of CA

CA was the first zinc metalloenzyme identified and many metallo variants of CA have been produced till date (*174*, *188*, *229*, *235-246*). Substitution of Zn^{2+} by Co^{2+} in hCA II revealed no changes in the structure of the enzyme. In contrast, significant structural changes were observed upon substitution of Zn^{2+} by Cu^{2+} forms presumably due to the 5-coordinate square planar geometry acquired by Cu^{2+} (*240*).

Enzyme activity measurements showed that the zinc enzyme is the most active form followed by the cobalt form (50 % of the zinc enzyme activity). Other metallo enzyme variants exhibited very minimal or no activity due to the different coordination geometries exhibited by their metal ions (*243*). For example, Cu(II) binds to hCA II in trigonal-bipyramidal geometry, Ni(II) and Mn(II) coordinate octahedrally. Any metal coordination

other than tetrahedral coordination was found to disturb the solvent network between the zinc and His64 of hCA II, thereby hindering the proton transfer (*235*). The decrease in the activity of the cobalt variant inspite of its slightly distorted tetrahedral geometry is because of its octahedral coordination when complexed with the bicarbonate ion (*188*, *247*).

1.1.10. Catalytic mechanism of CAs

The Catalysis of CO_2 hydration in all the CAs investigated till now requires Zn(II), which is situated at the bottom of a 15 Å deep active site cleft and is coordinated by three histidine residues (His94, His96 and His119) and a water molecule/ hydroxide ion (*49*, *54*, *56*, *20*, *65-68*, *77*, *248*). The water molecule bound to the catalytic zinc is engaged in hydrogen bonding with the hydroxyl moiety of Thr199, which in turn is bridged to the carboxylate moiety of Glu106. These interactions increase the nucleophilicity of the zinc-bound water molecule and also orient CO_2 for the nucleophilic attack. The enzyme in its active form has a hydroxide bound to Zn(II) (*54*, *56*, *20*, *64*, *65*, *248*) which acts as a strong nucleophile and attacks the CO_2 molecule bound in a hydrophobic pocket, leading to the formation of zinc bound bicarbonate. A water molecule displaces the bicarbonate ion into solution, leading to the inactive form of the enzyme (*20*, *64*, *65*) (Figure 1.23). The active form of the enzyme is then regenerated by a proton transfer reaction from the active site to the surrounding environment which is the rate limiting step in catalysis (*54*, *56*, *20*, *64*, *21*, *248-250*). The proton transfer occurs by Grotthuss diffusion through the hydrogen bonded water network, often called as a proton wire between the zinc bound water and His64 placed at the entrance of the active site (*16*) (Figure 1.24). The imidazole ring of His64 which is in the "in" conformation, once protonated, acquires an "out" conformation

to release the proton to the bulk solvent. Any mutation in the active site that perturbs His64 (*181*, *251*, *252*) or the proton wire significantly reduces the enzyme's turnover rate indicating the importance of proton shuttle in catalysis (*16*, *179*, *181*, *251*, *252*).

1.1.11. Structure-function relationships in CA isozymes

Structure-function relationships in CAs have been extensively studied by the aids of site directed mutagenesis, evaluation of catalytic properties and x-ray crystallographic studies. These studies have provided insights into assigning specific functions of the enzyme's active-site residues.

Site directed mutagenesis of amino acid residues that are directly coordinated to the Zn(II) ion (His to Ala) resulted in substantially increased dissociation constants of the metal ion (*176-178*, *198*, *237-239*, *253-255*). The X-ray crystallographic studies of His94Cys and His119Cys mutants revealed that these variants can coordinate to the metal ion, while His96Cys alone does not. This is due to the lack of plasticity provided by the beta sheet around the His residue to allow the thiolate to coordinate to Zn(II) (*198*, *237*). Studies suggested that substitution of the histidne residues, that are directly bound to zinc, by acidic residues such as Asp, Cys, or Glu resulted in improved affinity of the metal ion to CA relative to the substitution of neutral residues like alanine. However, the catalytic activity of the mutants with acidic residues was 3 orders of magnitude lower than that of the wild type enzyme. This is due to the increase in pK_a of the Zn(II)-bound water molecule as a consequence of an additional charge at the active site. This in turn destabilizes both Zn(II)-OH and the transition state for the hydration of CO_2. Based on

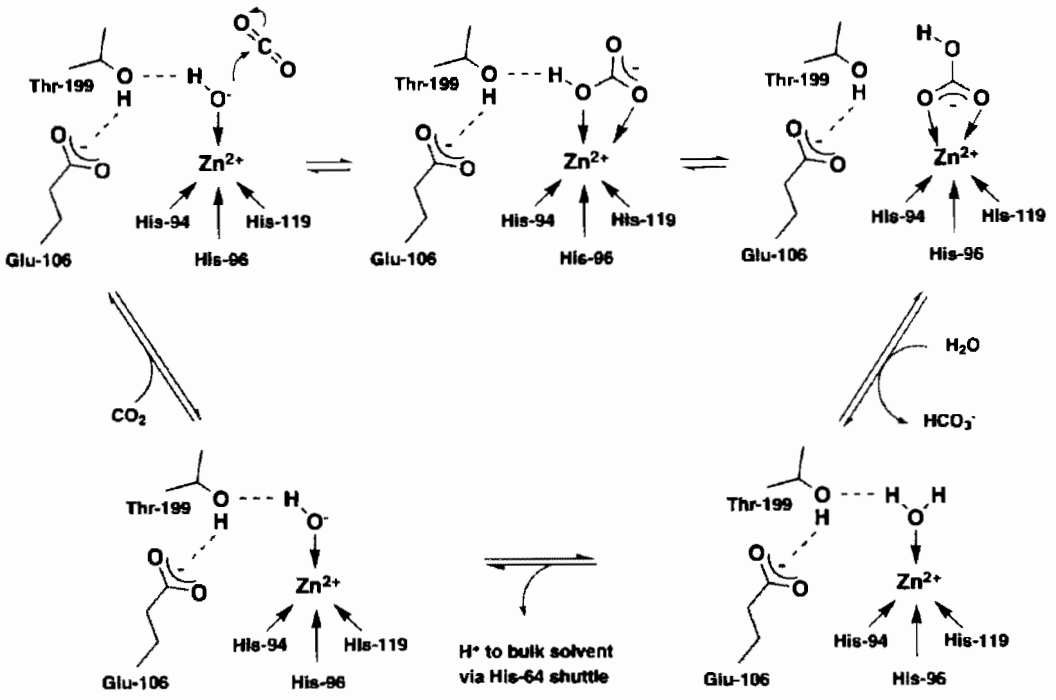

Figure 1.23. Catalytic mechanism of hCA.
Figure is adapted from reference (*16*).

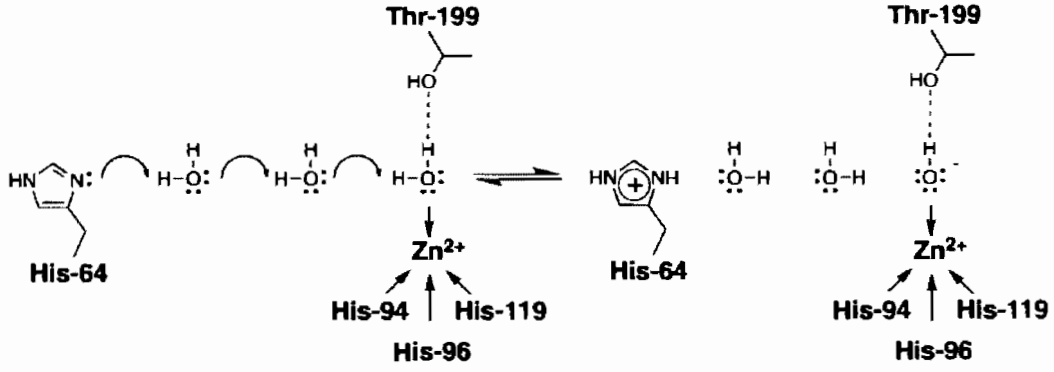

Figure 1.24. Proton translocation in hCA to regenerate active enzyme.
Figure is adapted from reference (*16*).

these studies, it was suggested that although histidine ligands do not participate in catalysis, they are important for maximizing the electrostatic stabilization of both the ground-state zinc-hydroxide and the negatively charged transition state (*119*, *256*).

Krebs et al. studied the functional importance of the conserved hydrophobic residues in hCA II by random mutagenesis followed by the investigation of catalytic activity, inhibitor binding and level of hCA II expression in *E. coli*. Their study revealed that the hydrophobic region is capable of accommodating residues of varied size, charge and hydrophobicity with little or no effect on the catalytic activity with the exception of substitutions for Thr199. Substitution of this residue with a residue lacking a hydroxyl group decreased the catalytic activity by almost 50 fold. This is due to the involvement of the hydroxyl group of threonine in the active site hydrogen bonded net work which is very crucial for the nuclophilic attack of the zinc hydroxide on the carbonyl moiety of the substrates CO_2 and esters (*173*, *205*, *257*). Mutation of Leu198 to Arg decreased the rate of CO_2 hydration more than that of the ester hydrolysis. Whereas the mutation of Trp209 decreased the ester hydrolysis, it had no effect on the CO_2 hydration. This showed that Trp209 is not the major determinant of the CO_2 association with the hydrophobic pocket of the enzyme (*257*).

Inhibition studies with mutants revealed that proper interaction of sulfonamide inhibitors with Thr199 is very important for their binding in contrast to Thr 200 mutants (*257*). Interestingly, it was found that introduction of positive charges at the active site lead to the enhanced binding presumably due to the favorable electrostatic interaction between the sulfonamide anion and the positive charges of the aminoacids. From the

protein expression levels of these mutants, it was found that when the non aromatic residues present in the beta sheet structures (residues 191-196 and 206-209) are mutated, it results in almost 10 fold decrease in protein expression (*257*). As these residues neither affected the catalysis nor inhibitor binding, but only the protein expression, it was concluded that these residues were conserved in order to ensure proper expression of hCA II . Hydrophobic residues in the active site of CA II are also important for proper protein folding as mutations in these regions lead to the formation of insoluble aggregates (*257*).

Mutation of any of the zinc bound histidine residues with alanine leads to almost 10^5 fold decrease in the metal affinity. Substitution of these His ligands with Asp, Glu, Gln, Asn or Cys decreased the zinc affinity to a large extent (*198, 238, 239, 241, 254, 255, 258*). Crystal structures of these variants revealed that as these side chains occupied a very different position from that of the imidazole nitrogen of His ligands, they could not properly coordinate the zinc ion (*259*). Mutation of any of the indirect ligands decreased the zinc affinity with the exception of E117Q (*176, 178, 197, 229, 253, 257, 260*). This variant showed increased kinetics of zinc binding but with substantial decrease in the catalytic activity and inhibitor binding. The k_{off} for the zinc dissociation from this variant is almost 10^6 fold higher as compared to that of the wild type enzyme with association rate constants reaching the diffusion controlled limit. As the side chain of the substituted lysine residue is in the same position as that of the side chain in the wild type, it was concluded that differences in the catalytic activity and inhibitor binding between the wild type and the mutant was due to the difference in the electrostatics rather than the structural effect (*229*). It was argued that E117Q substitution stabilized the anionic form of His119 by reversing

the polarity of the Q117-H119 hydrogen bond. The formation of the additional negative charge of His119 caused the pK_a of the the zinc bound solvent to increase which in turn led to the instability of the tetrahedral zinc complex (*229*). Hunt et al. (*242*) mutated the hydrophobic residues (Phe93, Phe95 and Trp97) of hCA II surrounding the zinc-binding site and found that substitution of these residues altered the structure of the enzyme such that the zinc ligands of the apo enzyme occupy a different orientation that does not support zinc binding and there by decreased the metal affinity of hCA II by as much as 100-fold (*240, 242, 261*).

Mutation of the residues that interact with the ligands bound to the metal rather than with the metal itself provided valuable information regarding the structure-function relation ships (*253-255*). Fierke and Christianson (*253-255, 262*) carried out mutation studies of Thr199 as it is close to the active site zinc and is also involved in hydrogen bond interaction with the zinc bound hydroxide ion. Of the four mutants with Thr 199 replaced by Cys, Asp, Glu and His, the first three showed similar or higher affinity for Zn(II) than the wild-type enzyme. The Thr199Glu mutant, in particular, resulted in a very high affinity for binding of Zn(II) (K_d = 20 fM) which is higher by an order of magnitude compared to the Thr199Asp mutant. These results clearly indicated the importance of the distance of separation between the metal and the ligand. The Thr199His mutant did not show any increase in affinity to zinc relative to the wild type enzyme due to rotation of the imidazole side chain away from the metal. Kiefer et al. (*254*) also found a 4 fold increase in the zinc binding affinity and a ten fold decrease in the catalytic activity upon substituting Cys for Thr199. Effect of the mutation of Gln92, Glu117 and Thr199 (whose side chains hydrogen

bond to the imidazole group of His residues and to the hydroxide group) on the thermodynamics and kinetics of metal binding, the pK_a of the water molecule bound to Zn(II), and the catalytic efficiency of hCA II was examined by Christianson and Fierke (*176-178*, *229*). Substitution of these residues with an Ala (Gln92Ala, Glu117Ala, and Thr199Ala) resulted in an order of magnitude decrease in the affinity of the protein for zinc. This effect of mutation is believed to be due to the decrease in entropy caused by the mutants.

Replacement of the proton shuttle residue His64 in hCA II to Ala reduced the enzymatic activity by 10-50 fold (*251*). Subsequently, it was found that this catalytic loss of the enzyme activity of His64Ala mutation in hCA II could be rescued by addition of an exogenous proton donor, 4-methylimidazole (4-MI), with a maximum activity of 40% of wild-type hCA II (*263*). The crystal structure of the rescued complex showed that 4-MI was bound in the active-site cavity of His64Ala hCA II, through pi stacking interactions with Trp5 and H-bonding interactions with water molecules. The crystal structure also showed that the conformation occupied by 4-MI in the rescued complexes mimicked the "out" conformation of His64 in the wild type enzyme (*263*)The compensation of the loss of catalytic activity by 4-MI in the absence of His64 suggested that the "out" conformation of His64 is effective in the transfer of protons between the zinc-bound solvent molecule and solution. In addition, His residues were introduced at different positions in the active-site cavity of hCA II and hCA III in order to study the kinetic significance of the location of proton shuttle. These studies showed that a histidine residue at sites other than position 64 (ie, His 67) is able to participate in proton transfer (*193*).

The absence of His64 makes mCA V a 20 fold less active protein than that of hCA II. Murine CA V has a tyrosine at this position which is a less efficient proton transfering residue (*39*, *260*). Mutational studies revealed that multiple residues, most importantly, Tyr131 and Lys91 in mCA V might act as proton shuttle residues in CA V (*44*). Heck et al. mutated Tyr64 and Tyr131 residues of mCA V with His and Ala respectively and investigated the catalytic rate of the mutants. As these mutant residues were replaced by those that are present in hCA II, with the hope of increasing the catalytic rate. However, in contrary to such expectation, neither of the mutatations enhanced the catalytic activity of mCA V (*260*).

Modification of cysteine residue of Phe65Ala/Tyr131Cys mutant of mCA V with 4-(chloromethyl) imidazole (4-CMI) resulted in a 3 fold increase in the proton transfer rate than the unmodified mutants (*38*, *264*). In order to understand the structural features that promote efficient proton transfer, crystal structure of Phe65Ala/Tyr131Cys-MI mCA V was investigated by Jude et al (*264*). Comparison of the active site of the mutants of mCA V with hCA II suggested two main differences: (1) The water bridge connecting the zinc bound water and the proton shuttle group adopts different channels towards the opposite side of the active site. (2) Three water molecules were found to present in the water bridge of Phe65Ala/Tyr131Cys -MI mCA V in contrast to two water molecules in hCA II. These differences are suggested to be responsible for the difference in the catalytic rate observed between several mCA V variants. For example, the decreased catalytic rate observed in Tyr64His/Tyr131Cys mutant of mCA V was explained better with the crystal structures. It has been proposed that the presence of bulky Phe65 perturbs the water bridge between

His64 and the proton shuttle residue, thereby decreasing the catalytic activity. However, it was found that the presence of bulky side chain of Phe95 did not show any difference in the catalytic activity between Phe65Ala/Tyr131Cys MI and Tyr131Cys-MI mCA V. This demonstrated that the presence of the bulky side chain of Phe65 does not perturb the proton transfer across the water bridge in Phe65Ala/Tyr131Cys-MI mCA V. In contrast to this result, the proton transfer rate of Cys131His mCA V was not enhanced. As the imidazole group of Cys131His mCA V is on a shorter side chain compared to that of Phe65Ala/Tyr131Cys-MI mCA V, it required an additional water molecule to join the water bridge connecting zinc bound solvent to the proton transfer residue. It is suggested that the unsatisfactory hydrogen bonded network for the water bridge could be one of the reasons for the lack of enhanced catalytic rate in this variant. The electron density map of Phe65Ala/Tyr131Cys-MI showed that Cys131-MI adopts two different conformations, and also appeared completely disordered suggesting the conformational mobility to some extent similar to that of the imidazole group of His64 in hCA II (*38*, *264*).

As the side chains of Trp5, Asn62, Ile91, and Phe131 of hCA II were found to extend in to the active site with distances ranging from 12.5 to 14.5 Å from the catalytic zinc, Elder et al. (*265*) replaced these residues with Cys and subsequently alkylated them with imidazole containing reagents in order to investigate their capacity to serve as an efficient proton transfer residues in catalysis. They found a two fold increase in the rate constant of proton transfer for the Phe131 modified mutants in comparison to the unmodified mutants. Other modified mutants showed almost 3 fold increase in the rate constants in comparison to the His64Ala mutant of hCA II. Though the distances of these

residues from zinc are comparable to the Cys131 of mCA V variant, chemical modification at these sites did not show any enhancement in the proton transfer rate. This was suggested to be due to the orientation of the modified side chains away from the metal or could be due to the electrostatic or hydrogen bonding interactions of the imidazole nitrogen of these residues (*264*).

In wild type hCA II, only minimal conformational changes of direct ligands takes place upon binding to the metal ion because the indirect residues favorably pre orient the metal-binding site and provide electrostatic stabilization of the metal ions (*119*, *185*). The hydrogen bonded network also plays a role in the rate of association of Zn(II). Experiments suggest that mutation of Glu117 with Ala, Gln, or Asp reduces the kinetics of zinc binding by a factor of 10^2 to 10^4 (*176*, *229*) but cause only a 10 fold loss in the catalytic activity relative to the wild type enzyme. The only exception to this observation is the Glu117Gln mutation where the catalytic activity is completely lost due to the increase in pK_a of the zinc bound water. This was suggested to be due to the following reasons. "(i) the reversal of polarity of the hydrogen bond between His119 and residue 117, (ii) stabilization of the negatively charged histidinate ligand, (iii) elevation of the pK_a of the Zn(II)-bound water, and (iv) the elimination of the reactivity of ZnII" (*119*, *229*). Based on the site directed mutagenesis of Thr199, it was also proposed that Thr199 is involved in the ground state stabilization of Zn(II)-OH and the transition state of the reaction pathway. Thr199Ala mutants resulted in a significant reduction in the catalytic activity due to the disruption of the hydrogen bond between the inhibitor and Thr (*119*, *177*).

Although the amino acid sequences of hCA I and hCA II are 60% identical (*266*, *267*) and the overall three dimensional structures are very similar (*174*, *204*), there are some isozyme-specific active site residues. For example, His200 in hCA I, which is replaced by Thr in most other CA enzymes. Another characteristic feature of hCA I is the presence of Val62 (which is Asn in other hCA isozymes) which is a hydrophobic residue in a hydrophilic part of the active site. Furthermore, His67 in hCA I is replaced by Asn in hCA II. To investigate the structural and functional importance of these residues, mutation studies were carried out. Mutation of His200 to Thr revealed that His200 in hCA I is involved in increasing the lifetime of the enzyme-bicarbonate complex and attenuation of the catalytic potential of hCA I (*268*). Based on the pH dependent esterase activity of wild type and His200Thr mutant, it was also found that His200 is involved in the stabilization of the zinc-bound water molecule (*268*). The acidity of the zinc-bound water molecule is believed to be at least 10 times lower in the presence of His200 than that with Thr200. Val62Asn and His67Asn mutants did not follow any specific pattern on the esterase activity and pK_a of the zinc-bound water. It was suggested that as these residues are more distant from the metal center than residue 200, their effects on the catalytic properties of the CA isozymes are probably less direct (*268*).

Residues Phe93, Phe95, and Trp97 located along the beta-strand of hCA II were found to contribute to the high zinc affinity and slow zinc dissociation rate constant of the enzyme (*261*). This feature was hypothesized either due to the ability of the above residues to restrict the conformational flexibility of the His residues coordinating the zinc ion or due to the contribution of their aromatic residues in decreasing the dielectric constant of the

active site thereby increasing the electrostatic interactions (*269*). The residues flanking the zinc ligands, His94 and His96 in a β-strand structure (Figure 1.25) form packing interactions with the hydrophobic core of the protein (*174*). Substitution of these residues with smaller amino acids were found to reduce the zinc affinity by 100-fold, and increase the zinc dissociation rate constants by 1000-fold (*261*). This was suggested to be either due to the loss of restriction of conformational flexibility of the zinc coordinating residues or the increase in the dielectric constant of the active site (*261*). In order to delineate which of the above two reasons are mor appropriate, six hCA II mutants that differ in size and hydrophobicity were substituted at positions 93, 95 and 97 and their metal specificity and stability were studied by Hunt et al (*242*). It was found that cobalt ion had the same affinity as that of zinc ion and the affinity decreases with decrease in hydrophobicity. But Cu^{2+} showed an opposite trend as its affinity increased with decrease in hydrophobicity. Their studies suggested that the stabilization of the tetrahedral metal ion geometry requires (i) hydrophobic residues, as observed in the case of Zn^{2+} and Co^{2+} bound to hCA II (*188*), and/or (ii) destabilizing the trigonal bipyramidal geometry as observed with Cu^{2+} (*235*) refuting the hypothesis that the increase in zinc coordination was due to the decreased dielectric constant of the metal resident pocket of the enzyme (*242*).

Cox et al (*240*) created three mutants (Phe93Ile/Phe95Met/Trp97Val, Phe93Ser/Phe95Leu/Trp97Met and Phe95Met/Trp97Val and determined their X-ray crystal structures to probe the roles of Phe93, Phe95 and Trp97 in modulating the metal affinity and specificity. Crystal structures of Phe93Ile/Phe95Met/Trp97Val and Phe95Met/Trp97Val hCA II revealed that the overall structures of these variants are similar

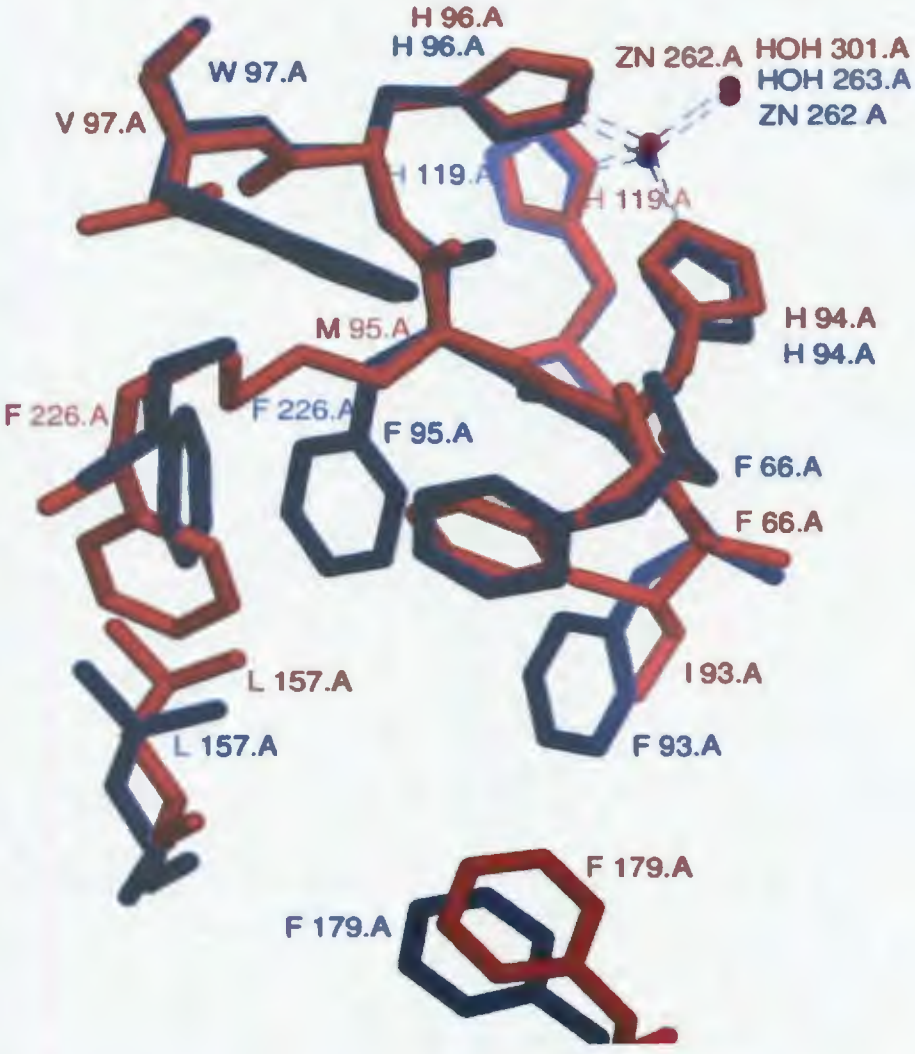

Figure 1.25. Overlay of the active site residues of the wild type and Phe93Ile/Phe95Met/Trp97Val hCA IIs.
Overlay of the active site residues of the wild type (blue) and Phe93Ile/Phe95Met/Trp97Val (red) hCA IIs. The PDB IDs of the wild type and mutant enzymes are 2CBA (*174*) and 1FQM (*240*). The structure was modeled using UCSF Chimera® software (*175*). Zinc ions are represented as spheres. Note the significant structural changes that occur because of the aminoacid substitutions.

to that of the wild-type hCA II. Only slight changes in the positions of His94 and His96 were observed. Substitution of bulky amino acids with smaller ones triggered slight

conformational changes in some amino acid side chains. As depicted in Figure 1.25, mutation resulted in the movement of Phe179 towards the void created by Phe93Ile substitution and Phe226 and Leu157 shifted toward the void created by the Phe95Met substitution in Phe93Ile/Phe95Met/Trp97Val mutants of hCA II. Similar structural changes, except for the movement of Phe179 were observed in the Phe95Met/Trp97Val double variant.

Comparison of the Phe93Ser/Phe95Leu/Trp97Met hCA II with the wild type enzyme revealed similar over all structure (*240*). However, the position of the zinc-bound water molecule is altered slightly which accounted for the reduction in CO_2 hydratase activity by this mutant (*240*, *261*). Residues Phe179, Val160, Phe66, and Phe226 make significant movements to partially fill the void created by the variant side chains (Figure 1.26). In addition, the water molecules 421 and 369 also help to fill the void created by the Phe95Leu and Trp97Met substitutions. It is revealed that aromatic residues Phe93, Phe95, and Trp97 serve as anchors and help to pre orient and stabilize the metal ligands for optimal zinc binding. Mutations of these residues weaken the anchor and are indicated by the conformational change of His94-Gln92 in the metal free form of the mutant Phe93Ile/Phe95Met/Trp97Val. It was concluded that the substitution of the bulky aromatic residues with small hydrophobic amino acid residues decreases the free energy barrier for adopting non tetrahedral metal coordination geometries which could account for the different metal ion specificities of these mutants (*240*).

1.1.12. NMR studies of CA isozymes

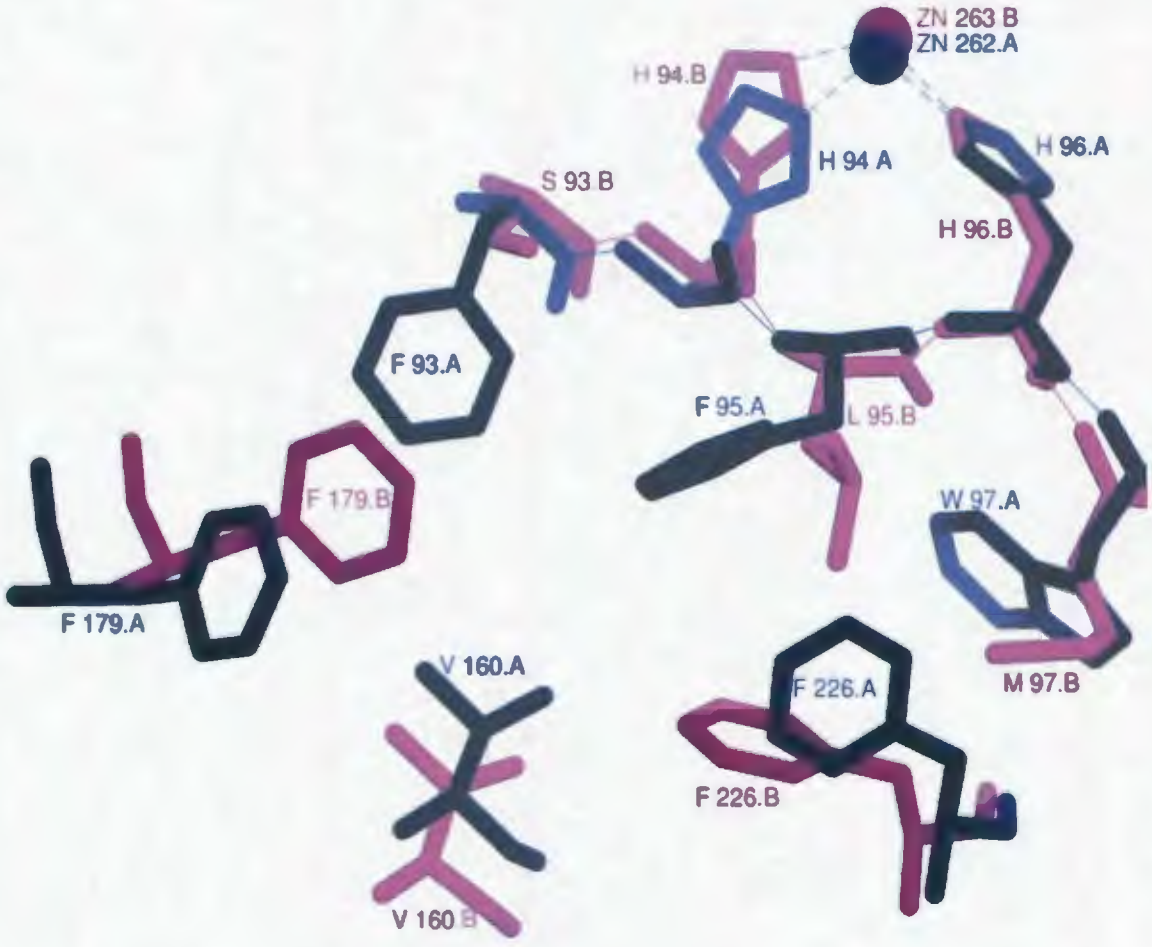

Figure 1.26. Overlay of the active site of wild-type and Phe93Ser/Phe95Leu/Trp97Met hCA IIs.
Overlay of the active site of wild-type (blue) and Phe93Ser/Phe95Leu/Trp97Met (majenta) hCA IIs. The PDB IDs of the wild type and mutant enzymes are 2CBA (*180*) and 1FQM (*240*). The structure was modeled using UCSF Chimera® software (*175*). Zinc ions are represented as spheres. Note the significant structural changes that occur because of the aminoacid substitutions.

In hCA XII His64 is believed to play the role of proton shuttle similar to that observed in hCA II. This is evidenced by a 10 fold decrease in the catalytic activity of the mutant His64Ala and His64Arg (*270*).

As mentioned earlier, the X-ray crystallographic studies provide useful information on the structure of native and mutant CAs in its free and ligand bound forms. However, information about the structural dynamics of enzyme and its bound inhibitor in solution phase cannot be obtained by such studies. NMR studies, which are very uselful in this aspect have been perfored to understand the solution structures as well to understand the kinetics and pathway of folding of CA I and CA II (*271-282*).

In order to understand the molecular basis for the marked changes in the catalytic activity and the affinity toward sulfonamides and other inhibitors of the carboxy methylated hCA I at His200 (*283-285*). Khalifah et al. (*245*) labeled this residue with ^{13}C enriched bromoacetate. The diamagnetic NMR studies on this derivative suggested that the carboxymethyl (Cm) carboxylate interacts with the active site zinc under specific pH conditions. This provided a molecular explanation for the catalytic activity and the active site ionization changes that result from the carboxymethylation. In order to understand the interaction of the carboxylate ion with the catalytic metal ion, ^{13}C NMR studies were conducted on the cobalt substituted hCA I and ^{13}C labeled carboxymethylated hCA I (*286, 287*). It was found that in hCA I complexed with inhibitor, the distance between the carboxylate carbon and the active site cobalt ion was in the range of 5-7 Å and when the inhibitor is absent, this distance was approximately 3.0-3.2 Å at pH 7.9, consistent with the coordination of the carboxylate to the metal. However, this distance increased to 4.8 Å when the pH was increased to 10. The carboxymethyl carboxylate coordinates to the active site metal at pH 8 and below, and it is displaced either by an increase of the pH or by addition of inhibitors that bind to the metal. It was suggested that the competition of the

intramolecular carboxylate with solvent hydroxyls and anions for binding at the zinc was the reason for the increase in the pK_a of the zinc bound water and the decrease in affinity toward anionic substrates and inhibitors. The close proximity of the carboxylate anion to the zinc was found to be responsible for the decrease in the catalytic activity of CmCA I at high pH (*245*).

^{15}N NMR studies by Kanamori and Roberts (*277*) demonstrated that the active site metal in CAs bind aryl sulfonamides in their anionic form through the sulfonamide nitrogen. They suggest that in order for arylsulfonamides to bind as anions to the zinc, deprotonation of sulfonamide group has to take place prior to binding. In addition, these studies found that the stoichiometry of the CA-aryl sulfonamide groups to be 1:1 (*288*) in contrast to the X-ray structures (*289*, *290*, *288*) which showed that one sulfonamide bound to the active site of hCA II and the other sulfonamide bound at the interface between two hCA II proteins in the crystal lattice. The internal motion of the bound inhibitors and the enzyme active site was also characterized by NMR (*271*, *274*, *275*). It was found that, in hCA I-benzene sulfonamide complex, the aromatic ring of benzene sulfonamides rotates rapidly on the NMR time scale. It was found that the internal mobility of the α-carbons in the enzyme is restricted upon binding of the inhibitor, ^{15}N [1H] NOE experiments qualitatively indicated the existence of some internal mobility of the bound inhibitor. Results from NMR studies suggest that internal motion of the enzyme and inhibitor should be taken into account while designing inhibitors as these factors would influence the binding of the ligand (*119*).

1.1.13. Inhibitors of CAs

Because of the role of CA isozymes in many pathological processes, it has been a therapeutic target for many years. Inhibition of CA isozymes have been found to and/or proposed to treat many disorders (*20*, *83*, *97*, *140*, *149*, *217*, *291-297*). CA inhibitors (CAIs) can be classified into three categories, namely, sulfonamides ($R\text{-}SO_2NH_2$), sulfonic acid derivatives ($R\text{-}SO_2\text{-}X$, $X * NH_2$), and small monoanions such as halides, azide, and thiocyanate (*119*). The sulfonamides and sulfonic acid derivatives have K_d values ranging from picomolar to micromolar, whereas the K_d for inorganic monoanions are in the micromolar to millimolar range (*119*).

The discovery by Mann and Keilin in 1940 (*298*) that sulfanilamides **(compound 1)** inhibit CAs was soon followed by the report by Krebs (*299*) that the unsubstituted aromatic sulfonamides ($ArSO_2NH_2$) act as strong CAIs, and that the potency of such compounds is drastically reduced by N-substitution of the sulfonamide moiety. This constituted the beginning of extensive structure–activity correlations, and paved the path of a great scientific adventure that led to important drugs, such as the antihypertensives (*300*), antiglaucoma agents (*301*, *302*, *300*), antithyroid drugs (*300*), the hypoglycemic sulfonamides (*303*) and novel anticancer agents (*304*). Extensive studies of their inhibitory potency, and physiological and pharmacological effects have been made which led to some valuable drugs during a short period of time (*65*).

A typical sulfonamide inhibitor is made up of a head group, ring group, tail group and secondary recognition group (*119*). The group attached to the sulfonamide is a 5- or 6-membered aromatic ring or fused ring system that mostly contains nitrogen, oxygen, and/or sulfur hetero atoms (*65*). The functional groups that are conjugated to the aromatic rings in

order to modulate the inhibitor properties such as pK_a and solubility are called "tails". The length of these groups varies from 1 to 100 Å and is expected to affect the in vitro and in vivo inhibition by changing the solubility, flexibility, polarity, and biocompatibility of the compound. These tails could also be used to recognize sites on the protein adjacent to the active site (*65*, *119*).

The crystallographic structure of hCAI and their binding to the zinc ion were analyzed by Liljas et al. in 1972 (*233*) and subsequently by many others (*182*, *226*, *305*, *306*). In all these structures, sulfonamides, in deprotonated state bind Zn(II) ion in a tetrahedral geometry (Figure 1.27) with the nitrogen atom of the sulfonamide moiety coordinated to Zn(II) (*307*). Anions bind either in tetrahedral geometry of the metal ion or as trigonal-bipyramidal adducts (*307*) (Figure 1.27). NMR spectroscopic studies by Kanamori and Roberts (*277*) showed that the mono-protonated and negatively charged nitrogen of the sulfonamide group binds to the metal ion. The X-ray crystallographic structures of CA complexed with sulfonamide inhibitors show that the sulfonamide is coordinated to the Zn(II) ion of CA in deprotonated form, and its NH moiety is involved in a hydrogen bond with the Oγ of Thr199, which in turn is involved in another hydrogen bond to the carboxylate group of Glu106. In addition, a hydrogen bond is observed between the oxygen atoms of the SO_2NH moiety also with the backbone NH moiety of Thr199 (*212*, *308*, *307*).

1.1.14. Development of CA inhibitors

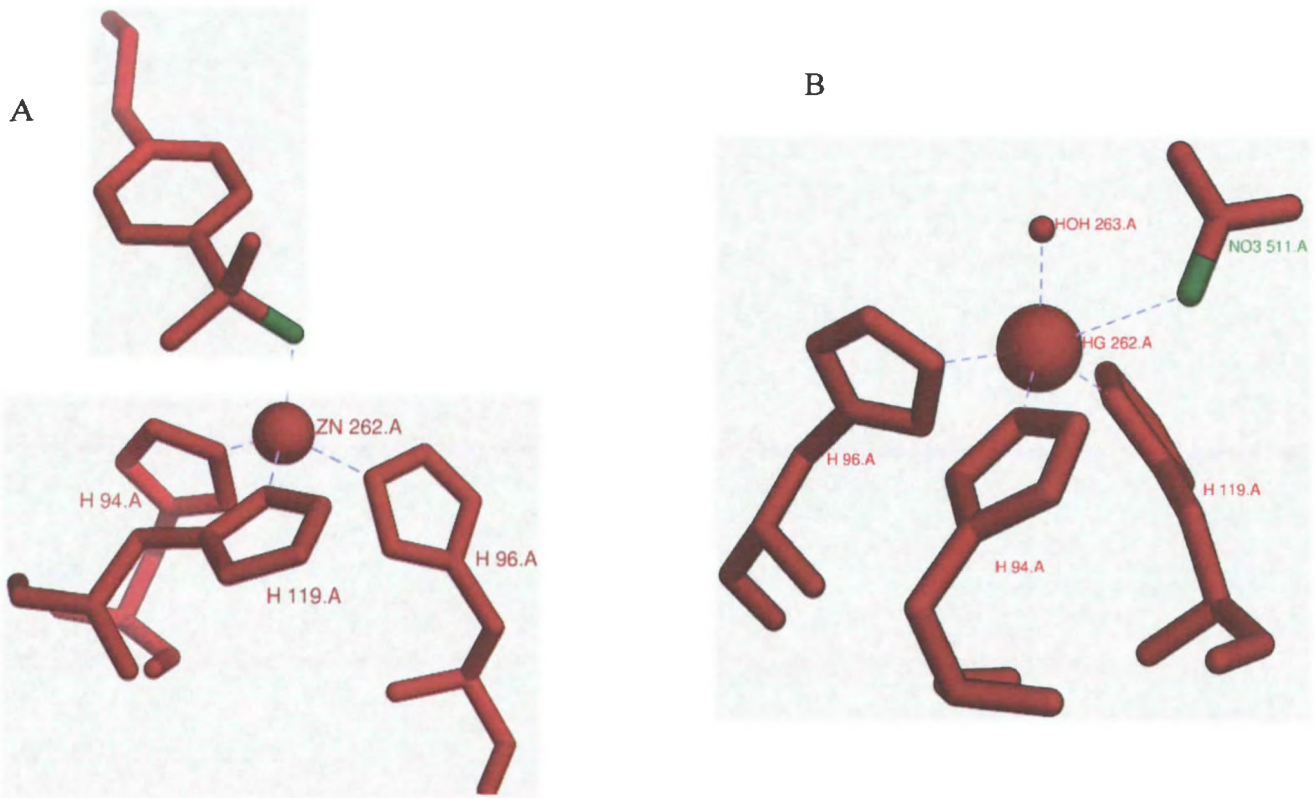

Figure 1.27. Active site geometry of hCA bound to inhibitors.
A shows that the sulfonamide inhibitor (PDB ID: 2NNG) (*309*) displaces the zinc bound water molecule thereby giving rise to a tetrahedral geometry. B shows that the anion NO_3^- binds in a trigonal bipyramidal geometry (PDB ID: 1CAN) (*310*) with out displacing the zinc bound water molecule. The structures were modeled using the above PDB IDs in UCSF Chimera software (*175*).

When CA inhibitors were given systemically, they inhibit different CA isozymes present in tissues other than that of the eye, and thus led to various side effects (*65*, *300*, *302*). But when the above clinically used inhibitors were given topically, they were not effective in reducing the IOP. This was later found to be due to inappropriate physicochemical properties of the CAIs that were available at that time, and thus initiated the discovery of topically acting sulfonamides, viz., dorzolamide **(compound 6)** and brinzolamide **(compound 7)** that entered in clinics in 1995 and 1999 repectively (*132*, *311*, *300*, *301*). The structures of CA inhibitors (compounds 1-7) are depicted in Figure 1.28.

Two main approaches were used for the design of anti glaucoma CA inhibitors. The first approach named as "ring approach" by Supran and coworkers involved exploring a large variety of ring systems on which the sulfonamide group was attached. Dorzolamide **(compound 6)** and brinzolamide **(compound 7)** were discovered based on this approach. The second approach named as the "tail approach" involved attaching water-solubilizing tails to aromatic/heterocyclic sulfonamides (*65*). This approach led to the development of many effective antiglaucoma sulfonamides as compared to dorzolamide **(compound 6)** and brinzolamide **(compound 7)** in animal models (*65*). Majority of the sulfonamides designed by the ring approach are bicyclic compounds, with at least one sulfur atom present in the rings. O-acyl- or O-alkyl sulfonyl derivatives of 6-hydroxy- benzothiazole-2-sulfonamide were the first candidates belonging to this family of sulfonamides **(compounds of type 8)**.

Even though these derivatives were very effective in reducing the IOP, they could not be developed for clinical applications as they were rapidly metabolized, and were found to be potent allergens in rabbits (*312*). It was found that the high electrophilic character of the heterocyclic ring was responsible for the side effects and hence attempts were made to

Sulfanilamide (compound 1)

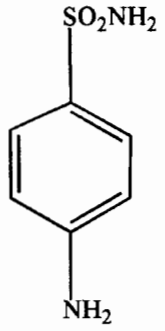

Acetazolamide (Compound 2)

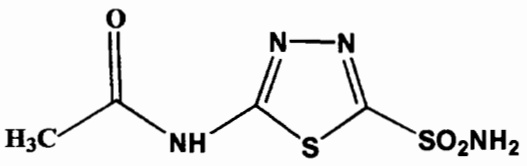

Methazolamide (Compound 3)

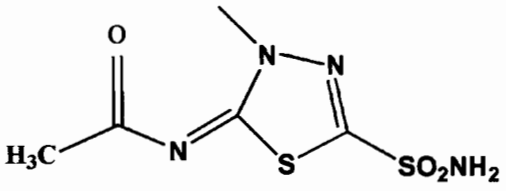

Ethoxzolamide (Compound 4)

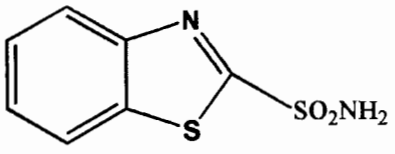

Dichlorophenamide (Compound 5)

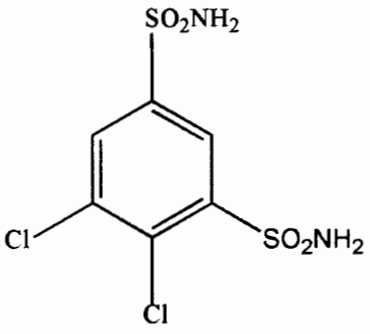

Dorzolamide (Compound 6)

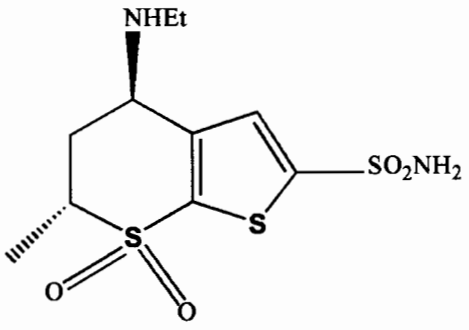

Brinzolamide (Compound 7)

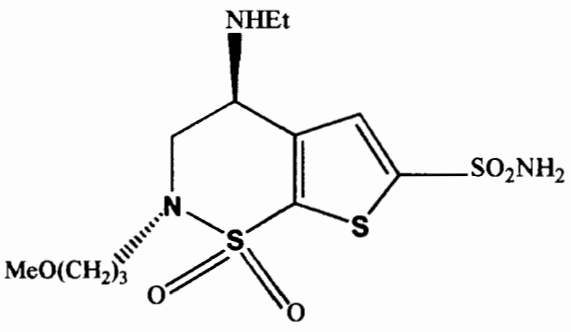

Figure 1.28. Structures of CA inhibitors (Compounds 1-7).

reduce the electrophilicity by incorporating other ring systems, such as benzo [b] thiophene-, benzofuran-, indole-, and thieno-thiophene **(compounds 9-13)**. These derivatives were also found to be potent allergens and were ineffective in humans (*313-315*). Subsequently, the same group reported a series of 4-substituted-thiophene-and -furan-2-sulfonamide derivatives which showed good CA inhibitory properties in rabbits without devoid of allergenic properties (*316*). Sulfonamides belonging to the thieno [2,3-b]thiopyran-2-sulfonamide class were among the most water soluble sulfonamides reported at that time **(compounds of type 14 and 15)** (*317, 316*). MK-927 **(compound 16)** was initially considered as the best inhibitor for clinical development, but subsequently the presence of a new chiral center was considered desirable,which ultimately led to the development of dorzolamide **(compound 6)** (*305*). Structures of compounds 8-16 are depicted in Figure 1.29. Both dorzolamide **(compound 6)** and Brinzolamide **(compound 7)** possesses chiral centers and the preparation of pure enantiomers is very expensive. Some dorzolamide like compounds that do not possess chiral centers have been reported by the Alcon group. These compounds bind hCA II and hCA IV in the nanomolar range and reduce IOP effectively (*318*). Whether these compounds would act as effective substituents of brinzolamide is not known yet (*65*).

The 'tail approach' developed in Supran's laboratory used known aromatic/heterocyclic sulfonamide scaffolds to which tails that induce water solubility were attached at the amino, hydroxy, imino, or hydrazino moieties of sulfonamide. This approach was considered much simpler as it allowed parallel synthesis leading to the preparation of a large number of derivatives (*133-137, 319-325*). Initially this approach involved the attachment of various aminoacids to the exocyclic acetyl group of acetazolamide. A

Compounds of type 8

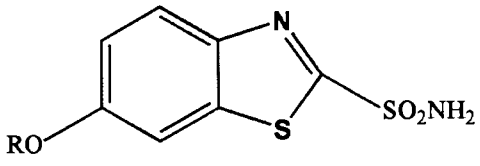

R= acyl, alkyl-SO_2

Compound 9

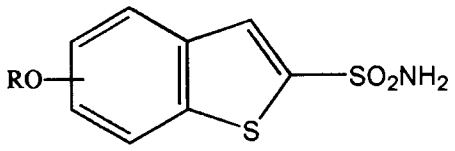

R=5-/6-substituted acyl, H

Compound 10

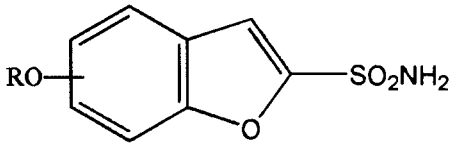

R=5-/6-substituted acyl, H

Compound 11

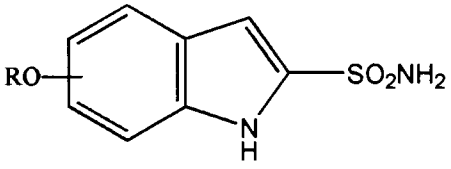

R=5-/6-substituted acyl, H

Compound 12

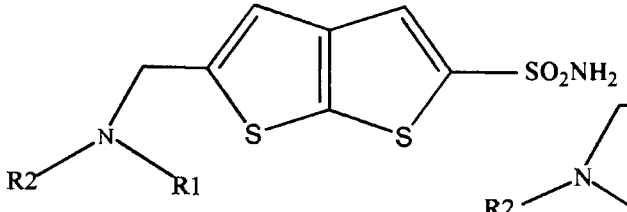

R1, R2 = H, alkyl etc

Compound 13

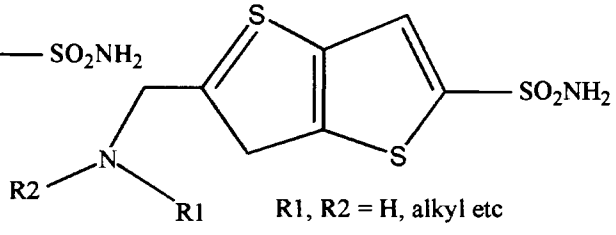

R1, R2 = H, alkyl etc

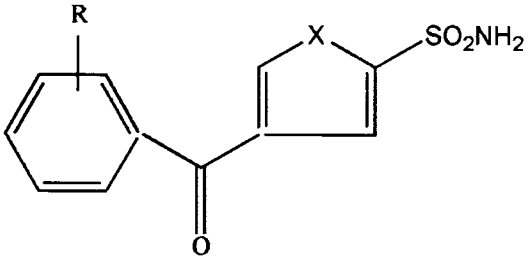

compounds of type 14: X=S, R= OH, OMe etc
compounds of type 15: X=O, R=OH, OMe etc

compound 16 (MK-927)

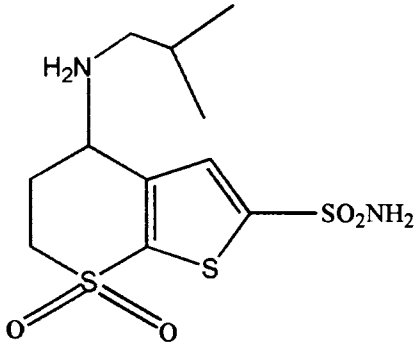

Figure 1.29. Structures of Some CA inhibitors(Compounds 8-16).

similar approach was used by Antonaroli et al. (*326*) using dioic fatty acids as their acylating agents.

Roy et al. (*327*) demonstrated a general strategy of inhibitor design by converting weak inhibitors of hCA II into very potent inhibitors. This approach involved attaching a metal chelating tether group, which extends beyond the active site pocket of the enzyme and interacts with the surface exposed histidine residues. Thus the weak inhibitors, benzene sulfonamide **(compound 17)** and para aminoethyl benzene sulfonamide **(compound 18)** were conjugated to the complex IDA-Cu^{2+} with a variety of spacers to generate the potent inhibitors. The structures of resultant conjugates **(compounds 19-21)** are shown in Figure 1.30.

Banerjee et al. (*328*) showed that the binding affinity of the active site directed ligand, benzenesulfonamide **(compound 17)**, is enhanced 40 fold if the latter is conjugated (via a spacer moiety) to iminodiacetate (IDA)-Cu^{2+}. A schematic representation of the two prong strategy is depicted by the cartoon in Figure 1.31. Whereas the second prong of the shorter ligand (L2) can easily loop around and interact at a complementary peripheral site, that of the longer spacer containing ligand (L1) fails to interact at the same or other complementary site on the surface of the enzyme. Based on the modeling data (Figure 1.31) they assigned His-4 as the most likely target for the interaction of IDA-Cu^{2+} of compound 19 (*329*). ITC experiments of hCA II with these two-prong inhibitors suggested that the binding energy is derived not only from the interactions at the active site region but also from the interactions of IDA-Cu^{2+} to the surface-exposed histidine residues.

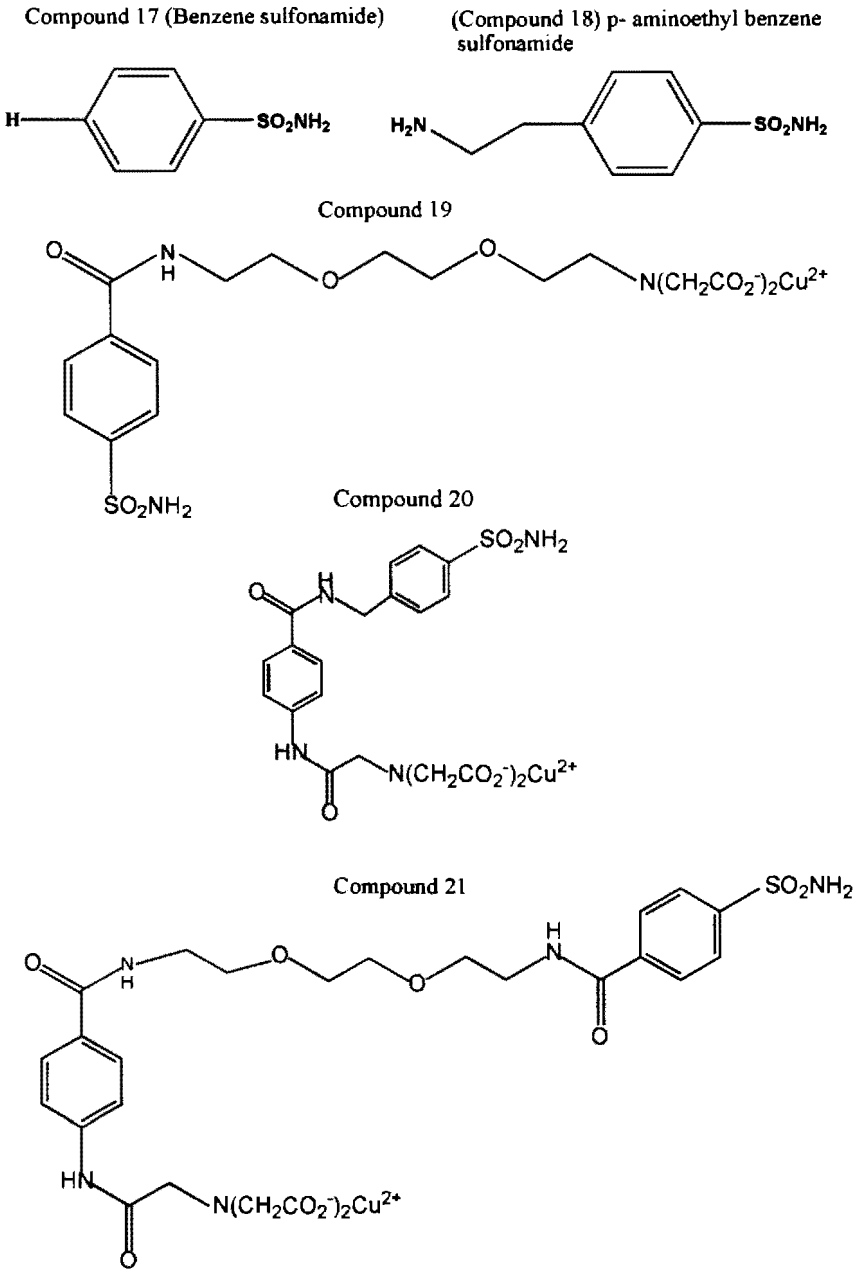

Figure 1.30. Structures of one and two prong inhibitors (Compounds 17-21).

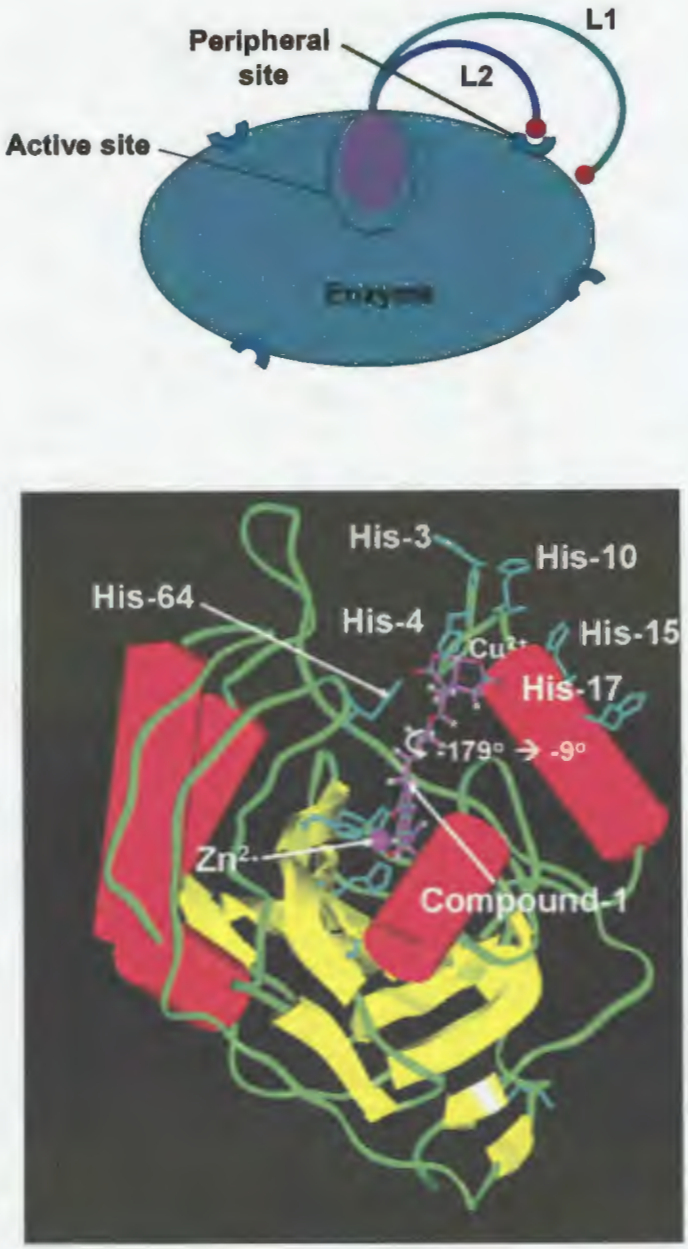

Figure 1.31. Representation of two prong approach.
Upper panel shows the schematic representation of two prong approach and the lower panel shows the modeling of the compound with hCA II. The Figure is adapted from reference (*329*).

It was initially believed that only aromatic sulfonamides could serve as potent CA inhibitors (*301*). However, it was later discovered that incorporating a "spacer" between the sulfonamide moiety and the ring could increase the affinity of inhibitors to CA.

Zonisamide (**compound 22**) (Figure 1.32), a tight binding inhibitor of hCA II has a methylene moiety between the aryl ring and the sulfonamide ring (*279*, *330*). It was also found that the meta-substituted sulfamates were more potent inhibitors of CA compared to the para-substituted analogues (*65*). The X-ray crystal structures of aryl sulfamates like topiramate (**compounds 23**) and EMATE (**compounds 24**), with hCA II revealed that although the K_i values of these two inhibitors were similar, their mode of binding in the CA active site was very different. Whereas several hydrogen bonds were found between topiramate and the hydrophilic face of the active site, EMATE (**compound 25**) made contacts only to the hydrophobic wall (*331-333*). Sulfamic acid and sulfamide also proved to be tight binding inhibitors of hCA I, hCA II, bCA II and bCAIV inspite of the removal of the aromatic ring (*334*, *335*, *308*, *332*). N- hydroxyl sulfamide is also a good inhibitor for hCA I, hCA II, hCA IX and hCA XII. X-ray structures of these compounds with hCA II show new hydrogen bonds that are not observed with aryl sulfonamides (*336*, *308*).

Trifluoromethanesulfonamide (**compound 25**) was found to be a potent inhibitor of hCA II in contrast to the low affinity of methane sulfonamide to hCA II (*337*). The high affinity of the fluorinated sulfonamide was attributed to its much lower pK_a value (6.3) than methane sulfonamide (10.8) (*337*). Extensive structure – activity relationship studies were also conducted by Scholz et al. (*337*) to describe the binding of aliphatic sulfonamides to hCA II. Their studies suggested that the potency of the inhibitor was dependent upon the substituents near the sulfonamide moiety and hydrophobicity of the

inhibitor. The inhibitor's affinity increases with increasing hydrophobicity of the aliphatic chain attached to the sulfonamide. This might increase the interaction of the inhibitor with the hydrophobic wall of the enzyme active which in turn would contribute to the stability of the complex.

Roughton and Booth (*338*) were the first to observe that small inorganic ions can inhibit CAs. Subsequently, several investigators reported the inhibition of CAs by anions (*199, 200, 339, 340*). The X-ray structural data of CAs bound to these anions show that most anions displace the Zn(II)-bound water and bind to the Zn(II) cofactor in a tetrahedral geometry (*174, 189, 193, 308, 310, 341-343*). Two anions, SCN and NO bind zinc in a distorted pentagonal geometry without displacing the water (*182, 310*).

As the CA isozymes possess high sequence as well as structural homology, designing inhibitors targeted to a particular isozyme has been a challenge over several decades (*65, 119, 324*). The side effects of the clinically used sulfonamide inhibitors such as acetazolamide **(compound 2)**, methazolamide **(compound 3)**, ethoxzolamide **(compound 4)** and dorzolamide **(compound 6)** have been attributed to the unwanted inhibition of hCA II, when other isozymes were targeted (*77*). As the affinity of sulfonamide inhibitors to hCA II and bCA IV was similar, distinguishing between these two isozymes has been the focus of research for many years. There has been some progress in the design of inhibitors with some selectivity towards CA I and CA IV (*65, 119, 344*).

CA I, in contrast to CA II possesses a number of histidine residues in the active site. The only His in the CA II active site apart from the histidine ligands, is His64, whereas in CA I, three other additional histidines, namely His67, His200 and His243, are present (*249*). Another difference between the two isozymes is the presence of a histidine cluster

Compound 22 (Zonisimide)

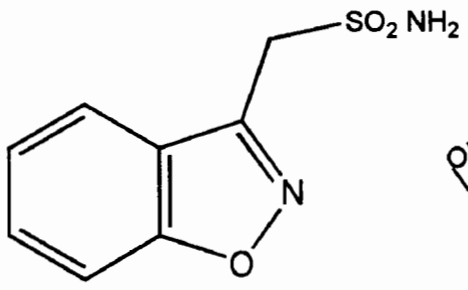

Compound 23 (Topiramate)

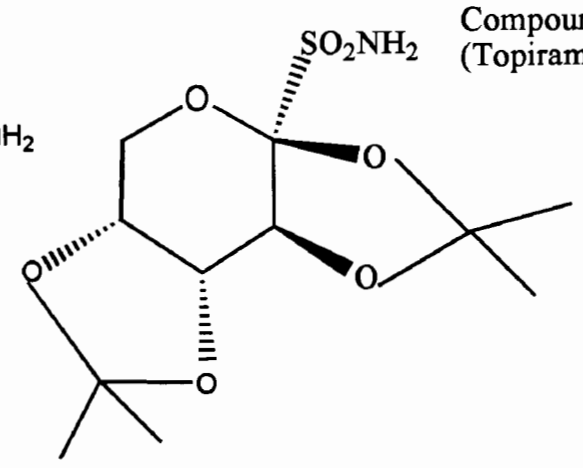

Compound 24 (EMATE)

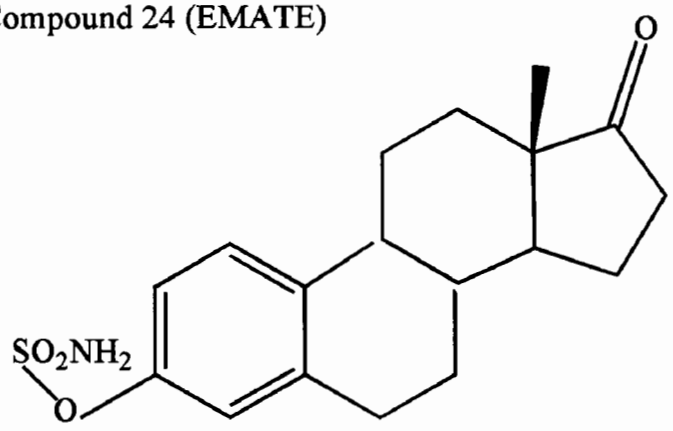

Compound 25 (Trifluoro methane sulfonamide)

$CF_3SO_2NH_2$

Figure 1.32. Structures of CA inhibitors (Compounds 22-25)

(His64, His4, His3, His10, His15, and His17) that extends from the middle of the active site to the rim of the cavity in CA II which is absent in CA I. Where as CA II has higher affinity for sulfonamides, CA I binds anions more tightly. This makes it difficult to design sulfonamide inhibitors that have higher affinity to CA I than to CA II (*302*, *345*, *334*).

Recently, Supran's group found that sulfonamides containing ureido or thioureido moieties **(compounds 26-30)** (Figure 1.33) bind with higher affinity to hCA I than hCA II (*65*, *346-348*). Banerjee et al. (*329*) found that DNSA **(compound 31)**, a fluorescent inhibitor of CA, binds more tightly to hCA I than to hCA II and it was proposed to be due to the difference in the structural feature or the active-site environment or a combination of both of these features.

The presence of four cysteine residues, which form two disulfide bonds, situated at the entrance of the active site cavity (Cys 6–Cys 11G and Cys 23–Cys 203) is the characteristic feature of the isozyme CA IV (*349*). The cysteine residues are located in the active site in a location similar to that of the histidine cluster in CA II and this difference is suggested to be the cause of the difference in affinity for sulfonamide inhibitors of these two isozymes (*65*, *249*). It was found that sulfonamides possessing heterocyclic or aromatic rings substituted with electron attracting groups like nitrogen bind with the highest affinity to CA II although these compounds have appreciable affinity to CAII and moderate affinity to CAI (*350-353*).

In contrast to other CAs, CA III is insensitive to sulfonamide inhibitors. His64, which is a proton shuttle residue in most other CAs is replaced by a less effective proton shuttle residue, lysine in CA III. The presence of a bulky side chain of Phe198 and the lower pK_a (5.5) of CA III are also considered to be responsible for the poor catalytic activity and insensitivity to sulfonamide inhibitors (*65*, *209*).

Due to the extracellular location of the membrane bound isozymes (CA IV, CA IX, CA XII, CA XIV), membrane-impermeant CAIs containing positively charged sulfonamides were designed and tested **(compounds 32-34)**. These compounds showed

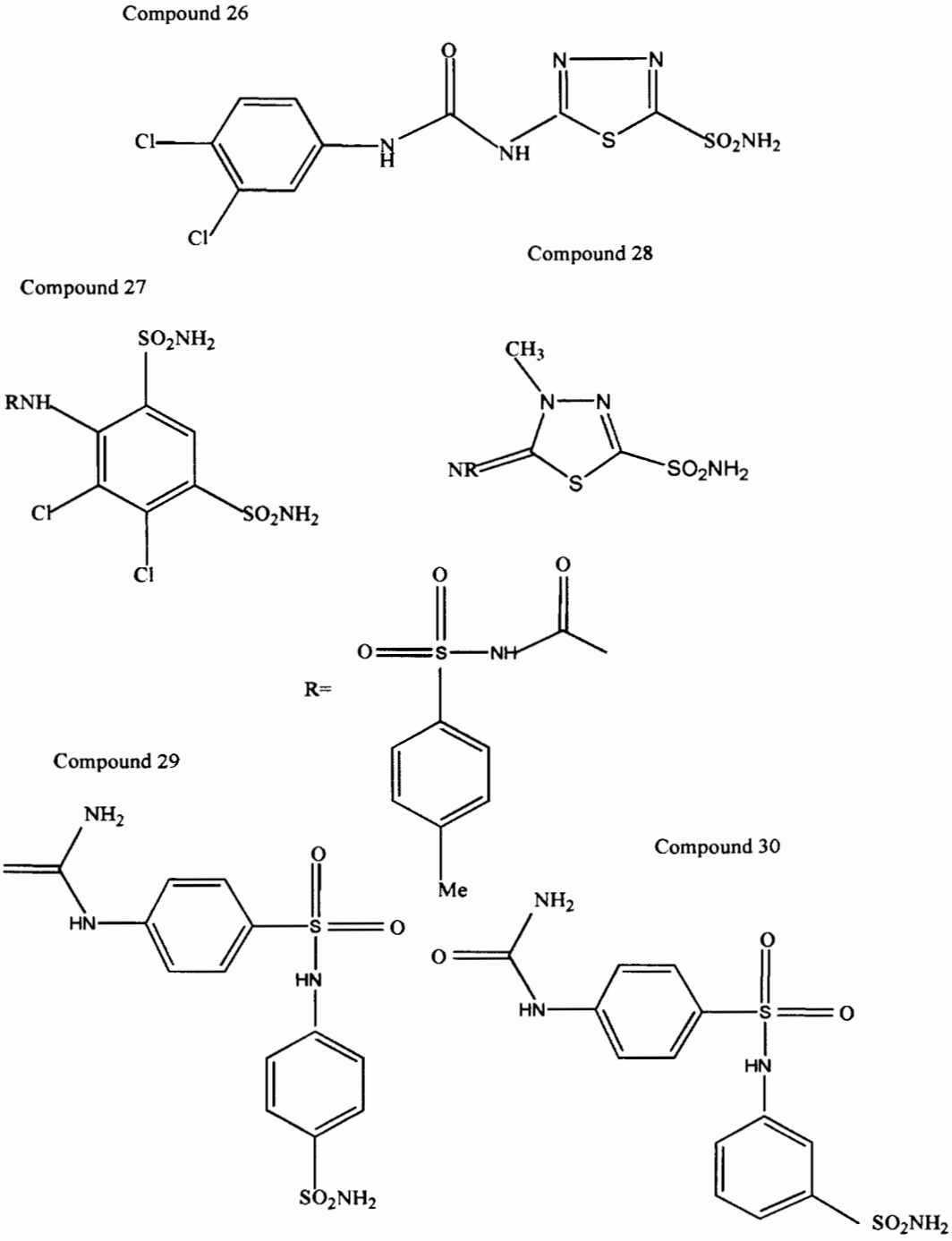

Figure 1.33. Structures of CA inhibitors containing Ureido and Thioureido moieties (Compounds 26-30).

membrane- impermeability because of their high molecular weights, and were selective towards CA IV in comparison with CA II. Unfortunately, their macromolecular nature and the allergic reactions induced by them in vivo prohibited the development of these inhibitors as drugs (*121*, *354-361*). Polar, salt like compounds such as quaternary ammonium sulfanilamide (QAS) **(compounds 35)** were also tested and showed membrane impermeability (*362*). The main draw back with this compound is its high toxicity in vertebrates (*300*). Using QAS as a lead compound, cationic sulfonamides were prepared. These compounds were moderately inhibitory towards CA II and CA IV (*354-356*). The inhibitory potency of these inhibitors were found to increase with increase in the length of the inhibitor. These inhibitors were found to specifically inhibit CA IV as compared to CA II, as they were unable to cross the plasma membrane (*357*, *358*).

CA inhibitors have been found to inhibit the growth of tumor cells both in vitro and in vivo (*142*, *165*, *297*, *363-366*). This is supposedly due to the inhibition of tumour associated CA isozymes (CA IX and CA XII) thereby reducing the supply of HCO_3^- for synthesizing nucleotides (*367*). CA isozymes have been shown to be involved in many tumors such as von hippel-lindau tumors (*368*), acinar-ductal carcinomas of the pancreas and auto immune/idiopathic chronic pancreatitis (*47*). Some CA isozymes like CA IX are predominantly expressed in cancer cells but are not found in their normal counterparts(*369*). Acetazolamide **(compound 2)**, in combination with cytotoxic agents such as alkylating agents, nucleoside analogs and platinum derivatives, showed anti cancer effects that are believed to be due to tumor cell acidification following CA inhibition (*370*). Methazolamide **(compound 3)** and ethoxzolamide **(compound 4)** were also found to inhibit the growth of human lymphoma cells (*367*). Compounds possessing both aromatic,

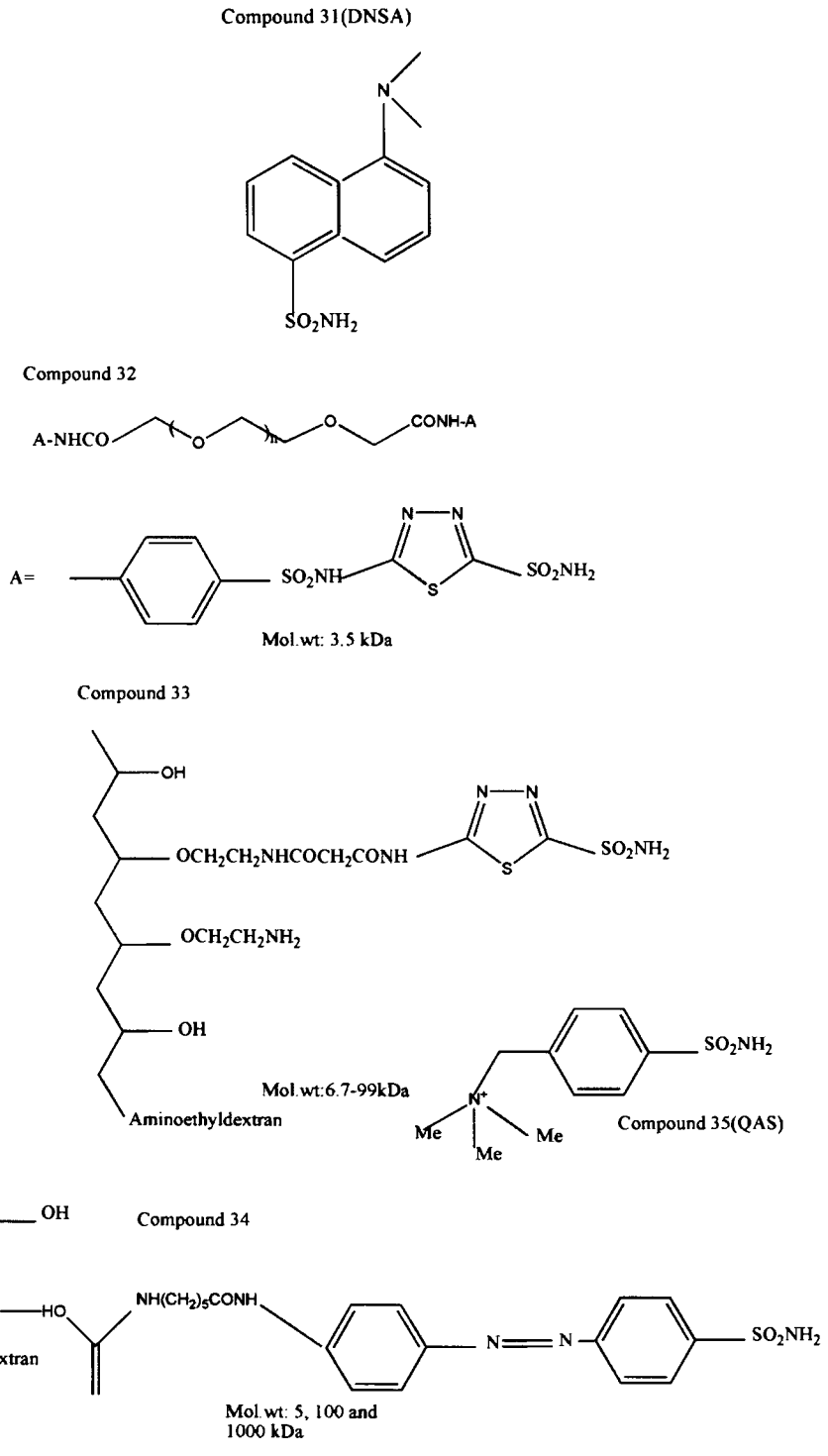

Figure 1.34. Structures of DNSA (Compound 31) and high molecular weight, positively charged CA inhibitors (Compounds 32-35).

as well as heterocyclic rings showed moderate anti tumor properties (*371*, *372*). When the aromatic rings possessing free amino, imino or hydrazino groups were converted into the corresponding N-morpholyl-thiocarbonylsulfenyl, or N,N-dimethyl/diethyl-thiocarbonylsulfenylamino-derivatives by reaction with dithiocarbamates in the presence of oxidizing agents (NaClO or iodine), they showed nanomolar affinity for hCA II and hCA IV, and also inhibited the growth of several tumor cell lines at concentrations as low as 10 nM (*373*, *374*).

In 2000, Owa's group reported an antitumor sulfonamide, E7070 (**compound 36**) which is in phase II clinical trials in Europe and United States (*304*, *375*). This inhibitor has a very strong binding affinity to hCA II (K_i=15 nM) and hCA IX (K_i =24 nM) (*296*). The X-ray crystal structure of hCA II with this inhibitor showed that the benzenesulfonamide head of the inhibitor binds Zn(II) with ionized sulfonamide moiety of the inhibitor similar to that found in other CA II-sulfonamide complexes. The bond distance between zinc and "N" of the sulfonamide is appreciaply shortened in this complex, which is considered as one of the reasons for the high affinity of the inhibitor to hCA II and hCA IX (*296*). In addition, three different conformations were observed for the chloro indole fragment of the inhibitor which interacts with different amino acid residues and water molecules compared to the other sulfonamide – CA complexes (*174*, *188*, *308*, *332*, *376*). Crystal structures showed that, one of the oxygen of the secondary sulfonamide moiety forms two hydrogen bonds with two active site water molecules and the endocyclic NH group of the inhibitor donates a hydrogen bond to a water molecule that is involved in hydrogen bonding with the secondary sulfonamide group. In addition, a weak hydrogen bonding interaction is seen between the chlorine atom and the -COOH group of Glu 69. An intramolecular hydrogen

bond between the second oxygen atom of the secondary sulfonamide moiety and the endocyclic NH group was seen in the second conformation. This NH group is also involved in another hydrogen bond with the $CONH_2$ group of Gln 92. A short hydrogen bond is also observed between the chlorine atom and the COOH group of Glu69. The third conformation showed a network of four hydrogen bonds involving one oxygen atom of the secondary sulfonamide moiety and three water molecules (*296*).

Inhibition profiles of hCA IX with a series of aromatic and heterocyclic sulfonamides revealed that both types of compounds have potent inhibitory properties. Mono/dihalogenated sulfanilamides and mono/dihalogenated aminobenzolamides showed inhibition profiles for hCA IX that are totally different from hCA I, II, and IV (*377*).

Inhibitors obtained by reaction of aromatic/heterocyclic sulfonamides incorporating amino groups with *N*, *N*-diphenyl carbamoyl chloride or diphenylacetyl chloride showed some isozyme selectivity towards hCA IX (*378*). A series of positively-charged, pyridinium derivatives of sulfanilamide, homosulfanilamide and 4-amino ethyl benzenesulfonamide of types (**componds of type 37-39**) selectively targeted hCA IX because of their membrane-impermeability (*379*). Supran's group reported a series of sulfonamide derivatives incorporating a hydrazine moiety in their structure, which was found to be beneficial for specifically targeting hCA IX as the susceptiblity of the hydrazine moiety to redox chemistry could be advantageous in the hypoxic environment present in some tumors. Among several inhibitors tested, compounds of type 40-42 showed inhibition constants in the range of 3 to 6 nM (*333*, *380*).

Of several aromatic and heteroaromatic sulfonamides that have been investigated, 1,3,4-thiadiazole/thiadiazoline-2-sulfonamides incorporating 5-acylamido or 5-

arylsulfonylamido moieties were found to be potent hCA XII inhibitors. But these compounds were also found to inhibit hCA I and II, with some selectivity towards hCA XII (*363*). CA inhibitors possessing sub-nano molar binding affinity towards hCA XII were first reported by Pastorekava et.al (*297*). Among a series of 2,3,5,6- tetrafluorophenyl-carboxamido/sulfonamido and pentafluoro- phenylureido- aromatic/heterocyclic sulfonamides tested, **compounds 43-48** showed very good hCA XII inhibitory properties, with K_i values in the range of 0.7–5.7 nM. Some of these inhibitors showed better affinity for hCA XII than for hCA II. Among these, **compound 46** is a potent inhibitor of both hCA IX and hCA XII.

In vivo studies of a series of thio ureido-substituted sulfonamides showed good inhibitory properties against hCA XII with binding affinities ranging from 1.5–144 nM. Some of these derivatives were found to be very effective in reducing elevated IOP in rabbits. This was the first study in which potent hCA XII inhibitors were designed and investigated in vivo (*381*). Innocenti et al. (*295*) reported the first anion inhibition studies of the hCA XII and hCA XIV. These studies revealed that halides (except fluoride), perchlorate, nitrate, and nitrite are very weak hCA XII inhibitors with inhibition constants ranging from 73–300 mM. Hydrogen sulfide was found to have moderate inhibition constant with hCA XII (K_i of 4.85 mM), whereas such as fluoride, cyanate, thiocyanate, inhibition constants in the range of 0.56–0.84 mM. Cyanide and azide were found to be the best of all with inhibition constants ranging from 1.0–80 μM. Human CA XII is resistant to inhibition by chloride, bromide and iodide similar to CA II. However it is inhibited by bicarbonate/carbonate in contrast to CA II, which is insensitive to these anions. In addition, hCA XII is inhibited by fluoride (K_i of 0.56 mM) and sulfate whereas hCA I and II are not

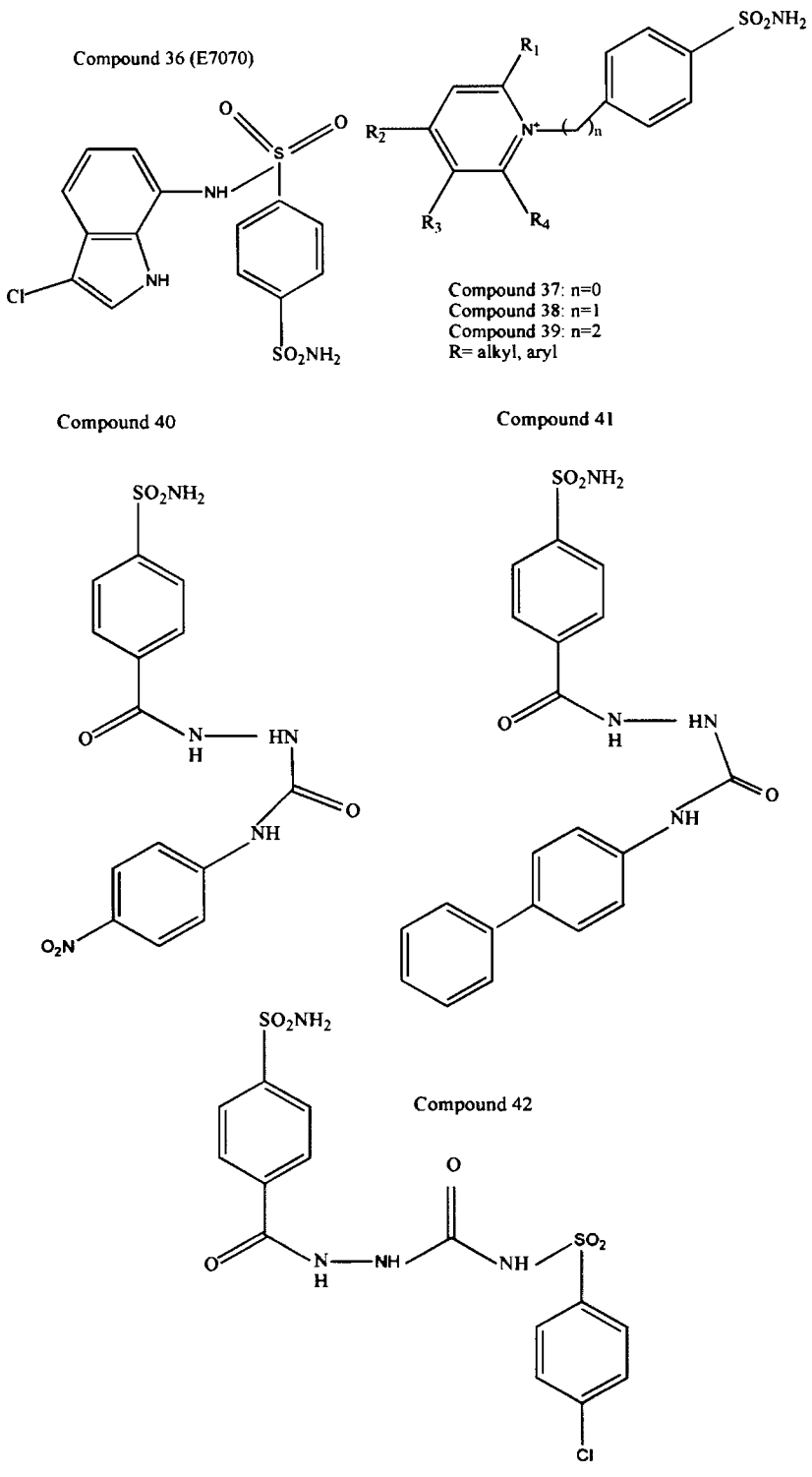

Figure 1.35. Structure of antitumor sulfonamide (compound 36) and CAIX inhibitors (Compounds 37-42).

Compound 43

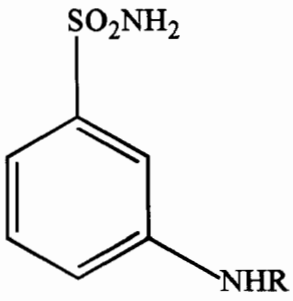

Compound 44

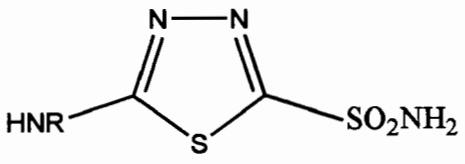

Compound 45

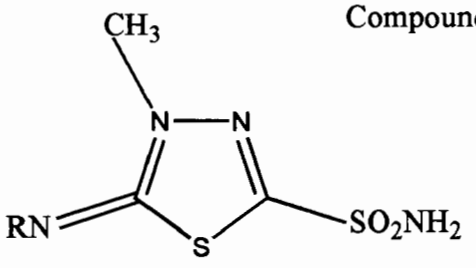

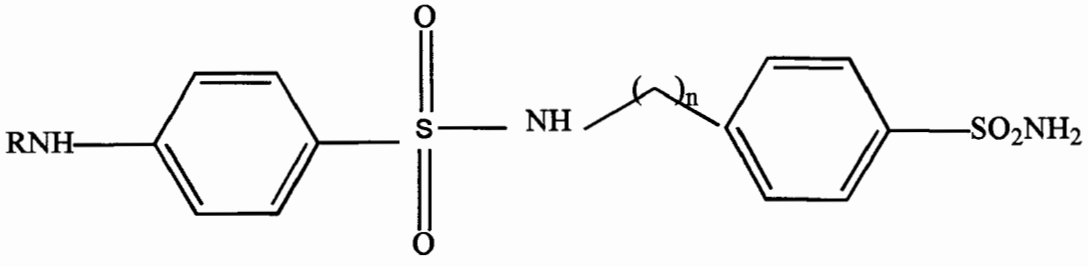

Compounds 43-48: R=H
Compound 46: n= 0
Compound 47: n=1
Compound 48: n=2

Figure 1.36. Structures of some hCA XII inhibitors (Compounds 43-48).

bicarbonate, carbonate, hydrogen sulfite, sulfate, sulfamide, sulfamate, phenylarsonic acid, and phenylboronic acid, showed good hCA XII inhibitory activity, with at all inhibited by these anions.

Lloyd et al. (*382*) reported the crystal structure of hCA II complexed with a sulphamate inhibitor, 667-coumate **(compound 49)** (Figure 1.37), which contains a coumarin ring. This inhibitor is in Phase 1 clinical trials for the treatment of breast cancer. The above inhibitor also inhibits steroid sulphatase, which promotes the production of oestrogenic steroid hormones that promote growth and development of breast cancers (*383*). The inhibitor also inhibits hCA II in vitro with IC_{50} values of 25 nM and 17 nM (*384, 385*). It is not known whether the anticancer activity of this inhibitor is due to the inhibition of hCA IX and XII or the inhibition of steroid sulphatase in cancer cells (*382*)or both. Crystal structure of the hCA II-667 coumate complex showed that the inhibitor interacts with the residues in the hydrophobic pocket inside hCA II, and is bound to the active-site zinc atom through the sulphamate group (Figure 1.37).

A secondary zinc binding site was also observed on the surface of the protein between His64 and His36 and a water molecule. This is in contrast with the EMATE structure, which is an aryl sulphamate ester (Figure 1.38), characterized by the absence of a second zinc binding site. The ring structure of 667-coumarin moiety was found to interact with the hydrophobic binding pocket of hCA II and is surrounded by the hydrophobic residues such as Val121, Phe131, Val135, Leu141, Leu198 and Pro202. This complex also has water molecules close to the ligand. While the ring in both EMATE and 667-coumate occupied the same positions in the hCA II active site pocket, the position of the side chain

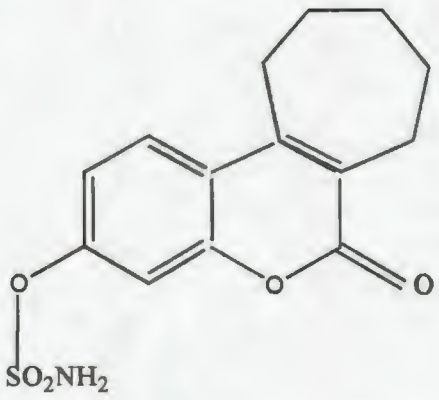

Compound 49 (667-coumate)

Figure 1.37. Structure of hCA II bound to 667-Coumate.
Structure of hCA II bound to 667-Coumate (PDB ID: 1TTM) (*382*). The zic ion and its three His ligands are shown in blue whereas the inhibitor, 667 coumate is shown in majenta. The structure is modeled using UCSF Chimera® software (*175*).

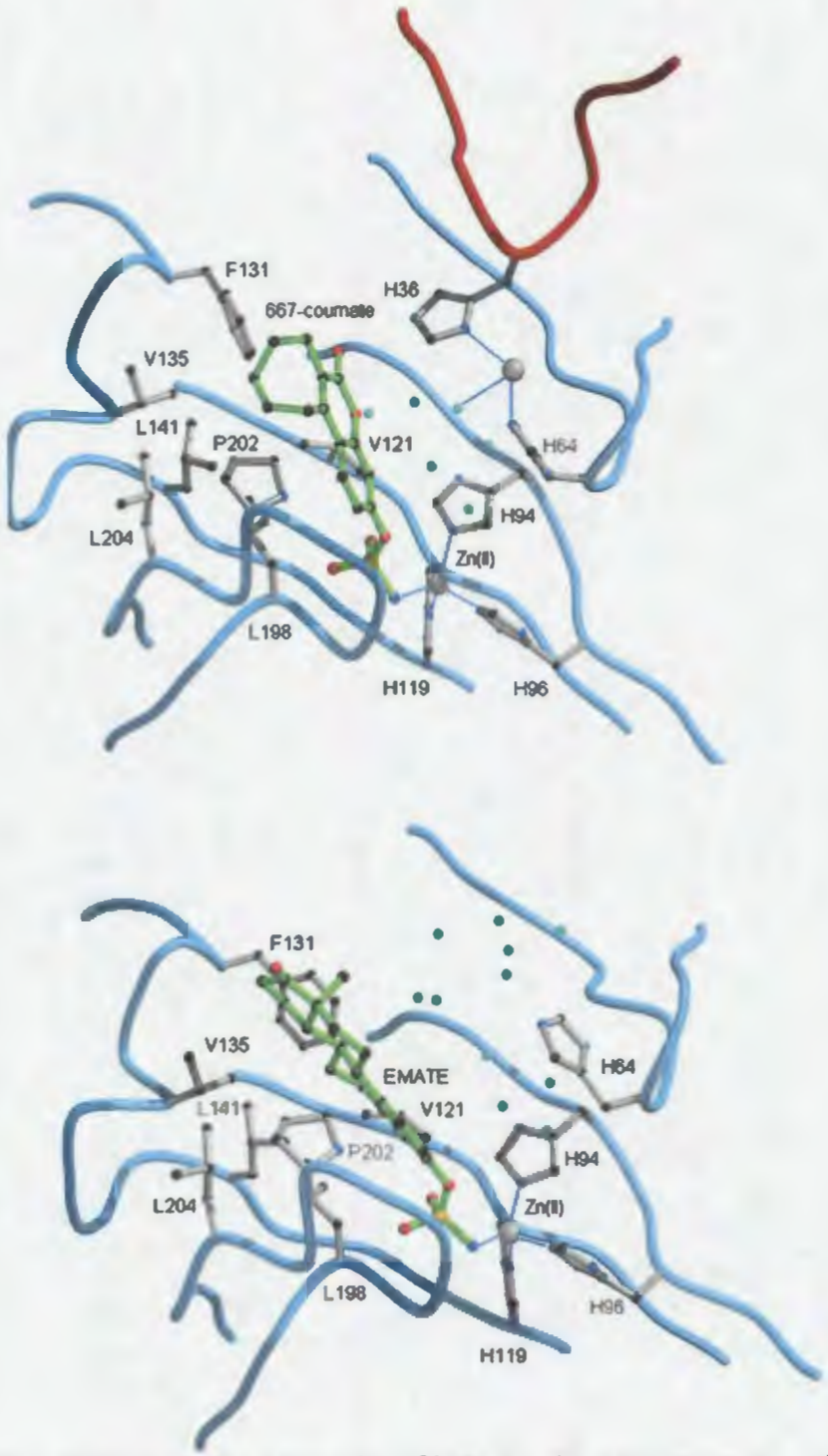

Figure 1.38. Close up view of the active site of hCA II with 667 –coumate and EMATE. Figure is adapted from reference (*382*).

of Phe 131 was found to be different in both the cases. Some conformational flexibility of the seven-membered ring of 667-coumate was also observed(*382*). Though this inhibitor was found to be extremely unstable leading to the release of sulphamic acid in solution and was rapidly cleared from the plasma ex vivo, the stability increased in whole blood. Pharmacokinetic studies showed an enhanced stability of 667- coumate in vivo and this has been ascribed to be binding of this inhibitor in the hydrophobic pocket of hCA II (*386*).Inhibition of hCA I and hCA II by a wide range of alternative arylsulfonic acid derivatives of formula R-SO_2-X **(compounds 50-61)** (Figure 1.39) have been investigated by Supuran and coworkers (*334*). They found that in contrast to sulfonamide-based inhibitors where there is little isozyme selectivity, numerous sulfonic acid derivatives showed significant selectivity (up to 20-fold) for either hCA I or hCA II. This study illustrated that sulfonamide head group is not necessary for effective inhibition of CA.

1.1.14.1. Fluorescent inhibitors of CA

5-dimethylaminonaphthalene-lsulfonamide (DNSA) **(compound 31)** was the first fluorescent compound identified to bind with bCA. This inhibitor forms a highly fluorescent complex with bCA leading to the increase in its quantuim yield upon binding coupled with a large blue shift in its emission maxima. The large emission blue shift is due to its binding in an extremely hydrophobic environment (*387*). The X-ray crystal structures of hCA II complexed with dansylamide (DNSA) showed that unlike other arylsulfonamide inhibitors of CA II, the naphthyl ring of DNSA binds in a hydrophobic pocket of the active site, making van der Waals contacts with Val121, Phe131, Val143, Leu98, and Trp209. This study indicated that binding of DNSA to hCA II requires a conformational change of Leu198 in order to accommodate DNSA (*179*)).

The quantum yield of DNSA bound to hCA I is about 4-fold higher than when bound to hCA II. Also, the binding affinity of this fluorescent probe to hCA I is stronger compared to hCA II. Banerjee et al. (*329*) performed detailed ligand binding and transient kinetic experiments to ascertain the structural-functional aspects based on the difference in the spectral and binding profiles of DNSA to hCA I and hCA II and found that the origin of the above differences lies in the difference in the microscopic sequence of steps involved in the enzyme-ligand interactions.

Cecchi et al. (*388*) in 2004 reported the synthesis of a series of sulfonamide inhibitors possessing fluorescent tails that selectively bound hCA IX under hypoxic conditions. Their studies identified a potent inhibitor, 4-sulfamoylphenylethylthioureido fluorescein, which was bound only to hypoxic tumors, overexpressing various CA isozymes such as hCA IX and hCA XII. This compound showed strong inhibition towards hCA II (K_i of 45nM) and hCA IX (K_i of 24 nM) (*164*, *192*). The X-ray crystal structure of the this inhibitor complexed with hCA II revealed a binding mechanism similar to that of other benzesulfonamides, with the ionized sulfonamide coordinated to the Zn^{2+} within the enzyme active site, and also involved in a network of hydrogen bonds with Thr199 and Glu106. The inhibitor made hydrophobic contacts with Gln92, Val121, Phe131, Val135, Leu198, Thr199, Thr200, and Pro202. The substituted 3-carboxy-amino-phenyl functionality was at van der Waals distance from Phe131, Gly132, and Val135. The bulky tricyclic fluorescein moiety was located at the rim of the active site, on the protein surface, and strongly interacted with the α-helix formed by residues Asp130-Val135. Model studies of hCA IX with the adduct of the inhibitor revealed the absence of these interactions. Instead, the carbonyl moiety of the fluorescein tail participates in a strong hydrogen bond

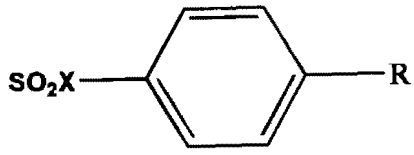

Compound 50 R=CH_3 X=OH

Compound 51 R=CH_3 X=SH

Compound 52 R=CH_3 X=N_3

Compound 53 R=CH_3 X=NO

Compound 54 R=CH_3 X=NCS

Compound 55 R=CH_3 X=$NHNH_2$

Compound 56 R=CH_3 X=NHOH

Compound 57 R=CH_3 X=NHOMe

Compound 58 R=CH_3 X=NHCl

Compound 59 R=COOH X=NCl_2

Compound 60 R=CH_3 X=NHCN

Compound 61 R=CH_3 X=$NHOCH_2COO^-$

Figure 1.39. Aryl sulfonamide inhibitors of CA (Compounds 50-61).

with the guanidinium moiety of Arg130, an amino acid characteristic of the hCA IX active site. This could be one of the reasons for the difference in the binding affinity of the inhibitor between hCA II and hCA IX (*389*).

1.1.15. Structural and functional consequences of nanoparticle adsorption on CA isozymes

Due to their potential diagnostic and therapeutic applications, nanoparticles have gained significant interest in recent years (*390-392*). Among nanoparticles, semiconductor quantum dots (Qds) offer added advantage due to their broad absorption and narrow emission bands, size tunable fluorescence emission spectra, longer fluorescence lifetimes, and resistance to photo bleaching (*393-399*). It has been recognized that as soon as the Qds enter into the blood stream, they are immediately coated with different types of proteins and depending on the surface properties of the Qds, the overall coating process is manifested by a combination of van der walls, electrostatic and hydrophobic interactions (*400-405*, *399*). The adsorption of proteins to the quantum dot surface leads to changes in the protein conformation and/or changes in the surface of the Qds (*406-412*). NMR data reveal that the silica nanoparticles exhibit completely different impact on the structure of hCA I and hCA II. Whereas hCA II interacts strongly with silica nanoparticles leading to an ensemble of molten globule like bound protein states, hCA I interacts (with similar silica nanoparticles) albeit weakly and leads to a small perturbation in the protein structure on a longer time scale. It is believed that the surface curvature of nanoparticles in conjunction with their complementary interactions with cognate proteins induce different types of conformational changes (*406*).

Billsten et al.(*413*) characterized the conformation of hCA II adsorbed on to silica nanoparticles. They used pseudo-wild type hCA II (hCA II_{pwt}) in which Cys206 is replaced by a serine. They also used two truncated forms in which the 4 and 16 N-terminal amino acids have been removed. GdmCl denaturation studies on the hCA II_{pwt} revealed the formation of a molten-globule type of equilibrium folding intermediate and a compact

residual structure of hCA II_{pwt} at moderate and high concentrations of GdmCl respectively. They compared these structures with the structures of the variants adsorbed on to silica nanoparticles with the use of circular dichroism (CD), intrinsic fluorescence, Anilino Naphthalene Sulfonamide (ANS) binding ability and inhibitor binding capacity. It was found that whereas the N-terminal truncated variants attain a molten-globule-like state after interaction with the silica nanoparticles, hCA II_{pwt} retained most of its native structure after adsorption to silica nanoparticles for 24 hrs (*414*). These different conformational effects between hCA II_{pwt} and the truncated forms upon silica nano particle adsorption were reasoned to be due to the difference in stability of the structure of the variants.

In order to further characterize the conformation that accompanies the adsorption, two tryptophan mutants, Trp16Cys and Trp97Cys along with the three above mentioned variants were investigated by differential scanning calorimetry (DSC) (*414*). They found that the two mutants attained a molten globule like state upon adsorption to the silica nanoparticles similar to the truncated variants. The conformation attained by hCA II_{pwt} according to the DSC profile was different from the above attained conformations and the native state in solution. These results indicated that the global stability of the protein in solution is an important parameter for the nature and degree of conformational changes upon adsorption. Although previous CD and fluorescence measurement studies suggested that the structure of hCA II_{pwt} was not at all or very minimally affected upon adsorption to silica nanoparticle, DSC studies showed that the melting temperature (T_m) of adsorbed hCA II_{pwt} is considerably lowered, suggesting that the surface alters the properties of the protein molecules. These studies showed that the main factor in determining the protein's conformational change upon adsorption to solid surfaces is its structural stability.

Using CD and fluorescence spectroscopy, Karlsson et al (*415*) explored the rate and extent of conformational changes of the above hCA II variants induced by adsorption to the solid surfaces. They found that hCA II first rapidly binds to the particle surface followed by a step wise conformational change. A schematic picture of the course of adsorption and subsequent conformational changes of the protein is depicted in Figure 1.40.

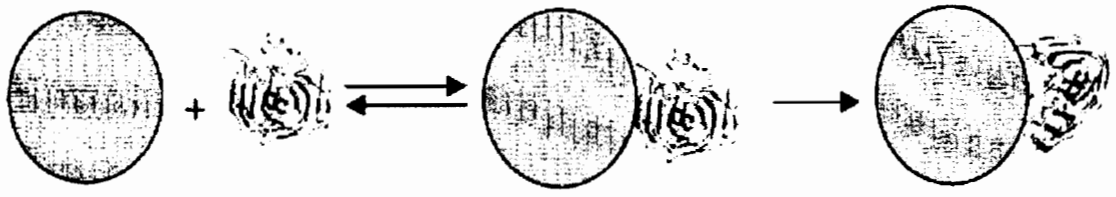

Figure 1.40. Step wise change in conformation of a protein upon adsorption to silica nanoparticles.
Figure is adapted from reference (415).

Enzyme activity measurements, CD, and ANS fluorescence measurements showed strong correlation between protein stability and the rate of conformational changes, with less stable variants showing a faster rate of conformational change upon adsorption to the nanoparticle surfaces. However, protein stability has no effect on conformation of the final state and a molten-globule-like state is adopted after prolonged incubation with particles in all cases. They also found that unlike chemical or thermal denaturation unfolding of the active site region takes place before the tertiary interactions are broken (*415*).

In order to obtain information regarding local structural alterations at the level of individual amino acid residues, NMR spectroscopy of the hCA I adsorbed to solid surfaces was studied by Lundqvist et al. (*416*) in addition to circular dichroism (CD), analytical ultracentrifugation (AUC), and gel permeation chromatography of both hCA I and hCA II adsorbed to solid surfaces. Results indicated that the adsorption of truncated 17hCA II to

the particles is relatively fast and that the protein loses all of its tertiary structure, during the first 24 h after mixing with the particles. The adsorption pattern of hCA I was different from that of truncated 17hCA II. Their NMR data revealed changes in the protein conformation, which was shown by the slow reduction in the total intensity of the NMR spectra after the initial (immediate) reduction upon addition of silica nanoparticles. However, some peaks indicative of flexible tertiary structure, were seen suggesting the appearance o f non–native tertiary conformations. They also found that hCA I was in equilibrium with the nanoparticles and the interaction caused variable degrees of conformational changes in the protein. The above study also led to another conclusion regarding the influence of particle curvature on the extent of conformational changes of hCA I. A 6 fold higher change in the secondary structure was observed with a 15 nm diameter particle compared to the 6 nm particles (*416*).

High resolution 2D 1H-15N NMR data obtained by studying hCA I and hCA II clearly showed very different impacts on their structure upon interaction with silica nanoparticles. Human CA II was found to bind strongly and lost its native structure in a rapid manner, forming an ensemble of non-native conformations. Prolonged incubation of hCA II with nanoparticles led to an ensemble of molten globule-like bound protein states. In contrary to hCA II, hCA I bound to nano particles very weakly. However, prolonged incubation caused gradual perturbation of its structure leading to non-native tertiary conformations (*406*).

Later studies revealed that upon prolonged incubation with nanoparticles, besides tertiary structural perturbations, perturbations of central β-strands were observed (*416*). NMR studies also revealed that whereas the N-terminus, loops, and peripheral secondary

structures adopted a native like conformation quickly after desorption from the silica particles, amino acids from the central β-strands were trapped in an ensemble of partially non-native conformations. This is because the highly dynamic nature of the loops and the N-terminus enabled them to adopt a native conformation relative to the less dynamic beta sheets in the center where the kinetic barriers for rearrangement would be very high (*417*, *416*). The catalytic activity of hCA I decreases with increase in the incubation period. However the desorbed hCA I showed catalytic activity similar to the native protein showing that the protein had adopted a near – native conformation after desorption (*418*).

Karlsson et al. (*419*) reported the first study for the direction of protein adsorption using silica nanoparticles and site-directed fluorescently labeled protein. They demonstrated that the N-terminal domain of hCA II specifically adsorbs the nano particles and the adsorption is strongly dependent on the pH. It was found that a specific histidine rich area is the dominating adsorption region at pH 6.3, whereas at higher pH values, when the histidnes are deprotonated, the nanoparticles are also adsorbed in the lysine and arginine rich region. Thus it was shown that the negatively charged silica nanoparticles specifically bind to the positively charged areas of the protein.

Karlsson et al. (*420*) further used nanoparticles with different surface properties (charge and hydrophobicity) and determined its influence on the stability, adsorption and desorption behavior of hCA II. They used three variants of hCA II, namely hCA II_{pwt} whose properties are similar to the wild type enzyme, S56N, the variant that has a lower thermodynamic stability as compared with hCA II_{pwt}, and the oxidized variant of Ala23Cys/Lys203Cys that has higher thermodynamic stability. As the surface properties of all the three variants are similar and their thermodynamic stabilities are different, it allowed

them to evaluate whether the adsorption/ desorption behavior of proteins are dependent on their stability and whether these features are influenced by nanoparticles with different surface properties. Of the four surfaces tested, they found that both the negatively charged and hydrophilic surfaced nanoparticles had the least denaturing effect and the more hydrophobic surface had the most denaturing effect. Correlations between the protein stability and kinetics of adsorption and the amount of adsorbed proteins were determined for all the above nano particles. Proteins with greater stability showed increased amplitude of the first kinetic phase of adsorption and a higher amount of adsorbed protein. Also, when washed with buffer, increased amount of protein was desorbed for proteins with maximal stability. All these outcomes have been explained in terms of the denaturing behavior of the three protein variants. For example, S56N was completely converted to a molten globule form within about 15 min after adsorption of negatively charged silica nano particles where as hCA II_{pwt} went through this transformation slowly (*420*).

Stiti et al. recently reported the synthesis of gold nanoparticle coated CA inhibitor that showed hCA IX specific inhibitory properties (*421*). The inhibitor selectively inhibited hCA IX over hCA I and II. Investigations of the penetrability of these CA inhibitors were performed by incubation of RBCs with sulfonamide inhibitors such as acetazolamide, and gold nano particle coated CA inhibitor. Due to the high diffusability of acetazolamide through membranes, it inhibited hCA I and hCA II after 30-60 min. In contrast, only negligible amounts of gold nanoparticle coated CA inhibitor was found with in RBCs even after 24 hrs of incubation. This proved that CA inhibitor coated Au NPs were unable to penetrate through biological membranes (*421*).

1.1.16. Denaturation and renaturation of CA isozymes

Detailed studies of the folding and unfolding of CA conducted over past several decades have given insights in to the pathway of their folding and the relationship between their structure and stability. According to Levinthal, a protein usually possesses one or more nucleation sites, which are referred to as "seeds". Seeds initiate folding by exchanging between random coil and ordered states. Usually hydrophobic residues are seen in these sites, which restrict the conformational space accessible to the protein by stabilizing the long range interactions and thereby decrease the entropy of the unfolded state (*422*).

1.1.16.1. Denaturation by guanidinium hydrochloride (GdmCl)

A stable, partially folded intermediate of bCA was first identified and characterized by Henkens et al (*423*). This intermediate possessed a compactness similar to the native enzyme, but with a fluctuating tertiary structure (*424*). They also found the presence of multiple kinetic intermediates in the folding pathway of hCA II from GdmCl. In order to confirm the presence of seeds in hCA II, they mutated Trp97 to Arg followed by denaturing the protein in 6.2M GdmCl. They observed a shift in the NMR resonances of 5 His residues namely 94, 96, 107, 119, and 122 of the mutant as compared to denatured wild-type hCA II. This showed that a residual structure of the denatured protein is present in this region, as a single point mutation altered the conformation of multiple amino acid residues in an unfolded protein (*425*).

Carlsson et al. engineered a cysteine group in the hydrophobic core of hCA II and attached a fluorescent probe to it with the intention of exploring the structural features of denatured and intermediate states in folding. The GdmCl denaturation studies of this

mutant indicated that the central beta strands of the enzyme remained folded even up till the denaturant concentration of 6M (*426-428*).

The studies of folding and unfolding using various denaturants indicated that the transition between the native and unfolded states of a protein occurs with the formation of a molten globule intermediate. This is an intermediate found in the folding and unfolding pathways, which is either an equilibrium intermediate and /or a kinetic intermediate (*429*, *430*). The compactness of a molten globule intermediate is somewhat similar to that of the native structure. It is characterized by a poor tertiary structure but significant secondary structure. The hydrophobic region of the molten globule state is exposed to the solvent in comparison to its native state (*119*, *431*). Studies on CA indicate the presence of this intermediate at 1 and 2 M concentrations of GdmCl (*423*, *424*). Absorbance and fluorescence studies of tryptophan residues of this intermediate indicated loss of tertiary structure (*432*, *427*). In addition, a red shift in the fluorescence emission maxima of the tryptophan was observed which indicated that the molten-globule state experiences a less hydrophobic environment compared to the native protein. Interestingly, a large negative ellipticity of the intermediate in the far-UV region was observed by Boren et al. (*433*) and Martensson et al. (*427*) for bCA II and hCA II respectively. This increase indicates the presence of extensive β-structure in the molten globule and was said to be due to the loss of interference from aromatic side chains in the symmetric environment of a molten globule. When the GdmCl concentration was increased, the negative ellipticity decreased indicating denaturation of CA II.

The increase in the quantum yield of ANS (from 0.004 in aqueous solution to 0.8 in the presence of CA) upon binding to hydrophobic residues of CA has been exploited in

monitoring the folding and unfolding of CAs. ANS binds strongly to bCA II in the molten-globule state with a fluorescence intensity that is much greater and more blue-shifted than when it is bound to the native or denatured protein (*434*, *430*). This result indicated that hydrophobic patches are formed concomitantly with an increase in compactness upon renaturation.

1.1.16.2. Denaturation of CA by other denaturants (Urea and Heat)

In contrast to the GdmCl induced denaturation of CAs, denaturation in the presence of urea followed a two state transition unfolding model with the absence of molten globule intermediate formation. This was explained to be due to the difference in the ionic character of the two denaturants (*435*, *436*). Temperature induced denaturation is often performed to determine T_m (*437*). Various methods are used to determine the T_m such as measuring the enzyme activity at various temperatures, absorbance and fluorescence changes, monitoring the secondary structure of protein using CD spectroscopy, and tertiary structural changes using DSC etc (*438-441*, *427*). The major problem associated with changes in temperature is protein aggregation due to conformational changes of the protein at high temperatures. This causes the hydrophobic areas to be exposed and leads to aggregation (*119*, *442*). The T_m of CA II was measured by its CO_2 hydration activity, tryptophan fluorescence, CD spectroscopy and 1D NMR and was found to be approximately equal to 64°C for hCA II. This value ranges 55 and 61 °C in bCA II (*119*, *427*, *439*, *440*).

1.1.16.3. Role of surface charges in refolding of CA

Gitlin et al. (*443*) studied the effect of surface charges on the refolding using bCA as a model protein. They used bCA and its derivative with all lysine groups acetylated

(bCA-Ac). Denaturation studies of these two proteins by urea, guanidinium chloride (GdmCl), heat, and sodium dodecyl sulfate demonstrated that increasing the net negative charge of the protein reduced its stability to urea, GdmCl, and heat, but increased its kinetic stability towards denaturation by SDS.

Denaturation of the above two proteins with urea revealed that where as the wild type unfolded with a two state transition, the bCA-Ac derivative unfolded with the formation of a stable intermediate. This was attributed to the destabilization of bCA-Ac due to changes in the surface charge. Denaturation by GdmCl revealed the presence of stable intermediate in both bCA and bCA-Ac with a three state denaturation. Comparison of the two transitions between the two proteins revealed that most of the destabilization of bCA-Ac occurred in the first transition, in which the tertiary structure of the protein was destroyed (*443*).

1.1.16.4. Role of zinc in CA refolding

As the presence of active site zinc zinc is very important for catalytic activity of CAs, its role in protein refolding was studied by many groups. Studies suggest that even though the final conformation of protein is not affected by the zinc ions, the kinetics of folding of CAs after denaturation with GdmCl is influenced by the metal (*444*, *423*, *432*). Whereas protein folding is completed within 10 min in the presence of zinc, it takes 20 min in its absence. The molten globule intermediate was seen irrespective of the presence or absence of zinc (*432*).

Studies suggest that folding of the molten globule can be induced by simple addition of equimolar amount of zinc (*445*). As soon as zinc is added it is found to bind the molten globule intermediate, and the region surrounding the metal ion gets compacted, as

confirmed by tryptophan fluorescence measurements. Following this, a functioning active center is formed, as confirmed by enzyme activity (*446*, *445*).

Avvaru et al. studied the role of zinc on the structure and stability of hCA II. To achieve this they prepared hCA II with (holo enzyme) and without (apoenzyme) zinc and compared their crystallographic structural features, backbone amide H/D exchange, and thermal stability (*447*). Crystalographic analysis of the apo and holo enzyme revealed the presence of the same ordered water structure as observed by Hakansson et al (*174*). However, they observed a 0.8 Å shift in the position of the zinc bound solvent towards the unoccupied zinc binding site. Their study confirned that neither zinc nor the zinc bound water has a major role in the formation and/or stability of the solvent network (*447*).

DSC studies revealed that the T_m of holo enzyme was 59° C while that of the apo-hCA II was 51° C. This showed the role of zinc in increasing the thermal stability of the enzyme. Studies revealed that although the residues in the vicinity of the zinc were not influenced by the removal of zinc, the thermal mobility in the region consisting of residues 147-189 was enhanced. However, it was found that the enthalpy of unfolding of both the protein forms were similar. They suggested that this could be due to the difference in the temperature required for the attainment of threshold vibration that triggers unfolding. This threshold was suggested to have been attained at an earlier temperature incase of the apo enzyme, presumably because it already possessed a higher thermal vibration in comparison to holo enzyme. Both the forms exhibited a two state unfolding upon denaturation (*447*).

Experiments were conducted on both holo- and apo-hCA II to understand the effects of the loss of zinc on the dynamics of hCA II. Similar to crystallographic studies, very little changes in the dynamics were observed for regions in the vicinity of zinc and the

hydrophobic environment of the active site. However, significant differences were observed in regions containing hydrophilic residues of the active site cavity such as Asn62 and the proton shuttling residue His64. This region was said to be destabilized in the absence of zinc. Inspite of the fact that CA refolds to its active state when denatured by GdmCl, denaturation by other means such as heat, urea, SDS or by change in pH does not yield a fully active protein upon refolding. This was mainly attributed to the intermolecular aggregation of CA. This aggregation of CA, according to Cleland and Wang (*448*), is due the interaction of molten globule intermediates. Their study suggested that at high GdmCl concentrations, the interaction between the hydrophobic regions of molten globule intermediates is prevented thereby preventing aggregation (*447*).

It was found by Karlsson et al. (*449*) that protein aggregation is suppressed in the presence of an engineered disulfide bond in hCA II. The presence of disulfide bond in Ala23Cys/Leu203Cys double mutant caused it to unfold and refold in a two state unfolding pathway without the formation of a molten globule intermediate. Due to the reduced tendency to form aggregates by this mutant, it yielded almost 95 % of the native protein upon denaturation. Their results suggested that the stabilization of the native state of CA helped to avoid the formation of molten globule intermediate and allowed to refold with high yield.

1.1.17. Methods to determine enzymatic activity

1.1.17.1. Indicator method

Several assays were developed to measure the activity of CA isozymes. Of these, indicator method was widely used because of its simplicity. In this method, the time taken for the pH of the reaction mixture to fall several units was measured using indicators such

as bromthymol blue or phenol red. There were several limitations to this method. High concentrations of the indicators used in this method served as inhibitors themselves. Moreover, in the broad pH range in which the observations were made, the changes in the hydrogen ion activity also affected the reaction rate. As a result, the measured reaction rate was not proportional to the true reaction rate (*24*).

1.1.17.2. Compound spectrophotometric assay

This assay, first published by Cutlo, is a coupled assay which is based on the measurement of the rate of carbon dioxide hydration reaction which leads to the generation of hydrogen ions. The hydrogen ion generation is then coupled to the reaction catalyzed by liver alcohol dehydrogenase (ADH).

$$\text{Ethanol} + \text{DPN} \longrightarrow \text{Acetaldehyde} + \text{DPNH} + H^{+} \qquad (1.4)$$

In this method, CA is mixed with a b uffer containing ethanol, alcohol dehydrogenase (ADH) and diphosphopyridine nucleotide. This causes the reaction 4 to move to the right with the appearance of absorption band of DPNH (reduced form of diphospho pyridine). Addition of carbon dioxide solution after the reaction has reached equilibrium generates excess hydrogen ions which force the reaction 4 towards the left side with decrease in the concentration of DPNH. The rate at which DPNH disappears is monitored spectrophotometrically at 340 nm. The rate limiting step in the above reaction that is the generation of hydrogen ions is equal to the rate of CA activity. This reaction is sensitive in the range of enzyme concentration of 10^{-7} to 10^{-5} M (*450*).

1.1.17.3. Rapid flow method

This method determines both the hydration and dehydration reaction catalyzed by CA, making use of indicators that sense the hydrogen ion activity in a flow apparatus. The

indicator that is widely used for this method in the p-nitro phenol whose pK_a is 7. The p-nitrophenolate ion is strongly colored at 470 nm. In a typical method, buffer, enzyme and indicator are mixed together as one solution and the substrate in a second solution. These solutions are simultaneously injected in a 2 mm capillary tube where the solutions are mixed by a turbulent flow. The flow is stopped after one minute and the decrease in absorbance of p-nitophenolate ions monitored spectrophotometrically at 400 nm (*450*).

1.1.17.4. Electrometric method

This method utilizes the change in the hydrogen ion concentration monitored by pH electrodes. In this method, the time taken for the decrease in pH of 0.02 M Tris-HCl buffer from 8.3 to 6.3 at 0 – 4 °C is determined upon addition of a saturated CO_2 solution in the absence and presence of CA is determined. This procedure involves bubbling of CO_2 gas into ice cold water for about 30 minutes prior to the assay. In the reaction blank, 6.0 mL of chilled 0.02 M Tris-HCl, pH 8.3 is mixed with 4.0 mL of ice cold CO_2 saturated solution with constant stirring and the time required for the pH to drop from 8.3 to 6.3 is recorded. The above experiment is repeated in the presence of CA and the activity of the enzyme is determined by the following equation:

$$\text{Unit of CA activity} = 2 \times (T_0\text{-}T)/T \qquad (1.5)$$

where T_0 and T are the time required to achieve the above pH drop in the absence and presence of the enzyme respectively (*451*).

1.1.17.5. Ester hydrolysis

The ability of CAs to hydrolyze esters has led to spectrophotometric methods that measure the hydrolysis of p-nitro phenyl acetate to p-nitro phenol and phenolate ion and is

monitored spectrophotometrically at 348 nm which is the isosbestic point for both p-nitro phenol and phenolate ion (*452*).

1.1.17.6. Stopped flow method

The CO_2 hydration reaction catalyzed by CAs is measured using stopped flow spectrometry by monitoring the change in absorbance using pH indicators as the reaction is catalyzed (*24*). In this method, saturated CO_2 solutions were prepared by bubbling CO_2 into water at 25^0C. This saturated solution of CO_2 was then diluted according to the requirement. The usual buffer-indicator pairs along with their pK_a values and the absorbance wavelength that are used in this method are listed below. 3,5-lutidine (pK_a 6.21) with p-nitrosophenol (pK_a 6.2, 400 nm) or with chlorphenol red (pK_a 6.3, 574 nm) ; imidazole (pK_a 7.14) or N-methylimidazole (pK_a 7.19) with p-nitrophenol (pK_a 7.15, 400 nm) ; 1,2-dimethylimidazole (pK_a 8.22) with metacresol purple (pK_a 8.3, 578 nm) ; bis-Tris-HCl (pK_a 6.60) with chlorphenol red (pK_a 6.3, 574 nm). MES (pK_a 6.1) and chlorophenol red (pK_a 7.1, 574 nm), MOPS (pK_a 7.2) with p-nitrophenol (pK_a 7.1, 400 nm), HEPES (pK_a 7.5) with phenol red (pK_a 7.5, 557 nm), TAPS (pK_a 8.4) with m-cresol purple (pK_a 8.3, 578 nm), and CHES (pK_a 9.3) and thymol blue (pK_a 8.9, 590 nm). Steady state linear rates were measured for the uncatalyzed reaction and the enzyme concentrations were adjusted such that the catalyzed reaction is atleast 10 fold greater than the uncatalyzed reaction. The initial rate obtained in absorbance per unit time is then converted into moles of substrate converted into product per liter per unit time by multiplication of the buffer factor. Initial rates for the enzyme-catalyzed reactions are obtained by subtracting the initial rate of the uncatalyzed reaction from the observed rate.

1.1.17.7. Mass spectrometry

This method is based on the principle of isotope exchange (in this case ^{18}O) caused by the CO_2 hydration and bicarbonate dehydration reaction at equilibrium (*453*) as depicted in eqn 6, 7 and 8.

$$CO^{18}O + H_2O \rightleftharpoons HCOOO^- + H^+ \rightleftharpoons COO + H2_{18}O \quad (1.6)$$

This method is capable of measuring two rates, first being the decrease in the rate of ^{18}O content (R_1) of CO_2 solution and second being the rate of proton transfer (RH_20) to the ^{18}O label at the active site of CA. A Solution containing all the reactants is kept in contact with a membrane that is permeable to gases and the CO_2 passes through the membrane and enters a mass spectrometer thereby providing a continuous measure of isotopic content of CO_2.

$$HOCO^{18}O^- + EZnH_2O \rightleftharpoons EZn^{18}OH^- + CO_2 + H_2O \quad (1.7)$$

$$EZn^{18}OH^- + BH \rightleftharpoons EZn^{18}OH_2 + B^- \rightleftharpoons EZnH_2O + H_2{}^{18}O + B^- \quad (1.8)$$

The first rate, R_1 is given by the following equation.

$$R_1/[E[= k^{ex}{}_{cat}\{S\}/(K_{eff}{}^S + [S]) \quad (1.9)$$

where [E] and [S] are the concentration of enzyme and substrate respectively. $k^{ex}{}_{cat}$ and $K_{eff}{}^S$ are the rate constants for maximal interconversion of the substrate and product, and apparent binding constant for CO_2 or bicarbonate to enzyme. The $k^{ex}{}_{cat}/K_{eff}{}^S$ ratio is equivalent to the k_{cat}/K_m for CO_2 hydration as measured by steady-state methods.

The second rate (R_{H2O}) is given by the following equation.

$$R_{H2O}/[E] = k_B/((1 + K_B/[H^+])(1 + [H^+]/K_E \quad (1.10)$$

Where k_B, K_B and and K_E are the rate constant of proton transfer to the zinc-bound hydroxide, ionization constant for the donor group and ionization constant of the zinc-bound water molecule respectively.

1.1.18. Assays for ligand binding

1.1.18.1. Thermodynamic assays

The spectrophotometric method for monitoring the esterase activity of CA is the widely used method to determine the inhibition constants (K_i) of the ligands (*176, 195, 196, 244, 339, 454-458*). The decrease in the esterase activity upon increase in inhibitor concentration is monitored spectrophotometrically and is plotted as a function of inhibitor concentration and is analyzed by the competitive displacement method to measure the inhibition constants. If the catalytic zinc is replaced by cobalt (Co II), direct binding constants of the ligand can be obtained by monitoring the absorption of cobalt. As the absorption spectrum of cobalt is very sensitive to changes in its coordination sphere, this method is widely used to determine the direct binding affinities of ligands without the need to determine the enzymatic activity (*200, 202, 339, 459*).

Fluorescence spectroscopy is also the most popular of all the techniques used to determine the dissociation constant of ligands to CA. This method utilizes the intrinsic fluorescence quenching of CA upon binding ligands and /or the increase in the fluorescence of ligands such as DNSA upon interaction with CA (*202, 222, 317, 328, 329, 387, 460-463*). The intrinsic fluorescence of CA has been contributed by the indole ring of tryptophans present in different chemical environments (*387*). Although 7 tryptophan residues are present in hCA II, only two (Trp97 and Trp245) contribute to almost 90 % of the total fluorescence intensity of hCA II. This has been attributed either due to the

electron transfer to neighboring protonated residues like arginine or energy transfer from one tryptophan to another that is adjacent to a quencher (*289*). Though this is a simpler method to determine the binding constants, this method has not been used extensively presumably due to the inner filter effect contributed by the increased absorption of inhibitors or due to the inability of the inhibitor to quench the fluorescence upon interaction (*119*).

Since DNSA can quench the tryptophan fluorescence as well as show an increase in its quantum yield upon binding to the active site pocket of CA, it has been widely used to determine its binding affinity with CAs as well as to determine the K_d of non fluorescent inhibitors. This is achieved by titrating the CA-DNSA mixture by the ligand of interest and monitoring the DNSA displacement from CA active site as revealed by the decrease in signal of DNSA at in the wavelength range of 458-468 nm upon excitation of the sample at 330 nm (*328*, *329*, *387*, *464*). Increase in the fluorescence anisotropy of the flurophore upon binding CAs has also been used to determine the K_d (*465*).

Isothermal titration calorimetry (ITC) has been widely used in studying the thermodynamics of CA-ligand interactions (*335*, *438*, *466-476*). The instrument contains a sample cell where the enzyme is loaded and a reference cell, both being maintained at same temperature. Titration of the enzyme in the sample cell by the ligand in the syringe either consumes (endothermic reaction) or releases heat (exothermic reaction). This change in heat is compensated by providing less power for exothermic reactions and more power for endothermic reactions to the sample cell so that the sample and reference cell are maintained at same temperature. This technique is useful for obtaining K_d and enthalpy of

binding. The standard free energy of binding is obtained from the association constant and the entropy is obtained by the following equation (*469*, *470*).

Circular dichroism spectroscopy is also a very useful technique to study alterations in the secondary structure of proteins. Use of CD for the CA ligand binding assays is very limited because of the moderate to strong absorption of aryl sulfonamides at 280 – 300 nm region (*477-479*). Apart from the techniques mentioned above, mass spectrometry has also been used to study the CA-ligand complexes (*480-493*).

1.1.18.2. Kinetic assays

The CO_2 hydration activity of CA is the conventionally used assay to determine the kinetics of ligand binding by measuring the change in the rate of CO_2 hydration in the presence of the ligand (*338*, *494*, *495*). As mentioned earlier this is achieved by using pH indicators (*195*, *199*, *201*, *455*, *496*, *497*). Following the report by Pocker and Stone (*498*) that bCA acts as an esterase and catalyzes the hydrolysis of p-NPA, this technique was also used to measure the kinetics of ligand binding by measuring the decrease in esterase activity as a function of time (*340*, *499-501*). Intrinsic tryptophan quenching by CA ligands has been used to measure the decay of fluorescence intensity as a function of time (*454*, *459*, *502*). Kinetics of ligand binding has also been determined by monitoring the decrease in the fluorescence intensity of enzyme –DNSA due to the competition of ligands for the same binding site (*387*, *459*).

1.1.19. Mechanism of ligand binding to CAs

Till date, two models have been used to fit the kinetics of association and dissociation of aryl sulfonamides to CA (*119*). The first model called the two state model (Figure 1.41A) involves the direct association of the inhibitor with the catalytic zinc of CA

in one step without the formation of a kinetically significant intermediate. For this to happen, the inhibitor and the CA both must be either in neutral or charged forms. In a two state model, the observed K_d can be calculated by the ratio of K_{off} and K_{on}.

In contrast to the two state model, a three state model proceeds in a two step manner (Figure 1.41B), with the formation of a kinetically significant intermediate. First, the inhibitor and CA associate and form a weak hydrophobic complex, followed by the interaction of the inhibitor with the catalytic zinc. Krishnamurthy et al. (*119*) showed that there are two possibilities in a three state model (Figure 1.42). The two possibilities differ only in the protonation states of the active forms of the aryl sulfonamide and CA. They refer to Scheme 2A as the neutral pathway and Figure 1.42B as the charged pathway.

King and Burgen (*459*) derived the following equation for the observed rate constant for association (k_{on})

$$k_{on} = k_1k_2/k_{-1} + k_2 \qquad (1.11)$$

Eqn 11 reduces to eqn 12 if the intermediate formed in Scheme 1.42B rapidly dissociates to reactants (that is $k_{-1}>>>k_2$) instead of proceeding towards the products.

$$k_{on} = k_1k_2/k_{-1} = Kk_2 \qquad (1.12)$$

Similarly, the observed rate constant for dissociation is given by eqn 1.13

When $k_{-1}>>>k_2$, eqn 33 simplifies to eqn 1.14.

$$k_{off} = k_{-1}k_{-2}/k_{-1} + k_2 \qquad (1.13)$$

$$k_{off} = k_{-2} \qquad (1.14)$$

All these equations were derived with the assumption that the reaction in Figure 1.41B is irreversible and goes to completion. The equations 1.11 and 1.13 suggest that whereas k_{on}

is dependent on the stability of the intermediates (K) and the rate constant to form the final product (k_2), k_{off} depends only on the rate constant to form the intermediate from the final product (k_{-2}).

Banerjee et al. determined the mechanism of DNSA binding to hCA I and hCA II (*329*). They found that the rate constant for the binding of DNSA exhibited a hyperbolic and a linear dependence for hCA I and hCA II respectively. The former suggested that the binding proceeds via two steps (Figure 1.42B) with the formation of a fast hCA I-DNSA encounter complex and a slow formation of hCA I-DNSA isomerized complex. The K_{obs} for this binding process, assuming the formation and dissociation of the encounter and isomerized complex are reversible, is given by the following eqn.

$$1/\tau_{obs} = \frac{k_2\,[DNSA]}{K_e + [DNSA]} + k_{-2} \quad (1.15)$$

In the case of hCA II-DNSA, the formation of the encounter complex was said to be slow and the formation of isomerization complex was very fast compared to that of the first step (k_1 and $k_{-1} < k_2$ and k_{-2}). K_{obs} in this case was given by the following equation.

$$1/\tau_{obs} = k_1[DNSA] + \frac{k_{-1}k_{-2}}{k_2 + k_{-2}} \quad (1.16)$$

They argued that the formation of isomerization complex is kinetically favorable but thermodynamically opposed in case of hCA II. However, the same was thermodynamically favorable and kinetically opposed in case of hCA I. Therefore, k_2/k_{-2} was said to be less favorable in the case of hCA II than with hCA I.

A: Two-state model

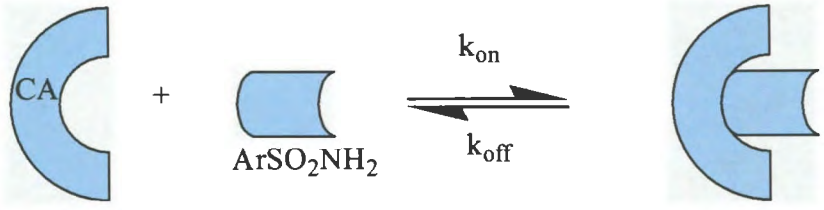

B: Three-state model

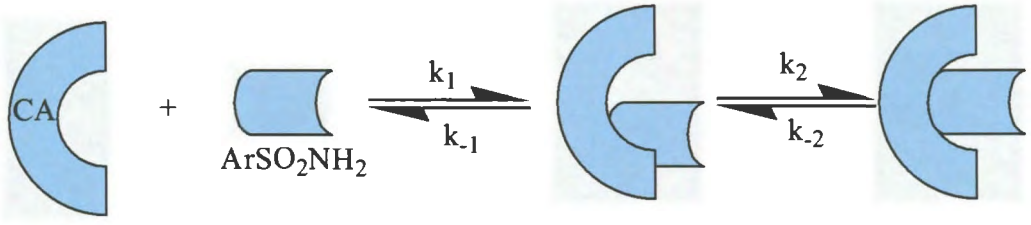

Figure 1.41. Two and three state models for the association of arylsulfonamides with CA. Figure adapted and modified from reference (119).

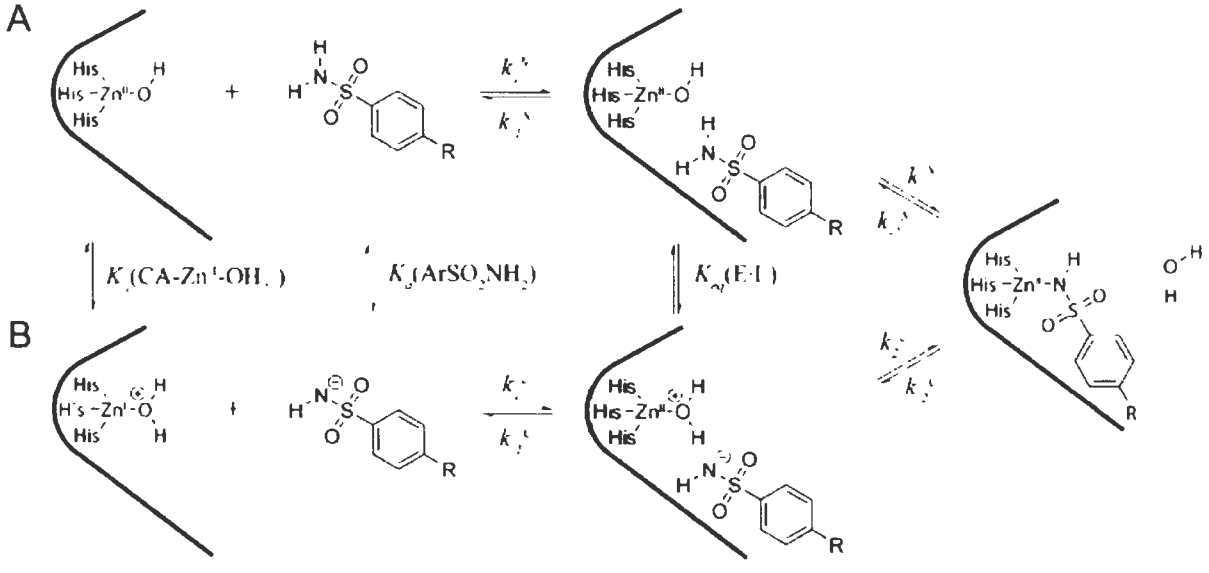

Figure 1.42. Three state model for the association of neutral and charged aryl sulfonamides with CA.
Figure is adapted from reference (119).

1.1.20. Isothermal titration calorimetric studies to study CA-ligand interactions

Krishnamurthy et al. in their comprehensive review of CA have compared the values of enthalpy and entropy of binding of various arylsulfonamides to CA II (*119*). They did not observe any corelation between the compared values of $\Delta H°_{obs}$, or $T\Delta S°$ and pK_a. Their comparison revealed that the binding of majority of aryl sulfonamides to CA II is enthalpically driven with a small contribution from entropy except for a few compounds such as ethoxzolamide, DNSA and dichlorophenamide that bind with favorable entropy which could be due to their extensive hydrophobic contacts with CA II. Interestingly, *p*-aminomethylbenzenesulfonamide binds CA II with lowest $\Delta H°_{obs}$ in comparison with all the aryl sulfonamides and was suggested that this could be due to the electrostatic repulsion between the positive charge of the $-CH_2NH_3^+$ moiety of the inhibitor and the positively charged active site of CA II. The unfavorable entropy of some of the inhibitors was due to the negative charge they possess which tends to orient towards the positively charged active site leading to entropic penalty. They also conclude that the complex formation between CA and inhibitor is dominated by hydrophobic forces, which is revealed by the negative change in heat capacity values (except benzene sulfonamide) when the $\Delta H°_{obs}$ values were plotted as a function of temperature.

Krishnamurthy et al used a series of fluorinated benzenesulfonamide ligands ($C_6H_nF_{5n}SO_2NH_2$) with bCA II (bCA) and determined their thermodynamic parameters for complex formation (*467*). This, along with their QSAR studies demonstrated that the increase in fluuorination, increased the hydrophobicity of the ligand, decreased the the Lewis basicity of the NH group of inhibitor to the zinc cofactor and also decreased strength

of the hydrogen bond network between the SO_2NH group and residues of the active site of CA thereby decreasing the binding affinity.

Studies of the binding isotherms for the association of bCA II with para substituted benzenesulfonamides containing chains of oligoglycine, oligosarcosine, and oligoethylene glycols of increasing chain lengths suggested that the dissociation constants were independent of chain length (*475*). As the chain length increased, the enthalpy became unfavorable and the entropy became favorable and there was a perfect compensation of entropy for enthalpy. They also found that the chain length did not have any influence on the change in enthalpy values. The authors explained the data based on a proposed model where the increase in chain length decreased the "tightness" of the protein-ligand interface which in turn led to favorable entropy and a less favorable enthalpy.

In light of these studies, the interaction of CA isozymes with ligands such as dansylamide derivatives (JB compounds), quantum dots, lipid nanoparticles were investigated. Detailed ligand binding, kinetic and thermodynamic experiments have been carried out to discern the effect of active site ligands and nanoparticles on hCA isozymes. In addition the influence of heat and chemical denaturants on the stability of hCA isozymes have been investigated.

CHAPTER 2. STATEMENT OF PROBLEM

The goal of this study is to investigate the effect of active site ligands and nanoparticle surfaces on hCA isozymes. In this pursuit, the binding of fluorescent probes to the recombinant form of hCAs was investigated via fluorescence spectroscopy and transient kinetic techniques. In addition, the influence of Qds, liposomes, heat and chemical denaturants on the structural – functional features of hCA isozymes have been investigated. Thermodynamic studies involving interaction of sulfonamide inhibitors to the hCA isozymes have also been investigated by performing ITC studies. These studies are summarized as follows:

(1) Steady state, transient kinetic and thermodynamic studies for the interaction of fluorescent probes with hCA isozymes.

(2) Ligand binding and ITC studies for the interaction of hCA-sulfonamide inhibitors

(3) Interaction of hCA isozymes to Qds and liposomes.

(4) Stability of hCA isozymes upon thermal and chemical denaturation.

These studies were designed to understand the mechanism of ligand binding to hCA isozymes towards finding applications in the rationale design of CA inhibitors as therapeutic agents. The stability studies were carried out to uncover the differences in the folding/unfolding mechanism of CAs.

CHAPTER 3. MATERIALS

Chloramphenicol, ampicillin, IPTG, Zinc sulphate, Tris-HCl, glycerol were from Life Science Resources, Milwaukee, WI. Yeast extracts, and tryptone were purchased from Becton Dickinson,Sparks, MD; Acetonitrile was from Aldrich Chemicals, Milwaukee,WI; HEPES, polylysine, phenyl methyl sulfonyl fluoride (PMSF), p-amino ethyl benzene sulfonamide-agarose, p-nitrophenyl acetate, MES, sodium mono hydrogen phosphate, sodium dihydrogen phosphate, DMSO, SDS-PAGE standards, bovine serum albumin, sodium chloride were obtained from Sigma-Aldrich (St. Louis, MO); All the chemicals needed for synthesis of JB2-48 were purchased from Aldrich Chemical Company, Milwaukee, WI. DNSA was purchased from Avocado Research Chemicals, Heysham, Lancashire, U.K.

The E. coli expression system BL21codon plus DE3(RIL) was from Stratagene, La Jolla, CA. The plasmid encoding the catalytic domain region of the human carbonic anhydrase XII gene was a generous gift from Dr. William Sly's laboratory at St. Louis University School of Medicine (St. Louis, MO). The plasmid encoding region of carbonic anhydrase II gene was a kind gift from Dr. Carol Fierke of University of Michigan, Ann Arbor, Michigan. The plasmid containing the coding sequence of hCA-I and hCA-VII (pCMV-SPORT6) was obtained from Open Biosystems, Hunsville, AL. The primers used for the PCR reactions were synthesized by Integrated DNA Technology (Coralville, IA). Cloned *Pfu* DNA polymerase and the BL21-CodonPlus® DE3 (RIL) *E. coli* cells were purchased from Stratagene (La Jolla, CA). Other restriction enzymes and T4 DNA ligase were obtained from New England Biolabs (Ipswich, MA). All other chemicals were of reagent grade, and were used without further purification.

CHAPTER 4. METHODS

4.1. Cloning, expression and purification of recombinant hCA isozymes

The cloning of hCA I and hCA XII were performed in Dr. Srivastava's laboratory at North Dakota State University by Donald Klocke. The cloning procedure for hCA I is detailed by Banerjee et al. (*329*). The cloning procedure for hCA VII and hCA XII are given as follows.

4.1.1. Cloning of hCA VII

The sequence encoding hCA VII was amplified from the plasmid pCMV sport 6 by the hot-start PCR method (*503*) using the sense and anti-sense primers, 5' – GGAATTCCATATGACCGGCCACCACGGCTGG 3'and 5' - CCGCTCGAGCTATCAGGCCCGGAAGGAGGCCTTTAC - 3', respectively. The sense primer contained the *Nde I* cleavage site (CATATG) and the antisense primer contained the *Xho I* cleavage site (GGATCC). The PCR reaction mixture contained the template DNA (~ 0.1 μg), primers (5 μL of 25 μM), dNTPs (0.5 μL of 100 mM), $MgCl_2$ (10 μL of 25 mM), and *Pfu* DNA polymerase (1 μL of 2.5 units) in a total volume of 50 μL. The PCR reaction conditions were set as follows: 1 min at 95 °C for denaturation, 1 min at 55 °C for annealing, 2 min at 72 °C for extension. This was repeated for a total number of 30 reaction cycles. An additional extension time of 20 min were allowed for the final products. *Nde I and BamH I* was used to digest the PCR reaction product and the pET-20b (+) plasmid expression vector. After digestion, both the product and vector were purified from an agarose gel using the Qiaquick® gel extraction kit (Qiagen; Valencia, CA). The purified products were ligated by T4 DNA ligase to form pET-hCA VII expression vector which was subsequently transformed into *E. coli* DH5α cells by standard molecular biology

protocol for plasmid propagation (*503*). The cloning of the coding regions of hCA VII in the pET-20b (+) vector was confirmed by sequencing of the plasmid at the University of Chicago Cancer Research Center (Chicago, IL).

4.1.2. Cloning of hCA XII

The sequence encoding hCA XII was amplified from the plasmid, pBShCA XII, obtained from Dr. William Sly's laboratory by the hot-start PCR method (*503*) using the sense and anti-sense primers, 5' - GGAATTCCATATGTCCAAGTGGACT - TATTTTGGTCC - 3'and 5' - CGGGATCCTCATCAGAAGGAGGTGTATACCA - 3', respectively. The sense primer contained the *Nde I* cleavage site (CATATG) and the antisense primer contained the *BamH I* cleavage site (GGATCC). The PCR reaction mixture contained the template DNA (~ 0.1 μg), primers (5 μL of 25 μM), dNTPs (0.5 μL of 100 mM), $MgCl_2$ (10 μL of 25 mM), and *Pfu* DNA polymerase (1 μL of 2.5 units) in a total volume of 50 μL. The PCR reaction conditions were set as follows: 1 min at 95 °C for denaturation, 1 min at 55 °C for annealing, 2 min at 72 °C for extension. This was repeated for a total number of 30 reaction cycles. An additional extension time of 20 min were allowed for the final products. *Nde I and BamH I* was used to digest the PCR reaction product and pET-20b (+) plasmid expression vector for hCA XII cloning. After digestion, both the product and vector were purified from an agarose gel using the Qiaquick® gel extraction kit (Qiagen; Valencia, CA). The purified products were ligated by T4 DNA ligase to form pET-hCA XII expression vector which was subsequently transformed into *E. coli* DH5α cells by standard molecular biology protocol for plasmid propagation (*503*). The cloning of hCA XII in the pET-20b (+) vector was confirmed by sequencing of the plasmid at the University of Chicago Cancer Research Center (Chicago, IL).

4.1.3. Expression and purification of hCA I, hCA II and hCA VII and hCA XII

The procedure for the expression and purification for hCA I and hCA II were followed as described by Banerjee et al.(*329*) with only minor modifications. The cloned plasmid containing the catalytic domain sequence of the hCA isozymes was transformed into *E.coli* BL21-CodonPlus® DE3 (RIL) cells by following the standard molecular biology protocol (*503*). The transformed cells were grown at 37 °C in LB medium, containing 100 μg/mL of ampicillin, 50 μg/mL of chloramphenicol, and 100 μM of $ZnSO_4$ until A_{600} was 0.8. For hCA XII, the temperature was then reduced to 18 °C until the absorbance reached 1.0 and was induced using 0.5 mM IPTG and 200 μM $ZnSO_4$. For hCA I, hCA II and hCA VII, the cells were grown until the A_{600} was 0.6 and was induced by the addition of 0.1 % IPTG and 100 μM $ZnSO_4$. After induction, the cells were allowed to grow at 18 °C (for hCA XII) and at 25 °C (for hCA I, hCA II and hCA VII) for 12 – 16 hours with constant shaking in an orbital shaker at 300 rpm. The cells were then centrifuged at 5000 rpm for 15 min. The cell pellet obtained after centrifugation was suspended in a buffer containing 20 mM Tris-SO_4 containing 0.5 mM EDTA and 0.25 % Triton X 100, pH 8.0. A total concentration of 1 mM PMSF dissolved in isopropanol is also added prior to sonication. The cells were then placed in an ice-cold bath and sonicated in branson bath sonifier for 10 min using 40 % duty cycle. After sonication, they were centrifuged at 15,000 rpm for 30 min and the supernatant was used for further purification.

For purification of the recombinant hCA XII from supernatant, p-AMBS-agarose was used as the column resin. The column was initially equilibrated with a buffer containing 20 mM Tris-SO_4 pH 8.0. The supernatant was mixed with the gel slurry and stirred for 2 hours and was loaded on a 2 x 12 cm column. The load flow through of the

column was discarded. The column was then washed with wash buffer containing 0.1 M Tris-SO_4, 0.2 M K_2SO_4 and 0.5 mM EDTA, pH 9.0 and another wash buffer having 0.1 M Tris-SO_4 and 0.2 M K_2SO_4, pH 7.0. The elution of the enzyme from the column was carried out using an elution buffer containing 0.1 M Tris-SO_4, 0.4 M KSCN and 0.5 mM EDTA, pH 6.8. All the fractions showing absorbance greater than 0.5 were pooled. The pooled fractions were then concentrated using a PM-10 membrane and dialyzed against 25 mM HEPES buffer pH 7.5.

4.1.4. SDS-PAGE analysis of purification

Continuous SDS-PAGE analysis of protein samples during the course of purification of the enzyme were performed, using the 12% resolving and 4% stacking gels by following the procedure from Maniatis laboratory manual (*503*). Briefly, a resolving gel containing 12% acrylamide + 0.1% SDS and a stacking gel containing 4% acrylamide + 0.1 % SDS were prepared in 1.5 M Tris-HCl, pH 8.8 and 0.5 M Tris-HCl pH 6.8 respectively. Equal amount of diluted protein and 2X loading dye containing 10% SDS, 25% glycerol, 5 mM β-mercaptoethanol, 0.015% bromophenol blue and 300 mM Tris-HCl, pH 6.8 were mixed together and denatured by boiling for 5 minutes at approximately 90 °C in water bath. The denatured protein samples were then loaded in the gel and run at 200 V in Tris-HCl-glycine buffer containing 0.1% SDS, 25 mM Tris-HCl, 190 mM glycine, pH 8.3. The gels were then stained with 0.1% coomassie blue in 10% acetic acid and 10% methanol for 15 min and destained by 10% acetic acid and 40% methanol. The enzyme purity was judged qualitatively by the intensity of the protein of interest in comparison with other bands in the gel.

4.1.5. Estimation of protein concentration

The concentration of hCAs was estimated by Bradford assay using BSA as a standard protein (*504*). These assays were performed in either a cuvette or micro plate using proteins diluted in Bradford reagent. This mixture was incubated for 5 min at room temperature and the absorbance was measured at 595 nm. The molar concentration of hCAs were determined by using their molecular mass of 30 KDa for hCA I, hCA II, hCA VII and 60 KDa for hCA XII.

4.1.6. Spectrophotometric assay for hCA catalyzed reaction

The activity of hCAs was routinely measured using the ester hydrolysis reaction catalyzed by CAs (*505*). Although this is not the physiological reaction catalyzed by CAs, this is a popular method to determine the CA activity. Stock solution of the ester, p-nitro phenyl acetate, prepared in 100 % acetonitrile was a colorless compound. Upon hydrolysis by CA, it forms p-nitro phenol and p-nitrophenolate ion giving rise to an yellow color. As the absorption maxima of both the products are different, the formation of yellow color was monitored spectrophotometrically at 348 nm as this wavelength is an isosbestic point for p-nitro phenol and p-nitrophenolate anion. The experiment was performed in 25 mM HEPES buffer, pH 7.0, containing 10% acetonitrile with 0.4 mM substrate at 25^0C. For experiments involving quantum dots and polylysine, the experiment was performed in 10 mM Tris buffer, pH 8.0, containing 10 % acetonitrile. The unit of enzyme activity is defined as one micromole of the substrate converted into product per minute under these experimental conditions.

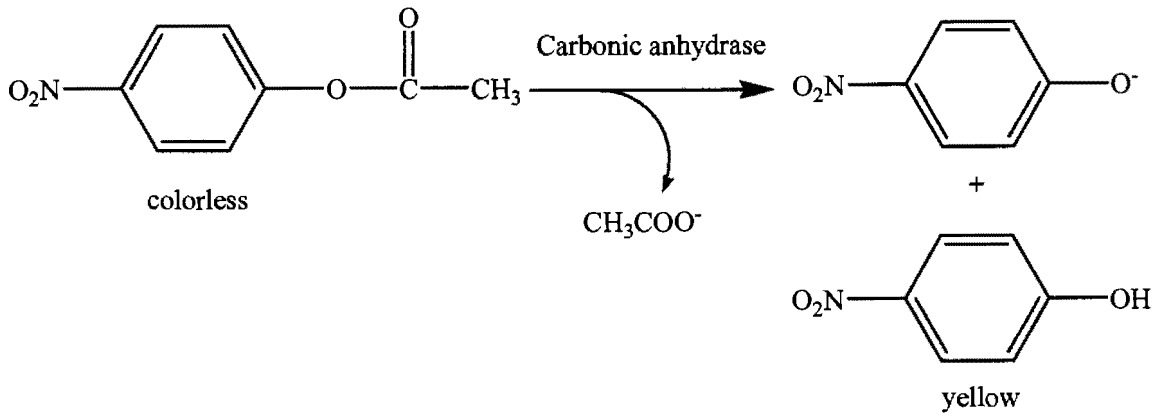

4.1.7. Determination of hCA activity by pH drop method

As the esterase activity of hCA VII and hCA XII was found to be poor, their enzyme activity was also measured by the pH drop method of Wilbur and Anderson (*451*). The time taken for the decrease in pH of 0.02 M Tris-HCl buffer from 8.3 to 6.3 at 0 – 4 °C upon addition of a saturated CO_2 solution in the absence and presence of CAs was determined. CO_2 gas was bubbled into ice cold water for about 30 minutes prior to the assay. The carbonated water was kept at 0 – 4 °C in an ice bath during the bubbling process. For the blank reaction, 6.0 mL of chilled 0.02 M Tris-HCl, pH 8.3 was mixed with 4.0 ml of ice cold CO_2 saturated solution with constant stirring and the time required for the pH to drop from 8.3 to 6.3 is recorded. The above experiment is repeated in the presence of CAs and the activity of the enzyme was determined by the following formula. where T_0 and T are the time required to achieve the above pH drop in the absence and presence of the enzyme respectively. The experiments were usually repeated two times and the results were averaged and rounded to the nearest value.

$$\text{Units of hCA activity} = T_0\text{-}T/T \times \text{mg hCA used} \qquad (4.1)$$

4.1.8. Characterization of fluorescent probes of CAs

Several fluorescent probes were synthesized by Jayati Banerjee from Dr. Mallik's lab. These probes named as JB2 compounds were characterized in the absence as well as in the presence of various CA isozymes using spectrophotometric, spectrofluorometric and transient kinetic techniques.

4.1.9. Spectrophotometric studies

All the absorption studies were performed on a Beckman DU 7400 spectrophotometer. The concentration of the probes and the buffer were the same as described for the spectrofluorometric studies. Stock solutions of all the probes and the standard were made in 100% DMSO, and were diluted in 25 mM HEPES buffer (pH = 7.0) containing 10% DMSO. The stock solutions were diluted to 5 μM and the absorption spectra were recorded.

4.1.10. Spectrofluorometric studies

All the spectrofluorometric studies were performed on Perkin–Elmer lambda 50-B spectrofluorometer equipped with a magnetic stirrer and thermostatic water bath. Stock solutions of all the probes and the standard were made in 100% DMSO, and were diluted in 25 mM HEPES buffer (pH = 7.0) containing 10% DMSO. The final concentration of the probes and CA were 5 μM and 10 μM respectively. The emission spectra were determined by fixing the excitation wavelength at the excitation maxima of the respective probes. The emission and the excitation slits were maintained at 9 mm and 2.5 mm. The PMT voltage was kept constant (800) throughout the experiment. Quinine was used as the standard fluorescent probe since its absorption maxima overlapped with almost all the probes.

4.1.11. Determination of the quantum yields of free and CA bound fluorescent probes

Quantum yield is defined as the ratio of the amount of light emitted from a sample to the amount of light absorbed by the sample.

QY= [# of fluorescence photons emitted /[# of incident photons absorbed]

The quantum yield of the probe in aqueous solution and when bound to CA was determined as follows.

1. Absorption spectrum of the sample was taken after blanking with the buffer containing 10% DMSO.
2. The optical density of the sample at the excitation wavelength was recorded.
3. The emission spectrum of the solvent was recorded.
4. The emission spectrum of the sample was taken.
5. Since the emission spectrum of solvent was almost near to zero, it was neglected.
6. The area under the emission peak was calculated.
7. The same procedure was repeated for the standard.
8. Quantum yield was determined using the following formula

$$QY = QY_s * I * OD_s * n_2/I_s * OD * n_{2s} \qquad (4.2)$$

Where is the quantum yield of the sample, I is the integrated intensity, OD is the optical density. The subscript "s" refers to the standard flurophore (quinine) with a quantum yield of 0.54.

4.1.12. Determination of the dissociation constant of the CA-JB complex

The dissociation constants of the hCA-JB complex was determined by titrating a fixed concentration of the enzyme (5 μM) with increasing concentrations of the probe (0-15 μM) in 25 mM HEPES containing 10% DMSO. Similar to DNSA, when excited at 330 nm, these fluorescent probes also undergo a blue shift in their emission maximum of 528

nm to approximately 470 nm upon binding to hCA (*387*). The corresponding intensity at 470 nm, after correcting for dilution was plotted as a function of JB concentration and their dissociation constants were determined by analyzing the classical binding model utilizing the quadratic equation (*506*) for the enzyme-ligand interactions with the help of Grafit 4.0 (Erithacus software)

$$\Delta F = (C * (L_{tot} + Kd + n*E_{tot}) - \sqrt{(E_{tot}*n + L_{tot} + K_d)^2 - 4E_{tot}*n*L_{tot}/2)} \qquad (4.2)$$

where ΔF is the change in signal of JB compound upon binding CA, E_{tot}, and L_{tot} refer to the total enzyme and total ligand concentration, K_d is the dissociation constant of the enzyme-ligand complex, n is stoichiometry of the enzyme-ligand complex and C is the change in amplitude of the signal. The dissociation constant of hCA I-JB2-48 complex was also by exciting the probe at 280 nm. A fixed concentration of the enzyme (2 μM) was titrated with increasing concentrations of the ligand in the standard HEPES buffer containing 10 % DMSO, pH 7.0. The initial reaction volume was 250 μl. The excitation and emission slits were 9 mm each. The decrease in fluorescence emission intensity of the protein and the increase in the fluorescence emission intensity of probe are monitored at 330 nm and 470 nm respectively and was plotted as a function of probe concentration. The dissociation constant was determined by analyzing the data with equation 4.2 with the help of Grafit 4.0 (Erithacus software).

4.1.13. Fluorescence Lifetime measurements

Fluorescence Lifetime measurements were performed on a custom design Photon Technology International (PTI) Fluorescence-Lifetime instrument. The excitation sources for measuring the time resolved fluorescence decay were the Light Emitting diodes (LEDs)

with maximum power outputs at 280 nm and 340 nm, respectively. Whereas the 280 nm LED was utilized to excite the intrinsic fluorescence of the protein (primarily contributed by the tryptophan residues), the 340 nm LED was utilized to excite JB2-48 fluorescent probe. The emitted light was detected (at right angle of the excitation source) by means of a stroboscopic emission monochromator configured at appropriate wavelengths. Dilute starch suspensions were used to collect the instrument response function (IRF). The data were collected in 200 channels and the integration time was set as 1 sec. Depending on the signal obtained 5-30 averages were performed for the samples to obtain better resolution of the fluorescence traces.

The time resolved fluorescence decay curves were analyzed to obtain the lifetimes of the fluorophores under different conditions by the aid of the PTI's software, Felix 32. The kinetic traces were fitted by the single and double exponential rate equations of the following format (Eqn. 4.3)

$$I(t) = \sum_{i=1}^{n} \alpha_i \exp(-t/\tau_i) \qquad (4.3)$$

where α_i and τ_i are amplitude and fluorescence lifetime for the i^{th} component, respectively. The relative contribution of component i(f_i) was calculated from the following relationship (Eqn. 4.4)

$$f_i = (\alpha_i \tau_i / \sum_{i=1}^{n} \alpha_i \tau_i) * 100\% \qquad (4.4)$$

The goodness of the exponential fit of fluorescence curves was determined by the reduced chi-square, the Durbin Watson, and Z values

4.1.14. Transient kinetic experiments

Transient kinetic experiments were performed on an Applied Photo physics SX-18 MV stopped-flow system, equipped with both absorption and fluorescence detecting photomultiplier tubes. The dead time of stopped flow was 1.3 msec. For fluorescence measurement, the light path was conFigured such that the fluorescence photomultiplier detected the emitting light via the 2 mm path length. The excitation wavelength was maintained at 336 nm, and a 395 nm cut-off filter was installed at the exit port of the cuvette to measure the time dependent increase in fluorescence intensity by a photomultiplier tube. All the stopped-flow experiments were performed in the single-mixing mode. In this mode, equal volumes of the reactants from syringes A and B were pushed under nitrogen pressure (100 Psi). This empties the old solution from the cuvette and the new solution is filled in the cuvette. Pseudo first order conditions ([S] >>> [E]) were maintained in all the transient kinetic experiments performed to determine the concentration dependence of the fluorescent probes (DNSA, and JB246) to hCA isozymes. All the transient kinetic experiments were performed at least in triplicate, and the resultant kinetic traces were averaged prior to analysis of the data by the SX-18MV software (version 4.42) developed by Applied Photo physics either using a single or double exponential rate equation. The single exponential rate equation is as follows.

$$Flu_t = Amp * \exp^{(-1/\tau)} + offset \qquad (4.5)$$

where Flu_t is the fluorescence at a given time. Amp and $1/\tau$ are the total amplitude and relaxation rate constant, respectively.

In the flurophore (F) concentration dependent relaxation kinetic data, the K_{obs} obtained at each individual concentration of the enzyme was plotted as a function of flurophore concentration and depending on whether there is a linear or hyperbolic

dependence of K_{obs} values with increasing flurophore concentration, the data were analyzed either according to one-step (for linear dependence) or two-step (for hyperbolic dependence) binding model (*119*, *329*). The one and two step models are schematically represented by schemes 4.1 and 4.2 respectively.

$$E + L \underset{K_r}{\overset{K_f}{\rightleftharpoons}} EL \qquad \text{(scheme 4.1)}$$

$$E + L \underset{K_e}{\rightleftharpoons} EL \underset{k_r}{\overset{k_f}{\rightleftharpoons}} EL^* \qquad \text{(scheme 4.2)}$$

In the above schemes, k_f and k_r represent the forward and reverse rate constants, respectively. The formation of EL complex in scheme 4.2 is assumed to satisfy rapid equilibrium condition with the dissociation constant of K_e.

The relationships between the relaxation rate constant ($1/\tau$) and the ligand concentration (under pseudo-first order conditions; [E] << [L]) are given in the following eqn 4.8 and 4.9 for one and two step model respectively.

$$1/\tau = k_f[L] + k_r \qquad (4.6)$$

$$1/\tau = \frac{k_{f2}[L]}{K_e + [L]} + k_{r2} \qquad (4.7)$$

4.1.15. Determination of dissociation off rates of hCA-fluorescent ligand (FL) complex.

Transient kinetic studies were also performed to determine the dissociation off rates (k_{off}) of hCA-DNSA and hCA-JB2 complexes with a competitive inhibitor of CA such as methazolamide. A mixture of the enzyme-DNSA or enzyme-JB2 complex was taken in one syringe and high concentration of methazolamide was taken in the other syringe and was

mixed together via the stopped-flow syringes. Methazolamide, being a competitive ligand of DNSA and JB2 compounds, displaces the fluorescent probes from the enzyme site, leading to the decrease in the intensity of the fluorescence signal of the enzyme-bound fluorescent probes. This is schematically shown in the following equation.

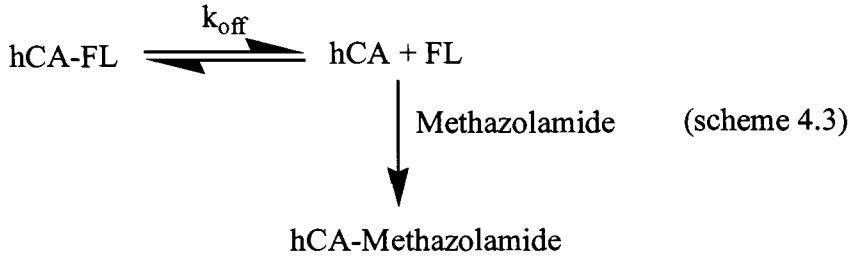

(scheme 4.3)

Thus the rate of formation of the enzyme-methazolamide complex would be limited by the rate of dissociation of the respective fluorophores from its enzyme site, yielding the magnitude of the dissociation "off-rate" (k_{off}) of the enzyme - flurophore complex.

4.1.16. pH Jump relaxation Studies

These experiments were performed by mixing a solution of the hCA I-JB2-48 complex, maintained at one pH, with a concentrated buffer at the other pH in the stopped-flow syringes, and recording the fluorescence change as described above. For a low to high pH jump, syringe A contained 2 μM CA I + 20 μM JB2-48 in 5 mM Acetate buffer at pH 5.0 containing 10% DMSO and syringe B contained 200 mM Tris at pH 9.0 with 10% DMSO. Upon mixing, the pH of the solution changed to pH 9.0. For a high to low pH jump experiment, syringe A contained 2 μM CA I + 20 μM JB2-48 in 5 mM Tris at pH 9.0 having 10% DMSO and syringe B contained 200 mM Acetate buffer at pH 5 with 10% DMSO. Upon mixing, the pH of the mixture changed to 5.0

4.1.17. Determination of inhibition constant for hCA I-Jb2 48 complex

The inhibition constant (K_i) was determined by monitoring the esterase reaction (*498*) in 25 mM HEPES buffer containing 10 % acetonitrile via Molecular Devices Spectra Max plus micro plate reader in a polystyrene micro plate in the absence and presence of inhibitor. The enzyme and p-NPA concentrations were kept at 2.75 μM and 1 mM respectively. The rate of enzyme catalysis was determined by taking the initial slopes of the reaction traces and is plotted as a function of inhibitor concentration.

As high concentrations of CA isozymes are taken to reliably measure the enzyme activity, it is always possible that part of the substrate and/or inhibitor is bound to the enzyme site. Since the data is to be analyzed by Michaelis-Menten equation which takes the free concentrations of the substrates and inhibitors, rather than their total concentrations, it was required to subtract the fraction of the bound species from their total concentrations. The free concentration of the inhibitors was thus calculated from the total concentration by complete solution of the quadratic equation, describing enzyme-inhibitor interaction. Eqn. 4.8 is a classic steady-state equation for the competitive inhibition of the enzyme,

$$V= V_{max}/1 + K_m/[S]\ (1 + [I]_f/K_i) \qquad (4.8)$$

where V is the velocity and V_{max} is the maximal velocity of the enzyme, $[I]_f$ is the free concentration of the inhibitor, [S] is the concentration of p-nitro phenyl acetate, K_m is the amount of pNPA required to half saturate hCA I and K_i is the inhibition constant to be determined. Due to the poor solubility of pNPA in buffer system, its concentration was kept at 1 mM which is less than the K_m value. This simplifies eqn 4.8 as follows.

$$V= V_{max} * [S]/K_m /(1 + [I]_f/K_i) \qquad (4.9)$$

The data were analyzed with the final form of the competitive steady-state model which is given as follows using the Graphit software.

$$v = v_0 * K_i/K_i + ([I]_t - 0.5 (([I]_t + [E]_t + K_i - \sqrt{([I]_t + [E]_t + K_i)^2 - 4 * [I]_t * [E]_t)}) \quad (4.10)$$

4.1.18. Molecular modeling studies

The molecular modeling studies were performed on a Silicon Graphics-O2 molecular modeling workstation with the aid of Accelrys software, InsightII (98). The coordinates for the X-ray crystallographic structures of bovine CA II complexed with DNSA (1okl.pdb) (*192*) and hCA I complexed with acetazolamide (1azm.pdb) (*507*) were downloaded from Research Collaboratory for Structural Bioinformatics (RCSB) Protein Data Bank. The backbones of these proteins were superimposed, and the DNSA was computationally transferred from bCA II to hCA I. The structure of JB2-48 was built on the backbone of the enzyme bound DNSA with the aid of the software builder under the InsightII (98) platform.

4.1.19. Determination of dissociation constants (K_d) of CA- sulfonamide inhibitor complexes by DNSA displacement method.

The binding affinity of certain non fluorescent inhibitors such as that of benzene sulfonamide, methazolamide, polylysine etc with hCA has been determined by monitoring the change in the signal of hCA-DNSA complex at 457 nm by competitive displacement of DNSA by these inhibitors. The experimental set up is similar to that as explained by Banerjee et al. (*328*). In a typical experiment, a fixed concentration of hCA-DNSA was titrated with increasing concentrations of the inhibitor. The excitation and emission wavelengths were maintained at 330 nm and 447 nm, respectively. As the inhibitor competitively displaces DNSA from hCA active site, fluorescence intensity of hCA-DNSA at 457 nm decreases. The change in the fluorescence intensity was plotted as a function of

inhibitor concentration and was analyzed by a modified form of the competitive binding model as elaborated by Banerjee et al. (*328*).

When two ligands (DNSA-D and methazolamide-M) compete for an enzyme active site (E), the K_d for the EM complex can be determined if the K_d of ED complex is already known. In an ideal situation, the total enzyme concentration should be far lower than its K_d with both D and M and also to the total ligand's concentration. If this ideal situation is met, the total concentrations of ligands can be taken as being equal to their free concentrations. However, if the enzyme-ligand dissociation constants are comparable to the initial concentrations of the enzyme and ligands, recourse can be made if the dissociation constant of the one-enzyme ligand complex is relatively higher than that of the other. In this situation, the competitive binding of DNSA (D) versus methazolamide (M) to the hCA (E) site can be represented by Eqn. 14.

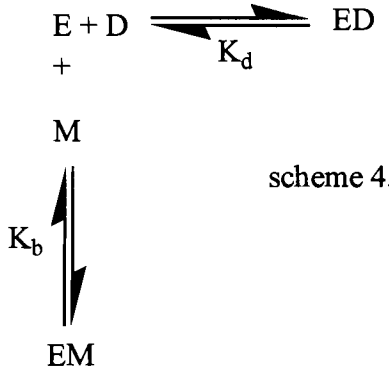

scheme 4.4

Eqn. 14

In scheme 4.4, K_d and K_b are the dissociation constants of the hCA -DNSA (ED) and hCA -methazolamide (EM) complexes, respectively and can be represented as follows.

$$K_d = [E][D]/[ED] = [E]([D]_t - [ED])/[ED] \quad (4.11)$$

$$K_b = [E][M]/[EM] = [E]([M]_t - [EM])/[EM] \qquad (4.12)$$

where E, D, and M are free concentrations of hCA, DNSA and methazolamide and $[E]_t$, $[D]_t$, and $[B]_t$ are the total concentrations.

When $[E]_t << [D]_t$, then $[D]_t$ can be taken to be the measure of [D], and by taking into account the mass balance ($[E]_t = [E] + [ED] + [EM]$), $[E]_t$ can be represented as follows

$$[E]_t = [EM] + \frac{K_b\,[EM]}{[M]_t - [EM]} + \frac{K_b\,[EM]\,[D]}{([M]_t - [EM])\,K_d} \qquad (4.13)$$

Eqn. 4.13 can be simplified to yield the dependence of [EB] on the concentrations and the binding constants of other species (Eqn. 4.14).

$$[EM] = ([E]_t + [M_t + K_b + (K_b/K_d)/[D]_t - \frac{\sqrt{([E]t + [M_t + K_b + (K_b/K_d)[D]_t)2 - 4[E]_t[M]_t}}{2} \qquad (4.14)$$

The binding isotherm is determined by plotting the the observed fluorescence (F_{obs}) as a function of the inhibitor ([M]) concentration as given by Eqn. 4.15

$$F_{obs} = \Delta F_{max}/[E]_t * ([E]_t - [EM]) \qquad (4.15)$$

where ΔF_{max} is the maximum change in fluorescence upon complete displacement of DNSA from the enzyme site.

4.1.20. Isothermal titration microcalorimetry

To determine the thermodynamic parameters for the binding of ligands with HCA isozymes, titration of the isozymes with ligands was performed via isothermal titration calorimetry (ITC). All calorimetric experiments were conducted on a VP-ITC isothermal

titration calorimeter. Before the titration, both the enzyme and the ligand solutions in respective buffers containing 10 % DMSO were thoroughly degassed in thermo vacuum and filtered with a 0.2 micron filter. The enzyme was taken in the sample cell (1.8 ml) and the ligand was taken in a syringe and 50 x 4 µl injections were made while the syringe was rotated at a constant speed of 310 rpm through out the titration to ensure proper mixing. Wiseman at al. describes the the instrumentation, experimental design and analysis in his comprehensive review (*469*). During titration, the reference cell was filled with 0.03% azide solution in water.

As the enzyme is titrated with the ligand, heat is released or absorbed. A thermoelectric device present in ITC measures the difference in temperature between the sample and the reference cell and is compensated by heating or cooling the sample cell thereby maintaining the temperature difference between the two cells constant. The heat released or absorbed upon titration of ligand is directly proportional to binding and as the reaction proceeds there is a decrease in this signal. Towards the completion of the reaction, the heat produced is due to the heat of dilution and is taken as a background signal. The raw calorimetric data was thus presented as the amount of heat produced per sec (after subtracting the back ground signal) upon injection of ligand. These heat signals are automatically integrated by the analysis software to give the amount of heat produced per injection and is plotted as a function of ligand concentration and analyzed by a single binding site model that is inbuilt in the origin 5.0 software. The average of heat produced per injection for the last 5 injections were taken as the back ground heat and was subtracted from all the injections. The final data represents the corrected amount of molar heat produced per injection as a function of molar ratio of ligand to hCA. For data analysis, all

the parameters (*n*, *K*a, and $\Delta H°_{obs}$) were allowed to vary and the standard errors were derived from the best fit of the experimental data.

The standard free energy ($\Delta G°$) was then calculated using either of the two following relation ships.

$$\Delta G^0 = -RT \ln K_a \qquad (4.16)$$

$$\Delta G^0 = \Delta H^\circ - T\,\Delta S^\circ \qquad (4.17)$$

The heat capacity change ($\Delta C_p°$) associated with hCA-ligand complex formation was calculated by repeating the titrations at different temperatures (15- 30 °C). The temperature dependent experiments were conducted in 25 mM Tris buffer, pH 7.5. The slope obtained by plotting $\Delta H°$ versus temperature gave the $\Delta C_p°$ value.

The enthalpic contributions that occur from the protonation or deprotonation of buffer species, were calculated by doing the ITC titration of hCA - ligand at different buffers (25 mM Tris and 25 mM phosphate and 25 mM HEPES pH 7.5) of varying ionization enthalpy (phosphate = 1.22 kcal/mol, HEPES = 5.1 kcal/mol, Tris-HCl = 11.51 kcal/mol) (*508-511*). The ionic strength of the buffers was adjusted by addition of K_2SO_4. The data were analyzed by the following relation ship.

$$\Delta H°_{obs} = \Delta H°_{int} + p\Delta H°_{ion} \qquad (4.18)$$

where p is the number of protons abstracted from the buffer media, $\Delta H°_{obs}$ is the observed enthalpy, $\Delta H°_{int}$ is the intrinsic enthalpy and $\Delta H°_{ion}$ is the buffer ionization enthalpy.

4.1.21. Interaction of quantum dots with hCA isozymes

4.1.21.1. Preparation of CdTe quantum dots:

The differently charged quantum dots were prepared in Dr. Weichen's laboratory at the Department of Physics, University of Texas at Arlington, TX.

4.1.21.2. Calculation of the electrostatic surface potential of hCA XII

The X-ray crystallographic coordinates of hCA XII were obtained from the Protein Data Bank (PDB ID: 1JCZ) (*49*). The electrostatic surface potential of hCA XII was calculated using the GRASP software program (*512*) on an SGI molecular modeling workstation.

4.1.21.3. UV/Vis spectra of quantum dots

All UV/Vis spectra were measured on a Molecular Devices SpectraMax® Plus micro plate reader using a quartz cuvette (1-cm path length). Spectra were measured after subtraction of a solvent background and the data are presented in standard absorbance units.

4.1.21.4. Spectrofluorometric measurements:

All the steady-state spectrofluorometric studies involving Qds were performed on a Perkin Elmer LS 50B spectrofluorometer, equipped with a magnetic stirrer and thermostated water bath. Unless otherwise mentioned, all the experiments involving Qds were performed utilizing 10 mM Tris, pH 8.0 as the Qds were found to be stable in this buffer. For experiments involving DNSA, 10% acetonitrile in addition to the above buffer was used. A stock of 1 mM DNSA was prepared in 10 mM HCl and was diluted into 10 mM Tris, pH 8.0, containing 10 % acetonitrile. The stock solution of polylysine was prepared in 25 mM HEPES pH 7.5. The emission spectrum of the enzyme was taken by fixing the excitation wavelength at 295 nm. Unless mentioned otherwise, the excitation and emission slits were kept at 5 mm each and the PMT voltage was set at 800.

4.1.21.5. Determination of binding isotherms for the interaction of hCA with Qds

The binding affinity of Qds to hCA XII was determined by titrating a fixed concentration of Qds with increasing concentrations of hCA in 10 mM Tris, pH 8.0. The excitation and emission wavelengths were set at 295 nm and 336 nm, respectively. A fixed concentration of Qds was titrated with known concentrations of hCAs. A blank titration of protein into buffer was subsequently performed in order to subtract the signal contributed by blank from that of the sample. The difference in the protein emission intensity at 336 nm was plotted as a function of the protein concentration and the dissociation constant of the hCA XII- Qds complex was determined as described by Qin and Srivastava (*506*). The concentration of Qds was allowed to vary without constraints in the fitting parameter as this would allow the estimation of its actual concentration.

4.1.21.6. Determination of the concentration of polylysine

The concentration of polylysine was determined by taking the average molecular weight of the macromolecule as being equal to 24,000 Da as per the manufacturer's specification. In all experiments reported herein the concentration of the entire (i.e., polymeric form) polylysine moiety rather than its monomeric lysine residue was taken.

4.1.21.7. Determination of the binding isothers of hCA XII-polylysine

The dissociation constant of polylysine to hCA XII was determined by monitoring the decrease in the tryptophan signal of hCA XII at 336 nm (λ_{ex} = 295 nm) upon titration of increasing concentrations of polylysine in 25 mM HEPES buffer pH 7.5. The decrease in the fluorescence of hCA XII upon interaction with polylysine was plotted as a function of polylysine concentration to determine the binding constants as described by Qin and Srivastava (*506*).

4.1.21.8. Determination of binding isotherms for hCA XII –polylysine in the presence of DNSA

The binding isotherm for the interaction of polylysine with hCA XII in the presence of DNSA was determined by titrating a fixed concentration of hCA XII (1 μM) and saturating concentration of DNSA (5 μM) by increasing concentrations of polylysine in 25 mM HEPES buffer containing 10 % acetonitrile, pH 7.5. The excitation wavelength was set at 330 nm and the decrease in the fluorescence emission intensity at 457 nm was monitored. A blank titration of polylysine in buffer was performed and the signal contributed by the blank was subtracted from that of the sample. The difference in the emission intensity at 457 nm was plotted as a function of polylysine concentration. The dissociation constant for the hCA XII-polylysine complex was determined via analysis of the data as described by Qin and Srivastava (*506*).

4.1.21.9. Determination of binding isotherm for the interaction of hCA XII with Qds^+ in the presence of DNSA

The binding isotherm for the interaction of Qds^+ with hCA XII in the presence of DNSA was determined by titrating a fixed concentration of hCA XII and saturating concentrations of DNSA by increasing concentrations of Qds^+ in 10 mM Tris-HCl buffer, pH 8.0, containing 10 % acetonitrile. The excitation and emission slits were kept at 10 mm each. The increase in the fluorescence intensity of Qds^+ (after subtracting the signal from free Qds^+) at 600 nm (λ_{ex} = 330 nm) is plotted as a function of Qds^+ concentration and the binding isotherm was analyzed as mentioned above.

4.1.21.10. Determination of binding isotherm for the interaction of hCA XII with DNSA in the presence of polylysine

The dissociation constant of hCA XII-DNSA complex in the presence of saturating concentrations of polylysine was determined by titrating a fixed concentration of hCA XII and saturating concentrations of polylysine by increasing concentrations of DNSA in 25 mM HEPES buffer, pH 7.5, containing 10 % acetonitrile. The increase in the fluorescence emission intensity of hCA XII-DNSA complex at 457 nm (λ_{ex} = 330 nm) was monitored and was plotted as a function of total concentration of DNSA. The binding isotherm was determined via analysis of the data as described above.

4.1.21.11. Catalytic activity of hCA XII in the presence of quantum dots

The catalytic activity of hCA XII was measured by the pH drop method (*451*) as explained above. Each activity measurement was performed in duplicate, and the resultant values were averaged. Since the enzyme activity thus calculated is in arbitrary unit, it is represented as the percent of the control activity (100%) in the absence of any ligand.

4.1.22. Interaction of liposomes with hCA XII

4.1.22.1. Liposome Preparation

Large unilamellar vesicles (LUVs) containing differently charged lipids were prepared by hydration, sonication, and extrusion of thin films, formed by mixing appropriate amounts of chloroformic solutions of desired lipids as described in the following sections.

4.1.22.1.1. Making dry film

Appropriate weights of respective lipids required to achieve their desired concentrations (4mM) were transferred (either as solids or as chloroform solutions) to a test tube. A 9:1 mixture of spectroscopic grade chloroform: methanol (total volume = 1 mL) was added to achieve complete dissolution of the lipids. The organic solvent was removed

under argon for 30 min. The thin film was kept under vacuum for 24 h to remove the residual organic solvent.

4.1.22.1.2. Hydration of the dry lipid film

This was accomplished simply by adding 500 ul of 25mM Hepes containing 150 mM NaCl pH 7.5 to the container of dry lipid. The temperature of the hydrating medium was kept at 60 degrees which is above the gel-liquid crystal transition temperature (Tc or Tm) of the lipid. After addition of the hydrating medium, the lipid suspension was maintained above the T_c during the hydration period. The lipid mixture was kept at 60 degrees for 1 hour and then slowly brought back to the room temperature. Next day, another 500µl of the hydrating medium which is preheated to 60 degrees was added and mixed together. This will yield LMVs (large multilamellar vesicles).

4.1.22.1.3. Extrusion

After hydration the liposomes were extruded. Lipid extrusion is a technique in which a lipid suspension is forced through a polycarbonate filter with a defined pore size to yield particles having a diameter near the pore size of the filter used. In this case we used a 100nm membrane filter to yield Large Unilamellar vesicles of this size. The lipids used in preparing liposomes with different charges are as follows. The liposomes were prepared with zwitterionic 1-palmitoyl-2-oleoyl-sn-glycero-3-phosphocholine (POPC) as a major (75–95%) component and other lipids contributing different net charges as minor components. Thus negatively charged liposomes were prepared by using either POPS (1-palmitoyl-2-oleoyl-sn-glycero-3-phospho-L-serine) or PIP2 (1,2-dioleoyl-sn-glycero-3-phosphoinositol-4,5-bisposphate) bearing -1 and -3 net charges, respectively, in their head groups at neutral pH. And EPOPC (1-palmitoyl- 2-oleoyl-sn-glycero-3-

ethylphosphocholine) bearing a + 1 net charge (EPOPC), on its head group at neutral pH was used to prepare positively charged liposomes. In all the liposomes 5 % Dansyl PE was used as a probe. For neutral liposomes we used only POPC as the major constituent along with 5 % Dansyl PE. The structures of the individual lipids are as follows.

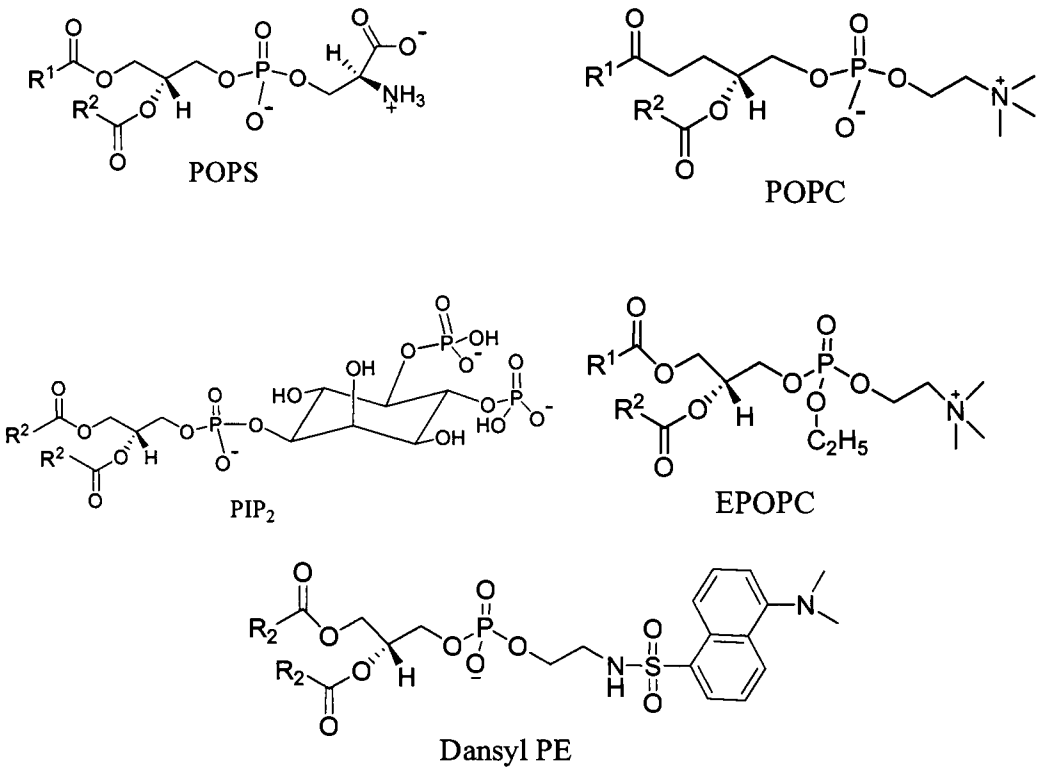

Figure 4.1. Structures of phospholipids

4.1.22.2. Determination of hCA XII–liposome interaction

All fluorescence measurements were performed using a LS-50B Perkin–Elmer spectroflourometer. Decrease in the intrinsic fluorescence of hCA XII upon interaction with differently charged liposomes was used as a signal in the determination of binding affinities of the hCA XII-liposome complex. The hCA XII was excited at 280 nm and the tryptophan quenching was monitored at 338 nm in 25 mM HEPES + 150 mM NaCl. The

decrease in the fluorescence intensity at 338 nm was plotted as a function of liposome concentration and the binding affinity was determined by analyzing the data using the classical binding model as described by Qin and Srivastava (*506*). Phosphate assay was used to determine the concentration of liposomes. Binding isotherms were also determined at different salt concentrations. The osmolality of the liposomes in these cases was adjusted with sucrose solution.

4.1.23. Thermal and chemical denaturation of hCA XII

4.1.23.1.Circular dichroism of CA isozymes

Circular dichroic (CD) spectra of the recombinant hCA isozymes were measured on J-815 spectropolarimeters (Tokyo, Japan) using a 1-mm path length quartz Cuvette and nitrogen flow rate of 20 $ft^3 hour^{-1}$. CA isozymes in the range of 6-12 μM were prepared either in 2.5 or 5 mM HEPES, pH 7.5. The spectrum of the buffer was subtracted from the spectra of protein. An average of at least 5 scans was taken for each sample and was smoothed by the fast Fourier transform utility of the Jasco analysis software.

4.1.23.2. Guanidinium chloride (GdmCl) and urea induced unfolding of hCA XII monitored by CD spectroscopy

Aliquotes of 6 μM hCA XII in 5 mM HEPES was mixed with increasing concentrations of GdmCl/Urea and was incubated at room temperature for 16 hours. The equilibrium unfolding of hCA XII was measured at 25°C by monitoring the changes in the ellipticity at 223 nm. For each sample an average of 5 scans were collected in a1-mm path length quartz cuvette. The ellipticity at 223 nm was plotted as a function of GdmCl concentration. As depicted in the following scheme, the unfolding of hCA XII takes place in a native-denatured two state equilibrium unfolding model.

$$N \underset{}{\overset{K}{\rightleftharpoons}} D$$

Where N represents the native form of protein and D represents the denatured form of protein.

According to this model, no stable intermediates are present between the native and the denatured states at equilibrium and that each state yields distinct experimental signals. Santoro and Bolen (*513*) described the two-state transition model by the following equation.

$$\text{Signal} = \frac{(S_u + m_u * [D] + (S_n + m_n * [D]) * e^{-(\Delta G_{n-u} + m_g * [D])/RT}}{1 + e^{-(\Delta G_{n-u} + m_g * [D])/RT}} \qquad (4.19)$$

In the above equation, m_u and S_u represent the slope and intercept of the linear portion of the plot at high denaturant concentrations, m_n and S_n are the slope and intercept of the linear portion at low denaturant concentrations, ΔG_u is the difference in free energy between the native and unfolded states in the absence of denaturant and mg is the slope of the line that describes the dependence of the observed ΔG on denaturant concentration.

4.1.23.3. Guanidinium chloride (GdmCl) and urea induced unfolding of hCA XII monitored by DNSA fluorescence

The stability of tertiary structure of hCA was determined utilizing the hCA bound DNSA fluorescence. A fixed concentration of hCA was mixed with saturating concentrations of DNSA and the fluorescence intensity of enzyme bound DNSA at 457 nm was monitored as a function of GdmCl concentration. The decrease in the fluorescence intensity was plotted against GdmCl concentrations and the data was analyzed by eqn 4.19.

4.1.23.4. Determination of melting temperatures of enzymes

The thermal unfolding of hCA XII and hCA II were performed on the Jasco J-815 spectropolarimeter (Tokyo, Japan), equipped with a peltier temperature control. Required concentrations of enzymes in 5 mM HEPES pH 7.5 were taken in a 1-mm path length quartz cuvette and heated from 25 to 95 °C at a rate of 30 degrees/hour or 90 degrees/hour and the ellipticity at 223 nm (θ_{223}) was monitored. Melting temperature (T_m) of the enzymes was determined by taking the midpoint of cooperative transition.

CHAPTER 5. RESULTS

5.1. Cloning, expression and purification of recombinant hCAs

5.1.1. Cloning, expression and purification of hCA VII

The coding sequence of hCA VII from the plasmid pCMV-SPORT 6 was amplified by the hot start PCR method (*514*) and cloned between the Nde I and Xho I sites of the pET-20b (+) vector. The vector containing the hCA VII coding sequence was then transformed into the BL21 codon plus DE3 (RIL) *E. coli* host cells, and over expressed by inducing with IPTG. After induction, the cells were grown at 25 °C for 16 hours which resulted in the expression of hCA VII in the soluble fraction of cell extract (crude extact). The protein was purified by affinity chromatography using the p-aminomethyl benzene-sulfonamide-agarose (pAMBS-agarose) column. In order to ensure proper binding of hCA VII to the column, the crude extract was mixed with the column material and was incubated at 4°C for 8 hours with slow stirring. The absence of enzyme activity in the load flow through (LFT) indicated the complete binding of hCA VII to the column matrix. The column was then washed with wash buffers (see section 4.1.3.) followed by elution of hCA VII with KSCN. Figure 5.1 represents the elution profiles of hCA VII where the absorbance of the eluted fractions at 280 nm is plotted as a function of the fraction number. All the fractions that showed absorbance greater than 0.5 were pooled, concentrated and dialyzed against 25 mM HEPES, pH 7.0. Whereas the specific activity of the crude extract was 3 units/mg, the specific cavity of the dialyzed sample was found to be 90.6 units/mg. This indicated that the protein is approximately 30 fold pure as compared to the crude extract. The dialyzed protein produced a single band on the SDS-PAGE (Figure 5.2) indicating the homogeneity of the purified enzyme. 15 mg of pure hCA VII was produce

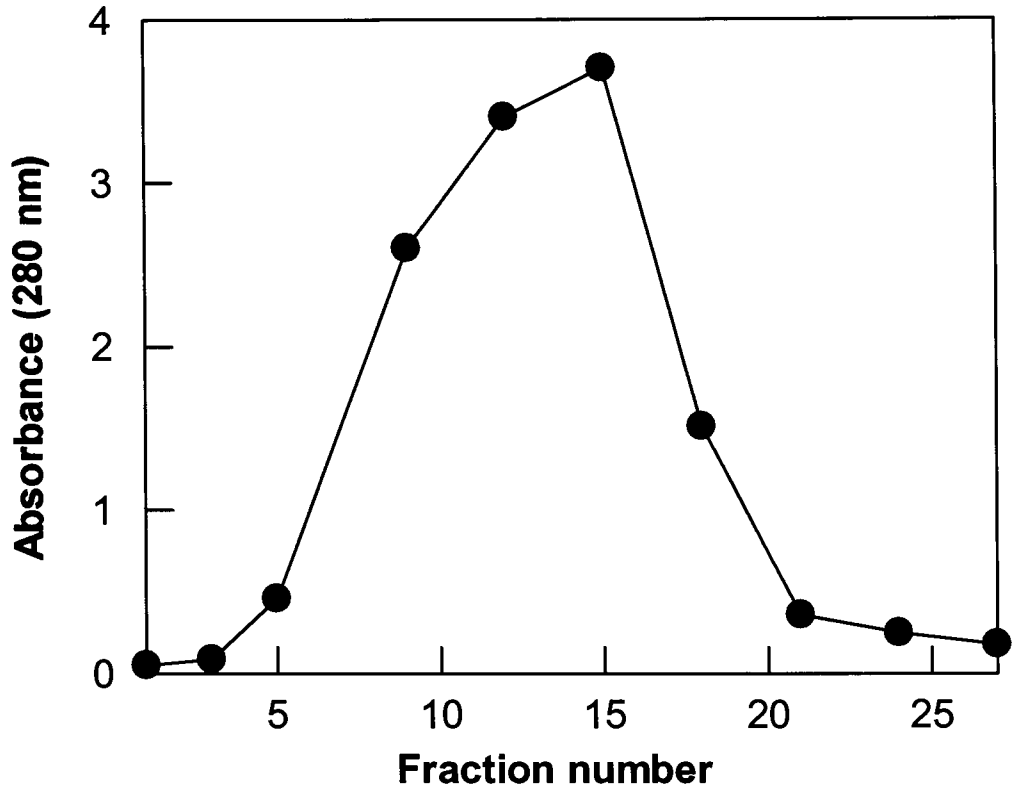

Figure 5.1. Elution profile of hCA VII from pAMBS-agarose column.
The protein was eluted with a buffer containing 0.4 M KSCN. The absorbance of the samples were measured at 280 nm and plotted with respect to its elution volume.

per liter of culture by this method.

5.1.2. Expression and purification of hCA XII

The pET-20b (+) vector containing the coding sequence for hCA XII was transformed in BL21 codon plus DE3 (RIL) *E. coli* host cells and induced with IPTG. After induction, the cells were grown at 18 °C for 16 hours, which resulted in the expression of

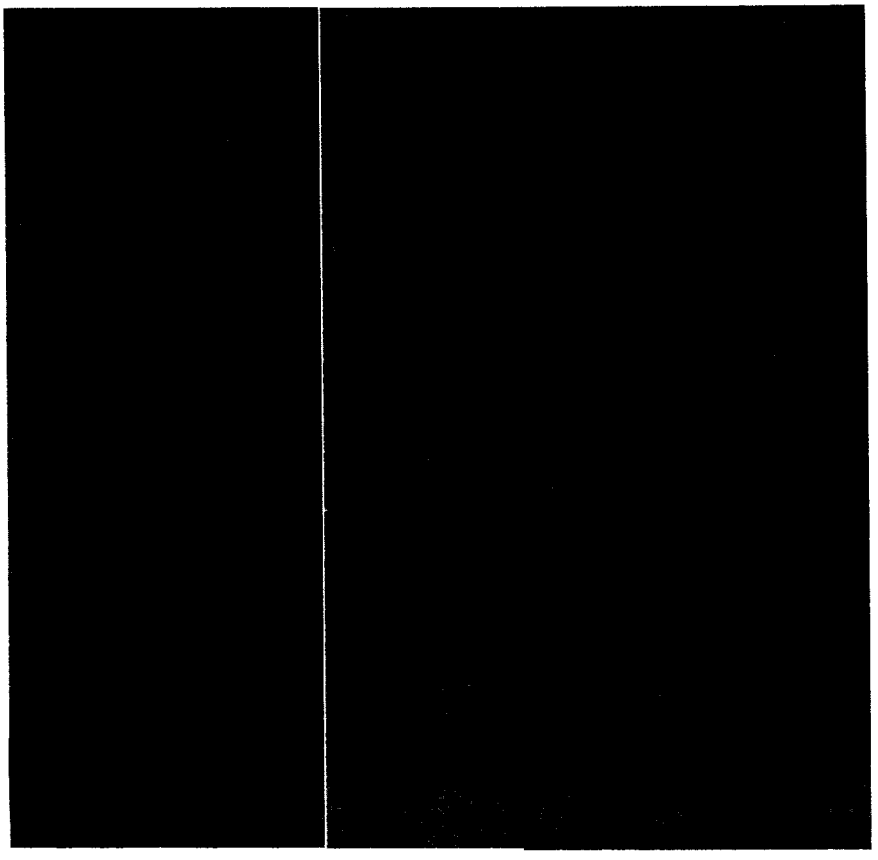

Figure 5.2. SDS-PAGE analysis of hCA VII at various stages of purification. SDS-PAGE was performed using a 12% resolving gel and 4% stacking gel and proteins were stained with coomassie blue. Lane 1: Crude extract, lane 2: Load Flow through, lane 3: Wash, lane 4: hCA VII, lane 5: Purified hCA I control (Mr. wt: 30, 000) (*207*).

hCA XII in the soluble fraction of cell extract (crude extact). The crude extract containing hCA XII, was purified by affinity chromatography using the pAMBS-agarose column. To ensure proper binding of hCA XII to the column matrix, the column material was mixed with the crude extract and incubated at 4°C for 16 hours with slow stirring. This ensured proper binding of hCA XII to the column as evident from SDS PAGE results (lane 2 of Figure 5.4) and was confirmed by the absence of enzymatic activity in the LFT.

Recombinant hCA XII was then eluted from the column with 0.4M KSCN. Figure 5.3 represents the elution profiles of hCA XII where the absorbance of the eluted fractions at 280 nm is plotted as a function of their fraction number. All the fractions that showed absorbance greater than 0.5 were pooled, concentrated and dialyzed against 25 mM HEPES, pH 7.0. The protein purified by this method was found to be pure as is evident from the SDS PAGE result (Figure 5.4). The total yield of the protein was found to be 4 mg per liter of the culture with a specific activity of 34 units/mg of protein. This shows that the protein is approximately 10 fold pure as compared to its crude extract with a specific activity of 3.1 units/mg of protein.

5.1.3. Determination of molecular weight of hCA XII

The secretory form of hCA XII was purified and crystallized by Whittingtan et al. with a reported molecular weight of 60, 000 (*49*). Except for a minor difference, the amino acid sequence of our hCA XII construct is essentially identical to that used for determining the crystal structure of the enzyme. The SDS-PAGE results of purified hCA XII showed a molecular weight of 30, 000 daltons. To confirm, if hCA XII exists as a homodimer in solution, gel filtration chromatography was performed using superdex-6 FPLC column. The gel filtration results confirmed that the molecular weight of hCA XII is approximately 60, 000 daltons.

The procedure for the expression and purification of hCA I and hCA II was followed as detailed by Banerjee et al. (*329*).

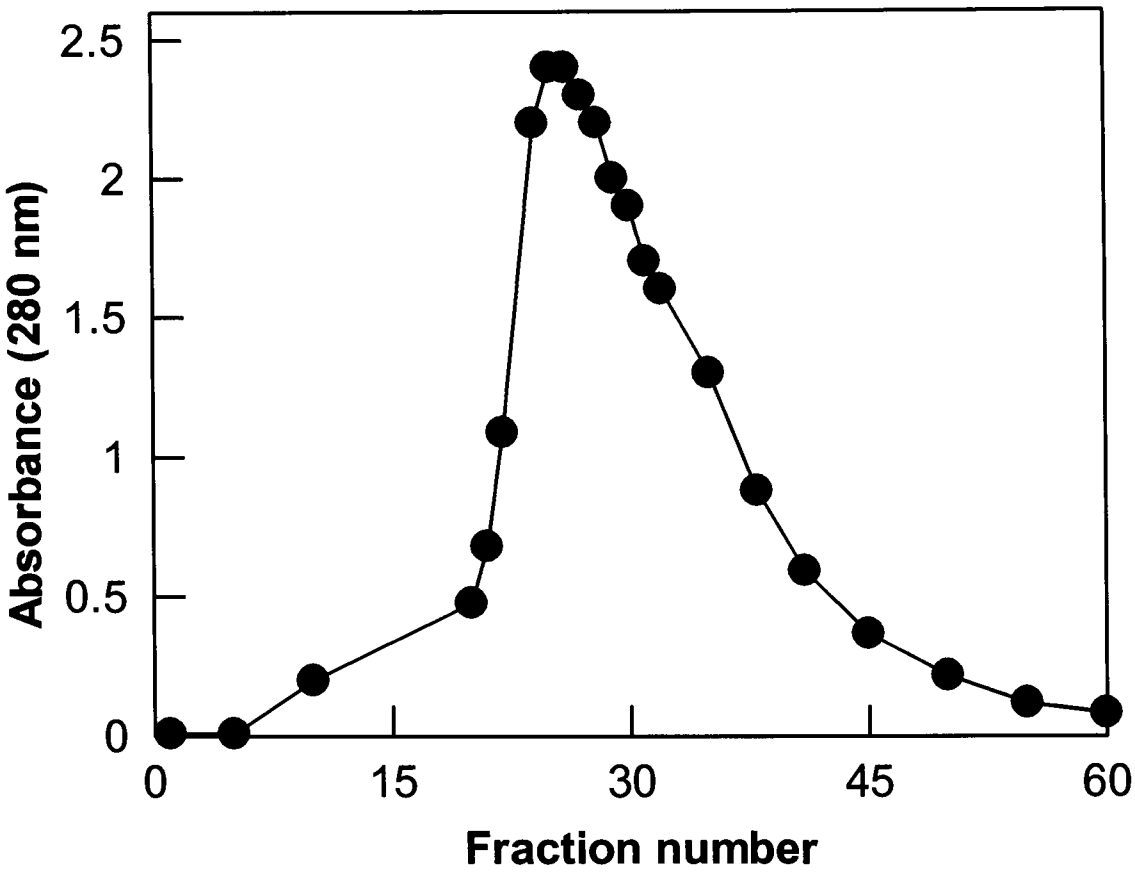

Figure 5.3. Elution profile of hCA XII from pAMBS-agarose column.
The protein was eluted with a buffer containing 0.4 M KSCN. The absorbance of the samples were measured at 280 nm and plotted with respect to its elution volume.

5.2. Comparison of the fluorescence spectral properties of DNSA and its derivatives upon interaction with hCA isozymes

In order to fulfill diverse cellular functions, different forms of the same enzyme (isoenzymes or isozymes) have been found to be expressed, often in different tissues, in a single organism (*28, 21, 97, 515-517*). This poses a main problem in using them as

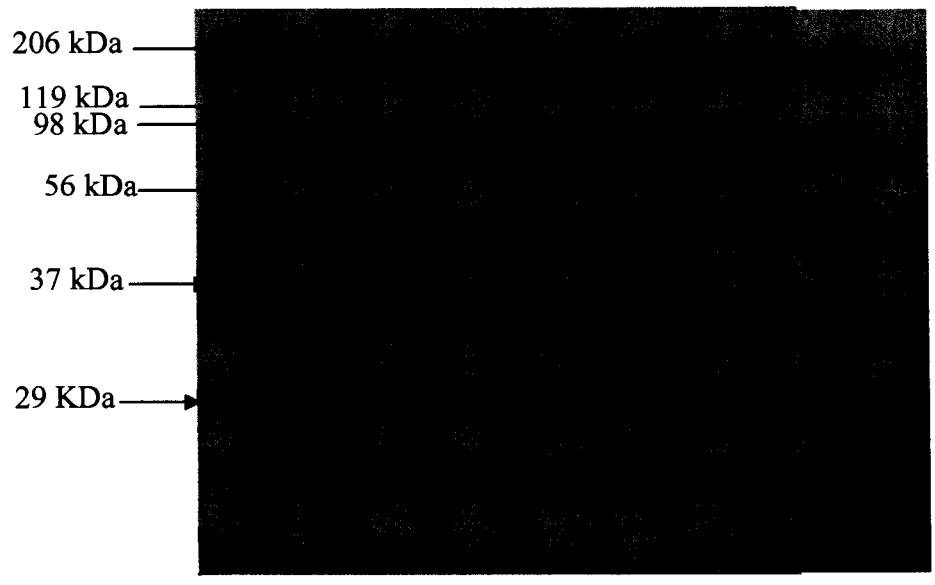

Figure 5.4. SDS-PAGE analysis of hCA XII at various stages of purification. SDS-PAGE was performed using a 12% resolving gel and 4% stacking gel and proteins were stained with coomassie blue. Lane 1: Perfect Protein™ ladder (EMD; Madison, WI), lane 2: crude extract, lane 3: LFT before incubating the crude extract with pAMBS column, lane 4: wash1, lane 5: wash 2, lane 6: LFT after incubating crude extract and pAMBS column for 16 hours, lane 7: pure hCA XII.

biomarkers (*65*). The catalytic properties of these isozymes are suited to the requirements of the cell/tissue in which they are expressed (*13*, *75*, *103*, *125*, *128*, *145*, *236*, *266*, *369*). At least 100 enzymes are known to exist in several molecular forms. Since all the isozymes catalyze the same chemical reaction, their active site pockets are markedly similar (*75*, *236*, *250*, *518*, *519*). Hence, targetting a particular isozyme from a pool of different isozymes in the physiological milieu remains a challenge till date despite enormous research effort in this field for several decades (*20*, *65*, *75*, *21*, *77*, *97*, *165*, *217*, *302*).

Human CAs which are ubiquitously distributed zinc containing metallo enzymes, have been the target for drug development for the last 6 decades (*20*, *64*, *21*, *97*, *217*, *22*). As mentioned in chapter 1, the existence of 16 isoenzymes of CA in the animal kingdom has been known so far with very different subcellular and tissue distributions (*22*). Like any other isozymes, the active sites of hCAs are remarkably similar making it difficult to selectively detect one isozyme from a mixture (*77*, *22*). However, a marked difference in the non-catalytic regions (e.g., the surface amino acid residues, peripheral active site pockets of isozymes, etc.) among these isozymes has been identified (*250*, *520*). Hence, it has been hypothesized that the isozyme selectivity among hCA isozymes is dictated by the difference in the surface distribution of amino acids as well as the distal (i.e., "entry") pockets of the isozymes. To test this hypothesis, spectral, kinetic, and thermodynamic studies were performed with hCA isozymes using DNSA and its derivatives.

DNSA is a widely used fluorescent sulfonamide inhibitor of CAs (*289*, *317*, *328*, *329*, *387*, *462*, *463*). The X-ray crystal structure of CA II complexed with DNSA showed that the inhibitor is deeply seated in the active site pocket of the enzyme (*192*). Other fluorescent probes of hCA have not been used extensively due to their challenging protocols and high synthetic cost (*521-523*). In addition, the quantum yields of these fluorescent probes are not significantly increased upon binding with CAs. The low sensitivity and high back ground of these flurophores prevented them from being used for transient kinetic and ligand binding studies. With these features in mind, a set of new fluorescent probes were synthesized by Dr. Sanku Mallik's group (Department of Pharmaceutical Sciences, NDSU) using DNSA as the parent compound. These fluorescent probes have extended structures (Figure 5.7) and therefore have the potential to interact

with the distal (i.e., "entry") pockets of the enzymes in addition to the active site residues, and thus were expected to distinguish the different isozymes of hCA. The changes in fluorescent spectral properties of these probes when complexed with hCAs have been compared with those obtained with DNSA (steady state and lifetime; section 5.2) followed by their kinetic (section 5.3) and thermodynamic (section 5.3 and section 5.4.1) studies. These studies were designed to substantiate or refute the hypothesis that isozyme selectivity is encoded by the non-catalytic regions of the enzymes.

5.2.1. Fluorescence spectral features of DNSA upon interaction with hCA isozymes

In contrast to the majority of sulfonamides that serve as potent inhibitors of hCA II (*137*, *524*, *525*), DNSA serves as a potent inhibitor of hCA I (*329*). The emission maximum of DNSA in water has been reported to shift from 580 nm to 468 nm (*387*), 458 nm and 455 nm upon binding to bCA, hCA I and hCA II (*329*) respectively.

Figure 5.5 shows the emission spectral changes of DNSA complexed with hCA I, II, VII and XII. Consistent with the literature data (*329*, *387*), the fluorescence emission maximum of DNSA underwent a blue shift with concomitant increase in its fluorescence intensity upon interaction with the above hCA isozymes. As can be seen from the Figure, the emission maximum of DNSA (λ_{ex} = 330 nm) was shifted from 580 nm to 470 nm upon interaction with hCA I, II and to 460 nm and 465 nm upon interaction with hCA VII and hCA XII respectively.

The fluorescence quenching of DNSA in aqueous solution and its varying range of enhancements when bound to the active site of different hCAs prompted the determination of its quantum yield in both the free and enzyme bound forms. These values are listed in the last row of Table 5.2. From the values presented in Table 5.2, it is clear that hCA I

exhibits a greater enhancement in the quantum yield of DNSA followed by hCA II, hCA VII and hCA XII. This is in accordance with the results obtained by Banerjee et al (*329*), who reported higher amplitude of fluorescence changes for DNSA when it is bound to hCA I than to hCA II. The fluorescent spectral changes exhibited by hCA bound DNSA were found to be qualitatively similar to those exhibited by other fluorescent probes such as amino naphthalene sulfonamide (ANS), 5-dimethyl amino naphthalene sulfonyl (DNS) L-proline, DNS-L-glycine, DNS- L-glutamic acid with hydrophobic proteins such as bovine serum albumin (BSA), apomyoglobin and apohemoglobin (*387, 526, 527*). In contrast to the high fluorescent complex exhibited by these fluorescent probes with the above mentioned proteins, they did not exhibit any change in their spectral properties in the presence of CAs. Chen et al (*387*) described the changes in the emission properties of DNSA upon interaction with bCA as partly due to the hydrophobicity and partly due to the zinc induced changes in the sulfonamide region of the inhibitor. The absence of sulfonamide group in the above compounds was considered to be one of the reasons for their fluorescent spectra remaining unchanged in the presence of hCAs despite the presence of large hydrophobic patches in them.

The differential increase in the fluorescence intensiy of DNSA by different hCA isozymes prompted the determination of their excited state lifetimes. This was performed with the intention of checking the possibility of selectively identifying a particular isozyme in a pool of different isozymes based on their lifetime properties. Figure 5.6 shows the fluorescence decay profiles of DNSA (λ_{ex} = 340 nm, λ_{em} = 470 nm) in the presence of hCA I (panel A), hCA II (panel B), hCA VII (panel C) and hCA XII (panel D). As can be seen from the Figure, the fluorescence decay of DNSA conformed to a biexponential process in

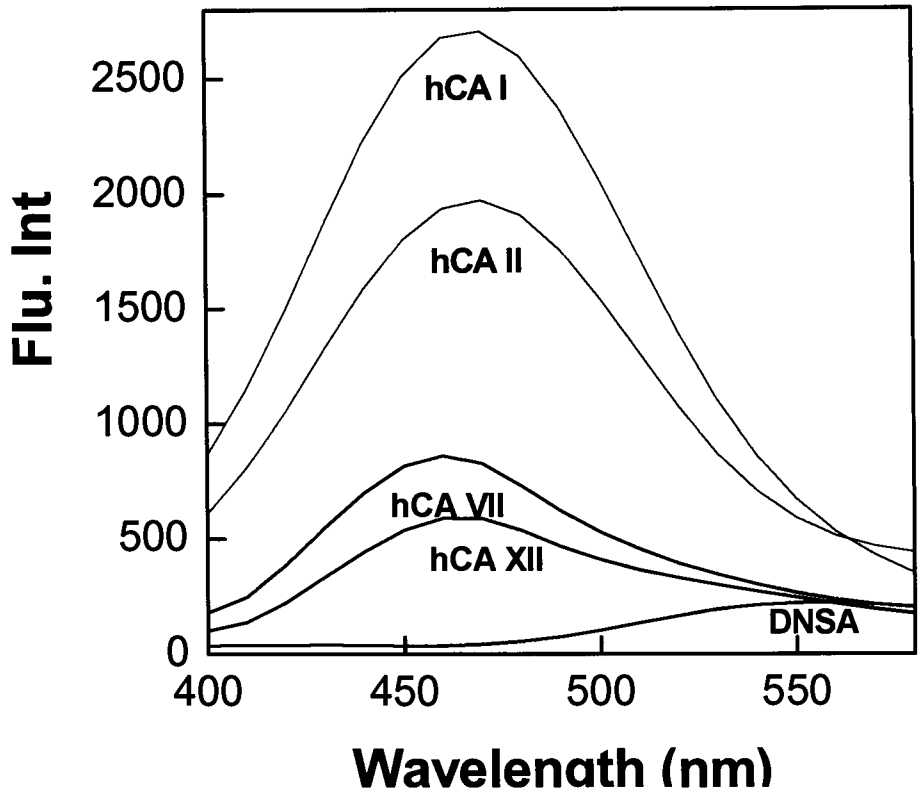

Figure 5.5. Fluorescence emission spectra of free and hCA bound DNSA.
The spectra of free DNSA and in the presence of hCA I, hCA II, hCA VII, hCA XII (λ_{ex} = 330 nm, λ_{em} = 400-600 nm) in 25 mM HEPES containing 10 % DMSO, pH 7.0 is shown. [DNSA] = 5 μM, [hCA] = 10 μM.

the presence of all hCA isozymes. These values are listed in Table 5.1. It is evident from the Table that except for hCA I, neither of the two lifetimes of DNSA are different between different hCA isozymes.

5.2.2. Fluorescence spectral features of JB2 compounds upon interaction with hCA isozymes

With the idea that fluorophores having extended structures could potentially interact with the distal (i.e., "entry") pockets, in addition to the active site residue of the enzymes,

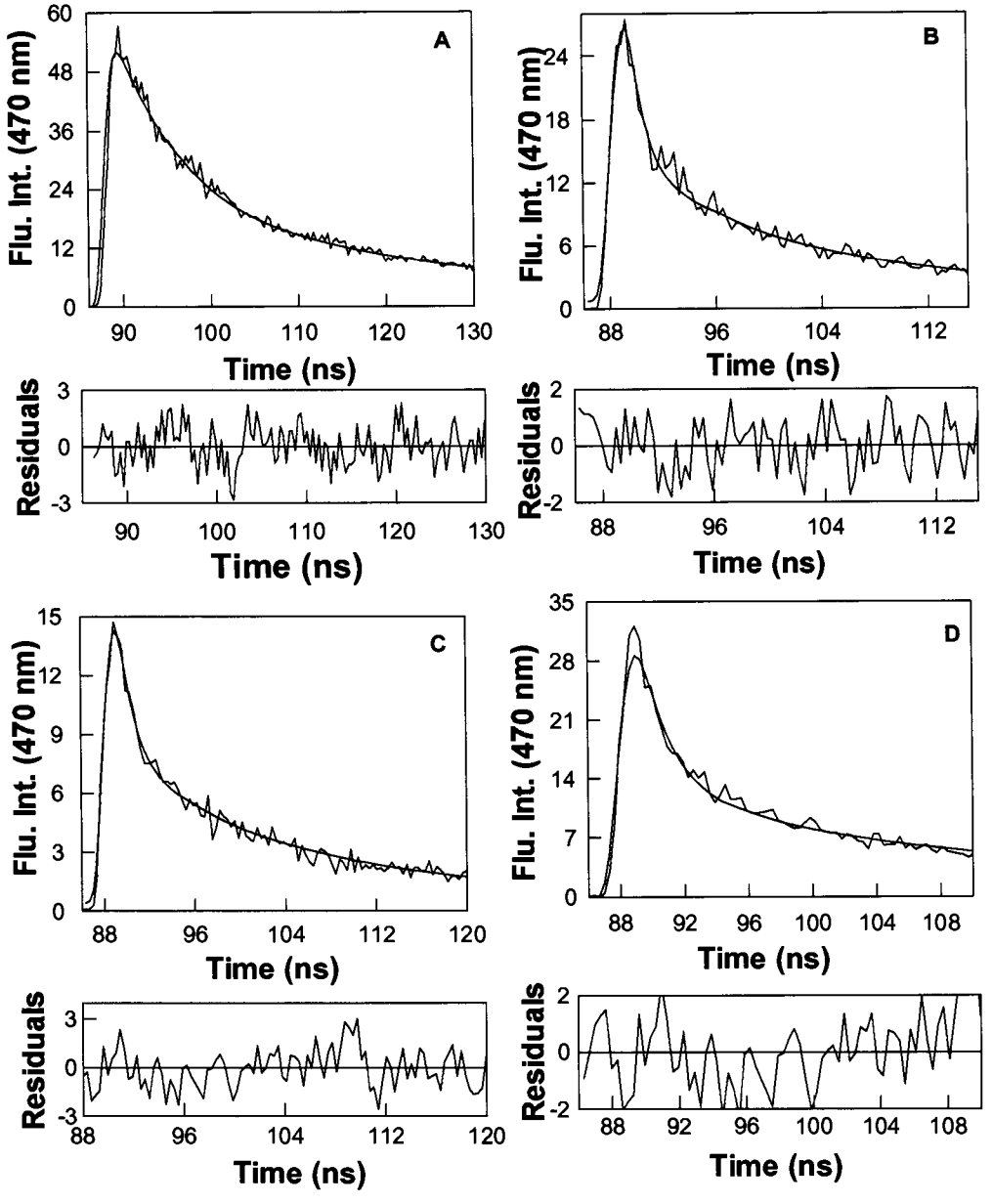

Figure 5.6. Fluorescence lifetime decay of DNSA bound to hCA isozymes.
The fluorescence lifetime decay profiles of DNSA (λ_{ex} = 340 nm, λ_{em} = 470 nm) bound to hCA I, hCA II, hCA VII, hCA XII and hCA sigma in 25 mM HEPES containing 10 % DMSO are shown in panels A, B, C, D and E respectively. The concentration of DNSA was maintained as 3 μM. [hCA I] = 15 μM, [hCA II] = 30 μM, [hCA VII] = 30 μM, [hCA XII] = 15 μM. The solid smooth lines are the best fit of the data for the double exponential rate equation with short (τ_1) and long (τ_2) lifetimes of 5.6 ± 0.66 and 17.53 ± 1.13 (Panel A), 0.9 ± 0.13 and 9.9 ± 0.26 (Panel B), 1.18 ± 0.13 and 13.84 ± 0.45 (Panel C), and 2.27 ± 0.84 and 17.27 ± 0.54 (Panel D) respectively. The residuals of the lifetime decays are shown at the bottom of each panel.

Table 5.1. Fluorescence lifetime of DNSA in the presence of hCA isozymes.

hCA isozyme	DNSA (τ_1) (ns)	DNSA (τ_2) (ns)
hCA I	5.6	17.5
hCA II	0.9	9.9
hCA VII	1.2	13.8
hCA XII	2.2	17.2
Sigma hCA	2.0	21

Summary of the lifetime data of DNSA (Figure 5.6) in the presence of hCA isozymes shows that DNSA exhibits similar lifetimes with all isozymes with the exception of hCA I. a series of newly synthesized fluorescence probes were prepared by derivatizing the amino group of aminonaphthalenesulfonamide with a variety of substituted benzaldehyde (ArCHO) moieties (*464*). The structures of these flurophores are depicted in Figure 5.7. As can be seen in the Figure, all the fluorescent probes have unsubstituted sulfonamides which enabled them to interact tightly with hCAs. Figure 5.8 depicts a model of the DNSA and probe JB2-48 in the active site pocket of hCA I. The modeling data shows that unlike its parent compound DNSA (which occupied only 1/3 of the enzyme's active site pocket) (*192*), JB2-48 filled nearly the entire (~15Å deep) hydrophobic pocket of hCA I. Hence, JB2-48 (and thus all similar probes) could be envisaged to experience "full" hydrophobicity of the enzyme's active site environment.

For all the experiments involving JB2 compounds, their stock solutions were prepared in 100 % DMSO and were diluted in required buffer solutions containing 10 % DMSO. In order to test the stability of JB2 compounds in 10 % DMSO at room

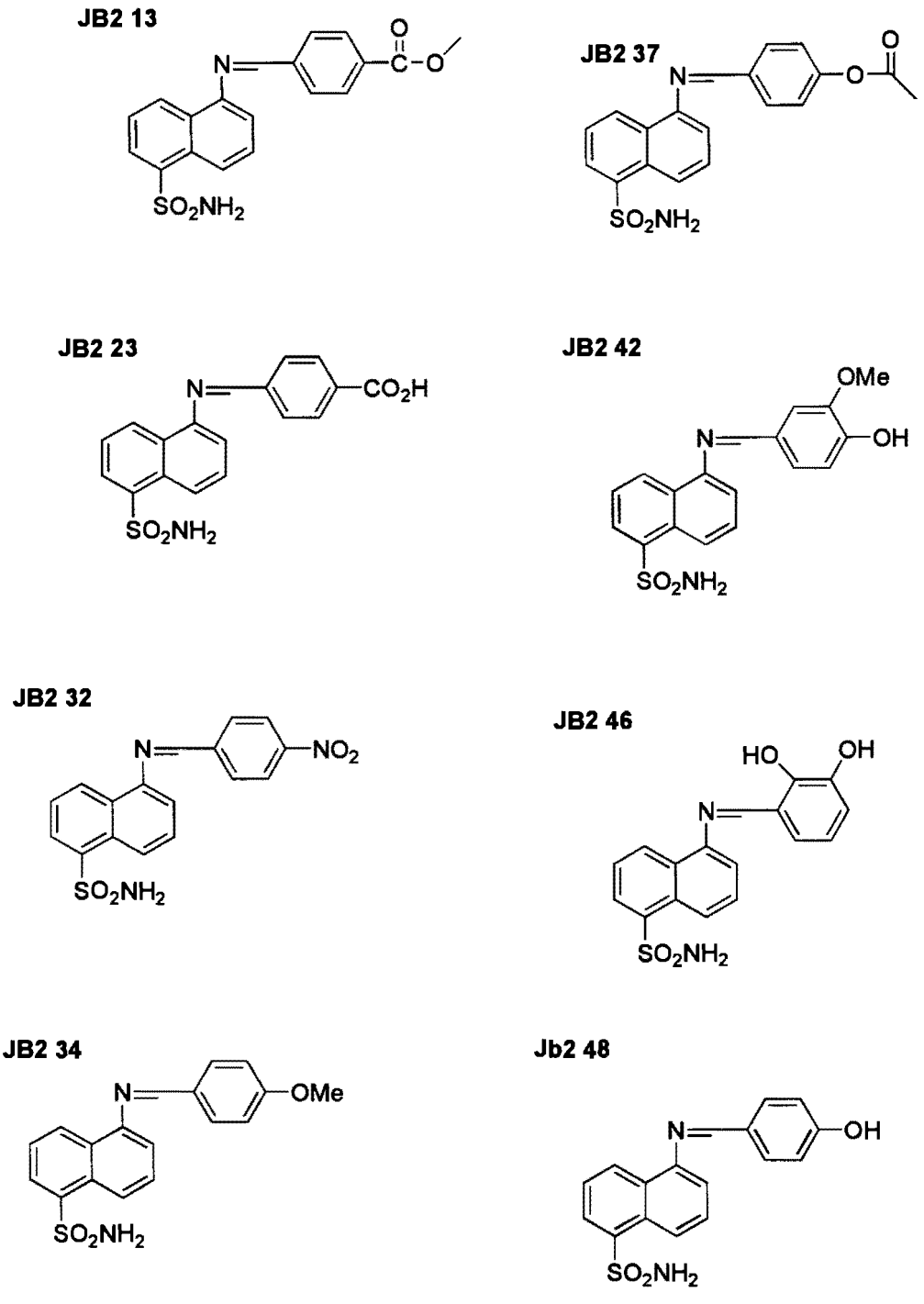

Figure 5.7. Structure of JB2 compounds

Figure 5.7. continued..

Jb2 52

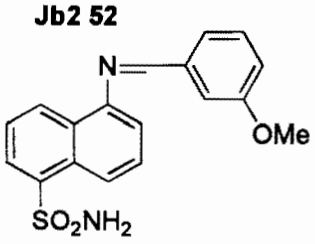

Jb2 53

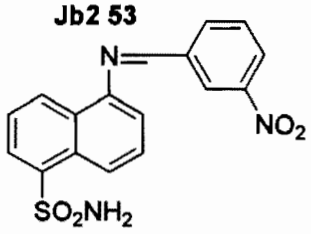

JB2 56

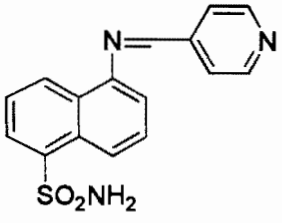

Jb2 57

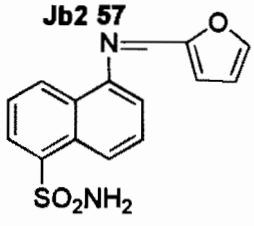

Jb2 65

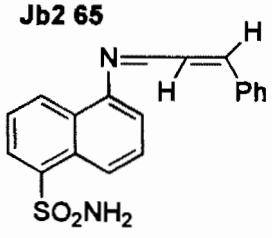

Jb2 66

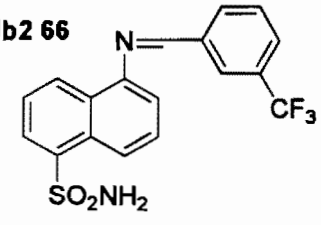

JB2 67

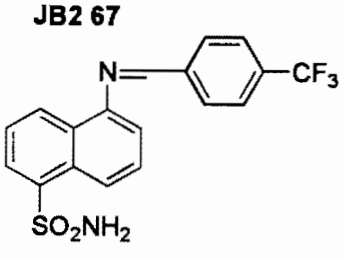

Jb2 76

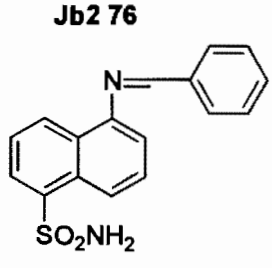

Figure 5.8. Comparison of the structures of hCA I-DNSA and hCA I-JB2-48 complex. Panel A shows the crystal structure of hCA I-DNSA complex (PDB ID: 1OKL) (192). The Figure was modeled using UCSF Chimera software. Panel B shows the molecular model of the occupancy of JB2-48 to the active site pocket of hCA I. The Figure was generated using Insight(98) software.

temperature, time dependent changes in UV-Vis spectra of JB2-48 was monitored. This was performed to ensure that the schiff base is not degraded into aldeheyde and amine over time in aqueous solution. The idea was that if the Schiff's base is hydrolyzed at a typical rate of 0.32 – 3.2 min^{-1} (*528*) , time dependent spectral changes will be observed. As is evident from Figure 5.9., no changes in the UV-Vis spectra of JB2-48 were observed for a period of 2 hours, attesting to the stability of these fluorophores in aqueous solutions with 10% DMSO.

In addition to testing the stability of the probes in the buffer solutions it was also necessary to determine whether the changes in fluorescence intensity of flurophores upon binding hCA isozymes (see Figure 5.11) originated from the binding of the parent (Schiff's base) compound or its hydrolyzed amine product. Toward this goal, stopped flow transient kinetic experiments were performed involving hCAs and JB2 compounds, JB2-46 and JB2-48. The enzyme and ligand were taken in separate syringes and the content of the syringes were mixed in the reaction chamber under high pressure, followed by monitoring the time dependent changes in the fluorescence of the ligand bound to hCA. As will be shown in next section (Figures 5.42, 5.44, 5.46, 5.48), the stopped flow trace for the binding of JB2-46 and JB2-48 with hCA isozymes under pseudo-first order condition yields rate constants which are at least 100 times faster than that expected for the rate of hydrolysis of the Schiff's base from aromatic aldehydes and aromatic amines (*528*). Clearly, the observed fluorescence changes associated with JB2-hCA interaction is a consequence of binding of the parent compound rather than its dissociated (hydrolyzed) amine product. In this regard, it should be pointed out that the sulfonamide moiety of the hCA inhibitors substituted with amino groups are poor inhibitors for CAs (particularly hCA II) (*340*). On the other hand

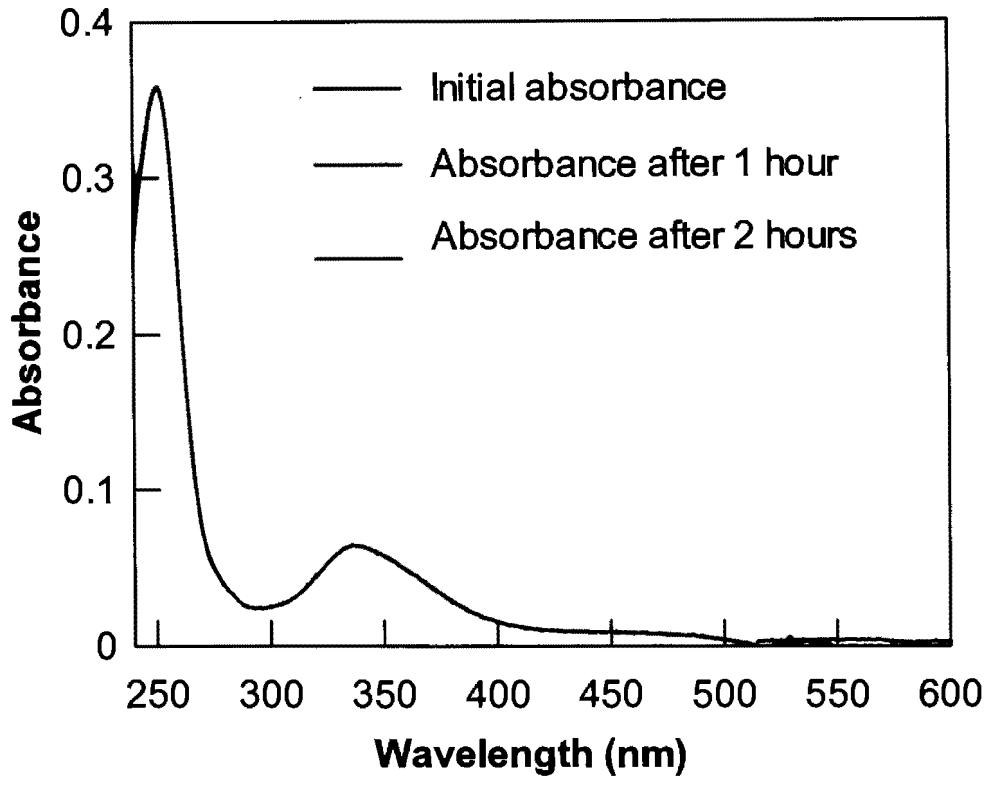

Figure 5.9. UV-Vis spectra of JB2-48 at different time intervals.
Absorption spectra of 5 μM JB2-48 in water containing 10% DMSO is shown at various time intervals (black: immediately after dissolution; red: after 1 h at room temperature; green: after 2 h at room temperature).

when the p-amino group is derivatized to form the amide moiety, its binding affinity increases by 1-2 orders of magnitude (*327*). Hence, even if a mixture of Schiff's base and free amine (albeit in low concentration) were present at equilibrium, the mass action would favor the binding of the Schiff's base (in preference to the amine derivative) to hCA II. Therefore, it was concluded that the observed fluorescence changes upon binding of probe JB2 probe to hCA isozymes is due to the binding of the parent compound and not its hydrolytic product. Based on these observations, it is clear that both free as well as the

enzyme bound form of the JB2 compound was fairly stable at the room temperature, and showed no evidence of degradation/hydrolysis during the course of any of the experiments reported herein.

Since all the experimental conditions required the use of 10 % DMSO to ensure the solubility of the compounds, it was of interest to know if this concentration of DMSO would have any effect on the catalytic activity of the enzyme. To probe this, the esterase activity of hCA I was monitored in the presence and absence of 10 % DMSO. From the analysis of the slope values of the data in Figure 5.10, it is evident that the effect of 10% DMSO on the catalytic activity of hCA I is insignificant (< 5 %).

As can be seen from Table 5.2, all of these probes have absorption maximum in the range of 330-370 nm. When the free forms of these probes (5 mM in 25 mM HEPES buffer, pH = 7.0, containing 10% DMSO) were excited at the wavelengths of their absorption maxima, most of the probes showed very weak fluorescence emission intensity. However, the fluorescence emission intensities of these probes were markedly enhanced in the presence of hCA isozymes. Representative emission spectra of one of the probes (JB2-48) in its free and the enzyme bound form are shown in the Figure 5.11. Comparison of the fluorescence profiles of free versus enzyme bound probes reveals that the emission intensities of the free probes are quenched in the aqueous solution. However, this is not a self-quenching process, since increasing the concentration of the probes in buffer solution resulted in proportional increase in the emission intensity. It is evident from the Figure that the emission maxima of JB2-48 is shifted from 528 nm to 470 nm in the presence of enzyme.This is in contrast to the emission maximum of the enzyme-bound DNSA as being

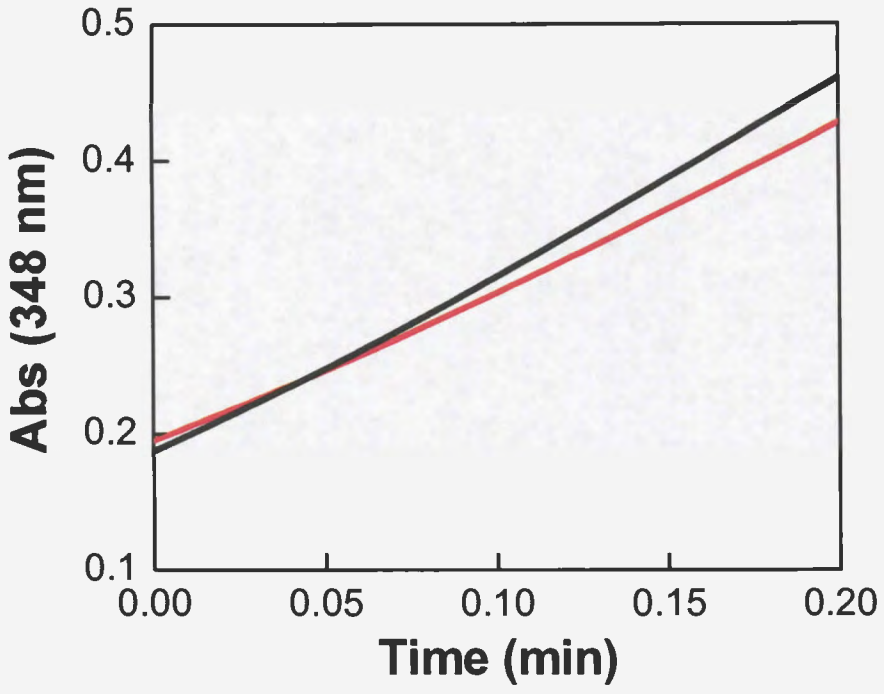

Figure 5.10. Comparison of the time courses of carbonic anhydrase catalyzed reaction in the absence and presence of DMSO.
The initial rate of hydrolysis of p-NPA by hCA I at 348 nm was measured in the absence (black) and presence (red) of 10% DMSO. [hCA I] = 2 μM, [p-NPA] = 1 mM. The initial rate of the reaction in the presence and absence of 10 % DMSO was found to be 59.5 milli units min^{-1} and 57 milli units min^{-1} respectively.

equal to 458 nm (*329*). In addition, the quantum yield of the enzyme bound JB2-48 (as compared to the free ligand) is increased by about 40 fold, and this feature allowed us to easily differentiate between the free versus the enzyme bound form of the ligand via spectrofluorometric and transient kinetic approaches (see below).

Table 5.2 shows the quantum yields of the free and enzyme bound fluorophores. As is evident from the Table, several of the fluorescent probes exhibited significant enhancements in quantum yields when bound to the enzymes. Infact, JB2-34, JB2-37, JB2-42, JB2-46, JB2-48, JB2-52, JB2-53, JB2-56, JB2-57 and JB2-76 exhibited muc

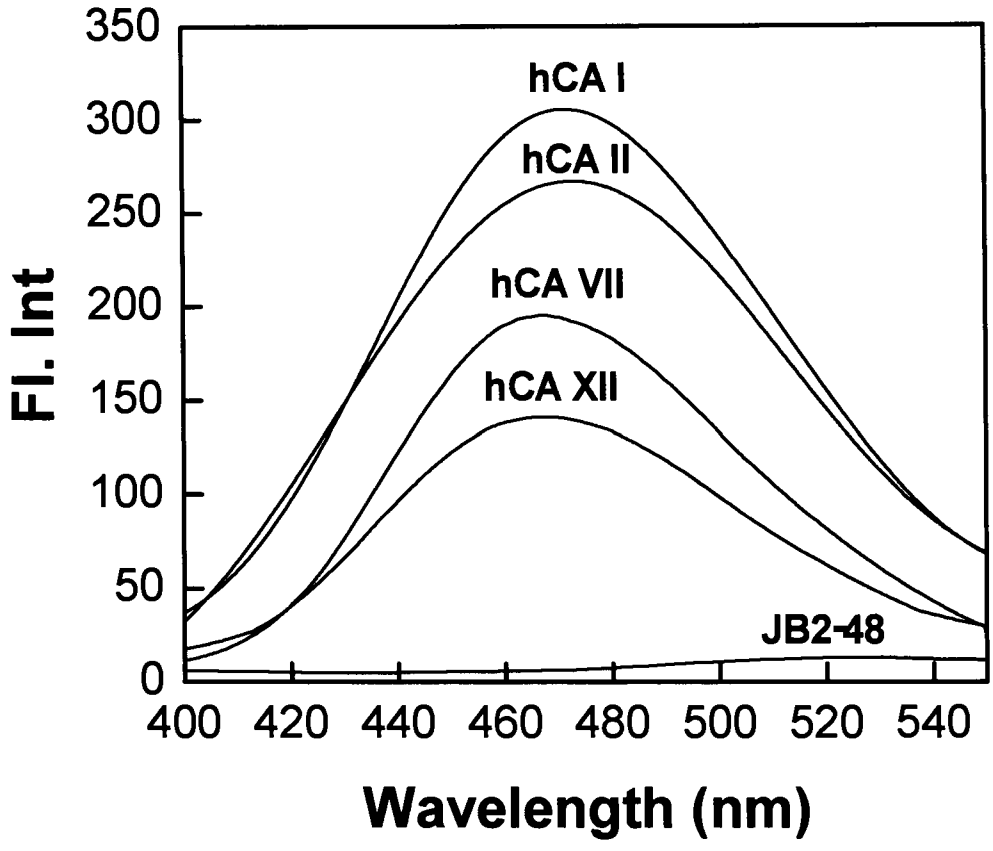

Figure 5.11. Fluorescence emission spectra of free and hCA bound JB2-48.
The spectra of free JB2-48 and in the presence of hCA I, hCA II, hCA VII, hCA XII (λ_{ex} = 336 nm, λ_{em} = 400-600 nm) in 25 mM HEPES containing 10 % DMSO, pH 7.0 is shown. [JB2-48] = 5 μM, [hCA] = 10 μM.

higher enhancements compared to that observed for DNSA. Another thing that needs to be mentioned here is the low background exhibited by these flurophores. In fact, the emission intensity of JB2-65 and JB2-66 in aqueous solution was too low to determine their quantum yield. In contrast, these compounds were highly fluorescent in the presence of hCA isozymes. Of all the probes used, where as JB2-23 and JB2-76 showed higher enhancements in quantum yield upon binding with hCA I as compared to that of hCA II, JB2-34 and JB2-57 showed higher enhancements with hCA VII compared to hCA I and II.

Other probes showed either slightly higher quantum yields with hCA II or nearly equal enhancements in the quantum yields with all the isozymes.

Of different fluorescent probes of Table 5.2, the quantum yield of enzyme bound JB2-48 was found to be much higher. Due to its low background and high quantum yield, the above fluorophore was considered ideal for undertaking fluorescence based studies in the presence f hCA isozymes. Toward this goal, the fluorescence lifetime properties of JB2-48 (λ_{ex} = 340 nm, λ_{em} = 470 nm) were investigated in the presence of hCA isozymes. Figure 5.12 shows the fluorescence decay profiles of JB2-48 bound to hCA I (panel A), hCA II (panel B), hCA VII (panel C) and hCA XII (panel D). The fluorescence lifetime values of enzyme bound JB2-48 are listed in Table 5.3. It is evident from the lifetime values listed in Table 5.1 and 5.3, that both DNSA and JB2-48 exhibited two lifetimes when bound to the enzyme, however unlike DNSA, the shorter lifetimes of JB2-48 are different with different hCAs showing that the isozymes could be selectively identified based on their lifetimes when bound to JB2-48.

5.2.2.1. Investigation of the contributions of hydrophobic and electrostatic interactions of ligand structures in stabilizing the enzyme-ligand complexes

It is well known that the aliphatic sulfonamides do not serve as potent inhibitors of carbonic anhydrases (*65*, *529*) and that the wide active site pocket of the enzyme needs to be occupied by bulky (viz., aromatic) groups of the ligand structures. Based on the structure-activity relationship, it has been apparent that both sulfonamide and aromatic moieties of ligands contribute to the overall binding energy of carbonic anhydrase-ligand complexes (*530-532*). However, no systematic studies have been conducted to assess the contributions of hydrophobic and electrostatic interactions of ligand structures in stabilizing the corresponding enzyme-ligand complexes.

Table 5.2. Comparison of the quantum yields of DNSA and JB2-48, free and bound to hCA isozymes.

Probes	λ_{abs}	λ_{em}	QY_{free}	$Q.Y_{CAI}$ bound probe	$Q.Y_{CAII}$ bound probe	$Q.Y_{CAVII}$ bound probe	$Q.Y_{hCA\ XII}$ bound probe	$Q.Y_{CAI}$ bound probe/ QY_{free}	$Q.Y_{CAII}$ bound probe/ QY_{free}	$Q.Y_{CAVII}$ bound probe/ QY_{free}	$Q.Y_{CAXII}$ bound probe/ QY_{free}
JB2-13	342	521.9	0.011	0.016	0.011	nd	nd	1.4	1.01	nd	nd
JB2-23	342	516.2	0.00097	0.022	0.013	0.0081	nd	22.4	13.3	8.4	nd
JB2-32	358	528.1	0.0013	0.016	0.010	0.0055	nd	12.	7.9	4.2	nd
JB2-34	330	519.2	0.00044	0.013	0.024	0.033	nd	30.7	55.2	75	nd
JB2-37	333	521.8	0.00094	0.044	0.062	0.033	nd	47.2	66.8	35	nd
JB2-42	342	519.6	0.0007	0.020	0.017	0.016	nd	28.4	23.9	23	nd
JB2-46	330	525.7	0.00092	0.036	0.045	0.013	0.005	39.5	49.2	14	5.4
JB2-48	336	527.7	0.0034	0.14	0.144	0.077	0.06	40.9	42.3	22	17.7
JB2-52	330	524.8	0.00090	0.07	0.064	0.033	nd	77.6	70.0	36	nd
JB2-53	330	528.1	0.0014	0.073	0.077	0.026	nd	53.1	55.8	19	nd
JB2-56	330	518.1	0.0025	0.116	0.107	0.037	nd	45.6	41.9	14	nd
JB2-57	330		0.00025	0.011	0.015	0.031	nd	47.7	60.5	127	nd
JB2-65	352	-	0	0.002	0.003	0.0058	nd	nd	nd	nd	nd
JB2-66	333	-	0	0.018	0.015	0.03	nd	nd	nd	nd	nd
JB2-67	336	526	0.0020	0.042	0.063	0.02	nd	20.4	30.1	11	nd
JB2-76	330	525.4	0.0023	0.073	0.041	0.035	nd	31.1	17.5	15	nd
Dansylamide	330	532.4	0.027	0.730	0.314	0.11	0.077	26.9	11.6	4.2	2.86

nd: not detected.

As JB2-48 has two ionizable groups (viz., the sulfonamide group of the naphthalene ring and the phenolic hydroxyl group), it was of interest to determine their pK_as and how they change in the presence of enzyme. In this endeavor, it was noted that the absorption maximum of JB2-48 increases at 336 nm as a function of the pH of the solution. In order to determine the pKa of JB2-48, the absorbance of a fixed concentration of JB2-48 (3 μM) was monitored as a function of the pH of the buffer medium. The absorbance was then plotted as a function of the pH value (Figure 5.13, panel A). and was analyzed according to the Henderson-Hasselbalch equation (solid smooth line) for two pK_a values of 6.5 and 10.2, respectively. Given that the pK_a value of sulfonamide group in "aqueous" benzenesulfonamide is 9.79 (*387*), the experimentally determined pK_a's of 6.5 and 10.2 were ascribed to the phenolic hydroxyl group and the sulfonamide moiety of JB2-48, respectively.

In order to determine how the pK_a of JB2-48 is altered in the presence of hCA I, fluorescence spectral changes of hCA I- JB2-48 complex was monitored as a function of pH of the buffer medium. The inset of Figure 5.13, panel B shows the representative fluorescence emission spectra (λ_{ex} = 336 nm) of the enzyme bound JB2-48 at pH 5.0 and 9.0. The data of Figure 5.13 reveals that the fluorescence emission intensity of the enzyme bound JB2-48 at pH 5.0 is significantly lower than that observed at pH 9.0. Panel B of Figure 5.13 shows the pH dependent changes in the fluorescence emission intensity of the enzyme-JB2-48 complex. The solid smooth line is the best fit of the data according to the Henderson-Hasselbalch equation for the pK_a value of 6.6. The latter value is similar to the pK_a derived from the pH dependent changes in the binding of DNSA with hCA I (pK_a = 6.3) and hCA II (pK_a = 6.4) (*329*).

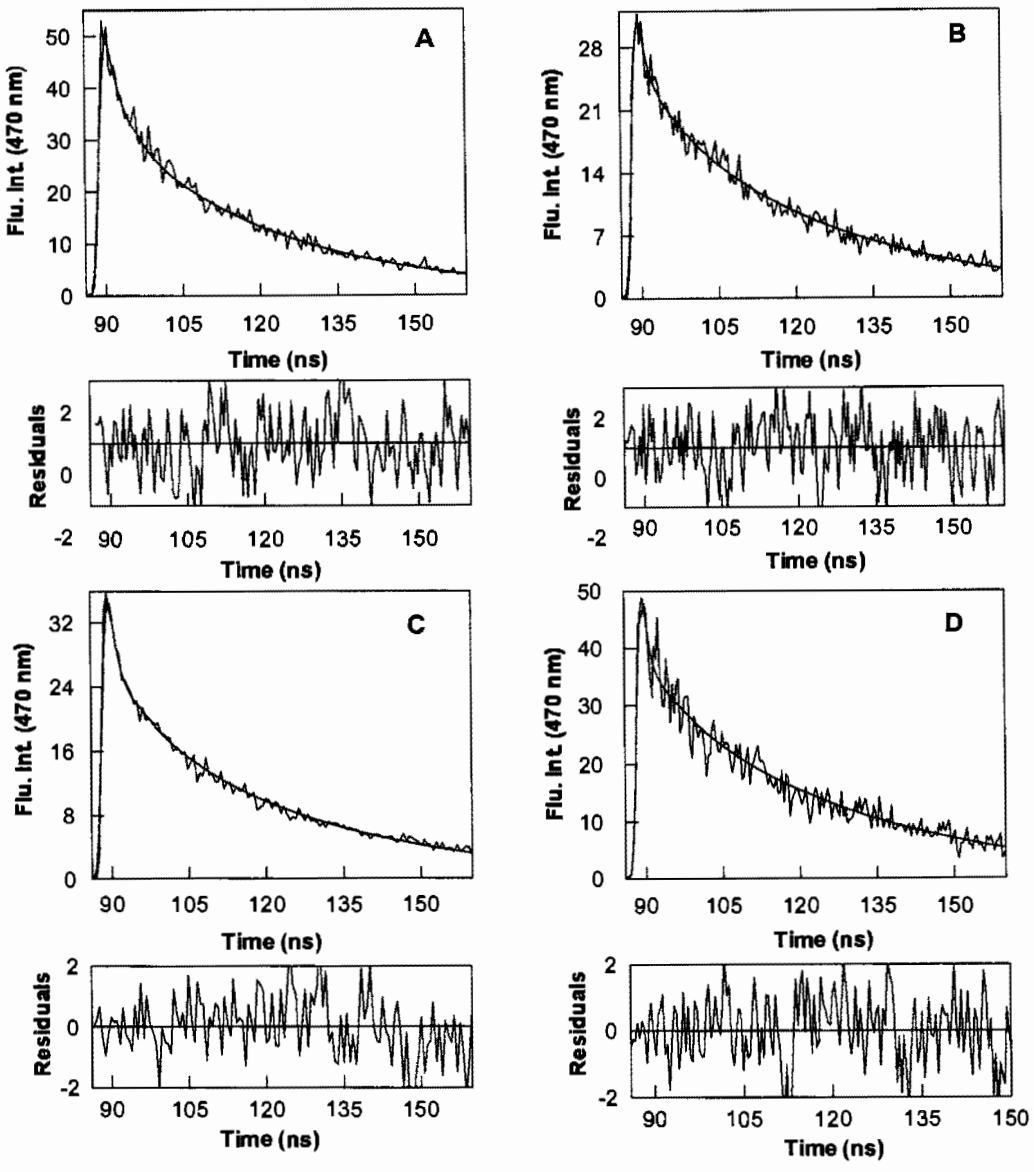

Figure 5.12. Fluorescence lifetime decay of JB2-48 bound to hCA isozymes.
The fluorescence lifetime decay profiles of JB2-48 (λ_{ex} = 340 nm, λ_{em} = 470 nm) bound to CAI, CAII, CAVII, hCA XII and hCA sigma in 25 mM HEPES containing 10 % DMSO are shown in panels A, B, C, D and E respectively. The concentration of JB2-48 was maintained as 4 μM. [CAI] = 50 μM, [CAII] = 50 μM, [CAVII] = 15 μM, [hCA XII] = 15 μM, [hCA sigma] = 50 μM. The solid smooth lines are the best fit of the data for the double exponential rate equation with short (τ_1) and long (τ_2) lifetimes of 13 ± 1.2 and 29.4 ± 3.8 (Panel A), 1.3 ± 0.4 and 23.5 ± 0.37 (Panel B), 2 ± 0.16 and 22.58 ± 0.1 (Panel C), 0.72 ± 0.28 and 25.6 ± 0.44 (Panel D) and 6.62 ± 1 and 25.3 ± 0.64 (Panel E) respectively. The residuals of the lifetime decays are shown at the bottom of each panel.

Table 5.3. Lifetime of JB2-48 in the presence of hCA isozymes.

hCA isozyme	JB-2-48 (τ_1) (ns)	JB-2-48 (τ_2) (ns)
hCA I	13	29.4
hCA II	1.3	23.5
hCA VII	2	22.5
hCA XII	0.72	25.6
Sigma hCA	6.6	25.3

Summary of the lifetime data of JB2-48 (Figure 5.12) in the presence of hCA isozymes is shown. Note that the shorter lifetime of JB2-48 is different in presence of different hCA isozymes.

On comparison of the titration results of Figures 5.13 A and B, it appears evident that the coordination of sulfonamide group of JB2-48 with the active site resident Zn^{2+} of hCA I (forming a Lewis acid-base pair) decreases its pK_a value by about 3 units. This is in accord with the widespread view that at neutral pH, the Zn^{2+} cofactor electrostatically interacts with the negatively charged nitrogen of aryl sulfonamide ligands in different isoforms of carbonic anhydrases (*204*, *277*, *278*, *533*) though the above coordination is also likely to decrease the pK_a value of the phenolic hydroxyl group of JB2-48 (due to an extended conjugation in the entire molecule), we could not reliably ascertain its magnitude. However, such a decrease is unlikely to be significant since the enzyme bound form of JB2-48 yields only one pK_a of 6.6. Hence, the pK_a of phenolic hydroxyl group of JB2-48 (in the enzyme bound form) remains unresolved from that given by the protonation/deprotonation of the sulfonamide moiety. It should be reiterated that the

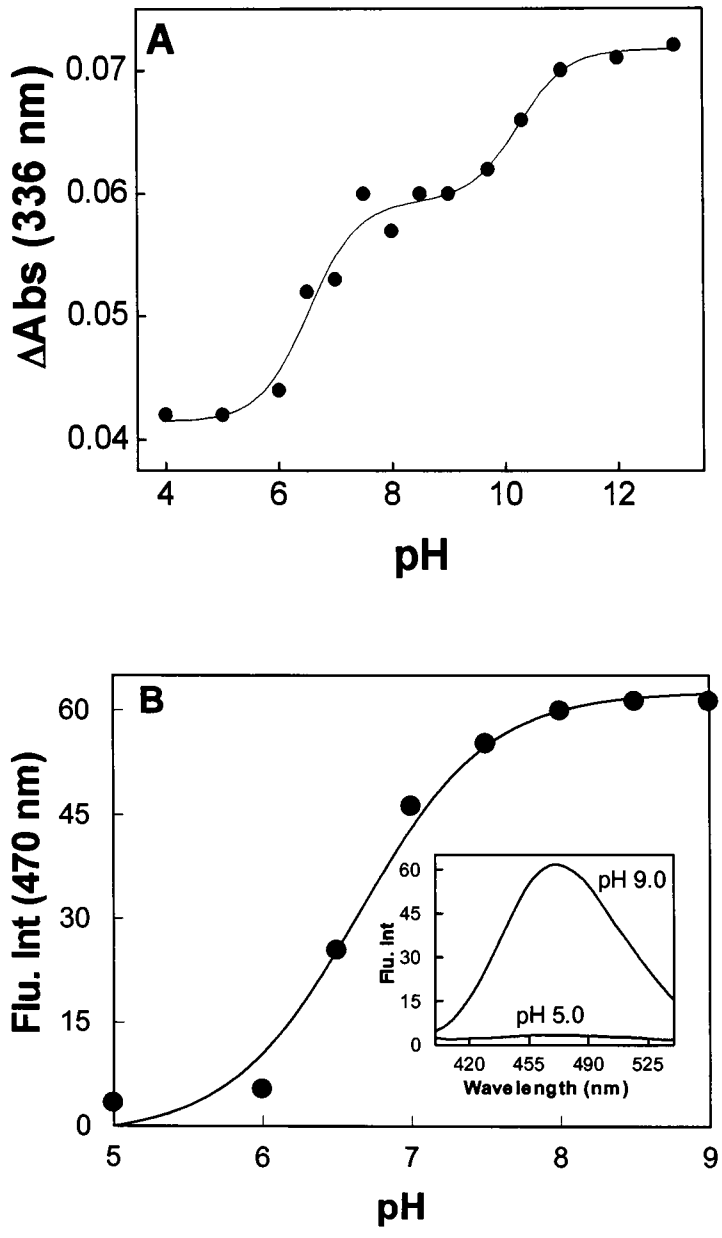

Figure 5.13. pK_a determination of free and hCA I bound JB2-48.
Panel A shows the absorbance of JB2-48 (3 μM) at 336 nm as a function of pH. The solid smooth line is the best fit of the data according to the modified form of HH equation yielding the pK_a values of 6.5 and 10.2 Panel B shows the pH-dependent changes in the fluorescence emission profile of the hCA I bound JB2-48. The main Figure shows the increase in fluorescence emission intensity of the enzyme bound JB2-48 (λ_{ex} = 336 nm, λ_{em} = 470 nm) as a function of pH. [hCA I] = 10 μM, [JB2-48] = 3 μM. The solid line is the best fit of the data according to the HH equation for the pKa value of 6.6 ± 0.1. The inset

shows the representative emission spectra of the enzyme bound JB2-48 complex at pH 5.0 and 9.0.
sulfonamide moiety of DNSA fluorophore (which is devoid of the phenolic hydroxyl group) also shows the pK_a of 6.3 when bound to hCA I (*329*). Irrespectively, a comparative account of the pK_a values of JB2-48 in free and the enzyme bound forms clearly attests to the fact that the sulfonamide as well as phenolic hydroxyl groups of the enzyme bound fluorophore remain fully protonated and deprotonated (ionized) at pH values 5.0 and 9.0, respectively, and at these pH extrema, the enzyme bound fluorophore exhibits minimum and maximum fluorescence intensities, respectively.

As many experiments involved pH dependent interaction of hCA I and JB2-48, it was considered whether or not the enzyme was active at different pH values, particularly under acidic conditions. To test this, 30 μM hCA I was incubated in acetate buffer, pH 5.0 for 1 hour at 4 ° C and then diluted 10 fold in 25 mM HEPES containing 10 % DMSO, pH 7.0 to measure its activity. As a control, 30 μM hCA I was incubated in HEPES buffer, pH 7.0 for 1 hour at 4 ° C and then diluted 10 fold in 25 mM HEPES containing 10 % DMSO, pH 7.0 to measure its activity. The activity of hCA I in the former (after incubating in a 25 mM acetate buffer, pH 5.0) and the later case (after incubating in a 25 mM HEPES buffer, pH 7.0) was found to be 33.6 and 34 milli units min^{-1} respectively suggesting that almost 98 % of hCA I remained active even after subjecting it to pH 5.0 for 1 hour. This confirmed that at this pH extreme, the catalytic activity of the enzyme remains unaffected during the time regime of all spectral, kinetic, and thermodynamic studies reported in this as well as in subsequent sections.

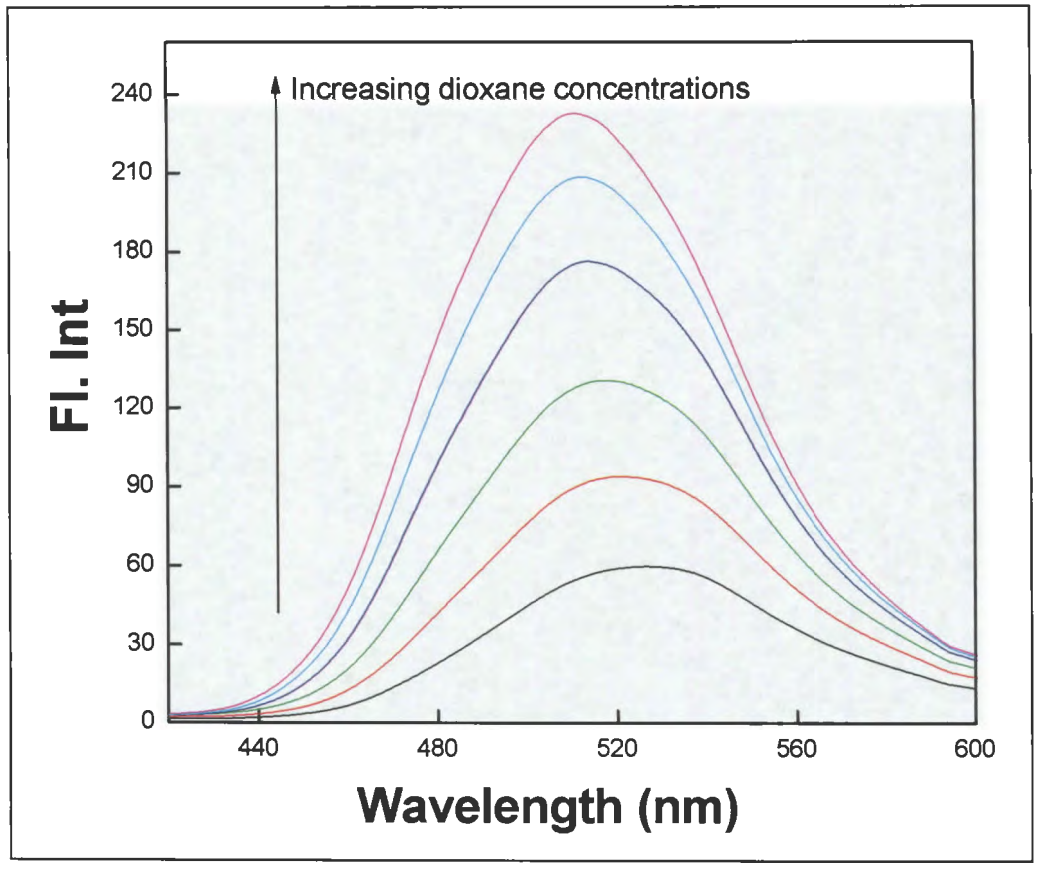

Figure 5.14. Emission spectra of JB2-13 in the presence of increasing concentrations of dioxane.
The emission intensities of 5 μM JB2-13 (λ_{ex} = 336 nm) in 25 mM aqueous HEPES buffer, pH 7.0.containing varying amounts of added dioxane are shown. The percentages of added dioxane are as follows: black- no dioxane, red- 9 % , green- 16 %, blue -23 %, cyan - 28 %, pink- 33 %

Table 5.4. Quantum yield of JB2-13 at different dioxane concentrations.

% dioxane	Qantum yield of JB2-13
0	0.007
9	0.012
16	0.019
23	0.028
28	0.036

33	0.043

Both structural as well as isothermal titration microcalorimetric (ITC) data for the binding of ligands to hCA I revealed that the active site pocket of the enzyme is predominantly hydrophobic (*203*, *309*). Therefore, the question arose whether the enhancements in the fluorescence quantum yields of the JB2 probes upon binding to hCA isozymes were due to changes in polarity of the solvent media. To probe this, the fluorescence emission spectra and quantum yields of one of those probes (JB2-13) in 25 mM HEPES buffer (pH = 7.0) as a function of increasing concentration of added dioxane (Fig. 5.14, Table 5.4) was determined. Note that as the hydrophobicity of the solvent medium increases, thefluorescence emission intensity as well as the quantum yield keep on increasing. In addition the emission maximum shifts from 523 nm to 510 nm.

In addition to JB2-13, the fluorescence emission spectra of JB2-48 was also monitored as a function of added dioxane concentration (from 0 to 90%) to probe as to the extent such hydrophobicity modulates the fluorescent properties of the enzyme bound JB2-48. Since 10% DMSO was used to solubilize the fluorophore, it was only possible to maintain the concentration of dioxane between 0 to 90%. As shown in Table 5.5 and Figure 5.15, as the concentration of dioxane increases, the fluorescence emission maximum of JB2-48 progressively shifts to blue. Clearly, the hydrophobicity of the active site pockets of hCA is responsible, at least in part, for the enhanced quantum yields and the blue shift in the emission maximum of the fluorescent probes in Table 5.2. However, the contribution of active site resident Zn^{2+} ion to the enhancement of the emission intensity could not be ascertained due to precipitation of Zn^{2+} - free (apo) hCA II in the presence of the parent compound DNSA. As sulfonamides are known to be weak binders of Zn^{2+} ions in solution,

it was not expected that the fluorescence emission spectra of the probes to be modulated by Zn^{2+} ions in aqueous solution. However, to confirm this expectation, a fixed concentration of JB2-46 was titrated with increasing concentrations of $ZnSO_4$. Poor solubility of $ZnSO_4$ in HEPES buffer at pH = 7.0 prevented deciphering the fluorescence spectra of the probes in the presence of various concentrations of Zn^{2+} ions at the above pH. Figure 5.16 shows the fluorescence emission spectra of JB2-46 (5 μM, λ_{ex} = 336 nm) in the absence (black trace) and presence of 25 mM (red trace) and 50 mM (blue trace) $ZnSO_4$ in water containing 10% DMSO. Clearly, the binding of Zn^{2+} to the probe does not produce spectral shifts or emission intensity increases as observed upon binding to hCAs. Hence, it is believed that the fluorescence spectral changes upon binding of different fluorophores to hCAs originated from a combined effect of the hydrophobicity of the active site pocket as well as the electronic contribution of Zn^{2+} at the sulfonamide binding region of the enzyme (see below).

To ascertain the effect of dioxane on the fluorescence lifetimes of JB2-48, experiments were performed at different concentrations of dioxane. It was observed that at all concentrations of dioxane, the excited state decay profile of JB2-48 (λ_{ex} = 340 nm, λ_{em} = 470 nm) conforms to a single lifetime with increasing magnitude as a function of the above solvent (Figure 5.17 and Table 5.5). This feature is consistent with the observation that the fluorescence emission intensity of the fluorophore increases with increase in the dioxane concentration. It should be pointed out that due to solubility issues, the above experiments could not be performed in different solvents to ascertain the contributions of hydrogen bonding and/or other microenvironment effect on the spectral features of JB2-48.

After determining the lifetimes of JB2-48 as a function of dioxane concentration, it

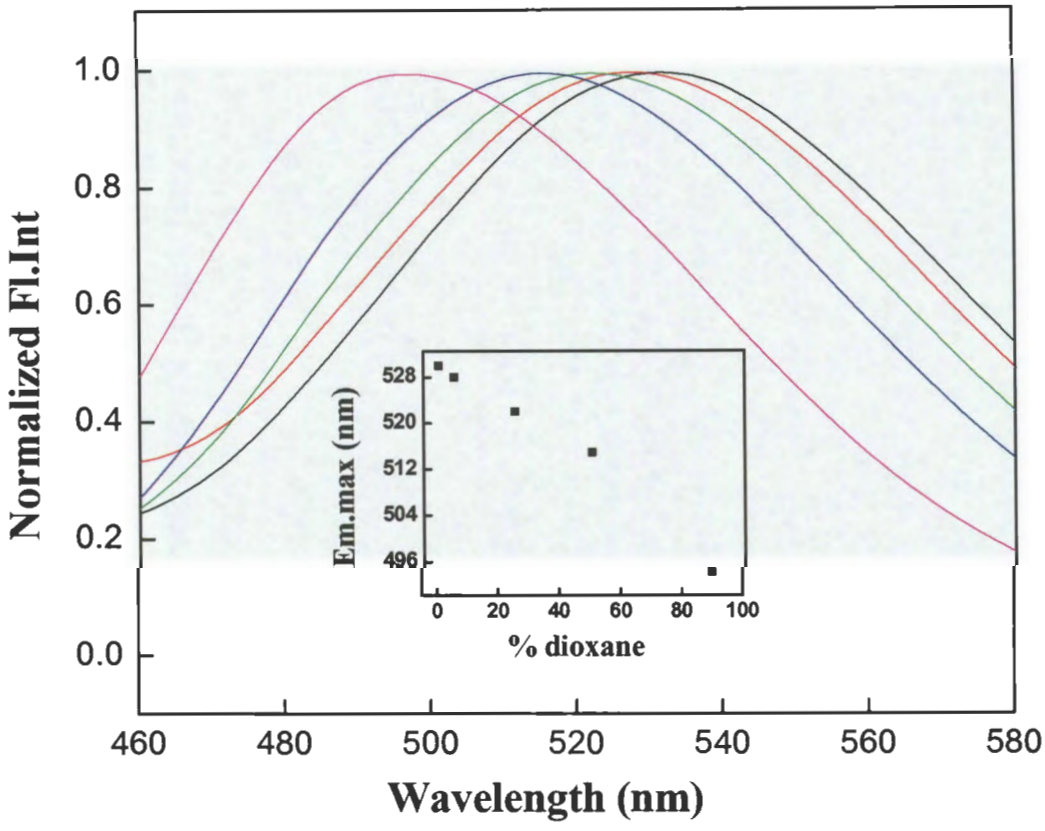

Figure 5.15. Fluorescence emission spectra of JB2-48 as a function of dioxane concentration.

The fluorescence emission spectra of JB2-48 (10 μM) as a function of dioxane concentration are shown. The spectrum of JB2-48 in 0 % ($\lambda_{em.\ max}$ = 528 nm), 5 % ($\lambda_{em.\ max}$ = 526 nm), 25 % ($\lambda_{em.\ max}$ = 522 nm), 50 % ($\lambda_{em.\ max}$ = 515 nm) and 90 % ($\lambda_{em.\ max}$ = 494 nm) dioxane are shown in black, red, green, blue and pink colors respectively. The excitation maximum was kept at 336 nm. The inset Figure shows the dependence of the emission maxima of JB2-48 on dioxane concentration.

was of intereset to ascertain what concentration of dioxane qualitatively mimics the hydrophocity of the enzyme's active site pocket. In this endeavor, the fluorescence lifetimes of the enzyme bound JB2-48 at neutral (pH 7.0), acidic (pH 5.0), and alkaline (pH 9.0) pH values were determined. By coincidence, it was noted that the fluorescence

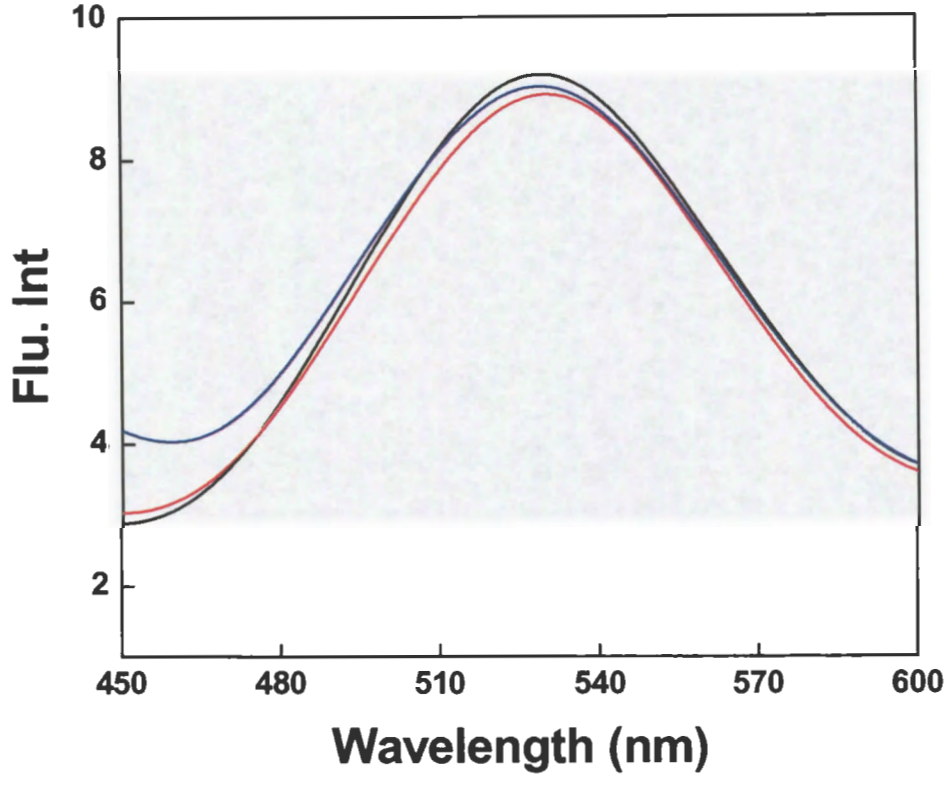

Figure 5.16. Fluorescence emission intensities of JB2-48 at different zinc concentrations. Fluorescence emission intensities of JB2-48 (5 μM, λ_{ex} = 336 nm) in the absence (black) and presence of 25 mM (red) and 50 mM (blue) $ZnSO_4$ in water containing 10% DMSO.

lifetime of JB2-48 in 90% dioxane (12.5 ± 0.1 ns; Table 5.5) was similar to the shorter lifetime of the enzyme bound fluorophore at pH 7.0 (see below). Figure 5.18 represents a comparative account of fluorescence decay profiles of JB2-48 bound to hCA I at pH 7.0 (panel A), pH 5.0 (panel B), and pH 9.0 (panel C). A comparison of the lifetime data of Figure 5.18 revealed that unlike the excited state decay profile of JB2-48 in the presence of 90% dioxane (conforming to the single lifetime profile of 12.5 ns), the hCA I bound form the fluorophore at pH 7.0 yields two lifetimes of 13.5 and 27.3 ns, respectively. Clearly,

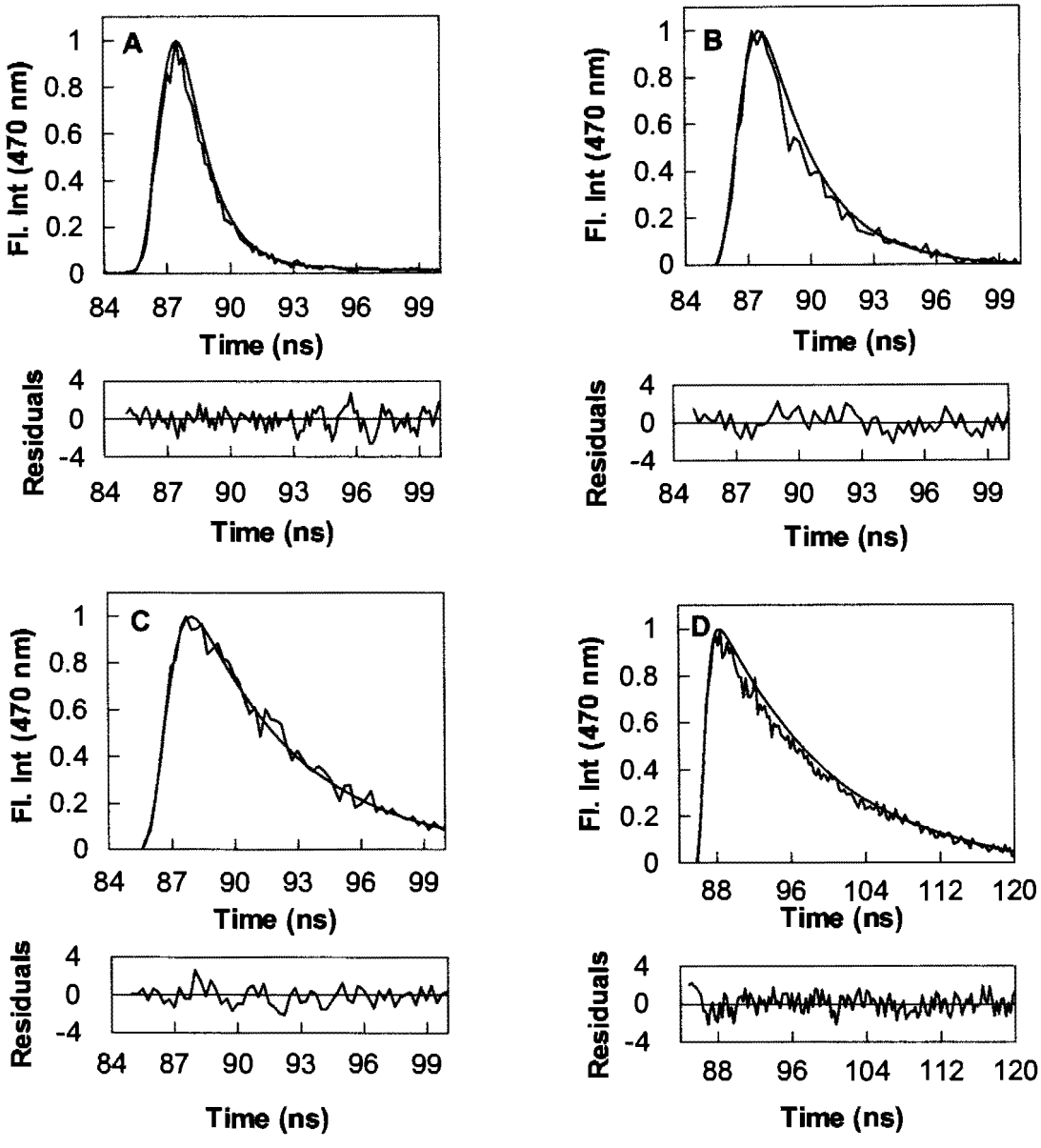

Figure 5.17. Effect of dioxane concentration on the fluorescence lifetimes of JB2-48 at 25 ° C.

Normalized fluorescence decay profiles of JB2-48 (λ_{ex} = 340 nm; λ_{em} = 470 nm) under different dioxane concentrations are presented. The solid smooth lines are the best fit of the data with the lifetime values as follows. Panel A – 0 % dioxane , τ = 1.2 ± 0.02 ns, Panel B – 25% dioxane (τ) = 2.4 ± 0.05ns; Panel C –50 % dioxane (τ) = 4.9 ± 0.09 ns; panel D - 75 % dioxane (τ) = 8.4 ± 0.1 ns and Panel E – 90 % dioxane (τ) = 12.5 ± 0.1 ns

Table 5.5. Fluorescence emission maxima and lifetimes of JB2-48 in dioxane

% Dioxane	Emission Maxima (nm)	Lifetime (ns)
0	528	1.2 ± 0.02
25	522	2.4 ± 0.05
50	515	4.9 ± 0.09
75	nd	8.4 ± 0.1
90	494	12.5 ± 0.1

All solutions contained 10% DMSO. λ_{ex} = 336 for determining emission maxima and 340 nm (LED source) for determining lifetimes. nd – not determined.

JB2-48 does not experience identical microscopic environment in 90% dioxane vis a vis that present at the active site pocket of hCA I at the neutral pH. However, since the shorter lifetime of the fluorophore in the presence of the enzyme (13.5 ns) is similar to that observed in the presence of 90% dioxane (12.5 ns), it was surmised that the shorter lifetime component is given by the microscopic state of the enzyme which harbors the protonated (i.e., non-ionic) form of the sulfonamide moiety of JB2-48. To test this hypothesis, the lifetime profiles of hCA I-JB2-48 complex at neutral pH with those determined at low (pH = 5.0; Figure 5.18B) and high pH (pH = 9.0; Figure 5.18C) values were compared. Such comparison revealed that unlike at neutral pH, the excited state fluorescence decay traces at low and high pH values conformed to single lifetimes with magnitudes of 14 and 20 ns, respectively. Note that the latter values are similar to the shorter (13.5 ns) and longer (27.3 ns) lifetime components for the excited state decay data of the enzyme bound JB2-48 at pH

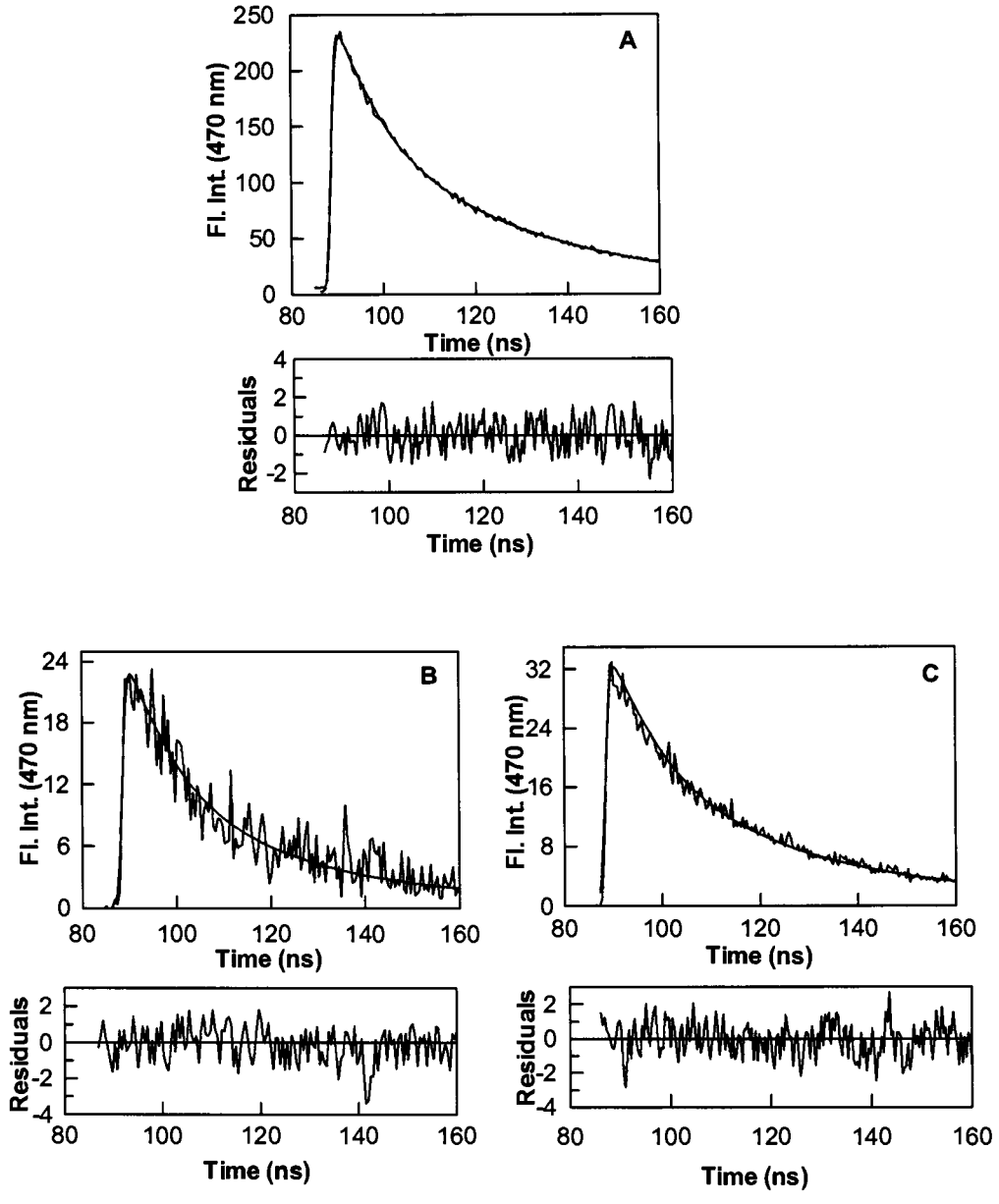

Figure 5.18. Effects of pH on the fluorescence lifetimes of hCA I bound JB2-48.
The excited state fluorescence decay profiles of JB2-48 –hCA I (λ_{ex} = 340 nm; λ_{em} = 470 nm) under different experimental conditions are presented. The concentrations of JB2-48 and hCA I were maintained at 4 μM and 50 μM, respectively. The solid smooth lines are the best fit of the data either for one (Panels B and C) or two (Panel A) lifetime profiles, and their residuals are shown at the bottom of each panel. The derived lifetimes for the data of individual panels are as follows: Panel A - hCA I bound JB2-48 at pH 7.0; two lifetimes, τ_1 = 13.5 ± 0.1 ns, τ_2 = 27.3 ± 0.4 ns; Panel B – hCA I bound JB2-48 at pH 5.0; single lifetime (τ) = 14 ± 0.6 ns; Panel C – hCA I bound JB2-48 at pH 9.0; single lifetime (τ) = 20 ± 0.7 ns.

7.0. Evidently, the prevalence of two lifetimes of the enzyme bound JB2-48 at the neutral pH, but single lifetimes at lower and higher pH values imply that ionized and neutral forms of sulfonamide moiety of JB2-48 are stabilized by the corresponding microscopic states of the enzyme. In one such state, the fluorescence properties of the enzyme bound JB2-48 is primarily given by the ligand harboring the neutral form of sulfonamide (i.e., at pH 5.0), where in the other state it is given by the negatively charged sulfonamide moiety (i.e., at pH 9.0) of the ligand.

Although the above experimental data led to the suggestion that the differential fluorescence profiles (including lifetimes) of JB2-48 under different environmental conditions were contributed by the hydrophobic and electrostatic interactions within the active site pocket of hCA I, the possibility that such changes originated from the restriction in rotational freedom between the two aromatic rings of the fluorophore as delineated in the case of green fluorescent protein (*534*) could not be ruled out. However, such possibility seemed unlikely since both parent fluorophore (DNSA) as well as its different derivatives showed increase in fluorescence as well as the blue shift in their emission maxima. In addition, pK_a measurement of free JB2-48 (Figure 5.13A) revealed that the phenolic hydroxyl group yields an unusually low pK_a (6.5 instead of 10 for phenol) value, presumably because of delocalization of the electrons (formed upon deprotonation of the phenolic hydroxyl group) via extended conjugation between the two aromatic rings as well as the terminal sulfonamide moiety. Hence, even the aqueous form of JB2-48 (at least at neutral and basic pH values) is likely to be devoid of the rotational freedom as noted with the individual fluorophoric units of green fluorescent protein (*534*). To substantiate or refute this conclusion, the fluorescence lifetimes of free JB2-48 (Figure 5.19) as well as its

enzyme bound form (Figure 5.20) at pH 7.0 as a function of temperature was determined. As shown in Table 5.6 and Figures 5.19 and 5.20, the increase in temperature from 25 to 40° C (the range where enzyme remains fully active) has practically no effect on the lifetimes of either free or the enzyme bound JB2-48. Hence, the enhancement in the fluorescence intensity of JB2-48 is not due to restriction in the rotational freedom (enhancing internal conversion) around the "bridged atoms" connecting the two aromatic rings of the fluorophore upon binding to the enzyme.

5.3. Binding and kinetic studies of hCA-ligand interactions

5.3.1. Binding isotherms of hCA-DNSA

Binding isotherms for the interaction of hCA isozymes with DNSA were obtained by titrating fixed concentrations of enzyme with increasing concentrations of the ligand via monitoring the increase in fluorescence intensity of the complex at 448 nm (λ_{ex} = 330 nm). This wavelenghth was choosen as the signal to noise ratio was maximal. The solid smooth lines of Figure 5.21 are the best fit of the experimental data for the dissociation constants of hCA I-DNSA, hCA II-DNSA, hCA VII-DNSA and hCA XII-DNSA complexes as being equal to 0.74 ± 0.08 μM, 3.69 ± 0.36 μM, 3.14 ± 0.17 μM and 0.06 ± 0.01 μM respectively. The K_d values obtained for hCA I and II were similar to that obtained by Banerjee et al. (*329*) but different from that obtained by Day et al (*473*). The latter authors determined the K_d value of bCA II-DNSA complex to be around 0.34 μM. This one order of magnitude difference between hCA II and bCA II could have occurred due to changes in experimental conditions and/or the difference in enzyme species. In fact, experiments conducted by Banerjee et al.(*329*) proved that the discrepancy is due to the above mentioned reasons.

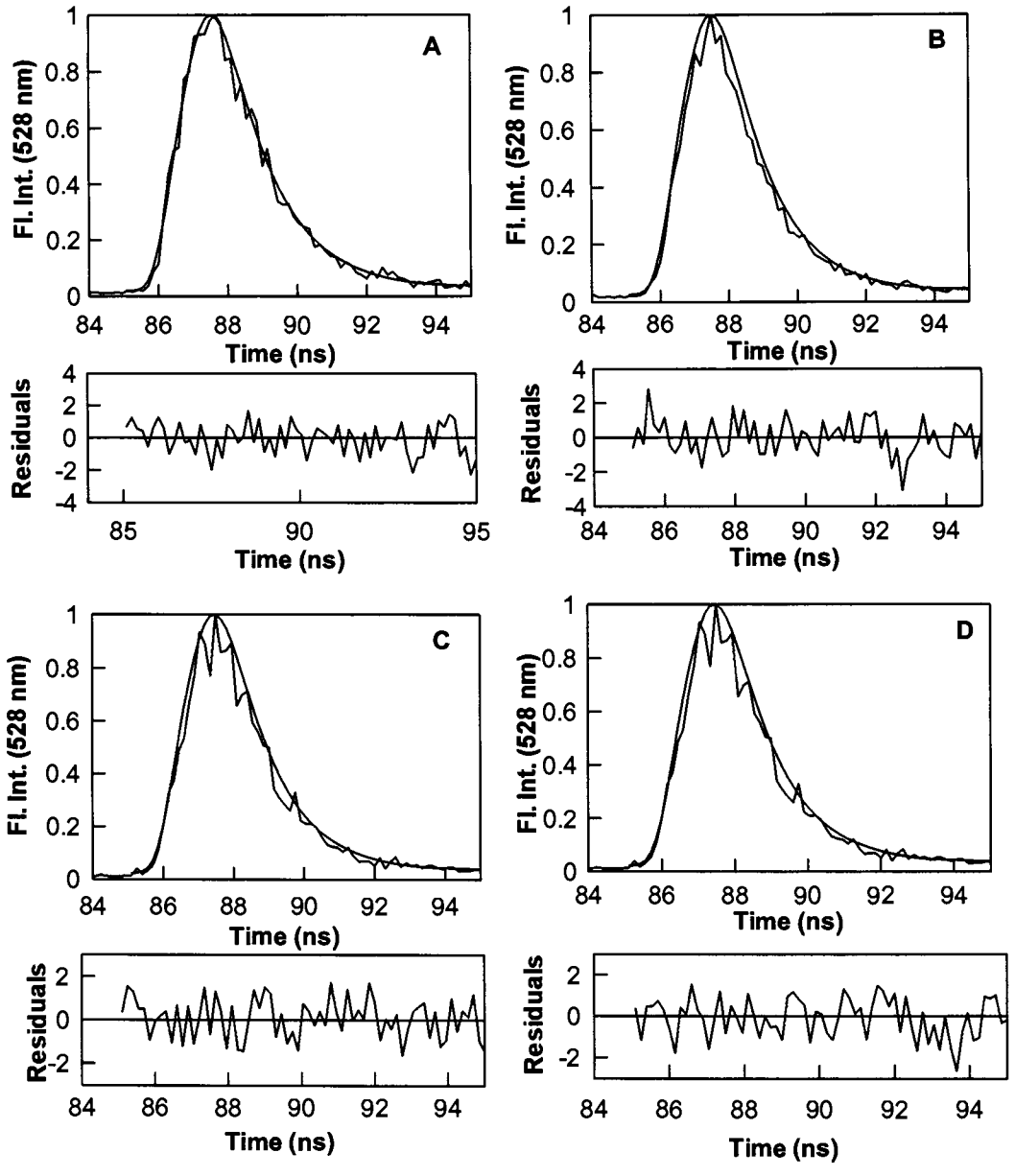

Figure 5.19. Effect temperature on the fluorescence lifetimes of JB2-48. Normalized fluorescence decay profiles of JB2-48 (λ_{ex} = 340 nm; λ_{em} = 470 nm) at different temperatures (Panel A- 30 ° C, Panel B- 35 ° C and Panel C- 40 ° C) are presented. The solid smooth lines are the best fit of the data with the lifetime values as follows. Panel A- (τ) = 1.3 ± 0.03 ns, Panel B (τ) = 1.3 ± 0.03 ns; Panel C (τ) = 1.2 ± 0.03. The goodness of the fit was determined by the residuals.

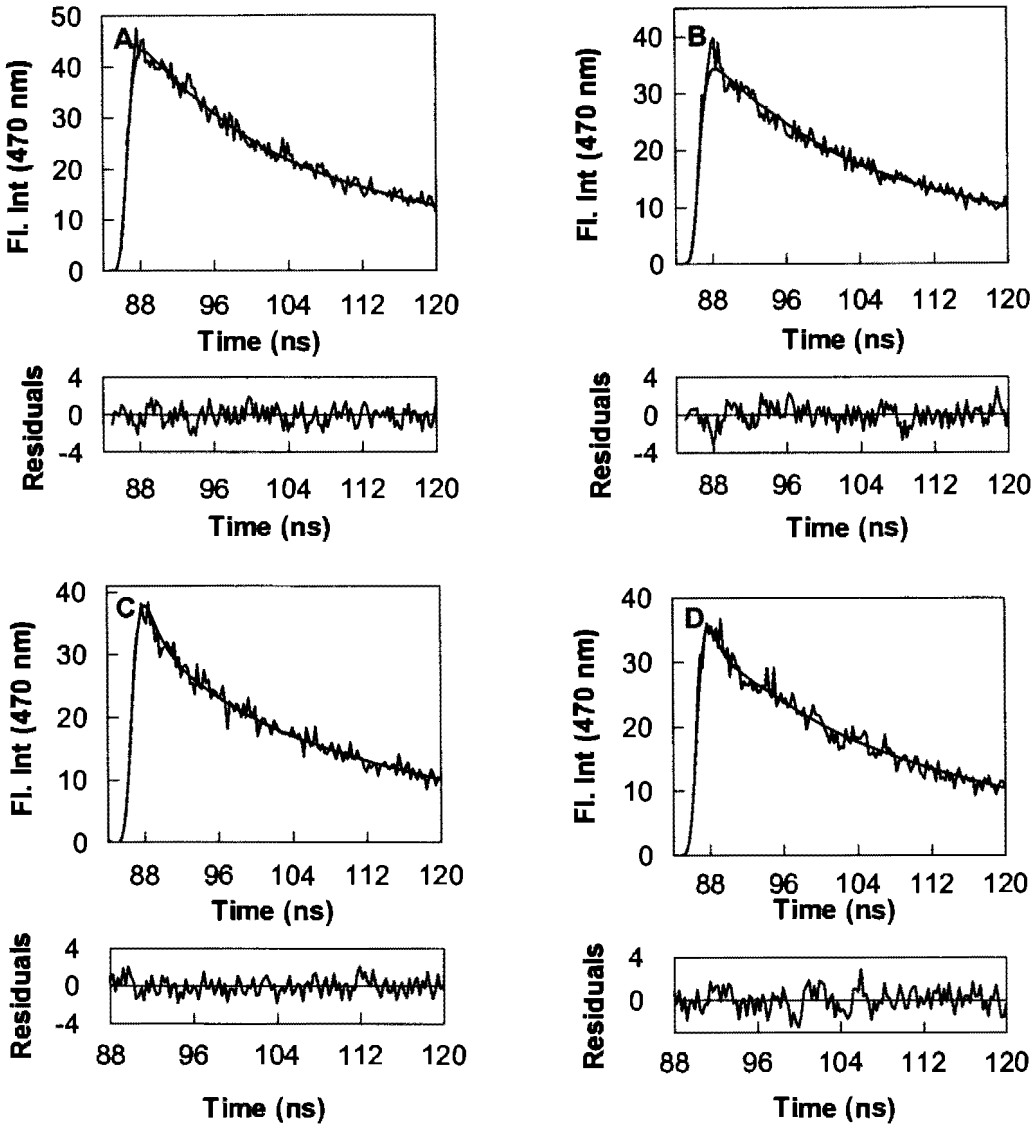

Figure 5.20. Effect temperature on the fluorescence lifetimes of hCA I bound JB2-48. Normalized fluorescence decay profiles of hCA I-JB2-48 complex (λ_{ex} = 340 nm; λ_{em} = 470 nm) at different temperatures (Panel A- 30 ° C, Panel B- 35 ° C and Panel C- 40 ° C) are presented. The solid smooth lines are the best fit of the data with the lifetime values as follows. Panel A- τ_1 = 12.7 ± 0.004 ns and τ_2 = 29.1 ± 0.007 ns , Panel B - τ_1 = 11.6 ± 0.1 ns and τ_2 = 28.6 ± 0.01 ns Panel C- τ_1 = 12.8 ± 0.2 ns and τ_2 = 28.7 ± 0.3 ns . The goodness of the fit was determined by the residuals.

Table 5.6. Effect of temperature on lifetimes of JB2-48.

Temperature (° C)	Free JB2-48	hCA I – JB2-48 complex	
	τ (ns)	τ_1 (ns)	τ_2 (ns)
25	1.2 ± 0.02	13.5 ± 0.1	27.3 ± 0.4
30	1.3 ± 0.03	12.7 ± 0.004	29.1 ± 0.01
35	1.3 ± 0.03	11.6 ± 0.1	28.6 ± 0.01
40	1.2 ± 0.03	12.8 ± 0.2	28.7 ± 0.3

The experiments were performed in 25 mM HEPES buffer, pH 7.0, containing 10% DMSO. λ_{ex} = 340 nm (LED) and λ_{em} = 470 nm. [JB2-48] = 35 μM for measuring the lifetimes of free fluorophore. [JB2-48] = 4 μM and [hCA I] = 50 μM for measuring the lifetimes of the enzyme bound fluorophore.

Upon comparison of the K_d values, it is evident that DNSA binds to hCA XII with atleast 10 fold higher affinity as compared to other isozymes. In addition, it binds with a higher affinity to hCA I as compared to hCA II, in contrast to most sulfonamide inhibitors. Banerjee et al (*329*) revealed that this discrepancy is due to the difference in the microscopic pathways of DNSA binding to hCA I and hCA II.

5.3.2. Binding isotherms of hCA- JB2 compounds

The dissociation constants of the hCA-JB2 complex were determined by titrating a fixed concentration of the enzyme with increasing concentrations of the JB2 probes and monitoring the increase in the emission intensity of the probe at 470 nm. The contribution of the free probe to the fluorescence intensity at 470 nm was subtracted by performing a blank titration in the buffer. The change in the fluorescence intensity at 470 nm was plotted

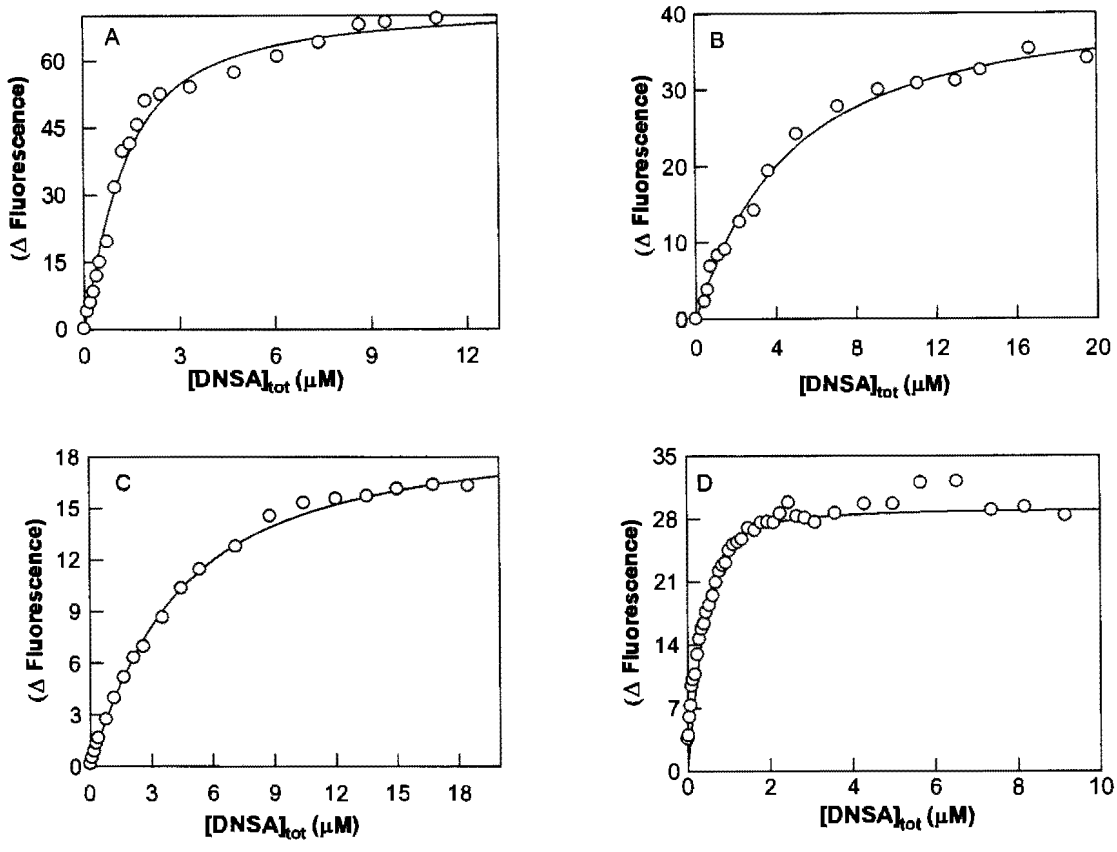

Figure 5.21. Binding isotherms for the interactions of DNSA with hCA isozymes. Panel A, B, C and D represents the binding isotherms for the interactions of DNSA with hCA I, hCA II, hCA VII and hCA XII respectively in 25 mM HEPES pH 7.0 containing 10 % acetonitrile. [hCA I] = 1 μM, [hCA II] = 1.5 μM, [hCA VII] = 2 μM, [hCA XII] = 1.25 μM. The increase in the fluorescence emission intensity of enzyme bound dansylamide at 448 nm (λ_{ex} = 330 nm) for the titration of fixed concentration of respective enzymes with increasing concentrations of dansylamide is shown. The solid smooth lines are the best fit of the data yielding the K_d values of 0.74 ± 0.08, 3.69 ± 0.36, 3.14 ± 0.17, 0.06 ± 0.01 for panels A, B, C and D respectively.

as a function of the probe concentration and analyzed according to the model described by Qin and Srivastava (*506*). The solid smooth lines of Figures 5.22-5.31 are the best fit of the data with the K_d values as listed in Table 5.7. The K_d values for DNSA and JB2 compounds with hCA isozymes suggest that where as majority of the probes are much better inhibitors of hCA I, II and VII than DNSA, they are weaker inhibitors for hCA XII

when compared with DNSA. The comparison of the K_d values of the probes between different hCAs revealed that they bind hCA VII with strongest affinity.

In order to complement the pH dependent lifetimes of hCA I-JB2-48 obtained in the previous section, it was of interest to determine their pH dependent binding affinities. This was required to probe the contributions of hydrophobic versus electrostatic interactions in the ground and putative transition states upon binding of JB2-48 to hCA I, respectively. Figure 5.32 shows the emission spectra of hCA I (λ_{ex} = 280 nm) in the presence of increasing concentrations of JB2-48 at pH 7.0. The intrinsic fluorescence of hCA I was contributed mainly by the enzyme resident tryptophan residues (*203*). As shown in Figure 5.32A, with increase in the concentration of JB2-48, whereas the fluorescence emission intensity of the tryptophan residues (λ_{em} = 330 nm) decreased (presumably due to the static quenching), the emission intensity of the probe (λ_{em} = 470 nm) increased. Given the changes in fluorescence signals at the above wavelengths, a fixed concentration of hCA I was titrated by increasing concentrations of the fluorophore to determine the binding constant of the enzyme-fluorophore complex in 25 mM HEPES, pH 7.0. Figure 5.32B shows the titration profiles for the binding of JB2-48 to hCA I by monitoring the intrinsic fluorescence of the enzyme (decrease in the fluorescence intensity at 330 nm; open circles) as well as the probe's signal (increase in the fluorescence at 470 nm; open triangle). The solid smooth lines are the best fit of the data for the dissociation constants of the enzyme-probe complex as being equal to 2.1 ± 0.2 and 2.3 ± 0.4 μM at 330 and 470 nm, respectively. Note that the K_d determined for hCA I-JB2-48 interaction by exciting the probe at 330 nm (Figure 5.23B) is similar to the K_d obtained by exciting at 280 nm indicating a common physical step. Similar experiments were performed to

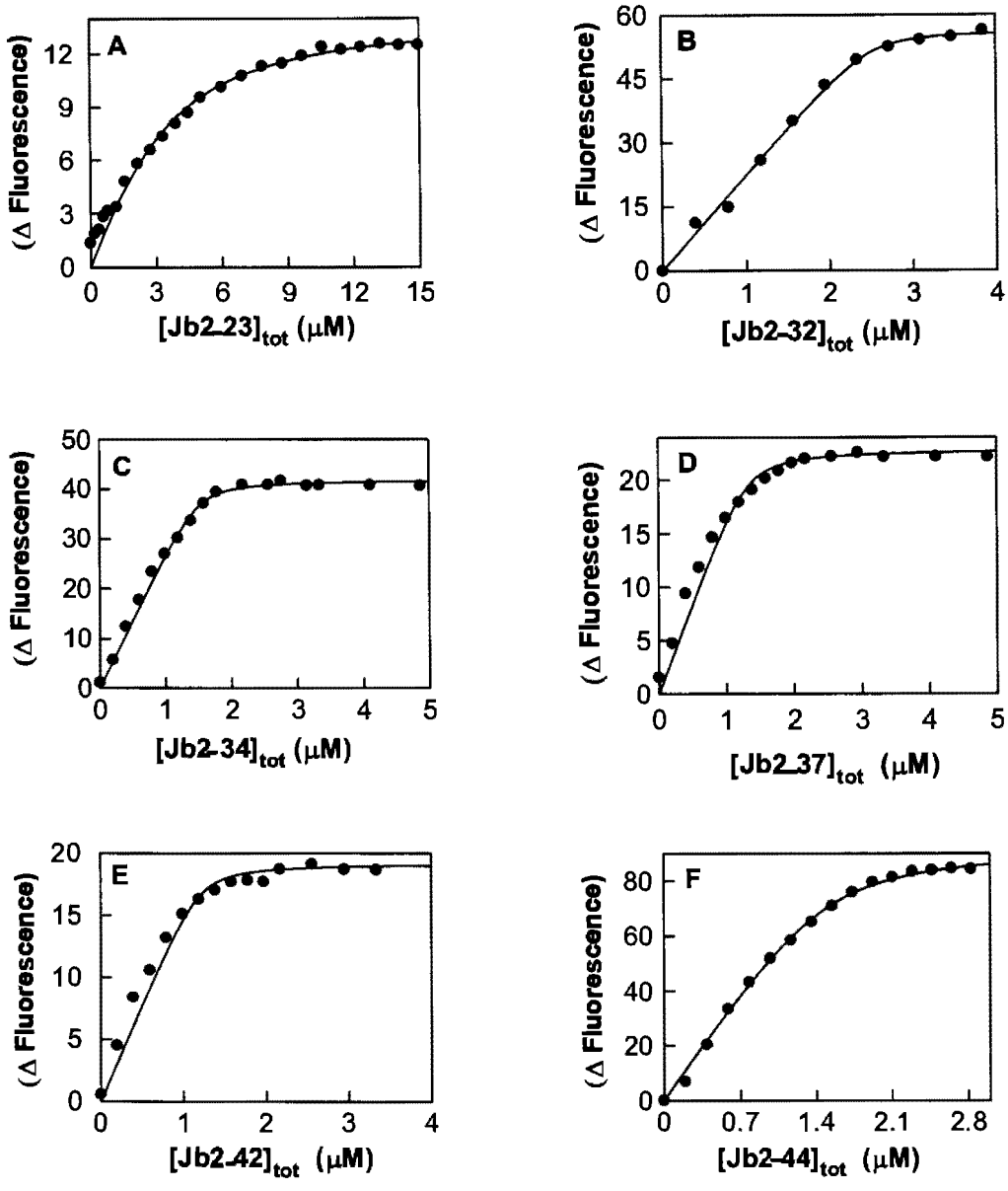

Figure 5.22. Binding isotherms for the interactions of hCA I with JB compounds. Panel A, B, C, D, E and F represents the binding isotherms for the interactions of hCA I with JB2-23, 32, 34, 37, 42 and 44 respectively in 25 mM HEPES pH 7.0 containing 10 % DMSO. [hCA I] = 1 μM. The increase in the fluorescence emission intensity of enzyme bound JB compounds at 470 nm (λ_{ex} = 330 nm) for the titration of fixed concentration of hCA I with increasing concentrations of JB compounds is shown. The solid smooth lines are the best fit of the data yielding the K_d values of 1.47 ± 0.24, 0.024 ± 0.02, 0.03 ± 0.01, 0.04 ± 0.02, 0.025 ± 0.04, 0.1 ± 0.02 for panels A, B, C, D, E and F respectively.

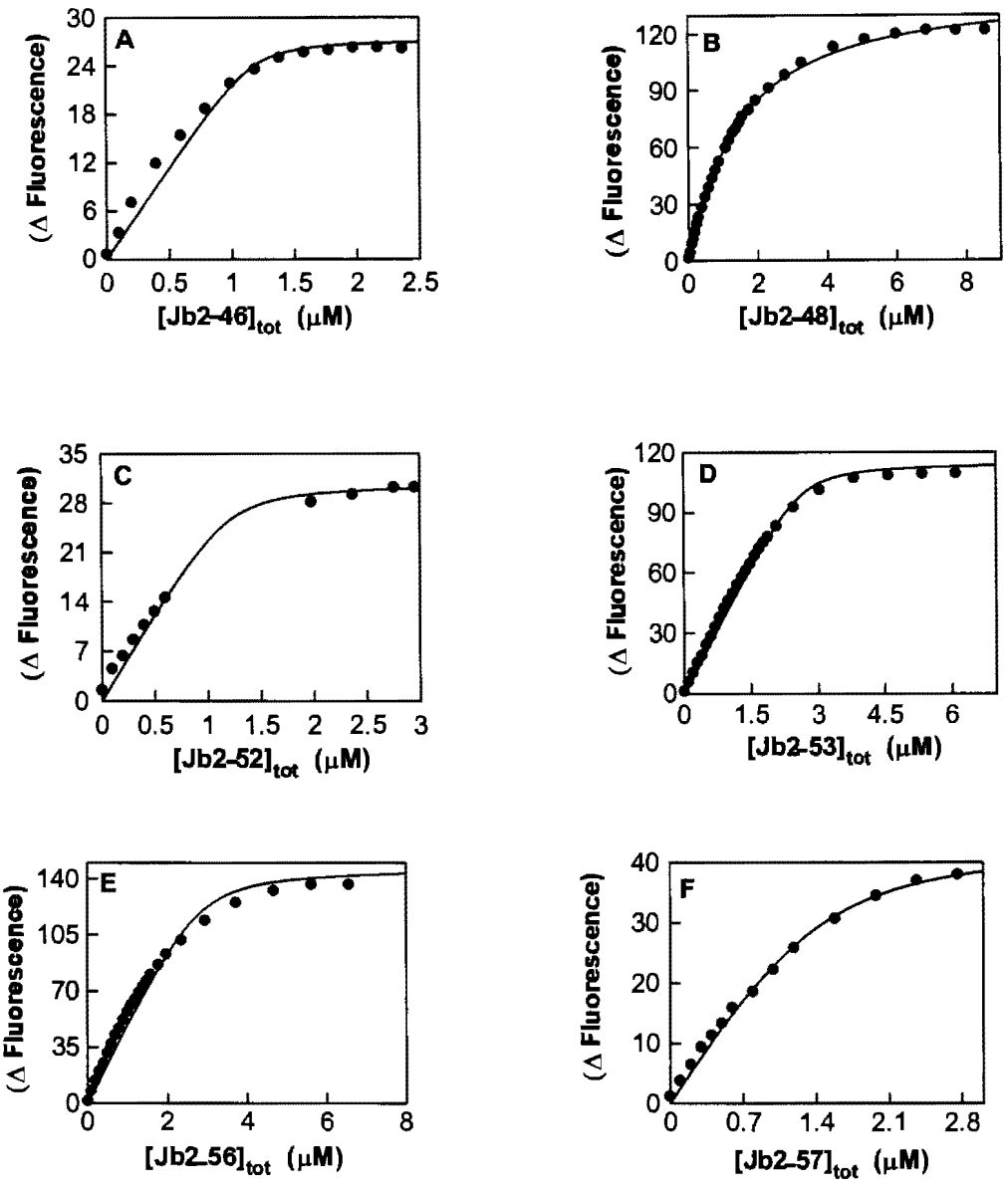

Figure 5.23. Binding isotherms for the interactions of hCA I with JB compounds. Panel A, B, C, D, E and F represents the binding isotherms for the interactions of hCA I with JB2-46, 48, 52, 53, 56 and 57 respectively in 25 mM HEPES pH 7.0 containing 10 % DMSO. [hCA I] = 1 μM. The increase in the fluorescence emission intensity of enzyme bound JB compounds at 470 nm (λ_{ex} = 330 nm) for the titration of fixed concentration of hCA I with increasing concentrations of JB compounds is shown. The solid smooth lines are the best fit of the data yielding the K_d values of 0.02 ± 0.02, 1.2 ± 0.02, 0.04 ± 0.03, 0.07 ± 0.02, 0.13 ± 0.09, 0.23 ± 0.06 for panels A, B, C, D, E and F respectively.

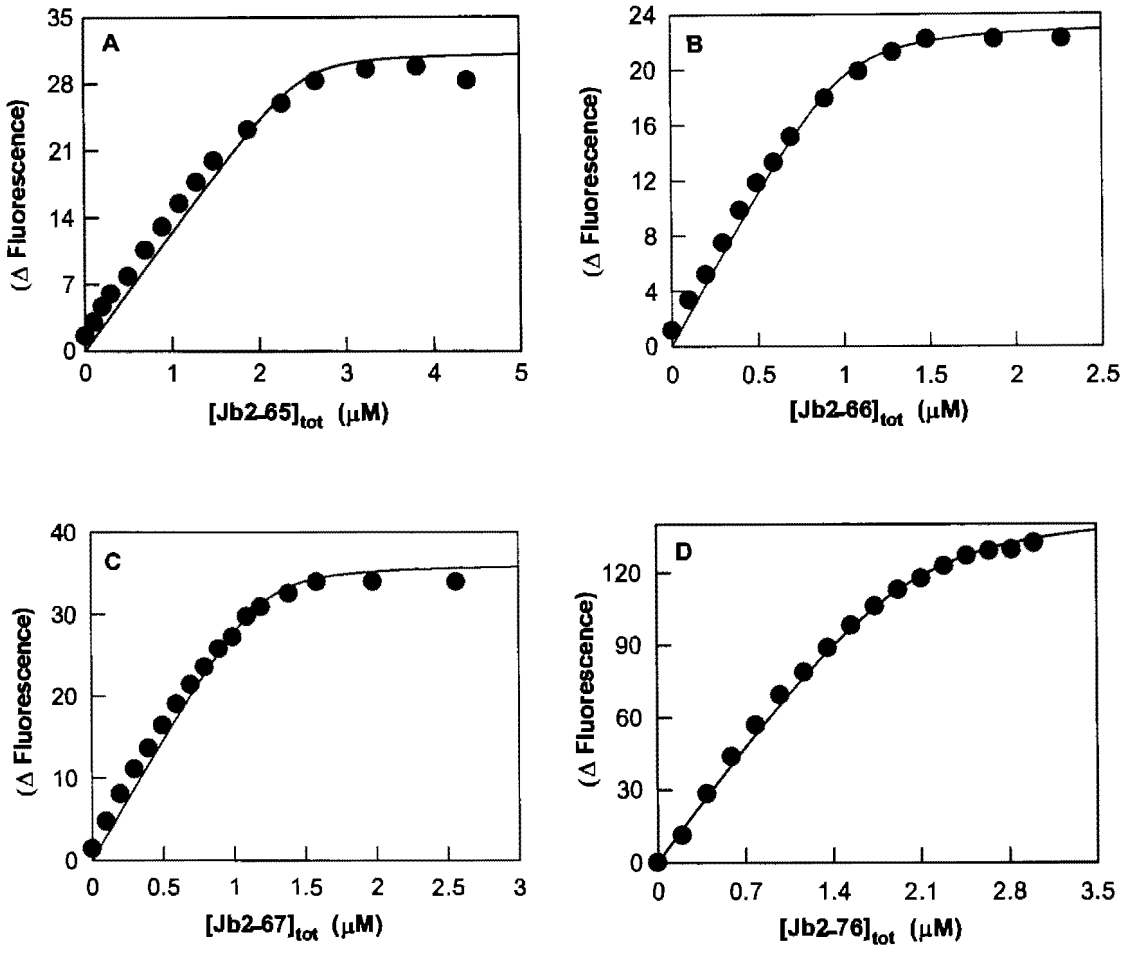

Figure 5.24. Binding isotherms for the interactions of hCA I with JB compounds. Panels A, B, C, and D represents the binding isotherms for the interactions of hCA I with JB2-65, 66, 67 and 76 respectively in 25 mM HEPES pH 7.0 containing 10 % DMSO. [hCA I] = 1 μM. The increase in the fluorescence emission intensity of enzyme bound JB compounds at 470 nm (λ_{ex} = 330 nm) for the titration of fixed concentration of hCA I with increasing concentrations of JB compounds is shown. The solid smooth lines are the best fit of the data yielding the K_d values of 0.027 ± 0.09, 0.034 ± 0.02, 0.026 ± 0.01, 0.12 ± 0.04 for panels A, B, C and D respectively.

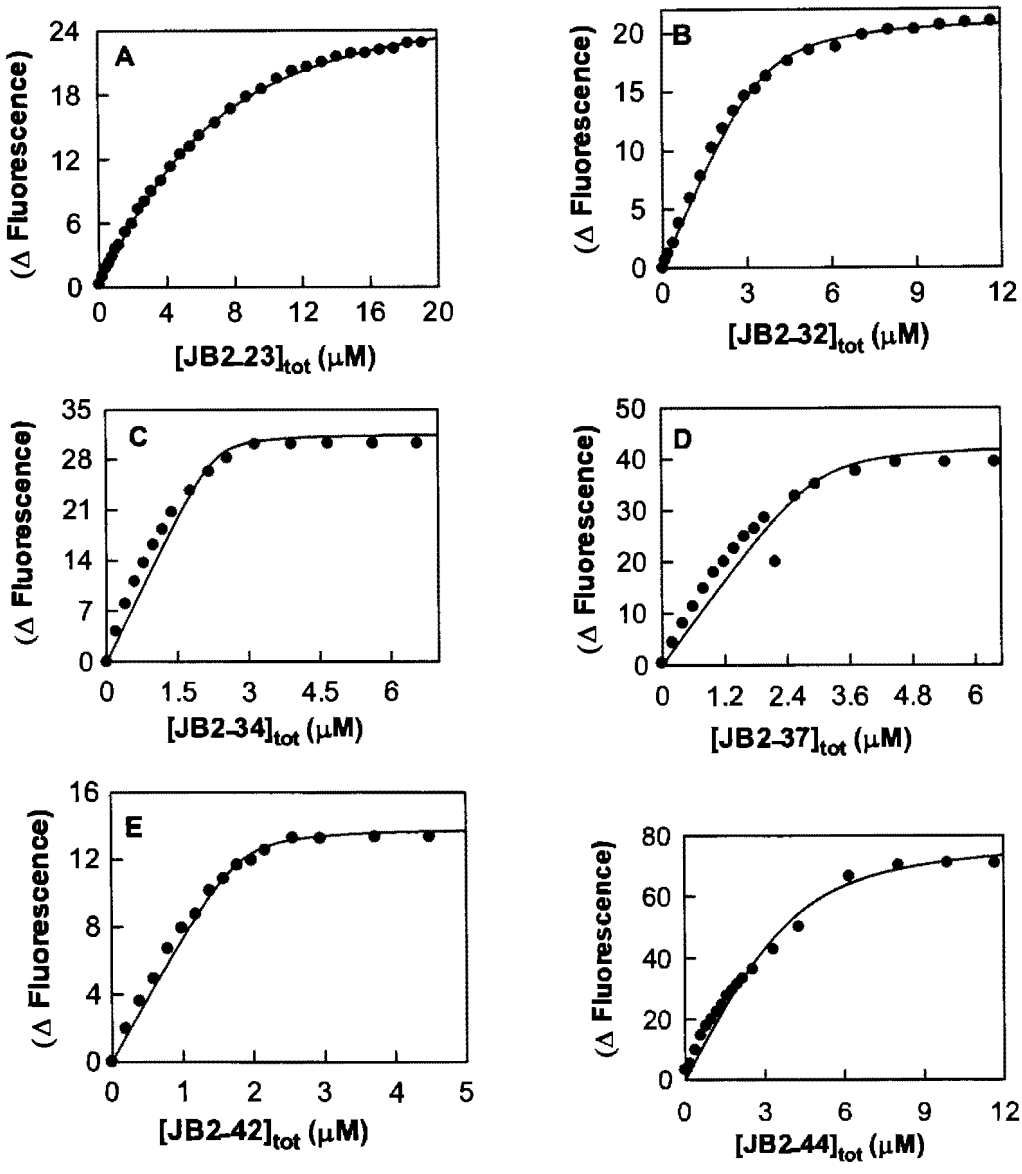

Figure 5.25. Binding isotherms for the interactions of hCA II with JB compounds. Panel A, B, C, D, E and F represents the binding isotherms for the interactions of hCA I with JB2-23, 32, 34, 37, 42 and 44 respectively in 25 mM HEPES pH 7.0 containing 10 % DMSO. [hCA I] = 1 μM. The increase in the fluorescence emission intensity of enzyme bound JB compounds at 470 nm (λ_{ex} = 330 nm) for the titration of fixed concentration of hCA I with increasing concentrations of JB compounds is shown. The solid smooth lines are the best fit of the data yielding the K_d values of 3.3 ± 0.12, 0.31 ± 0.04, 0.035 ± 0.03, 0.097 ± 0.2, 0.047 ± 0.02, 0.72 ± 0.2 for panels A, B, C, D, E and F respectively.

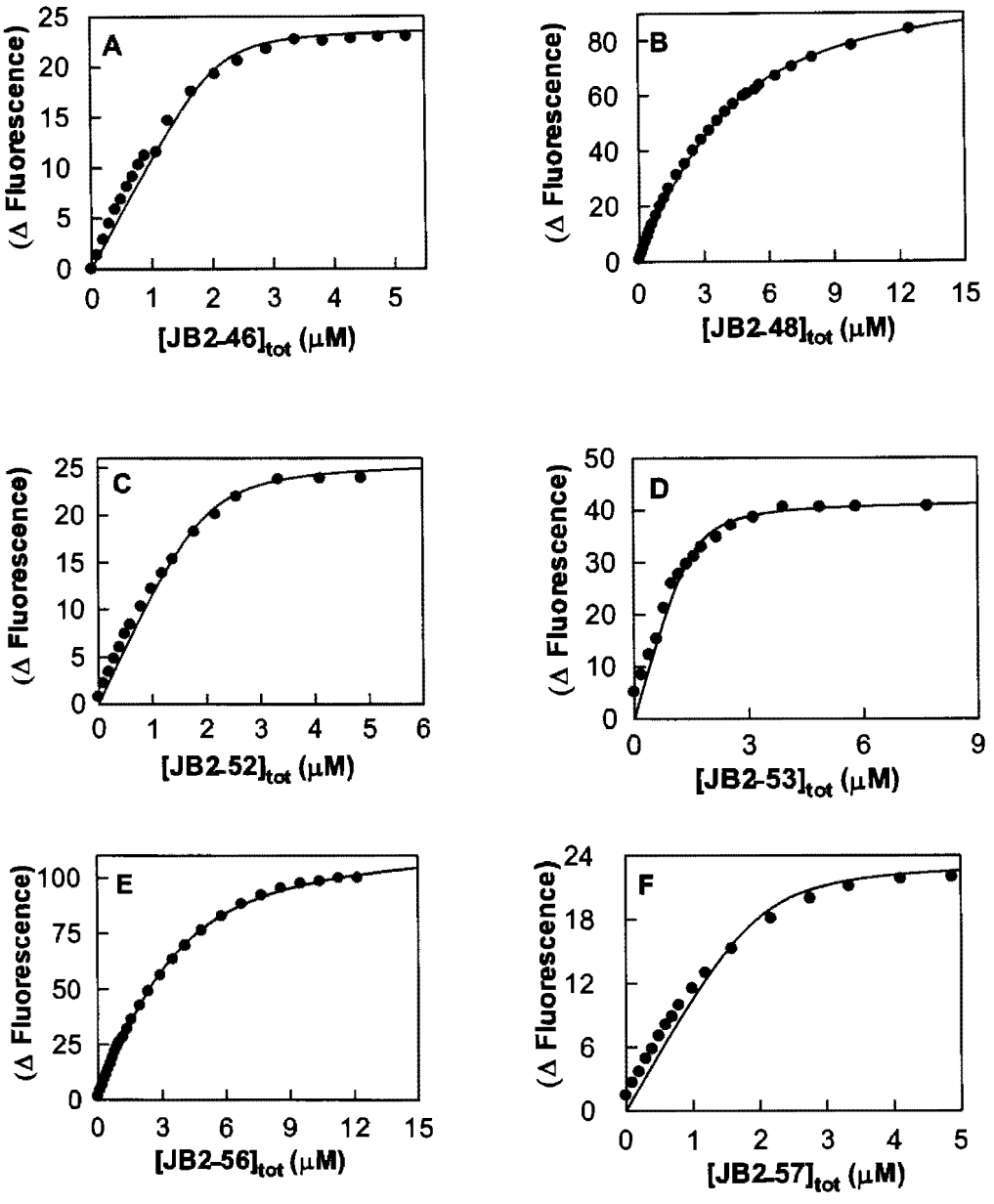

Figure 5.26. Binding isotherms for the interactions of hCA II with JB compounds. Panel A, B, C, D, E and F represents the binding isotherms for the interactions of hCA II with JB2-46, 48, 52, 53, 56 and 57 respectively in 25 mM HEPES pH 7.0 containing 10 % DMSO. [hCA I] = 1 μM. The increase in the fluorescence emission intensity of enzyme bound JB compounds at 470 nm (λ_{ex} = 330 nm) for the titration of fixed concentration of hCA I with increasing concentrations of JB compounds is shown. The solid smooth lines are the best fit of the data yielding the K_d values of 0.067 ± 0.07, 2.8 ± 0.07, 0.13 ± 0.06, 0.13 ± 0.04, 1.53 ± 0.08, 0.13 ± 0.1 for panels A, B, C, D, E and F respectively.

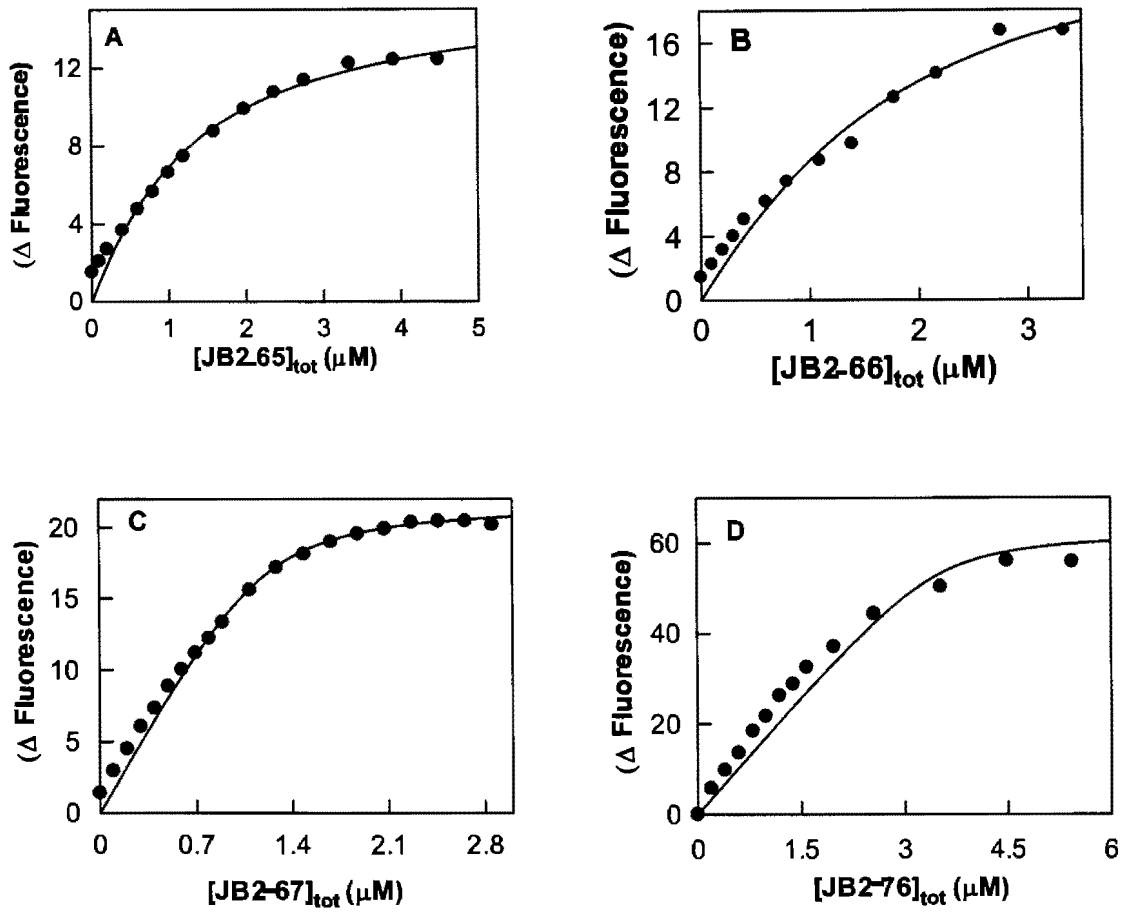

Figure 5.27. Binding isotherms for the interactions of hCA II with JB compounds. Panels A, B, C, and D represents the binding isotherms for the interactions of hCA II with JB2-65, 66, 67 and 76 respectively in 25 mM HEPES pH 7.0 containing 10 % DMSO. [hCA I] = 1 μM. The increase in the fluorescence emission intensity of enzyme bound JB compounds at 470 nm (λ_{ex} = 330 nm) for the titration of fixed concentration of hCA I with increasing concentrations of JB compounds is shown. The solid smooth lines are the best fit of the data yielding the K_d values of 1.0 ± 0.1, 0.96 ± 0.4, 0.086 ± 0.03, 0.096 ± 0..2 for panels A, B, C and D respectively.

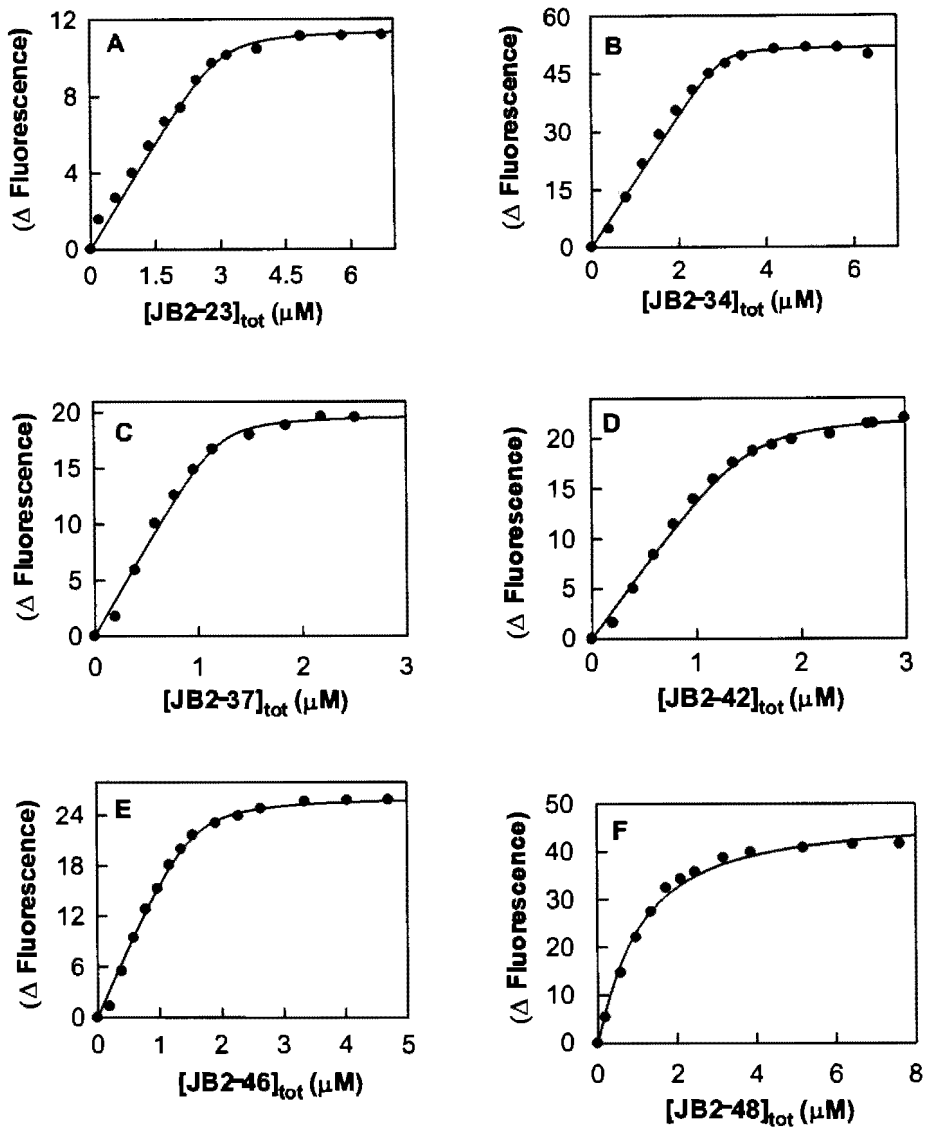

Figure 5.28. Binding isotherms for the interactions of hCA VII with JB compounds. Panel A, B, C, D, E and F represents the binding isotherms for the interactions of hCA VII with JB2-23, 34, 37, 42, 46 and 48 respectively in 25 mM HEPES pH 7.0 containing 10 % DMSO. The increase in the fluorescence emission intensity of enzyme bound JB compounds at 470 nm (λ_{ex} = 330 nm) for the titration of fixed concentration of hCA I with increasing concentrations of JB compounds is shown. The solid smooth lines are the best fit of the data yielding the K_d values of 0.067± 0.03, 0.023 ± 0.01, 0.027 ± 0.01, 0.063 ± 0.02, 0.077 ± 0.02, 0.83 ± 0.07 for panels A, B, C, D, E and F respectively.

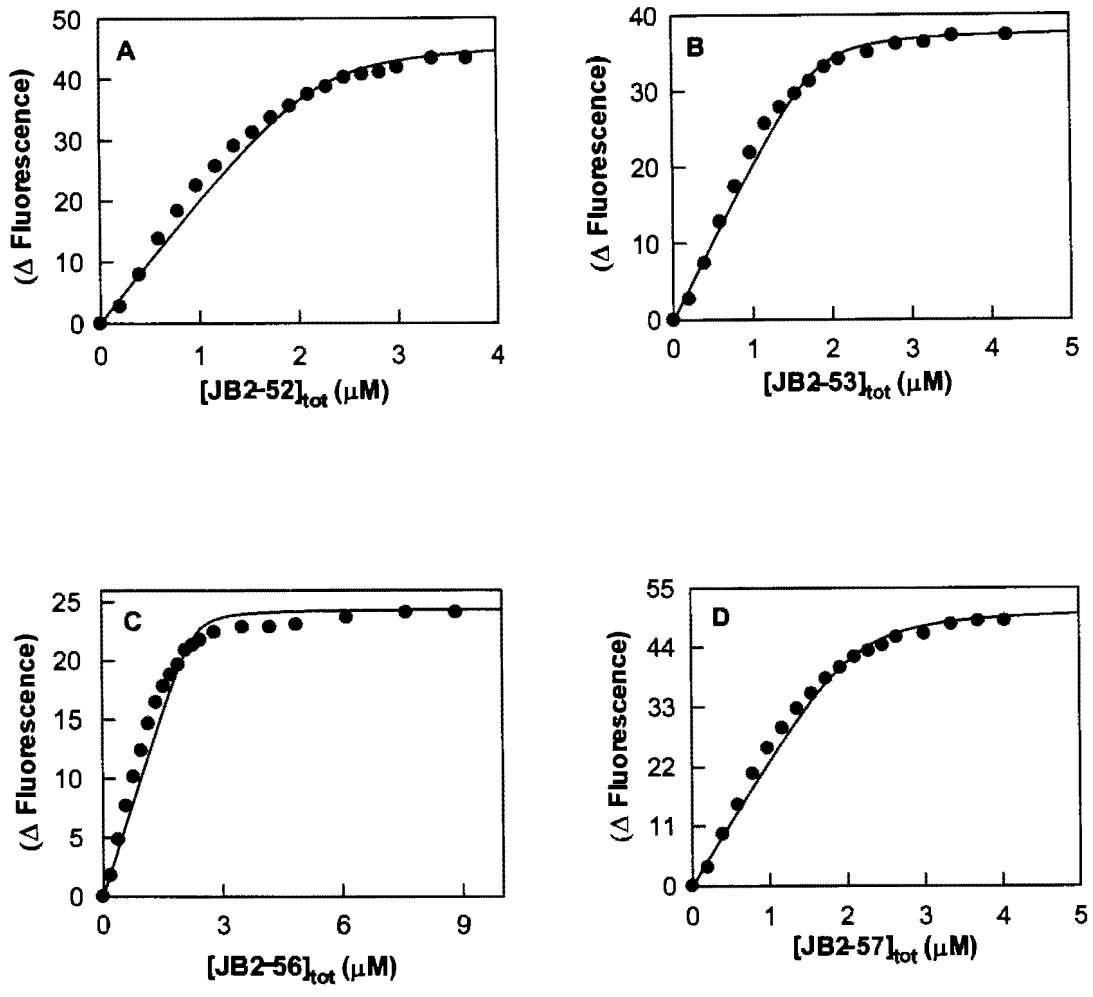

Figure 5.29. Binding isotherms for the interactions of hCA VII with JB compounds. Panels A, B, C, and D represents the binding isotherms for the interactions of hCA II with JB2-52, 53, 56 and 57 respectively in 25 mM HEPES pH 7.0 containing 10 % DMSO. The increase in the fluorescence emission intensity of enzyme bound JB compounds at 470 nm (λ_{ex} = 330 nm) for the titration of fixed concentration of hCA VII with increasing concentrations of JB compounds is shown. The solid smooth lines are the best fit of the data yielding the K_d values of 0.073 ± 0.04, 0.042 ± 0.02, 0.026 ± 0.01, 0.08 ± 0.03 for panels A, B, C and D respectively.

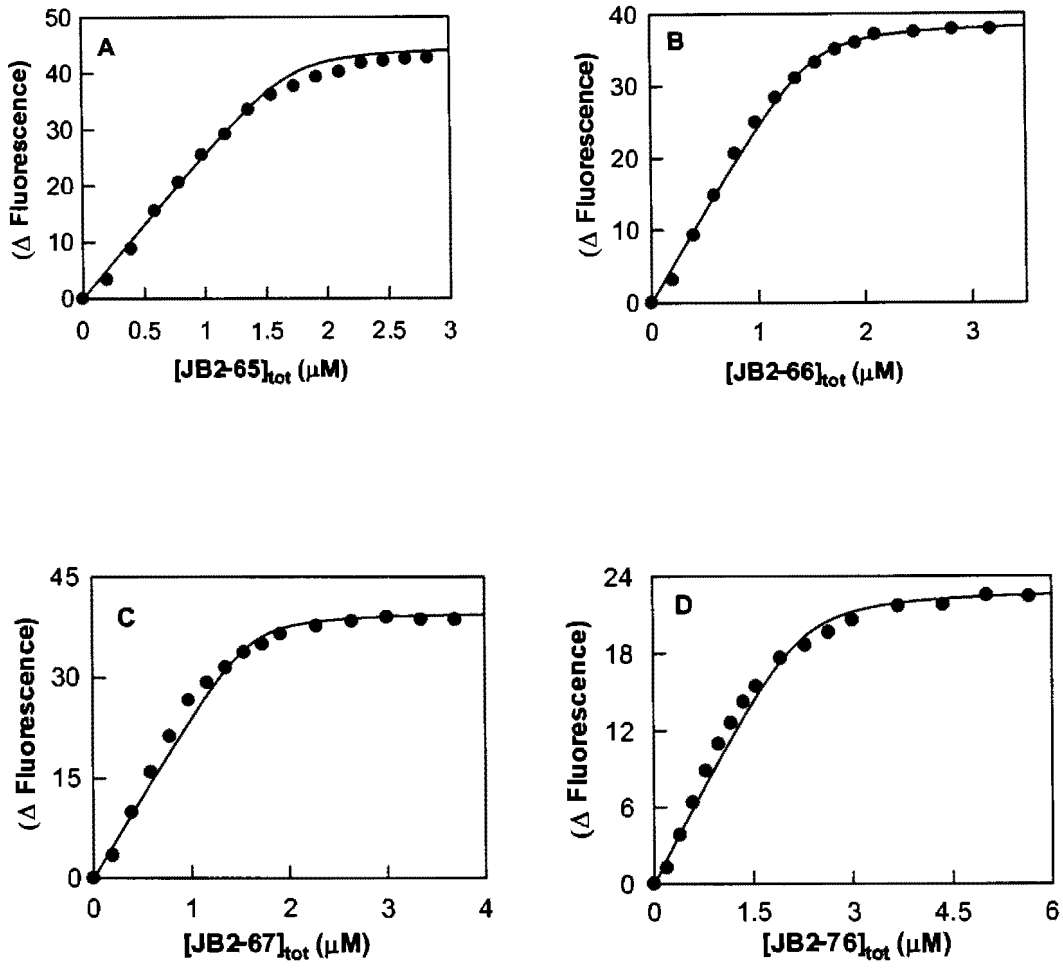

Figure 5.30. Binding isotherms for the interactions of hCA VII with JB compounds. Panels A, B, C, and D represents the binding isotherms for the interactions of hCA II with JB2-65, 66, 67 and 76 respectively in 25 mM HEPES pH 7.0 containing 10 % DMSO. The increase in the fluorescence emission intensity of enzyme bound JB compounds at 470 nm (λ_{ex} = 330 nm) for the titration of fixed concentration of hCA VII with increasing concentrations of JB compounds is shown. The solid smooth lines are the best fit of the data yielding the K_d values of 0.027 ± 0.02, 0.038± 0.01, 0.03 ± 0.01, 0.087 ± 0.03 for panels A, B, C and D respectively.

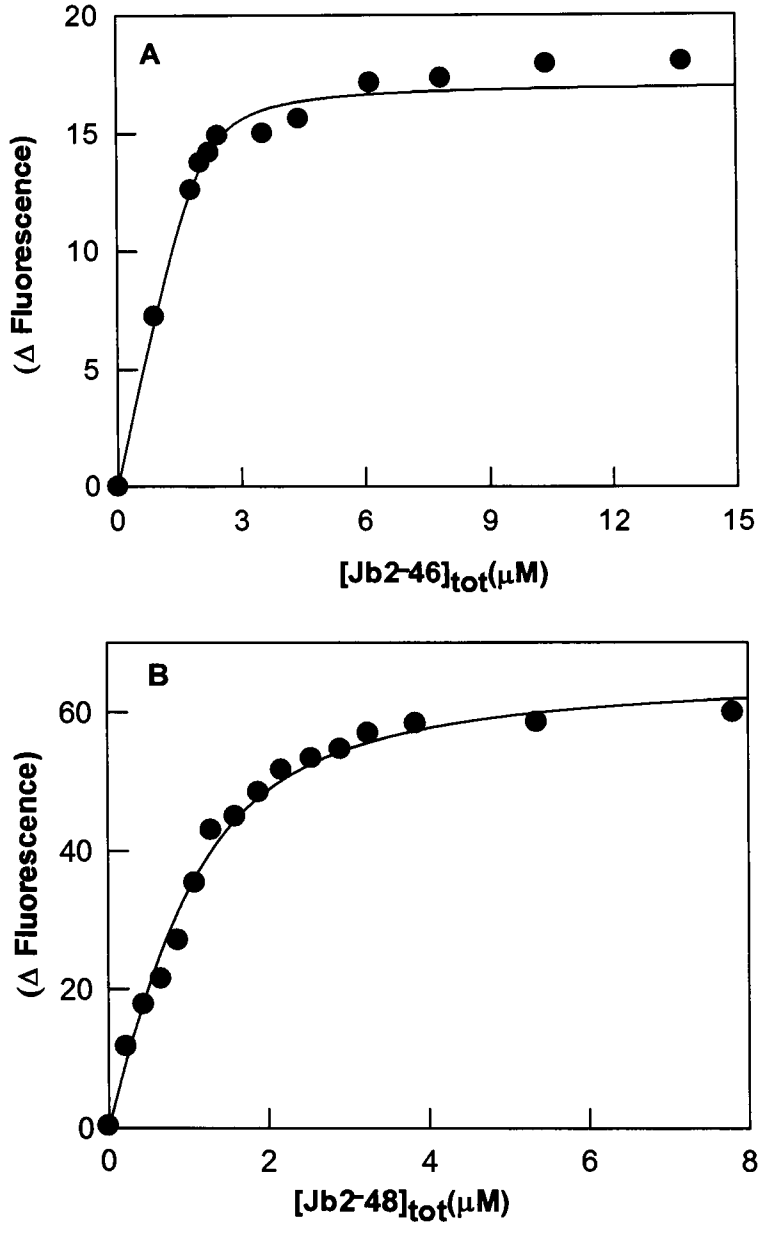

Figure 5.31. Binding isotherms for the interactions of hCA XII with JB2-46 and 48. Panels A and B represents the binding isotherms for the interactions of hCA XII with JB2-46 and 48 respectively in 25 mM HEPES pH 7.0 containing 10 % DMSO. The increase in the fluorescence emission intensity of enzyme bound JB compounds at 470 nm (λ_{ex} = 330 nm) for the titration of fixed concentration of hCA XII with increasing concentrations of JB compounds is shown. The solid smooth lines are the best fit of the data yielding the K_d values of 0.12 ± 0.03, 0.45 ± 0.06 for panels A and B respectively.

Table 5.7. Comparison of binding isotherm values for fluorescent probes with hCA isozymes.

Compound	hCA I K_d (μM)	hCA II K_d (μM)	hCA VII K_d (μM)	hCA XII K_d (μM)
JB2-23	1.4	3.3	0.066	nd
JB2-32	0.02	0.3	nd	nd
JB2-34	0.03	0.03	0.02	nd
JB2-37	0.04	0.1	0.026	nd
JB2-42	0.02	0.047	0.062	nd
JB2-44	0.1	0.7	nd	nd
JB2-46	0.03	0.06	0.07	0.12
JB2-48	1.2	2.8	0.83	0.45
JB2-52	0.04	0.13	0.072	nd
JB2-53	0.07	0.10	0.04	nd
JB2-56	0.1	1.5	0.025	nd
JB2-57	0.2	0.13	0.079	nd
JB2-65	0.02	1.02	0.027	nd
JB2-66	0.03	0.96	0.037	nd
JB2-67	0.02	0.08	0.03	nd
JB2-76	0.1	0.1	0.087	nd
Dansylamide	0.47	3.2	3	0.1

nd: not detectable

determine the binding affinity of JB2-48 for hCA I at pH 5.0 and 9.0, respectively (Figure 5.33). The binding affinity was determined by exciting the probe at 330 nm and monitoring the emission intensity at 470 nm in 25 mM acetate and 25 mM Tris buffer, both containing 10 % DMSO, at pH 5.0 and pH 9.0 respectively. These values are summarized in Table 5.8. Using the standard state as being equal to 1.0 M, the K_d values of Table 5.8 were

translated to the standard free energy changes (ΔG^o) for the enzyme-ligand interactions at 25°C (ΔG^o = -RT ln ($1/K_d$)), and these derived values are presented in the last column of Table 5.8. A casual perusal of the ΔG^o values of Table 5.8 reveals that the difference in the enzyme-JB2-48 binding energy ($\Delta\Delta G^o$) between the high and low pH values is 2.2 kcal/mol. Since at the above high and low pH values, the sulfonamide nitrogen of JB2-48 is expected to exist in fully ionized and neutral forms respectively, the calculated $\Delta\Delta G^o$ value serves as a measure of the electrostatic interactions between the active site resident Zn^{2+} cofactor and the negatively charged sulfonamide moiety of the fluorophore.

In order to discern if JB2-48 can inhibit the enzyme catalyzed reaction of hCA I, the enzyme activity was determined as a function of increasing concentration of JB2-48 using p-nitriphenyl acetate as the enzyme substrate. The enzyme concentration was maintained as 2 μM. The rates of enzyme catalyzed reactions were measured by following the hydrolysis of p-NPA at 348 nm in 25 mM HEPES + 10 % DMSO, pH 7.0. The initial rate of the reaction was measured by taking the slopes of the reaction traces. The solid smooth line of Figure 5.34 is the best fit of the data (*328*) yielding a K_i value of 2.7 ± 0.5 μM. It is to be noted that the K_d and K_i vales for hCA I-JB2-48 interaction are comparable, and thus they appear to originate from a common physical/binding step.

5.3.3. Transient kinetic studies for the binding of JB2-48 to hCA I:

Transient kinetic studies were performed for the binding of JB2-48 to hCA I at pH 5.0, 7.0, and 9.0. This was accomplished by mixing the above species via the stopped flow syringes, followed by monitoring the increase in fluorescence intensity of the probe (λ_{ex} = 336 nm, cutoff filter = 395 nm) as a function of time. Figures 5.35 and 5.36 show the

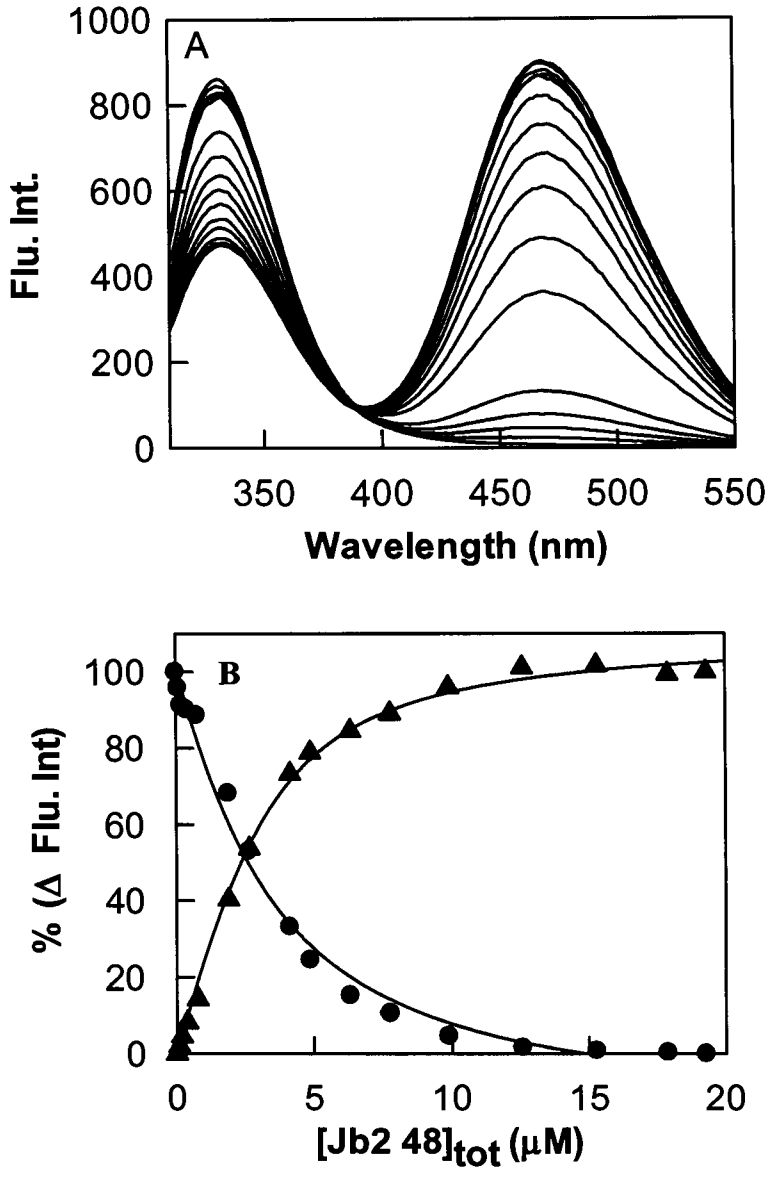

Figure 5.32. Fluorescence spectral changes upon binding of JB2-48 to hCA I.
Panel A shows the fluorescence emission spectra of hCA-I in the absence and presence of increasing concentrations of JB2-48. [hCA I] = 2 μM, [JB2-48] = 1 – 20 μM; λ_{ex} = 280 nm. Note that the titration of hCA I by JB2-48 results in a decrease in the fluorescence intensity at 330 nm, and increase in the fluorescence intensity at 470 nm. Panel B represents the binding isotherm for hCA I – JB2-48 interaction. The Figure shows the binding isotherms for the interaction of JB2-48 with hCA-I determined at 330 nm (dark circles- decreasing phase) and at 470 nm (dark triangles-increasing phase) in 25 mM HEPES buffer containing 10 % DMSO at pH 7.0. λ_{ex} = 280 nm; hCA I = 2 μM. The solid smooth lines are the best fit of the data for the K_d values of 2.1 ± 0.2 (330 nm plot) and 2.3 ± 0.4 μM (470 nm plot) respectively.

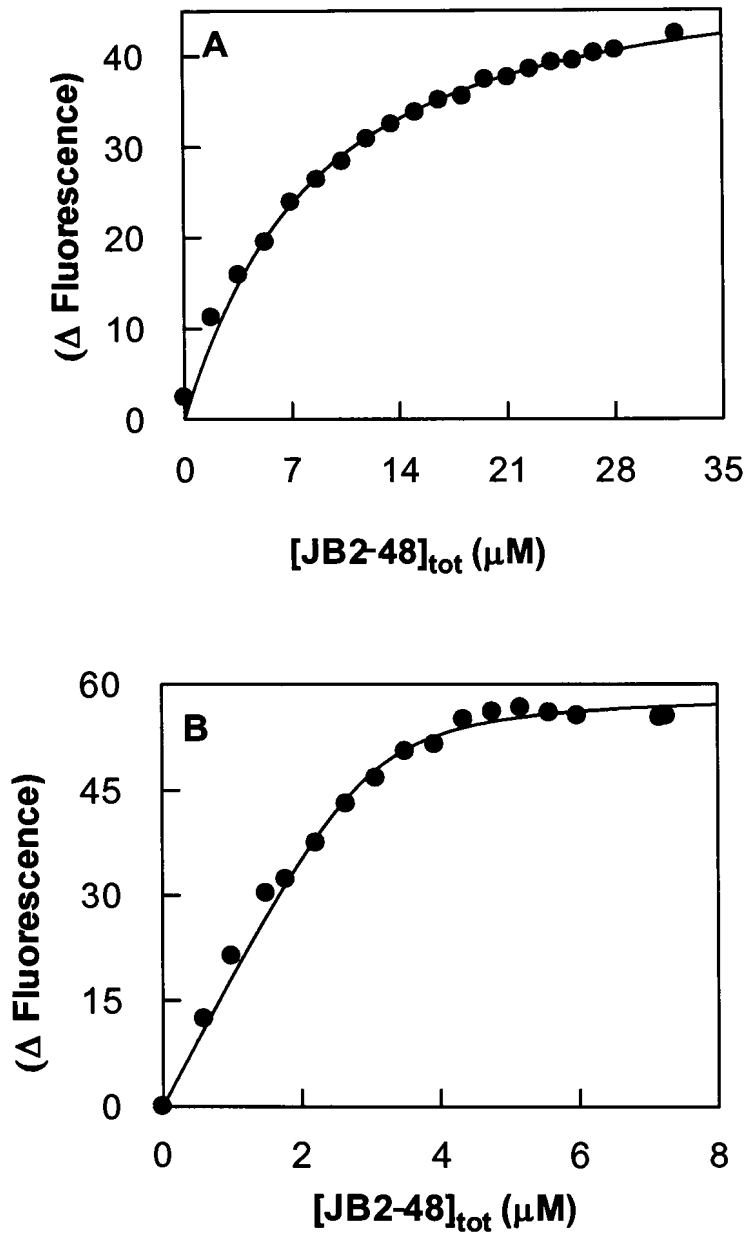

Figure 5.33. Binding isotherm for hCA I – JB2-48 interaction at pH 5.0 and 9.0.
The Figure shows the binding isotherms for the interaction of JB2-48 with hCA-I determined at at 470 nm in 25 mM acetate buffer containing 10 % DMSO at pH 5.0 (panel A) and 25 mM Tris buffer containing 10 % DMSO at pH 9.0. (Panel B). λ_{ex} = 330 nm, λ_{am} = 470 nm, hCA I = 2 μM. The solid smooth lines are the best fit of the data for the K_d values of 6.3 ± 0.4 and 0.14 ± 0.04 μM at pH 5.0 and 9.0 respectively.

Table 5.8. Binding of JB2-48 to hCA I as a function of pH.

pH	K_d	ΔG^o
5.0	6.0 μM	-7.1 kcal/mol
7.0	2.2 μM	-7.7 kcal/mol
9.0	0.14 μM	-9.3 kcal/mol

stopped flow traces for the binding of JB2-48 with hCA I under pseudo-first order condition ([JB2-48] >> hCA I]) at the above pH values. The solid smooth lines are the best fit of the data for the biphasic rate equation with fast and slow relaxation rate constants of 0.69 ± 0.003 and 0.35 ± 0.003 s^{-1} respectively at pH 7.0 (Figure 5.35) and single exponential rate equation with rate constants of 0.08 ± 0.004 and 0.37 ± 0.001 s^{-1} at pH 5.0 and 9.0 respectively (Figure 5.36). These rate constants at pH 5 and 9 translate into the activation energies ($\Delta G^{\ddagger} = -RT \ln (6.2 \times 10^{12}/k)$) of 18.9 and 18.0 kcal/mol respectively. In view of the earlier argument, the difference in the putative transition state jump from 9 to 5. An essentially identical experiment was performed for the mixing of hCA I-JB2-48 complex maintained at pH 5.0 with 200 mM Tris buffer of pH 9.0 (the pH of the mixture was 9.0). It is to be noted that the opposite pH jump (i.e., from 5.0 to 9.0) resulted in the time dependent increase in fluorescence of the enzyme-probe complex. Both the traces of Figure 5.37 conformed to the single exponential rate equation with rate constants of 0.078 ± .0005 and 0.67 ± 0.003 s^{-1} for the pH jump from 9 to 5 and that from 5 to 9, respectively. On the basis that the protonation/deprotonation reactions are diffusion

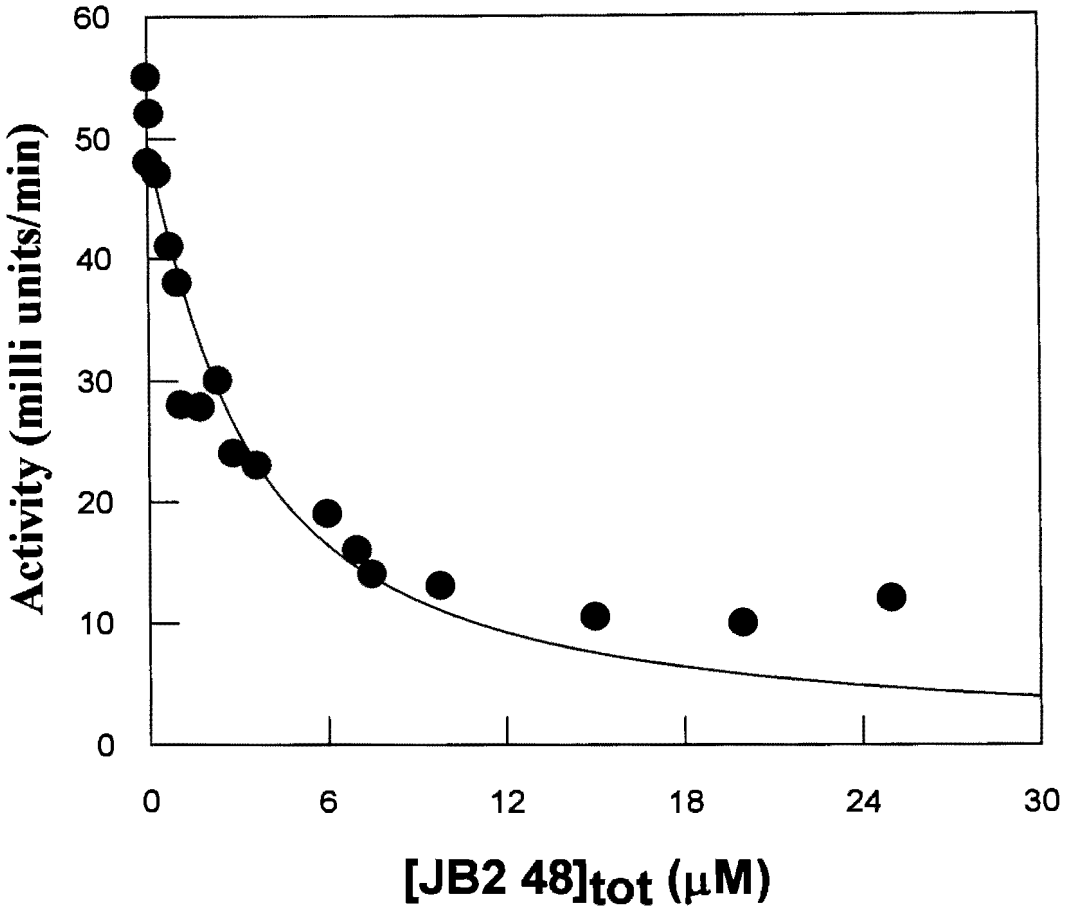

Figure 5.34. Steady-state kinetic data for the inhibition of hCA I by JB2-48.
The initial rate of hydrolysis of p-NPA by hCA I at 348 nm was measured as a function of JB2-48 concentration. [Enzyme] = 2 μM, [p-NPA] = 1 mM. The solid smooth line is the best fit of the data (*328*)with a K_i value of 2.7 ± 0.5 μM.

limited (*535*), the origin of the above rate constants must lie in the slow change in the electronic structure of the hCA I bound JB2-48, which is likely to originate from the readjustment/packing of the enzyme-ligand complex. This is further supported by the fact that the transient rate constants for the association of JB2-48 to hCA I at pH 5.0 and 9.0 (Figure 5.36) are comparable to those obtained from the pH jump experiments from 9 to 5 and from 5 to 9 (Figure 5.37), respectively (see Discussion).

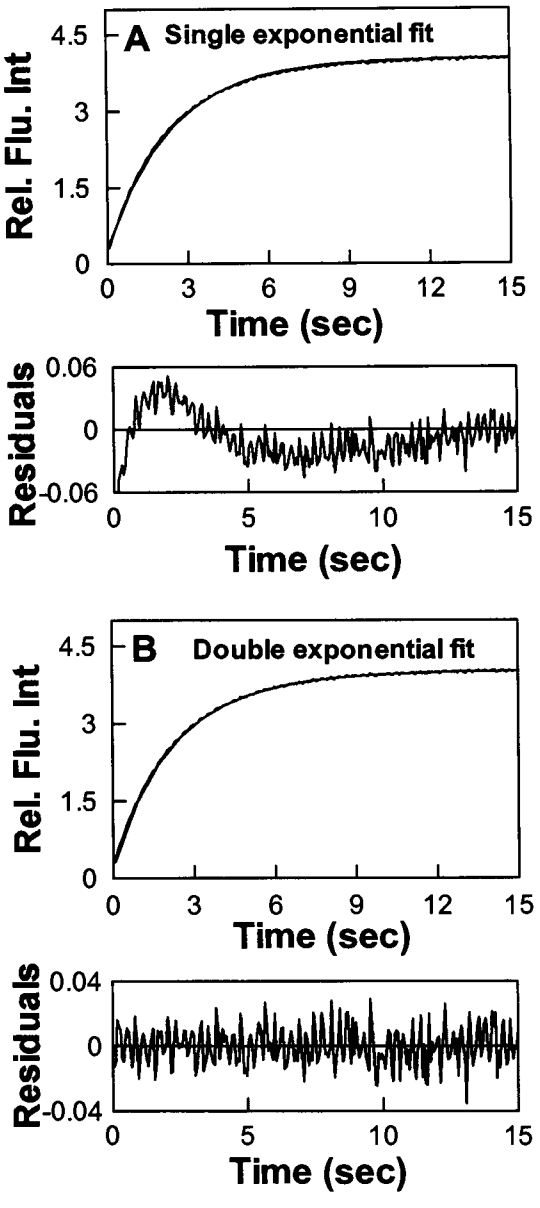

Figure 5.35. Transient kinetics for the binding of JB2-48 to hCA I at pH 7.0.
The stopped flow trace for the mixing of JB2-48 with hCA I in 25 mM HEPEs buffer pH 7.0 is shown (λ_{ex} = 336 nm, "cutoff" filter = 395 nm). The after-mixing concentrations of hCA I and JB2-48 were 1 and 30 μM, respectively. The data were analyzed by both single and double exponential rate equations (smooth lines). However, based on the residuals (bottom panels), the kinetic trace was judged to be biphasic in nature with fast and slow rate constants of 0.69 ± 0.003 and 0.35 ± 0.003 s^{-1}, respectively. The rate constants are the mean ± SD of three independent experiments.

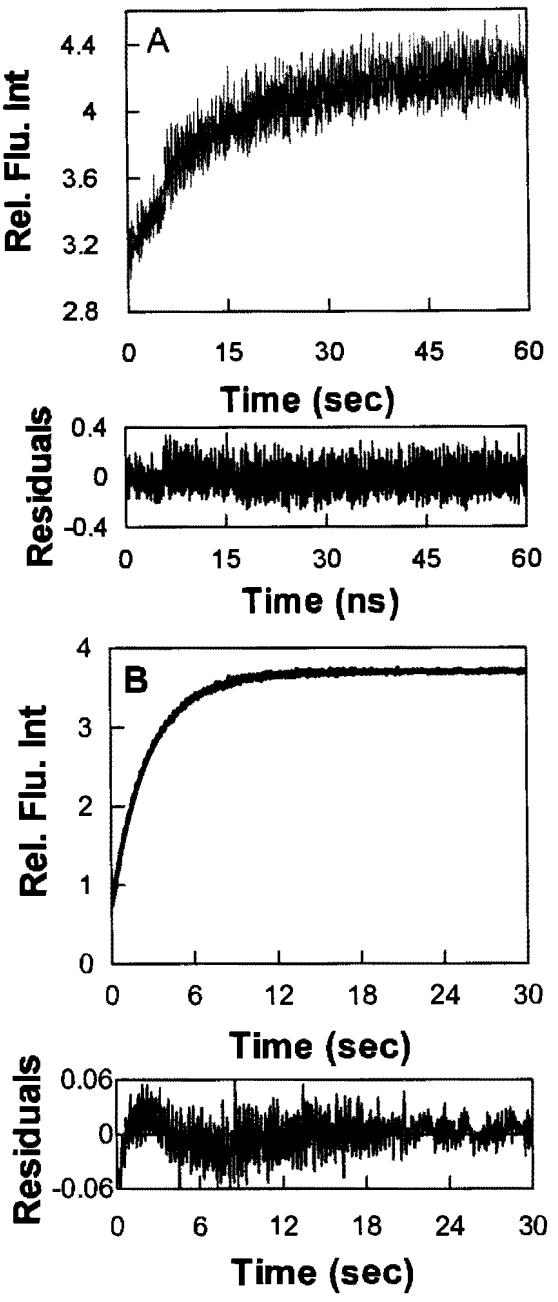

Figure 5.36. Transient kinetics for the binding of JB2-48 to hCA I at acidic and basic pH. The stopped flow traces for the mixing of JB2-48 with hCA I (λ_{ex} = 336 nm, "cutoff" filter = 395 nm) in 25 mM acetate and Tris buffer at pH 5.0 and 9.0 respectively are shown in Panels A and B, respectively.The after-mixing concentrations of hCA I and JB2-48 were 1 and 30 μM, respectively.The solid smooth lines are the best fit of the data according to the single exponential rate equation for the relaxation rate constants (k_{obs}) of 0.08 ± 0.004 and 0.37 ± 0.001 s^{-1} at pH 5.0 and 9.0, respectively.

5.3.4. Transient kinetic studies for the binding of DNSA and JB2 compounds with hCA isozymes

In order to delineate the difference in the microscopic pathways for the binding of DNSA and JB2 compounds by hCA isozymes, transient kinetic experiments were performed using these fluorescent compounds. The experimental set up was similar to that explained in the above section with the exception that 25 mM HEPES containing 10 % DMSO, pH 7.0 was the only buffer used in the following experiments.

5.3.4.1. Transient kinetic studies for the interaction of hCA with DNSA

The transient kinetic experiments for the binding of DNSA to hCA VII and hCA XII were investigated via the stopped flow system as described above.On the other hand, experiments involving JB2-46 has been performed with all hCA isozymes (hCA I, hCA II, hCA VII, hCA XII).

Figure 5.38A and 5.40A shows the representative stopped flow traces for the time dependent increase (k_{obs}) in the fluorescence signals upon interaction of hCA VII and hCA XII with DNSA under a pseudo first order condition. The solid smooth lines are the best fit of the data according to the single-exponential rate equation for the relaxation rate constants being equal to $0.25 \pm 0.003\ s^{-1}$ and $0.15 \pm 0.001\ s^{-1}$ indicating a similar association rate for both the isozymes.

Transient kinetic studies for the dissociation of DNSA from hCA VII and hCA XII active site were performed to obtain their dissociation "off rates". For this, hCA VII and hCA XII were mixed with saturating concentrations of DNSA in one syringe while the other syringe contained excessive (saturating) concentrations of either acetazolamide or benzene sulfonamide. As these two compounds are competitive inhibitors of hCA

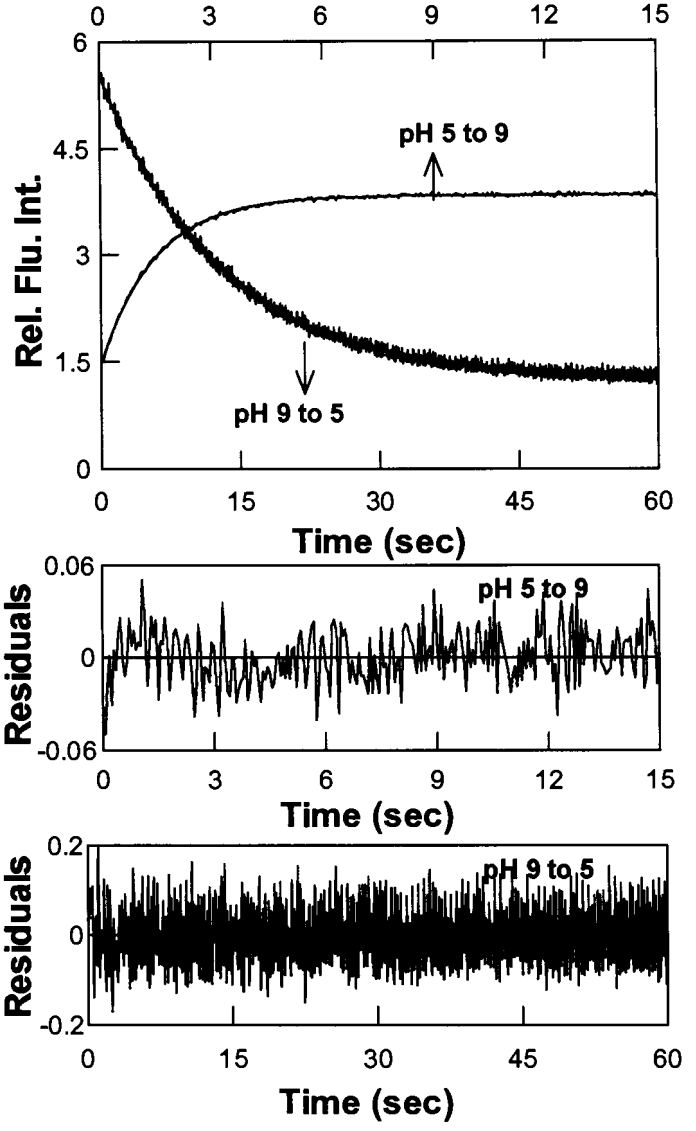

Figure 5.37. pH jump relaxation kinetic studies of hCA I bound JB2-48.
The stopped flow traces for the change in fluorescence of the hCA I-JB2-48 complex upon mixing (the after mixing concentrations of hCA I and JB2-48 being equal to 1 μM and 20 μM, respectively) with buffers of selected pH values are shown. The pH jump from 5 to 9 (increase in fluorescence) was accomplished by mixing the hCA I- JB2-48 complex in 5 mM acetate buffer (pH 5.0) with 200 mM Tris buffer (pH 9.0). The pH of the mixture was found to be 9.0. The pH jump from 9 to 5 (decrease in fluorescence) was accomplished by mixing the hCA I-JB2-48 complex in 5 mM Tris buffer (pH 9.0) with 200 mM acetate buffer (pH 5.0). The pH of the mixture was found to be 5.0. The solid smooth lines are the best fit of the data according to the single-exponential rate equation with the rate constants of 0.67 ± 0.003 s^{-1} and 0.078 ± 0.0005 s^{-1} for the pH jump experiments from 5 to 9 and from 9 to 5, respectively.

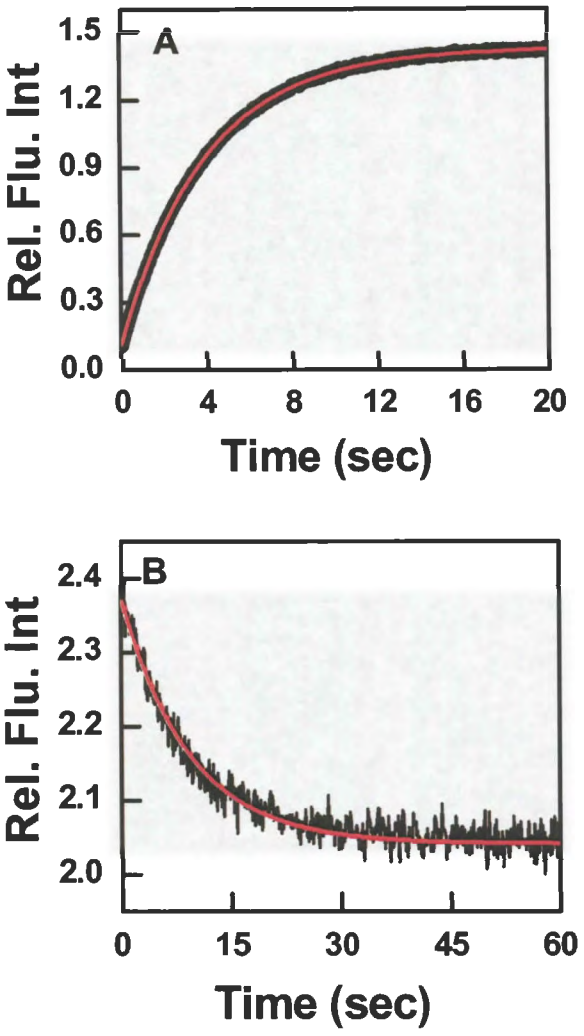

Figure 5.38. Stopped flow traces for the interaction of hCA VII with DNSA.
Panel A: Representative stopped-flow traces for the association of DNSA with hCA VII. The samples were excited at 330 nm. The after-mixing concentration of hCA VII and dansylamide were 1 μM and 6.79 μM respectively. The solid smooth line is the best fit of the experimental data according to the single exponential rate equation with rate constant of $0.25 \pm 0.003\ s^{-1}$
Panel B: Representative stopped-flow traces for the dissociation of dansylamide from the hCA VII-dansylamide complexes. 100 μM benzene sulfonamide was used to dissociate DNSA from hCA VII active site and the decrease in the fluorescence intensity of hCA VII-DNSA complex was monitored as a function of time. The after mixing concentrations of the individual species were as follows: [hCA VII] = 1 μM [dansylamide] = 10 μM, [benzenesulfonamide] = 100 μM. The solid smooth line is the best fit of the experimental data according to the single-exponential rate equation with the dissociation rate constant of $0.109 \pm 0.002\ s^{-1}$

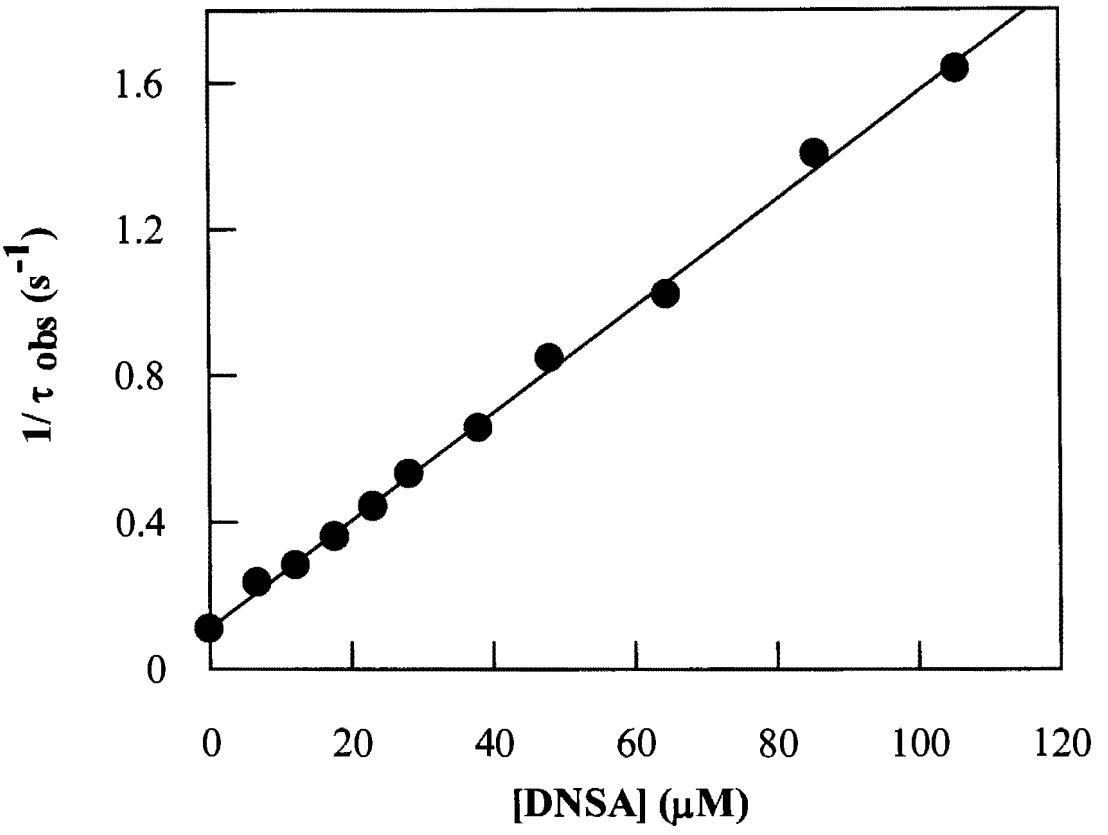

Figure 5.39. Dansylamide concentration dependence of the relaxation rate constants with hCA VII.
The relaxation rate constants (determined under a pseudo-first-order condition) for the binding of dansylamide with hCA VII was determined as a function of the DNSA concentration. The samples were excited at 330 nm. The after-mixing concentration of hCA VII was kept at 2 μM . The data at the zero concentration of dansylamide were taken from the dissociation off-rate measurements. The solid line is the linear regression analysis of the data for the intercept and slope values of 0.11 ± 0.01 $\mu M^{-1}s^{-1}$ and 0.014 ± 0.00004 s^{-1} respectively.

and are present at much higher concentrations than DNSA, mixing the ingredients of both the syringes led to the competitive displacement of DNSA from their respective enzyme sites causing a decrease in the fluorescence signal of the above. Since the rate of dissociation of DNSA from the active sites of the above hCAs would be limited by the formation of hCA- benzene sulfonamide or hCA -acetazolamide complex, this rate would

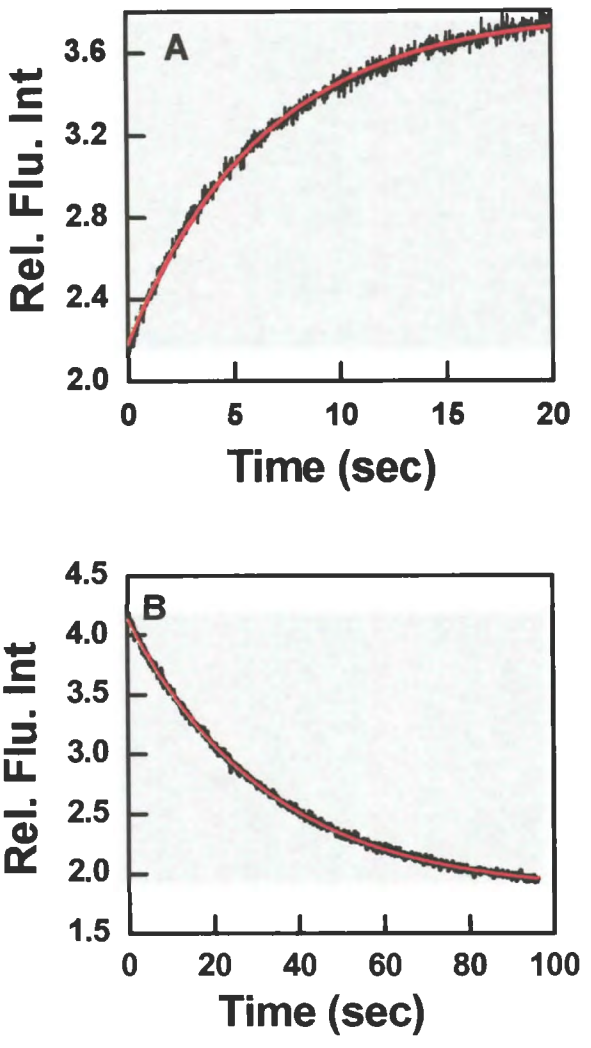

Figure 5.40. Stopped flow traces for the interaction of hCA XII with DNSA.
Panel A: Representative stopped-flow traces for the interaction of DNSA with hCA XII. The samples were excited at 330 nm. The after-mixing concentration of hCA XII and dansylamide were 1 μM and 4.25 μM respectively. The solid smooth line is the best fit of the experimental data according to the single exponential rate equation with rate constant of $0.15 \pm 0.001\ s^{-1}$
Panel B: Representative stopped-flow traces for the dissociation of dansylamide from the hCA VII-dansylamide complexes. 100 μM acetazolamide was used to dissociate DNSA from hCA XII active site and the decrease in the fluorescence intensity of hCA XII-DNSA complex was monitored as a function of time. The after mixing concentrations of the individual species were as follows: [hCA XII] = 1 μM [dansylamide] = 10 μM [acetazolamide] = 100 μM. The solid smooth line is the best fit of the experimental data according to the single-exponential rate equation with the dissociation rate constant of $0.003 \pm 0.001\ s^{-1}$

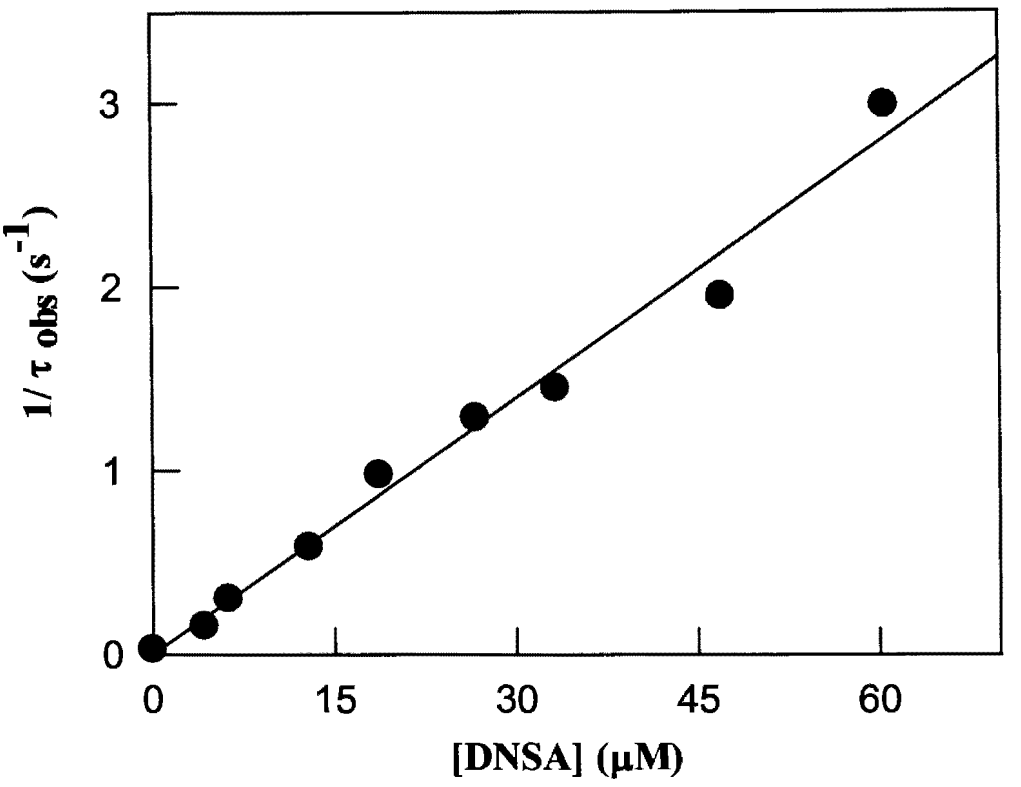

Figure 5.41. Dansylamide concentration dependence of the relaxation rate constants with hCA XII.
The relaxation rate constants (determined under a pseudo-first-order condition) for the binding of dansylamide with hCA XII was determined as a function of the DNSA concentration. The samples were excited at 330 nm. The after-mixing concentrations of hCA XII was kept at 2 μM respectively. The data at the zero concentration of dansylamide were taken from the dissociation off-rate measurements. The solid line is the linear regression analysis of the data for the intercept and slope values of $0.0015 \pm 0.06\ \mu M^{-1}s^{-1}$ and $0.0464 \pm 0.002\ s^{-1}$ respectively.

serve as a measure of dissociation off rate (k_{off}) of the hCA- methazolamide/benzene sulfonamide complex. Figure 5.38B and 5.40B represents the stopped flow traces for the dissociation of DNSA from hCA VII and hCA XII active site respectively. The solid smooth lines are the best fit of the experimental data for the dissociation "off-rates" of

DNSA from hCA VII and hCA XII as being equal to 0.109 ± 0.002 and 0.003 ± 0.0001 s^{-1}. It is evident from the dissociation off rate that the dissociation of DNSA from hCA XII active site is atleast 34 times slower than that from hCA VII.

Transient kinetic experiments for the association of DNSA to hCA VII and hCA XII were performed as a function of ligand concentration. All the k_{obs} values were determined under pseudo first order conditions and these values are plotted as a function of DNSA concentration as represented in Figure 5.39 (for hCA VII) and Figure 5.41 (for hCA XII). It can be seen from the Figures that the k_{obs} values are dependent on the DNSA concentration and increases linearly with respect to increase in DNSA concentration. The solid smooth lines are the best fits of the data for the linear regression analysis yielding the slope and intercept values as being equal to 0.014 ± 0.00004 $\mu M^{-1}s^{-1}$ and 0.11 ± 0.01 s^{-1} and 0.0464 ± 0.002 $\mu M^{-1}s^{-1}$ and 0.0015 ± 0.006 s^{-1} for hCA VII and hCA XII respectively. It should be noted that the intercepts obtained in both the cases are similar to the k_{off} values determined experimentally. The linear dependence exhibited above indicates that DNSA binds to hCA VII and hCA XII in a single step (see discussion).

5.3.4.2. Transient kinetic studies for the interaction of hCA to JB2-46

The transient kinetic experiments for the binding of JB2-46 with hCA I, hCA II, hCA VII and hCA XII were performed in a similar manner as mentioned for DNSA. The association rates as a function of JB2-46 concentration and the K_{off} for the dissociation of JB2-46 from the enzyme site were determined with all the isozymes.

Figures 5.42A, 5.44A, 5.46A and 5.48A shows the representative stopped flow traces for the time dependent increase in the fluorescence signals upon interaction of JB2-46 with hCA I, hCA II, hCA VII and hCA XII, respectively, under pseudo first order

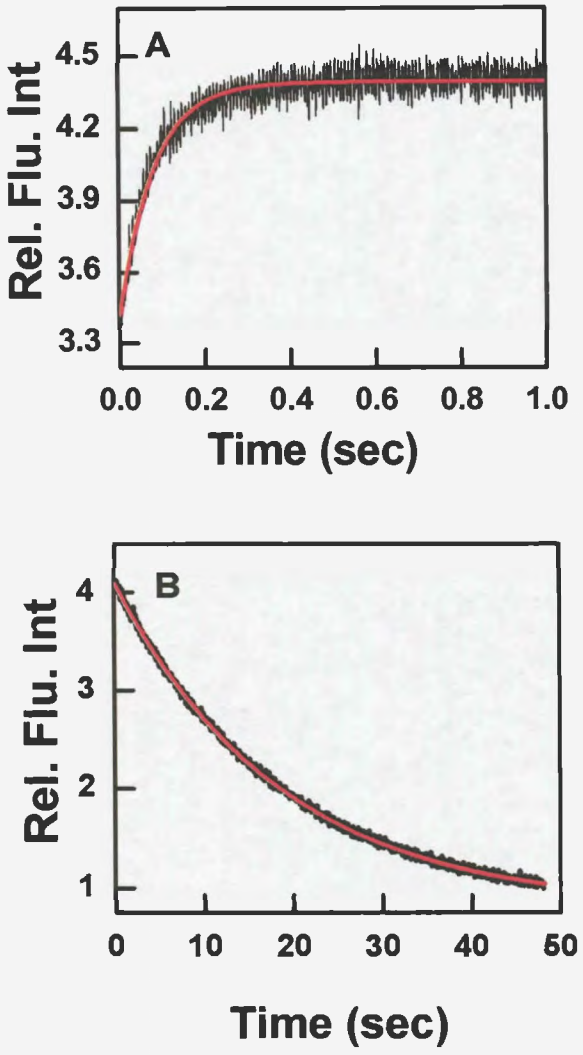

Figure 5.42. Stopped flow traces for the interaction of hCA I with JB2-46.
Panel A: Representative stopped-flow traces for the association of JB2-46 with hCA I. The samples were excited at 330 nm. The after-mixing concentration of hCA I and JB2-46 were 1 μM and 35 μM respectively. The solid smooth line is the best fit of the experimental data according to the single exponential rate equation with rate constant of 13 ± 0.02 s^{-1}.
Panel B: Representative stopped-flow traces for the dissociation of JB2-46 from the hCA I-JB2-46 complexes. 100 μM methazolamide was used to dissociate JB2-46 from hCA I active site and the decrease in the fluorescence intensity of hCA I-JB2-46 complex was monitored as a function of time. The aftermixing concentrations of the individual species were as follows: [hCA I] = 1 μM [JB2-46]) = 35 μM, [methazolamide] = 100 μM. The solid smooth line is the best fit of the experimental data according to the single-exponential rate equation with the dissociation rate constant of 0.055 ± 0.0004 s^{-1}.

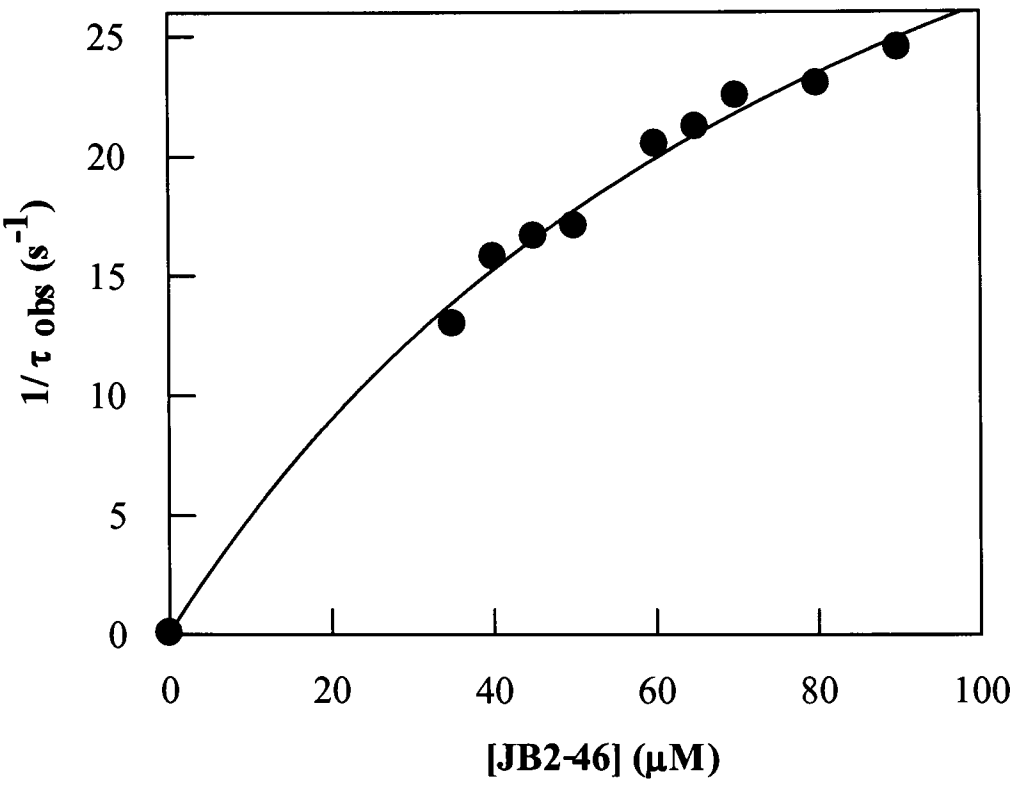

Figure 5.43. JB2-46 concentration dependence of the relaxation rate constants with hCA I. The relaxation rate constants (determined under a pseudo-first-order condition) for the binding of JB2-46 with hCA I was determined as a function of the JB2-46 concentration. The samples were excited at 330 nm. The after-mixing concentration of hCA I was kept at 1 μM. The data at the zero concentration of JB2-46 were taken from the dissociation off-rate measurements. The solid smooth line is the best fit of the data for the relaxation rate constants at the saturating concentration of JB2-46 ($1/\tau_{max}$), and the concentration of JB2-46 required to achieve half of the maximal saturation (K_e) as being equal to 92.9 s^{-1} and 50.58 μM respectively.

conditions. The solid smooth lines are the best fit of the data according to the single-exponential rate equation for the relaxation rate constants being equal to 13 s^{-1}, 17.8 s^{-1}, 0.51 s^{-1}, 0.73 s^{-1} respectively. The transient kinetic studies for the dissociation of JB2-46 from hCA active site were also performed. In this endeavor, hCA was mixed with saturating concentrations of JB2-46 and was taken in one syringe. The other syringe

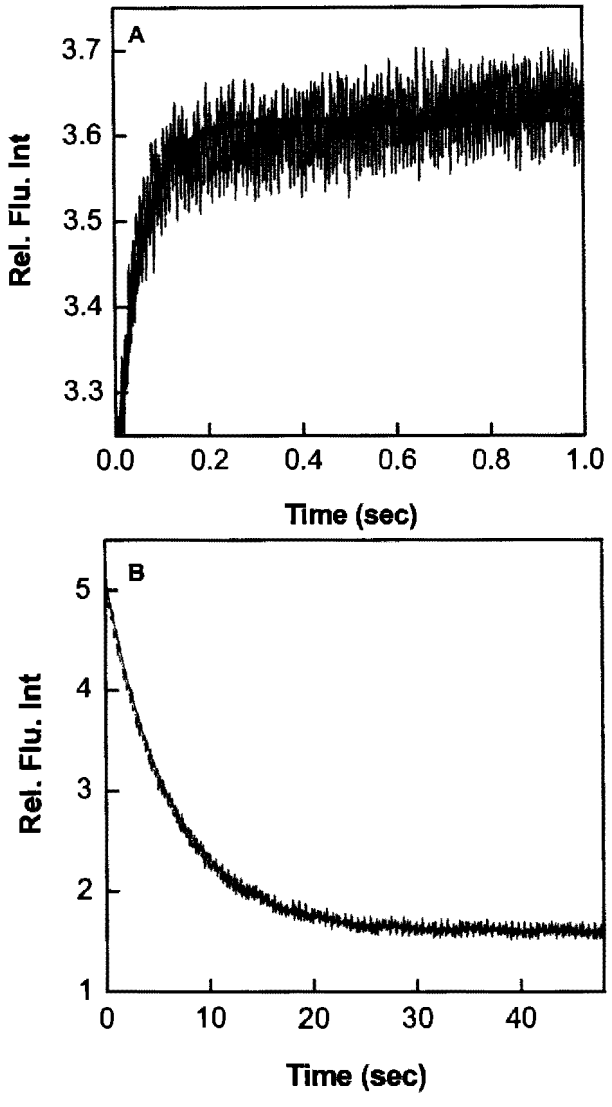

Figure 5.44. Stopped flow traces for the interaction of hCA II with JB2-46.
Panel A: Representative stopped-flow traces for the association of JB2-46 with hCA II I. The samples were excited at 330 nm. The after-mixing concentration of hCA II and JB2-46 were 1 μM and 32 μM respectively. The solid smooth line is the best fit of the experimental data according to the single exponential rate equation with rate constant of $17.8 \pm 0.132\ s^{-1}$
Panel B: Representative stopped-flow traces for the dissociation of JB2-46 from the hCA I-JB2-46 complexes. 100 μM methazolamide was used to dissociate JB2-46 from hCA I active site and the decrease in the fluorescence intensity of hCA I-JB2-46 complex was monitored as a function of time. The aftermixing concentrations of the individual species were as follows: [hCA I] = 1 μM [JB2-46] = 35 μM, [methazolamide] = 100 μM. The solid smooth line is the best fit of the experimental data according to the single-exponential rate equation with the dissociation rate constant of $0.1 \pm 0.004\ s^{-1}$.

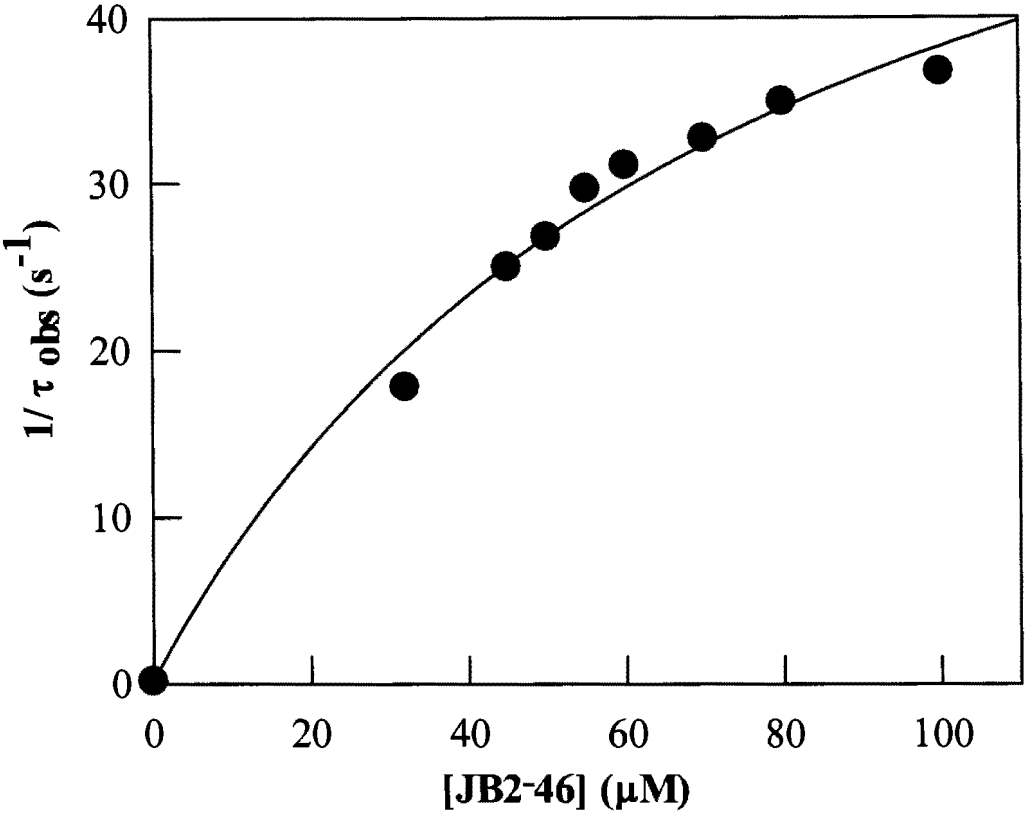

Figure 5.45. JB2-46 concentration dependence of the relaxation rate constants with hCA II. The relaxation rate constants (determined under a pseudo-first-order condition) for the binding of JB2-46 with hCA II was determined as a function of the JB2-46 concentration. The samples were excited at 330 nm. The after-mixing concentration of hCA II was kept at 1 μM. The data at the zero concentration of JB2-46 were taken from the dissociation off-rate measurements. The solid smooth line is the best fit of the data for the relaxation rate constants at the saturating concentration of JB2-46 ($1/\tau_{max}$), and the concentration of JB2-46 required to achieve half of the maximal saturation (K_e) as being equal to 66.6 ± 7.2 s^{-1} and 75.2 ± 15.2 μM respectively.

contained excessive (super saturating) concentrations of methazolamide. As methazolamide is a competitive inhibitor and is present in much higher concentrations than JB2-46, mixing the ingredients of both the syringes led to the competitive displacement of

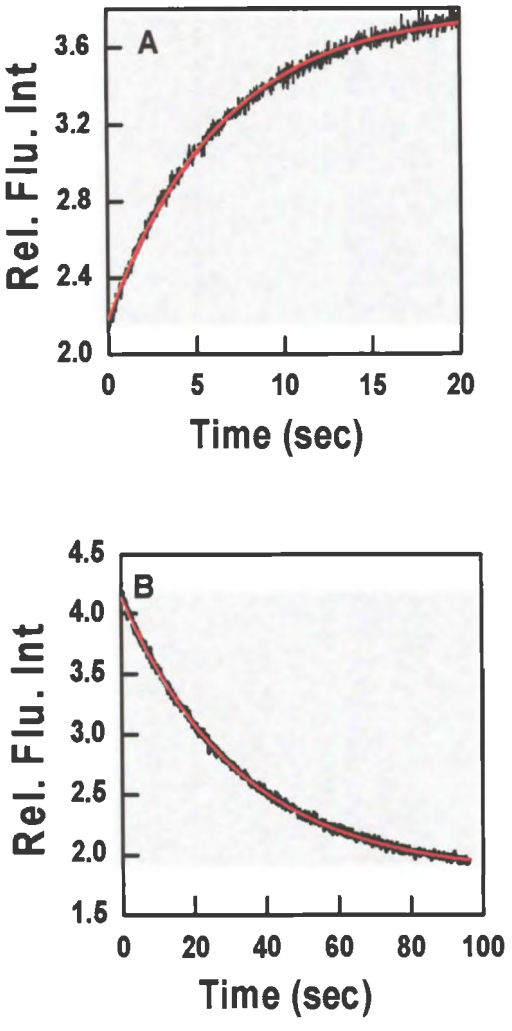

Figure 5.46. Stopped flow traces for the interaction of hCA VII with JB2-46.
Panel A: Representative stopped-flow traces for the association of JB2-46 with hCA VII. The samples were excited at 330 nm. The after-mixing concentration of hCA VII and JB2-46 were 2 μM and 10μM respectively. The solid smooth line is the best fit of the experimental data according to the single exponential rate equation with rate constant of $0.51 \pm 0.01\ s^{-1}$
Panel B: Representative stopped-flow traces for the dissociation of JB2-46 from the hCA VII-JB2-46 complexes. Methazolamide was used to dissociate JB2-46 from hCA VII active site and the decrease in the fluorescence intensity of hCA VII-JB2-46 complex was monitored as a function of time. The aftermixing concentrations of the individual species were as follows: [hCA VII] = 2 μM, [JB2-46] = 30 μM, [methazolamide] = 100 μM. The solid smooth line is the best fit of the experimental data according to the single-exponential rate equation with the dissociation rate constant of $0.006 \pm 0.002\ s^{-1}$

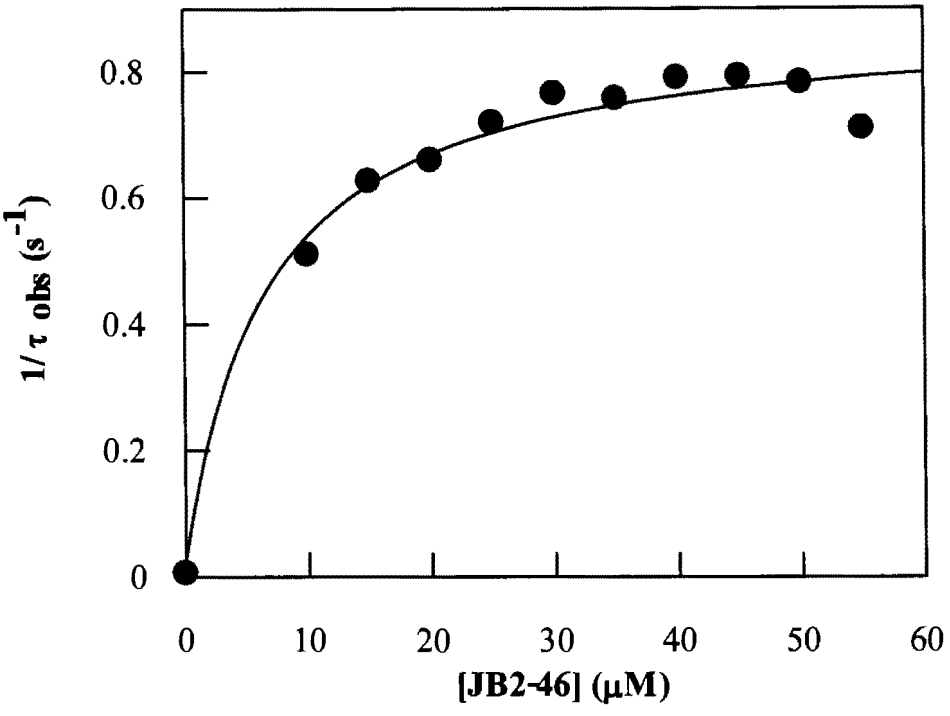

Figure 5.47. JB2-46 concentration dependence of the relaxation rate constants with hCA VII.

The relaxation rate constants (determined under a pseudo-first-order condition) for the binding of JB2-46 with hCA VII was determined as a function of the JB2-46 concentration. The samples were excited at 330 nm. The after-mixing concentration of hCA VII was kept at 1 μM. The data at the zero concentration of JB2-46 were taken from the dissociation off-rate measurements. The solid smooth line is the best fit of the data for the relaxation rate constants at the saturating concentration of JB2-46 ($1/\tau_{max}$), and the concentration of JB2-46 required to achieve half of the maximal saturation (K_e) as being equal to 0.86 ± 0.03 s^{-1} and 6.65 ± 1.3 μM respectively.

JB2-46 by methazolamide causing a decrease in the fluorescence signal of enzyme bound

JB2-46. As the rate of dissociation of JB2-46 from the active site of hCA would be limited

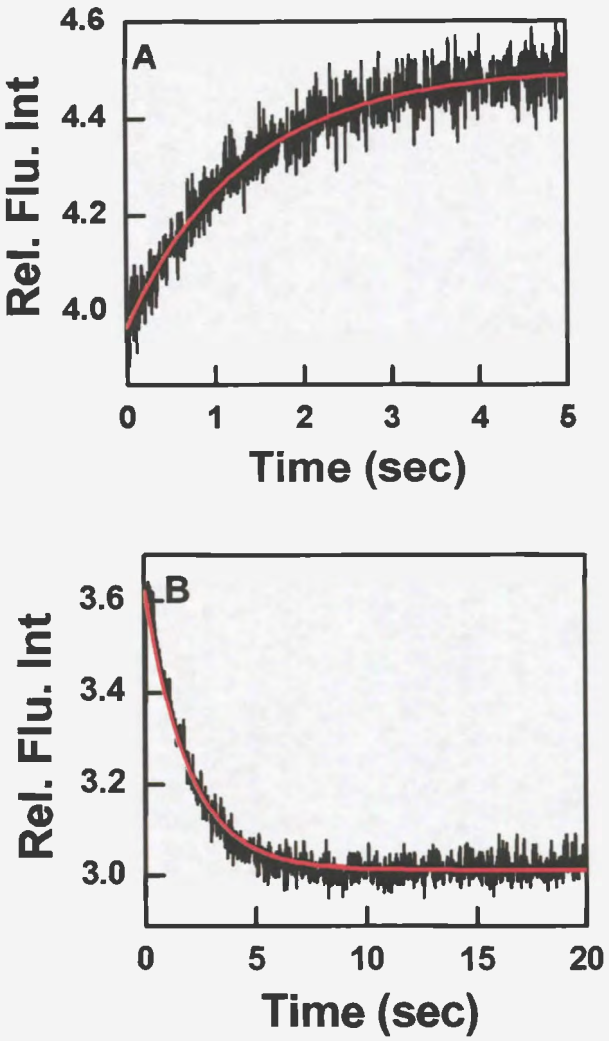

Figure 5.48. Stopped flow traces for the interaction of hCA XII with JB2-46.
Panel A: Representative stopped-flow traces for the association of JB2-46 with hCA XII. The samples were excited at 330 nm. The after-mixing concentration of hCA XII and JB2-46 were 2 μM and 10μM respectively. The solid smooth line is the best fit of the experimental data according to the single exponential rate equation with rate constant of $0.73 \pm 0.02\ s^{-1}$.
Panel B: Representative stopped-flow traces for the dissociation of JB2-46 from the hCA XII-JB2-46 complexes. 100 μM methazolamide was used to dissociate JB2-46 from hCA XII active site and the decrease in the fluorescence intensity of hCA XII-JB2-46 complex was monitored as a function of time. The aftermixing concentrations of the individual species were as follows: [hCA XII] = 2 μM, [JB2-46] = 30 μM, [methazolamide] = 100 μM. The solid smooth line is the best fit of the experimental data according to the single-exponential rate equation with the dissociation rate constant of $0.09 \pm 0.005\ s^{-1}$.

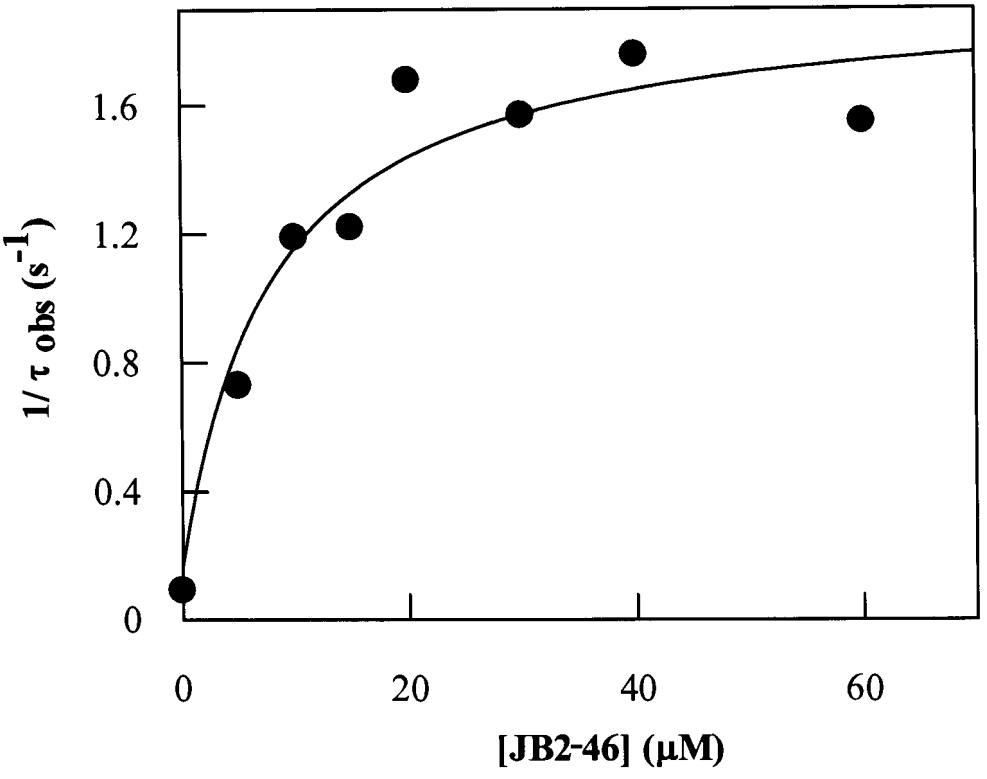

Figure 5.49. JB2-46 concentration dependence of the relaxation rate constants with hCA XII.

The relaxation rate constants (determined under a pseudo-first-order condition) for the binding of JB2-46 with hCA XII was determined as a function of the JB2-46 concentration. The samples were excited at 330 nm. The after-mixing concentration of hCA XII was kept at 1 μM. The data at the zero concentration of JB2-46 were taken from the dissociation off-rate measurements. The solid smooth line is the best fit of the data for the relaxation rate constants at the saturating concentration of JB2-46 ($1/\tau_{max}$), and the concentration of JB2-46 required to achieve half of the maximal saturation (K_e) as being equal to 1.7 ± 0.17 s^{-1} and 7.9 ± 2.1 μM respectively.

by the formation of hCA-methazolamide complex, this rate was used as a measure of dissociation off rate (k_{off}) of the hCA- JB2-46 complex. Figures 5.42B, 5.44B, 5.46B and 5.48B represents the stopped flow traces for the dissociation of JB2-46 from hCA I, hCA

II, hCA VII and hCA XII active site respectively. The solid smooth lines are the best fit of the experimental data for the dissociation "off-rates" of JB2-46 from hCA I, hCA II, hCA VII and hCA XII as being equal to 0.055 s^{-1}, 0.1 s^{-1}, 0.006 s^{-1}, and 0.09 s^{-1} respectively. It is evident from the dissociation off rates that the dissociation of JB2-46 from hCA VII active site is atleast 9 times slower than hCA I, 15 times slower than hCA II and 16 times slower than hCA XII.

Transient kinetic experiments for the association of JB2-46 to hCA isozymes were performed as a function of ligand concentration. All the k_{obs} values were determined under pseudo first order conditions and these values are plotted as a function of JB2-46 concentration as represented in Figure 5.43 (for hCA I), Figure 5.45 (hCA II), Figure 5.47 (for hCA VII) and Figure 5.49 (for hCA XII). It can be seen from the Figures that the K_{obs} values are dependent on the JB2-46 concentration with an increase in magnitude as the concentration of JB2-46 was increased. However, in contrast to DNSA, this increase conforms to hyperbolic dependence in all hCA isozymes. The data corresponding to zero concentration of JB2-46 was taken from the dissociation off rate measurements (Figure 5.42B, 5.44B, 5.46B, 5.48B). The solid smooth lines of Figures 5.43, Figure 5.45, Figure 5.47 and Figure 5.49 are the best fits of the data for the hyperbolic dependence of K_{obs} on JB2-46 yielding relaxation rate constants at the saturating concentration of JB2-46 ($1/\tau_{max}$) and the concentration of JB2-46 required to achieve half of the maximum saturation of the enzyme (K_e) as being equal to 92.9 s^{-1} and 50.8 μM (for hCA I), 66.6 s^{-1} and 75.2 μM (for hCA II), 0.86 s^{-1} and 6.65 μM (for hCA VII), 1.7s^{-1} and 7.9 μM (for hCA XII) respectively. The K_d values obtained using the the concentration dependence values for hCA – JB2-46 interaction was calculated to be 0.09 μM, 0.1 μM, 0.04 μM , 0.1 μM for

hCA I, II, VII and XII respectively. It should be noted that these values are qualitatively similar to those obtained from spectrofluorometric titrations (Table 5.7).

5.4. Thermodynamic studies of hCA-ligand interactions.

5.4.1. Thermodynamic analysis of the binding of JB2-48 by hCA I

The data from previous sections demonstrated that JB2-48 interacts with hCA I with good binding affinity, and that the K_d value obtained from the spectrofluorometric titrations (either by exciting at 280 nm and monitoring the tryptophan quenching or by exciting at 330 nm and monitoring probe's fluorescence) and the K_i obtained from the esterase activity of hCA I are similar suggesting that the binding in both cases originates from a common physical step. In this regard, it was of interest to determine the detailed thermodynamic parameters and how they change with respect to changes in temperature as well as the buffer media via isothermal titration calorimetric studies. The results obtained from these experiments was envisaged to provide valuable information regarding the changes in heat capactity associated with formation of enzyme-ligand complex and the protonation/deprotonation reactions associated with this interaction.

In a preliminary manner, it was evaluated whether the interaction of hCA I with JB2-48 produced heat signals, hCA I was titrated with the ligand via VP-ITC instrument at 25 °C. Figure 5.50 shows the titration of 25 μM hCA I with 49 x 4 μl injections of 500 μM JB2-48 in 25 mM Tris buffer at pH 7.5.Where as the upper panel shows the raw calorimetric data produced by the titration indicating the amount of heat produced, the lower panel represents the binding curve generated by plotting the area under each peak as a function of the molar ratio of JB2-48. It should be noted that, as the titration progresses, the amount of heat produced starts decreasing progressively. This is due to the saturation

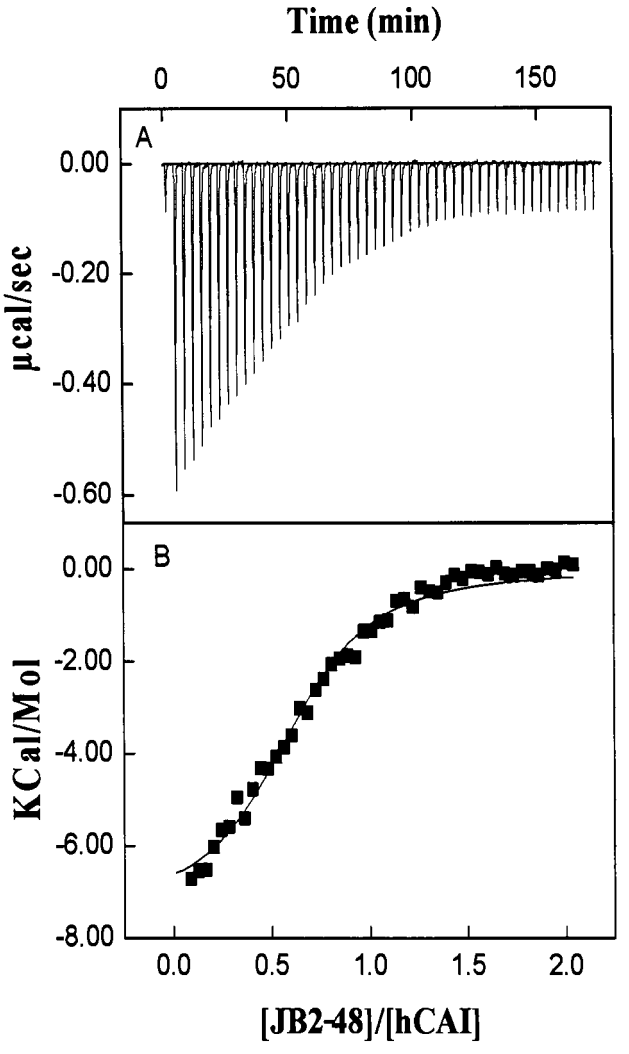

Figure 5.50. Isothermal titration calorimetric assay for the binding of JB2-48 to hCA I at 25 ° C in 25 mM HEPES buffer, pH 7.0.

Panel A of the Figure shows the raw data produced by the titration of 25 µM hCA I by injection of increasing concentrations of (49 x 4 µl injection from 500 µM) JB2-48. Panel B represents the binding curve generated by plotting the area under each peak as a function of molar ratio of JB2-48. The solid smooth line represents the best fit of the data analyzed by the single binding site model provided by the origin software. The analysis yielded the stoichiometry (n), association constant (K_a), and $\Delta H°_{obs}$ as being equal to 0.64, 3.41 x 10^5 M and -7.4 (kcal/ mol) respectively.

of the enzyme active site with the ligand, after which titration of ligand produced heat signals due to its interaction with buffer. The average of these signals was taken as a background signal and was subtracted from the raw data. The solid, smooth line of Figure 5.50 is the best fit of the data according to the model provided by Wiseman et al. (1989) (*469*), yielding values for the stoichiometry (n) of the hCA I-JB2-48 complex, the association constant (K_a), and the standard enthalpy change ($\Delta H°$) of 0.64, 3.41 x 10^5 M and -7.4 kcal/mol respectively. The free energy ($\Delta G°$) for the binding of hCA I to JB2-48 was calculated to be -7.49 kcal/mol. Based on the values of $\Delta H°$ and $\Delta G°$, $T\Delta S°$ was calculated to be 0.089 kcal/mol.

Given the values of $\Delta H°$ and $\Delta G°$, $T\Delta S°$, it is evident that the magnitude of $\Delta G°$ is dominated by the more favourable enthalpic contribution as compared to the entropic contribution. Thus, the interaction of hCA I-JB2-48 is enthalpically driven under the experimental conditions of Figure 5.50.

5.4.1.1. Effect of temperature on the binding of JB2-48 with hCA I

To investigate the effect of temperature on the binding of hCA I-JB2-48, titrations were carried out in 25 mM Tris-HCl buffer, pH 7.5, containing 10 % DMSO, over a range of temperatures from 15°C to 30°C. Figures 5.51 and 5.52 shows the thermodynamic profiles for the titration of 25 μM hCA I with 49 x 4 μl injections of 500 μM JB2-48 in the above buffer at pH 7.5 at temperatures 15°C and 30°C respectively. The thermodynamic parameters derived from the temperature dependent experiments are presented in Table 5.9. From the values presented in the Table, it is evident that $\Delta G°$ remains almost invariant at all temperatures, however, both $\Delta H°$ and $T\Delta S°$ decreases with increase in temperature. Figure 5.53 shows the plot of $\Delta H°$ as a function of temperature. It can be seen from the

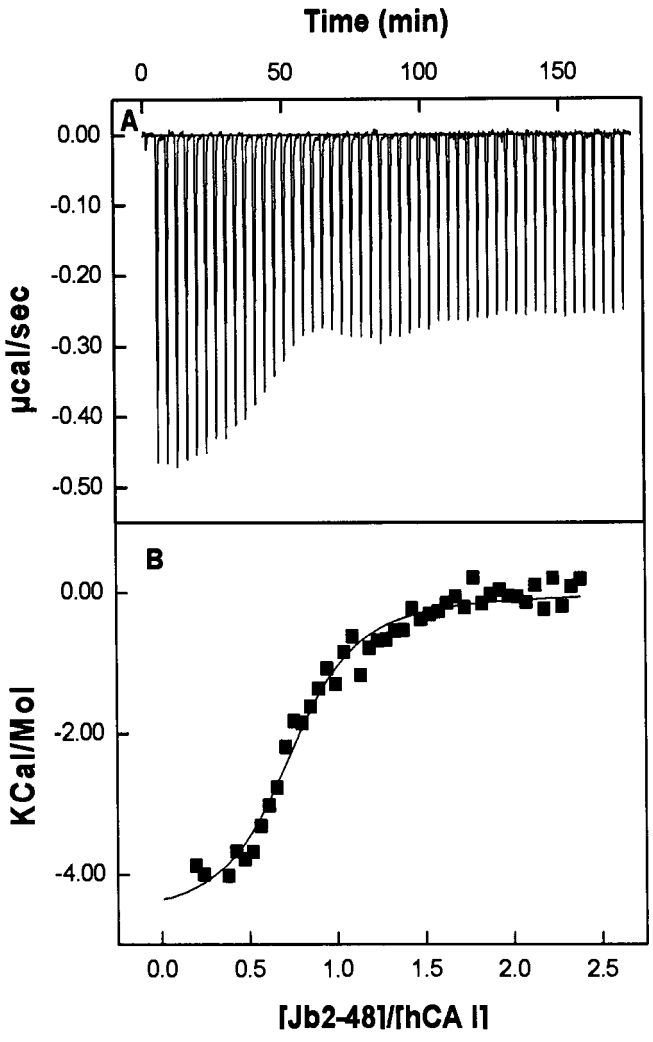

Figure 5.51. Isothermal titration calorimetric assay for the binding of JB2-48 to hCA I at 15 ° C in 25 mM HEPES buffer, pH 7.0.

Panel A of the Figure shows the raw data produced by the titration of 25 µM hCA I by injection of increasing concentrations (49 x 4 µl injection from 500 µM) of JB2-48. Panel B represents the binding curve generated by plotting the area under each peak as a function of molar ratio of JB2-48. The solid smooth line represents the best fit of the data analyzed by the single binding site model provided by the origin software. The analysis yielded the stoichiometry (n), association constant (K_a), and $\Delta H°_{obs}$ as being equal to 0.76, 6.15 x 10^5 M and -4.67 (kcal/ mol) respectively.

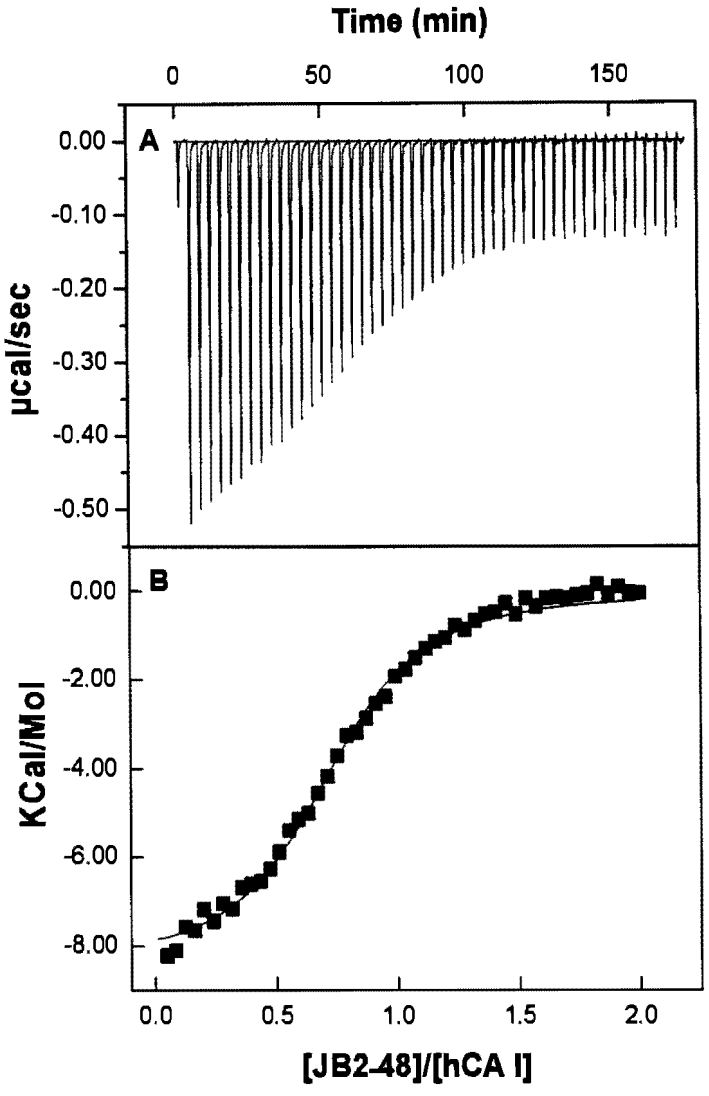

Figure 5.52. Isothermal titration calorimetric assay for the binding of JB2-48 to hCA I at 30 ° C in 25 mM HEPES buffer, pH 7.0.

Panel A of the Figure shows the raw data produced by the titration of 25 µM hCA I by injection of increasing concentrations of (49 x 4 µl injection from 500 µM) JB2-48. Panel B represents the binding curve generated by plotting the area under each peak as a function of molar ratio of JB2-48. The solid smooth line represents the best fit of the data analyzed by the single binding site model provided by the origin software. The analysis yielded the stoichiometry (n), association constant (K_a), and $\Delta H°_{obs}$ as being equal to 0.75, 6.86 x 10^5 M and -8.4 (kcal/ mol) respectively.

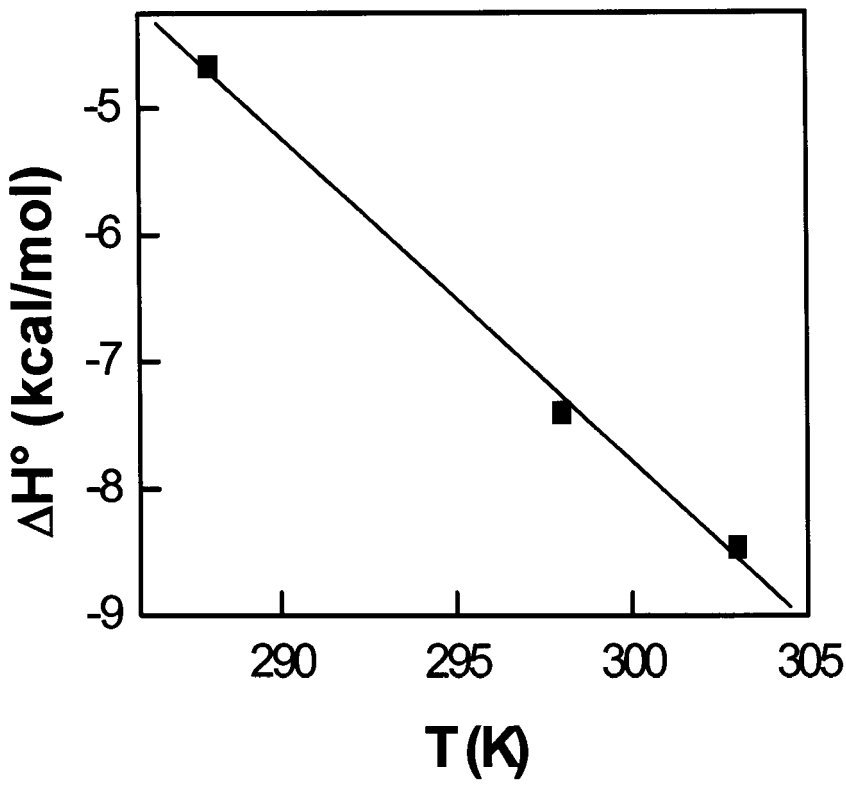

Figure 5.53. Effect of temperature on ΔH^0 for the interaction of JB2-48 with hCA I. The solid smooth line is the linear regression analysis of the experimental data for a slope (ΔC_p^0) of -0.25 ± 0.01 kcal mol^{-1} K^{-1} and an intercept (at 0°K) of 68.9 ± 3.87 kcal mol^{-1}.

Figure that $\Delta H°$ becomes more favourable (more negative) with increase in temperature. This is due to less favourable entropy at higher temperatures. The solid line of the Figure is the best fit for the linear regression analysis with the slope and intercept of -0.255 kcal/mol K^{-1} and 68.9 kcal/mol. Of these, where as the slope represents the ΔCp°, the intercept represents the value of the $\Delta H°$ when the temperature is 0 K. As will be discussed in the next chapter, a large negative ΔCp° value suggests that the binding of JB2-48 to the active site of hCA I is dominated by hydrophobic forces. In order to see the dependence of $\Delta H°$ and ΔG° on $T\Delta S°$, the data on Table 5.9. were plotted in Figure 5.54. From the Figure it is

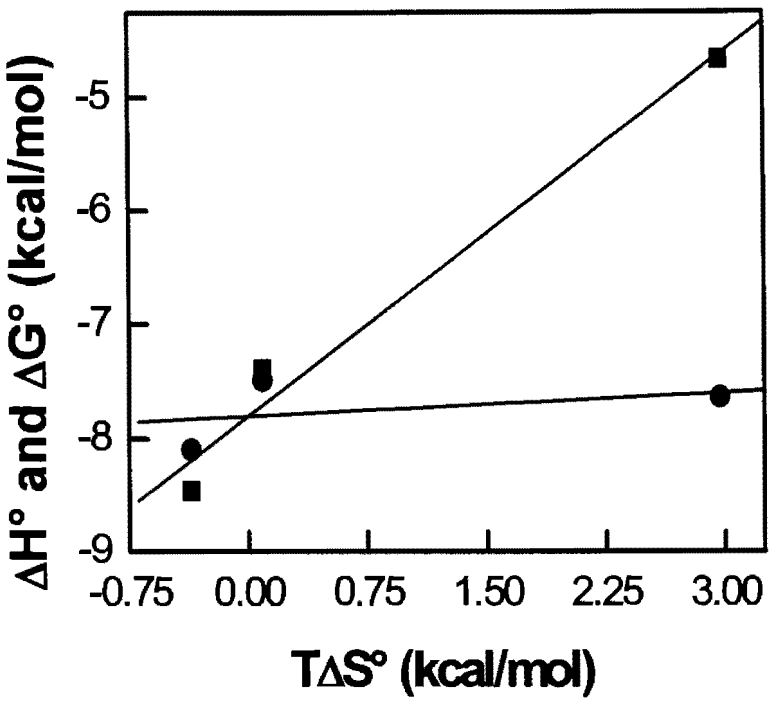

Figure 5.54. Enthalpy-entropy compensation plot for the binding of JB2-48 to hCA I in 25 mM Tris, 10% DMSO (pH 7.0).
The dependence of ΔG^0 and ΔH^0 on $T\Delta S^0$ is shown by circles and squares respectively. The linear regression analysis for the data of ΔH^0 versus $T\Delta S^0$ yields magnitudes of the slope and intercept of 1 ± 0.16 and -7.8 ± 0.2 kcal mol^{-1}, respectively.

evident that where as $\Delta G°$ remains invariant with changes in $T\Delta S°$, $\Delta H°$ increases linearly as a function of $T\Delta S°$ suggesting a strong enthalpy-entropy compensation. Also, note that $\Delta H° = \Delta G°$ when $T\Delta S° = 0$. The temperature at which $\Delta H° = \Delta G°$ could be calculated from the Figure and is found to be 300.7 K. At this temperature, the entropic contribution for the free energy of binding will be equal to zero.

5.4.1.2. Effect of buffer system on the the binding of JB2-48 to hCA I

From the literature evidence, it is apparent that the thermodynamic parameters obtained from the ITC experiments include the sum of all non covalent interactions

involved in forming a complex between an enzyme and ligand (*510*). For instance, the change in enthalpy measured by the ITC experiments includes contributions not only by the heat changes resulting from the formation or removal of non-covalent bonds between enzyme and ligand but also from those involving the interaction between the solvent and the solute molecules during the complex formation (*508*, *509*, *536*). Hence the observed enthalpic changes ($\Delta H°_{obs}$) include heat contributions resulting from binding ($\Delta H°_{bind}$), conformational changes ($\Delta H°_{conf}$), the heat of ionization ($\Delta H°_{ion}$) from the buffer as well as their interactants. The $\Delta H°_{obs}$ is thus expressed as follows.

$$\Delta H°_{obs} = \Delta H°_{bind} + \Delta H°_{conf} + n\Delta H°_{ion} \qquad \text{(Eq 5.1)}$$

The combination of heat changes due to binding and conformational changes can be taken as intrinsic enthalpy ($\Delta H°_{int} = \Delta H°_{bind} + \Delta H°_{conf}$). This modifies the above equation as follows.

$$\Delta H°_{obs} = \Delta H°_{int} + n\Delta H°_{ion} \qquad \text{(Eq 5.2)}$$

In the above equation n represents the number of protons consumed or released in the process of enzyme binding to a ligand. The proton consumption and release that takes place during binding has been investigated by many investigators (*508-510*, *537*, *536*) using different buffers of known ionization enthalpies.

To account for whether the binding of hCA I to JB2-48 involves proton consumption or release, the enthalpic changes were determined by using two buffers of different ionization enthalpies, viz.Tris-HCl ($\Delta H°_{ion}$ = 11.5 kcal mol^{-1}) and phosphate ($\Delta H°_{ion}$ = 1.2 kcal mol^{-1}). Figure 5.55 shows the titration of hCA I by JB2-48 in the phosphate buffer pH 7.5. The $\Delta H°_{obs}$ obtained with Tris-HCl (Figure 5.50) and phosphate buffer (Figure 5.55) indicates that the observed and the intrinsic enthalpies are comparable

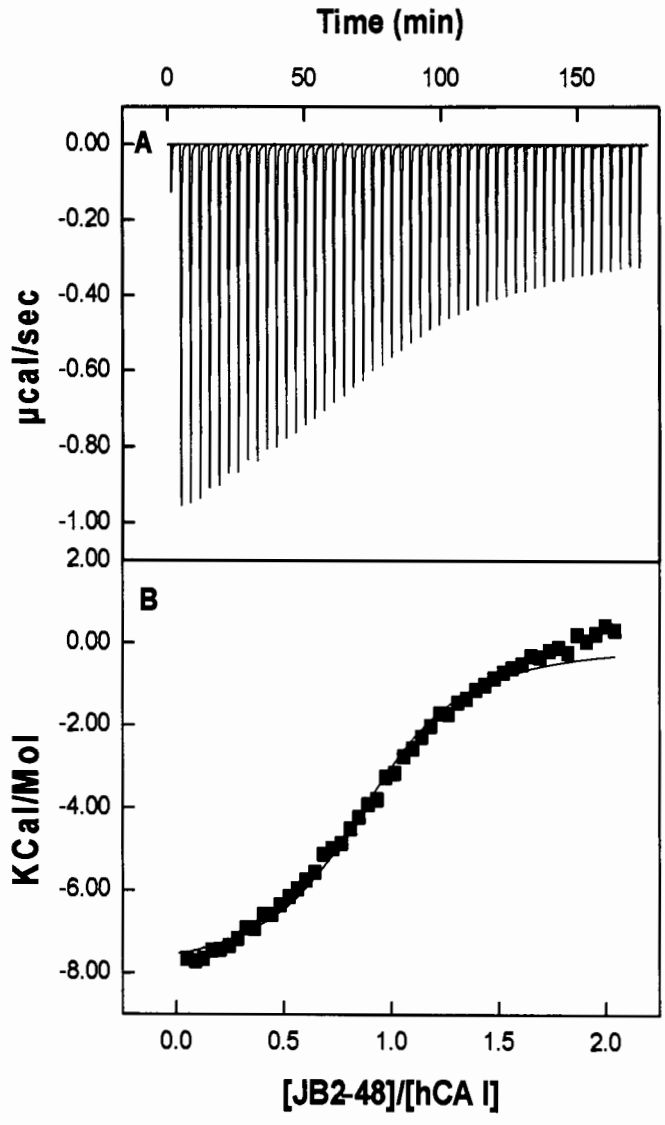

Figure 5.55. Isothermal titration calorimetric assay for the binding of JB2-48 to hCA I at 25 ° C in 25 mM phosphate buffer, pH 7.0.
Panel A of the Figure shows the raw data produced by the titration of 25 µM hCA I by injection of increasing concentrations of (49 x 4 µl injection from 500 µM) JB2-48. Panel B represents the binding curve generated by plotting the area under each peak as a function of molar ratio of JB2-48. The solid smooth line represents the best fit of the data analyzed by the single binding site model provided by the origin software. The analysis yielded the stoichiometry (n), association constant (K_a), and $\Delta H°_{obs}$ as being equal to 0.75, 6.86 x 10^5 M and -8.4 (kcal/ mol), respectively.

Table 5.9. Summary of the thermodynamic data for the interaction of JB2-48 with hCA I at different temperatures and buffer.

T (K)	n	K_a (x 100000 /M)	ΔH°_{obs} (kcal/ mol)	$T\Delta S^\circ$ (kcal /mol)	ΔG° (kcal /mol)
288[a]	0.76	6.15	-4.67	2.97	-7.64
298[a]	0.64	3.41	-7.4	0.089	-7.49
303[a]	0.75	6.86	-8.46	-0.36	-8.1
298[b]	0.92	4.54	-8.0	-0.31	-7.69

. [a] Tris buffer; [b] Phosphate buffer.

and no proton is consumed or released during the process. Upon binding of hCA, the sulfonamide inhibitors require a pH dependent deprotonation. Similarly, the active site zinc bound hydroxide must be protonated before it gets replaced by the amino group of sulfonamide (*65*, *21*, *119*, *22*). Thus the deprotonation of sulfonamide nitrogen is balanced by the protonation of the zinc bound hydroxide resulting in the net protonation/deprotonation value to be zero.

5.4.2. Thermodynamic analysis of the binding of sulfonamide inhibitors to hCA VII

5.4.2.1. Binding isotherms for hCA VII-sulfonamide inhibitors

The results of the binding isotherms of JB2 compounds with hCA isozymes (Table 5.7) revealed comparatively tighter binding of these probes with hCA VII. In order to see whether this phenomena is due to the extended structure of the probes or the intrinsic ability of hCA VII to bind sulfonamides more tightly as compared to the other isozymes, the binding of selective commercially available inhibitors with hCA VII were investigated and the resulting data were compared with that for hCA II(*538*), the most thoroughly studied isozyme of hCA.

The binding affinities for hCA VII-inhibitor complexes were determined by titrating a fixed concentration of hCA VII sataurated with DNSA by increasing

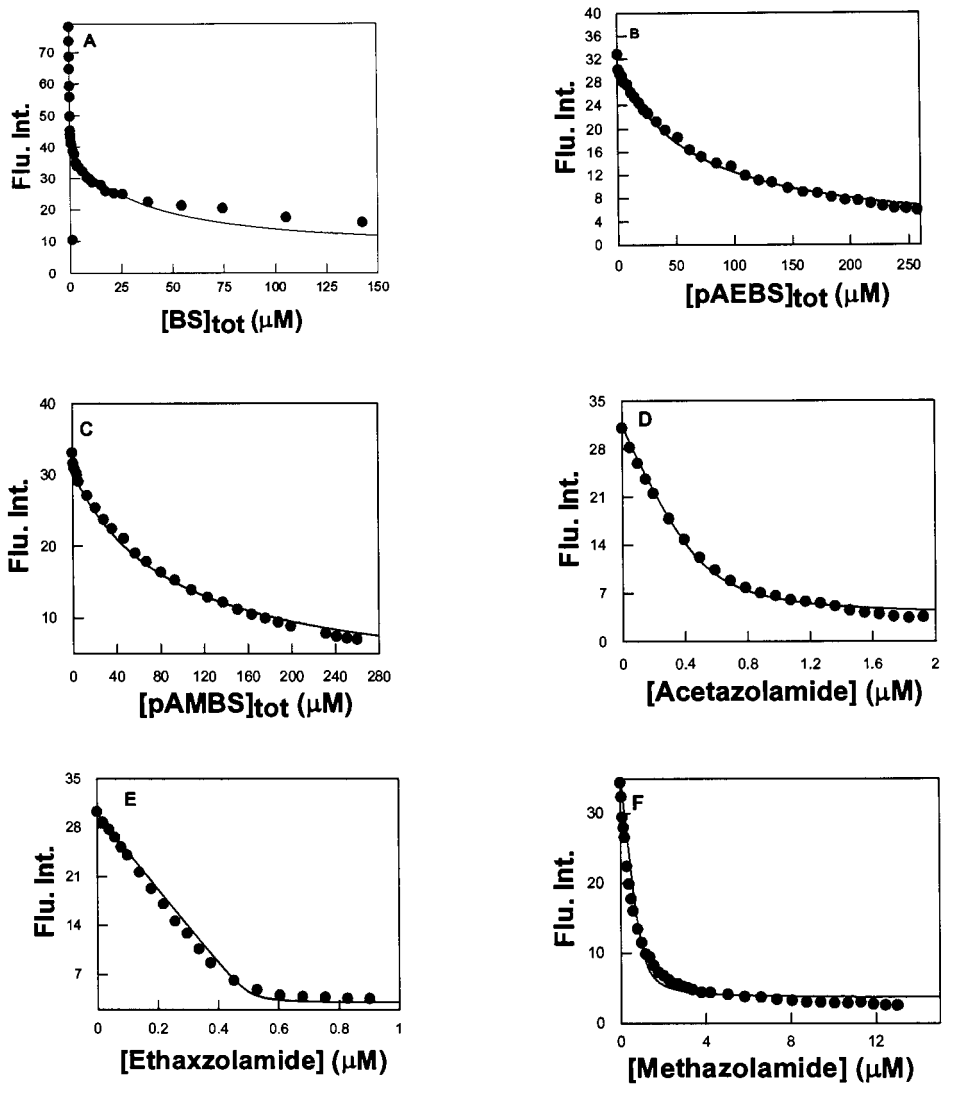

Figure 5.56. Binding isotherms for the interactions of hCA VII with sulfonamide compounds.
Panel A, B, C, D, E and F represents the binding isotherms for the interactions of hCA VII with BS, pAMBS, pAEBS, acetazolamide, ethaxazolamide and methazolamide respectively in 25 mM HEPES pH 7.0 containing 10 % DMSO. [hCA VII] = 0.6 μM. [DNSA] = 20 μM. The decrease in the fluorescence emission intensity of enzyme bound DNSA at 470 nm (λ_{ex} = 330 nm) with increasing concentrations of JB compounds is shown. The solid smooth lines are the best fit of the data yielding the K_d values of 1.4 ± 0.6, 8 ± 0.1, 11 ± 0.3, 0.04 ± 0.04, 0.08 ± 0.08, 0.04 ± 0.1 for panels A, B, C, D, E and F respectively.

Table 5.10. Inhibition data for sulfonamide inhibitors against hCA II (*65*, *538*) and hCA VII.

Inhibitor	K_d / K_i (μM) hCA II	K_d / K_i (μM) hCA VII
Benzene sulfonamide	0.66	1.4
pAEBS	4.3	8
pAMBS	nd	11
Acetazolamide	0.01	0.04
Ethoxzolamide	0.08	0.08
Methazolamide	0.007	0.04

nd: not detected

concentrations of inhibitors. The decrease in the fluorescence signal of hCA VII-DNSA (λ_{ex} = 330 nm, λ_{em} = 448 nm) upon competitive displacement of DNSA by the sulfonamide inhibitors was plotted as a function of the inhibitor concentration. The solid smooth lines of Figure 5.56 are the best fit of the data with the K_d values as listed in Table 5.10. From the K_d values listed in the Table, it is evident that except for methazolamide, all the inhibitors have comparable binding affinities for hCA VII and hCA II.

5.4.2.2. Isothermal titration calorimetric studies for the binding of benzene sulfonamide (BS) to hCA VII at different temperatures.

The energetics of binding of BS to hCA VII was delineated via the ITC method as a function of temperatures ranging from 15° C to 30° C. The results obtained were intended to be compared with those obtained for hCA II. As will be discussed below, despite the similar binding affinities of BS with both the isozymes (Table 5.10) and the high sequence (*43*, *539*, *22*) and structural similarity between hCA II (crystal structure)

(*174*) and hCA VII (homology modeling) (Figure 5.57), the thermodynamic parameters associated with their interactions are markedly different.

Figures 5.58 – 5.61 shows the ITC profiles for the titration of 10 μM hCA VII with 49 x 4 μl injections of 500 μM BS in 25 mM Tris buffer at pH 7.5 at temperatures ranging from 15°C to 30°C. The thermodynamic parameters derived from the temperature dependent experiments of hCA VII and hCA II are presented in Table 5.11 and Table 5.12 respectively. From the values presented in these Tables, it is evident that for hCA VII, where as ΔG° remains almost invariant at all temperatures, however, both $\Delta H°$ and $T\Delta S°$ decreases with increase in temperature. This is in contrast to hCA II where $\Delta H°$ and $T\Delta S°$ increase with increase in temperature. Figure 5.62 shows the plot of $\Delta H°$ as a function of temperature for hCA VII and hCA II. It is evident from the Figures that $\Delta H°$ becomes more favourable (more negative) with increase in temperature for hCA VII, however this is not the case in hCA II where $\Delta H°$ becomes more unfavourable (less negative) with increase in temperature. The favorable and unfavorable change in enthalpies in the case of hCA VII and hCA II respectively, are compensated by the temperature dependent entropies. The solid lines of the Figure 5.62 are the linear regression analysis of the data with the slope and intercept of -0.286 kcal mol^{-1} K^{-1} and 81.3 kcal/mol for hCA VII and 0.463 kcal mol^{-1} K^{-1}, and 148.5 kcal mol^{-1} for hCA II respectively. Of these, where as the slope represents the ΔCp°, intercept represents the value of the $\Delta H°$ when the temperature is 0 K. Note the difference in the ΔCp° values of hCA VII and hCA II. As will be discussed in the next chapter, the above differential thermodynamic parameters originate from subtle differences in the active site pockets of these isozymes.

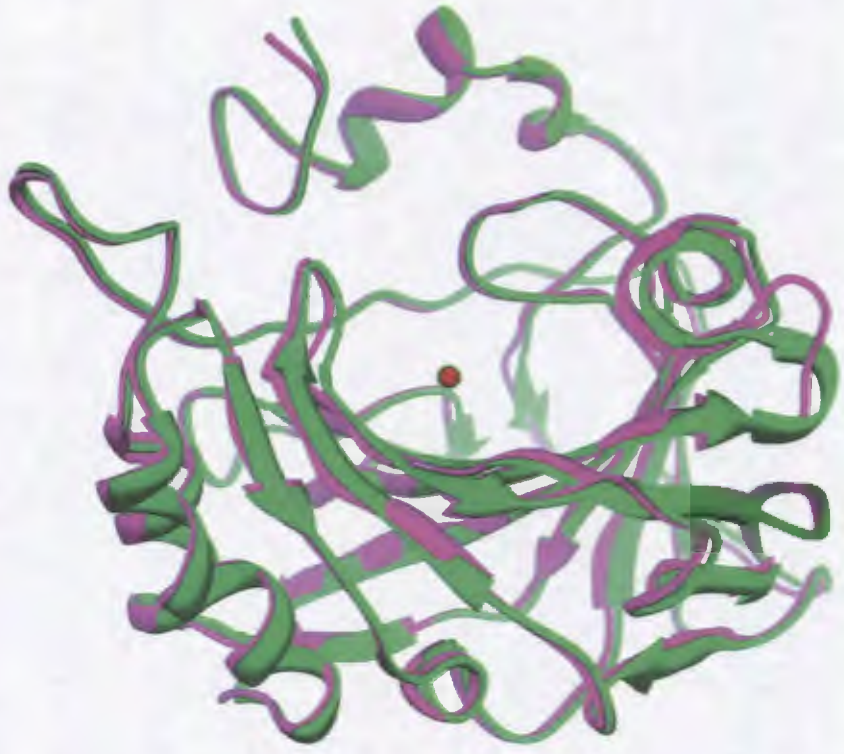

Figure 5.57. Comparison of the structures of hCA II and hCA VII.
The figure shows the overlay of structures of hCA II (green) (PDB ID: 2CBA) and hCA VII (pink) (homology modeled). The figure was modeled using UCSF Chimera software.

To discern the dependence of $\Delta H°$ and $\Delta G°$ on $T\Delta S°$ in hCA II and hCA VII, the data in Table 5.11 were plotted as shown in Figure 5.63. From this Figure it is evident that where as $\Delta G°$ remains invariant with changes in $T\Delta S°$, $\Delta H°$ increases linearly as a function of $T\Delta S°$ suggesting a strong enthalpy-entropy compensation. Also, note that $\Delta H° = \Delta G°$ when $T\Delta S° = 0$. The temperature at which $\Delta H° = \Delta G°$ could be calculated from the above Figures and was found to be 307 K for hCA VII and 302.6 K for hCA II (*538*). At this

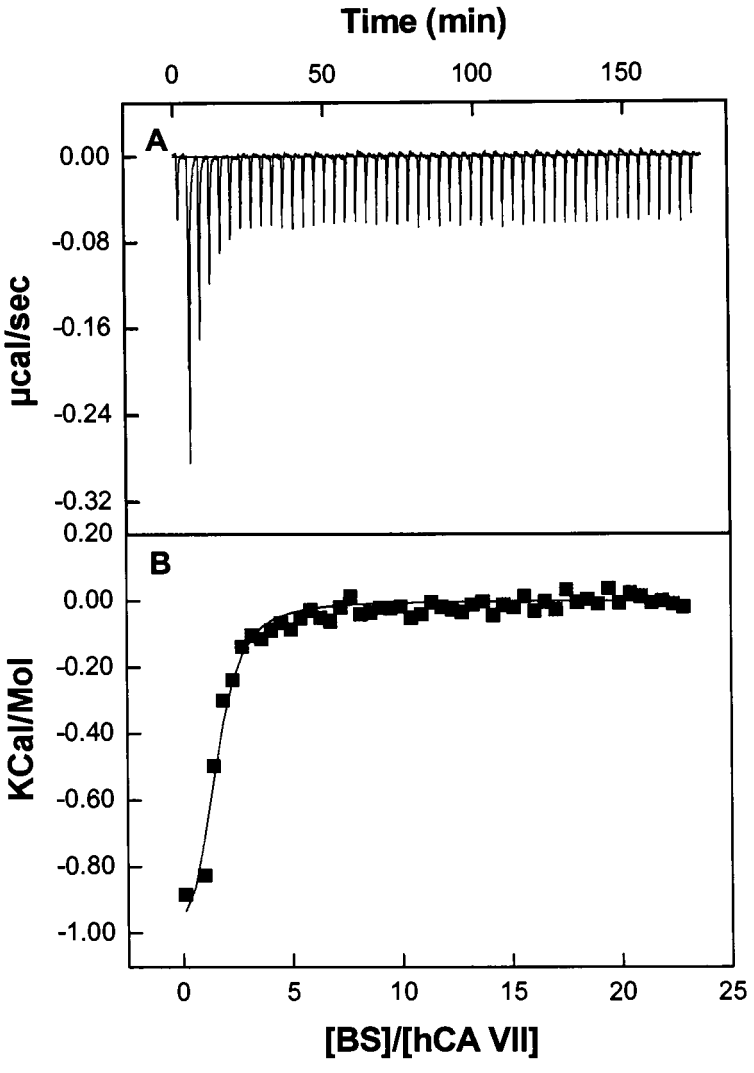

Figure 5.58. Isothermal titration calorimetric assay for the binding of BS to hCA VII at 15 ° C in 25 mM Tris buffer, pH 7.0.

Panel A of the Figure shows the raw data produced by the titration of 25 µM hCA VII by injection of increasing concentrations of (49 x 4 µl injection from 500 µM) BS. Panel B represents the binding curve generated by plotting the area under each peak as a function of molar ratio of BS. The solid smooth line represents the best fit of the data analyzed by the single binding site model provided by the origin software. The analysis yielded the stoichiometry (n), association constant (K_a), and $\Delta H°_{obs}$ as being equal to 1.42, 3.29 x 10^5 M and -1.1 (kcal/ mol), respectively.

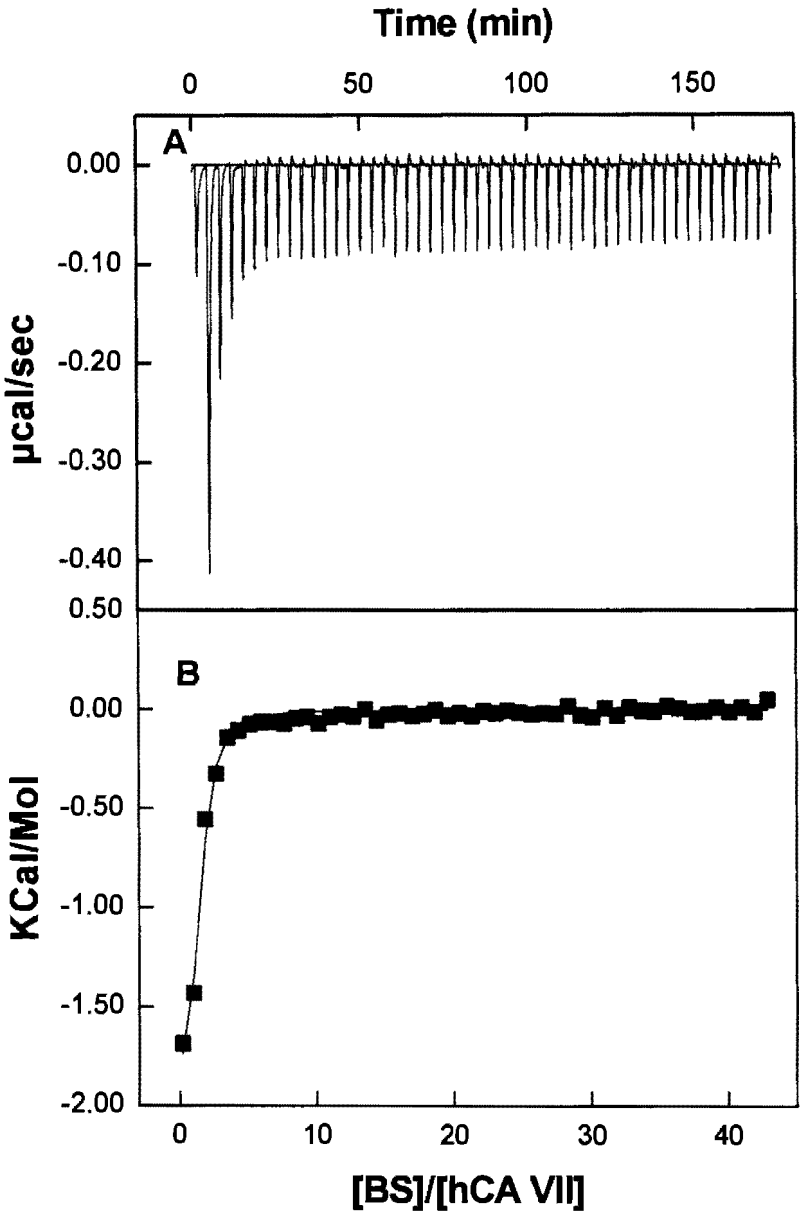

Figure 5.59. Isothermal titration calorimetric assay for the binding of BS to hCA VII at 20 ° C in 25 mM Tris, pH 7.0.

Panel A of the Figure shows the raw data produced by the titration of 25 µM hCA VII by injection of increasing concentrations of (49 x 4 µl injection from 500 µM) BS. Panel B represents the binding curve generated by plotting the area under each peak as a function of molar ratio of BS. The solid smooth line represents the best fit of the data analyzed by the single binding site model provided by the origin software. The analysis yielded the stoichiometry (n), association constant (K_a), and ΔH°_{obs} as being equal to 1.15, 3.06 x 10^5 M and -2.3 (kcal/ mol), respectively

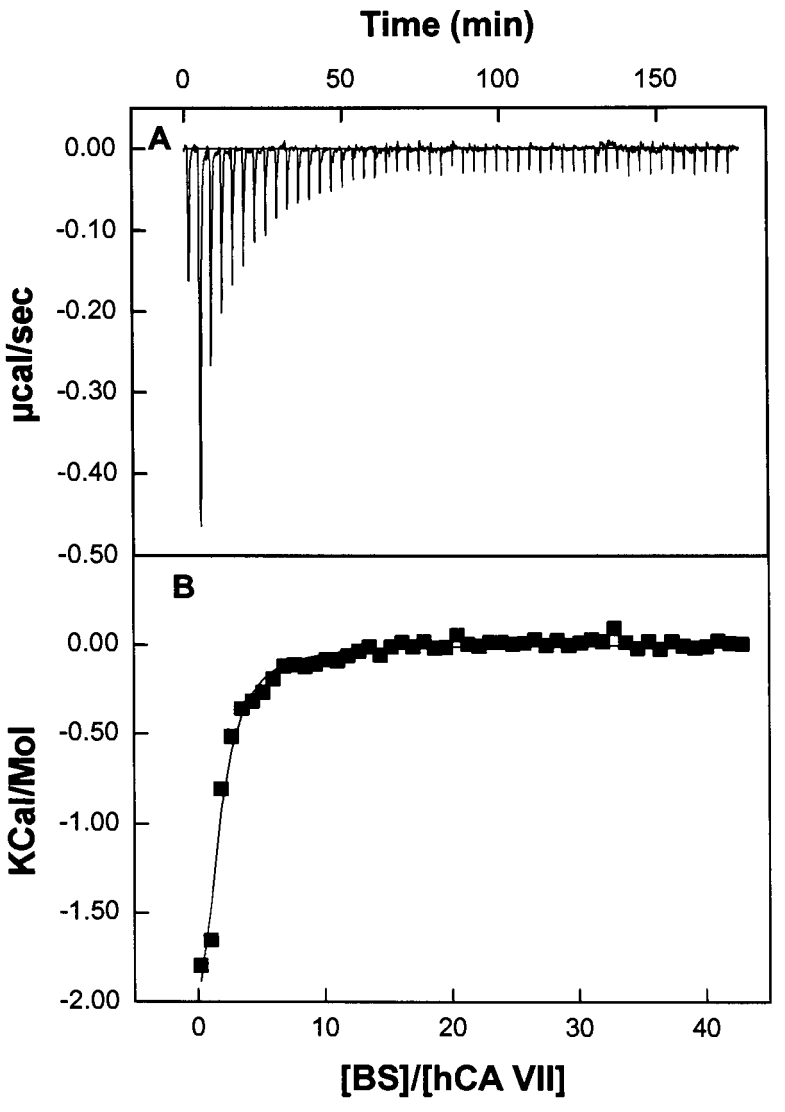

Figure 5.60. Isothermal titration calorimetric assay for the binding of BS to hCA VII at 25 ° C in 25 mM Tris, pH 7.0.

Panel A of the Figure shows the raw data produced by the titration of 25 µM hCA I by injection of increasing concentrations of (49 x 4 µl injection from 500 µM) JB2-48. Panel B represents the binding curve generated by plotting the area under each peak as a function of molar ratio of JB2-48. The solid smooth line represents the best fit of the data analyzed by the single binding site model provided by the origin software. The analysis yielded the stoichiometry (n), association constant (K_a), and $\Delta H°_{obs}$ as being equal to 1.12, 8.53 x 10^4 M and -4.4 (kcal/ mol), respectively.

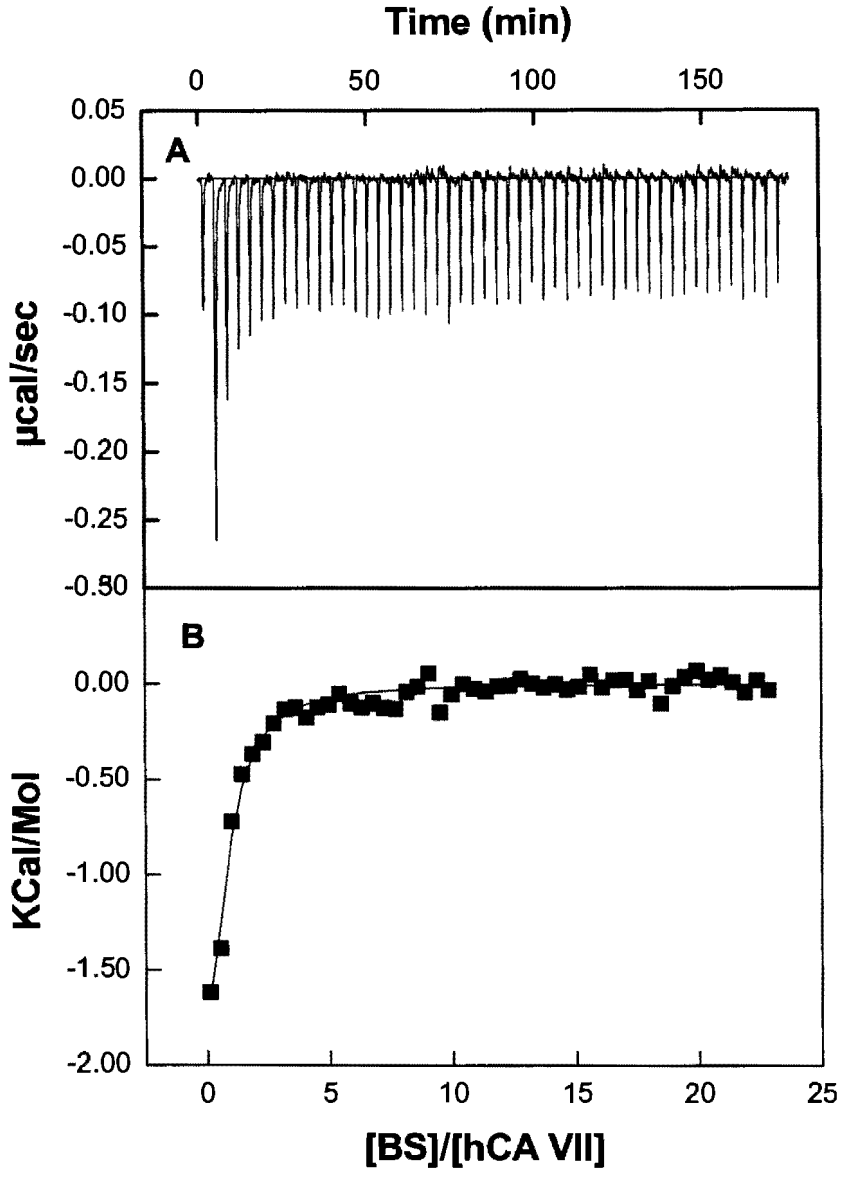

Figure 5.61. Isothermal titration calorimetric assay for the binding of BS to hCA VII at 30 ° C in 25 mM HEPES buffer, pH 7.0.

Panel A of the Figure shows the raw data produced by the titration of 25 µM hCA VII by injection of increasing concentrations of (49 x 4 µl injection from 500 µM) BS. Panel B represents the binding curve generated by plotting the area under each peak as a function of molar ratio of BS. The solid smooth line represents the best fit of the data analyzed by the single binding site model provided by the origin software. The analysis yielded the

stoichiometry (n), association constant (K_a), and $\Delta H°_{obs}$ as being equal to 0.4, 1.1 x 10^5 M and -5.3 (kcal/ mol), respectively.

Table 5.11. Summary of the thermodynamic data for the interaction of BS with hCA VII at different temperatures.

T (K)	n	K_a (M^{-1})	$\Delta H°_{obs}$ (kcal/ mol)	$T\Delta S°$ (kcal/mol)	$\Delta G°$ (kcal /mol)
288	1.42	3.3 x 10^5	-1.1	6.0	-7.17
293	1.15	3.0 x 10^5	-2.3	5.0	-7.31
298	1.12	8.5 x 10^4	-4.0	2.6	-6.6
303	0.4	1.1 x 10^5	-5.3	1.6	-6.9

Table 5.12. Summary of the thermodynamic data for the interaction of BS with hCA II at different temperatures.

T (K)	n	K_a (x $10^6 M^{-1}$)	$\Delta H°_{obs}$ (kcal/ mol)	$T\Delta S°$ (kcal/mol)	$\Delta G°$ (kcal /mol)
286.5	0.74	0.36	-16.5	-9.22	-7.28
290.8	0.77	0.72	-13.3	-5.50	-7.80
294.2	1.1	0.42	-12.8	-5.23	-7.57
298.2	0.76	1.65	-9.08	-0.6	-8.48
303.1	0.61	2.08	-7.34	1.42	-8.76
308.1	1.1	0.77	-6.88	1.42	-8.30

The Table 5.12 is adapted from reference (*538*)

temperature, the entropic contribution for the free energy of binding will be zero and the binding between BS and hCAs is solely contributed by $\Delta H°$. The zero entropy does not indicate the absence of any entropic changes, rather it indicates that the favourable entropic changes (ex: hydrophobic, vibrational entropy) are cancelled by the unfavorable entropic changes (ex: rotational, translational, and conformational entropy) (*540-542*).

5.4.2.3. Effect of buffer system on the binding of BS with hCA VII

It is well known that the binding of enzyme and ligand involves protonation-

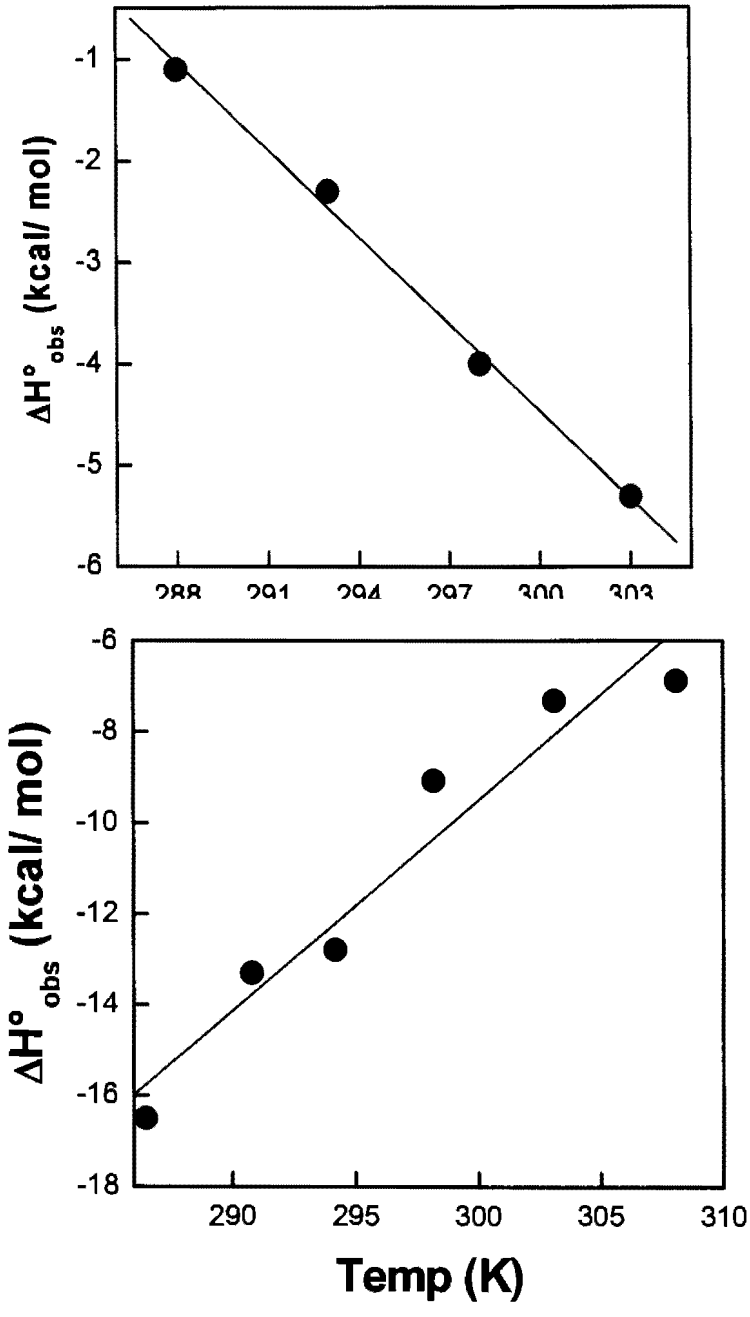

Figure 5.62. Effect of temperature on ΔH^0 for the interaction of benzenesulfonamide with hCA VII (upper panel) and hCA II (lower panel).
The solid smooth line is the linear regression analysis of the experimental data with a slope (ΔC_p^0) of -0.286 ± 0.01 kcal mol^{-1} K^{-1} and an intercept (at 0°K) of -81.3 ± 3.87 kcal mol^{-1} for hCA VII and a slope (ΔC_p^0) of 0.463 ± 0.06 kcal mol^{-1} K^{-1} and an intercept (at 0^0K) of -

148.5 ± 17.7 kcal mol^{-1} for hCA II. Lower panel of this Figure is modified from reference (*538*).

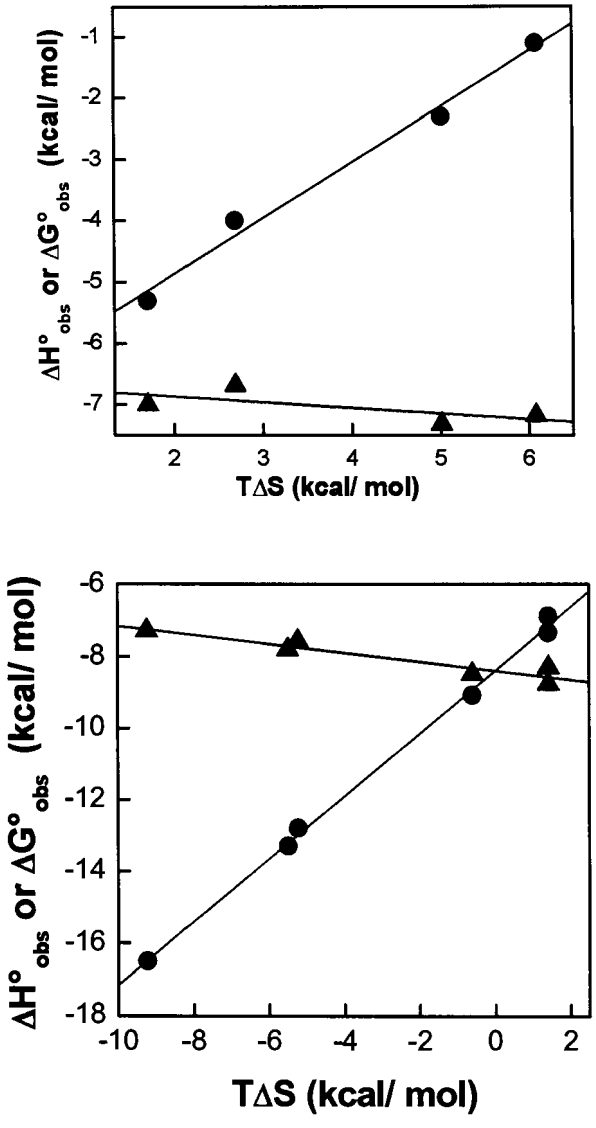

Figure 5.63. Enthalpy-entropy compensation plot for the binding of benzenesulfonamide to hCA VII and hCA II in 25 mM Tris, 10% DMSO (pH 7.0).
The dependence of ΔG^0 (triangle) and ΔH^0 (circle) on $T\Delta S^0$ is shown by triangles and circles, respectively. The linear regression analysis for the data of ΔH^0 versus $T\Delta S^0$ yields magnitudes of the slope and intercept of 0.9 ± 0.06 and -6.6 ± 0.29 kcal mol^{-1} for hCA VII (upper panel), 0 .88 ± 0.02 and -8.4 ± 0.1 kcal mol^{-1} for hCA II(lower panel) respectively. Lower panel of this Figure is modified from reference (*538*)

deprotonation of enzyme's amino acid residues. To determine if these process occur in the binding of BS to hCA VII, ITC experiments were performed in 3 different buffers of varying ionization enthalpies. The idea was that if there is a net change in protonation event upon binding, there will be an increase or decrease in the observed enthalpies of enzyme-ligand interactions in different buffer solutions.

The ITC experiments were performed in Tris-HCl ($\Delta H°_{ion}$ = 11.5 kcal mol^{-1}; Figures 5.60), HEPES ($\Delta H°_{ion}$ = 5.01 kcal mol^{-1}; Figure 5.64) and phosphate ($\Delta H°_{ion}$ = 1.2 kcal mol^{-1}; Figure 5.65) buffers (*510*), containing 10 % DMSO at pH 7.5. Table 5.13 and 5.14 lists the thermodynamic parameters for the binding of BS to hCA VII and hCA II.

When the $\Delta H°_{obs}$ obtained in these buffers were plotted as a function of their ionization enthalpies and analyzed using equation 5.2, it yielded the slope (n) and intercept ($\Delta H°_{int}$) values of 0.03 and -4.38 kcal/mol for hCA VII and -0.03 and -8.4 kcal/mol for hCA II respectively. This indicates that the observed and the intrinsic enthalpies are comparable and no proton is consumed or released during the binding process. This is presumably due to the fact that the protonation of the zinc bound hydroxide of hCA is cancelled by the deprotonation of the sulfonamide nitrogen of BS upon enzyme-ligand interaction.

5.4.2.4. Temperature dependence of the thermodynamic parameters of hCA VII-acetazolamide (AZM) interaction.

To investigate the effect of temperature on the binding of hCA VII to AZM, isothermal calorimetric titrations were performed at different temperatures ranging from 15° C to 30° C. The results obtained with acetazolamide were compared with those obtained for the binding of BS to hCA VII. Figures 5.66-5.69 shows the thermodynamic

profiles for the titration of 10 μM hCA VII with 49 x 4 μl injections of 500 μM AZM in 25 mM Tris buffer pH 7.5, at temperatures ranging from 15°C to 30°C. The thermodynamic parameters derived from the temperature dependent experiments of hCA VII are presented in Table 5.15. From the data of Table, it is evident that whereas ΔG° remains almost similar at all temperatures, both $\Delta H°$ and $T\Delta S°$ increase with increase in temperature. This is in contrast to the binding of BS to hCA VII where $\Delta H°$ and $T\Delta S°$ decrease with increase in temperature. Figure 5.70 shows the plot of $\Delta H°$ as a function of temperature. It is evident from the Figure that $\Delta H°$ becomes more unfavourable (less negative) with increase in temperature incase of AZM, unlike that observed with hCA VII – BS interaction. In the latter case $\Delta H°$ becomes more favourable (more negative) with increase in temperature. The favorable and unfavorable change in enthalpies in the case of BS and AZM are compensated by entropic changes in the opposite magnitude. The solid line of the Figure is the best fit for the linear regression analysis of the data with the slope and intercept of 0.14 kcal mol^{-1} K^{-1} and -46.96 kcal/mol respectively. Note the difference in the ΔCp° values for the interaction of BS and AZM with hCA VII. As will be discussed in the next chapter, negative and positive ΔCp° value suggests that the binding of inhibitor to the active site of the enzyme is dominated by hydrophobic and polar forces respectively.

In order to see the dependence of $\Delta H°$ and ΔG° on $T\Delta S°$, the data on Table 5.15 were plotted as shown in Figure 5.71. From the Figure it is evident that where as ΔG° remains invariant with changes in $T\Delta S°$, $\Delta H°$ increases linearly as a function of $T\Delta S°$ suggesting a strong enthalpy-entropy compensation.

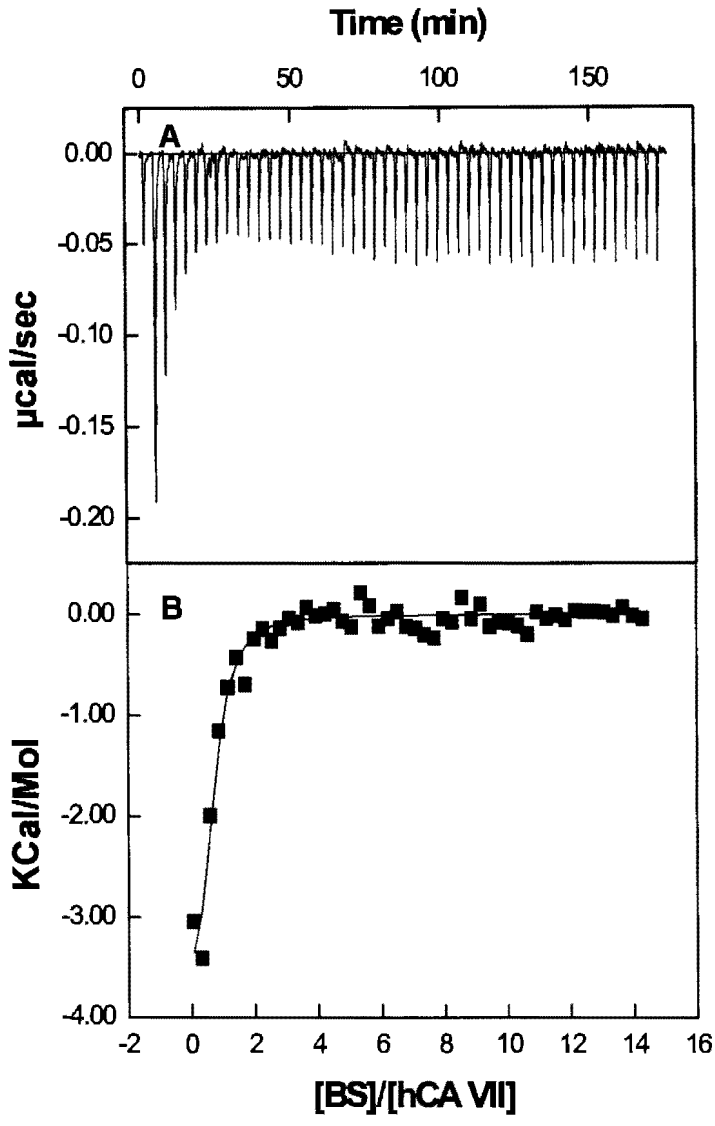

Figure 5.64. Isothermal Titration calorimetric assay for the binding of BS to hCA VII at 25 ° C in 25 mM HEPES, pH 7.0.

Panel A of the Figure shows the raw data produced by the titration of 25 µM hCA VII by injection of increasing concentrations of (49 x 4 µl injection from 500 µM) BS. Panel B represents the binding curve generated by plotting the area under each peak as a function of molar ratio of BS. The solid smooth line represents the best fit of the data analyzed by the single binding site model provided by the origin software. The analysis yielded the stoichiometry (n), association constant (K_a), and $\Delta H°_{obs}$ as being equal to 0.65, 1.1 x 10^6 M and -4.3 (kcal/ mol) respectively.

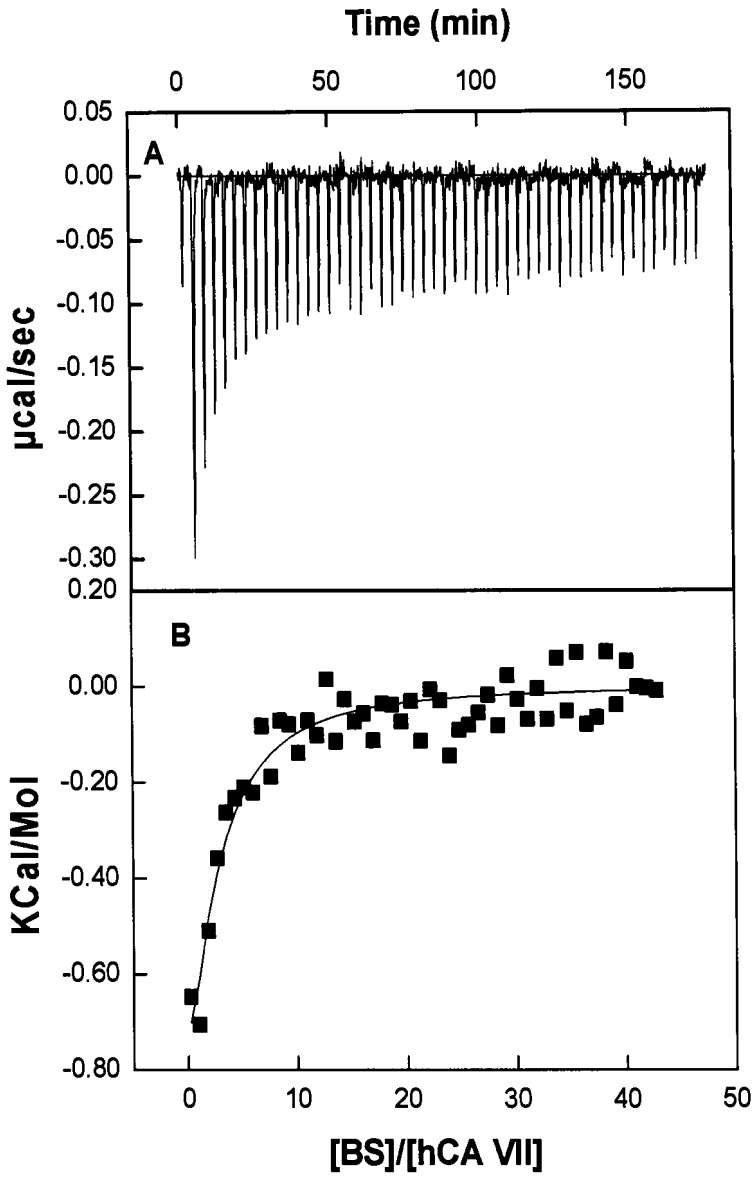

Figure 5.65. Isothermal titration calorimetric assay for the binding of BS to hCA VII at 25 ° C in 25 mM phosphate buffer, pH 7.0.
Panel A of the Figure shows the raw data produced by the titration of 25 µM hCA VII by injection of increasing concentrations of (49 x 4 µl injection from 500 µM) BS. Panel B represents the binding curve generated by plotting the area under each peak as a function of molar ratio of BS. The solid smooth line represents the best fit of the data analyzed by the single binding site model provided by the origin software. The analysis yielded the stoichiometry (n), association constant (K_a), and $\Delta H°_{obs}$ as being equal to 0.65, 1.1 x 10^6 M and -4.3 (kcal/ mol) respectively.

Table 5.13. Effect of buffer on the binding of benzenesulfonamide to hCA VII.

Ligand	Buffer	K_a (M^{-1})	$\Delta H°_{obs}$ (kcal/ mol)	$\Delta G°$ (kcal /mol)	n
BS	Phosphate	1.1×10^6	-4.3	-8.1	0.65
	HEPES	2.15×10^4	-4.3	-5.9	0.94
	Tris	8.5×10^4	-4.0	-6.6	1.12

Table 5.14. Effect of buffer on the binding of benzenesulfonamide to hCA II.

Ligand	Buffer	K_a (M^{-1})	$\Delta H°_{obs}$ (kcal/ mol)	$\Delta G°$ (kcal /mol)	n
BS	Phosphate	0.79×10^6	-8.2	-8.04	1.1
	HEPES	1.65×10^6	-9.08	-8.48	0.76
	Tris	1.54×10^6	-8.6	-8.6	0.9

The Table is adapted from reference (*538*)

Also, note that $\Delta H°$ = $\Delta G°$ (-8.23) when $T\Delta S°$ = 0. The temperature at which $\Delta H°$ = $\Delta G°$ could be calculated from the above Figure and is found to be 276 K. At this temperature, the entropic contribution of the free energy of binding is zero, and the binding between AZM and hCA VII is solely contributed by $\Delta H°$.

5.4.2.5. Effect of buffer system on the binding of BS with hCA VII

To compare the effect of buffer ions on the thermodynamic parameters for the interaction of BS and AZM to hCA VII, binding studies were performed in different buffer systems. As mentioned above, the enthalpy changes observed calorimetrically are not solely contributed by the breaking or making of non covalent bonds involved in the protein-ligand interactions (563-567), but are often contributed by the ionization enthalpy

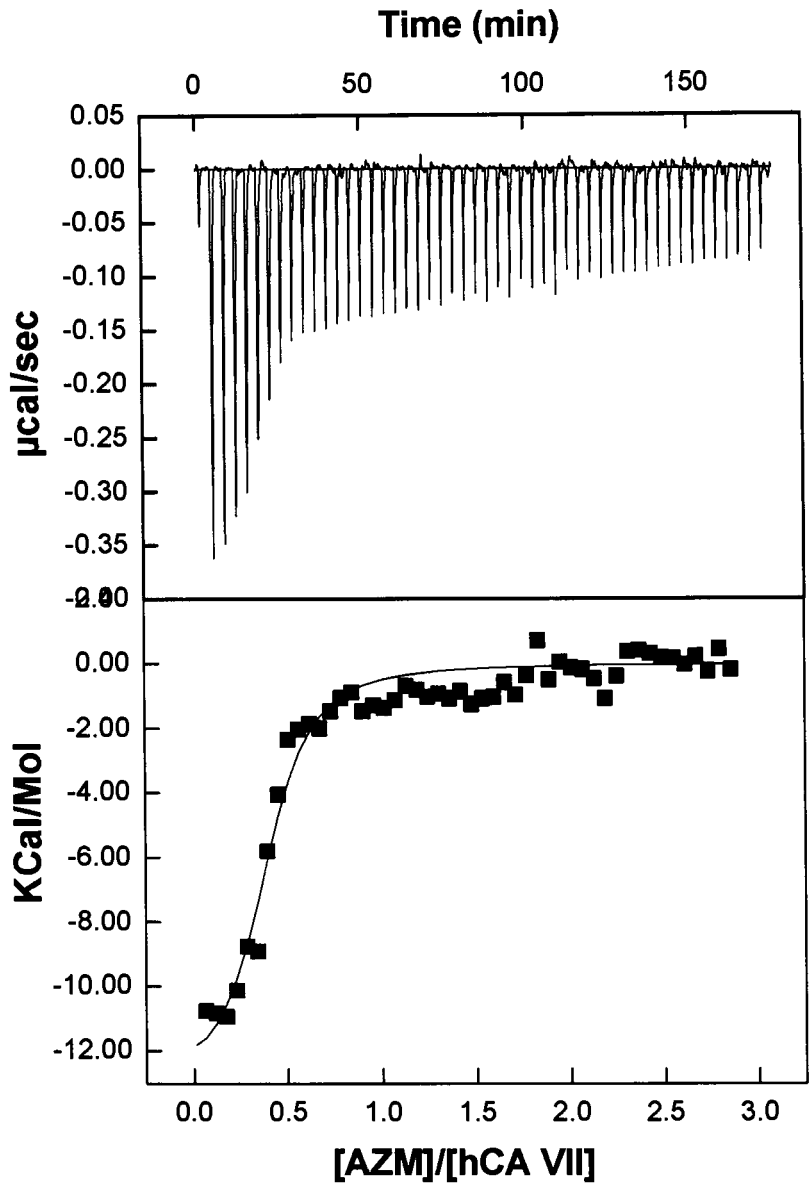

Figure 5.66. Isothermal titration calorimetric assay for the binding of AZM to hCA VII at 15 ° C in 25 mM Tris buffer, pH 7.0.

Panel A of the Figure shows the raw data produced by the titration of 25 µM hCA VII by injection of increasing concentrations of (49 x 4 µl injection from 500 µM) AZM. Panel B represents the binding curve generated by plotting the area under each peak as a function of molar ratio of AZM. The solid smooth line represents the best fit of the data analyzed by the single binding site model provided by the origin software. The analysis yielded the stoichiometry (n), association constant (K_a), and $\Delta H°_{obs}$ as being equal to 0.95, 3.5 x 10^6 M and -5.8 (kcal/ mol) respectively.

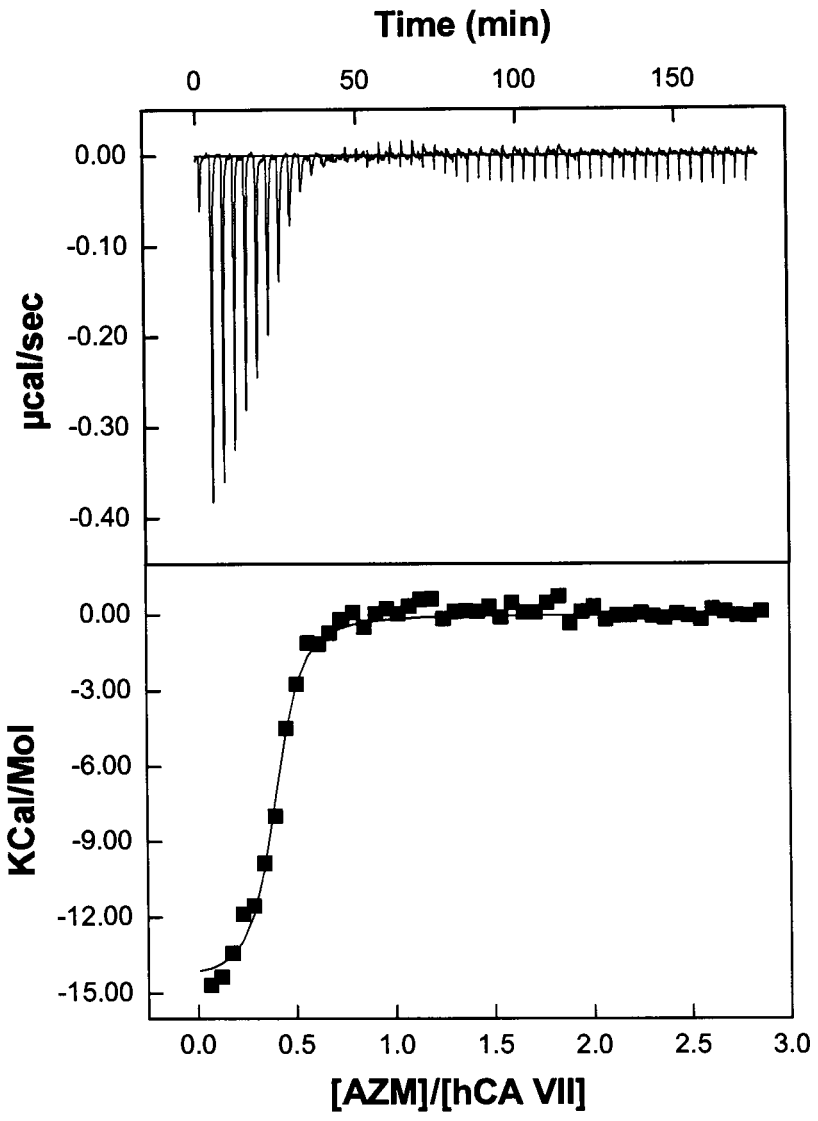

Figure 5.67. Isothermal titration calorimetric assay for the binding of AZM to hCA VII at 20 ° C in 25 mM Tris buffer, pH 7.0.
Panel A of the Figure shows the raw data produced by the titration of 25 µM hCA VII by injection of increasing concentrations of (49 x 4 µl injection from 500 µM) AZM. Panel B represents the binding curve generated by plotting the area under each peak as a function of molar ratio of AZM. The solid smooth line represents the best fit of the data analyzed by the single binding site model provided by the origin software. The analysis yielded the stoichiometry (n), association constant (K_a), and $\Delta H°_{obs}$ as being equal to 0.98, 7.5 x 10^5 M and –5.5 (kcal/ mol) respectively.

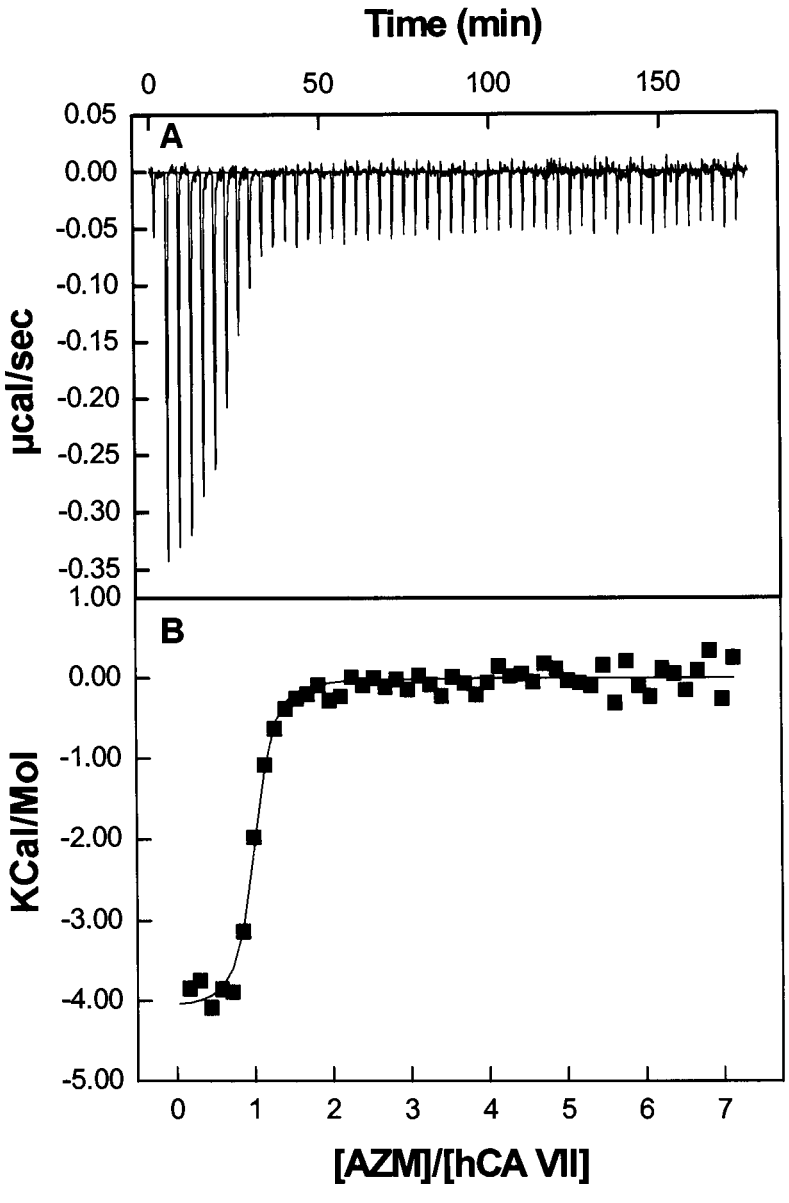

Figure 5.68. Isothermal titration calorimetric assay for the binding of AZM to hCA VII at 25 ° C in 25 mM Tris buffer, pH 7.0.
Panel A of the Figure shows the raw data produced by the titration of 25 µM hCA VII by injection of increasing concentrations of (49 x 4 µl injection from 500 µM) AZM. Panel B represents the binding curve generated by plotting the area under each peak as a function of molar ratio of AZM. The solid smooth line represents the best fit of the data analyzed by the single binding site model provided by the origin software. The analysis yielded the stoichiometry (n), association constant (K_a), and $\Delta H°_{obs}$ as being equal to 0.95, 6.5 x 10^6 M and -4.1 (kcal/ mol) respectively.

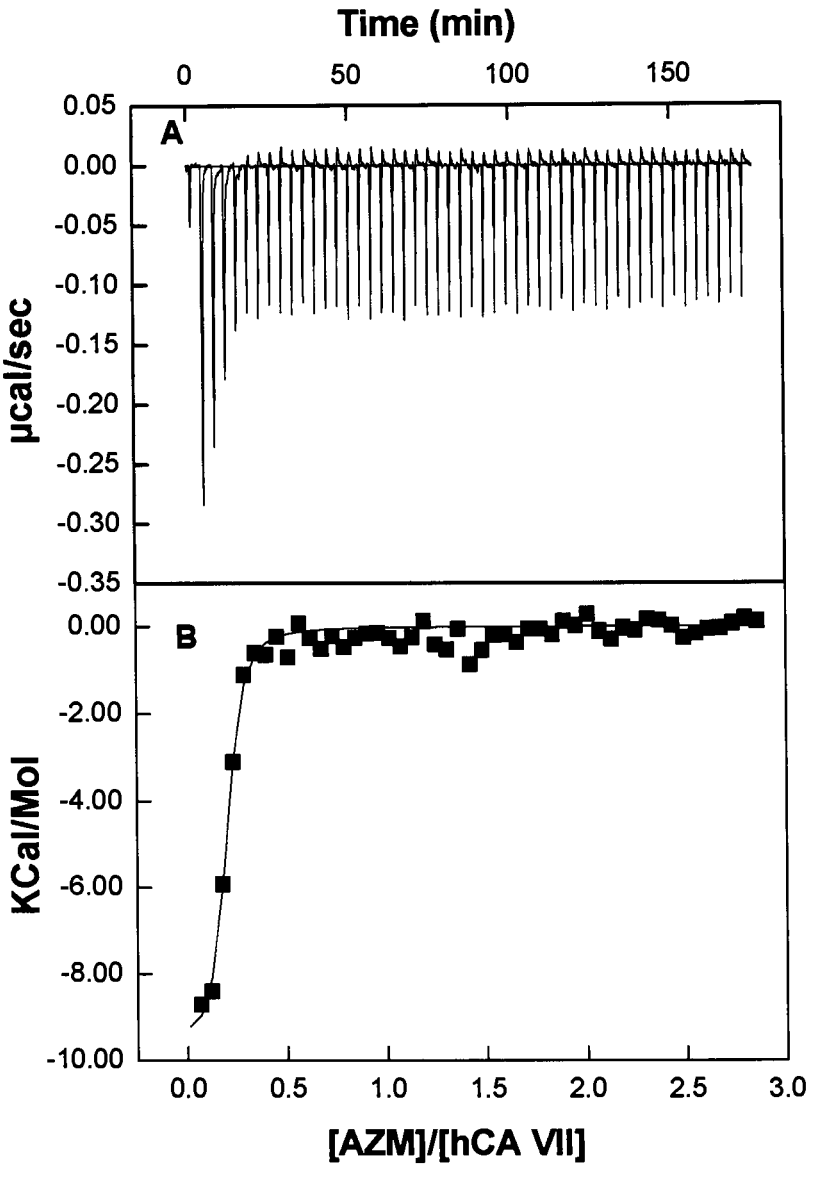

Figure 5.69. Isothermal titration calorimetric assay for the binding of AZM to hCA VII at 30 ° C in 25 mM Tris buffer, pH 7.0.

Panel A of the Figure shows the raw data produced by the titration of 25 µM hCA VII by injection of increasing concentrations of (49 x 4 µl injection from 500 µM) AZM. Panel B represents the binding curve generated by plotting the area under each peak as a function of molar ratio of AZM. The solid smooth line represents the best fit of the data analyzed by the single binding site model provided by the origin software. The analysis yielded the stoichiometry (n), association constant (K_a), and $\Delta H°_{obs}$ as being equal to 0.45, 4.2 x 10^6 M and -3.89 (kcal/ mol) respectively.

Table 5.15. Summary of the thermodynamic data for the interaction of AZM with hCA VII at different temperatures.

T (K)	n	K_a (M^{-1})	$\Delta H°_{obs}$ (kcal/ mol)	$T\Delta S°$ (kcal/mol)	$\Delta G°$ (kcal /mol)
288	0.95	3.5×10^6	-5.8	2.9	-8.7
293	0.98	7.5×10^5	-5.5	3.5	-9.0
298	0.95	6.5×10^6	-4.1	5.1	-9.2
303	0.45	4.2×10^6	-3.89	5.3	-9.1

of the buffer species. Hence it is important to consider the enthalpic contributions due to protonation-deprotonation of the buffer species and must be subtracted from ΔH^0_{obs} to obtain the intrinsic enthalpy (ΔH^0_{int}) of the complex.

To achieve this objective, ITC studies were peformed out in Tris-HCl ($\Delta H°_{ion}$ = 11.5 kcal mol^{-1}; Figure 5.68), HEPES ($\Delta H°_{ion}$ = 5.01 kcal mol^{-1}; Figure 5.72) and phosphate ($\Delta H°_{ion}$ = 1.2 kcal mol^{-1}; Figure 5.73) (*510*) buffers containing 10 % DMSO at pH 7.5. Table 5.16 lists the thermodynamic parameters for the binding of hCA VII with AZM. Casual perusal of the data on Table 5.16 indicates that the $\Delta H°_{obs}$ values remain invariant with changes in ionization enthalpy indicating that no proton is consumed or released during the process of binding.

5.5. Binding of hCA isozymes to nanoparticles

While working with different isoforms of hCAs, it was noted that the surface of hCA XII, the enzyme implicated in promoting hypoxic tumors (*49, 95, 97, 270, 294, 374*), harbors patches of positive and negative charges in the vicinity and opposite side of the enzyme's active site pocket (*49*), respectively. Such a distinct charge distribution on the surface of hCA XII prompted investigation of the role of electrostatic interaction of

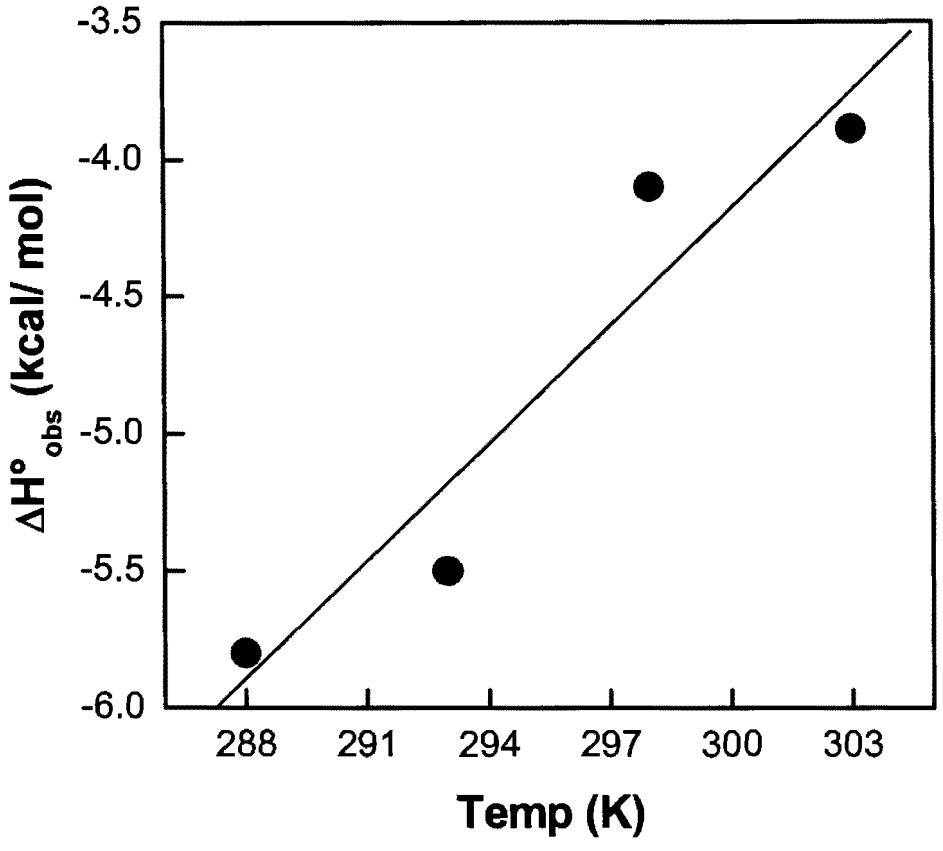

Figure 5.70. Effect of temperature on ΔH° for the interaction of AZM with hCA VII. The solid smooth line is the linear regression analysis of the experimental data for a slope (ΔC_p^{0}) of 0.14 ± 0.03 kcal mol^{-1} K^{-1} and an intercept (at $0^{0}K$) of -46.96 ± 9.6 kcal mol^{-1}.

charged macromolecules with oppositely charged Qds, polylysine and liposomes in modulating the enzyme's functional features.

Studies on the interaction of quantum dots (Qds) and proteins have gained significant attention in the past decade because of the potential of Qds as drug carriers and diagnostic tools (*390-392*). Qds are semi conductor nano crystals with unique properties as compared to the conventional fluorophores (*393-396, 398, 543*). The adsorption of proteins to Qds surface leads to the changes in the protein conformation and/or changes in the

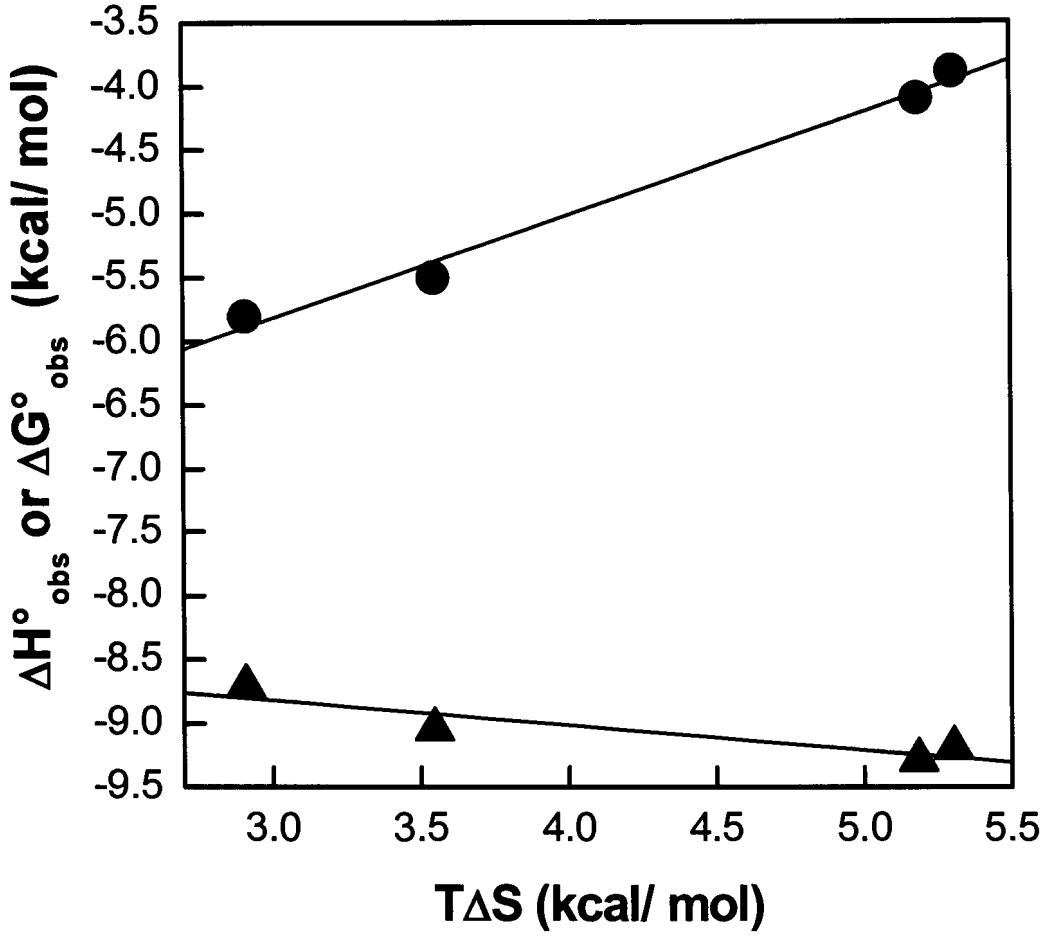

Figure 5.71. Enthalpy-entropy compensation plot for the binding of AZM to hCA VII in 25 mM Tris, 10% DMSO (pH 7.0).
The dependence of ΔG^0 and ΔH^0 on $T\Delta S^0$ is shown by circles and triangles, respectively. The linear regression analysis for the data of ΔH^0 versus $T\Delta S^0$ yields magnitudes of the slope and intercept of -0.19 ± 0.05 and -8.23 ± 0.25 kcal mol^{-1}, respectively.

surface of the nanoparticles (*406-411*). For example, the interaction of CdS-Qds with human hemoglobin results in a significant alteration of its secondary and tertiary structures. This in turn leads to quenching of the intrinsic fluorescence of the protein (*407*). In this paradigm, it has been noted that certain nanoparticle induced conformational changes in proteins are isozyme selective (*406*). For example, recent NMR data reveals

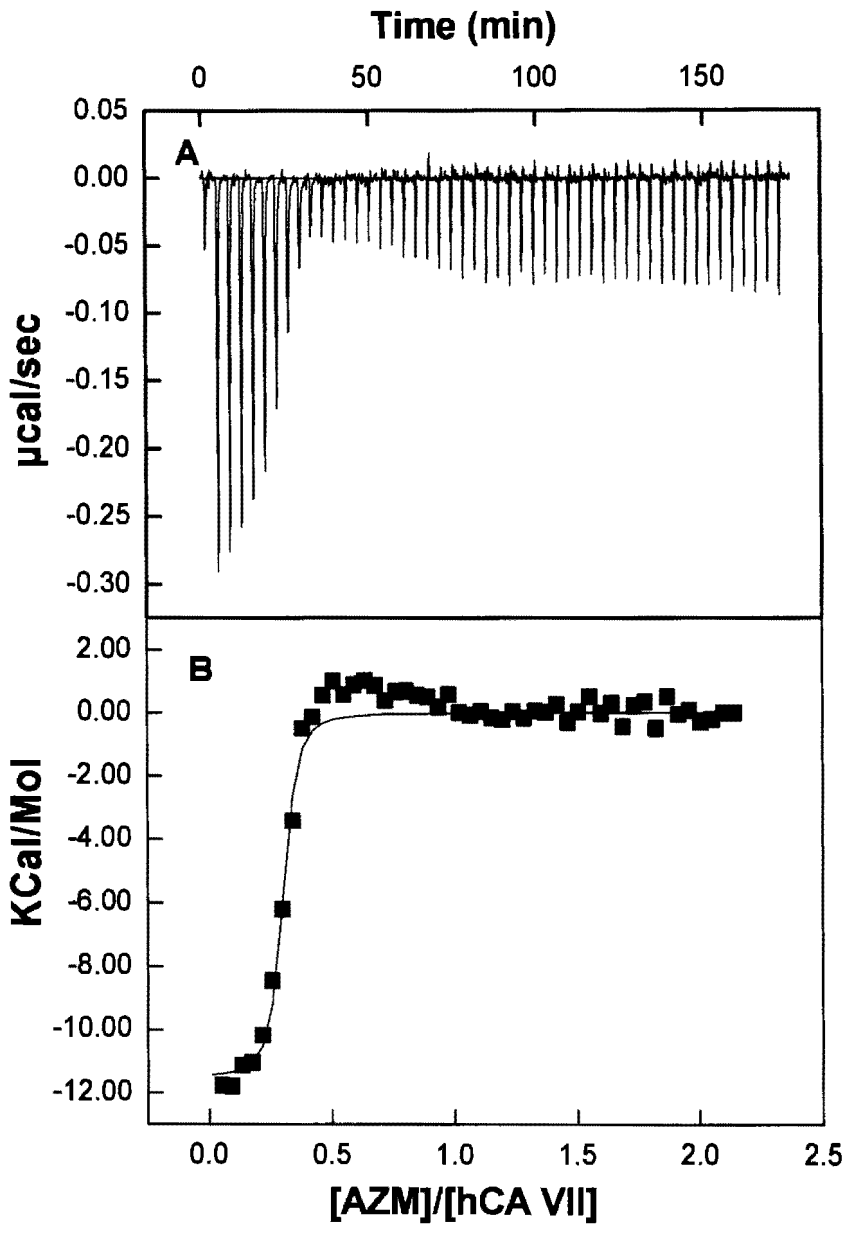

Figure 5.72. Isothermal titration calorimetric assay for the binding of AZM to hCA VII at 25 ° C in 25 mM HEPES buffer, pH 7.0.
Panel A of the Figure shows the raw data produced by the titration of 25 µM hCA VII by injection of increasing concentrations of (49 x 4 µl injection from 500 µM) AZM. Panel B represents the binding curve generated by plotting the area under each peak as a function of molar ratio of AZM. The solid smooth line represents the best fit of the data analyzed by the single binding site model provided by the origin software. The analysis yielded the stoichiometry (n), association constant (K_a), and $\Delta H°_{obs}$ as being equal to 0.75, 1.3 x 10^7 M and -4.3 (kcal/ mol) respectively.

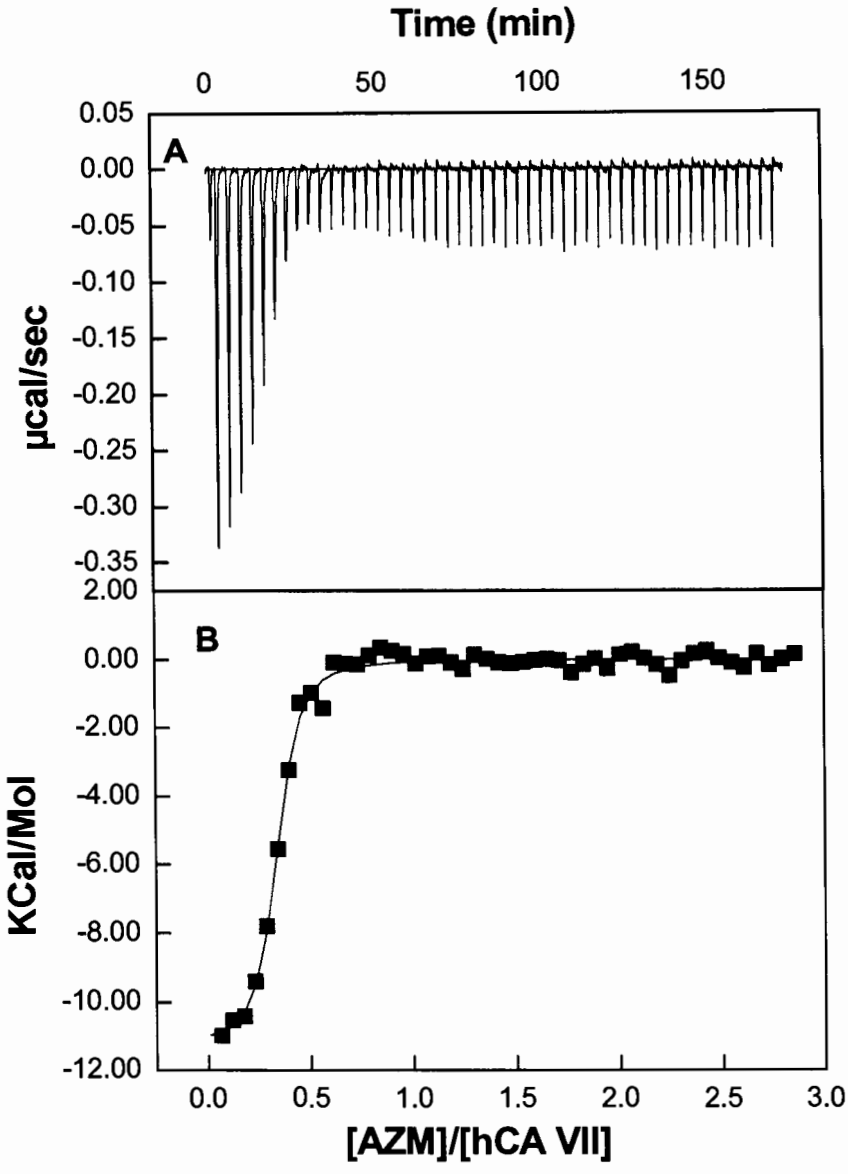

Figure 5.73. Isothermal titration calorimetric assay for the binding of AZM to hCA VII at 25 ° C in 25 mM phosphate buffer, pH 7.0.
Panel A of the Figure shows the raw data produced by the titration of 25 µM hCA VII by injection of increasing concentrations of (49 x 4 µl injection from 500 µM) AZM. Panel B represents the binding curve generated by plotting the area under each peak as a function of molar ratio of AZM. The solid smooth line represents the best fit of the data analyzed by the single binding site model provided by the origin software. The analysis yielded the stoichiometry (n), association constant (K_a), and $\Delta H°_{obs}$ as being equal to 0.8, 4.2 x 10^6 M and -4.4 (kcal/ mol) respectively.

Table 5.16. Effect of buffer on the thermodynamic parameters of hCA VII- AZM interaction.

Ligand	Buffer	K_a (M^{-1})	$\Delta H°_{obs}$ (kcal/ mol)	$\Delta G°$ (kcal/mol)	n
AZM	Phosphate	4.2×10^6	-4.4	-8.9	0.8
	HEPES	1.3×10^7	-4.3	-9.6	0.75
	Tris	6.5×10^6	-4.1	-9.2	0.95

that the silica nanoparticles exhibit completely different impacts on the structure of human carbonic anhydrase I (hCA I) versus human carbonic anhydrase II (hCA II). Whereas hCA II interacts strongly with silica nanoparticles leading to an ensemble of molten globule like bound protein states, hCA I interacts (with similar nanoparticles) albeit weakly and leads to a small perturbation in the protein structure on a longer time scale (*407*). Depending on the adsorption properties and conformational changes of proteins upon binding to the solid surfaces, the following classification was developed: proteins that do not adsorb to solid surfaces or do not show any conformational change upon adsorption are referred to as "hard" proteins and those that adsorb and show significant conformational change are termed as "soft" protein. Accordingly, hCA I and hCA II were designated as hard and soft proteins respectively (*407*). With these available literature evidences that confirm that Qds interact with hCAs, it was of interest to study the interaction of charged Qds with hCA isozymes with particular focus on hCA XII as it had the bipolar distribution of charges which would drive their binding. The influence of charged liposomes on the spectral, lifetime and other functional features were also studied to complement the results obtained from Qds. Studies with liposomes were of further interest to gain insight on the effect of

rigid (Qds) versus soft (liposomes) nanoparticles on the functional properties of the enzyme.

5.5.1. Interaction of hCA XII with differently charged Qds

5.5.1.1. Interaction of hCA XII with cationic Qds (Qds^+)

To gain insights into the distribution of charges on the surface of hCA XII, the electrostatic surface potential of the enzyme was determined using the X-ray crystallographic structural coordinates of Whittington *et al.* (PDB ID: 1JCZ) (*49*). As depicted in Figure 5.74, the electrostatic surface potential of hCA XII reveals that the surface of the enzyme is largely negatively charged, except in the vicinity of the active site, which is positively charged. This finding suggested that hCA XII had the potential to electrostatically interact with both positively and negatively charged surfaces with different orientations of the enzyme. More specifically, it appeared likely that the enzyme's active site region would interact with the negatively charged surfaces, whereas the opposite side of the enzyme would interact with the positively charged surfaces. Although the former orientation would likely inhibit the enzyme by occlusion of the active site pocket, the latter orientation would allow hCA XII to remain active while bound to the positively charged surface.

5.5.1.2. Absorption and emission spectra of Qds^+

To ascertain whether hCA XII could bind to a positively charged surface, the binding of the enzyme to cationic Qds of approximately 4.5 nm diameter was investigated. The positive charge on the cadmium telluride (CdTe) Qds was prepared by the conjugation of cystamine. Figure 5.75 shows the absorbance and fluorescence spectra of the Qds^+. The Qds^+ show a broad absorption band from 250 nm to approximately 600 nm.

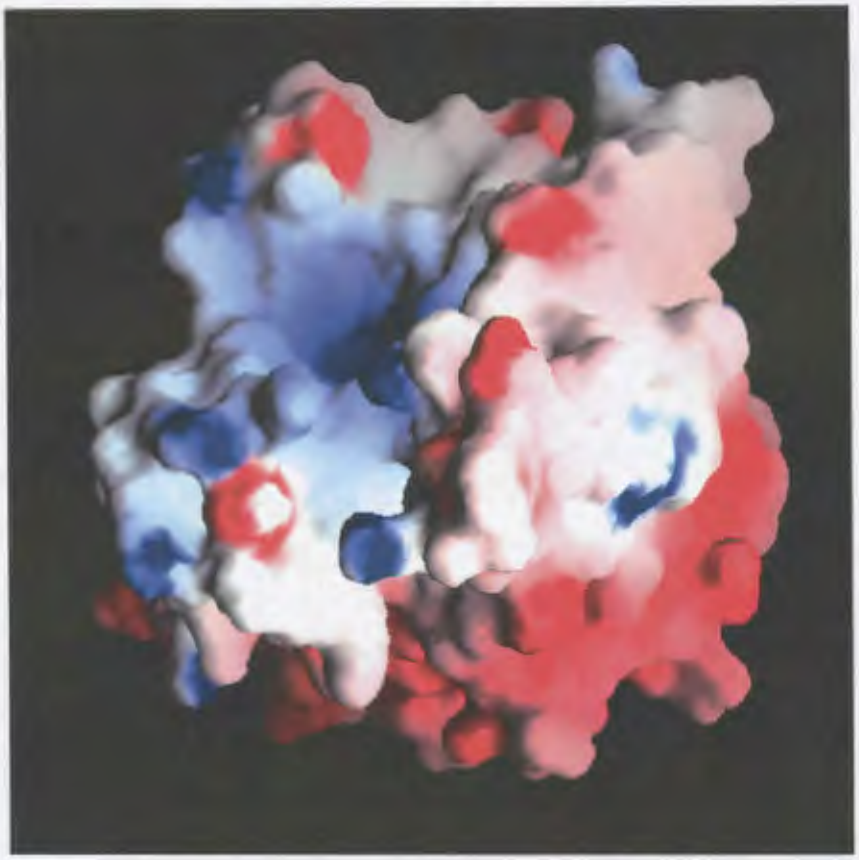

Figure 5.74. Electrostatic surface potential of hCA XII.
Electrostatic surface potential of the crystal structure of human carbonic anhydrase XII (PDB# 1JCZ) (*49*). The electrostatic potential of the enzyme surface was calculated using the GRASP utility of Insight® II software. Regions of negative charge are colored red and those of positive charge are colored blue.

Aside from the major peak in the UV region, a smaller peak was observed at 570 nm (Fig. 5.75, panel A). The latter peak was chosen for excitation of the Qds so as to avoid complications due to the absorbance of hCA XII in the ultraviolet region. When excited at 570 nm, Qds showed strong fluorescence with emission maximum at 610 nm (Fig. 5.75, panel B).

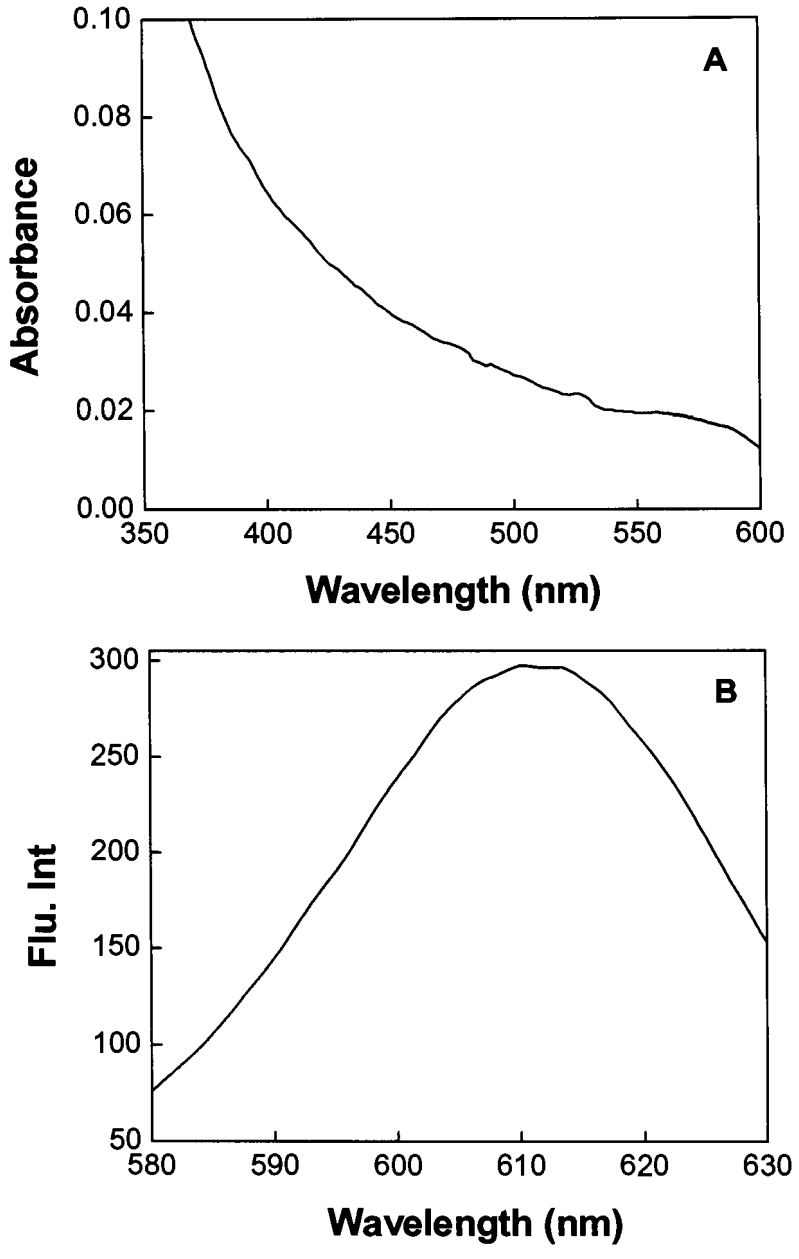

Figure 5.75. Absorption and emission properties of the CdTe/cys Qds in 10 mM Tris buffer pH 8.0.
Panel A depicts the absorbance of 0.75 μM CdTe/cys Qds in a 1 cm path length quartz cuvette whereas panel B depicts the steady-state fluorescence emission of 3.4 μM CdTe/cys Qds (excitation at 570 nm) in a 4 mm square quartz cuvette.

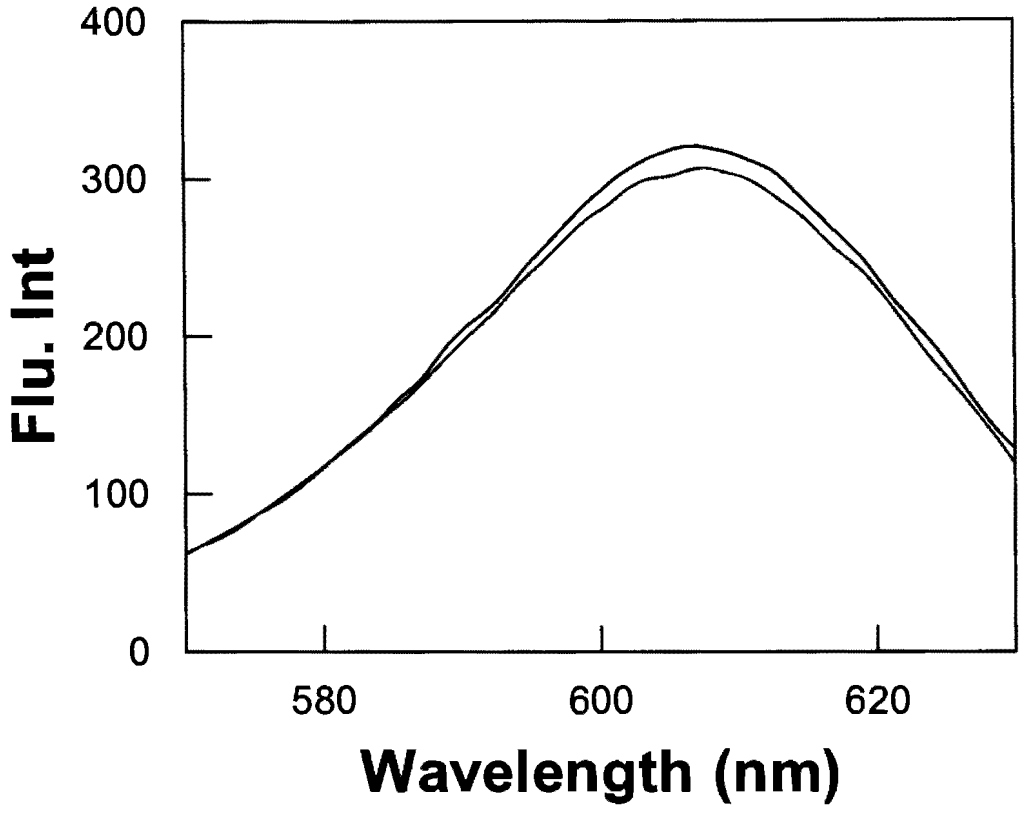

Figure 5.76. Steady-state fluorescence emission spectra of the Qds^{+}.
The solid green line depicts the spectrum of free Qds^{+} which overlays with the spectrum of CdTe/cys in the presence of 1 μM hCA XII. The solid black line indicates the fluorescence emission spectrum of Qds^{+} in the presence of 5 μM DNSA. All spectra were measured in 10 mM Tris, pH 8.0 containing 10% acetonitrile with an excitation wavelength of 500 nm.

5.5.1.3. Influence of hCA XII on the fluorescence emission spectrum of Qds^{+}

Figure 5.76 represents the emission spectra of Qds^{+} in the presence of stoichiometric concentrations of hCA XII. The Figure indicates that there is practically no change in fluorescence profile of Qds^{+} in the presence of hCA XII. This finding seemed to suggest that hCAXII was not binding to Qds^{+}, regardless of the favorable electrostatic surface potentials between the charged species. However, such observation was also possible if the interacting species did not alter the electronic transition of the Qds despite their physical interactions.

5.5.1.4. Influence of Qds^+ on the emission spectra of hCA XII

To probe whether the intrinsic fluorescence of hCA XII was influenced by the Qds^+, the fluorescence spectra of the enzyme was determined in the absence and presence of stoichiometric concentrations of Qds^+ (Figure 5.77A). In light of the X-ray crystallographic data, it is apparent that the enzyme harbors 8 tryptophan residues per subunit with varied degrees of exposures to the aqueous environment (*49*). These tryptophans upon excitation at 280 nm, exhibit an emission maximum at 336 nm. As the steady-state fluorescence emission of tryptophan is highly sensitive to changes in its microenvironment, it appeared plausible that this signal would change upon binding of hCA XII to the Qds^+. It was found that the steady-state fluorescence of the protein was indeed quenched in the presence of Qds^+, and it was confirmed that such a quenching was not an artifact of the inner filter effect since the absorption of the reaction mixture was less than 0.1. Evidently, the quenching of the enzyme's fluorescence by Qds^+ was due to hCA XII– Qds^+ interaction. This was not surprising since the electrostatic surface potential of hCA XII opposite to the active site pocket of the enzyme is predominantly negative (*49*). Hence, the hCA XII–Qds^+ interaction was envisaged to be caused by the electrostatic forces. To validate this, the spectrum of hCA XII–Qds^+ in the presence of 250 mM NaCl was recorded (Figure 5.77A). It was observed that the presence of NaCl restored the fluorescence emission peak of hCA XII (which was quenched by Qds^+).

The Qds^+ mediated quenching of hCA XII fluorescence was used for monitoring their binding affinities. However, in pursuit of this endeavor, it was realized that the titration of an increasing concentration of the Qds^+ to a fixed concentration of hCA XII

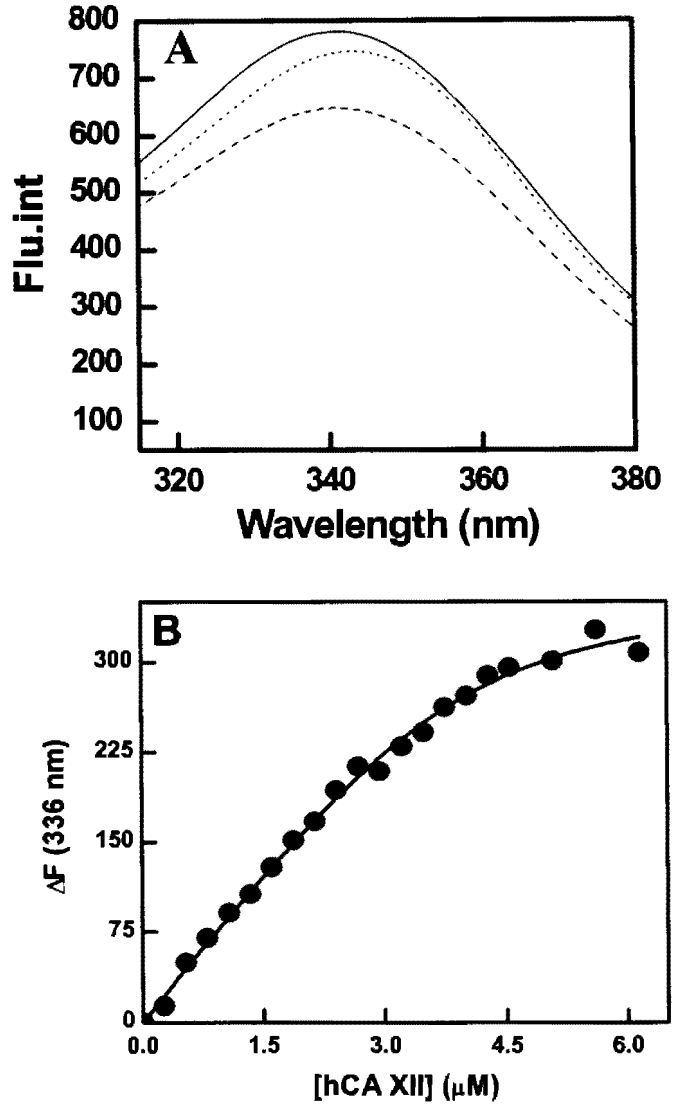

Figure 5.77. Fluorescence spectral changes upon binding of Qds^+ to hCA XII. Panel A shows the fluorescence emission spectra of hCA XII (solid line), hCA XII-Qds^+ (dashed line) and hCA XII-Qds^+ in the presence of 250 mM NaCl (dotted lines) in 10 mM Tris buffer pH 8.0. The fluorescence emission spectra of 0.2 μM hCA XII (solid line) (λ_{ex} = 295 nm; λ_{em} = 310 nm – 400 nm) was quenched in the presence of stoichiometric amounts of Qds^+ (dashed line). Panel B shows the binding isotherm for the interaction of hCA XII with Qds^+. A fixed concentration of the Qds^+ (0.96 μM) was titrated with increasing concentrations of hCA XII (λ_{ex}= 295 nm, λ_{em} = 336 nm) in 10 mM Tris buffer, pH 8.0. The data represent the magnitude of ΔF obtained by subtracting the fluorescence intensity of the mixture from that given by the protein itself under identical conditions as a function of protein concentration. The solid line is the best fit of the data (*506*) which provided a dissociation constant of 0.32 ± 0.16 μM, and a stoichiometry of hCA XII bound per Qds^+ as being equal to 4.

was not feasible. This was a consequence of the significant UV absorption of the Qds^+ (as evident by the spectra in panel A of Figure 5.75A). Since increasing concentrations of Qds^+ produces inner filter effect, it was expected to preclude the determination of reliable binding constant due to masking of the enzyme's tryptophan fluorescence emission. Hence, to determine the binding affinity of hCA XII for Qds^+, titration of a fixed concentration of Qds^+ with enzyme was performed while monitoring the fluorescence emission of hCA XII at 336 nm. The observed fluorescence was corrected by subtraction of the background signal obtained from the titration of hCA XII into buffer, and then plotted as a function of enzyme concentration (Figure 5.77B).

As shown in Figure 5.77B, the extent of quenching of the tryptophan signal exhibited a nearly linear dependence at lower concentration of hCA XII with the overall profile being hyperbolic in nature. This was suggestive of a very tight binding of the enzyme to the Qds^+ surface. However, under this situation, a significant fraction of free enzyme was envisaged to be complexed with Qds^+ during the entire course of the titration, and thus the total concentration of hCA XII could not be taken as the measure of its free concentration. This scenario led to the analysis of the titration data of Figure 5.77B by the quadratic equation which takes into account the bound versus free form of the titrant as described by Qin and Srivastava (*506*). The solid smooth line is the best fit of the data of Figure 5.77B for the dissociation constant and stoichiometry of the hCA XII–Qds^+ complex as being equal to 0.32 μM and 4 molecules of hCA XII subunit bound to per molecule of Qds^+, respectively. The stoichiometry of hCA XII - Qds^+ complex was determined using the molecular weight of dimeric hCA XII as being equal to 4. It was found that 4 moles of hCA XII is bound to 1 mole of Qds^+.

5.5.1.5. Effect of Qds^+ on the fluorescence lifetimes of hCA XII

Since the broad absorption band of Qds^+ overlaps with the fluorescence emission peak (336 nm) of hCA XII, the observed fluorescence quenching of hCA XII in the presence of Qds^+ was envisaged to be possibly due to the fluorescence resonance energy transfer (FRET) from the enzyme's tryptophan residues to Qds^+. To probe this possibility, the intrinsic fluorescence lifetime of hCA XII was determined in the absence and presence of Qds^+. In this experiment, a relatively high energy 280 nm LED was used as the excitation source, and the emission wavelength was set at 336 nm. Figure 5.78 shows the excited state lifetime traces of hCA XII in the absence and presence of Qds^+. Both these lifetime traces conformed to the biphasic rate equation yielding two lifetimes (τ_1 and τ_2). Whereas the analysis of the experimental data (solid smooth lines) for free hCA XII yielded the short (τ_1) and long (τ_2) lifetimes as being equal to 0.24 and 2.4 ns, respectively, those for the hCA XII– Qds^+ complex yielded the above parameters to be 0.22 and 2.3 ns, respectively. Note that these values are not too different, suggesting that Qds^+ mediated quenching is not due to perturbation of the excited state energy of the enzyme's intrinsic fluorophores. Evidently, there has been no FRET between the enzyme's tryptophan residues and the Qds^+. The fact that Qds^+ quench the intrinsic steady-state fluorescence of hCA XII but do not alter the lifetimes of the tryptophan moieties implies that the overall quenching process is a ground state phenomenon (*544*). The latter could be manifested either due to the formation of a complex with lower extinction coefficient or due to an impaired transition of the complex from the ground state to the excited state (*544*).

5.5.1.6. Effect of Qds^+ on the spectral features of hCA XII-ligand complex

To ascertain whether or not the electrostatic interaction between hCA XII and Qds^+ altered the structural–functional features of the enzyme, a series of experiments involving fluorescence inhibitor DNSA (DNSA) of the enzyme as well as polylysine as an analogous (positively charged) surface binding group of the enzyme we performed. DNSA is known to bind at the hydrophobic active site pocket of CA isozymes and such interaction results in a blue shift, with a marked increase in the fluorescence emission intensity of the fluorophores (*329*, *387*). Whereas free DNSA exhibits a fluorescence emission band at 536 nm (λ_{ex}=330 nm), the enzyme-bound form is characterized by a relatively intense emission band at 457 nm. It was reasoned that if a change in the active site structure of hCA XII were to occur upon binding to the Qds, the binding of DNSA to the hCA XII-Qds^+ complex would be altered.

The effect of binding of Qds^+ to hCA XII on the fluorescence properties of the enzyme-bound DNSA was investigated. The idea was to ascertain whether or not the distally (i.e., opposite to the active site pocket of the enzyme) bound Qds^+ somehow altered the microenvironment of the enzyme-bound DNSA (via long range conformational changes) and such feature modulated the spectral properties of the fluorophore. Toward this goal, a fixed concentration of hCA XII and saturating concentration of DNSA was titrated with increasing concentrations of Qds^+ and monitored the fluorescence emission profile of the hCA XII bound DNSA. As shown in Figure 5.79, as the concentration of Qds^+ increases, the fluorescence intensity of the hCA XII–DNSA complex at 457 nm (λ_{ex}=330 nm) decreases. This proceeds in concomitance with an increase in the fluorescence emission peak of Qds^+ at 600 nm. As a control, the above experiment was

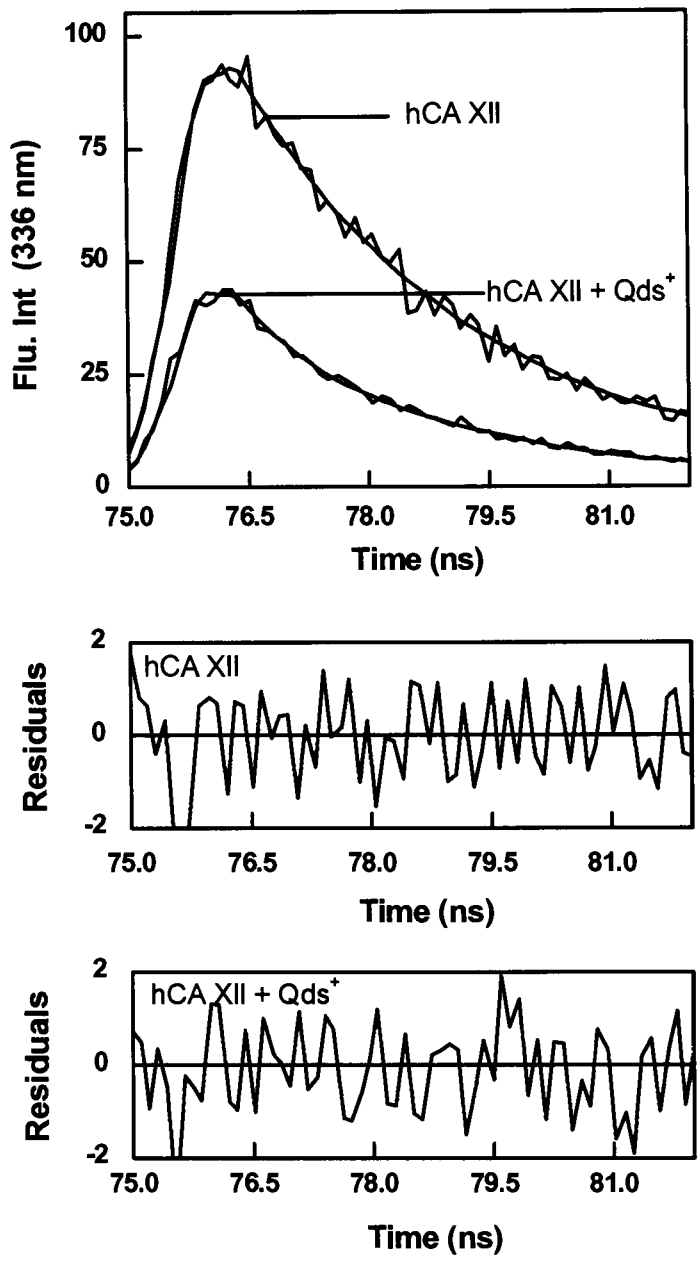

Figure 5.78. Excited state fluorescence decay profiles of hCA XII in the absence and presence of Qds^+.
[hCA XII] = 1 μM; [Qds^+] = 11 μM; λ_{ex} = 280 nm; λ_{em} = 336 nm. Other experimental conditions are same as in Figure 1. The solid smooth lines are the best fit of the data for the double exponential rate equation with $\tau_1 = 0.24 \pm 0.01$ ns and $\tau_2 = 2.4 \pm 0.01$ ns in the absence of Qds^+, and $\tau_1 = 0.22 \pm 0.01$ ns and $\tau_2 = 2.3 \pm 0.03$ ns in the presence of Qds^+. The bottom panels show the residuals of the fitted data.

performed in the absence of hCA XII, and it was observed that neither did Qds^+ quench the DNSA fluorescence around the 536 nm region nor did its fluorescence intensity increase at 600 nm. Hence, the Qds^+ mediated quenching of the DNSA fluorescence occurred only when the latter was bound to hCA XII, and the overall process was manifested via the direct (electrostatic) interaction between hCA XII and Qds^+. The data of Figure 5.79A further revealed that the fluorescence spectral changes adhered to a common isosbestic point only at higher concentration of Qds^+; no common isosbestic point was observed at lower concentrations of Qds^+. These features are more pronounced in the difference spectra (i.e., the spectra of the mixture minus the individual species) of Figure 5.79 B. It is believed that the lack of a common isosbestic point at lower concentration of Qds^+ is due to non-specific quenching of the 457 nm peak vis a vis the FRET between the enzyme-bound DNSA and Qds^+ (see below). However, at this time, possibility of changes in the binding affinity of DNSA for hCA XII (resulting in the re-equilibration of the free and enzymebound DNSA) under the influence of Qds^+ (see below) cannot be ruled out. The spectral titration results of Figure 5.79 A and B allowed for the determination of the binding affinity of Qds^+ to hCA XII in the presence of DNSA, and comparison of the above parameter with that obtained for the direct binding of free Qds^+ with the enzyme (i.e., 0.32 μM; panel B of Figure 5.77). Figure 5.79C shows the plot of ΔF600 (extracted from the difference spectra of Figure 5.79 B) as a function of Qds^+. The analysis of the experimental data by fixing the stoichiometry of 0.25 (i.e. 1 Qds^+ bound per enzyme subunit; panel B of Figure 5.79) yielded the dissociation constant of Qds^+ for the DNSA bound hCA XII as being equal to 0.09 μM. The latter value is about 4 fold lower than that

obtained for the binding of Qds^+ to the unliganded form of the enzyme. Evidently, the bound DNSA slightly increases the avidity of the enzyme for Qds^+.

The fact that the fluorescence emission peak of Qds^+ at 600 nm only increases when DNSA is bound to hCA XII (Figure 5.79A and B) and not with the free enzyme (data not shown) led to the suggestion that the excited state energy of the enzyme-bound DNSA was transferred to Qds^+ (i.e., the FRET effect). This was plausible since fluorescence emission maximum of the enzyme-bound DNSA (457 nm) coincided with the broad absorption/excitation band of Qds^+ in the above region. To substantiate the occurrence of FRET between the above species, the excited state fluorescence decay profiles of Qds^+ under different experimental conditions were compared (Figure 5.80). By using 340 nm LED as the excitation source and setting the emission monochromator at 600 nm, the time decay of the excited state fluorescence intensity of 1 μM free Qds^+ (control; panel A), in the presence of 25 μM hCA XII (panel B), in the presence of 25 μM DNSA (panel C), and in the presence of 3 μM hCA XII and 15 μM DNSA (panel D) were obtained. All the reaction traces conformed to the biphasic rate equation yielding two lifetimes, τ_1 and τ_2. Whereas the lifetimes of free Qds^+ and those in the presence of free hCA XII and free DNSA were found to be nearly identical (τ_1 and τ_2 falling in the range of 1.3 and 7.3 ns, respectively), the second (longer) lifetime (τ_2) of Qds^+in the presence of hCA XII– DNSA complex increased to 11.4 ns. Although the origin of the shorter lifetime component (τ_1) of Qds^+ is not very clear, the increase in the magnitude of τ_2 only in the presence of the enzyme-bound DNSA (but not with other components) substantiates the occurrence of FRET between the enzyme-bound DNSA and Qds^+.

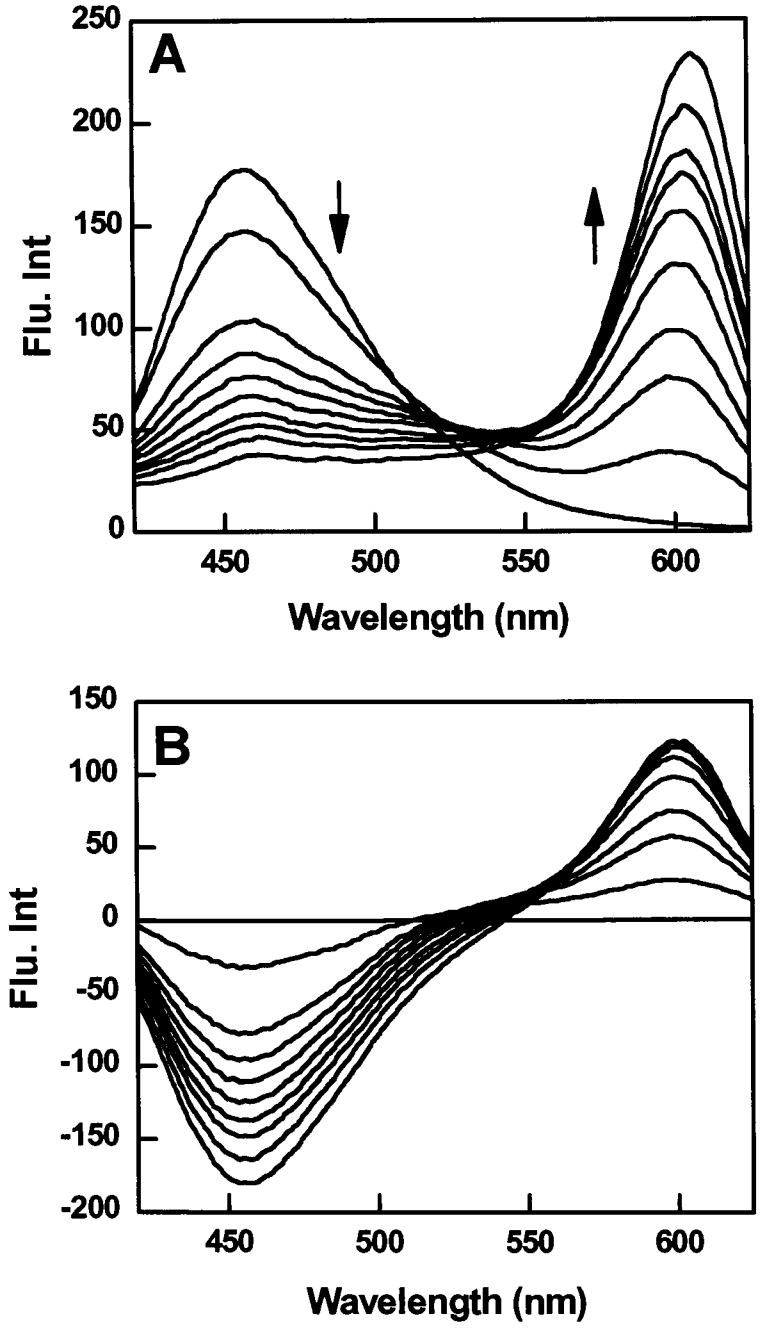

Figure 5.79. Fluorescence spectral changes for the interaction of Qds^{+} with hCA XII-DNSA complex.
Panel A shows the spectra of hCA XII-DNSA complex in the presence of increasing concentrations of Qds^{+} in 10 mM Tris-HCl buffer, pH 8.0 containing 10 % acetonitrile. [hCA XII] = 0.3 μM, [DNSA] = 2 μM, λ_{ex} = 330 nm. The decrease and increase in the fluorescence emission intensity at 457 and 600 nm, respectively, are shown by the arrows. Panel B shows the difference spectra, which were derived from the raw spectral data of Panel A minus the sum of the spectra of the individual components.

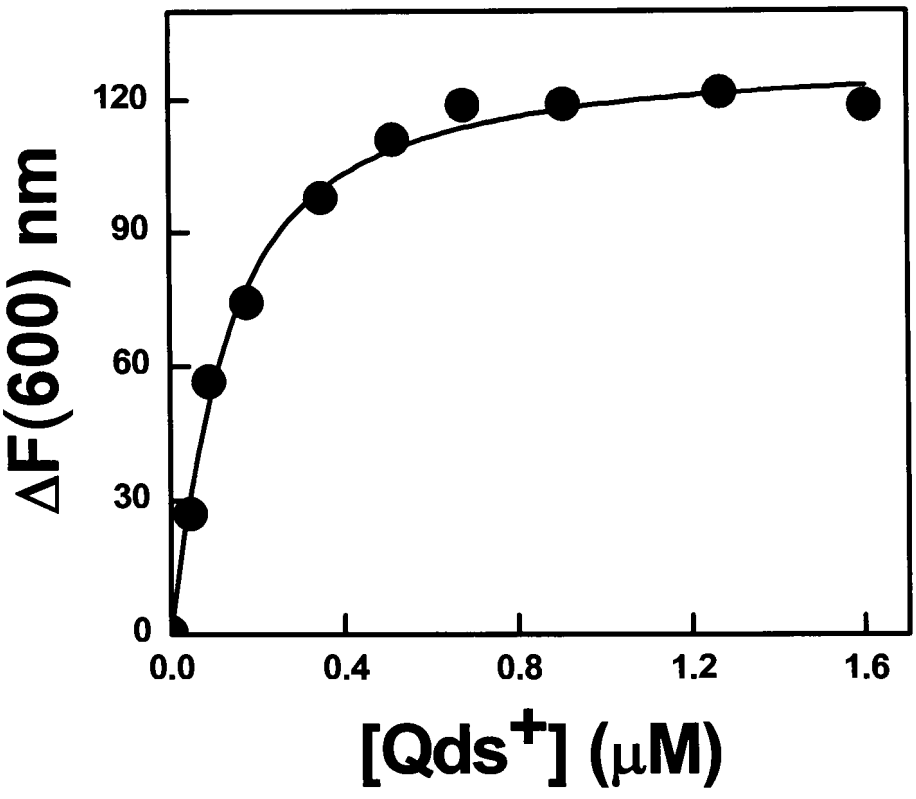

Figure 5.79 C. Binding isotherm for the interaction of Qds+ with hCA XII-DNSA complex.
The Figure shows the plot of ΔF_{600} (from Figure 5.79 A) as a function of Qds^+ concentration. The solid smooth line is the best fit of the data (by fixing the stoichiometry of 0.25) for the dissociation constant of hCA XII (DNSA)-Qds^+ complex as being equal to $0.09 \pm 0.01 \mu M$.

5.5.1.7. Effect of polylysine as the positively charged macromolecules

To assert the contribution of positive charges vis a vis the structural features of Qds^+ in eliciting the observed spectral changes (Figure 5.79 A and B) and/or the binding profiles of Qds^+ with hCA XII in the absence (Figure 5.77B) and presence (Fig. 5.79C) of DNSA, polylysine was utilized as the positively charged macromolecule. Toward this objective, the influence of binding of polylysine to hCA XII on the fluorescence emission profile of the enzyme-bound DNSA was first investigated. Figure 5.81 shows the

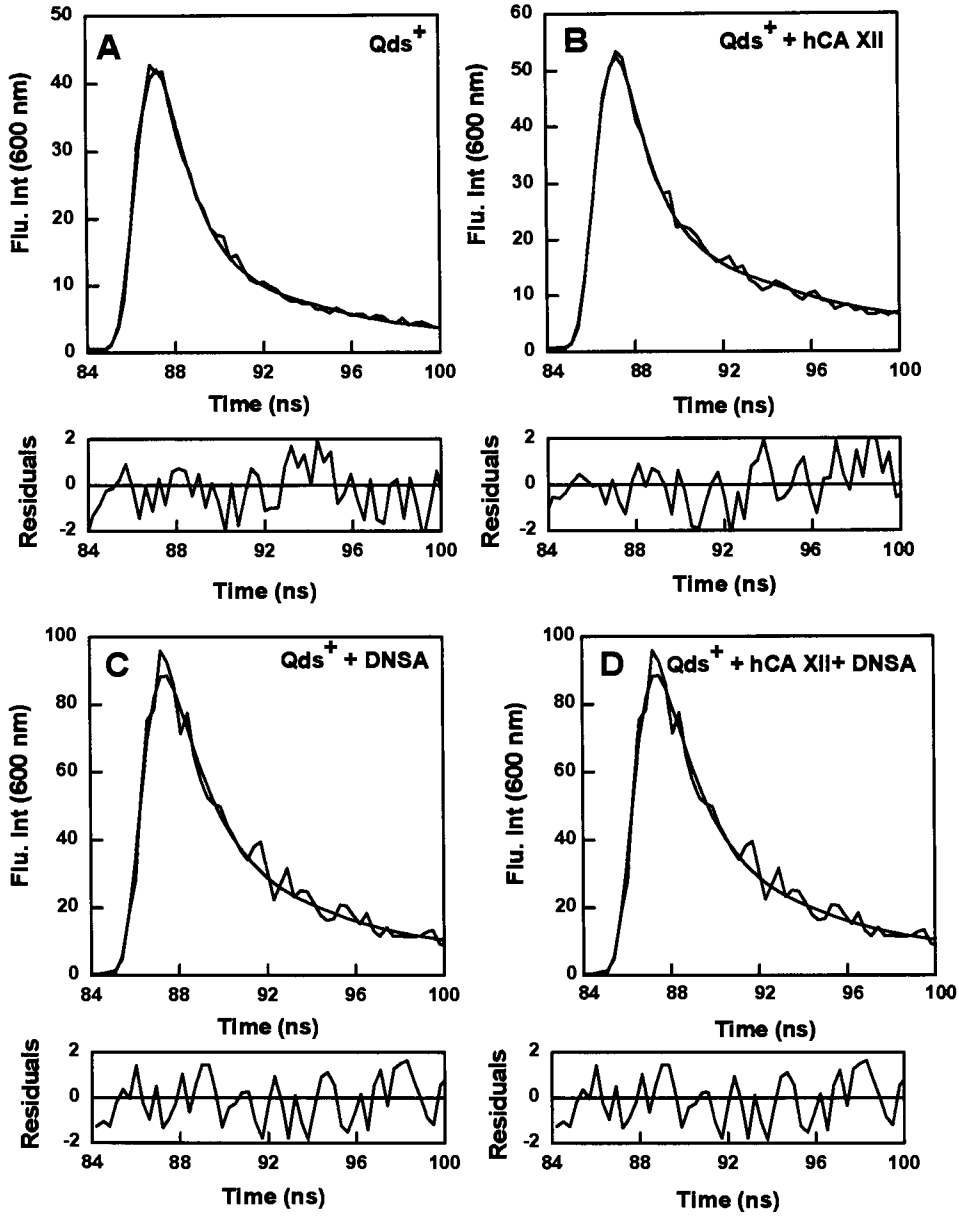

Figure 5.80. Fluorescence lifetimes of Qds^+ under various conditions.
Excited state fluorescence decay profiles of free Qds^+ (1 μM) (Panel A), Qds^+ (1 μM) in the presence of 25 μM hCA XII (Panel B), Qds^+ (1 μM) in the presence of 25 μM DNSA (Panel C), Qds^+ (1 μM) in the presence of 3 μM hCA XII and 15 μM DNSA (Panel D). The excitation and emission wavelengths were 340 nm and 600 nm, respectively. Other experimental conditions were same as in Figure 3. The solid smooth lines are the best fit of the data according to the double exponential rate equation for the data of different panels. Panel A: $\tau_1 = 1.3 \pm 0.01$ ns; $\tau_2 = 7.3 \pm 0.02$ ns; Panel B: $\tau_1 = 1.3 \pm 0.01$ ns ; $\tau_2 = 7.3 \pm 0.01$ ns. Panel C: $\tau_1 = 1.4 \pm 0.02$ ns; $\tau_2 = 7.4 \pm 0.01$ ns. Panel D: $\tau_1 = 1.4 \pm 0.02$ ns; $\tau_2 = 11.4 \pm 0.02$ ns. The bottom panels show the residuals of the fitted data.

fluorescence emission spectra of hCA XII bound DNSA (λ_{ex}=330 nm) as a function of increasing concentrations of intact polylysine molecule (rather than its monomeric amino acid residue; see methods). Note that as the concentration of polylysine increases, the fluorescence emission intensity of DNSA at 457 nm decreases. It should be pointed out that such a quenching of the enzyme-bound DNSA fluorescence (at 457 nm) has also been evident in the presence of Qds^+ (Figure 5.79A and B) although the latter has been demonstrated to proceed in concomitance with FRET between the above fluorophores. Evidently, the positive charges of the interacting macromolecules (contributed either by Qds^+ or polylysine) serve as the primary determinant in modulating the fluorescence properties of the enzyme-bound DNSA. Figure 5.81B shows the decrease in the fluorescence intensity of the enzyme-bound DNSA at 457 nm as a function of polylysine concentration. The binding isotherm was analyzed by the same quadratic equation which takes into account the bound versus free form of the titrant (*506*), and was used for analyzing the Qds^+-hCA XII binding data (see Figure 5.77B). The solid smooth line is the best fit of the data for the binding affinity of polylysine for hCA XII–DNSA conjugate as being equal to 6 μM.

At this juncture, it was of interest to see if the binding affinity of polylysine to hCA XII would be different in the absence of DNSA. This was essential to discern if the presence of DNSA influenced the binding affinity of polylysine even though the sites of binding of polylysine and DNSA on hCA XII was considered to be different. Towards achieving this goal, fluorescence emission spectra of hCA XII (λ_{ex} = 295 nm, λ_{em} = 336 nm) in the absence and presence of polylysine was obtained. It was found that similar to

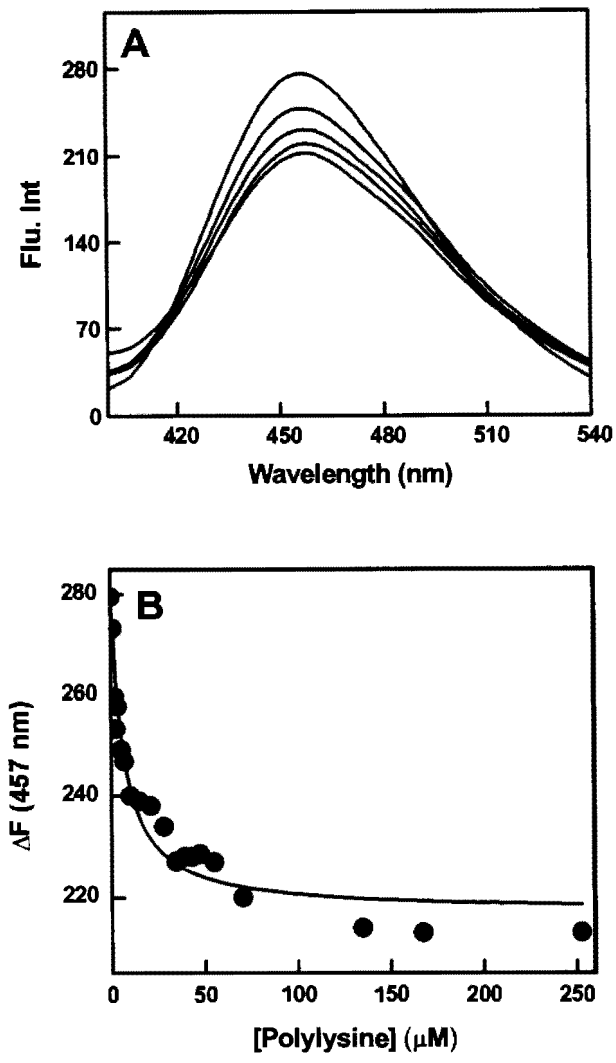

Figure 5.81. Fluorescence spectral changes upon binding of polylysine with hCA XII-DNSA complex.
Panel A shows the fluorescence emission spectra of hCA XII-DNSA complex in the presence of increasing concentrations of polylysine. The experiments were performed in 25 mM HEPES buffer, pH 7.5 containing 10% Acetonitrile. [hCA XII] = 1 μM, [DNSA] = 5 μM, polylysine = [1-253 μM], λ_{ex} = 330 nm. Panel B shows the binding isotherm for the interaction of polylysine with hCA XII- DNSA complex. The decrease in the fluorescence emission intensity of hCA XII-DNSA at 457 nm (derived from the data of Panel A) was plotted as a function of polylysine concentration. The solid smooth line is the best fit of the data for the dissociation constant of hCA XII(DNSA)-polylysine complex as being equal to 6 ± 0.9 μM.

Qds^+, polylysine induced quenching of the intrinsic fluorescence of hCA XII. This decrease in the fluorescence intensity of hCA XII upon addition of polylyine was used as a signal to determine their binding affinity. Figure 5.82 represents the fluorescence intensity of hCA XII as a function of increasing concentrations of polylysine. The solid smooth line of the Figure is the best fit of the data with the K_d value of 3.3 μM. Hence, the presence of DNSA did not significantly influence the binding affinity of hCA XII for polylysine. The question arose whether Qds^+ and polylysine-mediated quenching of the enzyme-bound DNSA fluorescence was partly due to the changes in the binding affinity of he enzyme–presence of carbonic anhydrase isozymes (*329*, *387*, *473*). The above possibility could not be substantiated or refuted in the presence of Qds^+ due to its high absorption as well as its interference in the fluorescence signal of the enzyme–DNSA complex. However, since the latter constraints were non-existent with polylysine, the influence of polylysine on the binding affinity of DNSA for hCA XII could not be determined.

Figure 5.83 shows the titration of a fixed concentration of hCA XII (0.2 μM) and saturating concentration of polylysine (25 μM) with increasing concentrations of DNSA (λ_{ex}=330 nm, λ_{em}=457 nm). The analysis of the experimental data yielded the binding affinity of DNSA for hCA XII (bound to polylysine) as being equal to 0.18 μM. It should be emphasized that this value is similar to the binding affinity of DNSA for free enzyme as being equal to 0.08 μM. Hence, the enzyme bound polylysine had practically no effect on the dissociation constant of the enzyme–DNSA complex.

5.5.1.8. Effect of Qds^+, polylysine and DNSA on the catalytic activity of hCA XII

Given that both Qds^+ and polylysine macromolecules interacted with hCA XII with comparable binding affinities, and both these macromolecules influenced the fluorescence emission profile of the enzyme-bound DNSA, we proceeded to determine whether or not

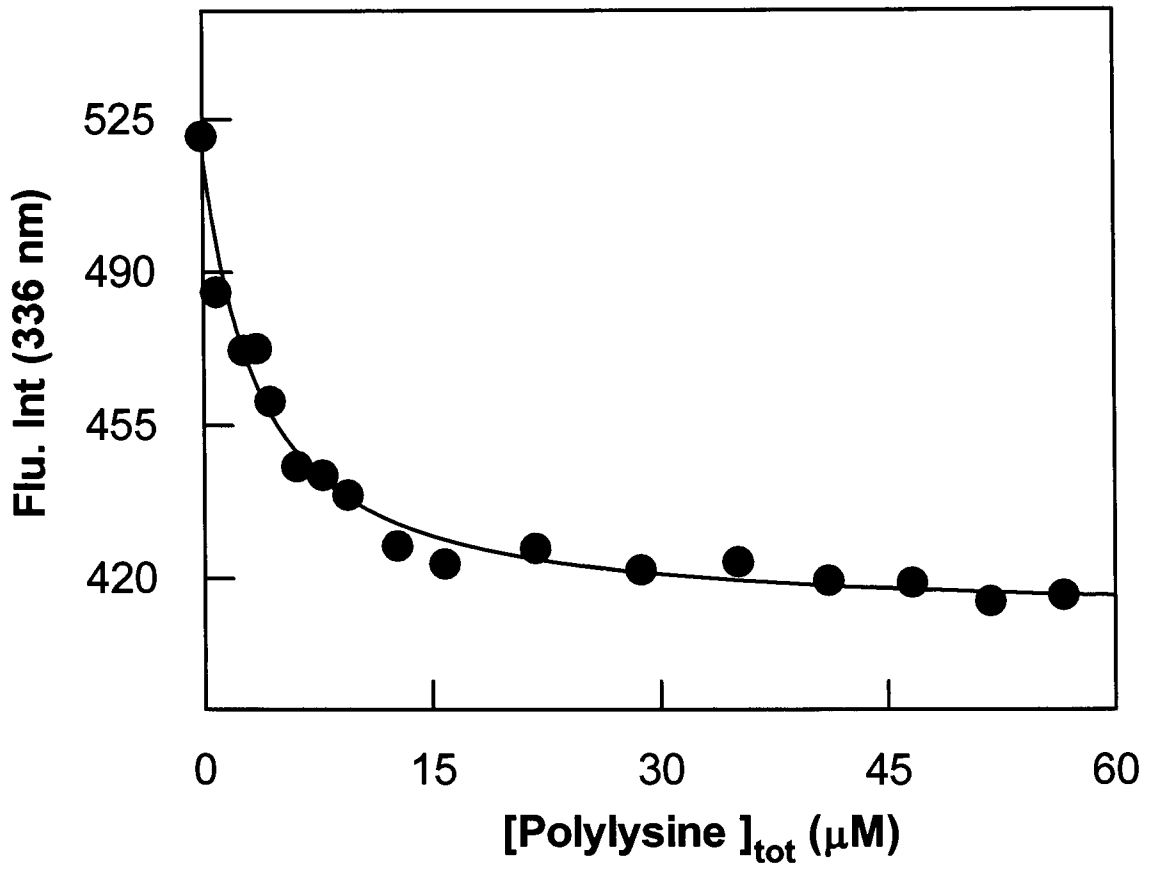

Figure 5.82. Binding isotherm for the interaction of hCA XII with polylysine.
The Figure shows the decrease in the fluorescence emission intensity of hCA XII at 336 nm (λ_{ex}= 280 nm) as a function of polylysine concentration. A fixed concentration of the hCA XII (0.95 μM) was titrated with increasing concentrations of polylysine (λ_{ex}= 280 nm, λ_{em} = 336 nm) in 25 mM HEPES buffer, pH 7.0. The solid line is the best fit of the data which provided a dissociation constant of 3.3 ± 0.48 μM.

they elicited similar or different influence on the catalytic activity of the enzyme. Toward

this goal, we measured the activity of hCA XII in the absence and presence of Qds^+, polylysine and DNSA via the pH drop method (*451*). The data are summarized in Table 5.17. Note that the activity of the enzyme drastically decreases in the presence of 5 μM DNSA. This was expected since DNSA is known to coordinate with the active site resident

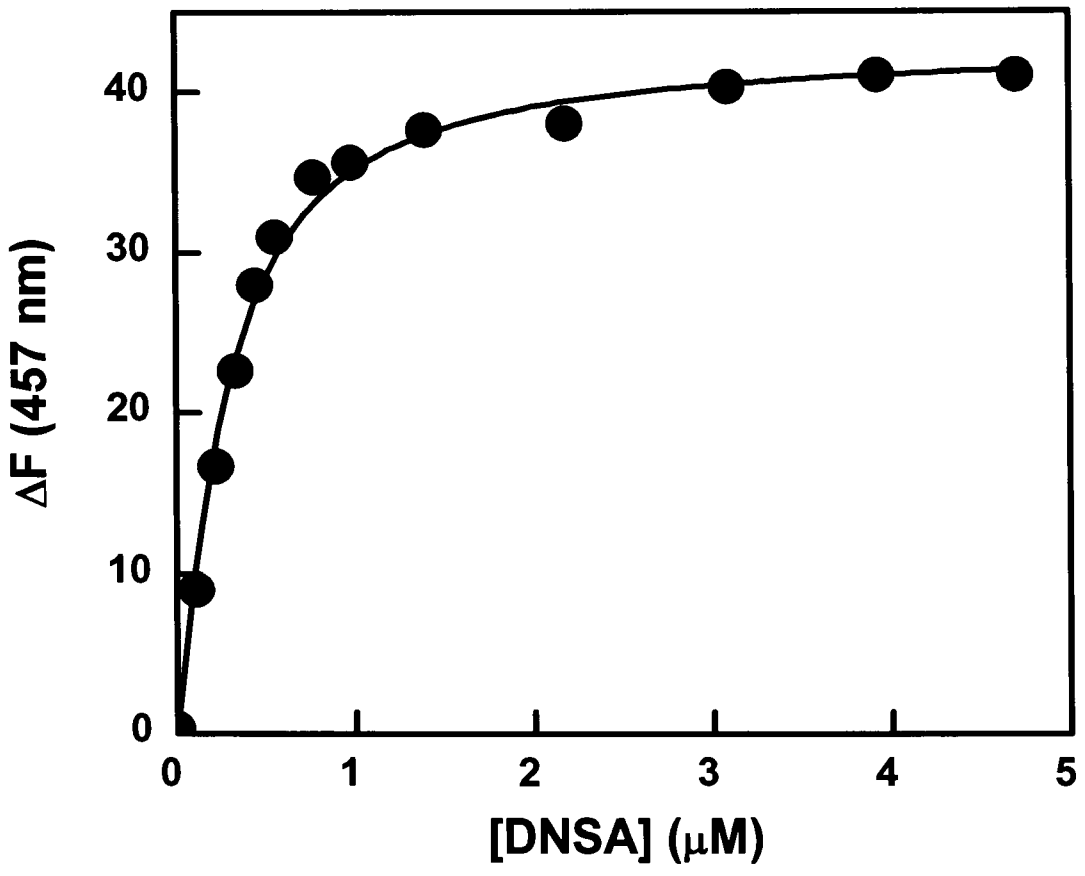

Figure 5.83. Effect of polylysine on the binding affinity of DNSA with hCA XII. A fixed concentration of hCA XII (0.2 μM) with saturating concentrations of polylysine (25 μM) was titrated with increasing concentrations of DNSA, and the increase in the fluorescence emission intensity of hCA XII-DNSA complex at 457 nm (λ_{ex} = 330 nm) was monitored. The solid smooth line is the best fit of the data for the K_d value of 0.18 ± 0.01 μM.

Zn^{2+}, and by doing so precludes the hydration reaction of CO_2. On the other hand, there was a very small decrease (approximately 7 to 10%) in the catalytic activity of the enzyme upon addition of saturating concentrations of either polylysine or Qds^+.Evidently, the catalytic machinery of hCA XII remained practically unaffected upon binding of the positively charged macromolecules. In contrast to these observations, it was of surprise to note that whereas the inhibitory effect of DNSA was overcome (by about 70%) by the presence of Qds^+, the presence of polylysine had no effect. Clearly, despite their marked similarity in binding to the surface of hCA XII, they elicited different influence in modulating the enzyme activity. As will be discussed in the next chapter, the above noted discriminatory effect of these cationic macromolecules is encoded in their rigid versus flexible structural features.

5.5.1.9. Interaction of Qds^+ with hCA I and hCA II

The electrostatic surface potential of hCA isozymes I and II revealed the presence of patches of anionic charges distributed on their surfaces. Hence, it was of interest to see whether these isozymes interact with Qds^+. In a preliminary manner, the fluorescence emission intensity of hCA I and II were monitored (λ_{ex} = 295 nm, λ_{em} (hCA I) = 330 nm, λ_{em} (hCA II) = 335 nm) upon addition of small amounts of Qds^+. This caused a quenching in the fluorescence signal of both the isozymes. It was confirmed that such a quenching was not an artifact of the inner filter effect since the absorption of the reaction mixture was less than 0.1. The decrease in emission intensity of hCA I and II upon addition of Qds^+ served as a signal for monitoring their binding. However, as mentioned above, prior to determining the binding affinity of hCA I and II for Qds^+, it was realized that the titration of an increasing concentration of the Qds^+ to a fixed concentration of the protein was not

feasible since this would lead to inner filter effect as a consequence of high UV absorption of the Qds^+ at 295 nm. Hence, the binding affinities were determined by a titration of a fixed concentration of Qds^+ with increasing concentrations of enzyme while monitoring the fluorescence emission of the respective proteins. The observed fluorescence was corrected by subtraction of a background titration of hCA I and II into buffer and then plotted as a function of the enzyme concentration.

As is evident from the data of Figure 5.84A and B, the fluorescence of hCA I exhibited a hyperbolic behavior in the presence of Qds^+. The solid smooth lines in Figure 5.84 represent the best fit of the data to the quadratic binding model as described by Qin and Srivastava which provided a K_d of 6.7 μM and 5.9 μM for hCA I and II respectively. The binding isotherms of Qds^+ with hCA I, hCA II and hCA XII are listed in Table 5.20. Clearly, Qds^+ bind with a much higher affinity to hCA XII as compared to hCA I and hCA II.

5.5.2. Interaction of hCA XII with anionic Qds (Qds^-)

5.5.2.1. Absorption and emission spectra of Qds^-

To ascertain whether hCA XII could bind to a negatively charged surface, the binding of the enzyme to Qds^- of approximately 4.5 nm diameter was investigated. The negative charge on the cadmium telluride (CdTe) Qds was prepared by the conjugation of thio glycolic acid. Figure 5.85 shows the absorbance and fluorescence spectra of the Qds^-. The Qds^- show a broad absorption band from 250 nm to approximately 600 nm. Aside from the major peak in the UV region, a smaller peak was observed at 575 nm (Fig. 5.85, panel A). The latter peak was chosen for excitation of the Qds^- so as to avoid complications due to the absorbance of hCA XII in the ultraviolet region. When excited at

570 nm, the steady-state fluorescence emission of the Qds^- was strong with an emission maximum of 602 nm (Fig. 5.85, panel B).

Table 5.17. Catalytic activity of hCA XII in the presence of different ligands.

Experimental condition[a]	% activity
Free hCA XII	100
hCA XII -DNSA	9
hCA XII-Qds^+	92
hCA XII-DNSA -Qds^+	72
hCA XII-Polylysine	91
hCA XII-DNSA-Polylysine	2

All experiments have been performed under identical conditions, and the enzyme activity is represented as the percent of the control activity in the absence of any added ligand.

[a] [DNSA]=5 μM, [polylysine]=25 μM, [Qds+]=10 μM.

5.5.2.2. Influence of Qds^- on the emission spectra of hCA XII

To probe whether the intrinsic fluorescence of hCA XII was influenced by the Qds^- the fluorescence spectra of the enzyme was determined in the presence of stoichiometric concentrations of Qds^-. This lead to the quenching of the tryptophan fluorescence of the protein. The decrease in the fluorescence of hCA XII upon addition of Qds^- served as a signal for monitoring the binding of hCA XII to Qds^-. It was noticed that, similar to Qds^+, Qds^- also contribute significant absorption at 295 nm. Hence, determination of the binding constant by titrating hCA XII with increasing concentrations of Qds^- would lead to inner filter effect and there by artifactually decrease the binding affinity. Because of this reason, it was decided that the binding isotherm for hCA XII-Qds^- will be determined by taking a fixed and low concentrations of Qds^- and titrated with known concentrations of hCA XII as

in the case for Qds^+. The observed fluorescence was corrected by subtraction of a background titration of hCA XII into buffer and then plotted as a function of the enzyme concentration (Figure 5.86).

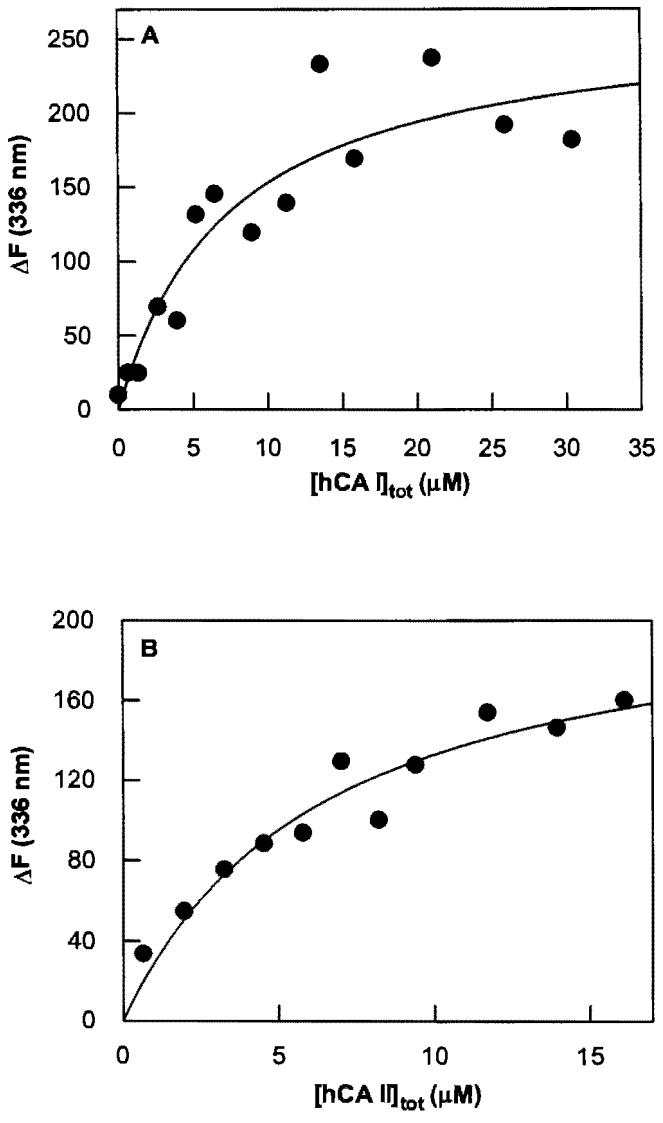

Figure 5.84. Binding isotherm for the interaction of Qds^+ with hCA I and hCA II. The Figure shows the decrease in the fluorescence emission intensity of hCA I (Panel A) and hCA II (Panel B) at 336 nm (λ_{ex}= 280 nm) as a function of Qds+ concentration. A fixed concentration of the Qds^- (0.17 μM) was titrated with increasing concentrations of hCA I and hCA II in 10 mM Tris buffer, pH 8.0. The solid line is the best fit of the data which provided a dissociation constant of 6.7 ± 2.6 μM and 5.9 ± 0.6 μM and stoichiometry of 7 and 4 for A and B, respectively.

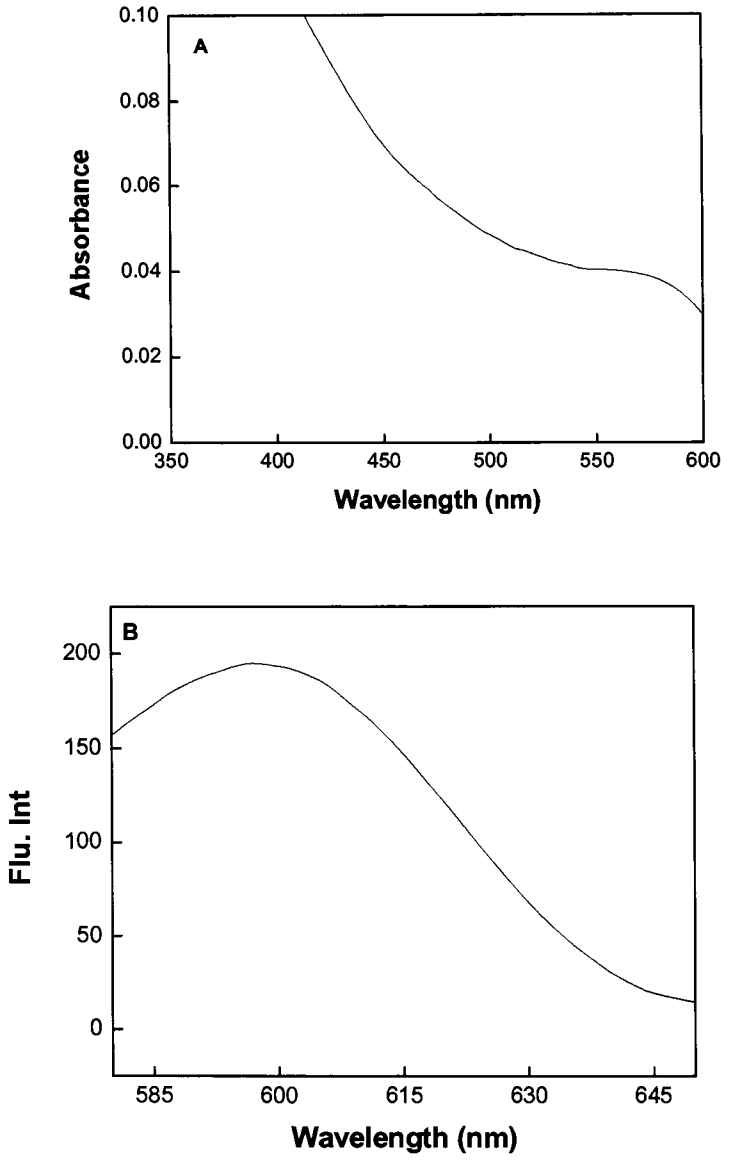

Figure 5.85. Absorption and emission properties of the CdTe/TGA Qds in 10 mM Tris buffer pH 8.0.
Panel A depicts the absorbance of 0.75 μM CdTe/TGA Qds in a 1 cm path length quartz cuvette whereas panel B depicts the steady-state fluorescence emission of 3 μM CdTe/TGA Qds (excitation at 570 nm) in a 4 mm square quartz cuvette.

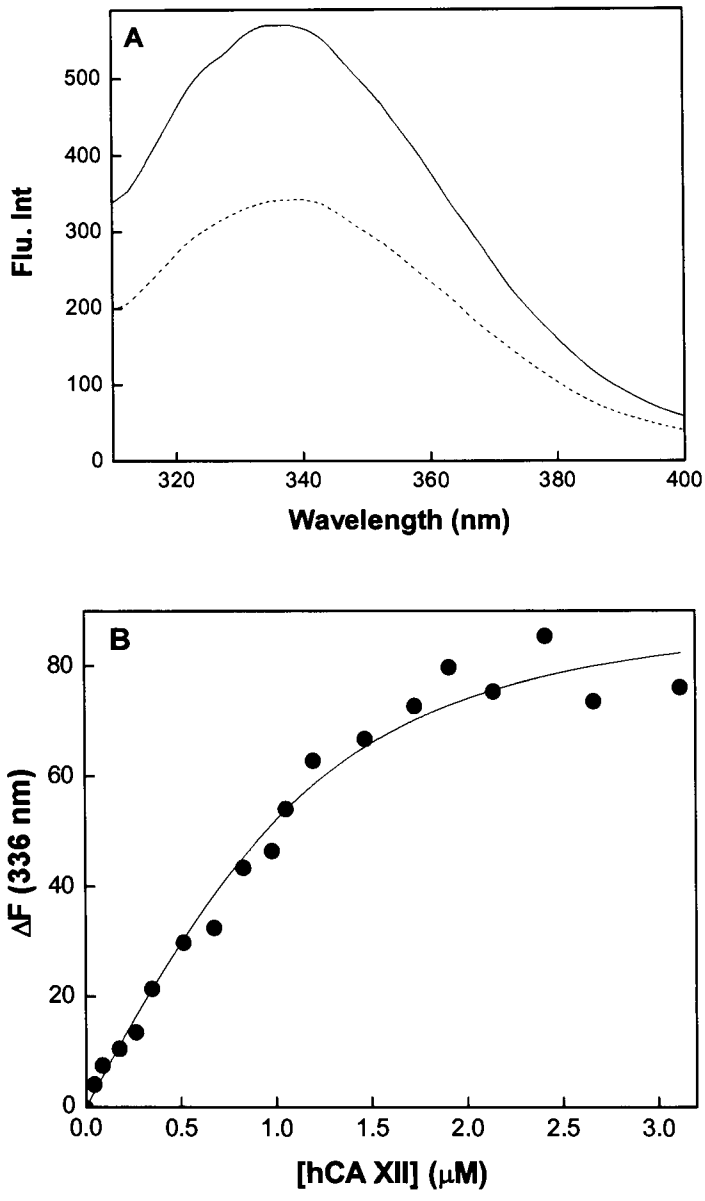

Figure 5.86. Fluorescence spectral changes upon binding of Qds^- to hCA XII. Panel A of Fig shows the fluorescence emission spectra of hCA XII and hCA XII-Qds^- in 10 mM Tris buffer pH 8.0. The fluorescence emission spectra of 0.2 μM hCA XII (solid line) (λ_{ex} = 295 nm; λ_{em} = 310 nm – 400 nm) was quenched in the presence of stoichiometric amounts of Qds^- (dashed line). Panel B shows the binding isotherm for the interaction of hCA XII with Qds^-. A fixed concentration of the Qds^- (0.64 μM) was titrated with increasing concentrations of hCA XII (λ_{ex}= 295 nm, λ_{em} = 336 nm) in 10 mM Tris buffer, pH 8.0. The data represent the magnitude of ΔF obtained by subtracting the fluorescence intensity of the mixture from that given by the protein itself under identical conditions as a function of protein concentration. The solid line is the best fit of the data (*38*) which provided a dissociation constant of 0.28 ± 0.06 μM, and a stoichiometry of hCA XII bound per Qds^- as being equal to 1.8.

As is evident from the data of Figure 5.86, the fluorescence of hCA XII exhibited a saturating (hyperbolic) behavior in the presence of Qds^-. This finding was consistent with the formation of a complex between hCA XII and Qds^-. For the analysis of the binding isotherm, it should be emphasized that although the concentration of hCA XII was known, we had no method to directly determine the concentration of Qds^-. Hence, it was not possible to ascertain *a priori* whether it was valid to assume that the total concentration of hCA XII was approximately equal to the free concentration of the enzyme throughout the titration. Therefore, a binding equation accounting for both the concentrations of the enzyme and the Qds had to be employed (*506*) to determine the dissociation constant (K_d). The solid smooth line in Figure 5.86 represents the best fit of the data to the quadratic binding model as described by Qin and Srivastava (*506*) which provided a dissociation constant (K_d) for and stoichiometry of the hCA XII–Qds^+ complex as being equal to 0.28 μM and 1.8 molecules of hCA XII subunit bound per molecule of Qds^-, respectively. The concentration of Qds^- calculated from this analysis was then utilized to determine the concentration of the Qds^- stock for further use.

5.5.2.3. Influence of hCA XII on the fluorescence emission spectra of Qds^-

Figure 5.87A represents the emission spectra of Qds^- in the presence of stoichiometric concentrations of hCA XII (λ_{ex} = 280 nm). Unlike Qds^+, the steady-state fluorescence intensity of Qds^- increased in presence of hCA XII. The decrease in the fluorescence intensity of hCA XII upon addition of Qds^- and the increase in the fluorescence intensity of Qds^- upon addition of hCA XII when excited at 280 nm suggested the possibility of energy transfer from the tryptophan residues of the protein to Qds. In order to substantiate or refute the above possibility, the fluorescence emission spectra of

Qds^- in the presence of hCA XII was monitored by exciting at 330 nm. This wavelength was chosen to avoid the possibility of energy transfer from tryptophan residues to Qds^-. As depicted in Fig 5.87 B, the fluorescence intensity of the Qds increase upon addition of hCA XII. This suggested that the increase in fluorescence intensity is not necessarily due to the energy transfer from the tryptophan residues but could be due to the increased passivity Qds^- upon interaction with hCA XII.

Since interaction of hCA XII to Qds^- changed the signal of the latter in contrast to Qds^+, it was of interest to determine its binding affinity with hCA XII utilizing this signal change. Towards this idea, a fixed concentration of hCA XII (0.75 μM) was titrated with increasing concentrations of Qds^- (λ_{ex} = 330 nm, λ_{em} =600 nm) and the increase in the fluorescence intensity of Qds^- (by subtracting the fluorescence intensity of the free Qds from tha given by the mixture) was plotted as a function of its concentration (Figure 5.88). The solid smooth line is the best fit of the data which provided a dissociation constant and a stoichiometry of 0.25 μM and 0.5 molecules of Qds^- bound per protein molecule.

5.5.2.4. Effect of Qds^- on the spectral features of hCA XII-DNSA complex

Since the data of Figure 5.86 and Figure 5.87 indicated that hCA XII was able to bind to Qds^-, it was of interest to determine whether the binding of hCA XII to Qds^- influences the active site structural and functional features of the enzyme. Towards achieving this goal, it was of interest to compare the binding affinity of hCA XII for the inhibitor, DNSA, in the absence and presence of Qds^-. Having established the binding affinity of free hCA XII for DNSA (Figure 5.79), the binding of DNSA by hCA XII in the presence of Qds^- was investigated. A fixed concentration of hCA XII (1 μM) was titrated with increasing concentrations of the Qds^- in the presence of a saturating concentration of

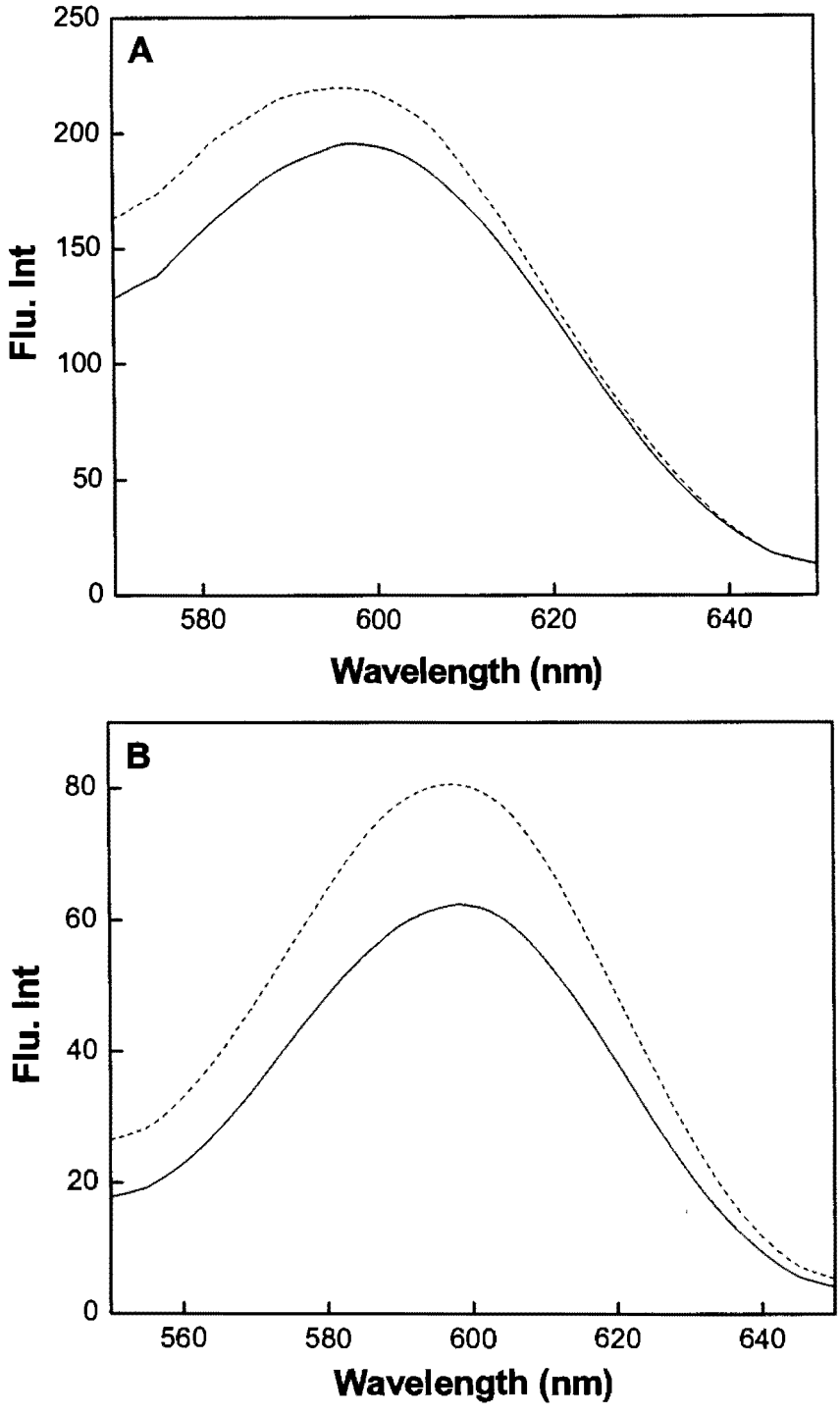

Figure5.87. Steady-state fluorescence emission spectra of the Qds^{-}.
The solid lines of Panel A and B represent the emission spectra of free Qds^{-} (0.2 μM) and the broken lines represent its emission spectra in the presence of stoichiometric amounts of hCA XII (Panel A: λ_{ex} = 280 nm; Panel B: λ_{ex} = 330 nm). All spectra were measured in 10 mM Tris, pH 8.0.

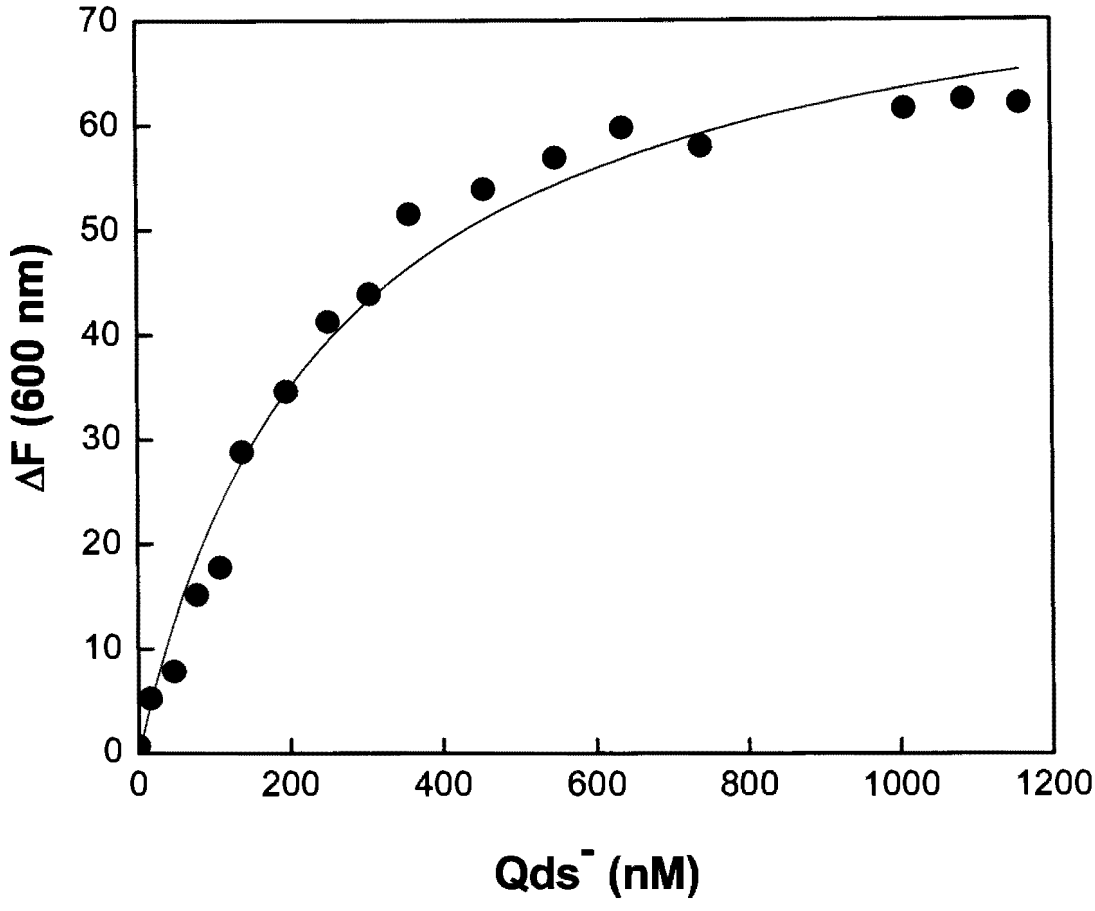

Figure5.88. Binding isotherm for the interaction of hCA XII with Qds^-.
A fixed concentration of the hCA XII (0.75 μM) was titrated with increasing concentrations of Qds^- (λ_{ex}= 330 nm, λ_{em} = 600 nm) in 10 mM Tris buffer, pH 8.0. The data represent the magnitude of ΔF obtained by subtracting the fluorescence intensity of the mixture from that given by the Qds^- itself under identical conditions as a function of Qds^- concentration. The solid line is the best fit of the data (*38*) which provided a dissociation constant of 0.25 ± 0.2 μM, and a stoichiometry of Qds^- bound per hCA XII as being equal to 0.5.

DNSA (5 μM) and the fluorescence of hCA XII-DNSA complex was monitored. The changes in steady-state fluorescence emission intensity as a function of the concentration of Qds are shown in Figure 5.89. As the concentration of Qds were increased, a decrease in the fluorescence intensity of the hCA XII-DNSA emission peak at 457 nm was observed.

Furthermore, after subtraction of the background signal of free Qds^-, an increase in the fluorescence emission intensity of the Qds was evident at 602 nm as a function of the concentration of Qds^-.

The decrease in the 457 nm peak apparent in Figure 5.89 suggested that DNSA was excluded from the hCA XII active site pocket in the presence of Qds^-. This observation was not surprising due to the fact that hCA XII exhibits a positive electrostatic potential in and around the active site which is a potential binding site for Qds^- binding. It is intuitively obvious that the binding of Qds to the active site would competitively displace the active site bound ligand DNSA there by leading to a decrease in the fluorescence signal at 457 nm. It needs to be mentioned that the decrease in the fluorescence intensity of the enzyme-DNSA complex in the presence of Qds^- could also be attributed to the decrease in the binding affinity of hCA XII for DNSA in the presence of Qds similar to Qds^+ . Therefore, an attempt was made to determine the binding affinity of hCA XII for DNSA in the presence of Qds^- by titration of DNSA into hCA XII in the presence of a saturating concentration of Qds^-, while monitoring the signal of the enzyme bound DNSA. However, no signal was observed for the hCA XII-DNSA complex which indicated that hCA XII could not bind DNSA while already bound to Qds^- or that the fluorescence of hCA XII-bound DNSA was quenched in the presence of the Qds^-.

Apart from the decrease in the fluorescence intensity of hCA XII-DNSA at 457 nm, an increase in the fluorescence intensity of Qds^- at 600 nm was also observed. This increase was similar to that observed for Qds^- interacting with hCA XII in the absence of DNSA. At this point, it was not feasible to rule out the possibility that the increase could

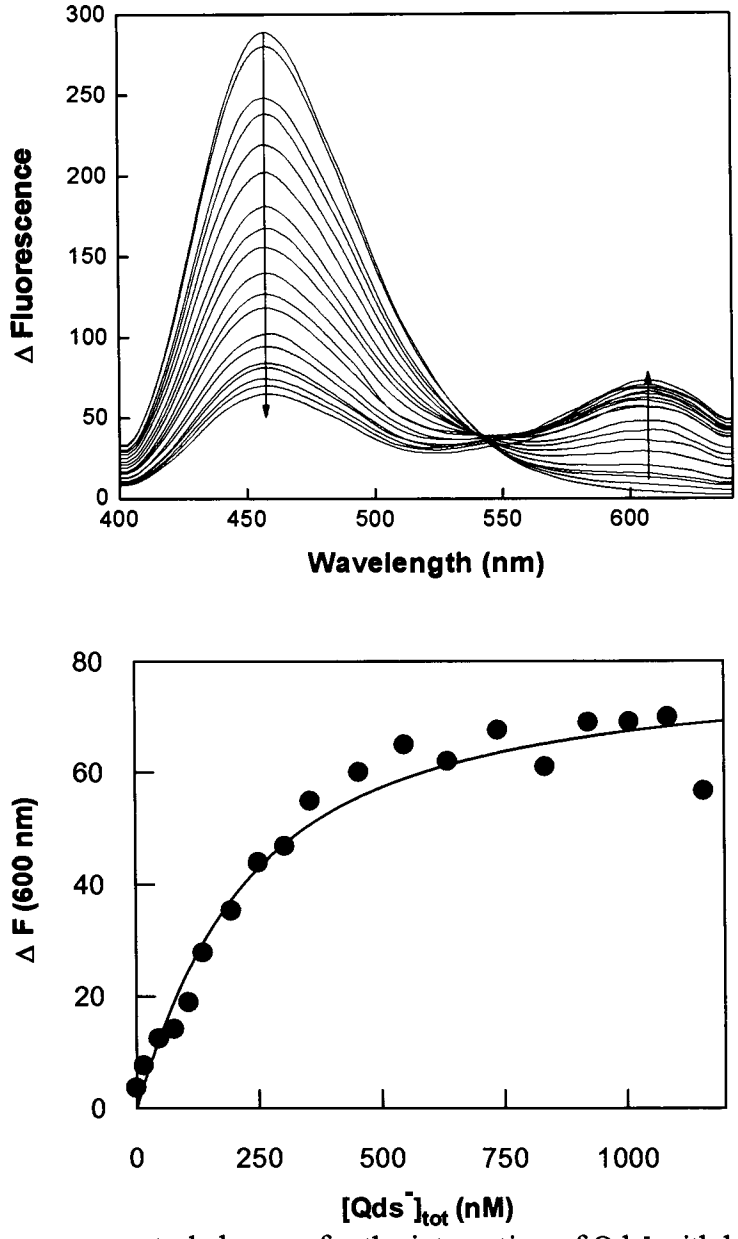

Figure 5.89. Fluorescence spectral changes for the interaction of Qds^- with hCA XII-DNSA complex.

Panel A shows the spectra of hCA XII-DNSA complex in the presence of increasing concentrations of Qds^- in 10 mM Tris-HCl buffer, pH 8.0 containing 10 % acetonitrile. [hCA XII] = 0.5 μM, [DNSA] = 3 μM, λ_{ex} = 330 nm. The decrease and increase in the fluorescence emission intensity at 457 and 600 nm, respectively, are shown by the arrows. The spectra is generated by subtracting the emission contributed by the free Qds^- in buffer from theat of the (hCA XII – DNSA)- Qds^- complex. Panel B shows plot of ΔF_{600} (from panel A) as a function of Qds^- concentration. The solid smooth line is the best fit of the data (by fixing the stoichiometry of 0.5, the value reciprocal of the experimentally determined stoichiometry of hCA XII-Qds^- complex) for the dissociation constant of hCA XII (DNSA)-Qds^- complex as being equal to 0.17 ± 0.03 μM.

also be due to the energy transfer from DNSA if the latter is still bound at or near the active site pocket. Irrespective of the mechanistic outcome, the binding affinity of Qds^- to hCA XII was determined by monitoring the increase in its fluorescence signal. As evident from Figure 5.89B, a hyperbolic dependence was obtained when the difference in the fluorescence intensity was plotted as a function of Qds^- concentration. The solid smooth line of Figure represents the best fit of the data with the K_d value of 0.17 μM. Note that this K_d is qualitatively similar to that obtained from Figure 5.86 and 5.88.

5.5.2.5. Effect of Qds^- on the fluorescence lifetimes of hCA XII

Since the broad absorption band of Qds^- overlaps with the emission peak (336 nm) of hCA XII, the observed fluorescence quenching of hCA XII in the presence of Qds^- and the fluorescence enhancement of the latter in the presence of hCA XII was envisaged to be possibly due to the fluorescence resonance energy transfer (FRET) from the enzyme's tryptophan residues to Qds^-. To probe this possibility, the intrinsic fluorescence lifetime of hCA XII was determined in the absence and presence of Qds^-. In this experiment, a relatively high energy 280 nm LED was used as the excitation source, and the emission wavelength was set at 336 nm. Figure 5.90 shows the excited state lifetime traces of hCA XII in the absence and presence of Qds^-. Both these lifetime traces conformed to the biphasic rate equation yielding two lifetimes (τ_1 and τ_2). Whereas the analysis of the experimental data (solid smooth lines) for free hCA XII yielded the short (τ_1) and long (τ_2) lifetimes as being equal to 0.24 and 2.4 ns, respectively, those for the hCA XII– Qds^+ complex yielded the above parameters to be 0.22 and 2.3 ns, respectively. Note that these values are not too different, suggesting that Qds^- mediated quenching is not due to perturbation of the excited state energy of the enzyme's intrinsic fluorophores. Evidently,

there has been no FRET between the enzyme's tryptophan residues and Qds^-. The fact that Qds^- quench the intrinsic steady-state fluorescence of hCA XII but do not alter the lifetimes of the tryptophan moieties implies that the overall quenching process is a ground state phenomenon (*544*).

5.5.2.6. Effect of hCA XII on the fluorescence lifetimes of Qds^-

In addition to the fluorescence lifetime measurements of hCA XII, the fluorescence lifetime of Qds^- in the presence and absence of hCA XII was also determined. In this experiment, a relatively high energy 340 nm LED was used as the excitation source, and the emission wavelength was set at 600 nm. Figure 5.91 shows the excited-state lifetime traces of Qds^- in the absence and presence of hCA XII. Both these lifetime traces conformed to the biphasic rate equation yielding two lifetimes (τ_1 and τ_2). Whereas the analysis of the experimental data (solid smooth lines) for free Qds^- yielded the short (τ_1) and long (τ_2) lifetimes as being equal to 1.8 and 17 ns, respectively, those for the hCA XII–Qds^- complex yielded the above parameters to be 3.3 and 20.98 ns, respectively. Note the increase in the lifetime of Qds^- upon interaction with hCA XII. The increase in lifetime corroborates well with the steady-state fluorescence increase and since the Qds^- were excited at 340 nm it is evident that there has been no FRET between the enzyme's tryptophan residues and the Qds^-. All these results suggest that the surface passivity of Qds^- is increased in the presence of hCA XII.

5.5.2.7. Effect of Qds^- on the catalytic activity of hCA XII and hCA XII-DNSA complex

Given that both Qds^+ and Qds^- interacted with hCA XII with good binding affinity, and influenced the fluorescence emission profile of the enzyme-bound DNSA, it was of

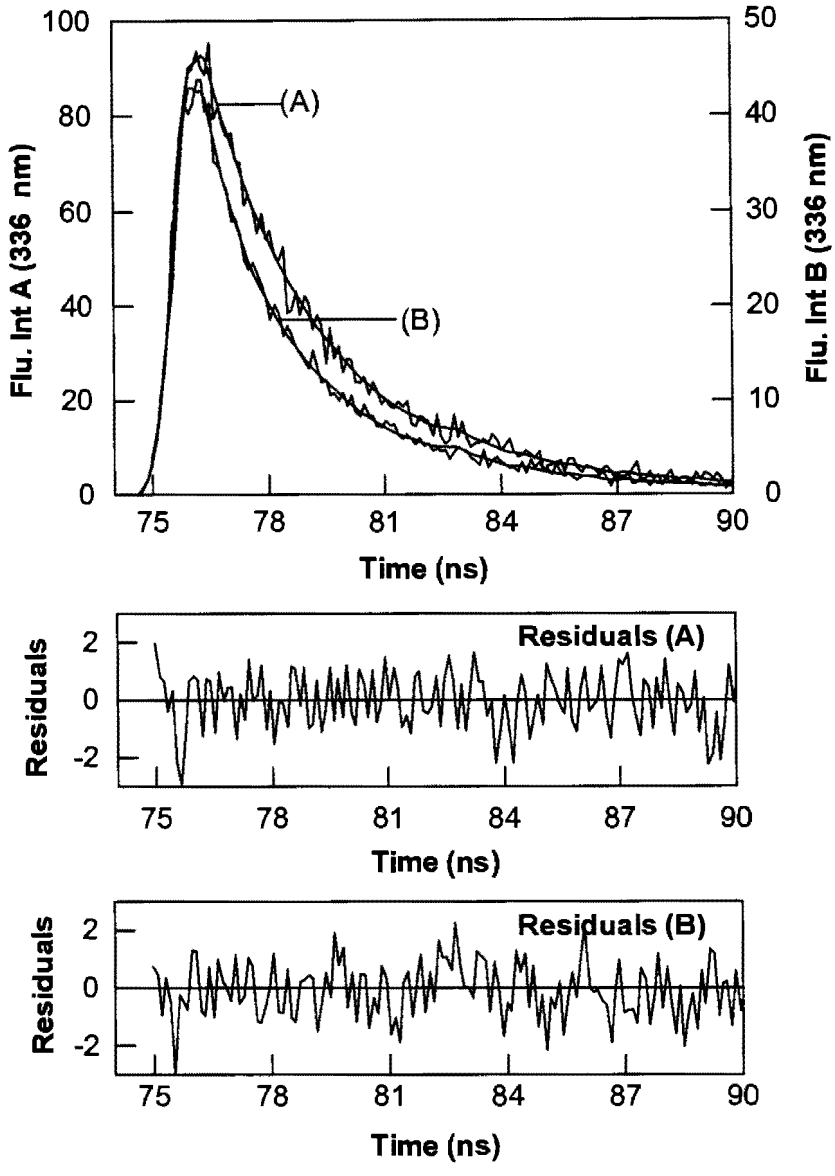

Figure 5.90. Fluorescence lifetimes of hCA XII in the presence and absence of Qds^-. Excited state fluorescence decay profiles of free hCA XII (2 μM) (A) and in the presence of Qds^- (20 μM). The excitation and emission wavelengths were 280 nm and 336 nm, respectively in 10 mM Tris pH 8.0. The solid smooth lines are the best fit of the data according to the double exponential rate equation for the data with lifetimes of $\tau_1 = 0.24 \pm 0.01$ ns; $\tau_2 = 2.4 \pm 0.02$ ns for A and $\tau_1 = 0.26 \pm 0.01$ ns ; $\tau_2 = 2.3 \pm 0.01$ ns for B. The bottom panels show the residuals of the fitted data.

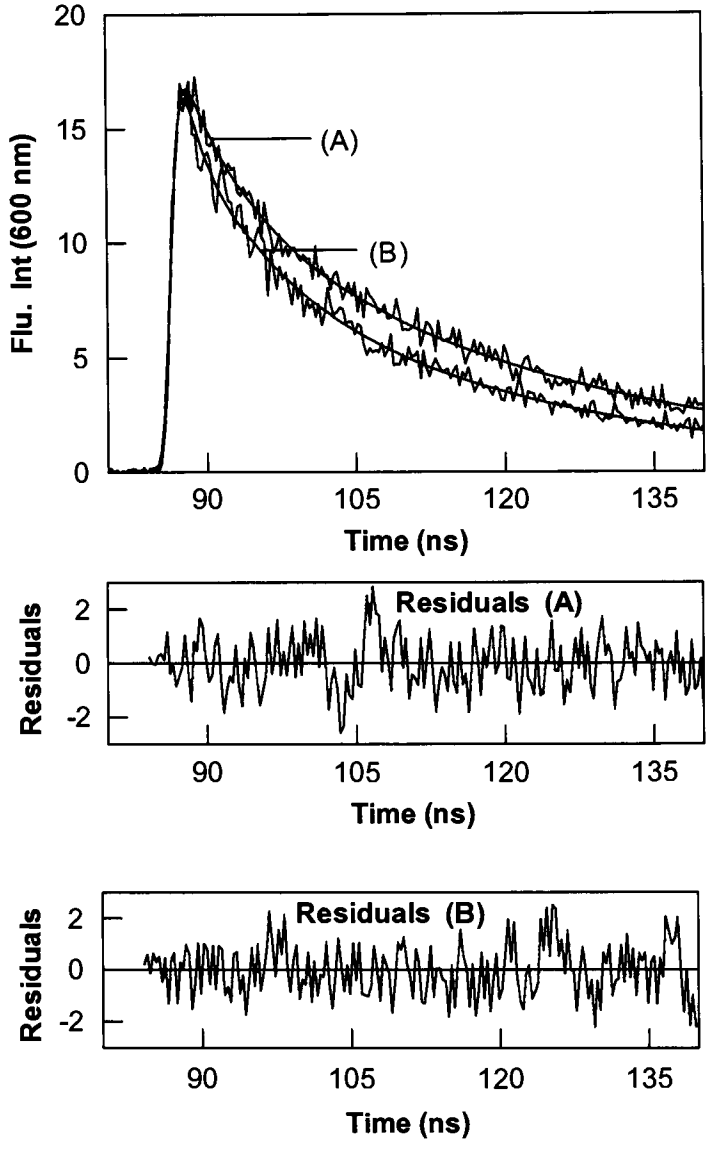

Figure 5.91.Fluorescence lifetimes of Qds^{-} in the presence and absence of hCA XII. Excited state fluorescence decay profiles of free Qds- (1 μM) (A) and in the presence of hCA XII (30 μM). The excitation and emission wavelengths were 340 nm and 600 nm, respectively in 10 mM Tris pH 8.0. The solid smooth lines are the best fit of the data according to the double exponential rate equation for the data with lifetimes of $\tau 1 = 1.8 \pm 0.01$ ns; $\tau 2 = 17 \pm 0.02$ ns for A and $\tau_1 = 3.3 \pm 0.03$ ns ; $\tau_2 = 20.98 \pm 0.06$ ns for B. The bottom panels show the residuals of the fitted data.

interest to determine whether or not they elicited similar or different influence on the catalytic activity of the enzyme. Toward this goal, the activity of hCA XII and hCA XII-DNSA were determined in the presence and absence of Qds^- via the pH drop method (*451*). The data are summarized in Table 5.18. Note that the activity of the enzyme decreases drastically in the presence of 5 μM DNSA. This was expected since DNSA is known to coordinate with the active site resident Zn^{2+}, and by doing so precludes the hydration reaction of CO_2. Contrary to the observation that the catalytic activity of hCA XII remained invariant in the presence of Qds^+, Qds^- totally abolished the enzyme activity upon addition of saturating concentrations of the latter to hCA XII. Also, addition of Qds^- to the hCA XII-DNSA complex did not have any effect on the enzyme activity. Evidently, Qds^- has a different effect on the active site features of hCA XII.

5.5.2.8. Interaction of Qds^- with hCA I and hCA II

The electrostatic surface potential of hCA isozymes I and II revealed the presence of patches of positive charges distributed on their surfaces. Hence, it was of interest to see whether these isozymes interact with Qds^-. In a preliminary manner, the fluorescence emission intensity of hCA I and II were monitored ((λ_{ex} = 295 nm, λ_{em} (hCA I) = 330 nm, λ_{em} (hCA II) = 335 nm) upon addition of small amounts Qds^-. This caused a quenching in the fluorescence signal of both the isozymes. It has been confirmed that such a quenching was not an artifact of the inner filter effect since the absorption of the reaction mixture was less than 0.1. The decrease in emission intensity of hCA I and II upon addition of Qds^- served as a signal for monitoring their binding. However, as mentioned above, prior to determining the binding affinity of hCA I and II for Qds^-, it was realized that the titration of an increasing concentration of the Qds^- to a fixed concentration of the protein was not

feasible as this would lead to inner filter effect as a consequence of high UV absorption of the Qds^- at 295 nm. Hence, the binding affinities were determined by a titration of a fixed concentration of Qds^- with increasing concentrations of enzyme while monitoring the fluorescence emission of the respective proteins. The observed fluorescence was corrected by subtraction of a background titration of hCA I and II into buffer and then plotted as a function of enzyme concentration.

As is evident from the data of Figure 5.92A and B, the fluorescence of hCA I exhibited a hyperbolic behavior in the presence of Qds^-. The solid smooth lines in Figure 5.92 represents the best fit of the data to the quadratic binding model as described by Qin and Srivastava which provided a K_d of 6.7 μM and 5.9 μM for hCA I and II respectively. The binding isotherms of Qds^- with hCA I, II and XII are listed in Table 5.20. Clearly, Qds^- bind with a much higher affinity to hCA XII as compared to hCA I and II.

5.5.3. Interaction of neutral Qds (ZnO/ethanol) with hCA isozymes

5.5.3.1. Absorption and emission spectra of neutral quantum dots (NQds)

Figure 5.93 shows the absorption and emission spectrum of NQds. These nanoparticles show broad absorption spectrum ranging from 260 nm to about 600 nm. When excited at 330 nm, they emitted fluorescence with an emission maxima of 520 nm.

5.5.3.2. Influence of hCA XII on the emission spectra of NQds

Figure 5.94A represents the emission spectra of NQds in the presence of stoichiometric concentrations of hCA XII (λ_{ex} = 280 nm). As is evident from the Figure, the emission spectrum of NQds increases only slightly in the presence of hCA XII.

Table 5.18. Catalytic activity of hCA XII in the presence of different ligands.

Experimental condition[a]	% activity
Free hCA XII	100
hCA XII-DNSA	9
hCA XII-Qds^-	2
hCA XII-DNSA–Qds^-	5

All experiments have been performed under identical conditions, and the enzyme activity is represented as the percent of the control activity in the absence of any added ligand.

[a] [DNSA]=5 μM, [Qds^-]=10 μM.

5.5.3.3. Influence of neutral Qds on the emission spectral properties of hCA XII

To probe whether the intrinsic fluorescence of hCA XII was influenced by NQds, the emission spectra of hCA XII was monitored in the presence and absence of NQds. As the stock solution of NQds showed a very high absorption, it was diluted almost 50 fold in 10 mM Tris buffer, pH 8.0. This reduced the amount of ethanol present in the working solution of NQds. The diluted solution of NQds has been used for all the experiments. As is evident from Figure 5.94B, that the emission intensity of hCA XII decreases upon addition of stoichiometric concentrations of NQds. The quenching of hCA XII fluorescence was confirmed to be not due to the inner filter effect by keeping their absorbance values much below 0.1. As these Qds have not been functionalized with any charged particles, the interaction between them is considered to be non-columbic in nature.

5.5.3.4. Effect of NQds on the spectral features of hCA XII-DNSA complex

Although hCA XII did not influence the emission spectra of NQds, the latter caused quenching of protein tryptophan fluorescence upon its addition to the enzyme. This

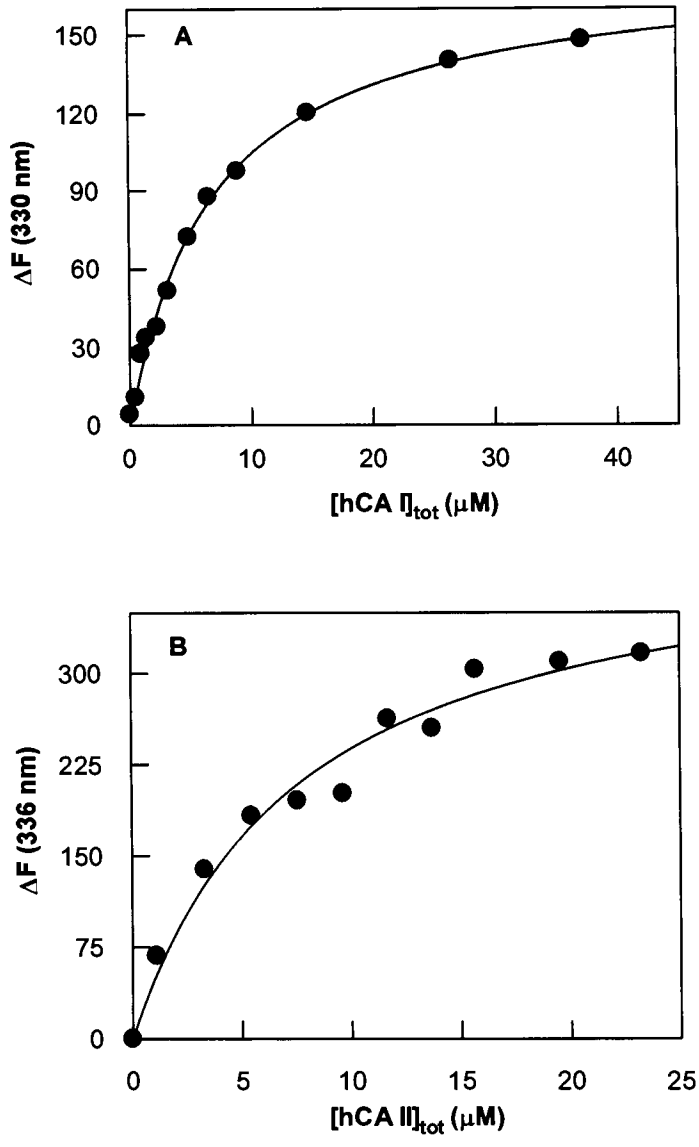

Figure 5.92. Binding isotherm for the interaction of Qds^- with hCA I and hCA II.
The Figure shows the decrease in the fluorescence emission intensity of hCA I (Panel A) and hCA II (Panel B) at 336 nm (λ_{ex}= 280 nm) as a function of Qds^- concentration. A fixed concentration of the Qds^- (0.17 μM) was titrated with increasing concentrations of hCA I and hCA II in 10 mM Tris buffer, pH 8.0. The solid line is the best fit of the data which provided a dissociation constant of 6.7 ± 0.6 μM and 7.6 ± 0.1 μM and stoichiometry of 2 and 4 for A and B respectively.

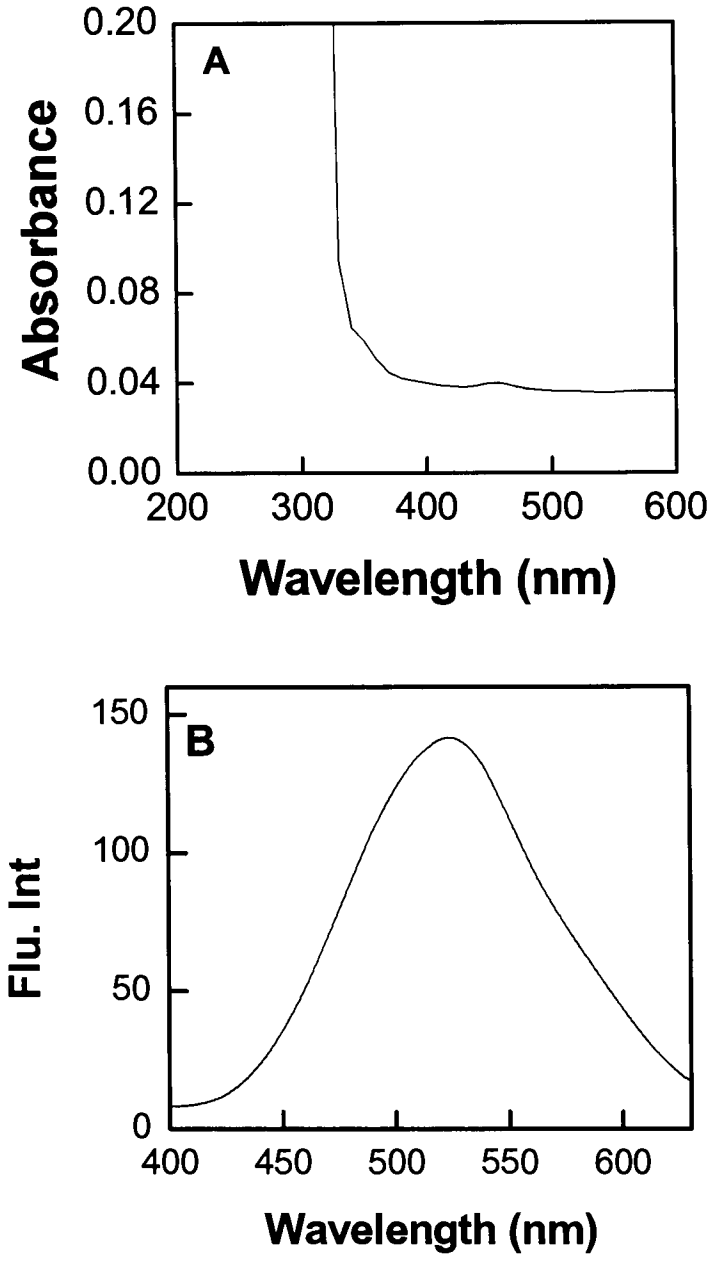

Figure 5.93. Absorption and emission properties of the ZnO/ethanol Qds in 10 mM Tris buffer pH 8.0.

Panel A depicts the absorbance of 0.2 μM of Qds in a 1 cm path length quartz cuvette whereas panel B depicts the steady-state fluorescence emission of 5 μM neutral Qds (excitation at 330 nm) in a 4 mm square quartz cuvette.

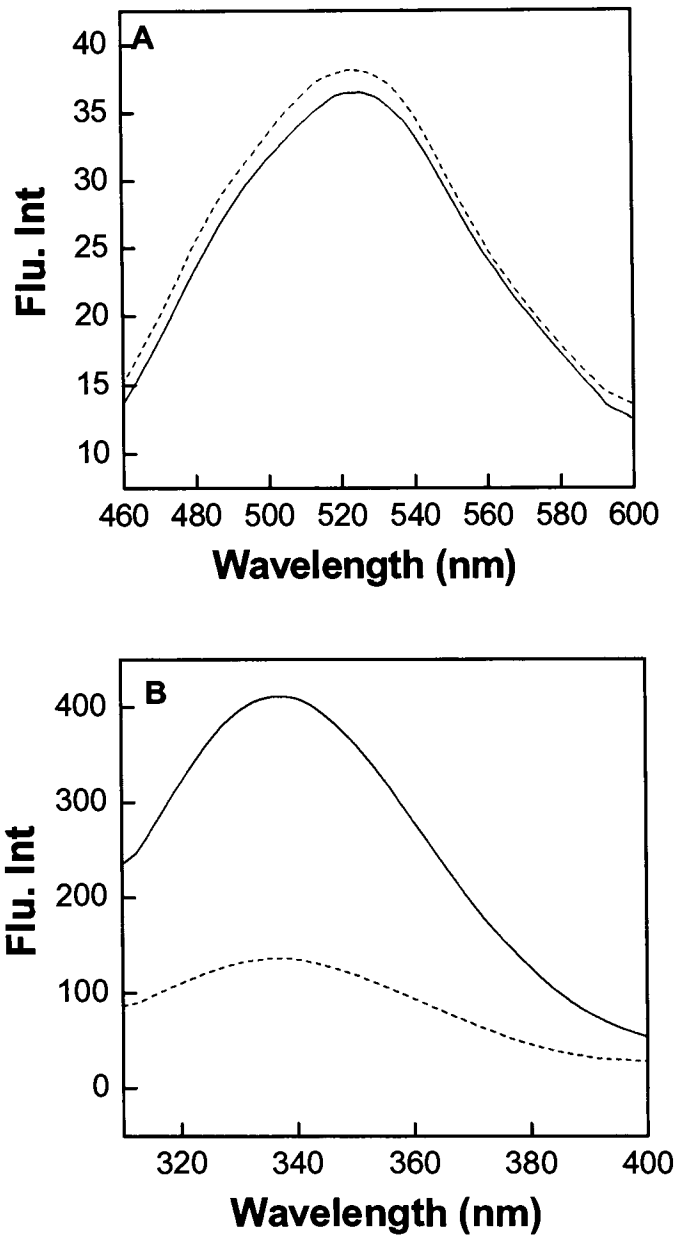

Figure 5.94. Spectral changes associated with hCA XII-NQd interaction.
Panel A of the Figure shows the fluorescence emission spectra of free and hCA XII bound NQds in 10 mM Tris buffer pH 8.0. The fluorescence emission spectra of 0.1 μM NQds (solid line) (λ_{ex} = 295 nm; λ_{em} = 310 nm – 400 nm) was unchanged in the presence of stoichiometric amounts of hCA XII (dashed line).
Panel B of the Figure shows the fluorescence emission spectra of hCA XII and hCA XII-Qds^- in 10 mM Tris buffer pH 8.0. The fluorescence emission spectra of 0.2 μM hCA XII (solid line) (λ_{ex} = 295 nm; λ_{em} = 310 nm – 400 nm) was quenched in the presence of stoichiometric amounts of Qds^- (dashed line).

suggested that in spite of the absence of any charged groups, NQds are able to interact with hCA XII. Hence, it was of interest to determine whether the binding of hCA XII to NQds influences the active site structural and functional features of the enzyme. Toward this goal, the binding of DNSA by hCA XII in the presence of NQds was investigated. A fixed concentration of hCA XII (1 μM) was titrated with increasing concentrations of the NQds in the presence of a saturating concentration of DNSA (5 μM) and the fluorescence of hCA XII-DNSA complex was monitored. The changes in steady-state fluorescence emission intensity as a function of the concentration of Qds are shown in Figure 5.95. As the concentration of Qds were increased, a decrease in the fluorescence intensity of the hCA XII-DNSA emission peak at 457 nm was observed. However, in contrast to the charged nanoparticles, no change in the fluorescence emission intensity of NQds was observed after subtraction of the background signal of free NQds.

The decrease in the 457 nm peak apparent in Figure 5.95 suggested that DNSA was either excluded or slightly displaced from the hCA XII active site pocket in the presence of NQds.

5.5.3.5. Effect of NQds on the catalytic activity of hCA XII and hCA XII-DNSA complex

Since the binding of DNSA to hCA XII results in inhibition of the enzyme, the effect of NQDs on the DNSA-inhibited enzyme activity was explored. The activity of a fixed concentration of hCA XII (0.25 μM) was measured in the absence and presence of NQds and/or DNSA using the pH drop assay (*451*). The data are summarized in Table 5.19. It is evident from the values of the Table, that the activity of hCA XII remained unchanged upon addition of NQds, indicating that the formation of the hCA XII-NQds

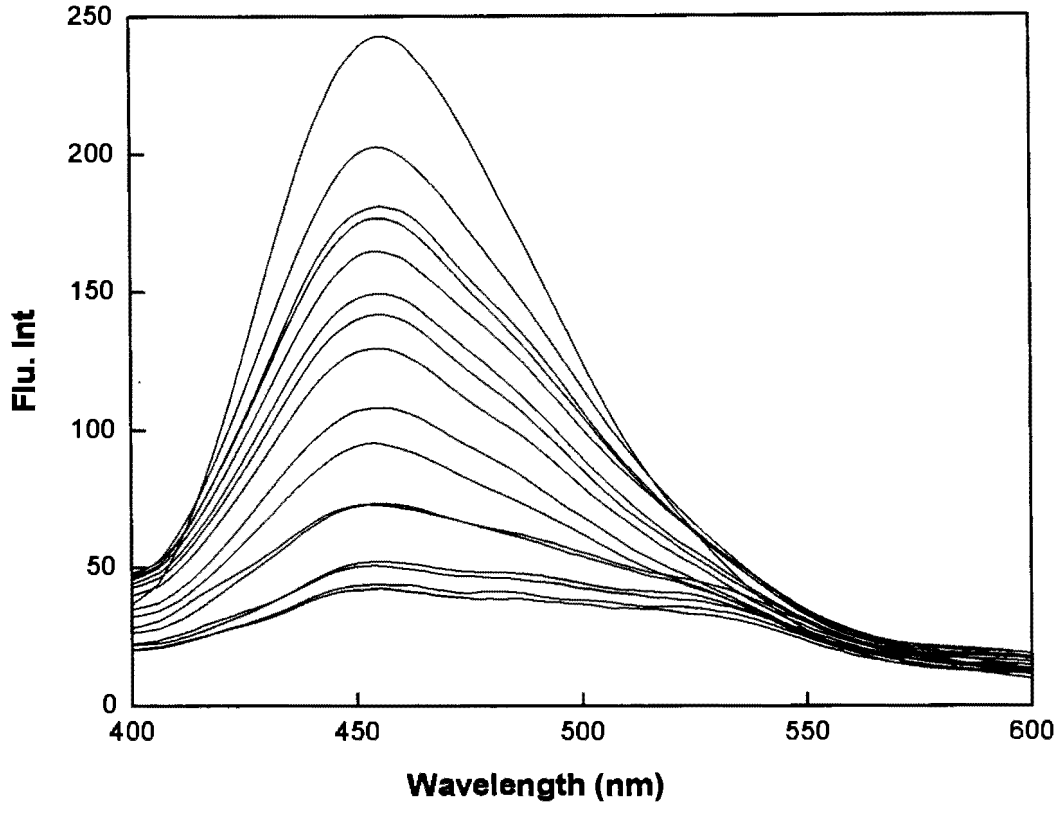

Figure 5.95. Fluorescence spectral changes for the interaction of NQds with hCA XII-DNSA complex.
The Figure shows the spectra of hCA XII-DNSA complex in the presence of increasing concentrations of NQds in 10 mM Tris-HCl buffer, pH 8.0 containing 10 % acetonitrile. [hCA XII] = 0.3 μM, [DNSA] = 2 μM, λ_{ex} = 330 nm. The spectrum is generated by subtracting the emission contributed by the free NQds in buffer from that of the (hCA XII – DNSA)- NQds complex.

complex did not inhibit the activity of the enzyme. In contrast, the treatment of hCA XII with DNSA resulted in a decrease in the activity of hCA XII by about 90% of the activity of the free enzyme. However, addition of NQds to hCA XII-DNSA complex did not have any effect on the observed inhibition of hCA XII by DNSA. This suggests that the binding

of NQds to hCA XII is very weak and does not influence the structural and functional properties to a large extent.

5.5.3.6. Binding isotherms for the interaction of hCA isozymes with NQds

The decrease in emission intensity of hCA isozymes upon interaction with NQds served as a signal for monitoring the binding of hCAs to NQds. However, significant absorption of NQds at 295 nm prevented the titration of an increasing concentration of the latter to a fixed concentration of protein was not possible. Therefore, it was decided that the binding isotherms will be determined by titration of a fixed concentration of NQds with increasing, known concentrations of hCA XII will be performed as in the case for charged Qds. The decrease in the fluorescence intensity of hCA I, II and XII at 330 nm, 332 nm and 336 nm (λ_{ex} = 295 nm) respectively was corrected by subtraction of a background titration of hCA isozymes into the buffer and then plotted as a function of enzyme concentration (Figure 5.95). As is evident from the data of Figure 5.95, the fluorescence of hCA isozymes exhibited a saturating (hyperbolic) behavior in the presence of NQds. For the analysis of the binding isotherm, it should be emphasized that although the concentration of hCAs were known, no direct method was available to determine the concentration of NQds. Hence, it could not be ascertained *a priori* whether it was valid to assume that the total concentration of hCAs were approximately equal to the free concentration of the enzyme throughout the titration. Therefore, a binding equation accounting for both the concentrations of the enzyme and the Qds had to be employed to determine the dissociation constant (K_d). The solid smooth lines in Figure 5.95 represents the best fit of the data to the quadratic binding model as described by Qin and Srivastava

(*506*) (Eq. 4.16), which provided a dissociation constants (K_d) of 9.3 μM, 14.7 μM and 18.4 μM respectively for hCA I, II and VII and a stoichiometry of 1 in all the cases.

Table 5.19. Catalytic activity of hCA XII in the presence of different ligands.

Experimental condition[a]	% activity
Free hCA XII	100
hCA XII-DNSA	9
hCA XII-NQds	98.5
hCA XII-DNSA–NQds	7

All experiments have been performed under identical conditions, and the enzyme activity is represented as the percent of the control activity in the absence of any added ligand.

[a] [DNSA]=5 μM, [NQds]=10 μM.

5.5.4. Interaction of liposomes with hCA XII

The experimental results from the interaction of Qds with hCA isozymes revealed that the charged Qds exhibit strong binding affinities for hCA XII as compared to that of other hCA isozymes. The basis for such interaction lied in the bipolar distribution of positive and negative charges near the active site and the opposite end of hCA XII, respectively. It was shown in section 5.5.1.1. and 5.5.1.7. that inspite of possessing the same charge, polylysine and Qds^+ influenced the spectral and ligand binding features differently. This difference was attributed to the difference in the surface properties of the two molecules vis a vis polylysine and Qds^+ which are considered to be flexible and rigid molecules respectively. Hence it was of interest to explore the electrostatic contributions of hCA XII with liposomes and its effect on the spectral, ligand binding and catalytic

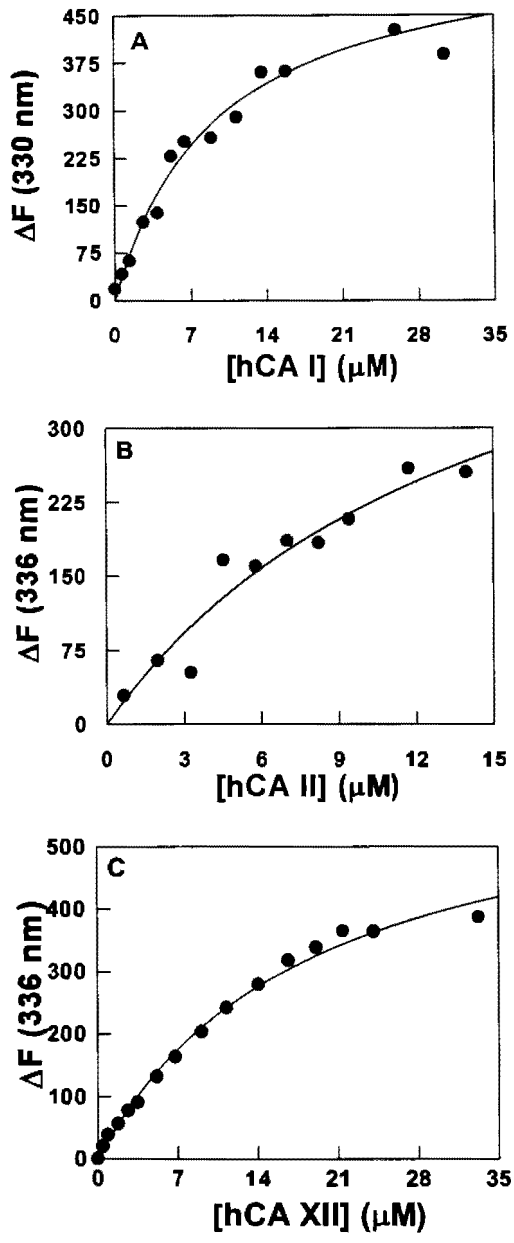

Figure 5.96. Binding isotherm for the interaction of NQds with hCA I and hCA II and hCA XII.

The Figure shows the decrease in the fluorescence emission intensity of hCA I (Panel A), hCA II (Panel B), hCA XII (Panel C) at 336 nm (λ_{ex}= 280 nm) as a function of Qds+ concentration. A fixed concentration of the NQds (0.11 μM) was titrated with increasing concentrations of hCAs (λ_{ex}= 280 nm, λ_{em} = 330 or 336 nm) in 10 mM Tris buffer, pH 8.0. The data represent the magnitude of ΔF obtained by subtracting the fluorescence intensity of the mixture from that given by the protein itself under identical conditions as a function of protein concentration. The solid line is the best fit of the data (*506*) which provided a dissociation constant of 9.3 ± 1.3 μM, 14.7 ± 5.2 μM, 18.4 ± 2 μM for Panels A, B and C respectively.

Table 5.20. Binding affinity (K_d) for Qds to hCA isozymes.

Isozyme	K_d (μM) Cationic	K_d (μM) Anionic	K_d (μM) Neutral
hCA I	13	6.8	9.3
hCA II	6.9	6.7	15
hCA XII	2.1	0.58	18.3

properties of the enzyme. This goal was pursued by preparing liposomes possessing a net positive, negative and neutral charge on their surface. As will be discussed below, the liposomes which are representative of flexible surfaces, exhibit a completely different effect on the ligand binding and catalytic features of the enzyme as compared to those observed with Qds which have rigid surface.

5.5.4.1. Interaction of anionic liposomes with hCA XII

Anionic liposomes (AL) were prepared by mixing either POPS (1-palmitoyl-2-oleoyl-sn-glycero-3-phospho-L-serine) or PIP_2 (1,2-dioleoyl-sn-glycero-3-phosphoinositol-4,5-bisposphate) with zwitterionic POPC (1-palmitoyl- 2-oleoyl-sn-glycero-3-phosphocholine) and dansyl-PE (1,2-dioleoyl-snglycero- 3-phosphoethanolamine-N (5-dimethylamino-1-naphthalenesulfonyl) as the reporter lipid. The concentrations of dansyl PE, POPS and PIP_2 were maintained throughout at 5 %, 25 % and 4 % respectively and the concentration of POPC was adjusted accordingly. It is to be noted that where as POPS possess a net charge of -1, PIP_2 possess a charge of -3 in its head group at neutral pH. The anionic liposomes containing POPS and PIP_2 will be designated as AL-POPS and AL-PIP_2 throughout the thesis.

Since the dansyl head group is highly sensitive to its microenvironment, it was included in the liposome preparation as a reporter group. It is known that DNSA binds to

all hCA isozymes through its sulfonamide nitrogen (*192, 387*), leading to a shift in its emission maxima with concomitant increase in the quantum yield. Since sulfonamide group of the probe is blocked (Figure 4.1) by conjugating it to a lipid tail which would prevent it from binding directly to the hCA active site. Thus, if at all there is any contribution of the probe to the overall binding of liposomes (presumably by interacting with hydrophobic residues of hCA by the dansyl head group) to the enzyme, it is expected to be very weak.

In a preliminary manner, it was found that addition of anionic, cationic and neutral liposomes to hCA XII quenched the fluorescence (λ_{ex} = 295 nm, λ_{em} = 336 nm) of the enzyme while the former did not exhibit any change in its fluorescence (after subtracting the contribution by the free liposomes) when excited either at 295 nm or 330 nm. Hence, the change in the fluorescence intensity of hCA XII upon interaction with liposomes was utilized to determine their binding affinities. Note that the fluorescence quenching of hCA XII by liposomes is a phenomena similar to that exhibited by Qds.

Figure 5. 97 represents the binding isotherm for the interaction of PIP_2 containing liposomes with hCA XII in 25 mM HEPES containing 150 mM NaCl, pH 7.5. It was noticed that, unlike Qds^-, liposomes do not absorb significantly at 295 nm. As increasing concentrations of liposomes would not artifactually lower the tryptophan peak, the binding isotherm was determined by titrating hCA XII with increasing concentrations of liposomes. The observed fluorescence was corrected by subtraction of a background titration of liposome into buffer and then plotted as a function of liposome concentration. The concentration of anionic lipid components of liposomes was taken as half of the total

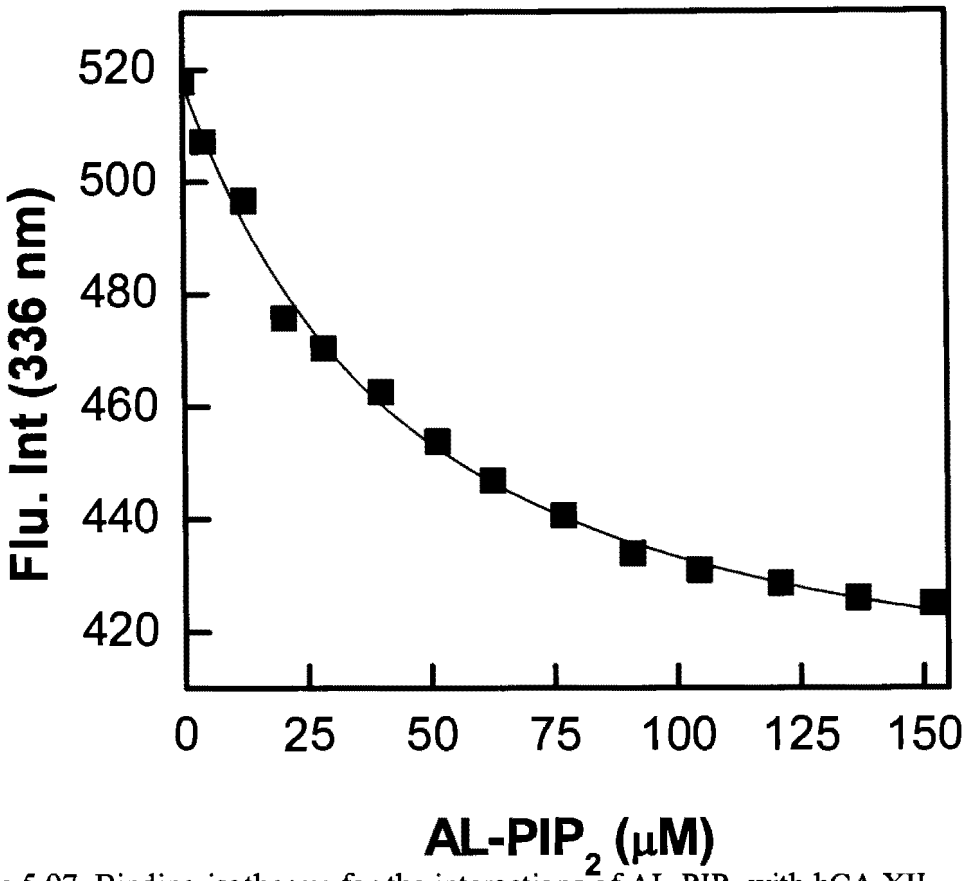

Figure 5.97. Binding isotherms for the interactions of AL-PIP_2 with hCA XII. The decrease in the fluorescence emission intensity of enzyme upon interacting with liposomes at 336 nm (λ_{ex} = 280 nm) for the titration of fixed concentration of hCA XII (1 μM) with increasing concentrations of liposomes are shown. The experiment was conducted in 25 mM HEPES containing 150 mM NaCl pH 7.5. The solid smooth lines are the best fit of the data yielding the K_d values of 0.29 ± 0.4, 3.3 ± 1.6, 13.4 ± 7.6, 35.4 ± 1.01 for panels A, B, C and D respectively.

concentration based on the fact that only the exposed lipids in the outer membrane leaflet would be available for interaction with enzyme.

As is evident from the data of Figure 5.97, the intrinsic fluorescence of hCA XII exhibits a saturating (hyperbolic) behavior as a function of increasing concentrations of liposomes. This observation suggests that a complex formation between hCA XII and liposomes does exist. For the analysis of the binding isotherm, the quadratic equation

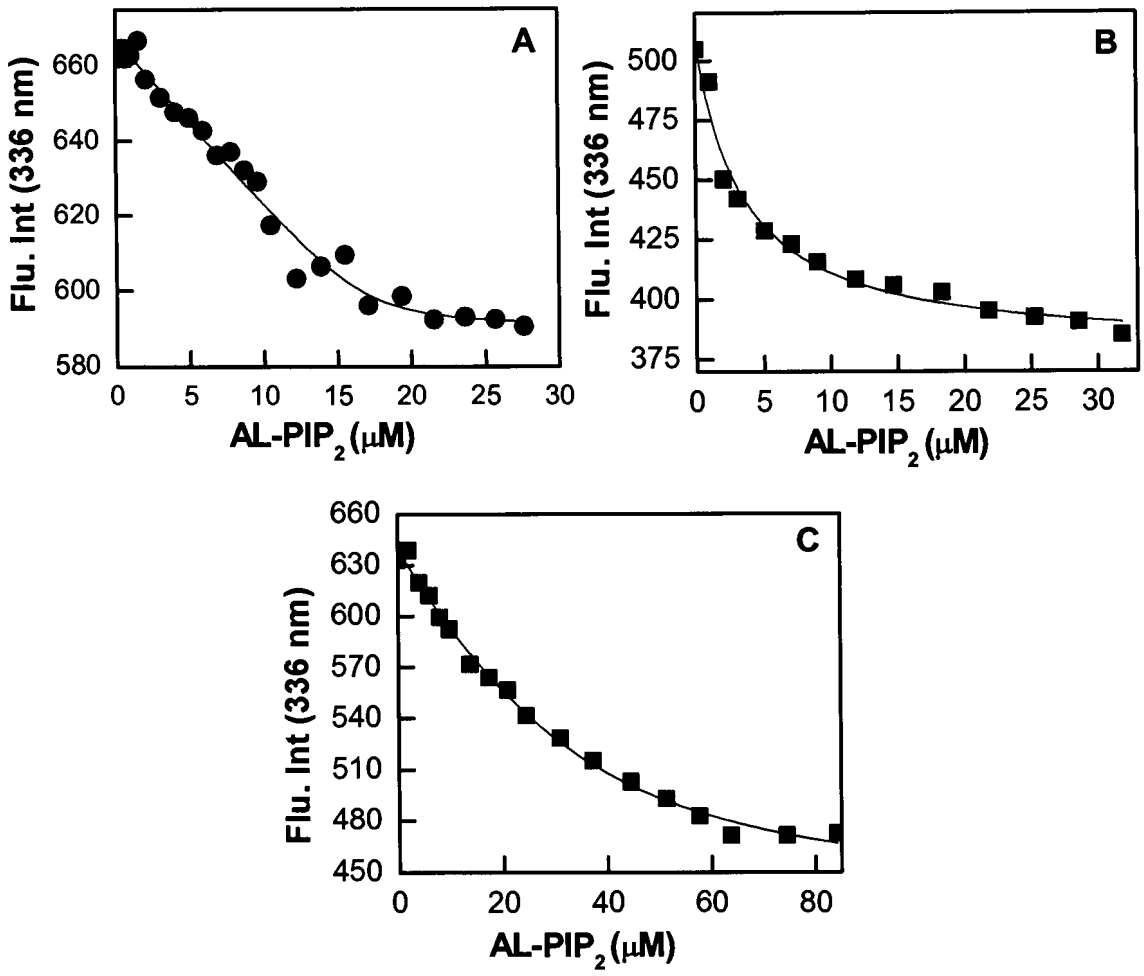

Figure 5.98. Binding isotherms for the interactions of AL-PIP2 with hCA XII at different salt concentrations.
Panel A, B and C represents the binding isotherms for the interactions of anionic liposomes with hCA XII at 25 mM HEPES pH 7.0 containing 25, 50 and 100mM NaCl respectively. The decrease in the fluorescence emission intensity of enzyme upon interacting with liposomes at 336 nm (λ_{ex} = 280 nm) for the titration of fixed concentration of hCA XII (1 μM) with increasing concentrations of liposomes are shown. The solid smooth lines are the best fit of the data yielding the K_d values of 0.29 ± 0.4, 3.3 ± 1.6 and 13.4 ± 7.6 for panels A, B and C respectively.

which takes into account the bound versus free form of the titrant such as described by Qin and Srivastava (*506*) was used. The solid smooth line in Figure 5.97 represents the best fit of the data to the quadratic binding model which provided a dissociation constant (K_d) for

and stoichiometry of the hCA XII–AL- PIP2 complex as being equal to 35.4 μM and 8 molecules of liposomes/hCA XII molecule.

Note that the binding constant derived from the above experiment is very weak (35 μM) compared to that obtained for Qds^- (Figures 5.86 and 5.88). However, it should be realized that the experimental set up for determination of binding isotherms for hCA XII with liposome and Qds are different. Whereas 25 mM HEPES containing 150 mM NaCl was used in the case of liposome, only 10 mM Tris was used in the case of Qds. As the liposomes were prepared in 150 mM NaCl, the above experimental set up required the use of the same concentration of NaCl in the buffer system so as to maintain the osmolarity. However, at this concentration, Na^+ and Cl^- ions present in the buffer system would interact with the negative and positive residues of protein respectively there by neutralizing the charge of hCA XII. As the interaction of hCA XII to AL- PIP2 is considered to be driven by electrostatic forces, use of 150 mM NaCl would have a direct impact on the hCA XII-liposome interaction. Hence, to probe the above feature, experiments were performed at different salt concentrations. However, prior to conducting the binding experiment, it was realized that the liposomes (that were prepared in 150 mM NaCl) would not be stable in a buffer containing lower concentration of salt. This is because, for a liposome molecule to be intact and stable, the osmolarity between its inner and outer mileu should be maintained equal. This was achieved by adjusting osmolarity of the exterior buffer solution by NaCl and sucrose. In this endeavor, different concentrations of NaCl and sucrose ranging from 0-150 mM were prepared in 25 mM HEPES solution and their osmolarities were measured via osmometer. The osmolarities obtained were then plotted as a function of NaCl and sucrose concentrations and were analyzed by the linear regression analysis.

Once the osmolarities for NaCl and sucrose solutions at different concentrations were known, the osmolarity of the liposome was adjusted accordingly with the sucrose solution.

Figure 5.98 represents the binding isotherms for the interaction of hCA XII- AL-PIP_2 as a function of NaCl concentration. Except for the change in NaCl concentration, the experimental setup and data analysis are exactly the same as that mentioned above. All the titration profiles exhibited a hyperbolic dependence with the K_d values of 0.29 μM, 3.3 μM, 13.4 μM at 25, 50 and 100 mM NaCl respectively. These data led to the suggestion that the binding of hCA XII and AL- PIP_2 is mediated via electrostatic interaction.

To probe if the above feature is a general phenomena for all negatively charged liposomes, liposomes containing an anionic lipid POPS (AL- POPS) were prepared. Figure 5.99 represents the binding isotherm of hCA XII- AL- POPS complex at various NaCl concentrations. The K_d for this complex was determined as explained above and was found to be 2.84 μM, 9.98 μM, 63.7 μM and 80.4 μM at 25, 50, 100 and 150 mM NaCl respectively. Note the increase in the binding affinity for hCA XII- AL- POPS as the concentration of NaCl is is decreased. A casual perusal of the K_d values between AL-POPS and AL- PIP2 suggest that both the liposomes exhibit a tighter binding affinity at lower salt concentration. However, the binding is much stronger in the case of AL- PIP2.

5.5.4.2. Interaction of cationic liposomes with hCA XII

Cationic liposomes (CL) were prepared by mixing EPOPC (1-palmitoyl-2-oleoyl-sn-glycero-3-ethylphosphocholine) with zwitterionic POPC (1-palmitoyl- 2-oleoyl-sn-glycero-3-phosphocholine) and dansyl-PE (1, 2-dioleoyl-snglycero- 3-phosphoethanolamine-N (5-dimethylamino-1-naphthalenesulfonyl) as the reporter lipid. The binding affinities of hCA XII to CL was quantified by monitoring the decrease in the

fluorescence signals of the enzyme's tryptophan/tyrosine residues. Figure 5.100 shows the binding isotherms at different salt concentrations and was found to be 1.47 μM, 2.93 μM, 5 μM, 6.7 μM at 30, 60, 105 and 150 mM NaCl respectively.

5.5.4.3. Interaction of neutral liposomes with hCA XII

Neutral liposomes are composed of a mixture of POPC (95 %) and dansyl PE (5%). Since the charged lipids present in the liposome preparations of AL and CL are considered to be the major driving force for their interaction with hCA XII, it was of interest to see how the binding is influenced if the charged lipids are excluded from the liposome prepartation. Similar to the charged liposomes, NL also quench the intrinsic fluorescence of hCA XII. This shows their ability to interact with each other irrespective of the presence of any net charge in the liposome although the possible binding site for NL with hCA XII is not known. The binding affinity for NL with hCA XII was determined as mentioned above (Figure 5.101) and was found to be 58μM.

5.5.4.4. Influence of liposomes on the functional features of hCA XII

As mentioned above, based on the bipolar distribution of charges on hCA XII structure, possible binding sites for AL and CL were assigned. Accordingly, AL and CL are considered to have the ability to electrostatically interact with the active site and surface of the enzyme opposite to the active site, respectively. It is clear from the Qds data (sections 5.5.1.-5.5.3.) that they electrostatically interact with the enzyme, and depending on the site of interaction, they differentially influence the catalytic activity and ligand binding features of the enzyme. As the Qds are representatives of the rigid surfaces, it was of interest to investigate whether the features exhibited by them are applicable to all molecules possessing similar charges or is dependent on the nature (rigid or flexible) of

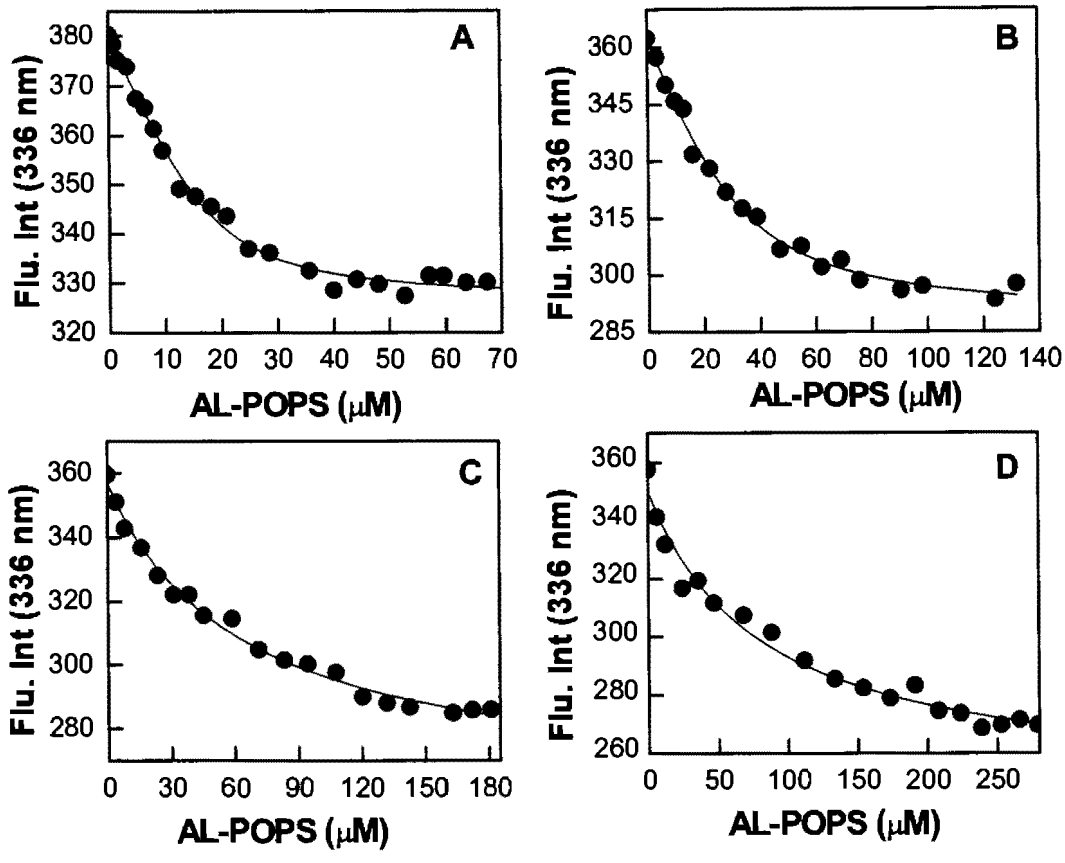

Figure 5.99. Binding isotherms for the interactions of AL-POPS with hCA XII at different salt concentrations.

Panel A, B, C and D represents the binding isotherms for the interactions of anionic liposomes with hCA XII at 25 mM HEPES pH 7.0 containing 25, 50, 100 and 150 mM NaCl respectively. The decrease in the fluorescence emission intensity of enzyme upon interacting with liposomes at 336 nm (λ_{ex} = 280 nm) for the titration of fixed concentration of hCA XII (1 μM) with increasing concentrations of liposomes are shown. The solid smooth lines are the best fit of the data yielding the K_d values of 2.84 ± 1.15, 9.98 ± 3.8, 63.7 ± 3.3, 80.4 ± 3.01 for panels A, B, C and D respectively.

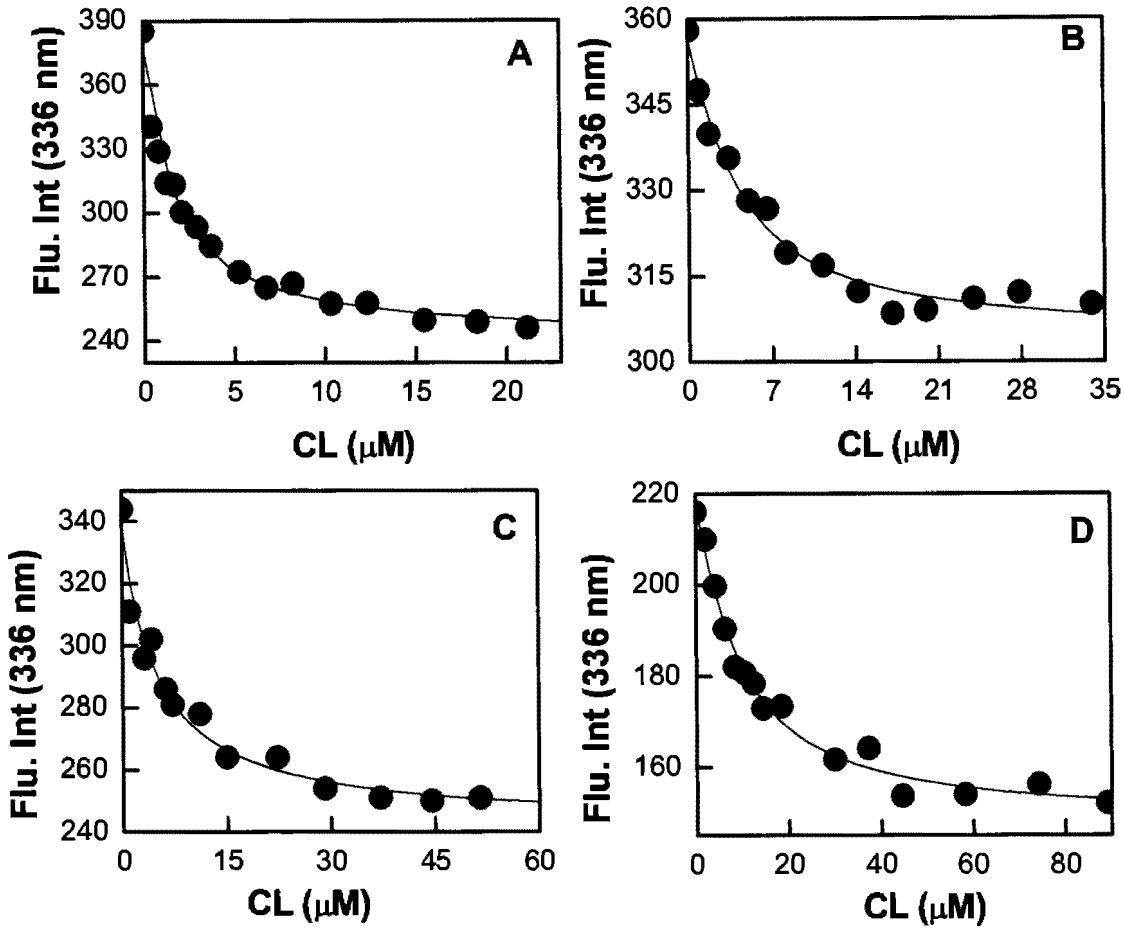

Figure 5.100. Binding isotherms for the interactions of CL with hCA XII at different salt concentrations.

Panel A, B, C and D represents the binding isotherms for the interactions of cationic liposomes with hCA XII at 25 mM HEPES pH 7.0 containing 30, 60, 105 and 150 mM NaCl respectively. The decrease in the fluorescence emission intensity of enzyme upon interacting with liposomes at 336 nm (λ_{ex} = 280 nm) for the titration of fixed concentration of hCA XII (1 μM) with increasing concentrations of liposomes are shown. The solid smooth lines are the best fit of the data yielding the K_d values of 1.47 ± 0.47, 2.93 ± 1.7, 5 ± 3.3, 6.7 ± 3.01 for panels A, B, C and D respectively.

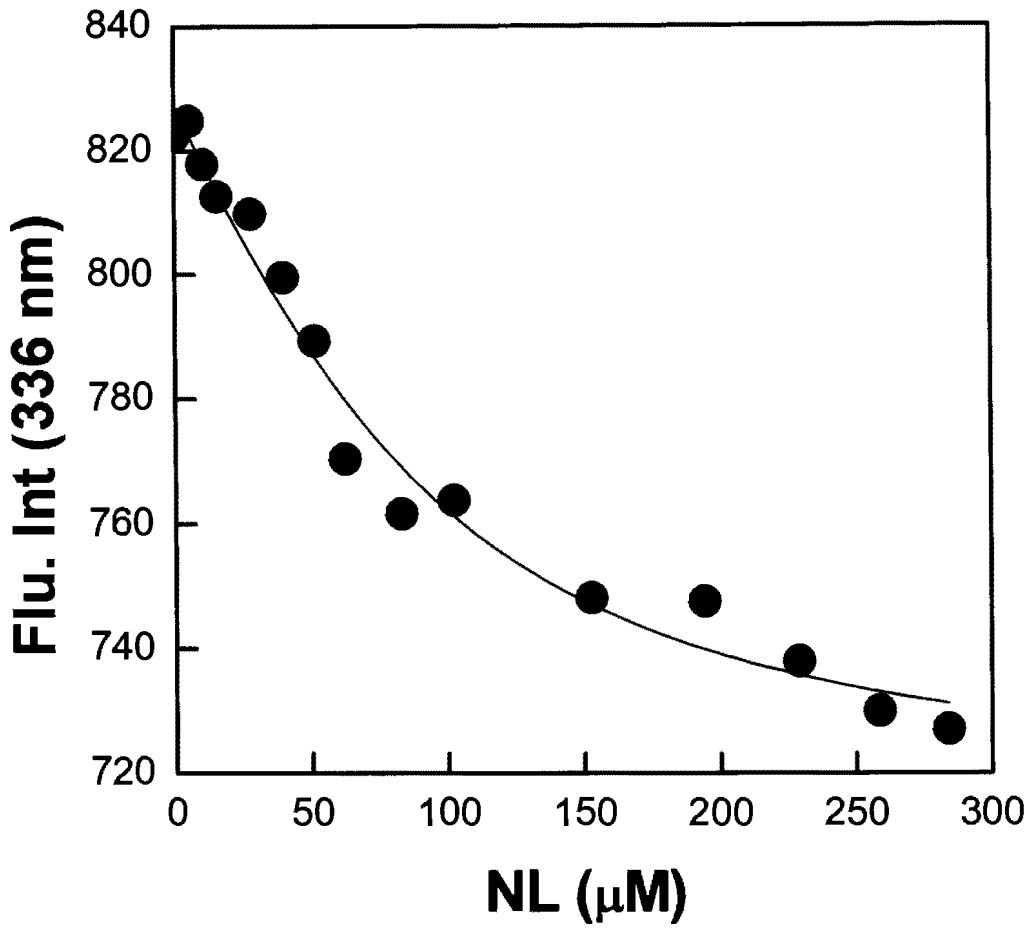

Figure 5.101. Binding isotherm for the interactions of NL with hCA XII in 25 mM HEPES pH 7.5.
The decrease in the fluorescence emission intensity of enzyme upon interacting with liposomes at 336 nm (λ_{ex} = 280 nm) for the titration of fixed concentration of hCA XII (1 μM) with increasing concentrations of liposomes are shown. The solid smooth line is the best fit of the data yielding the K_d value of 39.8 μM.

surface of the molecules carrying the charge. Towards this goal, the effects of differently charged liposomal surfaces on the catalytic and ligand binding properties of hCA XII were performed.

It was thought that measuring the binding affinity of hCA XII-DNSA in the presence of liposomes would be an ideal way to determine if the later had any influence on

the above features. Comparison of K_d values of hCA XII-DNSA in the presence and absence of liposomes would indicate whether the active site of hCA XII was influenced by the liposomes. However, it was realized that the experimental conditions used for the K_d determination of DNSA with hCA XII (Figure 5.21D; K_d = 0.06 μM) is different from that used for experiments involving liposomes. The later requires the use of NaCl and sucrose to maintain the osmolarity of liposomes in the buffer system. Therefore, the binding isotherm for hCA XII-DNSA was required to be determined before any comparison could be made between their K_d values. Figure 5.102 represents the binding isotherm for hCA XII-DNSA in the presence of 25 mM HEPES, 25 mM NaCl and 173 mM sucrose containing 10 % acetonitrile pH 7.5. Other experimental conditions were maintained to be the same as in Figure 5.21D. The solid smooth line represents the best fit of the data with a K_d value of 0.11 μM. Clearly their binding remains similar in both cases.

The binding isotherm for hCA XII-DNSA in the presence of CL was determined by titrating a fixed concentration of hCA XII containing saturating concentrations of CL with increasing concentrations of DNSA and the increase in the fluorescence intensity (after subtracting the contribution of free DNSA by titrating it with buffer) at 448 nm was plotted as a function aof DNSA concentration. The solid smooth line of Figure 5.103 represents the best fit of the data with a K_d value of 0.1 μM. This K_d is similar to that obtained in the absence of CL (K_d = 0.06 μM). Note that this feature is in contrast to that obtained for Qds^+ where the fluorescence intensity of enzyme bound DNSA decreases with increasing concentrations of Qds^+.

In addition to ligand binding, the catalytic activity of hCA XII was also measured in the presence of liposomes by the pH drop method. The experimental method is the same

as described in the previous section except that the buffers used for blank and test experiments contained 150 mM NaCl in addition to the Tris buffer. It was found that in the presence of CL, almost 96 % of the enzyme activity is retained suggesting that CL does not influence the ligand binding nor it influences the catalytic activity of the enzyme.

To quantitate if the binding of hCA XII to CL is influenced by the presence of DNSA, the binding affinity of the above complex (K_d = 1.47 μM) was measured in the presence of saturating concentrations of DNSA. This was performed by titrating increasing concentrations of CL to a fixed concentration of hCA XII containing a saturating concentration of DNSA, and the decrease in fluorescence intensity was measured as a function of CL concentration. The binding constant (K_d = 1.76 μM) determined from Figure 5.104 suggest that the presence of DNSA does not affect the interaction of CL to the enzyme. This also suggests that their binding sites are different.

As the active site and the region surrounding it are positively charged, AL were expected to interact at this region and such interaction was thought to have significant effects on the ligand binding and catalytic features of the enzyme. Contrary to our expectation, as shown in Figure 5.105, the binding affinity for hCA XII –DNSA interaction in the presence of saturating concentrations of AL was found to be 0.036 μM. This value is almost similar to that obtained in the absence of AL (K_d = 0.1 μM). Measurement of catalytic activity of hCA XII in the presence of AL- PIP2 suggested that they do not have any effect on the catalytic features of the enzyme . In addition, data on Figure 5.106, shows that the binding affinity of hCA XII-AL remains unaffected in the presence of an excess concentration of DNSA. These results are completely different from that obtained for hCA XII- Qds- interaction. As will be discussed in the next chapter the

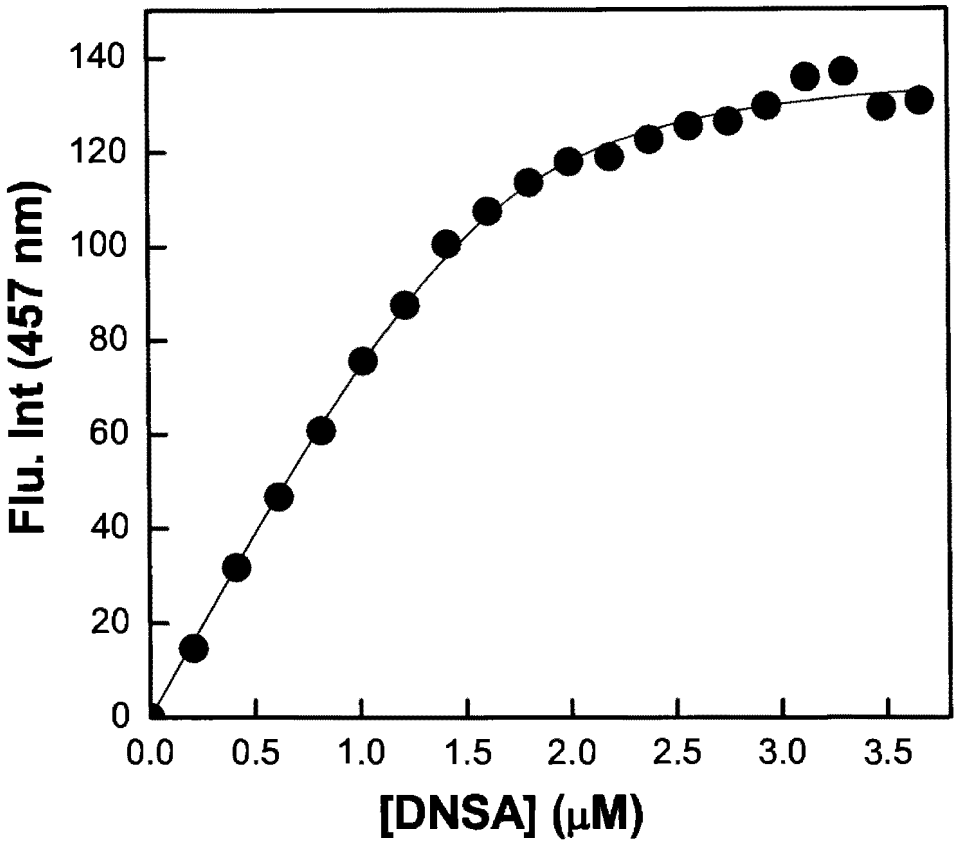

Figure 5.102. Binding isotherms for the interaction of DNSA with hCA XII.
The Figure represents the binding isotherm for the interactions of DNSA with hCA XII in 25 mM HEPES containing 25 mM NaCl and 173 mM sucrose containing 10 % acetonitrile at pH 7.5. [hCA XII] = 1.25 μM. The increase in the fluorescence emission intensity of enzyme bound dansylamide at 448 nm (λ_{ex} = 330 nm) for the titration of fixed concentration of hCA XII with increasing concentrations of dansylamide is shown. The solid smooth line is the best fit of the data yielding the K_d value of 0.1 ± 0.03 μM.

above differential feature is encoded in the "rigidity" versus "flexibility" of these

macromolecules.

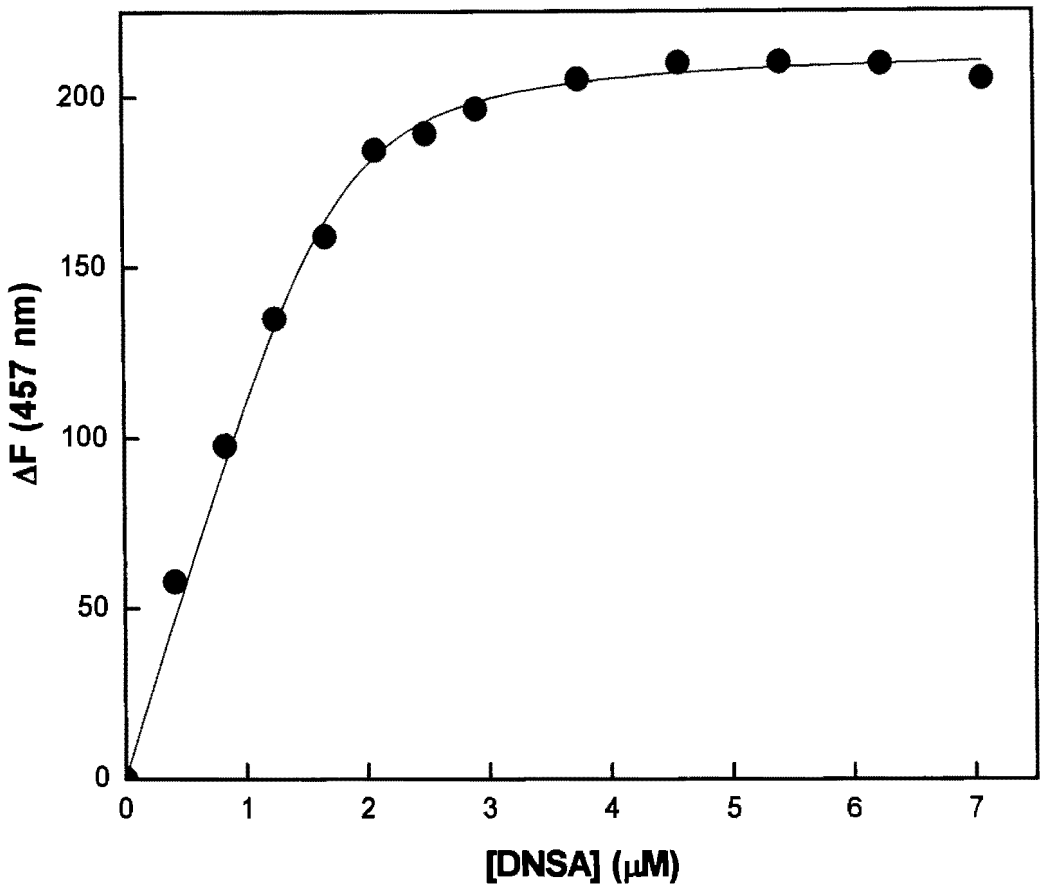

Figure 5.103. Effect of CL on the binding affinity of DNSA with hCA XII.
A fixed concentration of hCA XII (1.75 μM) with saturating concentrations of cationic liposome (25 μM) was titrated with increasing concentrations of DNSA, and the increase in the fluorescence emission intensity of hCA XII-DNSA complex at 457 nm (λ_{ex} = 330 nm) was monitored in 25 mM HEPES containing 25 mM NaCl + 10 % DMSO, pH 7.5. The solid smooth line is the best fit of the data for the K_d value of 0.10 ± 0.02 μM.

5.6. Thermal and Chemical stability of hCA isozymes

Protein refolding and unfolding are hallmark to understanding the transition from nascently synthesized protein chain to their three dimensional structures. Various techniques have been employed to study the above processess such as fluorescence, circular dichroism, NMR etc (*427, 438-441*). Although some studies have been conducted

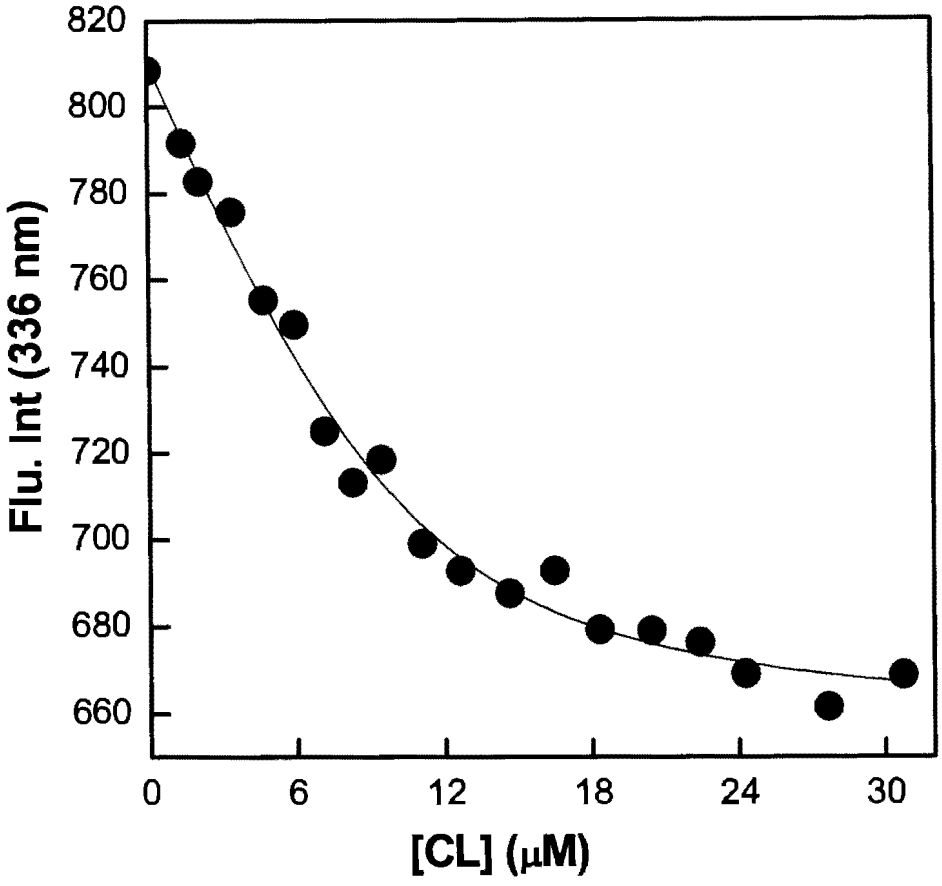

Figure 5.104. Effect of DNSA on the binding affinity of cationic liposomes with hCA XII. A fixed concentration of hCA XII (2 μM) with saturating concentrations of DNSA (10 μM) was titrated with increasing concentrations of cationic liposome, and the deccrease in the fluorescence emission intensity of hCA XII-liposome complex at 336 nm (λ_{ex} = 280 nm) was monitored in 25 mM HEPES containing 25 mM NaCl + 10 % DMSO, pH 7.5. The solid smooth line is the best fit of the data for the K_d value of 1.76 ± 1 μM.

on unfolding and refolding of hCA II (*423*, *424*, *426*, *428*, *429*, *431*, *432*, *434*, *435*), there has been no studies on tumorigenic hCA XII.

With the aim of understanding the the effects of temperature and denaturing agents (Urea and GdmCl) on the secondary and tertiary structural features of hCA XII, CD and

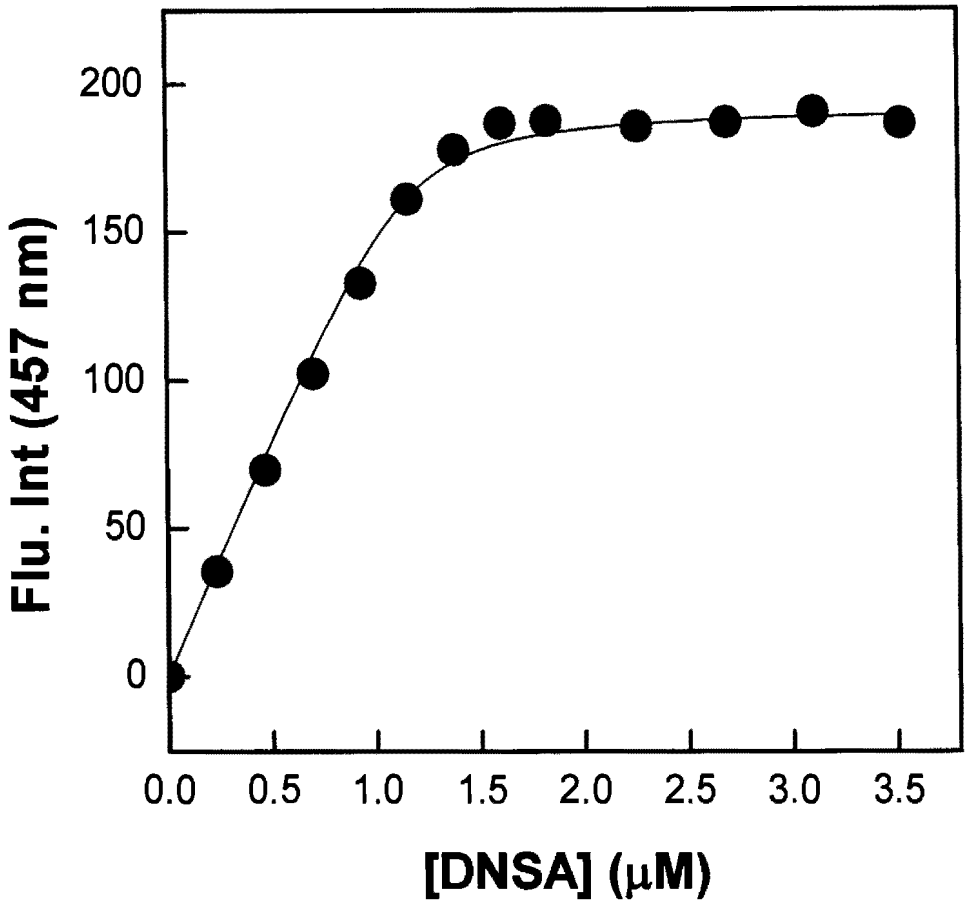

Figure 5.105. Effect of anionic liposomes on the binding affinity of DNSA with hCA XII. A fixed concentration of hCA XII (1.15 μM) with saturating concentrations of anionic liposome (25 μM) was titrated with increasing concentrations of DNSA, and the increase in the fluorescence emission intensity of hCA XII-DNSA complex at 457 nm (λ_{ex} = 330 nm) was monitored in 25 mM HEPES containing 25 mM NaCl + 10 % DMSO, pH 7.5. The solid smooth line is the best fit of the data for the K_d value of 0.036 ± 0.01 μM.

fluorescence spectroscopy methods were used. The results obtained from hCA XII were compared with that of the thoroughly studied hCA isozyme hCA II. Towards this objective, secondary structural features of the isozymes were examined by CD spectroscpy upon thermal and chemical denaturation, and tertiary structural features were examined by ligand binding studies with DNSA and by enzyme activity measurements.

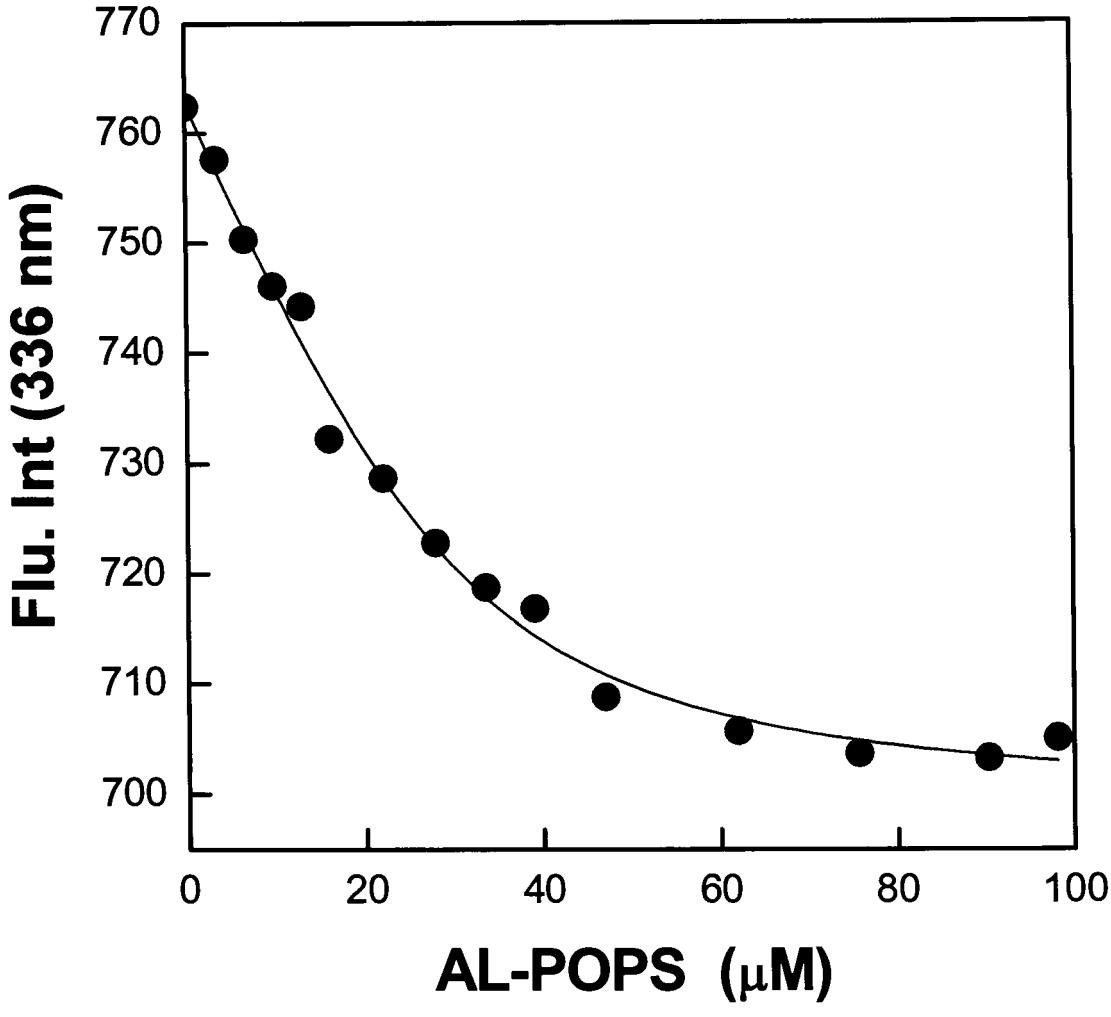

Figure 5.106. Effect of DNSA on the binding affinity of anionic liposomes with hCA XII. A fixed concentration of hCA XII (2 μM) with saturating concentrations of DNSA (10 μM) was titrated with increasing concentrations of anionic liposome, and the deccrease in the fluorescence emission intensity of hCA XII-liposome complex at 336 nm (λ_{ex} = 280 nm) was monitored in 25 mM HEPES containing 25 mM NaCl + 10 % DMSO, pH 7.5. The solid smooth line is the best fit of the data for the K_d value of 5.5 ± 2.89 μM.

5.6.1.Thermal stability of hCA XII and hCA II

Panel A of Figure 5.107 represents the far UV CD spectra of the native and thermally denatured hCA XII (6 μM). The CD spectrum of native hCA XII shows the typical elliptical spectra characteristic of a protein containing mixture of α-helices and β-sheets. The spectrum of the thermally denatured protein was measured after heating the native enzyme sample from 25°C to 80°C at a scan rate of 30°C / hour followed by cooling to the room tempertature. Comparison of this spectra with the native spectra clearly indicates that majority of the secondary structural features remain intact even after thermal denaturation at 80°C. Contrary to this, significant loss of secondary structure was observed incase of hCA II (6 μM) under the similar denaturation condition (Figure 5.107B).

In the light of the fact that the CD spectral profiles exhibited by the two isozymes for their native and denatured states were different, it was of interest to find their mid points of transition (T_m) from native to the denatured state, and also how the later changes occur as a function of the rate of heating. As is evident from the native CD spectra of hCA isozymes of Figure 5.107, they show a major minimum in ellipticity (θ) at 222 nm which is contributed by the α-helices. As denaturation of the protein would lead to a change in the signal at the above wavelength due to conversion of α-helices to randon coils, this signal was utilized to measure the secondary structural changes upon denaturation.

Figure 5.108 represents the change in θ_{222} for hCA isozymes upon heating. It is clearly evident from the Figure that the unfolding pathway of both the isozymes exhibits a sigmoidal dependence with a single cooperative transition from native to the denatured state. Panel A of the Figure shows thermal unfolding of hCA XII (6 μM) at a scan rate of 30 and 90 /hour. It is evident from the Figure that their mid point of transition at 53°C remains invariant with respect to the changes in the scan rates. Contrary to this, the T_m of

hCA II increases from 53°C to 60 °C as the scan rate is increased from 30°C to 90°C respectively. Note the presence of significant secondary structure at 80°C in the case of

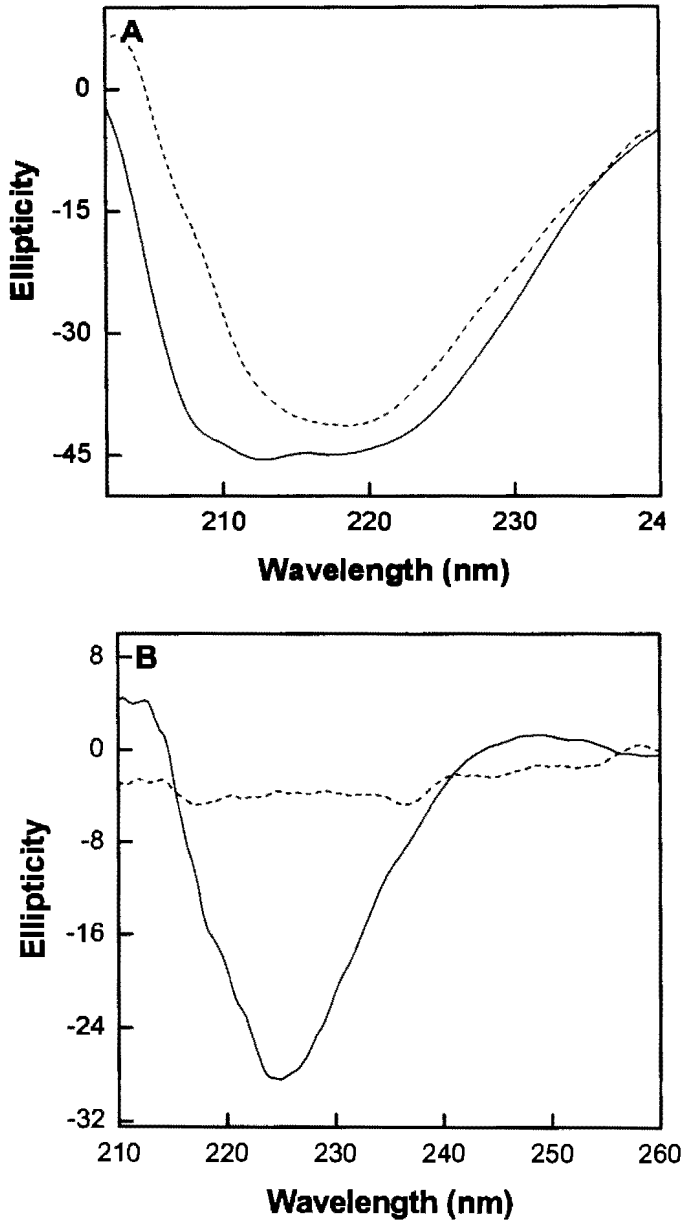

Figure 5.107. CD spectral features of native and thermally denatured hCA XII and hCA II. Panel A shows the CD scan of hCA XII in 5 mM HEPES at room temperature (solid) and thermally denatured hCA XII (dashed lines). Panel B shows the CD scan of hCA II in 5 mM HEPES at room temperature (solid) and thermally denatured hCA II (dashed lines).

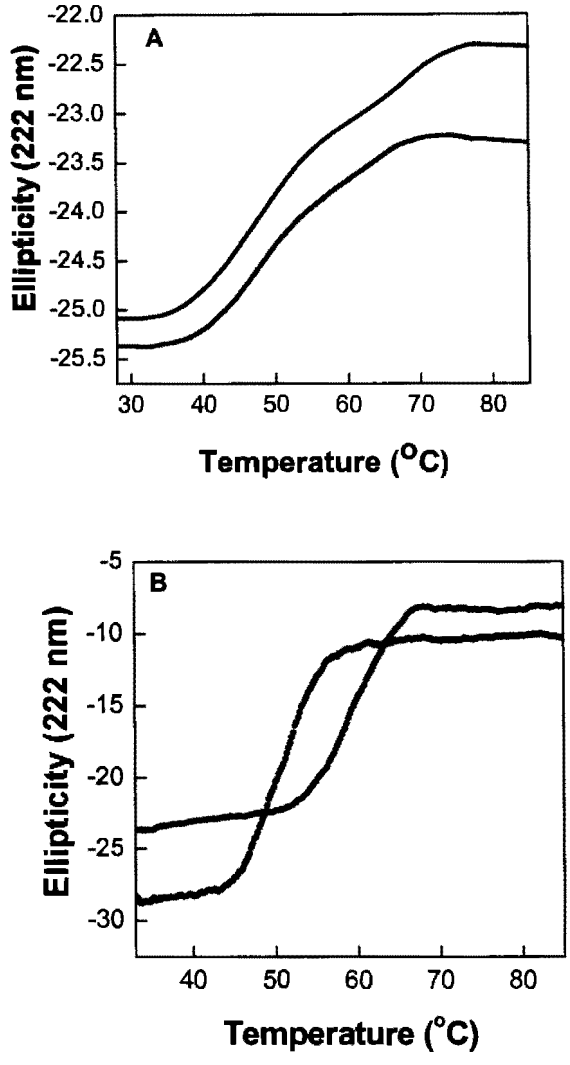

Figure 5.108. Thermal unfolding of hCA XII and hCA II at different scan rates. Panel A shows the thermal unfolding of hCA XII at 30 ° C/h (black) and 90 °C/h (blue) with a Tm of both scan rates at 53 °C. Panel B shows the thermal unfolding of hCA II at 30 ° C/h (black) and 90 °C/h (blue) with a Tm of 53°C and 60 °C respectively for black and blue respectively.

hCA XII, but a significant fraction of secondary structure is lost incase of hCA II between 58°C and 65°C.

As most of the secondary structure of hCA XII is retained, after thermal denaturation, it was of interst to find if the protein exhibits similar binding and catalytic

features as compared to the native enzyme. To this end, the CO_2 hydration activity and the DNSA binding ability of thermally denatured enzyme was examined as described in sections 4.1.7. and 4.1.12. The experimental results indicated that the thermally denatured protein could neither catalyze the CO_2 hydration reaction nor bind DNSA despite retaining significant secondary structure. This indicated that the tertiary structure of the enzyme was completely lost upon thermal denaturation.

5.6.2. Chemical unfolding of hCAs

Unfolding of hCAs was monitored using GdmCl or/Urea to discern the mechanism of their unfolding. The secondary structural perturbations for hCA XII and hCA II were examined by monitoring their far UV CD spectra as a function of the denaturant concentration. The samples of hCA were incubated with increasing concentrations of denaturants for 16 hours so that equilibrium is established. After 16 hours the ellipticity of the samples was monitored at 222 nm (θ_{222}) and plotted as a function of the denaturant concentration.

It is evident from the data of panel A of Figure 5.109, that the θ_{222} values decreased with increase in the denaturant concentration indicating perturbation of the secondary structure. Significant changes in the secondary structure were not observed till 2 M urea. Most of the changes occured after this point. Fully unfolded conformation of hCA XII was attained at 9 M concentration of urea. Panel B of Figure shows the changes in the θ_{222} with increase in GdmCl concentration. It was found that the significant secondary structure changes started to occur at 1M denaturant concentration. Both these data exhibited a sigmoidal profile and were well fitted by a two state model (see discussion). The solid smooth lines of the data represents the best fit of the data according to the equilibrium

folding-unfolding transition model of Santoro and Bolen (*513*) with the free energy of unfolding being ($\Delta G°_{n-u}$) -1.74 kcal mol^{-1} and -1.4 kcal mol^{-1} in the presence of urea and GdmCl respectively. The midpoint of transition was observed at approximately 4.5 and 2 M for Urea and GdmCl induced unfolding respectively. Note that unlike the temperature induced unfolding, there is a significant loss in the secondary structure upon chemical denaturation.

Figure 5.110 represents the far UV CD data for the equilibrium unfolding of hCA II at 222 nm in the presence of GdmCl. Similar to hCA XII, it was found that the secondary structure is progressively lost upon increase in the denaturant concentration, but unlike hCA XII it does not give rise to a smooth sigmoidal profile. A decrease in the CD signal at θ_{222} was observed till the denaturant concentration of 1.5M after which no change in the secondary structural signal was observed until 2M. When the GdmCl concentration was increased beyond 2M, further change in signal was observed. The data exhibited a profile that could be fit only by a three state transition model (*545*) (see discussion) indicating the presence of an intermediate in the unfolding pathway. The intermediate accumulates between a GdmCl concentration of 1.5 M and 2 M. This result is in accordance with others who observed the formation of a molten globule intermediate in the unfolding pathway of hCA II.

As DNSA binds to all hCAs leading to a change in its emission maximum and increase in the quantum yield, this served as an excellent probe to monitor tertiary structural changes upon denaturation of the enzyme by urea and GdmCl. Since DNSA

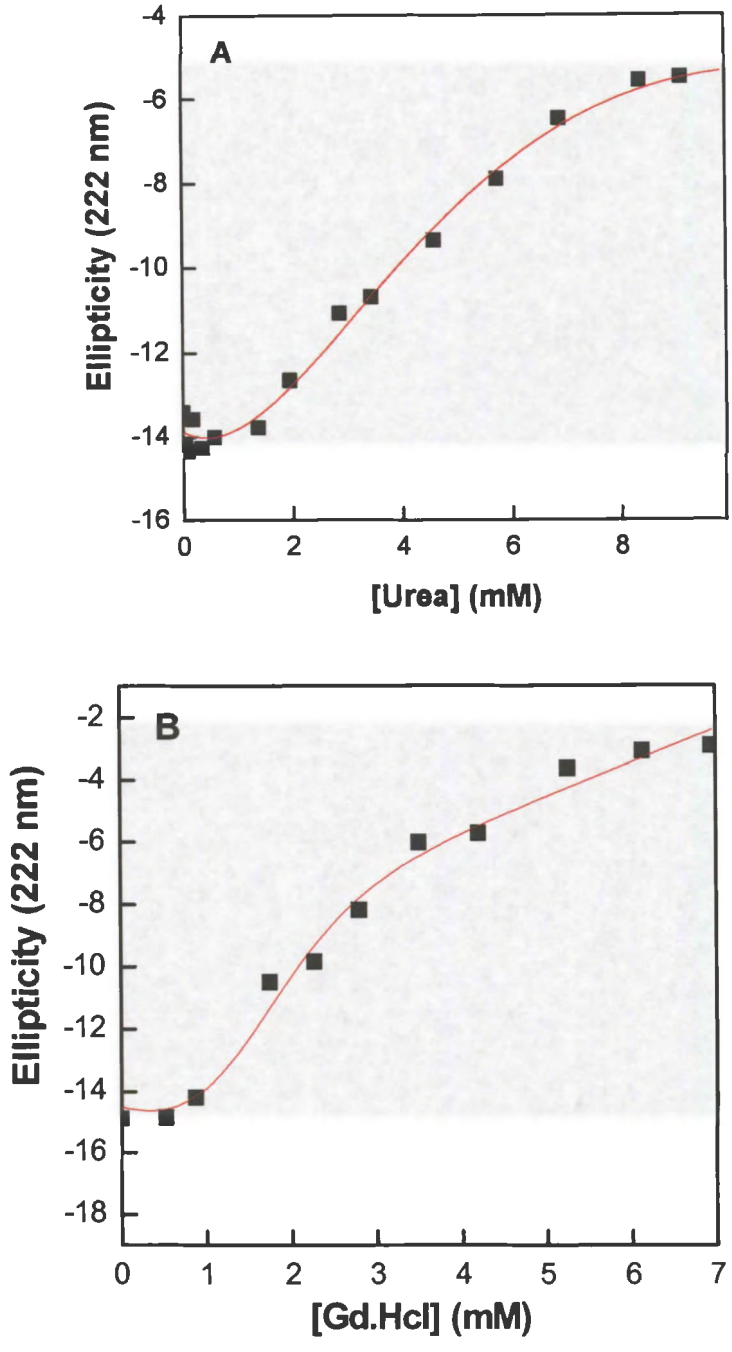

Figure 5.109. Urea and GdmCl induced CD unfolding profiles of hCA XII at 25°C. Urea and GdmCl dependent changes in the ellipticity of hCA XII at 222 nm is shown in panels A and B respectively. The solid smooth line in panels A and B is the best fit of the data for the $\Delta G^{\circ}_{n\text{-}u}$ values of -1.74 kcal mol^{-1} and -1.4 kcal mol^{-1} respectively.

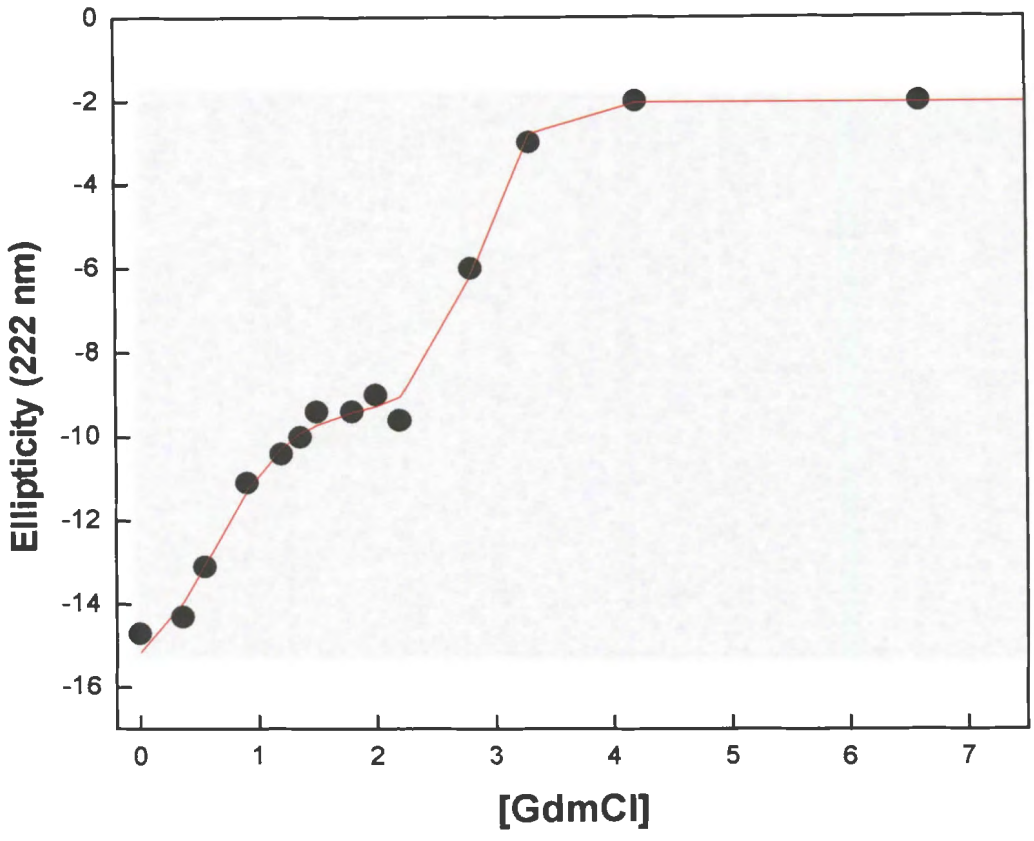

Figure 5.110. GdmCl induced CD unfolding profiles of hCA II at 25°C.
GdmCl dependent changes in the ellipticity of hCA II at 222 nm is shown. The solid smooth line is the best fit of the data for the $\Delta G°_{n\text{-}i}$ and $\Delta G°_{n\text{-}u}$ values of -1.15 kcal mol^{-1} and 2.84 kcal mol^{-1} respectively.

binds deep in the active site pocket of hCAs, any change in the tertiary structural features will be reflected in the fluorescence intensity of the enzyme bound DNSA. The unfolding of hCAs was measured by monitoring the changes in the fluorescence intensity of the enzyme bound DNSA at 457 nm as a function of increase in the concentrations of denaturants. It should be mentioned here that unlike CD measurements of unfolding, the samples were not incubated for 16 hours in this case. This was due to the observation that

the fluorescece change associated with tertiary structure unfolding happened instantly and did not change even after prolonged incubation times.

Panel A and B of Figure 5.111 shows the urea and GdmCl induced tertiary structure denaturation profiles of hCA XII respectively. Panel A of the Figure shows the effect of urea on the fluorescence emission intensity of enzyme bound DNSA at 457 nm. From the Figure it is evident that significant changes in emission intensity occur only after the urea concentration of 2 M and total tertiary structure is lost at a concentration of 4M urea with a midpoint of transition at 2.8 M. Denaturation with GdmCl shows that the above changes starts at very low concentrations of the denaturant (0.5M) and the total tertiary structure is lost at 2M GdmCl concentration with a midpoint of transition at 1M. Both the above data were well fitted by a two state model as mentioned above (Figure 5.109) yielding the free energy values of 2 and 3 kcal/mol for urea and GdmCl respectively.

Unlike CD spectral profiles, the unfolding of hCA II monitored by DNSA fluorescence exhibited a simple two state transition (Figure 5.112). From the Figure it is evident that the molten globule structure is attained at at denaturant concentration of 1.5M. As no significant changes in the fluorescence intensity take place after this point, it is concluded that the molten globule state does not retain the tertiary structure and thus not able to bind DNSA. The data was fit by a simple two state transition model yielding the free energy value of 3 $kcalmol^{-1}$. The mid point of transition was at 0.8M GdmCl.

It was of interest to determine if the chemically denatured proteins are able to refold if the denaturation concentration is decreased. The refolding of hCA isozymes were

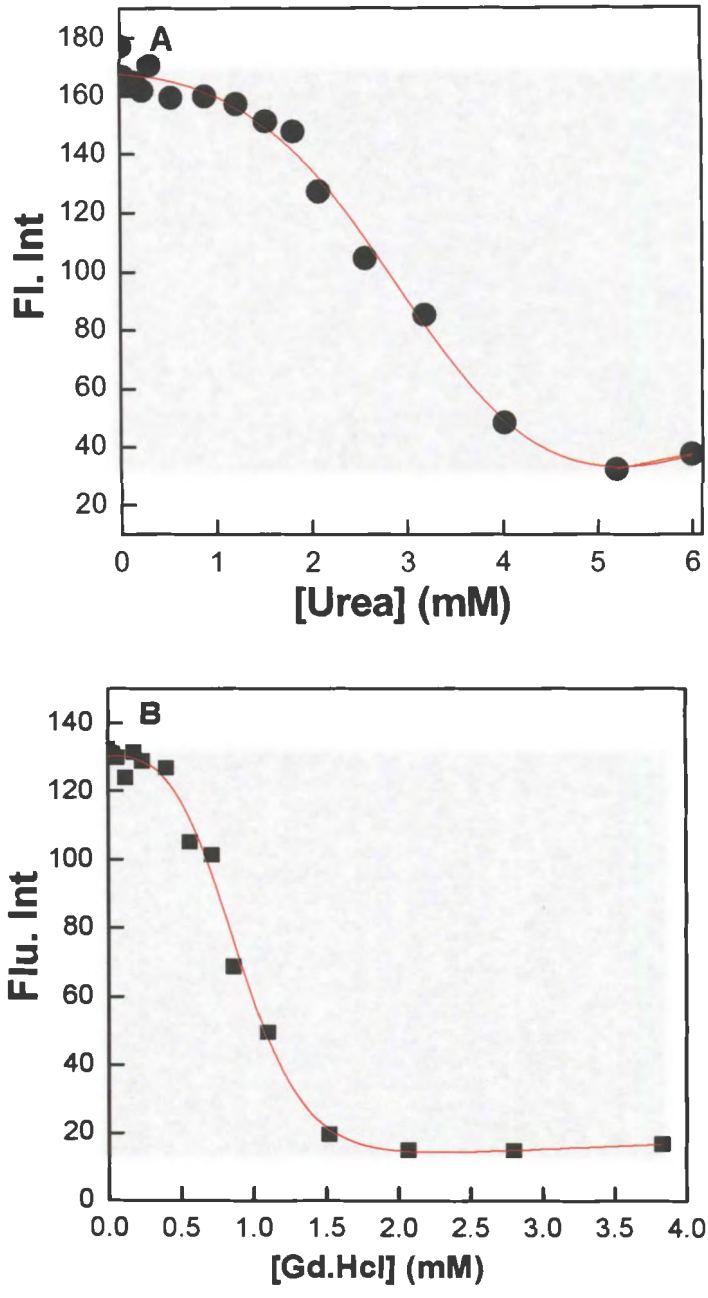

Figure 5.111. Guanidine hydrochloride induced unfolding profiles of hCA XII at 25°C. Panel A shows the unfolding profiles in the absence of mercaptoethanol. The decrease in the fluorescence intensity at 457 nm as a function of GdmCL concentration is shown. The solid smooth line in B is the best fit of the data for the ΔG°_{n-u} and m values of 3.09 kcal mol^{-1} and -2.8 kcal L mol^{-2}. Panel B shows the unfolding profiles in the presence of mercaptoethanol. The solid smooth line in B is the best fit of the data for the ΔG°_{n-u} and m values of 1.98 kcal mol^{-1} and -2.4 kcal L mol^{-2}

assessed by monitoring the fluorescence of active site ligand DNSA upon binding isozymes. Towards this goal, hCA containing 2M GdmCl was diluted 10 fold and its hCA fluorescence spectra in the presence of DNSA was compared with that of native hCA, hCA containing 2M GdmCl, hCA containing 0.2M GdmCl (Figure 5.113). It was found that in both hCA XII and hCA II, the fluorescence emission intensity of DNSA bound to hCA containing 0.2M GdmCl was similar to the snap diluted refolded proteins containing 0.2M GdmCl. From this it is evident that unlike thermal denaturation, chemical denaturation is reversible.

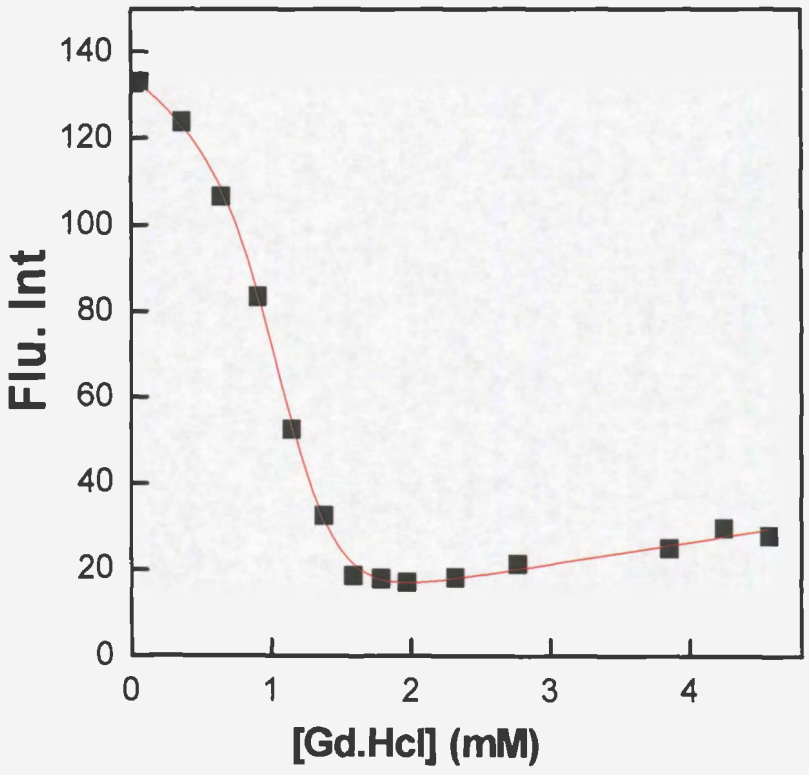

Figure 5.112. Guanidine hydrochloride induced unfolding profiles of hCA II at 25°C. The decrease in the fluorescence intensity at 457 nm as a function of GdmCl concentration is shown. The solid smooth line is the best fit of the data for the ΔG°_{n-u} value of 3.09 kcal mol^{-1}.

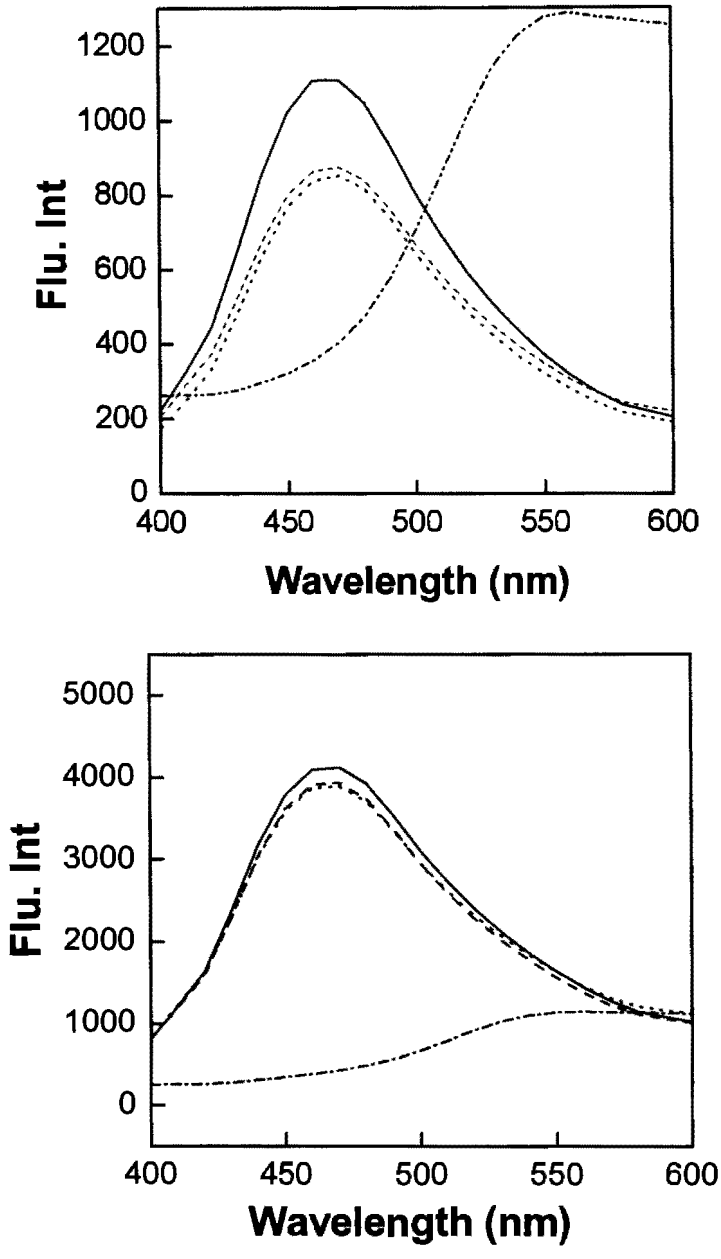

Figure 5.113. Refolding of hCA XII (upper panel) and hCA II (lower panel) after denaturation with GdmCl.
The Figure shows the refolding profiles of hCAs monitored using the hCA bound DNSA signal at 457 nm (λ_{ex} = 330 nm). The solid line in both panels shows the native hCAs bound to DNSA. The dashed lines show hCAs in the presence of 0.2 M GdmCl. The dash-dotted lines show hCAs in the presence of 2M GdmCl. The dotted lines represent the refolded protein.

CHAPTER 6. DISCUSSION

6.1. Influence of fluorescent probes on hCA isozymes

The experimental data presented for the interaction of fluorescent probes with hCA isozymes in chapter 5 led to the following conclusions: (1) Most of the JB2 fluorescent compounds showed higher enhancements in their quantum yields than DNSA upon binding to hCA isozymes. (2) The fluorescence lifetime and quantum yield of hCA I bound fluorescent probes (both DNSA and JB2-48) are higher as compared with other CA isozymes. (3) DNSA and JB2-48 has very strong binding affinity with hCA XII as compared to other isozymes. (4) Where as the K_{obs} values for the binding of DNSA to hCA isozymes exhibits a linear dependence (except hCA I), that of JB2-46 exhibits a hyperbolic dependence.

Studies on the interaction of JB2-48 with hCA I helped in deciphering the contributions of sulfonamide and hydrophobic regions of the ligand structure on the spectral, kinetic, and thermodynamic properties of the enzyme–ligand complex. Based on these studies the following conclusions were obtained. (1) Due to its size and extended conjugation, JB2-48 occupies nearly the entire active site pocket (about 15 Å deep) of hCA I, and this feature allows for deciphering the hydrophobic versus electrostatic contributions on the spectral, kinetic, and thermodynamic features of the enzyme–ligand complex. (2) Whereas the pKa of sulfonamide moiety of free JB2-48 is 10.2 that of the phenolic hydroxyl group is 6.5. (3) Depending upon the pH of the buffer media, the enzyme bound JB2-48 exists in either neutral (with sulfonamide group being fully protonated) or anionic form (pK_a=6.6), and these forms are stabilized by the cognate microscopic states of the

enzyme. (4) The neutral and anionic forms of the enzyme bound JB2-48 are distinguishable by their fluorescent lifetimes; whereas the fluorescent lifetime of the neutral form falls in the range of 12–14 ns, that of the anionic form is greater than 20 ns. Consistently, the anionic form of the enzyme bound JB2-48 is more fluorescent than its neutral counterpart. (5) Due to added electrostatic interaction (between the enzyme resident Zn^{2+} cofactor and the negatively charged sulfonamide group), the anionic form of JB2-48 is stabilized at the active site of hCA I by about 2.2 kcal/mol energy than its neutral form. (6) The rate of fluorescence changes accompanying the transient course of binding of JB2-48 to hCA I is about 5 fold faster with anionic than neutral form of the ligand, unraveling the fact that the putative transition state is about 0.9 kcal/mol more favorable with the anionic form of the ligand than the neutral form. (7) The similarity in the rate constants for the association of JB2-48 with hCA I (at acidic and basic pH values) with those derived from the pH jump experiments lead to the suggestion that the active site pocket of the enzyme undergoes slow restructuring during the course of the ligand binding.

The binding of both DNSA and JB2 compounds causes a blue shift in their emission maxima with concomitant increase in their quantum yields upon interacting with hCA isozymes. These fluorescence changes are considered to be due to the combination of the zinc induced changes in the electronic structure of the probes and the hydrophobic active site environment of the hCA isozymes. The idea that the disparity in the enhancements of quantum yields between enzyme bound DNSA and its derivatives could be due to the difference in their pK_a's at their respective enzyme sites was ruled out as the pK_a of DNSA at the active site of hCA I, hCA II (*329*) and the pK_a of JB2-48 at the active site of hCA I were found to be similar (pK_a = 6.3-6.6). The fact that DNSA occupies only

one third of the entire active site pocket of hCA II (Figure 5.8; upper panel) (*192*) reveals that it does not experience the full hydrophobicity of the enzyme's active site environment. This is in contrast to JB2 derivatives which has an extended structure and fills the entire active site pocket of hCA (Figure 5.8; lower panel) thus experiencing their full hydrophobicity. Hence the above difference is considered to arise due to the difference in the extent of hydrophobicity experienced by the two probes in the enzyme active site.

The substrate binding pocket of hCA II is lined by Val121, Phe131, Gly132, Lys133, Ala134, Lys135, Leu141, Val143, Leu198, Val207 and Trp209 (*174*). Compared to other sulfonamide inhibitors which usually contains a five or 6 membered aromatic ring, DNSA containing two fused aromatic rings binds in a different orientation in the active site pocket of hCA II. The naphthalene ring of the fluorophore undergoes a 54° twist as compared to the position of other aromatic rings so as to preferentially bind towards the more hydrophobic region of the enzyme. This process is accompanied by a conformational change in the active site residue Leu 198 to accommodate the binding. In addition it has been observed that mutation of Leu 198- Ala creates a void in the active site and results in tighter binding of DNSA (*192*). In light of these features, it is not surprising that hCA I binds more tightly to DNSA than hCA II (*329*) as the bulky residues like Val121, Phe131, Gly132, Lys133, Ala134 of hCA II are replaced by Ala, Leu, Ala, Ala and Gln respectively in hCA I (*203*). Also, Thr200 of hCA II is replaced by His in hCA I leading to a more hydrophobic environment and could possibly account for the high quantum yield and lifetime with the flurophores.

The substrate binding pocket of hCA XII (*49*) contains more polar and less bulky residues than hCA I (*203*) and hCA II (*173*). For instance, the presence of Ala131 widens

the active site canyon of hCA XII and it is said that this would help the enzyme to accommodate the bulky ligands more conveniently than other isozymes (*49*) and could be one of the reasons as to why hCA XII binds DNSA and JB2-48 more tightly than other isozymes. On the other hand presence of Ser132, Thr133, Ser135 in the substrate binding pocket reduces its hydrophobicity and might be responsible for the low quantum yield of bound flurophores. The reason as to why hCA VII binds DNSA weakly compared to other fluorescent probes listed in Table 5.7 is not clear at this point. Structural data of hCA VII with sulfonamide inhibitors would provide insights in to their binding mechanism.

The linear dependence exhibited by the k_{obs} values for the binding of DNSA to hCA VII and hCA XII reveals that their binding takes place in a single step as shown in scheme 4.1. According to this scheme, the final product is formed without the formation of any intermediate. However, it is also possible that the formation of the final product proceeds via the formation of an intermediate (scheme 4.2) still giving rise to a linear dependence of k_{obs} values for the binding. This has been elaborated by Banerjee et al. (*329*) for the binding of DNSA to hCA II. It is argued that the reaction can proceed with the formation of an intermediate giving rise to a linear dependence provided the first step (formation of EL complex) is much slower than the second step (formation of EL* complex).

If the second step is much faster than the first step, then the concentration of the isomerized complex at any given time could be considered negligible and this would reduce the over all binding mechanism to a single step process. Linear regression analysis of the transient kinetic data for the DNSA concentration dependent k_{obs} values obtained for hCA VII and hCA XII allowed the prediction of the binding constant of the hCA -

dansylamide complexes. It was found that the predicted K_d values ($K_d = k_r/k_f$) from the transient kinetic data (K_d= 7.8 μM for hCA VII and K_d= 0.032 μM for hCA XII) are in good agreement with the ones obtained from spectrofluorometric titrations (K_d= 3.1 μM for hCA VII and K_d= 0.06 μM for hCA XII) attesting to the consistency of the above model.

In contrast to DNSA, JB2-46 exhibited a hyperbolic dependence of its k_{obs} values for its binding with all hCA isozymes. This indicates that the reaction indeed proceeds with the formation of an intermediate and that the second step (formation of EL* complex- scheme 4.2) is slower than the first step (formation of EL complex - scheme 4.2). In this case, the observed rate constant is believed to be given by the second step. The K_d values predicted using the the concentration dependence values for hCA – JB2-46 interaction was calculated to be 0.09 μM, 0.1 μM, 0.04 μM , 0.1 μM for hCA I, II, VII and XII respectively. These values are similar to that obtained from the spectrofluorometric titrations (Table 5.7) validating our assumption that the second step is slow compared to that of the first step.

It is evident that DNSA (deeply seated active site ligand) binds to hCA VII and hCA XII in a single step whereas JB2-46 (with extended structure that could potentially interct with active site entry pocket residues in addition to the active site residues) binds in two steps. However the above observation could not be generalized for all the ligands with the above features. Infact, reports from Banerjee et al.(*329*) show that where as DNSA binds in a single step to hCA II, it binds in two steps with hCA I. It is said that of the three steps involved in the binding of a ligand to the enzyme, viz., desolvation, immobilization, and packing (*546*), the first two could possibly occur at the same rate and simultaneously.

However, packing takes comparatively longer time than the first two steps, as the enzyme and ligand needs to sample between all their conformational states to achieve an energetically stable and favorable state. This time depends on how well the enzyme can accommodate the ligand and also on the conformation of the ligand and the amino acid residues that interact with the ligand along with the flexibility of the enzyme. Thus whether the enzyme-ligand binding follows a one step or a two step binding completely depends on the enzyme conformation and the ligand structure.

The data presented in chapter 5 also revealed that the fluorescence spectral changes upon binding of JB2-48 to hCA I is contributed both by the hydrophobic environment of the enzyme's active site pocket as well as the electrostatic interaction between the active site resident Zn^{2+} cofactor and the negatively charged sulfonamide group of the ligand. Our temperature dependent lifetime data of both free and the enzyme bound JB2-48 (Table 5.6) as well as the pK_a values of free fluorophore eliminates the possibility that the enhancement in fluorescence of JB2-48 (upon binding to the enzyme site) is due to restriction in the rotational freedom between the two aromatic rings as observed with green fluorescent protein (*534*). It is believed that the fluorescence changes upon binding of JB2-48 (vis a vis dansylamide; (*329*)) to hCA I is more pronounced due to an extended conjugation of the π electrons between the two aromatic rings. The fact that the fluorescence intensity of JB2-48 increases with decrease in the solvent polarity (Figures 5.14 and 5.15) attests to the contribution of the hydrophobic active site environment of hCA I in enhancing the fluorescence emission intensity of the ligand. In addition to this, the negative ΔC_p value exhibited upon analysis of $\Delta H°$ values for the interaction of hCA I with JB2-48 at different temperatures attests to the fact that the binding is driven by

hydrophobic forces. However, since the fluorescence emission intensity of the enzyme bound JB2-48 is significantly higher at neutral and basic pH values (as compared to that that obtained in the presence of 90% dioxane) implies that aside from hydrophobicity, some additional factor(s) of the enzyme site phase is involved in enhancing the fluorescence intensity of the ligand. Based on the structural as well as the spectroscopic data (*173*, *210*, *277*, *278*, *529*), it appeared evident that such an "additional factor" is the electrostatic interaction between the active site resident Zn^{2+} and the negatively charged sulfonamide group of the ligand. Hence, it is not surprising that the decrease in pH diminishes the fluorescence emission intensity of the enzyme bound JB2-48 (Figure 5.13).

In view of the fact that the pK_a value of the enzyme bound JB2-48 is equal to 6.6, it is conceivable that the enzyme bound form of the above ligand would remain in fully protonated and ionized states at pH 5 and 9, respectively. This feature is further corroborated by the lifetime measurements of JB2-48 under different experimental conditions (Figures 5.17 and 5.18). Since the lifetime of "free" JB2-48 in 90% dioxane (τ = 12.5 ns) is similar to the lifetime of the enzyme bound JB2-48 at pH 5.0 (τ = 14 ns), it supports the notion (rather quantitatively) that the fluorescence profile of the enzyme bound ligand at pH < pK_a is dominated by the hydrophobic interaction within the enzyme's active site pocket. This is in contrast to the lifetime of the enzyme bound JB2-48 at pH 9.0 being equal to 20 ns (Figure 5.18) supports our hypothesis that at pH > pK_a, the fluorescence profile of the enzyme bound ligand is contributed by a combination of hydrophobic and electrostatic interactions. Hence, it is not surprising that at pH 7.0 (i.e., pH ≈ pK_a), the enzyme bound JB2-48 yields two lifetimes of 13.5 ns (τ_1) and 27.3 (τ_2), of which τ_1 and τ_2 are similar to the lifetimes of the enzyme bound ligand at pH 5.0 (or the

free ligand in the presence of 90% dioxane) and at pH 9.0, respectively. Since under physiological conditions CAs are known to bind one molecule of arylsulfonamide ligand per monomeric unit of the enzyme (*38, 49, 119, 173, 192, 203, 210, 212, 290, 309*), it appears plausible that τ_1 and τ_2 are associated with the two alternative microscopic states of the enzyme (see the cartoon of Figure 6.1).

The question arose whether the two microscopic states of the hCA I, harboring neutral versus anionic forms of JB2-48, respectively, are representative of the alternative conformational states of the enzyme. In pursuit of answering this question, we note that the observed rate constants during the pH jump experiments (Figure 5.37) are several orders of magnitude lower than those expected for the simple protonation/deprotonation (which are considered to be the diffusion limited process) step of the sulfonamide group of the enzyme bound ligand. Evidently, the protonation/deprotonation of the enzyme-bound ligand may not be the rate limiting step of the fluorescence changes during the pH jump experiments. The overall rate is neither expected to be contributed by the rate of decay of the excited state of the enzyme bound fluorophores since the lifetimes of the enzyme bound JB2-48 falls in the range of nanoseconds. However, one can argue that the slower rate constant for the increase in the fluorescence of the enzyme bound JB2-48, particularly during the 9→5 pH jump experiment (k_{obs} = 0.08 s^{-1}), is due to slow (rate limiting) breakdown of the Zn^{2+}-(anionic) sulfonamide bond of the ligand prior to the diffusion limited protonation step. Unfortunately, the above possibility falls short in explaining the comparably lower rate of fluorescence changes (k_{obs} = 0.67 s^{-1}) during the 5→ 9 pH jump experiment. Aside from these, the observed rate constants for the association of JB2-48 to

hCA I at pH 5 (k_{obs} = 0.08 s^{-1}) and 9 (k_{obs} = 0.37 s^{-1}) (Figure 5.36) are similar to the rate constants for the 9→5 and 5→9 pH jump experiments, respectively. Such a similarity in

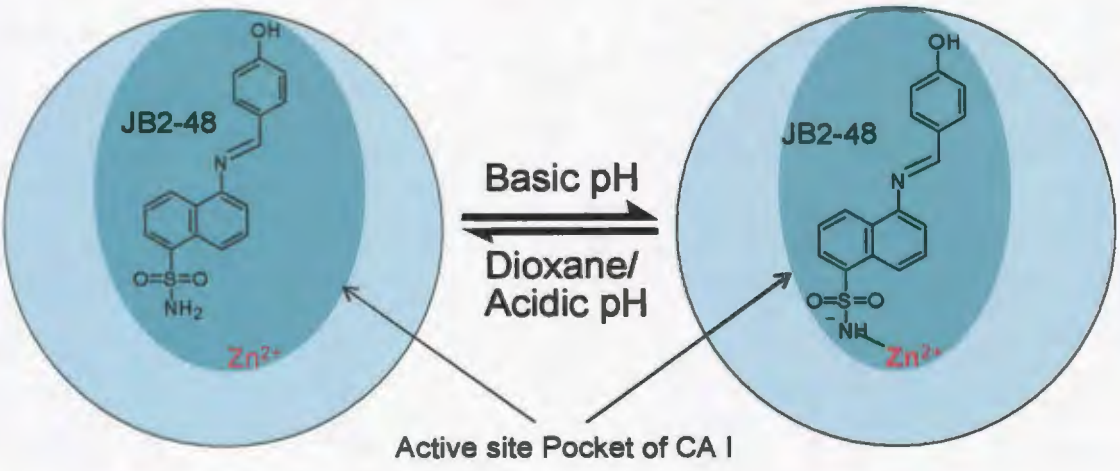

Figure 6.1. Cartoon showing the stabilization of neutral and anionic forms of JB2-48 at complementary microscopic states of hCA I.
The factors affecting the reversible transition between the two forms of the enzyme-ligand complexes are shown.

the rate constants has been somewhat surprising since these experiments are mechanistically different. In one case, the transient course of the fluorescence changes (as a function of pH) occur due to the association of the ligand to the enzyme, but in other case, the overall process is manifested via the protonation/deprotonation of the enzyme bound ligand. These arguments, in conjunction with our earlier transient kinetic studies for the binding of dansylamide to hCA I and hCA II (*329*), prompted to propose that the two alternative microscopic states of the hCA I (Figure 6.1) are representative of two alternatively conformational states of the enzyme which stabilize neutral and anionic forms of the ligand, and the transition between the above states serve as the rate limiting step during the pH dependent experiments. It should be emphasized that the conformational

changes during the ligand binding and/or the pH jump experiments need not be extensive to be deciphered via the fluorescence techniques – they can just be subtle and/or dynamic in nature to elicit the fluorescence changes reported herein.

The mechanistic conclusion derived herein has potential to find applications in the rationale design of hCA inhibitors as therapeutic agents. It appears evident that the potency of an arylsulfonamide inhibitor of hCAs can be increased by incorporating non polar groups toward the exterior region of the active site pocket as well as by introducing the electronic withdrawing groups on the aromatic ring(s) of the inhibitor (*65*, *77*, *309*, *530-532*). The latter groups would facilitate the deprotonation of the sulfonamide moiety (of the inhibitor) such that it's anionic form would interact more strongly with the Zn^{2+} cofactor, and the overall structure would be stabilized by the cognate microscopic/conformational state of the enzyme. As long as the newly incorporated groups do not pose steric hindrance within the active site pocket of the enzyme, nor do they alter the formal charges on the Zn^{2+} cofactor, the resultant inhibitors would exhibit high potencies. On the other hand, any factor which impairs deprotonation of the sulfonamide moiety would populate the other conformational state of the enzyme with weaker inhibitory potency.

6.2. Thermodynamic parameters for the interaction of sulfonamide inhibitors with hCA VII

The experimental evidence presented in chapter 5 (section 5.3) provide the following insights on the interaction of hCA VII with sulfonamide inhibitors, BS and AZM: (1) Increase in temperature decreases the $\Delta H°$ for the binding of BS to hCA VII (Table 5.11) where as it increases for the binding with hCA II (Table 5.12). (2) A negative change in heat capacity slope ($\Delta C_p° = -0.286$ kcal mol^{-1} K^{-1}) is involved in the binding of

BS with hCA VII where as it is the reverse in case of its binding with hCA II (ΔC_p° = 0.463 kcal mol^{-1} K^{-1}) (3) Temperature independent enthalpy-entropy compensation to the over all binding free energy has been observed in both the cases. (4) The binding of BS to both the isozymes has no effect on buffer ionization enthalpy (Tables 5.13 and 5.14).

The results obtained for the binding of AZM with hCA VII gave rise to the following conclusions: (1) contrary to the binding of hCA VII with BS, its binding to AZM resulted in an increase in ΔH^0 with increase in temperature (Table 5.15) giving rise to a positive change in heat capacity (ΔC_p° = 0.14 kcal mol^{-1} K^{-1}) upon binding. (2) Similar to the results obtained for the binding of hCA VII with BS, its binding to AZM did not have any effect on the buffer ionization enthalpy (Table 5.16) (3) A perfect enthalpy-entropy compensation that is independent of temperature was observed in both the cases.

In addition to the above, it was found that both the isozymes bind the above inhibitors with a stoichiometry of approximately 1. This is consistent with the NMR studies which found that the stoichiometry of the CA-aryl sulfonamide groups to be 1:1 (*277*) in contrast to the X-ray structures (*290*) which showed that one sulfonamide bound to the active site of hCA II and the other sulfonamide bound at the interface between two hCA II proteins in the crystal lattice.

Although BS inhibits both hCA II and hCA VII with comparable binding affinities (Table 5.10), the thermodynamic parameters associated with their interaction are different. Whereas the binding of BS with hCA II is enthalpically driven at low tempeatures, it is entropically driven for its binding with hCA VII. This resulted in a strong positive change in heat capacity (ΔC_p^0 = 0.463 kcal mol^{-1} K^{-1}) in the former case where as a negative heat capacity (ΔC_p° = -0.286 kcal mol^{-1} K^{-1}) in the latter case.

Edsall (*547*) was the first to recognize the effect of transfering the hydrophobic groups of a solute to a more polar environment. He found that doing so leads to an increase in the heat capacity of the solute. Followed by his observation many researchers (*548-552*) focused on understanding the nature of the hydrophobic effect of water. As water molecules has the ability to form hydrogen bonds, they tend form highly ordered structures around non polar groups. The above phenomenon was reasoned to be due to the formation of ordered water structures surrounding the non polar groups like "cages" (*548-552*). This ordered structure of water molecule decreases the entropy of the system thereby preventing the occurrence of spontaneous reactions according to the second law of thermodynamics. Thus when the highly ordered hydrogen bonded structures between water and non polar groups possessing a low entropy and high heat capacity, is released from the non polar groups, it results in an increase in entropy and decrease in the heat capacity (*553*, *554*, *548*).

In light of the above facts, it is evident that the binding of a ligand to a protein is will also be accompanied by a change in the heat capacity. The nature and the magnitude of those changes depend on the changes in the solvation properties of the interacting partners. A positive increase in ΔC_p value suggests that the hydrophobic groups of the protein are exposed to the polar environment where as a negative ΔC_p suggests burial of the above groups in a non polar environment. Accordingly, it can be said that hydrophobic interactions stabilize the ligand binding in the case of hCA VII-BS interaction, where as the binding of hCA II to BS and hCA VII to acetazolamide is stabilized by polar interactions.

Many researchers have predicted the magnitude of ΔC_p for enzyme–ligand interactions (*555*, *550-552*) by calculating the differences between the water-accessible polar and nonpolar surface areas of enzyme, ligand and enzyme-ligand complexes based on the structural data of the enzyme ligand complexes. This was not possible in the present study as the crystal structure of hCA VII is not available.

The fact that the enthalpy of binding of the above ligands to hCA VII and hCA II did not vary with change in buffer ionization enthalpy indicates that no significant change in protonation event takes place during binding. However, X-ray crystallographic (*49*, *226*, *290*, *382*) and NMR studies (*273*, *275-277*) suggest that the active site metal in CAs bind aryl sulfonamides in their anionic form through the sulfonamide nitrogen. It also suggests that in order for arylsulfonamides to bind as anions to the zinc, deprotonation of sulfonamide group has to take place prior to binding. This suggested that the proton that is released from the Zn^{2+}-bound water of the hCA active site into the buffer media is compensated by another proton being abstracted from the sulfonamide group of the ligand resulting in no net change in protonation event during binding.

The temperature dependent studies for the interaction of sulfonamide inhibitors indicated that irrespective of the temperature, the $\Delta G°$ values remained nearly identical in all cases suggesting a perfect compensation of entropy for enthalpy and vice versa. This could arise due to subtle changes in the position of amino acid residues and the solvent molecules at the interface of the interacting partners (titration calorimetric studies). From the enthalpy-entropy compensation plots it is evident that the temperature at which $\Delta H° = \Delta G°$ was found to be 307 K, 302.6 K and 276 K for the binding of BS with hCA VII, hCA II and for the binding of AZM with for hCA VII respectively. Based on the fact that D*S*° is

a combination of all the favorable and unfavorable entropic contributions, it can be said that at above temperatures the favorable (solvent displacement, vibrational entropy) and unfavorable entropic contributions (loss of rotational, translational and rotational entropy) balance each other such that $\Delta H^{\circ} = \Delta G^{\circ}$.

6.3. Effect of nanoparticles on hCA isozymes

A cumulative account of the experimental data presented herein leads to the following conclusions. (1) Qds^{+} and polylysine (representative of cationic macromolecules) electrostatically interact on the surface of the protein opposite to the active site pocket of hCA XII. (2) The binding of hCA XII to both the charged particles perturbed the intrinsic fluorescence emission of hCA XII without altering the fluorescence emission of the charged particles. (3) Neither of these cationic macromolecules influence the catalytic activity of the "free" (i.e., unliganded) enzyme. (4) DNSA bound to hCAXII transfers the excited state energy to Qds^{+} within the hCA XII-Qds^{+} complex (5) Qds^{+} and polylysine exhibit different influence on the fluorescence emission properties of the enzymebound DNSA (one of the potent inhibitors of the enzyme). (6) Whereas the inhibitory effect of DNSA is overcome upon binding of Qds^{+} to the enzyme's surface, it remains unchanged upon binding of polylysine. Evidently, Qds^{+} and polylysine differently modulate the microenvironment of the enzyme's active site pocket (via the long range interaction), and such feature is likely to be encoded in the "rigidity" versus "flexibility" of these cationic macromolecules. (6) Qds^{+} binds hCA XII with strong binding affinity as compared to hCA I and hCA II.

The fact that the intrinsic tryptophan fluorescence of hCA XII was quenched upon binding of the enzyme to the Qds^{+} and plolysine suggested their plausible interaction. This

was not surprising in the light of the oppositely charged surfaces between hCA XII and the Qds^+, which could promote electrostatically-mediated interactions between the above species. The latter feature is evident by the fact that the increase in the ionic strength of the buffer media abolishes the Qds^+ mediated quenching of the intrinsic fluorescence of the enzyme. It can be surmised that upon binding of hCA XII to Qds^+, the active site pocket of the enzyme would likely be oriented away from the surface of the latter. This is because the positive charges of the Qds would interact with the negative charges of the opposite face of the enzyme. In addition, neither the binding of DNSA nor the enzyme activity is altered particularly in the presence of polylysine. This would not be the case if the enzyme was oriented such that the active site pocket was oriented towards the QD surface as this would occlude the accessibility of the substrate during catalysis. Hence it is tempting to speculate that these cationic macromolecules interact on the enzyme surface opposite to the active site pocket of the enzyme.

Due to "colorless" nature of polylysine, it has been possible to decipher its influence on the fluorescence spectral profiles of the enzyme-bound DNSA and determine the dissociation constant of the enzyme–DNSA complex. Literature evidences (*329*, *387*, *464*, *473*, *556*, *557*) suggest that the fluorescence spectral changes of free DNSA upon binding with carbonic anhydrases are contributed both bythe hydrophobicity of the enzyme's active site pocket as well as the interaction of the deprotonated amide nitrogen of the sulfonamide group of the fluorophore to the enzyme resident Zn2+ cofactor. Hence, the apparent quenching of the fluorescence intensity (λ_{ex}=330 nm, λ_{em}=457 nm) of the enzyme-bound DNSA upon titration with polylysine (Figure 5.81A) can occur due a variety of reasons: (1) decrease in the binding affinity of DNSA for hCA XII in the

presence of polylysine. Since the fluorescence intensity of free DNSA is significantly lower than that of its enzyme-bound form (*328*, *387*, *473*, *556*, *557*), its dissociation from the enzyme site (induced by polylysine) would result in the decrease in the fluorescence emission intensity. (2) Distortion of interaction between the enzyme resident Zn^{2+} cofactor and the amide nitrogen of DNSA. (3) Increase in polarity of the enzyme's active site pocket. However, irrespective of the mechanistic origin for the polylysine induced quenching of the DNSA fluorescence, the overall process must be coordinated via the long range (possibly subtle) changes in the protein conformation. Of different plausible reasons for the polylysine-mediated quenching of the enzyme-bound DNSA fluorescence, the decrease in the binding affinity of the enzyme–DNSA complex (reason #1) is unlikely. This is because the Kd value for hCA XII–DNSA complex (0.08 μM) remains practically unchanged in the presence of saturating concentration of polylysine (K_d=0.18 μM). Furthermore, the effect of polylysine in distorting the interaction between the enzyme-bound Zn^{2+} cofactor and the sulfonamide nitrogen of the fluorophore (reason #2) is also unlikely since the activity of the DNSA inhibited enzyme is not regained in the presence of polylysine (note that this is in contrast to the restoration of the DNSA inhibited activity of the enzyme in the presence of Qds^{+}; Table 5.17). Hence, the polylysine-mediated quenching of the enzyme-bound DNSA fluorescence is, at the best, due to an increase in the polarity (reason#3) of the enzyme's active site pocket. The latter can easily happen due to an increase in the extent of hydration of the active site pocket (in the vicinity of boundDNSA) via polylysine induced subtle changes in the enzyme conformation.

Unlike polylysine, Qds^{+} induces marked changes in the fluorescence profile of the enzyme-bound DNSA. This is also because Qds^{+} itself is a fluorescent macromolecule and

it accepts excited state energy from the enzyme-bound DNSA (the FRET effect). Hence, the magnitude of quenching of the enzyme-bound DNSA fluorescence (around the 450 nm region) is likely to be caused by a combination of the Qds+ mediated changes in the active site environment of the enzyme (akin to that noted with polylysine) and the FRET between the two fluorophores. This is further supported by the fact that Qds^+ dependent fluorescence spectral changes of the enzyme-bound DNSA (Figure 5.79) is devoid of a clean isosbestic point around the 540 nm region. Since we could not determine the binding affinity of DNSA for hCA XII in the presence of Qds+ (due to its interference in the observed fluorescence signal), the observed spectral changes of Figure 5.79 can also be contributed by a partial dissociation of DNSA from the enzyme site. However, in marked contrast to polylysine, the presence of Qds^+ overcomes the DNSA dependent inhibition of the enzyme (Table 5.17). Whether it is caused by the distortion and/or displacement of DNSA from the enzyme site, it appears likely that the binding of Qds^+ to hCA XII induces more pronounced changes at the active site pocket of the enzyme than its cationic macromolecular counterpart — polylysine. The question arises why similarly charged cationic macromolecules (Qds^+ and polylysine) differently influence the microenvironment of the enzyme's active site? In attempting to answer this question, it was noted that whereas Qds^+ is a representative of a "rigid" charge carrier, polylysine is a "flexible" cationic macromolecule. Hence, the binding of hCA XII on the Qds^+ surface can result in the bending/flexing of the enzyme structure, resulting in the long range influence on the structural feature of the enzyme's active site pocket. On the other hand, due to flexible nature of polylysine, its binding with the enzyme can result in readjusting its structure. In view of these arguments, we propose that the Qds^+ mediated changes (via

long range interaction) at the active site pocket of the enzyme abolishes the interaction of the Zn2+ cofactor with the sulfonamide nitrogen of DNSA. This occurs presumably due to creation of new binding site of DNSA that is somewhat removed from its original binding site at the active site pocket of the enzyme. As a consequence, Zn^{2+}-OH is generated at the active site, and it serves as the Lewis acid–base pair in facilitating the hydration of CO_2 (see the cartoon of Figure 6.2). Being small molecules, CO_2 and H_2O can easily diffuse in the vicinity of the Zn^{2+} cofactor, promoting the carbonic anhydrase catalyzed reaction. This is in marked contrast to the miniscule influence of polylysine on the configuration of DNSA within the enzyme's active site pocket, and thus it does not facilitate the enzyme catalysis. The effects of differently functionalized nanoparticles (as well as their shapes and sizes) on the structural–functional features of enzymes has been reviewed by Wu et al.(*558*). Depending on the nature of the enzymes and complementarily charged nanoparticles, the electrostatic interactions can range from being silent to inhibition and inactivation of enzymes. For example, Rotello and his collaborators (*559*) have elegantly demonstrated that the electrostatic interaction between anionic gold nanoparticles and chymotrypsin results in the instantaneous inhibition of the enzyme activity followed by its inactivation on a longer time scale. The latter effect has been found to proceed in concomitance with changes in the secondary structural feature of the enzyme. Among carbonic anhydrase isozymes, the interaction between negatively charged silica nanoparticles and hCA II has been reported by Karlsson and Carlsson (*419*). These, in conjunction with other literature data (*406-411*), strengthen our deduction that the changes in the functional features of hCA XII are manifested via the structural changes in the protein, and the latter occurs via the long range interaction, akin to the allosteric

modulation of the enzymatic function (*560*). Whether or not the discriminatory influence of the "rigid" versus "flexible" macromolecules on hCA XII is unique needs more investigation.

The binding affinity values obtained for the interaction of Qds^{+} with hCA I and II revealed that although these nanoparticles have the ability to interact with the above isozymes, their binding affinities were many fold lower as compared with hCA XII. This is not surprising as the negatively charged residues in these proteins were "scattered" as compared to "clustered" in hCA XII.

A comprehensive account of the experimental data described in the earlier section for the interaction of hCA XII with QDS- has lead to several conclusions. (1) hCA XII is able to bind to negatively charged Qds through electrostatic interactions to form hCA XII-Qds^{-} complex. (2) The binding of hCA XII to Qds^{-} perturbed the intrinsic fluorescence emission of hCA XII and increased the fluorescence emission intensity of the Qds^{-}. (3) Interaction of Qds^{-} to hCA XII increased its fluorescence lifetime. (4) The binding of Qds^{-} to hCA XII-DNSA complex displaces DNSA from the active site pocket. (5) The activity of hCA XII is completely abolished upon interaction with Qds^{-} (6) Qds^{-} binds hCA XII with strong binding affinity as compared to hCA I and II.

The quenching of the intrinsic tryptophan fluorescence of hCA XII upon interaction with Qds- suggested their plausible interaction. The interaction was further confirmed by the increase in the fluorescence intensity of Qds^{-} upon addition of hCA XII. In view of the positive electrostatic potentials of the active site pocket of hCA XII (*555*) (Figure 5.74), it is not surprising that the Qds^{-} electrostatically interact with hCA XII. It can be surmised that upon binding of hCA XII to Qds^{-} to the active site pocket of the enzyme would likely

be oriented towards the surface of the latter. This is because the negative charges of the Qds would interact with the positive charges of the active site pocket of the enzyme. Support for this orientation of hCA XII is provided by the observation that the binding of the enzyme to the Qds^- abolishes the catalytic activity. This would not be the case if the enzyme was oriented such that the active site pocket was oriented away from Qds^- surface as this would not occlude the accessibility of the substrate during catalysis as seen in Qds^+. The conclusion that the orientation the Qds^- bound hCA XII is such that the active site pocket of the enzyme is towards the surface of the Qds^- is valid as the binding of the later displaces DNSA from the enzyme active site as is evidenced by the decrease in the fluorescence intensity of enzyme-DNSA complex at 457 nm with the addition of Qds^-. It can be argued that the decrease in the fluorescence intensity at 457 nm could not be taken in to consideration to arrive at a conclusion that DNSA is displaced from the enzyme active site as it could happen even if it is bound at a different site through long range allosteric effect as is the case for Qds^+. However, if this is the case, given the fact that the excitation spectrum of DNSA over laps with the emission spectrum of Qds^-, it is reasonable to assume that this would transfer its excitation energy to Qds^- leading to an increase in the quantum yield of Qds^-. Figure 5.88 and Figure 5.99 shows that the amplitude of the increase in the fluorescence intensity of Qds^- in the presence of hCA XII and hCA XII-DNSA complex are qualitatively similar. These along with the fact that a clear isosbestic point (unlike Qds^+; Figure 5.79) is observed for the spectral data of Figure 5.89 strenthens the conclusion that Qds^- binds near the active site and displaces the active site ligand DNSA.

In contrast to the Qds^+, the interaction of hCA XII with Qds^- led to the enhancement of the fluorescence intensity of the later. In addition, the fluorescence lifetime of Qds^- increased in the presence of hCA XII. Since the fluorescence excitation spectra of hCA XII overlaps with the emission spectra of the Qds^-, it was initailly thought that this increase could be due to the FRET from the protein to the Qds^-. This possibility was ruled out by the observation that the fluorescence intensity of Qds^- increases even when excited at 330 nm (Figure 5.87B). At this wavelenght, the protein tryptophn residues will not be excited and hence there is no possibility of FRET from hCA XII to Qds^-.This is also supported by the fact that the protein exhibits similar lifetime in the presence and absence of Qds^-. The fluorescence lifetime value of the protein would have reduced in case of energy transfer. All these features attest to the fact that FRET from protein to Qds^- is not the reason for the observed enhancement in the fluorescence intensity of Qds^- in presence of hCA XII. It has been shown in literature that when CdS nano particles were polmerized with acrylic acid, the fluorescence intensity of the former is increased. It has also been established that increasing the thickness of the nanoparticle surface decreases the surface defects thereby increasing its stability and fluorescence emission intensity. Based on these facts it is proposed that the electrostatic interaction of the amino groups of the positively charged amino acids in the active site of hCA XII to the TGA group present on the surface of the Qds^- increases the surface passivity of the Qds^- by eliminating its surface defects thereby causing an enhancement in its fluorescence emission intensity. However, it is not clear at this point as to why the fluorescence intensity of Qds^+ and Nqds are unchanged upon interaction with hCA XII.

The binding affinity values obtained for the interaction of Qds^- with hCA I and hCA II revealed that although these nanoparticles have the ability to interact with the above isozymes, their binding affinities were many fold lower as compared with hCA XII. This is not surprising as the positively charged residues in these proteins were "scattered" as compared to "clustered" in hCA XII.

Studies on the interaction of Nqds with hCA isozymes led to the following conclusions: (1) The interaction of hCAXII with the Nqds perturbed the intrinsic fluorescence emission of hCAXII without altering the fluorescence emission of the Nqds. (3) Nqds does not have any influence on the catalytic activity of hCA XII (3) The fluorescence emission intensity of hCA XII- DNSA complex decreases in the presence of Nqds. (4) The inhibitory effect of DNSA is not overcome by the addition of Nqds to the hCA XII-DNSA complex. (5) The binding affinity of Nqds is similar with all the isozymes.

The fact that the addition of Nqds to hCA XII decreased the fluorescence intensity of the later suggested plausible interaction between the two, albeit weakly as compared to charged Qds. This is evident by comparing the binding affinities of hCA XII with charged and neutral Qds as listed in Tables 5.17-5.19. The binding affinity of Nqds with hCA XII is atleast 30 fold less as compared to charged Qds. In addition, the binding affinity values listed in the Table 5.20 reveals that where as the charged quantum dots bind very tightly with hCA XII, and weakly with hCA I and hCA II, the Nqds bind with similar affinities to all the isozymes.

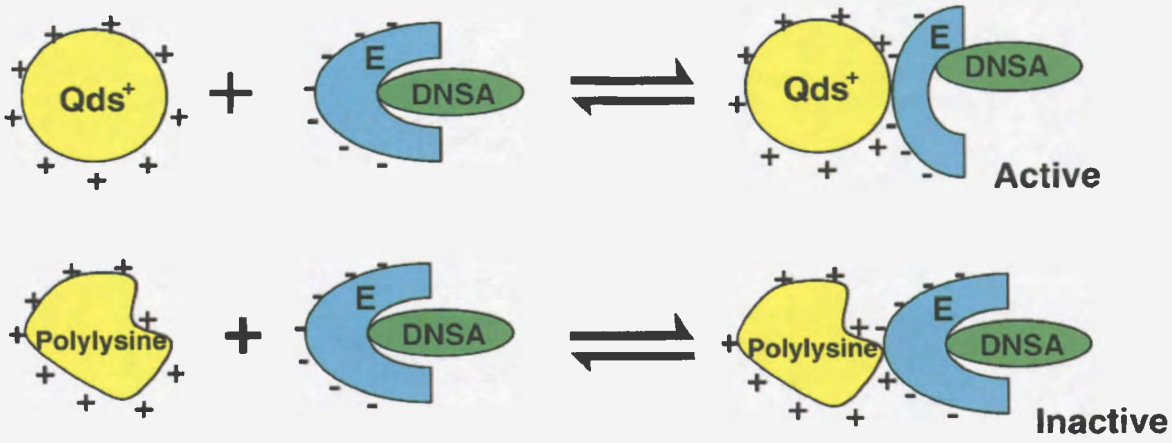

Figure 6.2. Diagrammatic representations for the differential influence of Qds^{+} and polylysine on the microenvironment of the active site pocket of hCA XII.
It is surmised that unlike polylysine, the binding of Qds^{+} to hCA XII alters the microenvironment of the enzyme's active site pocket, resulting in reorientation of the Zn^{2+} ligated DNSA and thus overcoming the inhibitory effect of DNSA. Since such changes are not manifested upon binding of polylysine to hCA XII (DNSA) complex and thus the enzyme remains inhibited.

Inspite of the weak binding, addition of Nqds to the hCA XII-DNSA complex decreases the fluorescence intensity of the complex at 457 nm (Figure 5.95). This quenching could occur due to the due to any/all of the following reasons: (1) Loss of tertiary structure of hCA XII in the presence of Nqds. (2) Competitive displacement of DNSA from the enzyme active site by Nqds. (3) Distortion of interaction between the enzyme resident Zn2+ cofactor and the amide nitrogen of DNSA, still having hydrophobic contact with the enzyme. (4) DNSA is slightly displaced from the active site without disturbing the interaction of the amide nitrogen of the sulfonamide moiety with the Zn^{2+}. Of the possible reasons mentioned above, reasons 1 and 2 are unlikely as the presence of Nqds does not have any influence on the catalytic activity of the enzyme. Reason 3 is also

unlikely, as the presence of Nqds did not reverse the DNSA induced inhibition of hCA XII. Hence, reason 4 seem to be a likely possibility as the decrease in fluorescence intensity could have happened due to the slight displacement of DNSA to the hydrophilic area of the active site. However, this displacement is not sufficient such that the DNSA and Nqds are in a proximal distance for an efficient FRET to occur from the former to the later.

Some of the features exhibited by Nqds are similar to that exhibited by Qds^{+} except that the effect of Qds^{+} was more pronounced on the binding of the active site ligand DNSA. This difference could have occurred due to the difference in the strength of the interaction, the site of interaction and size between the two Qds.

It is a well known fact that the three dimensional structure of the protein is only barely stable (*561*, *562*) as the favorable interactions that stabilize its structure is in most cases compensated by the unfavorable interactions and this is the reason why their interaction with solid surfaces easily disturbs its tertiary structure and as a consequence its function. However, there are many instances where the above interaction leaves the protein functional and this usually depends on the size of the nanoparticle and the site of its interaction in a protein (*561*). For instance it has been demonstrated that differently charged mixed monolayer protected gold clusters have different effects on the functional features of chymotrypsin (*559*). Whereas the interaction of cationic gold clusters with chymotrypsin did not affect the catalytic activity of the protein, interaction with anionic gold clusters inhibited its activity. This is due to its interaction with the positively charged residues present in the active site of the protein. It has also been evidenced that as the size of the nanoparticles increases it has large influence on the structure and function of proteins (*410*, *411*, *563*). For example, investigation on the structure and cataltic activity of

lysozyme (*410*) with silica nano particles ranging in size from 4 nm to 100 nm revealed that the smaller nanoparticles had least influence on the the structure and activity of lysozyme. In light of these literature evidences, it is concluded that the site of nanoparticle interaction on the hCA XII and the strength of the interaction between the two are responsible for its influence on the structural and functional features of the enzyme. As all the Qds used are approximately of the same size that possibility is ruled out.

Studies on the interaction of polylysine and Qds^{+} with hCA XII suggested these two molecules had an entirely different influence on the structural and regulatory features of the enzyme. This has been explained based on the difference in the surface properties (rigidity Vs flexibility) of both the particles. This feature was further explored by using differently charged liposomes. If the surface charges were the only determinants for their interaction and their effects on the enzyme, both Qds and liposomes would yield the similar results. On contrary, if the surface properties were responsible for the above effects, a totally different feature will be exhibited by the two molecules on hCA XII. The interaction of differently charged liposomes on hCA XII gave rise to the following conclusions: (1) The interaction of hCAXII with the liposomes perturbed the intrinsic fluorescence emission of the protein without altering the fluorescence emission of the liposomes. (2) hCA XII interacts with all the lipid membranes, albeit efficiently to positively and negatively charged membranes compared to neutral membranes. (3) The binding affinity for the interaction of hCA XII with charged liposomes decreases with increase in NaCl concentartion. (4) Despite the interaction of charged liposomes with hCA XII, they do not alter the binding affinity of the flurogenic ligand, DNSA, to hCA XII. Neither are the binding affinities of charged liposomes to hCA XII altered in presence of

saturating concentrations of dansylamide. (5) Interaction of none of the liposomes to hCA XII alters its catalytic activity.

Clear evidence has been provided in the previous chapter that the addition of liposomes to hCA XII quenches the tryptophan fluoescence of the protein. This suggested that the two species are interacting with each other. Liposomes in contrast to Qds, does not absorb to a large extent at 280 nm. So the observed quenching was not a result of inner filter effect. The fluorescence quenching observed with hCA XII upon addition of liposomes could be attributed to the change in the microenvironment of the tryptophan residues of hCA XII as a result of their interaction with liposomes. The fact that the interaction between hCA XII and charged liposomes becomes weak with increase in NaCl concentration suggested that the above interaction is driven by the favourable electrostatic forces. Given the fact that hCA XII is characterized by the bipolar distribution of charged residues, it is reasonable to assume that the positive and negative patches present on the active site of hCA XII and the surface of the enzyme opposite to the active site interacts with negative and positively charged liposomes respectively.

The fact that the catalytic activity of hCA XII remained unaffected in the presence of cationic liposomes was not surprising as the similarly charged Qd with rigid surface properties had the same effect. It needs to be mentioned that although the former feature is similar, in contrast to Qds^{+}, CL were unable to relieve the inhibition of the enzyme caused by DNSA. In the case of Qds^{+} it was argued that inspite of this observation, DNSA was not displaced from the active site as was evidenced by the lack of an isosbestic point in the spectral data of Figure 5.79. Since the fluorescence emission of free DNSA exhibits a maximum at 536 nm, the increase in the fluorescence band at the above wavelength was

responsible for precluding clean isosbestic points upon titration of hCA XII-DNSA complex by the Qds (Figure 5.79). If not for the activity of the hCA XII-Qds^+ complex (Table 5.17), it would have been very tempting to argue that the loss of DNSA from the enzyme phase was due to the direct displacement of the inhibitor upon binding of Qds^+ to the hCA XII-DNSA complex. In addition to the above feature, the CL and DNSA does not influence the binding of each other to hCA XII as was confirmed by the similar binding isotherms of DNSA to hCA XII in the presence and absence of of saturating concentrations of CL and vice versa. The observation that the activity of hCA XII and hCA XII-DNSA complex remains unaltered in the presence of CL, and their binding affinities remain the same in each others presence suggests that inspite of the interaction of CL to hCA XII, it does not modify the structural features of the enzyme active site to an extent that will alter its functional properties.

The observation that the AL did not have any effect on the catalytic properties of hCA XII and did not change its binding affinity to DNSA was totally unexpected. In addition, it was found that the binding affinity of AL to hCA XII was also unaffected in the presence of DNSA. This raised a question as to whether these particles are interacting at a different site. But it was realized that the the dansyl probe present in the liposome would not be able to electrostatically interact with the active site metal as its sulfonamide nitrogen is conjugated with the tail part of the DPE lipid although it interacts at the active site. This along with the fact that the liposomes are flexible molecules could be responsible for not affecting the functional features of the enzyme.

The differential influence of Qds^- and ALs on the structure and function of hCA XII could be explained as follows. The positive electrostatic potential of hCA XII around

the active site of hCA XII formed favorable interactions with both the nano particles. However, these two nanoparticles are characterized by a marked difference in the rigidity as well as the surface curvature. Because of this feature, where as the Qds^- binds and inactivates the enzyme, the liposomes possessing flexible surface in addition to a very minimal surface curvature does not influence the structural and functional properties of the enzyme irrespective of their site of interaction. This differential feature exhibited by the rigid and flexible particles on the catalytic features of the enzyme has been observed by many researchers (*564-566*). In case of protein-liposome interaction, both the interacting partners being flexible in nature are able to adjust their conformations and such a phenomenon has been describes as the "bending-dominated deformation" of flexible LNPs and "stretching dominated response" of the intrinsically flexible protein (*567*). In contrast to this, nano particles binding to proteins are often known to either denature or inactivate the protein based on the size, and site of interaction (*410*, *411*, *561*, *563*, *564*).

6.4. Stability of human carbonic anhydrases

Fluorescence (of hCA bound DNSA) and CD studies have been used in conjugation with enzyme activity measurements to study the secondary and tertiary structural unfolding of hCA isozymes (hCA II and hCA XII) upon thermal and chemical denaturation. These studies gave rise to the following conclusions. (1) Where as significant loss of secondary structure is observed for hCA II after thermal denaturation, it remained intact for hCA XII. (2) The thermally denatured hCA XII neither catalyzed the CO_2 hydration reaction nor bound to DNSA despite retaining significant secondary structure (3) The T_m of hCA II increased with increase in the scan rate for thermal unfolding. However, it remained the same for hCA XII (4) Whereas the unfolding of hCA XII follows a simple

two state model from native to unfolded state, hCA II unfolded with the formation of stable intermediate.

It was apparent from the CD data of hCA II, (Figure 5.107) that heat induced unfolding of the protein results in loss of its secondary structure. It is a well known fact that upon chemical and thermal unfolding proteins undergoes a change in secondary structure which is usually reflected in their CD signal. Unlike many proteins, the CD spectra of native and thermally denatured hCA XII remained more or less similar suggesting the following possibilities. (1) The protein is thermally very stable and is not denatured upon heating. (2) The protein is denatured but the denaturation is reversible (3) The protein is denatured and the denatured protein retains native like secondary structure. Of these the first possibility is ruled out based on the fact that after heat treatment, the protein neither possessed the ability to catalyze the CO_2 hydration reaction nor bind DNSA. This suggested that the protein is indeed denatured. The second possibility is also ruled out due to the reason mentioned above. If the denaturation is reversible, the protein should behave identical in terms of its ability to catalyze its physiological reaction and should be able to bind DNSA giving rise to an increase in the quantum yield of the later. (3) The third possibility appeared feasible as the complete loss of tertiary structure would prevent the enzyme from interacting with its substrates and ligands. It can be envisioned from the previous chapters that a partial loss of tertiary structure need not necessarily affect the CO_2 hydration reaction although the DNSA signal is quenched. This is because the substrates of the enzyme (CO_2 and H_2O) are very small molecules and they make only a few direct contacts with the enzymes active site, such as the formation of the Zn^{2+}-bound hydroxide. Hence partial loss might still keep the enzyme active. On the other hand, the

partial loss could still result in quenching of the DNSA signal as this loss could be adequate to prevent binding of DNSA to hCA XII. This is because DNSA is much larger than CO_2 and H_2O and makes more extensive contacts with the enzyme. Any small change in the active site could cause a shift in the positions of the side chains of amino acids that would interact with DNSA precluding it from binding to the active site. Based on the above facts it was concluded that there is a complete loss of tertiary structure of hCA XII upon heating the sample.

Increasing the temperature of the protein sample causes rapid vibration of the protein molecules and as a result weakens the bonds that are responsible for maintaining the tertiary structure initially. This is followed by the disruption of the hydrogen bonds that stabilize the helical structure making the protein molecules more flexible and as a result the hydrophobic groups that are burried are now exposed leading to the intermolecular hydrophobic bonding causing aggregation of proteins (*119*, *442*, *568*). This aggregation was evident by the precipitate formation in the case of hCA II when heated. According to Eyring theory, the folded and the unfolded states are assumed to be in equilibrium through out the experiment (*569*). As enzyme precipitation would disrupt the equilibrium between the native and unfolded forms at higher temperatures, the measured T_m could not be taken as a true measure of the temperature where 50 % of the protein exists in folded and unfolded state. This is evident by the different T_m values exhibited by hCA II as the rate of heating is varied. The absence of protein precipitation during thermal denaturation is considered as one of the reasons for exhibiting similar T_m when the heating rate is varied for hCA XII.

The stability of a protein in the native state is only marginally favored as the energetic difference between the forces that favor the folded state and the forces that oppose the same is very small (*570-575, 553*). The strength and the nature of the interactions favoring or opposing the native folded state depend on the solvent in which it is present. This intricate balance between the interactions could easily be disturbed to favor the unfolded state by denaturants such as urea and GdmCl. GdmCl stabilizes the unfolded state by involving in hydrogen bonding interactions with the amide groups of the protein (*568*). In order to effectively compete with the binding sites occupied by water, a high concentration of denaturant is required. Urea is said to act as a chaotrophic agent disturbing the hydrogen bond interactions of the protein leading to its denaturation. Two mechanisms have been hypothesized for the above process. (1) urea disturbs the network of hydrogen bonds surrounding the hydrophobic side chains, thereby creating a polar environment around the nonpolar amino acids (2) Urea directly interacts with the protein by hydrogen bonding thereby disturbs the intramolecular hydrogen bonding. Although both Urea and GdmCl can denature the proteins, the later served as a better denaturant comparatively. This is evident by comparing the midpoint of transitions from native to denatured state in the unfolding induced by the above denaturants. Where as the midpoint of transition for urea induced unfolding (Figures 5.109A and 5.111A) occurs only at a urea concentration of 4 M, it occurs at 2 M for GdmCl (Figures 5.109B, 5.110, 5.111B). It is evident from the Figures 5.109 and 5.111, that the unfolding of hCA XII follows a smooth sigmoidal transiton from native to unfolded states upon increasing the denaturant concentration, where as it is complex in the case of hCA II. The CD data in Figure 5.110 shows that as the denaturant concentration is increased from 0-1 M, the negative ellipticity

decreases and then remains constant till a denaturation concentration of 2M. Further increase in denaturant concentration lead to progressive decrease in the negative ellipticity. This suggested that the unfolding of hCA II proceeded with the formation of an intermediate in contrast to hCA XII. Intermediate formation in the unfolding and refolding pathways of hCA II has been observed by many researchers (*119*, *424*, *429*, *431*). This intermediate named as a molten globule intermediate although retains native like secondary structures does not retain the tertiary structure and hence does not show any catalytic activity. This explains why the GdmCl induced unfolding of hCA II monitored by increasing the enzyme bound DNSA signal showed a simple sigmoidal transition (implying a two state transition from native to unfolded state) with out any intermediate formation in contrast to its secondary structure unfolding. Although this is the case, it can still be considered to unfold with the formation of an intermediate and that intermediate does not bind DNSA as its tertiary structure is lost.

In light of these facts it was concluded that the unfolding of hCA II proceeds with the formation of intermediate in contrast to hCA XII.

From the results section it is evident that whereas the temperature induced infolding of hCA isozymes is irreversible (*119*, *440*), the unfolding induced by chemical denaturants are reversible. This has been observed by many researchers for hCA (*119*, *442*, *576*, *577*). For the aggregated protein to refold, it is first required to break the intermolecular hydrophobic bonds which are energetically unfavorable and unlikely. On the other hand absence of aggregation in the later case helps them to refold rapidly once the concentration of denaturant is lowered.

REFERENCES

1. Bohr, C. (1909) Article in Nagel's Handbuch der Physiol 1, 54-222.
2. Buckmaster, G. A. (1917) On the capacity of blood and haemoglobin to unite with carbon dioxide, J. Physiol. (Lond.) 51, 164-175.
3. Buckmaster, G. A. (1917) The relations of carbon dioxide in the blood, J. Physiol. (Lond.) 51, 105-110.
4. Bayliss, S. W. M. (1915) Principles of general physiology. Longmans, Green, and co.
5. Mellanby, J., and Thomas, C. J. (1920) The carbon dioxide carrying power of the constituents of plasma. The alkali reserve of blood, J. Physiol. (Lond.) 54, 178-191.
6. Haldane, J. (1922) Respiration. Yale university press, New Haven.
7. Parsons, T. R. (1919) The reaction and carbon dioxide carrying power of blood-a mathematical treatment: Part I, J. Physiol. (Lond.) 53, 42-59.
8. Henderson, L. J. (1928) Blood. A Study in General Physiology. Newhaven.
9. Peters, J. P. and van Slyke, D. D. (1931) Carbonic Acid and Acid-Base Balance: Quantitative Interpretations Clinical Chemistry. Williams and Wilkins, London.
10. Dodgson, S. J. (1991) The Carbonic anhydrases: cellular physiology and molecular genetics. Springer.
11. Meldrum, N. U., and Roughton, F. J. (1933) Carbonic anhydrase. Its preparation and properties, J. Physiol. (Lond.) 80, 113-142.
12. Donald. D Van Slyke, and James A. Hawkins. (1930) Studies of gas and electrolyte equilibria in blood: xvi. the evolution of carbon dioxide from blood and buffer solutions, J. Biol. Chem. 87, 265-279.
13. Tashian, R.E., M. C., , G. S., and Scandalios, J. G. (1977) Evolution and regulation of

carbonic anhydrase isozymes in Isozymes: current topics in biological and medical research, Volume 2edited by Mario C. Rattazzi, Gregory S. Whitt, John G. Scandalios, p 184. Liss., in .

14. Fernley, R. T., Wright, R. D., and Coghlan, J. P. (1979) A novel carbonic anhydrase from the ovine parotid gland, *FEBS Lett 105*, 299-302.
15. Lindskog, S. (1997) Structure and mechanism of carbonic anhydrase, *Pharmacol. Ther 74*, 1-20.
16. Christianson, D. W., and Cox, J. D. (1999) Catalysis by metal-activated hydroxide in zinc and manganese metalloenzymes, *Annu. Rev. Biochem 68*, 33-57.
17. Mitsuhashi, S., Mizushima, T., Yamashita, E., Yamamoto, M., Kumasaka, T., Moriyama, H., Ueki, T., Miyachi, S., and Tsukihara, T. (2000) X-ray structure of beta-carbonic anhydrase from the red alga, Porphyridium purpureum, reveals a novel catalytic site for CO(2) hydration, *J. Biol. Chem 275*, 5521-5526.
18. Alber, B. E., and Ferry, J. G. (1994) A carbonic anhydrase from the archaeon Methanosarcina thermophila, *Proc. Natl. Acad. Sci. U.S.A 91*, 6909-6913.
19. Roberts, S. B., Lane, T. W., and Morel, F. M. M. (1997) Carbonic anhydrase in the marine diatom Thalassiosira Weisflogi (Bacillariophyceae), *J Phycol 33*, 845-850.
20. Supuran, C. T. (2008) Carbonic anhydrases: novel therapeutic applications for inhibitors and activators, *Nat Rev Drug Discov 7*, 168-181.
21. Supuran, C. T. (2008) Carbonic anhydrases--an overview, *Curr. Pharm. Des 14*, 603-614.
22. Chegwidden, W. R., Carter, N. D., and Edwards, Y. H. (2000) The carbonic anhydrases: new horizons. Birkhäuser.

23. Tashian, R. E. (1992) Genetics of the mammalian carbonic anhydrases, *Adv. Genet 30*, 321-356.

24. Khalifah, R. G. (1971) The carbon dioxide hydration activity of carbonic anhydrase. I. Stop-flow kinetic studies on the native human isoenzymes B and C, *J. Biol. Chem 246*, 2561-2573.

25. Ren, X., and Lindskog, S. (1992) Buffer dependence of CO2 hydration catalyzed by human carbonic anhydrase I, *Biochim. Biophys. Acta 1120*, 81-86.

26. Carter, N., Shiels, A., and Tashian, R. (1978) Carbonic anhydrase III isoenzyme from human and bovine muscle [proceedings], *Biochem. Soc. Trans* 552-553.

27. Holmes, R. S. (1977) Purification, molecular properties and ontogeny of carbonic anhydrase isozymes. Evidence for A, B and C isozymes in avian and mammalian tissues, *Eur. J. Biochem 78*, 511-520.

28. Tashian, R.E. , M. C., Hewell Emmettt, D., and Scandalios, J. G. (1977) Isozymes: current topics in biological and medical research, *Alan R. Lin. Inc, New York* 79-100.

29. Whitney, P. L., and Briggle, T. V. (1982) Membrane-associated carbonic anhydrase purified from bovine lung, *J. Biol. Chem 257*, 12056-12059.

30. Wistrand, P. J., and Knuuttila, K. G. (1989) Renal membrane-bound carbonic anhydrase. Purification and properties, *Kidney Int 35*, 851-859.

31. Zhu, X. L., and Sly, W. S. (1990) Carbonic anhydrase IV from human lung. Purification, characterization, and comparison with membrane carbonic anhydrase from human kidney, *J. Biol. Chem 265*, 8795-8801.

32. Baird, T. T., Waheed, A., Okuyama, T., Sly, W. S., and Fierke, C. A. (1997) Catalysis and inhibition of human carbonic anhydrase IV, *Biochemistry 36*, 2669-2678.

33. Dodgson, S. J., Forster, R. E., Storey, B. T., and Mela, L. (1980) Mitochondrial carbonic anhydrase, *Proc. Natl. Acad. Sci. U.S.A 77*, 5562-5566.

34. Shah, G. N., Hewett-Emmett, D., Grubb, J. H., Migas, M. C., Fleming, R. E., Waheed, A., and Sly, W. S. (2000) Mitochondrial carbonic anhydrase CA VB: differences in tissue distribution and pattern of evolution from those of CA VA suggest distinct physiological roles, *Proc. Natl. Acad. Sci. U.S.A 97*, 1677-1682.

35. Fujikawa-Adachi, K., Nishimori, I., Taguchi, T., and Onishi, S. (1999) Human mitochondrial carbonic anhydrase VB. cDNA cloning, mRNA expression, subcellular localization, and mapping to chromosome x, *J. Biol. Chem 274*, 21228-21233.

36. Nagao, Y., Platero, J. S., Waheed, A., and Sly, W. S. (1993) Human mitochondrial carbonic anhydrase: cDNA cloning, expression, subcellular localization, and mapping to chromosome, *Proc. Natl. Acad. Sci. U.S.A* 7623-7627.

37. Parkkila, A. K., Scarim, A. L., Parkkila, S., Waheed, A., Corbett, J. A., and Sly, W. S. (1998) Expression of carbonic anhydrase V in pancreatic beta cells suggests role for mitochondrial carbonic anhydrase in insulin secretion, *J. Biol. Chem 273*, 24620-24623.

38. Boriack-Sjodin, P. A., Heck, R. W., Laipis, P. J., Silverman, D. N., and Christianson, D. W. (1995) Structure determination of murine mitochondrial carbonic anhydrase V at 2.45-A resolution: implications for catalytic proton transfer and inhibitor design, *Proc. Natl. Acad. Sci. U.S.A 92*, 10949-10953.

39. Heck, R. W., Tanhauser, S. M., Manda, R., Tu, C., Laipis, P. J., and Silverman, D. N. (1994) Catalytic properties of mouse carbonic anhydrase V, *J. Biol. Chem 269*, 24742-24746.

40. Murakami, H., and Sly, W. S. (1987) Purification and characterization of human salivary carbonic anhydrase, *J. Biol. Chem 262*, 1382-1388.

41. Parkkila, S., Parkkila, A. K., Vierjoki, T., Ståhlberg, T., and Rajaniemi, H. (1993) Competitive time-resolved immunofluorometric assay for quantifying carbonic anhydrase VI in saliva, *Clin. Chem 39*, 2154-2157.

42. Sok, J., Wang, X. Z., Batchvarova, N., Kuroda, M., Harding, H., and Ron, D. (1999) CHOP-Dependent stress-inducible expression of a novel form of carbonic anhydrase VI, *Mol. Cell. Biol 19*, 495-504.

43. Montgomery, J. C., Venta, P. J., Eddy, R. L., Fukushima, Y. S., Shows, T. B., and Tashian, R. E. (1991) Characterization of the human gene for a newly discovered carbonic anhydrase, CA VII, and its localization to chromosome 16, *Genomics 11*, 835-848.

44. Earnhardt, J. N., Qian, M., Tu, C., Laipis, P. J., and Silverman, D. N. (1998) Intramolecular proton transfer from multiple sites in catalysis by murine carbonic anhydrase V, *Biochemistry 37*, 7649-7655.

45. Pastorek, J., Pastoreková, S., Callebaut, I., Mornon, J. P., Zelník, V., Opavský, R., Zat'ovicová, M., Liao, S., Portetelle, D., and Stanbridge, E. J. (1994) Cloning and characterization of MN, a human tumor-associated protein with a domain homologous to carbonic anhydrase and a putative helix-loop-helix DNA binding segment, *Oncogene 9*, 2877-2888.

46. Opavský, R., Pastoreková, S., Zelník, V., Gibadulinová, A., Stanbridge, E. J., Závada, J., Kettmann, R., and Pastorek, J. (1996) Human MN/CA9 gene, a novel member of the carbonic anhydrase family: structure and exon to protein domain relationships,

Genomics 33, 480-487.

47. Türeci, O., Sahin, U., Vollmar, E., Siemer, S., Göttert, E., Seitz, G., Parkkila, A. K., Shah, G. N., Grubb, J. H., Pfreundschuh, M., and Sly, W. S. (1998) Human carbonic anhydrase XII: cDNA cloning, expression, and chromosomal localization of a carbonic anhydrase gene that is overexpressed in some renal cell cancers, *Proc. Natl. Acad. Sci. U.S.A 95*, 7608-7613.

48. Ivanov, S. V., Kuzmin, I., Wei, M. H., Pack, S., Geil, L., Johnson, B. E., Stanbridge, E. J., and Lerman, M. I. (1998) Down-regulation of transmembrane carbonic anhydrases in renal cell carcinoma cell lines by wild-type von Hippel-Lindau transgenes, *Proc. Natl. Acad. Sci. U.S.A 95*, 12596-12601.

49. Whittington, D. A., Waheed, A., Ulmasov, B., Shah, G. N., Grubb, J. H., Sly, W. S., and Christianson, D. W. (2001) Crystal structure of the dimeric extracellular domain of human carbonic anhydrase XII, a bitopic membrane protein overexpressed in certain cancer tumor cells, *Proc. Natl. Acad. Sci. U.S.A 98*, 9545-9550.

50. Lehtonen, J., Shen, B., Vihinen, M., Casini, A., Scozzafava, A., Supuran, C. T., Parkkila, A., Saarnio, J., Kivelä, A. J., Waheed, A., Sly, W. S., and Parkkila, S. (2004) Characterization of CA XIII, a novel member of the carbonic anhydrase isozyme family, *J. Biol. Chem 279*, 2719-2727.

51. Mori, K., Ogawa, Y., Ebihara, K., Tamura, N., Tashiro, K., Kuwahara, T., Mukoyama, M., Sugawara, A., Ozaki, S., Tanaka, I., and Nakao, K. (1999) Isolation and characterization of CA XIV, a novel membrane-bound carbonic anhydrase from mouse kidney, *J. Biol. Chem 274*, 15701-15705.

52. Fujikawa-Adachi, K., Nishimori, I., Taguchi, T., and Onishi, S. (1999) Human

carbonic anhydrase XIV (CA14): cDNA cloning, mRNA expression, and mapping to chromosome 1, *Genomics 61*, 74-81.

53. Kaunisto, K., Parkkila, S., Rajaniemi, H., Waheed, A., Grubb, J., and Sly, W. S. (2002) Carbonic anhydrase XIV: luminal expression suggests key role in renal acidification, *Kidney Int 61*, 2111-2118.

54. Hilvo, M., Tolvanen, M., Clark, A., Shen, B., Shah, G. N., Waheed, A., Halmi, P., Hänninen, M., Hämäläinen, J. M., Vihinen, M., Sly, W. S., and Parkkila, S. (2005) Characterization of CA XV, a new GPI-anchored form of carbonic anhydrase, *Biochem. J 392*, 83-92.

55. Tashian, R. E., Hewett-Emmett, D., Carter, N., and Bergenhem, N. C. (2000) Carbonic anhydrase (CA)-related proteins (CA-RPs), and transmembrane proteins with CA or CA-RP domains, *EXS* 105-120.

56. Smith, K. S., and Ferry, J. G. (2000) Prokaryotic carbonic anhydrases, *FEMS Microbiol. Rev 24*, 335-366.

57. Strop, P., Smith, K. S., Iverson, T. M., Ferry, J. G., and Rees, D. C. (2001) Crystal structure of the "cab"-type beta class carbonic anhydrase from the archaeon Methanobacterium thermoautotrophicum, *J. Biol. Chem 276*, 10299-10305.

58. Cherniad'ev, I. I., Terekhova, I. V., Komarova, I. M., Doman, N. G., and Goronkova, O. I. (1975) [Role of carbonic anhydrase in photosynthesis], *Dokl. Akad. Nauk SSSR 223*, 501-503.

59. Cronk, J. D., Endrizzi, J. A., Cronk, M. R., O'neill, J. W., and Zhang, K. Y. (2001) Crystal structure of E. coli beta-carbonic anhydrase, an enzyme with an unusual pH-dependent activity, *Protein Sci 10*, 911-922.

60. Kimber, M. S., and Pai, E. F. (2000) The active site architecture of Pisum sativum beta-carbonic anhydrase is a mirror image of that of alpha-carbonic anhydrases, *EMBO J 19*, 1407-1418.

61. Cox, E. H., McLendon, G. L., Morel, F. M., Lane, T. W., Prince, R. C., Pickering, I. J., and George, G. N. (2000) The active site structure of Thalassiosira weissflogii carbonic anhydrase 1, *Biochemistry 39*, 12128-12130.

62. Smith, K. S., and Ferry, J. G. (1999) A plant-type (beta-class) carbonic anhydrase in the thermophilic methanoarchaeon Methanobacterium thermoautotrophicum, *J. Bacteriol 181*, 6247-6253.

63. Klengel, T., Liang, W., Chaloupka, J., Ruoff, C., Schröppel, K., Naglik, J. R., Eckert, S. E., Mogensen, E. G., Haynes, K., Tuite, M. F., Levin, L. R., Buck, J., and Mühlschlegel, F. A. (2005) Fungal adenylyl cyclase integrates CO2 sensing with cAMP signaling and virulence, *Curr. Biol 15*, 2021-2026.

64. Supuran CT., Scozzafava, A., Conway, J. Carbonic anhydrase - Its inhibitors and activators., *CRC Press, Boca Raton (FL).*

65. Supuran, C. T., Scozzafava, A., and Casini, A. (2003) Carbonic anhydrase inhibitors, *Med Res Rev 23*, 146-189.

66. Nishimori, I., Vullo, D., Innocenti, A., Scozzafava, A., Mastrolorenzo, A., and Supuran, C. T. (2005) Carbonic anhydrase inhibitors. The mitochondrial isozyme VB as a new target for sulfonamide and sulfamate inhibitors, *J. Med. Chem 48*, 7860-7866.

67. Nishimori, I., Minakuchi, T., Onishi, S., Vullo, D., Scozzafava, A., and Supuran, C. T. (2007) Carbonic anhydrase inhibitors. DNA cloning, characterization, and

inhibition studies of the human secretory isoform VI, a new target for sulfonamide and sulfamate inhibitors, *J. Med. Chem 50*, 381-388.

68. Vullo, D., Voipio, J., Innocenti, A., Rivera, C., Ranki, H., Scozzafava, A., Kaila, K., and Supuran, C. T. (2005) Carbonic anhydrase inhibitors. Inhibition of the human cytosolic isozyme VII with aromatic and heterocyclic sulfonamides, *Bioorg. Med. Chem. Lett 15*, 971-976.

69. Thiry, A., Dogné, J., Masereel, B., and Supuran, C. T. (2006) Targeting tumor-associated carbonic anhydrase IX in cancer therapy, *Trends Pharmacol. Sci 27*, 566-573.

70. Whittington, D. A., Grubb, J. H., Waheed, A., Shah, G. N., Sly, W. S., and Christianson, D. W. (2004) Expression, assay, and structure of the extracellular domain of murine carbonic anhydrase XIV: implications for selective inhibition of membrane-associated isozymes, *J. Biol. Chem 279*, 7223-7228.

71. Kisker, C., Schindelin, H., Alber, B. E., Ferry, J. G., and Rees, D. C. (1996) A left-hand beta-helix revealed by the crystal structure of a carbonic anhydrase from the archaeon Methanosarcina thermophila, *EMBO J 15*, 2323-2330.

72. Iverson, T. M., Alber, B. E., Kisker, C., Ferry, J. G., and Rees, D. C. (2000) A closer look at the active site of gamma-class carbonic anhydrases: high-resolution crystallographic studies of the carbonic anhydrase from Methanosarcina thermophila, *Biochemistry 39*, 9222-9231.

73. Innocenti, A., Zimmerman, S., Ferry, J. G., Scozzafava, A., and Supuran, C. T. (2004) Carbonic anhydrase inhibitors. Inhibition of the zinc and cobalt gamma-class enzyme from the archaeon Methanosarcina thermophila with anions, *Bioorg. Med.*

Chem. Lett 14, 3327-3331.

74. So, A. K., Espie, G. S., Williams, E. B., Shively, J. M., Heinhorst, S., and Cannon, G. C. (2004) A novel evolutionary lineage of carbonic anhydrase (epsilon class) is a component of the carboxysome shell, *J. Bacteriol 186*, 623-630.

75. Lindskog, S., and Silverman, D. N. (2000), in The Carbonic Anhydrases: New Horizons., Chegwidden, W. R., Carter, N. D., Edwards, Y. H., Eds., . Birkhauser Verlag , Basel, Switzerland.,, in .

76. Parkkila, S. (2000) An overview of the distribution and function of carbonic anhydrase in mammals, *EXS* 79-93.

77. Supuran CT., Scozzafava, A., Conway, J. Carbonic anhydrase - Its inhibitors and activators. CRC Press, Boca Raton (FL).

78. Penschow, J. D., Giles, M. E., Coghlan, J. P., and Fernley, R. T. (1997) Redistribution of carbonic anhydrase VI expression from ducts to acini during development of ovine parotid and submandibular glands, *Histochem. Cell Biol 107*, 417-422.

79. Parkkila, S., Parkkila, A. K., Juvonen, T., and Rajaniemi, H. (1994) Distribution of the carbonic anhydrase isoenzymes I, II, and VI in the human alimentary tract, *Gut 35*, 646-650.

80. Parkkila, S., Kaunisto, K., Rajaniemi, L., Kumpulainen, T., Jokinen, K., and Rajaniemi, H. (1990) Immunohistochemical localization of carbonic anhydrase isoenzymes VI, II, and I in human parotid and submandibular glands, *J. Histochem. Cytochem 38*, 941-947.

81. Kitade, K., Nishita, T., Yamato, M., Sakamoto, K., Hagino, A., Katoh, K., and Obara,

Y. (2003) Expression and localization of carbonic anhydrase in bovine mammary gland and secretion in milk, *Comp. Biochem. Physiol., Part A Mol. Integr. Physiol 134*, 349-354.

82. KELENTEY, B., FOLDES, I., LIPAK, J., KOCSAR, L., and CSONGOR, J. (1961) Carbonic anhydrase inhibition and changes in the permeability of the blood--brain--cerebrospinal fluid--aqueous barrier. Studies on the haematoencephalic barrier. VII, *Acta Physiol Acad Sci Hung 20*, 81-88.

83. Gray, W. D., Maren, T. H., Sisson, G. M., and Smith, F. H. (1957) Carbonic anhydrase inhibition. VII. Carbonic anhydrase inhibition and anticonvulsant effect, *J. Pharmacol. Exp. Ther 121*, 160-170.

84. Lakkis, M. M., O'Shea, K. S., and Tashian, R. E. (1997) Differential expression of the carbonic anhydrase genes for CA VII (Car7) and CA-RP VIII (Car8) in mouse brain, *J. Histochem. Cytochem 45*, 657-662.

85. Taniuchi, K., Nishimori, I., Takeuchi, T., Fujikawa-Adachi, K., Ohtsuki, Y., and Onishi, S. (2002) Developmental expression of carbonic anhydrase-related proteins VIII, X, and XI in the human brain, *Neuroscience 112*, 93-99.

86. Leppilampi, M., Saarnio, J., Karttunen, T. J., Kivelä, J., Pastoreková, S., Pastorek, J., Waheed, A., Sly, W. S., and Parkkila, S. (2003) Carbonic anhydrase isozymes IX and XII in gastric tumors, *World J. Gastroenterol 9*, 1398-1403.

87. Hynninen, P., Vaskivuo, L., Saarnio, J., Haapasalo, H., Kivelä, J., Pastoreková, S., Pastorek, J., Waheed, A., Sly, W. S., Puistola, U., and Parkkila, S. (2006) Expression of transmembrane carbonic anhydrases IX and XII in ovarian tumours, *Histopathology 49*, 594-602.

88. Klatte, T., Belldegrun, A. S., and Pantuck, A. J. (2008) The role of carbonic anhydrase IX as a molecular marker for transitional cell carcinoma of the bladder, *BJU Int 101 Suppl 4*, 45-48.

89. Swinson, D. E. B., Jones, J. L., Richardson, D., Wykoff, C., Turley, H., Pastorek, J., Taub, N., Harris, A. L., and O'Byrne, K. J. (2003) Carbonic anhydrase IX expression, a novel surrogate marker of tumor hypoxia, is associated with a poor prognosis in non-small-cell lung cancer, *J. Clin. Oncol 21*, 473-482.

90. Niemelä, A. M., Hynninen, P., Mecklin, J., Kuopio, T., Kokko, A., Aaltonen, L., Parkkila, A., Pastorekova, S., Pastorek, J., Waheed, A., Sly, W. S., Orntoft, T. F., Kruhøffer, M., Haapasalo, H., Parkkila, S., and Kivelä, A. J. (2007) Carbonic anhydrase IX is highly expressed in hereditary nonpolyposis colorectal cancer, *Cancer Epidemiol. Biomarkers Prev 16*, 1760-1766.

91. Beasley, N. J., Wykoff, C. C., Watson, P. H., Leek, R., Turley, H., Gatter, K., Pastorek, J., Cox, G. J., Ratcliffe, P., and Harris, A. L. (2001) Carbonic anhydrase IX, an endogenous hypoxia marker, expression in head and neck squamous cell carcinoma and its relationship to hypoxia, necrosis, and microvessel density, *Cancer Res 61*, 5262-5267.

92. Pastoreková, S., Parkkila, S., Parkkila, A. K., Opavský, R., Zelník, V., Saarnio, J., and Pastorek, J. (1997) Carbonic anhydrase IX, MN/CA IX: analysis of stomach complementary DNA sequence and expression in human and rat alimentary tracts, *Gastroenterology 112*, 398-408.

93. Winum, J., Rami, M., Scozzafava, A., Montero, J., and Supuran, C. (2008) Carbonic anhydrase IX: a new druggable target for the design of antitumor agents, *Med Res*

Rev 28, 445-463.

94. Kivela, A., Parkkila, S., Saarnio, J., Karttunen, T., Kivela, J., Parkkila, A., Bartosova, M., Mucha, V., Novak, M., Waheed, A., Sly, W., Rajaniemi, H., Pastorekova, S., and Pastorek, J. (2005) Expression of von Hippel-Lindau tumor suppressor and tumor-associated carbonic anhydrases IX and XII in normal and neoplastic colorectal mucosa, *World J. Gastroenterol 11*, 2616-2625.
95. Watson, P. H., Chia, S. K., Wykoff, C. C., Han, C., Leek, R. D., Sly, W. S., Gatter, K. C., Ratcliffe, P., and Harris, A. L. (2003) Carbonic anhydrase XII is a marker of good prognosis in invasive breast carcinoma, *Br. J. Cancer 88*, 1065-1070.
96. Potter, C. P. S., and Harris, A. L. (2003) Diagnostic, prognostic and therapeutic implications of carbonic anhydrases in cancer, *Br. J. Cancer 89*, 2-7.
97. Supuran, C. T. (2007) Carbonic anhydrases as drug targets--an overview, *Curr Top Med Chem 7*, 825-833.
98. Hilvo, M., Innocenti, A., Monti, S. M., De Simone, G., Supuran, C. T., and Parkkila, S. (2008) Recent advances in research on the most novel carbonic anhydrases, CA XIII and XV, *Curr. Pharm. Des 14*, 672-678.
99. Kummola, L., Hämäläinen, J. M., Kivelä, J., Kivelä, A. J., Saarnio, J., Karttunen, T., and Parkkila, S. (2005) Expression of a novel carbonic anhydrase, CA XIII, in normal and neoplastic colorectal mucosa, *BMC Cancer 5*, 41.
100. Henry, R. P., and Swenson, E. R. (2000) The distribution and physiological significance of carbonic anhydrase in vertebrate gas exchange organs, *Respir Physiol 121*, 1-12.
101. Edsall, J.T. (1968) Carbon dioxide, carbonic acid, and the bicarbonate ion: Physical

properties and kinetics of interconversion, in CO2: Chemical, Biochemical, and Physiological Aspects Forster, R.E., Edsall, J.T., Otis, A.B., Roughton, F.J.W. (Eds.),, pp 15-28. Washington, DC., in ., in .

102. Stadie, W. C., and O'Brien, H. (1933) The catalysis of hydration by carbondioxide and dehydration of carbonic acid by an enzyme isolated from red blood cells, *Journal of Biological Chemistry 103*, 521 -529.

103. Esbaugh, A. J., and Tufts, B. L. (2006) The structure and function of carbonic anhydrase isozymes in the respiratory system of vertebrates, *Respir Physiol Neurobiol 154*, 185-198.

104. Swenson, E.R. (2000) Respiratory and renal roles of carbonic anhydrase in gas exchange and acid base regulation., in The Carboic Anhydrases: New Horizons Chegwidden, W.R., Carter, N.D., Edwards, Y.H. (Eds.), pp 281–342. Birkhauser Verlag, , Boston, in .

105. Christiansen, J., Douglas, C. G., and Haldane, J. S. (1914) The absorption and dissociation of carbon dioxide by human blood, *J. Physiol. (Lond.) 48*, 244-271.

106. Geers, C., and Gros, G. (2000) Carbon dioxide transport and carbonic anhydrase in blood and muscle, *Physiol. Rev 80*, 681-715.

107. Chegwidden, W.R., and Carter, N.D. (2000) Introduction to the carbonic anhydrases., in The Carbonic Anhydrases: New Horizons Chegwidden, W.R., Carter, N.D., Edwards, Y.H. (Eds.), pp 13–28. Birkhauser Verlag Basel, Boston, in .

108. Effros, R. M., Chang, R. S., and Silverman, P. (1978) Acceleration of plasma bicarbonate conversion to carbon dioxide by pulmonary carbonic anhydrase, *Science 199*, 427-429.

109. Cameron, J. N., and Wood, C. M. (1985) Apparent H+ Excretion and CO2 Dynamics Accompanying Carapace Mineralization in the Blue Crab (Callinectes Sapidus) Following Moulting, *J Exp Biol 114*, 181-196.

110. Goreau, T. F. (1959) The physiology of skeleton formation in corals. I. A method for measuring the rate of calcium deposition by corals under different conditions., *Biol Bull 116*, 59-75.

111. Henry, R. P. (1984) The function of invertebrate carbonic anhydrase in ion transport, *Ann. N. Y. Acad. Sci 429*, 544-546.

112. Kingsley, R. J., and Watabe, N. (1987) Role of carbonic anhydrase in calcification in the gorgonianLeptogorgia virgulata, *J. Exp. Zool. 241*, 171-180.

113. Lucas, J. M., and Knapp, L. W. (1997) A physiological evaluation of carbon sources for calcification in the octocoral Leptogorgia virgulata (Lamarck), *J. Exp. Biol 200*, 2653-2662.

114. Gay, C. V., Anderson, R. E., Schraer, H., and Howell, D. S. (1982) Identification of carbonic anhydrase in chick growth-plate cartilage, *J. Histochem. Cytochem 30*, 391-394.

115. Väänänen, H. K. (1984) Immunohistochemical localization of carbonic anhydrase isoenzymes I and II in human bone, cartilage and giant cell tumor, *Histochemistry 81*, 485-487.

116. Marie, P. J., and Hott, M. (1987) Histomorphometric identification of carbonic anhydrase in fetal rat bone embedded in glycolmethacrylate, *J. Histochem. Cytochem 35*, 245-250.

117. Vaananen, H. K., and Parvinen, E. K. Localization of carbonic anhydrase Isozymes

in calcified tissues, in The carbonic anhydrases, Cellular physiology and molecular genetics Dodgson, S. J., Tashian, R. E., Gros, G., and Carter, N. D. Plenum press, Newyork and London., in .

118. Wistrand, P. J., Schenholm, M., and Lönnerholm, G. (1986) Carbonic anhydrase isoenzymes CA I and CA II in the human eye, *Invest. Ophthalmol. Vis. Sci 27*, 419-428.

119. Krishnamurthy, V. M., Kaufman, G. K., Urbach, A. R., Gitlin, I., Gudiksen, K. L., Weibel, D. B., and Whitesides, G. M. (2008) Carbonic anhydrase as a model for biophysical and physical-organic studies of proteins and protein-ligand binding, *Chem. Rev 108*, 946-1051.

120. Alward, W. L. (1998) Medical management of glaucoma, *N. Engl. J. Med 339*, 1298-1307.

121. Maren, T. H., Conroy, C. W., Wynns, G. C., and Godman, D. R. (1997) Renal and cerebrospinal fluid formation pharmacology of a high molecular weight carbonic anhydrase inhibitor, *J. Pharmacol. Exp. Ther 280*, 98-104.

122. Sun, M., and Alkon, D. L. (2002) Carbonic anhydrase gating of attention: memory therapy and enhancement, *Trends Pharmacol. Sci 23*, 83-89.

123. Sun, M. K., and Alkon, D. L. (2001) Pharmacological enhancement of synaptic efficacy, spatial learning, and memory through carbonic anhydrase activation in rats, *J. Pharmacol. Exp. Ther 297*, 961-967.

124. Parkkila, S., and Parkkila, A. K. (1996) Carbonic anhydrase in the alimentary tract. Roles of the different isozymes and salivary factors in the maintenance of optimal conditions in the gastrointestinal canal, *Scand. J. Gastroenterol 31*, 305-317.

125. Parkkila, S., Parkkila, A. K., Lehtola, J., Reinilä, A., Södervik, H. J., Rannisto, M., and Rajaniemi, H. (1997) Salivary carbonic anhydrase protects gastroesophageal mucosa from acid injury, *Dig. Dis. Sci 42*, 1013-1019.

126. Dodgson, S. J., and Forster, R. E. (1986) Inhibition of CA V decreases glucose synthesis from pyruvate, *Arch. Biochem. Biophys 251*, 198-204.

127. Dodgson, S. J., and Forster, R. E. (1986) Carbonic anhydrase: inhibition results in decreased urea production by hepatocytes, *J. Appl. Physiol 60*, 646-652.

128. Lynch, C. J., Fox, H., Hazen, S. A., Stanley, B. A., Dodgson, S., and Lanoue, K. F. (1995) Role of hepatic carbonic anhydrase in de novo lipogenesis, *Biochem. J 310 (Pt 1)*, 197-202.

129. Splendiani, G., and Condò, S. (2006) [Diuretic therapy in heart failure], *G Ital Nefrol 23 Suppl 34*, S74-76.

130. Kyllönen, M. S., Parkkila, S., Rajaniemi, H., Waheed, A., Grubb, J. H., Shah, G. N., Sly, W. S., and Kaunisto, K. (2003) Localization of carbonic anhydrase XII to the basolateral membrane of H+-secreting cells of mouse and rat kidney, *J. Histochem. Cytochem 51*, 1217-1224.

131. Mincione, F., Scozzafava, A., and Supuran, C. T. (2007) The development of topically acting carbonic anhydrase inhibitors as anti-glaucoma agents, *Curr Top Med Chem 7*, 849-854.

132. Sugrue, M. F. (2000) Pharmacological and ocular hypotensive properties of topical carbonic anhydrase inhibitors, *Prog Retin Eye Res 19*, 87-112.

133. Scozzafava, A., Menabuoni, L., Mincione, F., Briganti, F., Mincione, G., and Supuran, C. T. (1999) Carbonic anhydrase inhibitors. Synthesis of water-soluble,

topically effective, intraocular pressure-lowering aromatic/heterocyclic sulfonamides containing cationic or anionic moieties: is the tail more important than the ring?, *J. Med. Chem 42*, 2641-2650.

134. Scozzafava, A., Briganti, F., Mincione, G., Menabuoni, L., Mincione, F., and Supuran, C. T. (1999) Carbonic anhydrase inhibitors: synthesis of water-soluble, aminoacyl/dipeptidyl sulfonamides possessing long-lasting intraocular pressure-lowering properties via the topical route, *J. Med. Chem 42*, 3690-3700.
135. Ilies, M., Supuran, C. T., Scozzafava, A., Casini, A., Mincione, F., Menabuoni, L., Caproiu, M. T., Maganu, M., and Banciu, M. D. (2000) Carbonic anhydrase inhibitors: sulfonamides incorporating furan-, thiophene- and pyrrole-carboxamido groups possess strong topical intraocular pressure lowering properties as aqueous suspensions, *Bioorg. Med. Chem 8*, 2145-2155.
136. Scozzafava, A., Menabuoni, L., Mincione, F., Briganti, F., Mincione, G., and Supuran, C. T. (2000) Carbonic anhydrase inhibitors: perfluoroalkyl/aryl-substituted derivatives of aromatic/heterocyclic sulfonamides as topical intraocular pressure-lowering agents with prolonged duration of action, *J. Med. Chem 43*, 4542-4551.
137. Scozzafava, A., Menabuoni, L., Mincione, F., and Supuran, C. T. (2002) Carbonic anhydrase inhibitors. A general approach for the preparation of water-soluble sulfonamides incorporating polyamino-polycarboxylate tails and of their metal complexes possessing long-lasting, topical intraocular pressure-lowering properties, *J. Med. Chem 45*, 1466-1476.
138. Winum, J., Casini, A., Mincione, F., Starnotti, M., Montero, J., Scozzafava, A., and Supuran, C. T. (2004) Carbonic anhydrase inhibitors: N-(p-sulfamoylphenyl)-alpha-

D-glycopyranosylamines as topically acting antiglaucoma agents in hypertensive rabbits, *Bioorg. Med. Chem. Lett 14*, 225-229.

139. Gao, B., Clermont, A., Rook, S., Fonda, S. J., Srinivasan, V. J., Wojtkowski, M., Fujimoto, J. G., Avery, R. L., Arrigg, P. G., Bursell, S., Aiello, L. P., and Feener, E. P. (2007) Extracellular carbonic anhydrase mediates hemorrhagic retinal and cerebral vascular permeability through prekallikrein activation, *Nat. Med 13*, 181-188.
140. Cox, S. N., Hay, E., and Bird, A. C. (1988) Treatment of chronic macular edema with acetazolamide, *Arch. Ophthalmol 106*, 1190-1195.
141. Supuran, C. T., Di Fiore, A., and De Simone, G. (2008) Carbonic anhydrase inhibitors as emerging drugs for the treatment of obesity, *Expert Opin Emerg Drugs 13*, 383-392.
142. Supuran, C. T. (2003) Carbonic anhydrase inhibitors in the treatment and prophylaxis of obesity, *Expert Opin. Ther. Patents 13*, 1545-1550.
143. De Simone, G., and Supuran, C. T. (2007) Antiobesity carbonic anhydrase inhibitors, *Curr Top Med Chem 7*, 879-884.
144. Riihonen, R., Supuran, C. T., Parkkila, S., Pastorekova, S., Väänänen, H. K., and Laitala-Leinonen, T. (2007) Membrane-bound carbonic anhydrases in osteoclasts, *Bone 40*, 1021-1031.
145. Kenny, A. D. (1991) Role of carbonic anhydrase in bone, *SAAS Bull. Biochem. Biotech. 4*, 6-12.
146. Hsieh, M., Chen, K., Chiou, H., and Hsieh, Y. (2010) Carbonic anhydrase XII promotes invasion and migration ability of MDA-MB-231 breast cancer cells through the p38 MAPK signaling pathway, *Eur. J. Cell Biol 89*, 598-606.

147. Proescholdt, M. A., Mayer, C., Kubitza, M., Schubert, T., Liao, S., Stanbridge, E. J., Ivanov, S., Oldfield, E. H., Brawanski, A., and Merrill, M. J. (2005) Expression of hypoxia-inducible carbonic anhydrases in brain tumors, *Neuro-oncology 7*, 465-475.

148. Pastorekov, S., and Vada, J. Z. (2004) Carbonic anhydrase IX (CA IX) as a potential target for cancer therapy, *Cancer Therapy 2*, 245-262.

149. Pastorekova, S., Zatovicova, M., and Pastorek, J. (2008) Cancer-associated carbonic anhydrases and their inhibition, *Curr. Pharm. Des 14*, 685-698.

150. Dorai, T., Sawczuk, I., Pastorek, J., Wiernik, P. H., and Dutcher, J. P. (2006) Role of carbonic anhydrases in the progression of renal cell carcinoma subtypes: proposal of a unified hypothesis, *Cancer Invest 24*, 754-779.

151. Ord, J. J., Agrawal, S., Thamboo, T. P., Roberts, I., Campo, L., Turley, H., Han, C., Fawcett, D. W., Kulkarni, R. P., Cranston, D., and Harris, A. L. (2007) An investigation into the prognostic significance of necrosis and hypoxia in high grade and invasive bladder cancer, *J. Urol 178*, 677-682.

152. Swietach, P., Vaughan-Jones, R. D., and Harris, A. L. (2007) Regulation of tumor pH and the role of carbonic anhydrase 9, *Cancer Metastasis Rev 26*, 299-310.

153. Hutchison, G. J., Valentine, H. R., Loncaster, J. A., Davidson, S. E., Hunter, R. D., Roberts, S. A., Harris, A. L., Stratford, I. J., Price, P. M., and West, C. M. L. (2004) Hypoxia-inducible factor 1alpha expression as an intrinsic marker of hypoxia: correlation with tumor oxygen, pimonidazole measurements, and outcome in locally advanced carcinoma of the cervix, *Clin. Cancer Res 10*, 8405-8412.

154. Trastour, C., Benizri, E., Ettore, F., Ramaioli, A., Chamorey, E., Pouysségur, J., and Berra, E. (2007) HIF-1alpha and CA IX staining in invasive breast carcinomas:

prognosis and treatment outcome, *Int. J. Cancer 120*, 1451-1458.

155. Koukourakis, M. I., Giatromanolaki, A., Sivridis, E., Pastorek, J., Karapantzos, I., Gatter, K. C., and Harris, A. L. (2004) Hypoxia-activated tumor pathways of angiogenesis and pH regulation independent of anemia in head-and-neck cancer, *Int. J. Radiat. Oncol. Biol. Phys 59*, 67-71.

156. Hussain, S. A., Ganesan, R., Reynolds, G., Gross, L., Stevens, A., Pastorek, J., Murray, P. G., Perunovic, B., Anwar, M. S., Billingham, L., James, N. D., Spooner, D., Poole, C. J., Rea, D. W., and Palmer, D. H. (2007) Hypoxia-regulated carbonic anhydrase IX expression is associated with poor survival in patients with invasive breast cancer, *Br. J. Cancer 96*, 104-109.

157. Maxwell, P. H., Wiesener, M. S., Chang, G. W., Clifford, S. C., Vaux, E. C., Cockman, M. E., Wykoff, C. C., Pugh, C. W., Maher, E. R., and Ratcliffe, P. J. (1999) The tumour suppressor protein VHL targets hypoxia-inducible factors for oxygen-dependent proteolysis, *Nature 399*, 271-275.

158. Semenza, G. L. (2007) Hypoxia and cancer, *Cancer Metastasis Rev 26*, 223-224.

159. Pouysségur, J., Dayan, F., and Mazure, N. M. (2006) Hypoxia signalling in cancer and approaches to enforce tumour regression, *Nature 441*, 437-443.

160. Brahimi-Horn, M. C., and Pouysségur, J. (2007) Oxygen, a source of life and stress, *FEBS Lett 581*, 3582-3591.

161. Jaakkola, P., Mole, D. R., Tian, Y. M., Wilson, M. I., Gielbert, J., Gaskell, S. J., Kriegsheim Av, Hebestreit, H. F., Mukherji, M., Schofield, C. J., Maxwell, P. H., Pugh, C. W., and Ratcliffe, P. J. (2001) Targeting of HIF-alpha to the von Hippel-Lindau ubiquitylation complex by O2-regulated prolyl hydroxylation, *Science 292*,

468-472.

162. Hon, W., Wilson, M. I., Harlos, K., Claridge, T. D. W., Schofield, C. J., Pugh, C. W., Maxwell, P. H., Ratcliffe, P. J., Stuart, D. I., and Jones, E. Y. (2002) Structural basis for the recognition of hydroxyproline in HIF-1 alpha by pVHL, *Nature 417*, 975-978.

163. Ratcliffe, P. J., Pugh, C. W., and Maxwell, P. H. (2000) Targeting tumors through the HIF system, *Nat. Med 6*, 1315-1316.

164. Svastová, E., Hulíková, A., Rafajová, M., Zat'ovicová, M., Gibadulinová, A., Casini, A., Cecchi, A., Scozzafava, A., Supuran, C. T., Pastorek, J., and Pastoreková, S. (2004) Hypoxia activates the capacity of tumor-associated carbonic anhydrase IX to acidify extracellular pH, *FEBS Lett 577*, 439-445.

165. Pastorekova, S. & Pastorek, J. (2004), in Carbonic Anhydrase — Its Inhibitors and Activators(eds Supuran, C. T., Scozzafava, A. & Conway, J.), pp 255–281. CRC, Boca Raton., in .

166. Dubois, L., Douma, K., Supuran, C. T., Chiu, R. K., van Zandvoort, M. A. M. J., Pastoreková, S., Scozzafava, A., Wouters, B. G., and Lambin, P. (2007) Imaging the hypoxia surrogate marker CA IX requires expression and catalytic activity for binding fluorescent sulfonamide inhibitors, *Radiother Oncol 83*, 367-373.

167. Takacova, M., Barathova, M., Hulikova, A., Ohradanova, A., Kopacek, J., Parkkila, S., Pastorek, J., Pastorekova, S., and Zatovicova, M. (2007) Hypoxia-inducible expression of the mouse carbonic anhydrase IX demonstrated by new monoclonal antibodies, *Int. J. Oncol 31*, 1103-1110.

168. Pastorekova, S., Ratcliffe, P. J., and Pastorek, J. (2008) Molecular mechanisms of carbonic anhydrase IX-mediated pH regulation under hypoxia, *BJU Int 101 Suppl 4*,

8-15.

169. Innocenti, A., Vullo, D., Scozzafava, A., Casey, J. R., and Supuran, C. (2005) Carbonic anhydrase inhibitors. Interaction of isozymes I, II, IV, V, and IX with carboxylates, *Bioorg. Med. Chem. Lett 15*, 573-578.

170. Vince, J. W., and Reithmeier, R. A. (1998) Carbonic anhydrase II binds to the carboxyl terminus of human band 3, the erythrocyte C1-/HCO3- exchanger, *J. Biol. Chem 273*, 28430-28437.

171. Raghunand, N., Gatenby, R. A., and Gillies, R. J. (2003) Microenvironmental and cellular consequences of altered blood flow in tumours, *Br J Radiol 76 Spec No 1*, S11-22.

172. Puscas, I., Coltau, M., Maghiar, A., and Domuta, G. (2000) Cysteamine, the most potent ulcerogenic drug known so far, powerfully activates carbonic anhydrase I, II and IV. In vitro and in vivo studies, *Exp. Toxicol. Pathol 52*, 431-435.

173. Eriksson, A. E., Jones, T. A., and Liljas, A. (1988) Refined structure of human carbonic anhydrase II at 2.0 A resolution, *Proteins 4*, 274-282.

174. Håkansson, K., Carlsson, M., Svensson, L. A., and Liljas, A. (1992) Structure of native and apo carbonic anhydrase II and structure of some of its anion-ligand complexes, *J. Mol. Biol 227*, 1192-1204.

175. Pettersen, E. F., Goddard, T. D., Huang, C. C., Couch, G. S., Greenblatt, D. M., Meng, E. C., and Ferrin, T. E. (2004) UCSF Chimera--a visualization system for exploratory research and analysis, *J Comput Chem 25*, 1605-1612.

176. Kiefer, L. L., Paterno, S. A., and Fierke, C. A. (1995) Hydrogen bond network in the metal binding site of carbonic anhydrase enhances zinc affinity and catalytic

efficiency, *Journal of the American Chemical Society 117*, 6831-6837.

177. Krebs, J. F., Ippolito, J. A., Christianson, D. W., and Fierke, C. A. (1993) Structural and functional importance of a conserved hydrogen bond network in human carbonic anhydrase II, *J. Biol. Chem 268*, 27458-27466.

178. Lesburg, C. A., and Christianson, D. W. (1995) X-ray crystallographic studies of engineered hydrogen bond networks in a protein-zinc binding site, *Journal of the American Chemical Society 117*, 6838-6844.

179. Nair, S. K., and Christianson, D. W. (1991) Unexpected pH-dependent conformation of His-64, the proton shuttle of carbonic anhydrase II, *Journal of the American Chemical Society 113*, 9455-9458.

180. Krebs, J. F., Fierke, C. A., Alexander, R. S., and Christianson, D. W. (1991) Conformational mobility of His-64 in the Thr-200----Ser mutant of human carbonic anhydrase II, *Biochemistry 30*, 9153-9160.

181. Scolnick, L. R., and Christianson, D. W. (1996) X-ray crystallographic studies of alanine-65 variants of carbonic anhydrase II reveal the structural basis of compromised proton transfer in catalysis, *Biochemistry 35*, 16429-16434.

182. Eriksson, A. E., Kylsten, P. M., Jones, T. A., and Liljas, A. (1988) Crystallographic studies of inhibitor binding sites in human carbonic anhydrase II: a pentacoordinated binding of the SCN- ion to the zinc at high pH, *Proteins 4*, 283-293.

183. Liang, J. Y., and Lipscomb, W. N. (1990) Binding of substrate CO2 to the active site of human carbonic anhydrase II: a molecular dynamics study, *Proc. Natl. Acad. Sci. U.S.A 87*, 3675-3679.

184. Boriack, P. A., Christianson, D. W., Kingery-Wood, J., and Whitesides, G. M. (1995)

Secondary interactions significantly removed from the sulfonamide binding pocket of carbonic anhydrase II influence inhibitor binding constants, *J. Med. Chem 38*, 2286-2291.

185. Christianson, D. W., and Fierke, C. A. Carbonic anhydrase: evolution of the zinc binding site by nature and by design. Text.

186. Stein, P. J., Merrill, S. P., and Henkens, R. W. (1977) Carbon-13 nuclear magnetic relaxation study on cobalt carbonic anhydrase: evidence on the location of enzyme bound carbon dioxide and bicarbonate(1-) ion, *Journal of the American Chemical Society 99*, 3194-3196.

187. Williams, T. J., and Henkens, R. W. (1985) Dynamic 13C NMR investigations of substrate interaction and catalysis by cobalt(II) human carbonic anhydrase I, *Biochemistry 24*, 2459-2462.

188. Håkansson, K., and Wehnert, A. (1992) Structure of cobalt carbonic anhydrase complexed with bicarbonate, *J. Mol. Biol 228*, 1212-1218.

189. Kumar, V., and Kannan, K. K. (1994) Enzyme-substrate interactions. Structure of human carbonic anhydrase I complexed with bicarbonate, *J. Mol. Biol 241*, 226-232.

190. Lindahl, M., Svensson, L. A., and Liljas, A. (1993) Metal poison inhibition of carbonic anhydrase, *Proteins 15*, 177-182.

191. Jain, A., Whitesides, G. M., Alexander, R. S., and Christianson, D. W. (1994) Identification of two hydrophobic patches in the active-site cavity of human carbonic anhydrase II by solution-phase and solid-state studies and their use in the development of tight-binding inhibitors, *J. Med. Chem 37*, 2100-2105.

192. Nair, S. K., Elbaum, D., and Christianson, D. W. (1996) Unexpected binding mode of

the sulfonamide fluorophore 5-dimethylamino-1-naphthalene sulfonamide to human carbonic anhydrase II. Implications for the development of a zinc biosensor, *J. Biol. Chem 271*, 1003-1007.

193. Fisher, Z., Hernandez Prada, J. A., Tu, C., Duda, D., Yoshioka, C., An, H., Govindasamy, L., Silverman, D. N., and McKenna, R. (2005) Structural and kinetic characterization of active-site histidine as a proton shuttle in catalysis by human carbonic anhydrase II, *Biochemistry 44*, 1097-1105.
194. Silverman, D. N., and Lindskog, S. (1988) The catalytic mechanism of carbonic anhydrase: implications of a rate-limiting protolysis of water, *Accounts of Chemical Research 21*, 30-36.
195. Kernohan, J. (1964) The activity of bovine carbonic anhydrase in imidazole buffers, *Biochimica et Biophysica Acta (BBA) - Specialized Section on Enzymological Subjects 81*, 346-356.
196. Coleman, J. E. (1967) Mechanism of action of carbonic anhydrase. Subtrate, sulfonamide, and anion binding, *J. Biol. Chem 242*, 5212-5219.
197. Liang, Z., Xue, Y., Behravan, G., Jonsson, B. H., and Lindskog, S. (1993) Importance of the conserved active-site residues Tyr7, Glu106 and Thr199 for the catalytic function of human carbonic anhydrase II, *Eur. J. Biochem 211*, 821-827.
198. Kiefer, L. L., and Fierke, C. A. (1994) Functional characterization of human carbonic anhydrase II variants with altered zinc binding sites, *Biochemistry 33*, 15233-15240.
199. Kernohan, J. C. (1965) The pH -activity curve of bovine carbonic anhydrase and its relationship to the inhibition of the enzyme by anions, *Biochim. Biophys. Acta 96*, 304-317.

200. Lindskog, S. (1966) Interaction of cobalt(II)--carbonic anhydrase with anions, *Biochemistry 5*, 2641-2646.

201. Lindskog, S., and Thorslund, A. (1968) On the interaction of bovine cobalt carbonic anhydrase with sulfonamides, *Eur. J. Biochem 3*, 453-460.

202. Taylor, P. W., King, R. W., and Burgen, A. S. (1970) Influence of pH on the kinetics of complex formation between aromatic sulfonamides and human carbonic anhydrase, *Biochemistry 9*, 3894-3902.

203. Kannan, K. K., Ramanadham, M., and Jones, T. A. (1984) Structure, refinement, and function of carbonic anhydrase isozymes: refinement of human carbonic anhydrase I, *Ann. N. Y. Acad. Sci 429*, 49-60.

204. Kannan, K. K., Notstrand, B., Fridborg, K., Lövgren, S., Ohlsson, A., and Petef, M. (1975) Crystal structure of human erythrocyte carbonic anhydrase B. Three-dimensional structure at a nominal 2.2-A resolution, *Proc. Natl. Acad. Sci. U.S.A 72*, 51-55.

205. Kannan, K. K., Petef, M., Fridborg, K., Cid-Dresdner, H., and Lövgren, S. (1977) Structure and function of carbonic anhydrases. Imidazole binding to human carbonic anhydrase B and the mechanism of action of carbonic anhydrases, *FEBS Lett 73*, 115-119.

206. SHAW, C. R., SYNER, F. N., and TASHIAN, R. E. (1962) New genetically determined molecular form of erythrocyte esterase in man, *Science 138*, 31-32.

207. Chegwidden, W. R., Wagner, L. E., Venta, P. J., Bergenhem, N. C., Yu, Y. S., and Tashian, R. E. (1994) Marked zinc activation of ester hydrolysis by a mutation, 67-His (CAT) to Arg (CGT), in the active site of human carbonic anhydrase I, *Hum.*

Mutat 4, 294-296.

208. Ferraroni, M., Tilli, S., Briganti, F., Chegwidden, W. R., Supuran, C. T., Wiebauer, K. E., Tashian, R. E., and Scozzafava, A. (2002) Crystal structure of a zinc-activated variant of human carbonic anhydrase I, CA I Michigan 1: evidence for a second zinc binding site involving arginine coordination, *Biochemistry 41*, 6237-6244.
209. Eriksson, A. E., and Liljas, A. (1993) Refined structure of bovine carbonic anhydrase III at 2.0 A resolution, *Proteins 16*, 29-42.
210. Duda, D. M., Tu, C., Fisher, S. Z., An, H., Yoshioka, C., Govindasamy, L., Laipis, P. J., Agbandje-McKenna, M., Silverman, D. N., and McKenna, R. (2005) Human carbonic anhydrase III: structural and kinetic study of catalysis and proton transfer, *Biochemistry 44*, 10046-10053.
211. Waheed, A., Okuyama, T., Heyduk, T., and Sly, W. S. (1996) Carbonic anhydrase IV: purification of a secretory form of the recombinant human enzyme and identification of the positions and importance of its disulfide bonds, *Arch. Biochem. Biophys 333*, 432-438.
212. Stams, T., Nair, S. K., Okuyama, T., Waheed, A., Sly, W. S., and Christianson, D. W. (1996) Crystal structure of the secretory form of membrane-associated human carbonic anhydrase IV at 2.8-A resolution, *Proc. Natl. Acad. Sci. U.S.A 93*, 13589-13594.
213. Krebs, J. F., Rana, F., Dluhy, R. A., and Fierke, C. A. (1993) Kinetic and spectroscopic studies of hydrophilic amino acid substitutions in the hydrophobic pocket of human carbonic anhydrase II, *Biochemistry 32*, 4496-4505.
214. Nair, S. K., Ludwig, P. A., and Christianson, D. W. (1994) Two-Site Binding of

Phenol in the Active Site of Human Carbonic Anhydrase II: Structural Implications for Substrate Association, *Journal of the American Chemical Society 116*, 3659-3660.

215. Hilvo, M., Baranauskiene, L., Salzano, A. M., Scaloni, A., Matulis, D., Innocenti, A., Scozzafava, A., Monti, S. M., Di Fiore, A., De Simone, G., Lindfors, M., Jänis, J., Valjakka, J., Pastoreková, S., Pastorek, J., Kulomaa, M. S., Nordlund, H. R., Supuran, C. T., and Parkkila, S. (2008) Biochemical characterization of CA IX, one of the most active carbonic anhydrase isozymes, *J. Biol. Chem 283*, 27799-27809.
216. Alterio, V., Hilvo, M., Di Fiore, A., Supuran, C. T., Pan, P., Parkkila, S., Scaloni, A., Pastorek, J., Pastorekova, S., Pedone, C., Scozzafava, A., Monti, S. M., and De Simone, G. (2009) Crystal structure of the catalytic domain of the tumor-associated human carbonic anhydrase IX, *Proc. Natl. Acad. Sci. U.S.A 106*, 16233-16238.
217. Supuran, C. T., and Scozzafava, A. (2007) Carbonic anhydrases as targets for medicinal chemistry, *Bioorg. Med. Chem 15*, 4336-4350.
218. Russ, W. P., and Engelman, D. M. (2000) The GxxxG motif: a framework for transmembrane helix-helix association, *J. Mol. Biol 296*, 911-919.
219. Senes, A., Gerstein, M., and Engelman, D. M. (2000) Statistical analysis of amino acid patterns in transmembrane helices: the GxxxG motif occurs frequently and in association with beta-branched residues at neighboring positions, *J. Mol. Biol 296*, 921-936.
220. Xue, Y., Liljas, A., Jonsson, B. H., and Lindskog, S. (1993) Structural analysis of the zinc hydroxide-Thr-199-Glu-106 hydrogen-bond network in human carbonic anhydrase II, *Proteins 17*, 93-106.
221. Xue, Y., Vidgren, J., Svensson, L. A., Liljas, A., Jonsson, B. H., and Lindskog, S.

(1993) Crystallographic analysis of Thr-200-->His human carbonic anhydrase II and its complex with the substrate, HCO3-, *Proteins 15*, 80-87.

222. Kim, C., Chang, J. S., Doyon, J. B., Baird, Fierke, C. A., Jain, A., and Christianson, D. W. (2000) Contribution of Fluorine to Protein−Ligand Affinity in the Binding of Fluoroaromatic Inhibitors to Carbonic Anhydrase II, *Journal of the American Chemical Society 122*, 12125-12134.
223. Stams, T., Chen, Y., Boriack-Sjodin, P. A., Hurt, J. D., Liao, J., May, J. A., Dean, T., Laipis, P., Silverman, D. N., and Christianson, D. W. (1998) Structures of murine carbonic anhydrase IV and human carbonic anhydrase II complexed with brinzolamide: molecular basis of isozyme-drug discrimination, *Protein Sci 7*, 556-563.
224. Boriack-Sjodin, P. A., Zeitlin, S., Chen, H. H., Crenshaw, L., Gross, S., Dantanarayana, A., Delgado, P., May, J. A., Dean, T., and Christianson, D. W. (1998) Structural analysis of inhibitor binding to human carbonic anhydrase II, *Protein Sci 7*, 2483-2489.
225. Cappalonga Bunn, A. M., Alexander, R. S., and Christianson, D. W. (1994) Mapping Protein-Peptide Affinity: Binding of Peptidylsulfonamide Inhibitors to Human Carbonic Anhydrase II, *Journal of the American Chemical Society 116*, 5063-5068.
226. Vidgren, J., Liljas, A., and Walker, N. P. (1990) Refined structure of the acetazolamide complex of human carbonic anhydrase II at 1.9 A, *Int. J. Biol. Macromol 12*, 342-344.
227. Christianson, D. W., and Alexander, R. S. (1989) Carboxylate-histidine-zinc interactions in protein structure and function, *Journal of the American Chemical*

Society 111, 6412-6419.

228. Christianson, D. W. (1991) Structural biology of zinc, *Adv. Protein Chem 42*, 281-355.

229. Huang, C. C., Lesburg, C. A., Kiefer, L. L., Fierke, C. A., and Christianson, D. W. (1996) Reversal of the hydrogen bond to zinc ligand histidine-119 dramatically diminishes catalysis and enhances metal equilibration kinetics in carbonic anhydrase II, *Biochemistry 35*, 3439-3446.

230. Riccardi, D., König, P., Guo, H., and Cui, Q. (2008) Proton transfer in carbonic anhydrase is controlled by electrostatics rather than the orientation of the acceptor, *Biochemistry 47*, 2369-2378.

231. Fisher, S. Z., Maupin, C. M., Budayova-Spano, M., Govindasamy, L., Tu, C., Agbandje-McKenna, M., Silverman, D. N., Voth, G. A., and McKenna, R. (2007) Atomic crystal and molecular dynamics simulation structures of human carbonic anhydrase II: insights into the proton transfer mechanism, *Biochemistry 46*, 2930-2937.

232. Fisher, S. Z., Tu, C., Bhatt, D., Govindasamy, L., Agbandje-McKenna, M., McKenna, R., and Silverman, D. N. (2007) Speeding up proton transfer in a fast enzyme: kinetic and crystallographic studies on the effect of hydrophobic amino acid substitutions in the active site of human carbonic anhydrase II, *Biochemistry 46*, 3803-3813.

233. Liljas, A., Kannan, K. K., Bergstén, P. C., Waara, I., Fridborg, K., Strandberg, B., Carlbom, U., Järup, L., Lövgren, S., and Petef, M. (1972) Crystal structure of human carbonic anhydrase C, *Nature New Biol 235*, 131-137.

234. Lindahl, M., Liljas, A., Habash, J., Harrop, S., and Helliwell, J. R. (1992) The

sensitivity of the synchrotron Laue method to small structural changes: binding studies of human carbonic anhydrase II (HCAII), *Acta Crystallogr B Struct Sci 48*, 281-285.

235. Håkansson, K., Wehnert, A., and Liljas, A. (1994) X-ray analysis of metal-substituted human carbonic anhydrase II derivatives, *Acta Crystallogr. D Biol. Crystallogr 50*, 93-100.

236. Kannan, K. K. (1981) Structure and function of carbonic anhydrases, *Biomol. Struct., Conform., Funct., EVol., Proc. Int. Symp. 1*, 165-181.

237. Ippolito, J. A., and Christianson, D. W. (1994) Structural consequences of redesigning a protein-zinc binding site, *Biochemistry 33*, 15241-15249.

238. Kiefer, L. L., Ippolito, J. A., Fierke, C. A., and Christianson, D. W. (1993) Redesigning the zinc binding site of human carbonic anhydrase II: structure of a His2Asp-Zn2+ metal coordination polyhedron, *Journal of the American Chemical Society 115*, 12581-12582.

239. Alexander, R. S., Kiefer, L. L., Fierke, C. A., and Christianson, D. W. (1993) Engineering the zinc binding site of human carbonic anhydrase II: Structure of the His-94.fwdarw.Cys apoenzyme in a new crystalline form, *Biochemistry 32*, 1510-1518.

240. Cox, J. D., Hunt, J. A., Compher, K. M., Fierke, C. A., and Christianson, D. W. (2000) Structural Influence of Hydrophobic Core Residues on Metal Binding and Specificity in Carbonic Anhydrase II†,‡, *Biochemistry 39*, 13687-13694.

241. Lesburg, C. A., Huang, C., Christianson, D. W., and Fierke, C. A. (1997) Histidine → Carboxamide Ligand Substitutions in the Zinc Binding Site of Carbonic Anhydrase II

Alter Metal Coordination Geometry but Retain Catalytic Activity†, *Biochemistry 36*, 15780-15791.

242. Hunt, J. A., Ahmed, M., and Fierke, C. A. (1999) Metal binding specificity in carbonic anhydrase is influenced by conserved hydrophobic core residues, *Biochemistry 38*, 9054-9062.

243. Lindskog, S., and Nyman, P. O. (1964) Metal binding properties of human erythrocyte carbonic anhydrases, *Biochim. Biophys. Acta 85*, 462-474.

244. McCall, K. A., and Fierke, C. A. (2000) Colorimetric and fluorimetric assays to quantitate micromolar concentrations of transition metals, *Anal. Biochem 284*, 307-315.

245. Khalifah, R. G., Rogers, J. I., Harmon, P., Morely, P. J., and Carroll, S. B. (1984) Paramagnetic 1H and 13C NMR studies on cobalt-substituted human carbonic anhydrase I carboxymethylated at active site histidine-200: molecular basis for the changes in catalytic properties induced by the modification, *Biochemistry 23*, 3129-3136.

246. Demille, G. R., Larlee, K., Livesey, D. L., and Mailer, K. (1979) Conformational change in carbonic anhydrase studied by perturbed directional correlations of gamma rays, *Chemical Physics Letters 64*, 534-539.

247. Yachandra, V., Powers, L., and Spiro, T. G. (1983) X-ray absorption spectra and the coordination number of zinc and cobalt carbonic anhydrase as a function of pH and inhibitor binding, *Journal of the American Chemical Society 105*, 6596-6604.

248. Lane, T. W., and Morel, F. M. (2000) A biological function for cadmium in marine diatoms, *Proc. Natl. Acad. Sci. U.S.A 97*, 4627-4631.

249. Briganti, F., Mangani, S., Orioli, P., Scozzafava, A., Vernaglione, G., and Supuran, C. T. (1997) Carbonic anhydrase activators: X-ray crystallographic and spectroscopic investigations for the interaction of isozymes I and II with histamine, *Biochemistry 36*, 10384-10392.

250. Stams. T., and Christianson D.W. X-ray crystallographic studies of mammalian carbonic anhydrase isozymes, in In The Carbonic Anhydrases – New Horizons; Chegwidden W.R., Edwards, Y., Carter, N. Eds.;, pp 159-74. Birkhäuser Verlag, 2000, Basel., in .

251. Tu, C. K., Silverman, D. N., Forsman, C., Jonsson, B. H., and Lindskog, S. (1989) Role of histidine 64 in the catalytic mechanism of human carbonic anhydrase II studied with a site-specific mutant, *Biochemistry 28*, 7913-7918.

252. Jackman, J. E., Merz, K. M., and Fierke, C. A. (1996) Disruption of the active site solvent network in carbonic anhydrase II decreases the efficiency of proton transfer, *Biochemistry 35*, 16421-16428.

253. Ippolito, J. A., and Christianson, D. W. (1993) Structure of an engineered His3Cys zinc binding site in human carbonic anhydrase II, *Biochemistry 32*, 9901-9905.

254. Kiefer, L. L., Krebs, J. F., Paterno, S. A., and Fierke, C. A. (1993) Engineering a cysteine ligand into the zinc binding site of human carbonic anhydrase II, *Biochemistry 32*, 9896-9900.

255. Ippolito, J. A., Baird, T. T., McGee, S. A., Christianson, D. W., and Fierke, C. A. (1995) Structure-assisted redesign of a protein-zinc-binding site with femtomolar affinity, *Proc. Natl. Acad. Sci. U.S.A 92*, 5017-5021.

256. Kimura, E., Shiota, T., Koike, T., Shiro, M., and Kodama, M. (1990) A zinc(II)

complex of 1,5,9-triazacyclododecane ([12]aneN3) as a model for carbonic anhydrase, *Journal of the American Chemical Society 112*, 5805-5811.

257. Krebs, J. F., and Fierke, C. A. (1993) Determinants of catalytic activity and stability of carbonic anhydrase II as revealed by random mutagenesis, *J. Biol. Chem 268*, 948-954.

258. McCall, K. A., and Fierke, C. A. (2004) Probing determinants of the metal ion selectivity in carbonic anhydrase using mutagenesis, *Biochemistry 43*, 3979-3986.

259. Hurst, T. K., Wang, D., Thompson, R. B., and Fierke, C. A. (2010) Carbonic anhydrase II-based metal ion sensing: Advances and new perspectives, *Biochim. Biophys. Acta 1804*, 393-403.

260. Heck, R. W., Boriack-Sjodin, P. A., Qian, M., Tu, C., Christianson, D. W., Laipis, P. J., and Silverman, D. N. (1996) Structure-based design of an intramolecular proton transfer site in murine carbonic anhydrase V, *Biochemistry 35*, 11605-11611.

261. Hunt, J. A., and Fierke, C. A. (1997) Selection of carbonic anhydrase variants displayed on phage. Aromatic residues in zinc binding site enhance metal affinity and equilibration kinetics, *J. Biol. Chem 272*, 20364-20372.

262. Christianson, D. W., and Fierke, C. A. (1996) Carbonic Anhydrase:□ Evolution of the Zinc Binding Site by Nature and by Design, *Accounts of Chemical Research 29*, 331-339.

263. Duda, D., Tu, C., Qian, M., Laipis, P., Agbandje-McKenna, M., Silverman, D. N., and McKenna, R. (2001) Structural and kinetic analysis of the chemical rescue of the proton transfer function of carbonic anhydrase II, *Biochemistry 40*, 1741-1748.

264. Jude, K. M., Wright, S. K., Tu, C., Silverman, D. N., Viola, R. E., and Christianson,

D. W. (2002) Crystal structure of F65A/Y131C-methylimidazole carbonic anhydrase V reveals architectural features of an engineered proton shuttle, *Biochemistry 41*, 2485-2491.

265. Elder, I., Han, S., Tu, C., Steele, H., Laipis, P. J., Viola, R. E., and Silverman, D. N. (2004) Activation of carbonic anhydrase II by active-site incorporation of histidine analogs, *Arch. Biochem. Biophys 421*, 283-289.

266. Tashian, R. E. (1989) The carbonic anhydrases: widening perspectives on their evolution, expression and function, *Bioessays 10*, 186-192.

267. Hewett-Emmett, D. and Tashian, R. E. (1991) Structure and evolutionary origins of the carbonic anhydrase multigene family, in The carbonic anhydrases: cellular physiology and molecular genetics (Dodgson, S. J., Tashian, R. E., Gros, G. & Carter, N. D., eds), pp 15-32. Plenum, New York., in .

268. Engstrand, C., Jonsson, B. H., and Lindskog, S. (1995) Catalytic and inhibitor-binding properties of some active-site mutants of human carbonic anhydrase I, *Eur. J. Biochem 229*, 696-702.

269. Yamashita, M. M., Wesson, L., Eisenman, G., and Eisenberg, D. (1990) Where metal ions bind in proteins, *Proc. Natl. Acad. Sci. U.S.A 87*, 5648-5652.

270. Ulmasov, B., Waheed, A., Shah, G. N., Grubb, J. H., Sly, W. S., Tu, C., and Silverman, D. N. (2000) Purification and kinetic analysis of recombinant CA XII, a membrane carbonic anhydrase overexpressed in certain cancers, *Proc. Natl. Acad. Sci. U.S.A 97*, 14212-14217.

271. Culf, A. S., Gerig, J. T., and Williams, P. G. (1997) Tritium NMR studies of the human carbonic anhydrase I-benzenesulfonamide complex, *J. Biomol. NMR 10*, 293-

299.

272. Gerig, J. T., and Moses, J. M. (1987) Aromatic ring dynamics in a carbonic anhydrase-inhibitor complex, *J. Chem. Soc., Chem. Commun.* 482-484.

273. Jarvet, J., Olivson, A., Mets, U., Pooga, M., Aguraiuja, R., and Lippmaa, E. (1989) 13C and 15N NMR and time-resolved fluorescence depolarization study of bovine carbonic anhydrase--4-methylbenzenesulfonamide complex, *Eur. J. Biochem 186*, 287-290.

274. Veenstra, D. L., and Gerig, J. T. (1998) Fluorine NMR studies of the human carbonic anhydrase-3,5-difluorobenzenesulfonamide complex, *Magnetic Resonance in Chemistry 36*, S169-S178.

275. Dugad, L. B., and Gerig, J. T. (1988) NMR studies of carbonic anhydrase-4-fluorobenzenesulfonamide complexes, *Biochemistry 27*, 4310-4316.

276. Dugad, L. B., Cooley, C. R., and Gerig, J. T. (1989) NMR studies of carbonic anhydrase-fluorinated benzenesulfonamide complexes, *Biochemistry 28*, 3955-3960.

277. Kanamori, K., and Roberts, J. D. (1983) Nitrogen-15 nuclear magnetic resonance study of benzenesulfonamide and cyanate binding to carbonic anhydrase, *Biochemistry 22*, 2658-2664.

278. Blackburn, G. M., Mann, B. E., Taylor, B. F., and Worrall, A. F. (1985) A nuclear-magnetic-resonance study of the binding of novel N-hydroxybenzenesulphonamide carbonic anhydrase inhibitors to native and cadmium-111-substituted carbonic anhydrase, *Eur. J. Biochem 153*, 553-558.

279. Luy, B. (2007) Approaching the megadalton: NMR spectroscopy of protein complexes, *Angew. Chem. Int. Ed. Engl 46*, 4214-4216.

280. Sprangers, R., and Kay, L. E. (2007) Quantitative dynamics and binding studies of the 20S proteasome by NMR, *Nature 445*, 618-622.

281. Venters, R. A., Farmer, B. T., Fierke, C. A., and Spicer, L. D. (1996) Characterizing the use of perdeuteration in NMR studies of large proteins: 13C, 15N and 1H assignments of human carbonic anhydrase II, *J. Mol. Biol 264*, 1101-1116.

282. Sethson, I., Edlund, U., Holak, T. A., Ross, A., and Jonsson, B. H. (1996) Sequential assignment of 1H, 13C and 15N resonances of human carbonic anhydrase I by triple-resonance NMR techniques and extensive amino acid-specific 15N-labeling, *J. Biomol. NMR 8*, 417-428.

283. Khalifah, R. G., and Edsall, J. T. (1972) Carbon dioxide hydration activity of carbonic anhydrase: kinetics of alkylated anhydrases B and C from humans (metalloenzymes-isoenzymes-active sites-mechanism), *Proc. Natl. Acad. Sci. U.S.A 69*, 172-176.

284. Whitney, P. L. (1970) Inhibition and modification of human carbonic anhydrase B with bromoacetate and iodoacetamide, *Eur. J. Biochem 16*, 126-135.

285. Taylor, P. W., and Burgen, A. S. (1971) Kinetics of carbonic anhydrase-inhibitor complex formation. a comparison of anion- and sulfonamide-binding mechanisms, *Biochemistry 10*, 3859-3866.

286. Bertini, I., Canti, G., Luchinat, C., and Mani, F. (1981) Hydrogen-1 NMR spectra of the coordination sphere of cobalt-substituted carbonic anhydrase, *Journal of the American Chemical Society 103*, 7784-7788.

287. Bertini, I., and Luchinat, C. (1983) Cobalt(II) as a probe of the structure and function of carbonic anhydrase, *Accounts of Chemical Research 16*, 272-279.

288. Kim, C., Chandra, P. P., Jain, A., and Christianson, D. W. (2001) Fluoroaromatic−Fluoroaromatic Interactions between Inhibitors Bound in the Crystal Lattice of Human Carbonic Anhydrase II, *Journal of the American Chemical Society 123*, 9620-9627.

289. Mårtensson, L. G., Jonasson, P., Freskgård, P. O., Svensson, M., Carlsson, U., and Jonsson, B. H. (1995) Contribution of individual tryptophan residues to the fluorescence spectrum of native and denatured forms of human carbonic anhydrase II, *Biochemistry 34*, 1011-1021.

290. Jude, K. M., Banerjee, A. L., Haldar, M. K., Manokaran, S., Roy, B., Mallik, S., Srivastava, D. K., and Christianson, D. W. (2006) Ultrahigh resolution crystal structures of human carbonic anhydrases I and II complexed with "two-prong" inhibitors reveal the molecular basis of high affinity, *J. Am. Chem. Soc 128*, 3011-3018.

291. Parkkila, S., Rajaniemi, H., Parkkila, A. K., Kivela, J., Waheed, A., Pastorekova, S., Pastorek, J., and Sly, W. S. (2000) Carbonic anhydrase inhibitor suppresses invasion of renal cancer cells in vitro, *Proc. Natl. Acad. Sci. U.S.A 97*, 2220-2224.

292. Pastorekova, S., Kopacek, J., and Pastorek, J. (2007) Carbonic anhydrase inhibitors and the management of cancer, *Curr Top Med Chem 7*, 865-878.

293. Thiry, A., Dogné, J., Supuran, C. T., and Masereel, B. (2007) Carbonic anhydrase inhibitors as anticonvulsant agents, *Curr Top Med Chem 7*, 855-864.

294. Vullo, D., Innocenti, A., Nishimori, I., Pastorek, J., Scozzafava, A., Pastoreková, S., and Supuran, C. T. (2005) Carbonic anhydrase inhibitors. Inhibition of the transmembrane isozyme XII with sulfonamides-a new target for the design of

antitumor and antiglaucoma drugs?, *Bioorg. Med. Chem. Lett 15*, 963-969.

295. Innocenti, A., Vullo, D., Pastorek, J., Scozzafava, A., Pastorekova, S., Nishimori, I., and Supuran, C. T. (2007) Carbonic anhydrase inhibitors. Inhibition of transmembrane isozymes XII (cancer-associated) and XIV with anions, *Bioorg. Med. Chem. Lett 17*, 1532-1537.

296. Abbate, F., Casini, A., Owa, T., Scozzafava, A., and Supuran, C. T. (2004) Carbonic anhydrase inhibitors: E7070, a sulfonamide anticancer agent, potently inhibits cytosolic isozymes I and II, and transmembrane, tumor-associated isozyme IX, *Bioorg. Med. Chem. Lett 14*, 217-223.

297. Pastorekova, S., Vullo, D., Casini, A., Scozzafava, A., Pastorek, J., Nishimori, I., and Supuran, C. T. (2005) Carbonic anhydrase inhibitors: Inhibition of the tumor-associated isozymes IX and XII with polyfluorinated aromatic/heterocyclic sulfonamides, *J Enzyme Inhib Med Chem 20*, 211-217.

298. Mann, T., and Keilin, D. (1940) Sulphanilamide as a Specific Inhibitor of Carbonic Anhydrase, *Nature 146*, 164-165.

299. Krebs, H. A. (1948) Inhibition of carbonic anhydrase by sulphonamides, *Biochem. J 43*, 525-528.

300. Maren, T. H. (1967) Carbonic anhydrase: chemistry, physiology, and inhibition, *Physiol. Rev 47*, 595-781.

301. Maren, T. H. (1976) Relatons between structure and biological activity of sulfonamides, *Annu. Rev. Pharmacol. Toxicol 16*, 309-327.

302. Supuran, C. T., and Scozzafava, A. (2000) Carbonic anhydrase inhibitors and their therapeutic potential, *Expert Opin. Ther. Patents 10*, 575-600.

303. Drews, J. (2000) Drug discovery: a historical perspective, *Science 287*, 1960-1964.

304. Owa, T., and Nagasu, T. (2000) Novel sulphonamide derivatives for the treatment of cancer, *Expert Opin. Ther. Patents 10*, 1725-1740.

305. Baldwin, J. J., Ponticello, G. S., Anderson, P. S., Christy, M. E., Murcko, M. A., Randall, W. C., Schwam, H., Sugrue, M. F., Springer, J. P., and Gautheron, P. (1989) Thienothiopyran-2-sulfonamides: novel topically active carbonic anhydrase inhibitors for the treatment of glaucoma, *J. Med. Chem 32*, 2510-2513.

306. Merz, K. M., Murcko, M. A., and Kollman, P. A. (1991) Inhibition of carbonic anhydrase, *Journal of the American Chemical Society 113*, 4484-4490.

307. Lindahl, M., Vidgren, J., Eriksson, E., Habash,J., Harrop, S., Helliwell, J., Liljas, A., Lindeskog, M., Walker, N. (1991) Crystallographic studies of carbonic anhydrase inhibition, in In: Botre` F, Gros G, StoreyBT, editors. Carbonic anhydrase., pp pp 111–118. Weinheim: VCH., in .

308. Abbate, F., Supuran, C. T., Scozzafava, A., Orioli, P., Stubbs, M. T., and Klebe, G. (2002) Nonaromatic sulfonamide group as an ideal anchor for potent human carbonic anhydrase inhibitors: role of hydrogen-bonding networks in ligand binding and drug design, *J. Med. Chem 45*, 3583-3587.

309. Srivastava, D. K., Jude, K. M., Banerjee, A. L., Haldar, M., Manokaran, S., Kooren, J., Mallik, S., and Christianson, D. W. (2007) Structural analysis of charge discrimination in the binding of inhibitors to human carbonic anhydrases I and II, *J. Am. Chem. Soc 129*, 5528-5537.

310. Mangani, S., and Håkansson, K. (1992) Crystallographic studies of the binding of protonated and unprotonated inhibitors to carbonic anhydrase using hydrogen

sulphide and nitrate anions, *Eur. J. Biochem 210*, 867-871.

311. Silver, L. H. (2000) Dose-response evaluation of the ocular hypotensive effect of brinzolamide ophthalmic suspension (Azopt). Brinzolamide Dose-Response Study Group, Surv Ophthalmol 44 Suppl 2, S147-153.

312. Woltersdorf, O. W., Schwam, H., Bicking, J. B., Brown, S. L., deSolms, S. J., Fishman, D. R., Graham, S. L., Gautheron, P. D., Hoffman, J. M., and Larson, R. D. (1989) Topically active carbonic anhydrase inhibitors. 1. O-acyl derivatives of 6-hydroxybenzothiazole-2-sulfonamide, *J. Med. Chem 32*, 2486-2492.

313. Graham, S. L., Hoffman, J. M., Gautheron, P., Michelson, S. R., Scholz, T. H., Schwam, H., Shepard, K. L., Smith, A. M., Smith, R. L., and Sondey, J. M. (1990) Topically active carbonic anhydrase inhibitors. 3. Benzofuran- and indole-2-sulfonamides, *J. Med. Chem 33*, 749-754.

314. Prugh, J. D., Hartman, G. D., Mallorga, P. J., McKeever, B. M., Michelson, S. R., Murcko, M. A., Schwam, H., Smith, R. L., Sondey, J. M., and Springer, J. P. (1991) New isomeric classes of topically active ocular hypotensive carbonic anhydrase inhibitors: 5-substituted thieno[2,3-b]thiophene-2-sulfonamides and 5-substituted thieno[3,2-b]thiophene-2-sulfonamides, *J. Med. Chem 34*, 1805-1818.

315. Graham, S. L., Shepard, K. L., Anderson, P. S., Baldwin, J. J., Best, D. B., Christy, M. E., Freedman, M. B., Gautheron, P., Habecker, C. N., and Hoffman, J. M. (1989) Topically active carbonic anhydrase inhibitors. 2. Benzo[b]thiophenesulfonamide derivatives with ocular hypotensive activity, *J. Med. Chem 32*, 2548-2554.

316. Hartman, G. D., Halczenko, W., Prugh, J. D., Smith, R. L., Sugrue, M. F., Mallorga, P., Michelson, S. R., Randall, W. C., Schwam, H., and Sondey, J. M. (1992)

Thieno[2,3-b]furan-2-sulfonamides as topical carbonic anhydrase inhibitors, *J. Med. Chem 35*, 3027-3033.

317. Ponticello, G. S., Freedman, M. B., Habecker, C. N., Lyle, P. A., Schwam, H., Varga, S. L., Christy, M. E., Randall, W. C., and Baldwin, J. J. (1987) Thienothiopyran-2-sulfonamides: a novel class of water-soluble carbonic anhydrase inhibitors, *J. Med. Chem 30*, 591-597.

318. Chen, H., Gross, S., Liao, J., McLaughlin, M., Dean, T., Sly, W. S., and May, J. A. (2000) 2H-Thieno[3,2-e]- and [2,3-e]-1,2-thiazine-6-sulfonamide 1,1-dioxides as ocular hypotensive agents: synthesis, carbonic anhydrase inhibition and evaluation in the rabbit, *Bioorganic & Medicinal Chemistry 8*, 957-975.

319. Borras, J., Scozzafava, A., Menabuoni, L., Mincione, F., Briganti, F., Mincione, G., and Supuran, C. T. (1999) Carbonic anhydrase inhibitors: synthesis of water-soluble, topically effective intraocular pressure lowering aromatic/heterocyclic sulfonamides containing 8-quinoline-sulfonyl moieties: is the tail more important than the ring?, *Bioorg. Med. Chem 7*, 2397-2406.

320. Menabuoni, L., Scozzafava, A., Mincione, F., Briganti, F., Mincione, G., and Supuran, C. T. (1999) Carbonic anhydrase inhibitors. Water-soluble, topically effective intraocular pressure lowering agents derived from isonicotinic acid and aromatic/heterocyclic sulfonamides: is the tail more important than the ring?, *J. Enzym. Inhib 14*, 457-474.

321. Supuran, C. T., Scozzafava, A., Menabuoni, L., Mincione, F., Briganti, F., and Mincione, G. (1999) Carbonic anhydrase inhibitors. Part 71. Synthesis and ocular pharmacology of a new class of water-soluble, topically effective intraocular pressure

lowering sulfonamides incorporating picolinoyl moieties, *Eur J Pharm Sci 8*, 317-328.

322. Scozzafava, A., Menabuoni, L., Mincione, F., Mincione, G., and Supuran, C. T. (2001) Carbonic anhydrase inhibitors: synthesis of sulfonamides incorporating dtpa tails and of their zinc complexes with powerful topical antiglaucoma properties, *Bioorg. Med. Chem. Lett 11*, 575-582.

323. Mincione, G., Menabuoni, L., Briganti, F., Mincione, F., Scozzafava, A., and Supuran, C. T. (1999) Carbonic anhydrase inhibitors. Part 79. Synthesis of topically acting sulfonamides incorporating GABA moieties in their molecule, with long-lasting intraocular pressure-lowering properties, *Eur J Pharm Sci 9*, 185-199.

324. Renzi, G., Scozzafava, A., and Supuran, C. T. (2000) Carbonic anhydrase inhibitors: topical sulfonamide antiglaucoma agents incorporating secondary amine moieties, *Bioorg. Med. Chem. Lett 10*, 673-676.

325. Casini, A., Scozzafava, A., Mincione, F., Menabuoni, L., Ilies, M. A., and Supuran, C. T. (2000) Carbonic anhydrase inhibitors: water-soluble 4-sulfamoylphenylthioureas as topical intraocular pressure-lowering agents with long-lasting effects, *J. Med. Chem 43*, 4884-4892.

326. Antonaroli, S., Bianco, A., Brufani, M., Cellai, L., Lo Baido, G., Potier, E., Bonomi, L., Perfetti, S., Fiaschi, A. I., and Segre, G. (1992) Acetazolamide-like carbonic anhydrase inhibitors with topical ocular hypotensive activity, *J. Med. Chem 35*, 2697-2703.

327. Roy, B. C., Banerjee, A. L., Swanson, M., Jia, X. G., Haldar, M. K., Mallik, S., and Srivastava, D. K. (2004) Two-prong inhibitors for human carbonic anhydrase II, *J.*

Am. Chem. Soc 126, 13206-13207.

328. Banerjee, A. L., Swanson, M., Roy, B. C., Jia, X., Haldar, M. K., Mallik, S., and Srivastava, D. K. (2004) Protein surface-assisted enhancement in the binding affinity of an inhibitor for recombinant human carbonic anhydrase-II, *J. Am. Chem. Soc 126*, 10875-10883.

329. Banerjee, A. L., Tobwala, S., Ganguly, B., Mallik, S., and Srivastava, D. K. (2005) Molecular basis for the origin of differential spectral and binding profiles of dansylamide with human carbonic anhydrase I and II, *Biochemistry 44*, 3673-3682.

330. De Simone, G., Di Fiore, A., Menchise, V., Pedone, C., Antel, J., Casini, A., Scozzafava, A., Wurl, M., and Supuran, C. T. (2005) Carbonic anhydrase inhibitors. Zonisamide is an effective inhibitor of the cytosolic isozyme II and mitochondrial isozyme V: solution and X-ray crystallographic studies, *Bioorg. Med. Chem. Lett 15*, 2315-2320.

331. Abbate, F., Winum, J., Potter, B. V. L., Casini, A., Montero, J., Scozzafava, A., and Supuran, C. T. (2004) Carbonic anhydrase inhibitors: X-ray crystallographic structure of the adduct of human isozyme II with EMATE, a dual inhibitor of carbonic anhydrases and steroid sulfatase, *Bioorg. Med. Chem. Lett 14*, 231-234.

332. Casini, A., Antel, J., Abbate, F., Scozzafava, A., David, S., Waldeck, H., Schäfer, S., and Supuran, C. T. (2003) Carbonic anhydrase inhibitors: SAR and X-ray crystallographic study for the interaction of sugar sulfamates/sulfamides with isozymes I, II and IV, *Bioorg. Med. Chem. Lett 13*, 841-845.

333. Winum, J., Vullo, D., Casini, A., Montero, J., Scozzafava, A., and Supuran, C. T. (2003) Carbonic anhydrase inhibitors. Inhibition of cytosolic isozymes I and II and

transmembrane, tumor-associated isozyme IX with sulfamates including EMATE also acting as steroid sulfatase inhibitors, *J. Med. Chem 46*, 2197-2204.

334. Briganti, F., Pierattelli, R., Scozzafava, A., and Supuran, C. (1996) Carbonic anhydrase inhibitors. Part 37. Novel classes of isozyme I and II inhibitors and their mechanism of action. Kinetic and spectroscopic investigations on native and cobalt-substituted enzymes, *European Journal of Medicinal Chemistry 31*, 1001-1010.
335. Franchi, M., Vullo, D., Gallori, E., Antel, J., Wurl, M., Scozzafava, A., and Supuran, C. T. (2003) Carbonic anhydrase inhibitors: inhibition of human and murine mitochondrial isozymes V with anions, *Bioorg. Med. Chem. Lett 13*, 2857-2861.
336. Temperini, C., Winum, J., Montero, J., Scozzafava, A., and Supuran, C. T. (2007) Carbonic anhydrase inhibitors: the X-ray crystal structure of the adduct of N-hydroxysulfamide with isozyme II explains why this new zinc binding function is effective in the design of potent inhibitors, *Bioorg. Med. Chem. Lett 17*, 2795-2801.
337. Scholz, T. H., Sondey, J. M., Randall, W. C., Schwam, H., Thompson, W. J., Mallorga, P. J., Sugrue, M. F., and Graham, S. L. (1993) Sulfonylmethanesulfonamide inhibitors of carbonic anhydrase, *J. Med. Chem 36*, 2134-2141.
338. Roughton, F. J., and Booth, V. H. (1946) The manometric determination of the activity of carbonic anhydrase under varied conditions, *Biochem. J 40*, 309-319.
339. Prabhananda, B. S., Rittger, E., and Grell, E. (1987) Kinetics and mechanism of anionic ligand binding to carbonic anhydrase, *Biophys. Chem 26*, 217-224.
340. Pocker, Y., and Dickerson, D. G. (1968) The catalytic versatility of erythrocyte carbonic anhydrase. V. Kinetic studies of enzyme-catalyzed hydrations of aliphatic

aldehydes, *Biochemistry 7*, 1995-2004.

341. Jönsson, B. M., Håkansson, K., and Liljas, A. (1993) The structure of human carbonic anhydrase II in complex with bromide and azide, *FEBS Lett 322*, 186-190.

342. Temperini, C., Innocenti, A., Guerri, A., Scozzafava, A., Rusconi, S., and Supuran, C. T. (2007) Phosph(on)ate as a zinc-binding group in metalloenzyme inhibitors: X-ray crystal structure of the antiviral drug foscarnet complexed to human carbonic anhydrase I, *Bioorg. Med. Chem. Lett 17*, 2210-2215.

343. Kumar, V., Kannan, K. K., and Sathyamurthi, P. (1994) Differences in anionic inhibition of human carbonic anhydrase I revealed from the structures of iodide and gold cyanide inhibitor complexes, *Acta Crystallogr. D Biol. Crystallogr 50*, 731-738.

344. Maren, T. H., and Conroy, C. W. (1993) A new class of carbonic anhydrase inhibitor, *J. Biol. Chem 268*, 26233-26239.

345. Bertini, I., Luchinat, C., and Scozzafava, A. (1982) Carbonic anhydrase: An insight into the zinc binding site and into the active cavity through metal substitution, in Biochemistry, pp 45-92., in .

346. Scozzafava, A., and Supuran, C. T. (1998) Carbonic Anhydrase Inhibitors: Ureido and Thioureido Derivatives of Aromatic Sulfonamides Possessing Increased Affinities for Isozyme I. A Novel Route To 2,5-Disubstituted-L,3,4-Thiadiazoles Via Thioureas, and Their Interaction with Isozymes I, II - and IV - PB - Informa Healthcare, *Journal of Enzyme Inhibition and Medicinal Chemistry 13*, 103.

347. Supuran, C. T., Scozzafava, A., Jurca, B. C., and Ilies, M. A. (1998) Carbonic anhydrase inhibitors - Part 49: Synthesis of substituted ureido and thioureido derivatives of aromatic/heterocyclic sulfonamides with increased affinities for

isozyme I, *European Journal of Medicinal Chemistry 33*, 83-93.

348. Scozzafava, A., and Supuran, C. T. (1999) Carbonic anhydrase inhibitors. Arylsulfonylureido- and arylureido-substituted aromatic and heterocyclic sulfonamides: towards selective inhibitors of carbonic anhydrase isozyme I, *J. Enzym. Inhib 14*, 343-363.

349. Kim, G., Selengut, J., and Levine, R. L. (2000) Carbonic anhydrase III: the phosphatase activity is extrinsic, *Arch. Biochem. Biophys 377*, 334-340.

350. Supuran, C., Nicolae, A., and Popescu, A. (1996) Carbonic anhydrase inhibitors. Part 35. Synthesis of Schiff bases derived from sulfanilamide and aromatic aldehydes: the first inhibitors with equally high affinity towards cytosolic and membrane-bound isozymes, *European Journal of Medicinal Chemistry 31*, 431-438.

351. Supuran, C., Popescu, A., Ilisiu, M., Costandache, A., and Banciu, M. (1996) Carbonic anhydrase inhibitors. Part 36. Inhibition of isozymes I and II with Schiff bases derived from chalkones and aromatic/heterocyclic sulfonamides, *European Journal of Medicinal Chemistry 31*, 439-447.

352. Supuran, C., Scozzafava, A., Popescu, A., Bobes-Tureac, R., Banciu, A., Creanga, A., Bobes-Tureac, G., and Banciu, M. (1997) Carbonic anhydrase inhibitors. Part 43. Schiff bases derived from aromatic sulfonamides: towards more specific inhibitors for membrane-bound versus cytosolic isozymes, *European Journal of Medicinal Chemistry 32*, 445-452.

353. Popescu, A., Simion, A., Scozzafava, A., Briganti, F., and Supuran, C. T. (1999) Carbonic Anhydrase Inhibitors. Schiff Bases of some Aromatic Sulfonamides and Their Metal Complexes: Towards More Selective Inhibitors of Carbonic Anhydrase

Isozyme IV - PB - Informa Healthcare, *Journal of Enzyme Inhibition and Medicinal Chemistry 14*, 407.

354. Supuran, C. T., Manole, G., Dinculescu, A., Schiketanz, A., Gheorghiu, M. D., Puscas, I., and Balaban, A. T. (1992) Carbonic anhydrase inhibitors. V: Pyrylium salts in the synthesis of isozyme-specific inhibitors, *J Pharm Sci 81*, 716-719.

355. Supuran, C., and Clare, B. (1995) Carbonic anhydrase inhibitors. Part 24. A quantitative structure-activity relationship study of positively charged sulfonamide inhibitors, *European Journal of Medicinal Chemistry 30*, 687-696.

356. Supuran, C. T., Ilies, M. A., and Scozzafava, A. (1998) Carbonic anhydrase inhibitors -- Part 29 1: Interaction of isozymes I, II and IV with benzolamide-like derivatives, *European Journal of Medicinal Chemistry 33*, 739-751.

357. Supuran, C. T., Scozzafava, A., Ilies, M. A., and Briganti, F. (2000) Carbonic anhydrase inhibitors: synthesis of sulfonamides incorporating 2,4,6-trisubstituted-pyridinium-ethylcarboxamido moieties possessing membrane-impermeability and in vivo selectivity for the membrane-bound (CA IV) versus the cytosolic (CA I and CA II) isozymes, *J. Enzym. Inhib 15*, 381-401.

358. Scozzafava, A., Briganti, F., Ilies, M. A., and Supuran, C. T. (2000) Carbonic anhydrase inhibitors: synthesis of membrane-impermeant low molecular weight sulfonamides possessing in vivo selectivity for the membrane-bound versus cytosolic isozymes, *J. Med. Chem 43*, 292-300.

359. Lucci, M. S., Tinker, J. P., Weiner, I. M., and DuBose, T. D. (1983) Function of proximal tubule carbonic anhydrase defined by selective inhibition, *Am J Physiol Renal Physiol 245*, F443-449.

360. Tinker, J. P., Coulson, R., and Weiner, I. M. (1981) Dextran-bound inhibitors of carbonic anhydrase, *J. Pharmacol. Exp. Ther 218*, 600-607.

361. Heming, T. A., Geers, C., Gros, G., Bidani, A., and Crandall, E. D. (1986) Effects of dextran-bound inhibitors on carbonic anhydrase activity in isolated rat lungs, *J. Appl. Physiol 61*, 1849-1856.

362. Henry, R. P. (1996) Multiple roles of carbonic anhydrase in cellular transport and metabolism, *Annu. Rev. Physiol 58*, 523-538.

363. Ozensoy, O., Puccetti, L., Fasolis, G., Arslan, O., Scozzafava, A., and Supuran, C. T. (2005) Carbonic anhydrase inhibitors: inhibition of the tumor-associated isozymes IX and XII with a library of aromatic and heteroaromatic sulfonamides, *Bioorg. Med. Chem. Lett 15*, 4862-4866.

364. Puccetti, L., Fasolis, G., Cecchi, A., Winum, J., Gamberi, A., Montero, J., Scozzafava, A., and Supuran, C. T. (2005) Carbonic anhydrase inhibitors: synthesis and inhibition of cytosolic/tumor-associated carbonic anhydrase isozymes I, II, and IX with sulfonamides incorporating thioureido-sulfanilyl scaffolds, *Bioorg. Med. Chem. Lett 15*, 2359-2364.

365. Owa, T., Yoshino, H., Okauchi, T., Yoshimatsu, K., Ozawa, Y., Sugi, N. H., Nagasu, T., Koyanagi, N., and Kitoh, K. (1999) Discovery of novel antitumor sulfonamides targeting G1 phase of the cell cycle, *J. Med. Chem 42*, 3789-3799.

366. Leese, M. P., Leblond, B., Smith, A., Newman, S. P., Di Fiore, A., De Simone, G., Supuran, C. T., Purohit, A., Reed, M. J., and Potter, B. V. L. (2006) 2-substituted estradiol bis-sulfamates, multitargeted antitumor agents: synthesis, in vitro SAR, protein crystallography, and in vivo activity, *J. Med. Chem 49*, 7683-7696.

367. Chegwidden, W. R., and Spencer, I. M. (1995) Sulphonamide inhlbitors of carbonic anhydrase inhibit the growth of human lymphoma cells in culture, *Inflammopharmacology 3*, 231-239.

368. Chegwidden, W.R., Spencer, I.M., Supuran, C.T. The roles of carbonic anhydrase isozymes in cancer. In: Xue G, Xue Y, Xu Z, Hammond G.L, Lim H.A, editors. Gene families: Studies of DNA, RNA, enzymes, and proteins. Singapore: World Scientific; 2001. pp 157–169., in .

369. Robertson, N., Potter, C., and Harris, A. L. (2004) Role of Carbonic Anhydrase IX in Human Tumor Cell Growth, Survival, and Invasion, *Cancer Research 64*, 6160-6165.

370. Teicher, B. A., Liu, S. D., Liu, J. T., Holden, S. A., and Herman, T. S. (1993) A carbonic anhydrase inhibitor as a potential modulator of cancer therapies, *Anticancer Res 13*, 1549-1556.

371. Supuran, C. T., and Scozzafava, A. (2000) Carbonic anhydrase inhibitors--Part 94. 1,3,4-thiadiazole-2-sulfonamidederivatives as antitumor agents?, *Eur J Med Chem 35*, 867-874.

372. Supuran, C. T., and Scozzafava, A. (2000) Carbonic anhydrase inhibitors: aromatic sulfonamides and disulfonamides act as efficient tumor growth inhibitors, *J. Enzym. Inhib 15*, 597-610.

373. Scozzafava, A., and Supuran, C. T. (2000) Carbonic anhydrase inhibitors: synthesis of N-morpholyl-thiocarbonylsulfenylamino aromatic/heterocyclic sulfonamides and their interaction with isozymes I, II and IV, *Bioorganic & Medicinal Chemistry Letters 10*, 1117-1120.

374. Supuran, C. T., Briganti, F., Tilli, S., Chegwidden, W. R., and Scozzafava, A. (2001)

Carbonic anhydrase inhibitors: sulfonamides as antitumor agents?, *Bioorg. Med. Chem 9*, 703-714.

375. Ozawa, Y., Sugi, N. H., Nagasu, T., Owa, T., Watanabe, T., Koyanagi, N., Yoshino, H., Kitoh, K., and Yoshimatsu, K. (2001) E7070, a novel sulphonamide agent with potent antitumour activity in vitro and in vivo, *Eur. J. Cancer 37*, 2275-2282.

376. Grüneberg, S., Wendt, B., and Klebe, G. (2001) Subnanomolar Inhibitors from Computer Screening: A Model Study Using Human Carbonic Anhydrase II, *Angew. Chem. Int. Ed. Engl 40*, 389-393.

377. Ilies, M. A., Vullo, D., Pastorek, J., Scozzafava, A., Ilies, M., Caproiu, M. T., Pastorekova, S., and Supuran, C. T. (2003) Carbonic anhydrase inhibitors. Inhibition of tumor-associated isozyme IX by halogenosulfanilamide and halogenophenylaminobenzolamide derivatives, *J. Med. Chem 46*, 2187-2196.

378. Vullo, D., Franchi, M., Gallori, E., Pastorek, J., Scozzafava, A., Pastorekova, S., and Supuran, C. T. (2003) Carbonic anhydrase inhibitors: inhibition of the tumor-associated isozyme IX with aromatic and heterocyclic sulfonamides, *Bioorg. Med. Chem. Lett 13*, 1005-1009.

379. Pastorekova, S., Casini, A., Scozzafava, A., Vullo, D., Pastorek, J., and Supuran, C. T. (2004) Carbonic anhydrase inhibitors: the first selective, membrane-impermeant inhibitors targeting the tumor-associated isozyme IX, *Bioorg. Med. Chem. Lett 14*, 869-873.

380. Winum, J., Scozzafava, A., Montero, J., and Supuran, C. T. (2009) Inhibition of carbonic anhydrase IX: a new strategy against cancer, *Anticancer Agents Med Chem 9*, 693-702.

381. Mincione, F., Starnotti, M., Masini, E., Bacciottini, L., Scrivanti, C., Casini, A., Vullo, D., Scozzafava, A., and Supuran, C. T. (2005) Carbonic anhydrase inhibitors: design of thioureido sulfonamides with potent isozyme II and XII inhibitory properties and intraocular pressure lowering activity in a rabbit model of glaucoma, *Bioorg. Med. Chem. Lett 15*, 3821-3827.

382. Lloyd, M. D., Pederick, R. L., Natesh, R., Woo, L. W. L., Purohit, A., Reed, M. J., Acharya, K. R., and Potter, B. V. L. (2005) Crystal structure of human carbonic anhydrase II at 1.95 A resolution in complex with 667-coumate, a novel anti-cancer agent, *Biochem. J 385*, 715-720.

383. Woo, L. L., Purohit, A., Malini, B., Reed, M. J., and Potter, B. V. (2000) Potent active site-directed inhibition of steroid sulphatase by tricyclic coumarin-based sulphamates, *Chem. Biol 7*, 773-791.

384. Vicker, N., Ho, Y., Robinson, J., Woo, L. L. W., Purohit, A., Reed, M. J., and Potter, B. V. L. (2003) Docking studies of sulphamate inhibitors of estrone sulphatase in human carbonic anhydrase II, *Bioorg. Med. Chem. Lett 13*, 863-865.

385. Ho, Y. T., Purohit, A., Vicker, N., Newman, S. P., Robinson, J. J., Leese, M. P., Ganeshapillai, D., Woo, L. W. L., Potter, B. V. L., and Reed, M. J. (2003) Inhibition of carbonic anhydrase II by steroidal and non-steroidal sulphamates, *Biochem. Biophys. Res. Commun 305*, 909-914.

386. Ireson, C. R., Chander, S. K., Purohit, A., Parish, D. C., Woo, L. W. L., Potter, B. V. L., and Reed, M. J. (2004) Pharmacokinetics of the nonsteroidal steroid sulphatase inhibitor 667 COUMATE and its sequestration into red blood cells in rats, *Br. J. Cancer 91*, 1399-1404.

387. Chen, R. F., and Kernohan, J. C. (1967) Combination of bovine carbonic anhydrase with a fluorescent sulfonamide, *J. Biol. Chem 242*, 5813-5823.

388. Cecchi, A., Hulikova, A., Pastorek, J., Pastoreková, S., Scozzafava, A., Winum, J., Montero, J., and Supuran, C. T. (2005) Carbonic anhydrase inhibitors. Design of fluorescent sulfonamides as probes of tumor-associated carbonic anhydrase IX that inhibit isozyme IX-mediated acidification of hypoxic tumors, *J. Med. Chem 48*, 4834-4841.

389. Alterio, V., Vitale, R. M., Monti, S. M., Pedone, C., Scozzafava, A., Cecchi, A., De Simone, G., and Supuran, C. T. (2006) Carbonic anhydrase inhibitors: X-ray and molecular modeling study for the interaction of a fluorescent antitumor sulfonamide with isozyme II and IX, *J. Am. Chem. Soc 128*, 8329-8335.

390. Bruchez, M., Moronne, M., Gin, P., Weiss, S., and Alivisatos, A. P. (1998) Semiconductor nanocrystals as fluorescent biological labels, *Science 281*, 2013-2016.

391. Chan, W. C., and Nie, S. (1998) Quantum dot bioconjugates for ultrasensitive nonisotopic detection, *Science 281*, 2016-2018.

392. Michalet, X., Pinaud, F. F., Bentolila, L. A., Tsay, J. M., Doose, S., Li, J. J., Sundaresan, G., Wu, A. M., Gambhir, S. S., and Weiss, S. (2005) Quantum dots for live cells, in vivo imaging, and diagnostics, *Science 307*, 538-544.

393. Wu, X., Liu, H., Liu, J., Haley, K. N., Treadway, J. A., Larson, J. P., Ge, N., Peale, F., and Bruchez, M. P. (2003) Immunofluorescent labeling of cancer marker Her2 and other cellular targets with semiconductor quantum dots, *Nat Biotech 21*, 41-46.

394. Alivisatos, A. P. (1996) Semiconductor Clusters, Nanocrystals, and Quantum Dots, *Science 271*, 933-937.

395. Murray, C. B., Kagan, C. R., and Bawendi, M. G. (2000) Synthesis and characterization of monodisperse nanocrystals and close packed nanocrystal assemblies, *Annu. Rev. Mater. Sci. 30*, 545-610.

396. Dabbousi, B. O., Rodriguez-Viejo, J., Mikulec, F. V., Heine, J. R., Mattoussi, H., Ober, R., Jensen, K. F., and Bawendi, M. G. (1997) (CdSe)ZnS Core–Shell Quantum Dots: Synthesis and Characterization of a Size Series of Highly Luminescent Nanocrystallites, *The Journal of Physical Chemistry B 101*, 9463-9475.

397. Gaponenko, S. V. (1998) Optical Properties of Semiconductor Nanocrystals 1st ed. Cambridge University Press., in .

398. Resch-Genger, U., Grabolle, M., Cavaliere-Jaricot, S., Nitschke, R., and Nann, T. (2008) Quantum dots versus organic dyes as fluorescent labels, *Nat. Methods 5*, 763-775.

399. Lynch, I., Dawson, K. A., and Linse, S. (2006) Detecting cryptic epitopes created by nanoparticles, *Sci. STKE 2006*, pe14.

400. Shao, L., Dong, C., Sang, F., Qian, H., and Ren, J. (2009) Studies on interaction of CdTe quantum dots with bovine serum albumin using fluorescence correlation spectroscopy, *J Fluoresc 19*, 151-157.

401. You, C., Arvizo, R. R., and Rotello, V. M. (2006) Regulation of [small alpha]-chymotrypsin activity on the surface of substrate-functionalized gold nanoparticles, *Chem. Commun.* 2905-2907.

402. Irle, S., Zheng, G., Elstner, M., and Morokuma, K. (2003) Formation of Fullerene Molecules from Carbon Nanotubes: A Quantum Chemical Molecular Dynamics Study, *Nano Lett. 3*, 465-470.

403. Erlanger, B. F., Chen, B., Zhu, M., and Brus, L. (2001) Binding of an Anti-Fullerene IgG Monoclonal Antibody to Single Wall Carbon Nanotubes, *Nano Lett. 1*, 465-467.

404. Chen, R. J., Zhang, Y., Wang, D., and Dai, H. (2001) Noncovalent sidewall functionalization of single-walled carbon nanotubes for protein immobilization, *J. Am. Chem. Soc 123*, 3838-3839.

405. Hong, R., Emrick, T., and Rotello, V. M. (2004) Monolayer-controlled substrate selectivity using noncovalent enzyme-nanoparticle conjugates, *J. Am. Chem. Soc 126*, 13572-13573.

406. Lundqvist, M., Sethson, I., and Jonsson, B. (2005) High-resolution 2D 1H-15N NMR characterization of persistent structural alterations of proteins induced by interactions with silica nanoparticles, *Langmuir 21*, 5974-5979.

407. Shen, X., Liou, X., Ye, L., Liang, H., and Wang, Z. (2007) Spectroscopic studies on the interaction between human hemoglobin and CdS quantum dots, *J Colloid Interface Sci 311*, 400-406.

408. Norde, W., and Giacomelli, C. E. (2000) BSA structural changes during homomolecular exchange between the adsorbed and the dissolved states, *J. Biotechnol 79*, 259-268.

409. Wu, X., and Narsimhan, G. (2008) Effect of surface concentration on secondary and tertiary conformational changes of lysozyme adsorbed on silica nanoparticles, *Biochim. Biophys. Acta 1784*, 1694-1701.

410. Vertegel, A. A., Siegel, R. W., and Dordick, J. S. (2004) Silica nanoparticle size influences the structure and enzymatic activity of adsorbed lysozyme, *Langmuir 20*, 6800-6807.

411. Shang, W., Nuffer, J. H., Dordick, J. S., and Siegel, R. W. (2007) Unfolding of ribonuclease A on silica nanoparticle surfaces, *Nano Lett 7*, 1991-1995.

412. Wang, L., Chen, H., Wang, L., Li, L., Xu, F., Liu, J., and Zhu, C. (2004) Preparation and Application of a Novel Composite Nanoparticle as a Protein Fluorescence Probe, Analytical Letters 37, 213.

413. Billsten, P., Freskgård, P. O., Carlsson, U., Jonsson, B. H., and Elwing, H. (1997) Adsorption to silica nanoparticles of human carbonic anhydrase II and truncated forms induce a molten-globule-like structure, *FEBS Lett 402*, 67-72.

414. Billsten, P., Carlsson, U., Jonsson, B. H., Olofsson, G., Höök, F., and Elwing, H. (1999) Conformation of Human Carbonic Anhydrase II Variants Adsorbed to Silica Nanoparticles, *Langmuir 15*, 6395-6399.

415. Karlsson, M., Mårtensson, L., Jonsson, B., and Carlsson, U. (2000) Adsorption of Human Carbonic Anhydrase II Variants to Silica Nanoparticles Occur Stepwise:□ Binding Is Followed by Successive Conformational Changes to a Molten-Globule-like State, *Langmuir 16*, 8470-8479.

416. Lundqvist, M., Sethson, I., and Jonsson, B. (2004) Protein adsorption onto silica nanoparticles: conformational changes depend on the particles' curvature and the protein stability, *Langmuir 20*, 10639-10647.

417. Kjellsson, A., Sethson, I., and Jonsson, B. (2003) Hydrogen exchange in a large 29 kD protein and characterization of molten globule aggregation by NMR, *Biochemistry 42*, 363-374.

418. Lundqvist, M., Sethson, I., and Jonsson, B. (2005) Transient interaction with nanoparticles "freezes" a protein in an ensemble of metastable near-native

conformations, *Biochemistry 44*, 10093-10099.

419. Karlsson, M., and Carlsson, U. (2005) Protein adsorption orientation in the light of fluorescent probes: mapping of the interaction between site-directly labeled human carbonic anhydrase II and silica nanoparticles, *Biophys. J 88*, 3536-3544.

420. Karlsson, M., Ekeroth, J., Elwing, H., and Carlsson, U. (2005) Reduction of irreversible protein adsorption on solid surfaces by protein engineering for increased stability, *J. Biol. Chem 280*, 25558-25564.

421. Stiti, M., Cecchi, A., Rami, M., Abdaoui, M., Barragan-Montero, V., Scozzafava, A., Guari, Y., Winum, J., and Supuran, C. T. (2008) Carbonic anhydrase inhibitor coated gold nanoparticles selectively inhibit the tumor-associated isoform IX over the cytosolic isozymes I and II, *J. Am. Chem. Soc 130*, 16130-16131.

422. Levinthal, C. Are there pathways for protein folding?, *J. Chim. Phys. 65*, 44-45.

423. Henkens, R. W., Kitchell, B. B., Lottich, S. C., Stein, P. J., and Williams, T. J. (1982) Detection and characterization using circular dichroism and fluorescence spectroscopy of a stable intermediate conformation formed in the denaturation of bovine carbonic anhydrase with guanidinium chloride, *Biochemistry 21*, 5918-5923.

424. Dolgikh, D. A., Kolomiets, A. P., Bolotina, I. A., and Ptitsyn, O. B. (1984) 'Molten-globule' state accumulates in carbonic anhydrase folding, *FEBS Lett 165*, 88-92.

425. Henkens, R. W.; Oleksiak, T. P. In Carbonic Anhydrase: From Biochemistry and Genetics to Physiology and Clinical Medicine; Botre`, F., Gros, G., Storey, B. T., Eds.; VCH: New York, 1991.

426. Svensson, M., Jonasson, P., Freskgård, P. O., Jonsson, B. H., Lindgren, M., Mårtensson, L. G., Gentile, M., Borén, K., and Carlsson, U. (1995) Mapping the

folding intermediate of human carbonic anhydrase II. Probing substructure by chemical reactivity and spin and fluorescence labeling of engineered cysteine residues, *Biochemistry 34*, 8606-8620.

427. Mårtensson, L. G., Jonsson, B. H., Freskgård, P. O., Kihlgren, A., Svensson, M., and Carlsson, U. (1993) Characterization of folding intermediates of human carbonic anhydrase II: probing substructure by chemical labeling of SH groups introduced by site-directed mutagenesis, *Biochemistry 32*, 224-231.

428. Carlsson, U., Aasa, R., Henderson, L. E., Jonsson, B. H., and Lindskog, S. (1975) Paramagnetic and fluorescent probes attached to "buried" sulfhydryl groups in human carbonic anhydrases. Application to inhibitor binding, denaturation and refolding, *Eur. J. Biochem 52*, 25-36.

429. Ohgushi, M., and Wada, A. (1983) 'Molten-globule state': a compact form of globular proteins with mobile side-chains, *FEBS Lett 164*, 21-24.

430. Ptitsyn, O. B., Pain, R. H., Semisotnov, G. V., Zerovnik, E., and Razgulyaev, O. I. (1990) Evidence for a molten globule state as a general intermediate in protein folding, *FEBS Lett 262*, 20-24.

431. Fink, A. L. (1995) Molten globules, *Methods Mol. Biol 40*, 343-360.

432. Yazgan, A., and Henkens, R. W. (1972) Role of zinc (II) in the refolding of guanidine hydrochloride denatured bovine carbonic anhydrase, *Biochemistry 11*, 1314-1318.

433. Borén, K., Andersson, P., Larsson, M., and Carlsson, U. (1999) Characterization of a molten globule state of bovine carbonic anhydrase III: loss of asymmetrical environment of the aromatic residues has a profound effect on both the near- and far-UV CD spectrum, *Biochim. Biophys. Acta 1430*, 111-118.

434. Semisotnov, G. V., Rodionova, N. A., Razgulyaev, O. I., Uversky, V. N., Gripas', A. F., and Gilmanshin, R. I. (1991) Study of the ?molten globule? intermediate state in protein folding by a hydrophobic fluorescent probe, *Biopolymers 31*, 119-128.

435. Bushmarina, N. A., Kuznetsova, I. M., Biktashev, A. G., Turoverov, K. K., and Uversky, V. N. (2001) Partially folded conformations in the folding pathway of bovine carbonic anhydrase II: a fluorescence spectroscopic analysis, *Chembiochem 2*, 813-821.

436. Borén, K., Grankvist, H., Hammarström, P., and Carlsson, U. (2004) Reshaping the folding energy landscape by chloride salt: impact on molten-globule formation and aggregation behavior of carbonic anhydrase, *FEBS Lett 566*, 95-99.

437. Creighton, T. E. Proteins: Structures and Molecular Properties.,2nd ed.; W. H. Freeman and Company: New York, 1993.

438. Jelesarov, I., and Bosshard, H. R. (1999) Isothermal titration calorimetry and differential scanning calorimetry as complementary tools to investigate the energetics of biomolecular recognition, *J. Mol. Recognit 12*, 3-18.

439. Almstedt, K., Lundqvist, M., Carlsson, J., Karlsson, M., Persson, B., Jonsson, B., Carlsson, U., and Hammarström, P. (2004) Unfolding a folding disease: folding, misfolding and aggregation of the marble brain syndrome-associated mutant H107Y of human carbonic anhydrase II, *J. Mol. Biol 342*, 619-633.

440. Lavecchia, R., and Zugaro, M. (1991) Thermal denaturation of erythrocyte carbonic anhydrase, *FEBS Lett 292*, 162-164.

441. Bull, H. B., and Breese, K. (1973) Thermal stability of proteins, *Arch. Biochem. Biophys 158*, 681-686.

442. McCoy, L. F., and Wong, K. P. (1981) Renaturation of bovine erythrocyte carbonic anhydrase B denatured by acid, heat, and detergent, *Biochemistry 20*, 3062-3067.

443. Gitlin, I., Gudiksen, K. L., and Whitesides, G. M. (2006) Effects of surface charge on denaturation of bovine carbonic anhydrase, *Chembiochem 7*, 1241-1250.

444. Wong, K. P., and Hamlin, L. M. (1975) The role of Zn(II) on the folding of bovine carbonic anhydrase B, *Arch. Biochem. Biophys 170*, 12-22.

445. Andersson, D., Hammarström, P., and Carlsson, U. (2001) Cofactor-induced refolding: refolding of molten globule carbonic anhydrase induced by Zn(II) and Co(II), *Biochemistry 40*, 2653-2661.

446. Bergenhem, N., and Carlsson, U. (1989) The role of the metal ion in the refolding of denatured bovine Co(II)-carbonic anhydrase II, *Biochimica et Biophysica Acta (BBA) - Protein Structure and Molecular Enzymology 998*, 277-285.

447. Avvaru, B. S., Busby, S. A., Chalmers, M. J., Griffin, P. R., Venkatakrishnan, B., Agbandje-McKenna, M., Silverman, D. N., and McKenna, R. (2009) Apo-human carbonic anhydrase II revisited: implications of the loss of a metal in protein structure, stability, and solvent network, *Biochemistry 48*, 7365-7372.

448. Cleland, J. L., and Wang, D. I. (1990) Refolding and aggregation of bovine carbonic anhydrase B: quasi-elastic light scattering analysis, *Biochemistry 29*, 11072-11078.

449. Karlsson, M., Mårtensson, L., Olofsson, P., and Carlsson, U. (2004) Circumnavigating misfolding traps in the energy landscape through protein engineering: suppression of molten globule and aggregation in carbonic anhydrase, *Biochemistry 43*, 6803-6807.

450. Forster, R.E. (1991) The Carbonic Anhydrases: Cellular physiology and molecular

genetics (Dodgson, S. J., Tashian, R. E.,Gros, G., and Carter, N. D., Eds.) pp. 79–98, Plenum, New York.

451. WILBUR, K. M., and ANDERSON, N. G. (1948) Electrometric and colorimetric determination of carbonic anhydrase, *J. Biol. Chem 176*, 147-154.

452. Verpoorte, J. A., Mehta, S., and Edsall, J. T. (1967) Esterase activities of human carbonic anhydrases B and C, *J. Biol. Chem 242*, 4221-4229.

453. Silverman, D. N. (1982) Carbonic anhydrase: oxygen-18 exchange catalyzed by an enzyme with rate-contributing proton-transfer steps, *Meth. Enzymol 87*, 732-752.

454. King, R. W., and Burgen, A. S. (1970) Sulphonamide complexes of human carbonic anhydrases. Ultraviolet difference spectroscopy, *Biochim. Biophys. Acta 207*, 278-285.

455. LINDSKOG, S. (1963) Effects of pH and inhibitors on some properties related to metal binding in bovine carbonic anhydrase, *J. Biol. Chem 238*, 945-951.

456. Kaiser, E. T., and Lo, K. (1969) Carbonic anhydrase catalyzed hydrolysis of 2-hydroxy-5-nitro-.alpha.-toluenesulfonic acid sultone, *Journal of the American Chemical Society 91*, 4912-4918.

457. Taylor, J. S., Mushak, P., and Coleman, J. E. (1970) Electron spin resonance studies of carbonic anhydrase: transition metal ions and spin-labeled sulfonamides, *Proc. Natl. Acad. Sci. U.S.A 67*, 1410-1416.

458. Olander, J., Bosen, S. F., and Kaiser, E. T. (1973) Binding of two sulfonamides to carbonic anhydrase,, *Journal of the American Chemical Society 95*, 1616-1621.

459. King, R. W., and Burgen, A. S. (1976) Kinetic aspects of structure-activity relations: the binding of sulphonamides by carbonic anhydrase, *Proc. R. Soc. Lond., B, Biol. Sci*

193, 107-125.

460. Kernohan, J. C. (1970) Fluorescence technique for studying the binding of sulphonamide and other inhibitors to carbonic anhydrase, *Biochem. J 120*, 26P.

461. Agrò, F., Morpurgo, L., and Mondovi, B. (1974) Effect of metal binding on the intrinsic fluorescence of bovine carbonic anhydrase, *Biophys. Chem 2*, 151-157.

462. Jain, A., Huang, S. G., and Whitesides, G. M. (1994) Lack of Effect of the Length of Oligoglycine- and Oligo(ethylene glycol)-Derived para-Substituents on the Affinity of Benzenesulfonamides for Carbonic Anhydrase II in Solution, *Journal of the American Chemical Society 116*, 5057-5062.

463. Grzybowski, B. A., Ishchenko, A. V., Kim, C., Topalov, G., Chapman, R., Christianson, D. W., Whitesides, G. M., and Shakhnovich, E. I. (2002) Combinatorial computational method gives new picomolar ligands for a known enzyme, *Proc. Natl. Acad. Sci. U.S.A 99*, 1270-1273.

464. Banerjee, J., Haldar, M. K., Manokaran, S., Mallik, S., and Srivastava, D. K. (2007) New fluorescent probes for carbonic anhydrases, *Chem. Commun.* 2723-2725.

465. Thompson, R. B., Maliwal, B. P., and Fierke, C. A. (1999) Selectivity and sensitivity of fluorescence lifetime-based metal ion biosensing using a carbonic anhydrase transducer, *Anal. Biochem 267*, 185-195.

466. Whitesides, G. M., and Krishnamurthy, V. M. (2005) Designing ligands to bind proteins, *Q. Rev. Biophys 38*, 385-395.

467. Krishnamurthy, V. M., Bohall, B. R., Kim, C., Moustakas, D. T., Christianson, D. W., and Whitesides, G. M. (2007) Thermodynamic parameters for the association of fluorinated benzenesulfonamides with bovine carbonic anhydrase II, *Chem Asian J 2*,

94-105.

468. Talhout, R., Villa, A., Mark, A. E., and Engberts, J. B. F. N. (2003) Understanding binding affinity: a combined isothermal titration calorimetry/molecular dynamics study of the binding of a series of hydrophobically modified benzamidinium chloride inhibitors to trypsin, *J. Am. Chem. Soc 125*, 10570-10579.

469. Wiseman, T., Williston, S., Brandts, J. F., and Lin, L. N. (1989) Rapid measurement of binding constants and heats of binding using a new titration calorimeter, *Anal. Biochem 179*, 131-137.

470. Khalifah, R. G., Zhang, F., Parr, J. S., and Rowe, E. S. (1993) Thermodynamics of binding of the CO2-competitive inhibitor imidazole and related compounds to human carbonic anhydrase I: an isothermal titration calorimetry approach to studying weak binding by displacement with strong inhibitors, *Biochemistry 32*, 3058-3066.

471. Pierce, M. M., Raman, C. S., and Nall, B. T. (1999) Isothermal titration calorimetry of protein-protein interactions, *Methods 19*, 213-221.

472. DiTusa, C. A., Christensen, T., McCall, K. A., Fierke, C. A., and Toone, E. J. (2001) Thermodynamics of metal ion binding. 1. Metal ion binding by wild-type carbonic anhydrase, *Biochemistry 40*, 5338-5344.

473. Day, Y. S. N., Baird, C. L., Rich, R. L., and Myszka, D. G. (2002) Direct comparison of binding equilibrium, thermodynamic, and rate constants determined by surface- and solution-based biophysical methods, *Protein Sci 11*, 1017-1025.

474. Melkko, S., Scheuermann, J., Dumelin, C. E., and Neri, D. (2004) Encoded self-assembling chemical libraries, *Nat. Biotechnol 22*, 568-574.

475. Krishnamurthy, V. M., Bohall, B. R., Semetey, V., and Whitesides, G. M. (2006) The

paradoxical thermodynamic basis for the interaction of ethylene glycol, glycine, and sarcosine chains with bovine carbonic anhydrase II: an unexpected manifestation of enthalpy/entropy compensation, *J. Am. Chem. Soc 128*, 5802-5812.

476. A new, general method for the determination of binding constants: photoacoustic titration of dansylamide with carbonic anhydrase. Text.

477. Bayley, P., and Anson, M. (1975) Stopped-flow circular dichroism: a rapid kinetic study of the binding of a sulphonamide drug to bovine carbonic anhydrase, *Biochem. Biophys. Res. Commun 62*, 717-722.

478. Gianazza, E., Sirtori, C. R., Castiglioni, S., Eberini, I., Chrambach, A., Rondanini, A., and Vecchio, G. (2000) Interactions between carbonic anhydrase and its inhibitors revealed by gel electrophoresis and circular dichroism, *Electrophoresis 21*, 1435-1445.

479. Freskgård, P. O., Mårtensson, L. G., Jonasson, P., Jonsson, B. H., and Carlsson, U. (1994) Assignment of the contribution of the tryptophan residues to the circular dichroism spectrum of human carbonic anhydrase II, *Biochemistry 33*, 14281-14288.

480. Deng, G., and Sanyal, G. (2006) Applications of mass spectrometry in early stages of target based drug discovery, *J Pharm Biomed Anal 40*, 528-538.

481. Nesatyy, V. J. (2002) Mass spectrometry evaluation of the solution and gas-phase binding properties of noncovalent protein complexes, *International Journal of Mass Spectrometry 221*, 147-161.

482. Daniel, J. M., Friess, S. D., Rajagopalan, S., Wendt, S., and Zenobi, R. (2002) Quantitative determination of noncovalent binding interactions using soft ionization mass spectrometry, *International Journal of Mass Spectrometry 216*, 1-27.

483. Purcell, A. W., and Gorman, J. J. (2004) Immunoproteomics: Mass spectrometry-based methods to study the targets of the immune response, *Mol. Cell Proteomics 3*, 193-208.

484. Naylor, S., and Kumar, R. (2003) Emerging role of mass spectrometry in structural and functional proteomics, *Adv. Protein Chem 65*, 217-248.

485. Sickmann, A., Mreyen, M., and Meyer, H. E. (2003) Mass spectrometry--a key technology in proteome research, *Adv. Biochem. Eng. Biotechnol 83*, 141-176.

486. Mann, M., Hendrickson, R. C., and Pandey, A. (2001) Analysis of proteins and proteomes by mass spectrometry, *Annu. Rev. Biochem 70*, 437-473.

487. Hofstadler, S. A., and Sannes-Lowery, K. A. (2006) Applications of ESI-MS in drug discovery: interrogation of noncovalent complexes, *Nat Rev Drug Discov 5*, 585-595.

488. Loo, J. A. (2003) The tools of proteomics, *Adv. Protein Chem 65*, 25-56.

489. Aebersold, R., and Mann, M. (2003) Mass spectrometry-based proteomics, *Nature 422*, 198-207.

490. Nousiainen, M., Derrick, P. J., Lafitte, D., and Vainiotalo, P. (2003) Relative affinity constants by electrospray ionization and Fourier transform ion cyclotron resonance mass spectrometry: calmodulin binding to peptide analogs of myosin light chain kinase, *Biophys. J 85*, 491-500.

491. Aebersold, R. (2003) A mass spectrometric journey into protein and proteome research, *J. Am. Soc. Mass Spectrom 14*, 685-695.

492. Regan, C. K., Craig, S. L., and Brauman, J. I. (2002) Steric effects and solvent effects in ionic reactions, *Science 295*, 2245-2247.

493. Gronert, S. (2001) Mass spectrometric studies of organic ion/molecule reactions,

Chem. Rev 101, 329-360.

494. Roughton, F. J., and Booth, V. H. (1946) The effect of substrate concentration, pH and other factors upon the activity of carbonic anhydrase, *Biochem. J 40*, 319-330.

495. Kiese, M. (1941) Kinetica of carbonic anhydrase I, *Biochem. Z. 307*, 400-413.

496. KERNOHAN, J. C., FORREST, W. W., and ROUGHTON, F. J. (1963) The activity of concentrated solutions of carbonic anhydrase, *Biochim. Biophys. Acta 67*, 31-41.

497. Kernohan, J. C. (1966) A method for studying the kinetics of the inhibition of carbonic anhydrase by sulphonamides, *Biochim. Biophys. Acta 118*, 405-412.

498. Pocker, Y., and Stone, J. T. (1965) The Catalytic Versatility of Erythrocyte Carbonic Anhydrase. The Enzyme-Catalyzed Hydrolysis of p-Nitrophenyl Acetate, *Journal of the American Chemical Society 87*, 5497-5498.

499. Pocker, Y., and Stone, J. T. (1968) The catalytic versatility of erythrocyte carbonic anhydrase. VI. Kinetic studies of noncompetitive inhibition of enzyme-catalyzed hydrolysis of p-nitrophenyl acetate, *Biochemistry 7*, 2936-2945.

500. Pocker, Y., and Storm, D. R. (1968) Catalytic versatility of erythrocyte carbonic anhydrase. IV. Kinetic studies of enzyme-catalyzed hydrolyses of p-nitrophenyl esters, *Biochemistry 7*, 1202-1214.

501. Pocker, Y., and Stone, J. T. (1968) Catalytic versatility of erythrocyte carbonic anhydrase. VII. Kinetic studies of esterase activity and competitive inhibition by substrate analogs, *Biochemistry 7*, 3021-3031.

502. Taylor, P. W., King, R. W., and Burgen, A. S. (1970) Kinetics of complex formation between human carbonic anhydrases and aromatic sulfonamides, *Biochemistry 9*, 2638-2645.

503. Sambrook, J., Fritsch, E. F., and Maniatis, T. (2000) Molecular cloning: A Laboratory Manual, Cold Spring Harbor Laboratory Press, Plainview, NY.

504. Bradford, M. M. (1976) A rapid and sensitive method for the quantitation of microgram quantities of protein utilizing the principle of protein-dye binding, *Anal. Biochem 72*, 248-254.

505. Pocker, Y., and Stone, J. T. (1967) The Catalytic Versatility of Erythrocyte Carbonic Anhydrase. III. Kinetic Studies of the Enzyme-Catalyzed Hydrolysis of p-Nitrophenyl Acetate*, *Biochemistry 6*, 668-678.

506. Qin, L., and Srivastava, D. K. (1998) Energetics of two-step binding of a chromophoric reaction product, trans-3-indoleacryloyl-CoA, to medium-chain acyl-coenzyme-A dehydrogenase, *Biochemistry 37*, 3499-3508.

507. Chakravarty, S., and Kannan, K. K. (1994) Drug-protein interactions. Refined structures of three sulfonamide drug complexes of human carbonic anhydrase I enzyme, *J. Mol. Biol 243*, 298-309.

508. Beschiaschvili, G., and Seelig, J. (1992) Peptide binding to lipid bilayers. Nonclassical hydrophobic effect and membrane-induced pK shifts, *Biochemistry 31*, 10044-10053.

509. Doyle, M. L., Louie, G., Dal Monte, P. R., and Sokoloski, T. D. (1995) Tight binding affinities determined from thermodynamic linkage to protons by titration calorimetry, *Meth. Enzymol 259*, 183-194.

510. Morin, P. E., and Freire, E. (1991) Direct calorimetric analysis of the enzymatic activity of yeast cytochrome c oxidase, *Biochemistry 30*, 8494-8500.

511. Jelesarov, I., and Bosshard, H. R. (1994) Thermodynamics of ferredoxin binding to

ferredoxin:NADP+ reductase and the role of water at the complex interface, *Biochemistry 33*, 13321-13328.

512. Nicholls, A., Sharp, K. A., and Honig, B. (1991) Protein folding and association: insights from the interfacial and thermodynamic properties of hydrocarbons, *Proteins 11*, 281-296.

513. Santoro, M. M., and Bolen, D. W. (1988) Unfolding free energy changes determined by the linear extrapolation method. 1. Unfolding of phenylmethanesulfonyl alpha-chymotrypsin using different denaturants, *Biochemistry 27*, 8063-8068.

514. Sambrook, J., Fritsch, E., and Maniatis, T. (1989) Molecular Cloning: A Laboratory Manual second ed. Cold Spring Harbor Laboratory, Cold spring Harbor, NY.

515. McCawley, L. J., and Matrisian, L. M. (2001) Matrix metalloproteinases: they're not just for matrix anymore!, *Curr. Opin. Cell Biol 13*, 534-540.

516. Coussens, L. M., Fingleton, B., and Matrisian, L. M. (2002) Matrix metalloproteinase inhibitors and cancer: trials and tribulations, *Science 295*, 2387-2392.

517. Stöcker, W., Grams, F., Baumann, U., Reinemer, P., Gomis-Rüth, F. X., McKay, D. B., and Bode, W. (1995) The metzincins--topological and sequential relations between the astacins, adamalysins, serralysins, and matrixins (collagenases) define a superfamily of zinc-peptidases, *Protein Sci 4*, 823-840.

518. Bode, W., Fernandez-Catalan, C., Tschesche, H., Grams, F., Nagase, H. and Maskos, K. (1999) Structural properties of matrix metalloproteinases., *Cell. Mol. Life Sci. 55*, 639-652.

519. Sang, Q.A. and Douglas, D.A. (1996) Computational sequence analysis of matrix

metalloproteinases., *J. Protein Chem. 15*, 137-160.

520. Banerjee, A. L., Eiler, D., Roy, B. C., Jia, X., Haldar, M. K., Mallik, S., and Srivastava, D. K. (2005) Spacer-based selectivity in the binding of "two-prong" ligands to recombinant human carbonic anhydrase I, *Biochemistry 44*, 3211-3224.
521. Takaoka, Y., Tsutsumi, H., Kasagi, N., Nakata, E., and Hamachi, I. (2006) One-pot and sequential organic chemistry on an enzyme surface to tether a fluorescent probe at the proximity of the active site with restoring enzyme activity, *J. Am. Chem. Soc 128*, 3273-3280.
522. Fierke, C. A., and Thompson, R. B. (2001) Fluorescence-based biosensing of zinc using carbonic anhydrase, *Biometals 14*, 205-222.
523. Thompson, R. B., Whetsell, W. O., Maliwal, B. P., Fierke, C. A., and Frederickson, C. J. (2000) Fluorescence microscopy of stimulated Zn(II) release from organotypic cultures of mammalian hippocampus using a carbonic anhydrase-based biosensor system, *J. Neurosci. Methods 96*, 35-45.
524. Supuran, C. T., and Scozzafava, A. (2002) Applications of carbonic anhydrase inhibitors and activators in therapy, , *Expert Opin. Ther. Pat. 12*, 217-242.
525. Vullo, D., Franchi, M., Gallori, E., Antel, J., Scozzafava, A., and Supuran, C. T. (2004) Carbonic anhydrase inhibitors. Inhibition of mitochondrial isozyme V with aromatic and heterocyclic sulfonamides, *J. Med. Chem 47*, 1272-1279.
526. Weber, G., and Young, L. B. (1964) Fragmentation of bovine serum albumin by pepsin. II. Isolation, aminoacid composition and physical properties of the fragments, *J. Biol. Chem 239*, 1424-1431.
527. Chen, R. F. (1967) Fluorescence of dansyl amino acids in organic solvents and

protein solutions, *Archives of Biochemistry and Biophysics 120*, 609-620.

528. Cordes, E. H., and Jencks, W. P. (1962) On the Mechanism of Schiff Base Formation and Hydrolysis1, *Journal of the American Chemical Society 84*, 832-837.

529. Coleman, J. E. (1975) Chemical reactions of sulfonamides with carbonic anhydrase, *Annu Rev Pharmacol 15*, 221-242.

530. Gupta, S. P. (2003) Quantitative structure-activity relationships of carbonic anhydrase inhibitors, *Prog Drug Res 60*, 171-204.

531. Vedani, A., and Meyer, E. F. (1984) Structure-activity relationships of sulfonamide drugs and human carbonic anhydrase C: modeling of inhibitor molecules into the receptor site of the enzyme with an interactive computer graphics display, *J Pharm Sci 73*, 352-358.

532. Menziani, M. C., De Benedetti, P. G., Gago, F., and Richards, W. G. (1989) The binding of benzenesulfonamides to carbonic anhydrase enzyme. A molecular mechanics study and quantitative structure-activity relationships, *J. Med. Chem 32*, 951-956.

533. Tripp, B. C., Smith, K., and Ferry, J. G. (2001) Carbonic Anhydrase: New Insights for an Ancient Enzyme ,, *Journal of Biological Chemistry 276*, 48615 -48618.

534. Gepshtein, R., Huppert, D., and Agmon, N. (2006) Deactivation mechanism of the green fluorescent chromophore, *J Phys Chem B 110*, 4434-4442.

535. G. G. Hammes, Thermodynamics and Kinetics for the Biological Sciences. John Wiley & Sons Inc. (2000), New York.

536. Lin, L. N., Mason, A. B., Woodworth, R. C., and Brandts, J. F. (1991) Calorimetric studies of the binding of ferric ions to ovotransferrin and interactions between binding

sites, *Biochemistry 30*, 11660-11669.

537. Jelesarov, I., and Bosshard, H. R. (1994) Thermodynamics of ferredoxin binding to ferredoxin:NADP+ reductase and the role of water at the complex interface, *Biochemistry 33*, 13321-13328.

538. Banerjee, A.L. (2006) Enzyme Ligand Interactions in Carbonic Anhydrase Isozymes. North Dakota State University.

539. Tashian, R. E., Venta, P. J., Nicewander, P. H., and Hewett-Emmett, D. (1990) Evolution, structure, and expression of the carbonic anhydrase multigene family, *Prog. Clin. Biol. Res 344*, 159-175.

540. Sturtevant, J. M. (1977) Heat capacity and entropy changes in processes involving proteins, *Proc. Natl. Acad. Sci. U.S.A 74*, 2236-2240.

541. Spolar, R. S., and Record, M. T. (1994) Coupling of local folding to site-specific binding of proteins to DNA, *Science 263*, 777-784.

542. Srivastava, D. K., Wang, S., and Peterson, K. L. (1997) Isothermal titration microcalorimetric studies for the binding of octenoyl-CoA to medium chain acyl-CoA dehydrogenase, *Biochemistry 36*, 6359-6366.

543. Chen, W. (2008) Nanoparticle fluorescence based technology for biological applications, *J Nanosci Nanotechnol 8*, 1019-1051.

544. J.R. Lakowicz, Principles of Fluorescence Spectroscopy, 2nd ed., Kluwer Academic/ Plenum Publishers, New York, 1999.

545. Hecky, J., and Müller, K. M. (2005) Structural perturbation and compensation by directed evolution at physiological temperature leads to thermostabilization of beta-lactamase, *Biochemistry 44*, 12640-12654.

546. Morton, A., Baase, W. A., and Matthews, B. W. (1995) Energetic origins of specificity of ligand binding in an interior nonpolar cavity of T4 lysozyme, *Biochemistry 34*, 8564-8575.

547. (1935) Apparent Molal Heat Capacities of Amino Acids and Other Organic Compounds, *J. Am. Chem. Soc. 57*, 1506–1507.

548. Tanford, C. 1980. The Hydrophobic Effect, 2d ed., Wiley, New York.

549. Privalov, P. L. (1979) Stability of proteins: small globular proteins, *Adv. Protein Chem 33*, 167-241.

550. Spolar, R. S., Ha, J. H., and Record, M. T. (1989) Hydrophobic effect in protein folding and other noncovalent processes involving proteins, *Proc. Natl. Acad. Sci. U.S.A 86*, 8382-8385.

551. Murphy, K. P., Xie, D., Garcia, K. C., Amzel, L. M., and Freire, E. (1993) Structural energetics of peptide recognition: angiotensin II/antibody binding, *Proteins 15*, 113-120.

552. Makhatadze, G. I., and Privalov, P. L. (1990) Heat capacity of proteins. I. Partial molar heat capacity of individual amino acid residues in aqueous solution: hydration effect, *J. Mol. Biol 213*, 375-384.

553. Dill, K. A. (1990) Dominant forces in protein folding, *Biochemistry 29*, 7133-7155.

554. Rowe, E. S., Zhang, F., Leung, T. W., Parr, J. S., and Guy, P. T. (1998) Thermodynamics of membrane partitioning for a series of n-alcohols determined by titration calorimetry: role of hydrophobic effects, *Biochemistry 37*, 2430-2440.

555. Makhatadze, G. I., and Privalov, P. L. (1993) Contribution of hydration to protein folding thermodynamics. I. The enthalpy of hydration, *J. Mol. Biol 232*, 639-659.

556. Fierke, C. A., Calderone, T. L., and Krebs, J. F. (1991) Functional consequences of engineering the hydrophobic pocket of carbonic anhydrase II, *Biochemistry 30*, 11054-11063.

557. Nair, S. K., Krebs, J. F., Christianson, D. W., and Fierke, C. A. (1995) Structural basis of inhibitor affinity to variants of human carbonic anhydrase II, *Biochemistry 34*, 3981-3989.

558. Wu, Z., Zhang, B., and Yan, B. (2009) Regulation of enzyme activity through interactions with nanoparticles, *Int J Mol Sci 10*, 4198-4209.

559. Fischer, N. O., McIntosh, C. M., Simard, J. M., and Rotello, V. M. (2002) Inhibition of chymotrypsin through surface binding using nanoparticle-based receptors, *Proc. Natl. Acad. Sci. U.S.A 99*, 5018-5023.

560. Monod, J., Wyman, J., and Changeux, J. P. (1965) On the nature of allosteric transitions: a plausible model, *J. Mol. Biol 12*, 88-118.

561. Lynch, I., and Dawson, K. A. Protein-nanoparticle interactions, *Nano Today 3*, 40-47.

562. Kumar, S., and Nussinov, R. (2001) How do thermophilic proteins deal with heat?, *Cell. Mol. Life Sci 58*, 1216-1233.

563. Fei, L., and Perrett, S. (2009) Effect of nanoparticles on protein folding and fibrillogenesis, *Int J Mol Sci 10*, 646-655.

564. Ganguly, B., and Srivastava, D. K. (2008) Influence of "Flexible" versus "Rigid" Nanoparticles on the Stability of Matrix Metalloproteinase-7, *J Biomed Nanotechnol 4*, 457-462.

565. Hantgan, R. R., Stahle, M. C., Connor, J. H., Horita, D. A., Rocco, M., McLane, M. A., Yakovlev, S., and Medved, L. (2006) Integrin alphaIIbbeta3:ligand interactions

are linked to binding-site remodeling, *Protein Sci 15*, 1893-1906.

566. Ohki, S., and Arnold, K. (2008) Experimental evidence to support a theory of lipid membrane fusion, *Colloids Surf B Biointerfaces 63*, 276-281.

567. Sanii, B., Smith, A. M., Butti, R., Brozell, A. M., and Parikh, A. N. (2008) Bending membranes on demand: fluid phospholipid bilayers on topographically deformable substrates, *Nano Lett 8*, 866-871.

568. Creighton, T. E. Proteins: Structures and Molecular Properties., 2nd ed.; W. H. Freeman and Company: New York, 1993.

569. Pollak, E., and Talkner, P. (2005) Reaction rate theory: what it was, where is it today, and where is it going?, *Chaos 15*, 26116.

570. Razvi, A., and Scholtz, J. M. (2006) Lessons in stability from thermophilic proteins, *Protein Sci 15*, 1569-1578.

571. KAUZMANN, W. (1959) Some factors in the interpretation of protein denaturation, *Adv. Protein Chem 14*, 1-63.

572. Rose, G. D., and Wolfenden, R. (1993) Hydrogen bonding, hydrophobicity, packing, and protein folding, *Annu Rev Biophys Biomol Struct 22*, 381-415.

573. Pace, C. N., Shirley, B. A., McNutt, M., and Gajiwala, K. (1996) Forces contributing to the conformational stability of proteins, *FASEB J 10*, 75-83.

574. Honig, B. (1999) Protein folding: from the levinthal paradox to structure prediction, *J. Mol. Biol 293*, 283-293.

575. Creighton, T.E. Folding and binding., *Curr. Opin. Struct. Biol. 2*, 1-5.

576. Jonasson, P., Aronsson, G., Carlsson, U., and Jonsson, B. H. (1997) Tertiary structure formation at specific tryptophan side chains in the refolding of human carbonic

anhydrase II, *Biochemistry 36*, 5142-5148.

577. Semisotnov, G. V., Uversky, V. N., Sokolovsky, I. V., Gutin, A. M., Razgulyaev, O. I., and Rodionova, N. A. (1990) Two slow stages in refolding of bovine carbonic anhydrase B are due to proline isomerization, *J. Mol. Biol 213*, 561-568.